UNIVERSIDADE DE LISBOA
INSTITUTO SUPERIOR TÉCNICO

Semi-active systems for structural vibration mitigation

Fernando Virgílio Pires de Oliveira

Supervisor: Doctor Afzal Suleman

Co-Supervisor: Doctor Paulo Jorge Gil de Morais

Thesis approved in public session to obtain the PhD degree in
Mechanical Engineering

Jury final classification: Pass with Merit

Jury

Chairperson: Chairman of the IST Scientific Board

Members of the Committee

Doctor Nuno Manuel Mendes Maia
Doctor Miguel Afonso Dias de Ayala Botto
Doctor Afzal Suleman
Doctor Francisco Manuel Gonçalves Alves Salgado
Doctor Carlos Manuel Ramos Moutinho
Doctor Paulo Jorge Gil de Morais

2015

UNIVERSIDADE DE LISBOA

INSTITUTO SUPERIOR TÉCNICO

Semi-active systems for structural vibration mitigation

Fernando Virgílio Pires de Oliveira

Supervisor: Doctor Afzal Suleman

Co-Supervisor: Doctor Paulo Jorge Gil de Morais

Thesis approved in public session to obtain the PhD degree in
Mechanical Engineering

Jury final classification: Pass with Merit

Jury

Chairperson: Chairman of the IST Scientific Board

Members of the Committee

Doctor Nuno Manuel Mendes Maia, Professor Associado (com Agregação) do Instituto Superior Técnico da Universidade de Lisboa

Doctor Miguel Afonso Dias de Ayala Botto, Professor Associado (com Agregação) do Instituto Superior Técnico da Universidade de Lisboa

Doctor Afzal Suleman, Professor Associado (com Agregação) do Instituto Superior Técnico da Universidade de Lisboa

Doctor Francisco Manuel Gonçalves Alves Salgado, Investigador Principal do Laboratório Nacional de Engenharia Civil, I.P.

Doctor Carlos Manuel Ramos Moutinho, Professor Auxiliar da Faculdade de Engenharia da Universidade do Porto

Doctor Paulo Jorge Gil de Morais, Investigador Auxiliar do Laboratório Nacional de Engenharia Civil, I.P.

Funding Institution
Fundação para a Ciência e a Tecnologia

2015

The research presented in this dissertation has been performed under the partnership agreement between the Laboratório Nacional de Engenharia Civil (LNEC) and Instituto Superior Técnico (IST). The work was performed at LNEC, with its resources and also with the resources provided by the Mechanical Engineering Department of IST and Instituto de Engenharia Mecânica (IDMEC), which are located in Lisbon, Portugal.

LABORATÓRIO NACIONAL DE ENGENHARIA CIVIL

TÉCNICO LISBOA

This dissertation was funded by Fundação para a Ciência e a Tecnologia (FCT) of the Ministério da Educação e Ciência of Portugal under the grant SFRH/BD/84769/2012.

FCT Fundação para a Ciência e a Tecnologia
MINISTÉRIO DA EDUCAÇÃO E CIÊNCIA

Fernando Virgílio Pires de Oliveira

Laboratório Nacional de Engenharia Civil
Centro de Instrumentação Científica
Núcleo de Sistemas Eletrotécnicos e Mecânicos
Av. do Brasil, 101
1700-066 Lisboa, Portugal
Phone: +351218443494
email: fvoliveira@lnec.pt
URL: http://www.lnec.pt/organizacao/cic/nsem

To my family and

to all who helped me in this journey

Resumo

Título: Modelação de Sistemas Semi-ativos para a mitigação de vibrações em estruturas

Nome: Fernando Virgílio Pires de Oliveira

Doutoramento: Engenharia Mecânica

Orientador: Doutor Afzal Suleman

Co-Orientador: Doutor Paulo Jorge Gil de Morais

Resumo

Nos últimos anos foram propostos novos conceitos para controlo de vibrações de estruturas sujeitas a ações sísmicas. No caso particular de estruturas com isolamento de base requerem-se sistemas amortecedores que reduzam os deslocamentos ao nível do sistema de isolamento sem aumentar as respostas da superstrutura. Neste trabalho é explorada a hipótese da utilização de amortecedores de característica variável que usam a informação das respostas estruturais para ajuste da força dissipativa. Várias estratégias de controlo foram identificadas e sistematizadas para aplicação a este contexto. Estratégias que têm em consideração as não linearidades e atrasos no tempo foram formuladas e estudadas. Esquemas baseados no seguimento de força que compreendem um controlador linear tal como, a ação integral, o regulador linear quadrático e o controlador preditivo, juntamente com um algoritmo de ajuste da entrada no amortecedor, a estratégia baseada na linearização por realimentação e o controlo por modo de deslizamento são considerados na resolução deste problema. O controlo colocado é proposto numa perspetiva de evitar as limitações na medição e facilitar a sua implementação. É proposto um método de sintonia dos parâmetros do controlador dada a variabilidade da ação sísmica e as não linearidades envolvidas. São efetuadas simulações numéricas e uma campanha experimental utilizando modelos representativos para avaliar o desempenho da solução proposta. Como resultado das comparações efetuadas, uma estratégia em particular apresentou um bom desempenho, o que permite definir indicações para aplicações à escala real.

Palavras Chave:

Controlo semi-ativo; Controlador com ação integral; Regulador linear quadrático; Controlo preditivo; Controlo por linearização através da realimentação não-linear da saída; Proteção sísmica; Isolamento de base híbrido; Mitigação de vibrações; Amortecedores do tipo viscoso; Amortecedores Magneto-Reológicos.

Abstract

Title: Semi-active systems for structural vibration mitigation

Name: Fernando Virgílio Pires de Oliveira

PhD Degree in: Mechanical Engineering

Supervisor: Doctor Afzal Suleman

Co-Supervisor: Doctor Paulo Jorge Gil de Morais

Abstract

In recent years new concepts for vibration control of structures when subjected to earthquakes have been proposed. In base-isolated structures damping systems which can reduce the base isolator displacements without increasing superstructure response have been required. Controllable dampers that use the structural response information to adapt themselves are exploited in this work. Several control strategies were identified and systematised for use in this context. Strategies that take into account the non-linearities and time delays are formulated. Force tracking schemes comprising a linear controller such as the integral controller, the linear quadratic regulator and the model predictive controller plus a "clipped" algorithm, a nonlinear output feedback controller as well as the sliding mode control are considered to tackle this problem. Collocated control is proposed to avoid the measurement limitations and facilitate the technological development of semi-active systems. A tuning method to adjust the controller parameters is proposed to account the variability of the ground motion and the nonlinearities. Numerical simulations and an experimental campaign using representative models was performed to evaluate the performance of those strategies. As a result of this comparative study one particular strategy showed good performance leading to important guidelines for real scale implementation.

Keywords:

Semi-active control; Integral controller; Linear quadratic regulator; Predictive control; Nonlinear output feedback control; Seismic protection; Hybrid base-isolation; Vibration mitigation; Fluid viscous dampers; Magneto-Rheological dampers.

Acknowledgements

This work is the result of an effort carried out not only by the author, but also by some people and institutions that contribute and motivate the author to finalize this journey. The author would like to express his gratitude and acknowledgement to everybody that, in one way or another, contributed to this work and helped him to develop it in its present stage. In the following lines are expressed the author's recognition to those that much contribute to this work:

- To the Laboratório Nacional de Engenharia Civil (LNEC), where the work was developed, to whom the author acknowledges in the person of the Board of Directors (actual and previous ones), for providing the main conditions for this research work, namely the research grant provided, the facilities, the materials and staff, which undoubtedly contributed to his formation;
- To the Instituto de Engenharia Mecânica (IDMEC) and Instituto Superior Técnico (IST) for providing also several resources and financial support to develop this work;
- To the Fundação para a Ciência e a Tecnologia (FCT), for financial support through grant reference number SFRH/BD/84769/2012;
- To the supervisors, Prof. Afzal Suleman and Eng. Paulo Morais, by their excellent guidance, discussions, for always being available, and for keep him encouraged with his care and friendship;
- To the Director of the Centro de Instrumentação Científica from LNEC, Eng. Carlos Oliveira Costa, for providing all the resources accessible in the development of the work;
- To Eng. Francisco Carvalhal, who support and express his interest in this theme since the beginning of this journey, as the department Director and member of LNEC's Board of Directors, and later with who the author had fruitful discussions and learned in a wide range of topics;
- To Eng. Almeida Santos, Eng. Almeida Garrett, Eng. João Palma and Mr. João Paixão from LNEC, for their kind help in developing the electronic equipments and interfaces, and for always being available in keeping the experimental installation working;
- To Eng. Alfredo Campos Costa and Eng. Paulo Candeias from LNEC, for providing the experimental installation at Ferry Borges building to develop this work; their kindly support, interest, advices and several fructuous discussions were also important; also

to Eng. António Correia, to the laboratory technicians staff, Mr. Artur Santos, Mr. Rúben Santos and Eng. Susana Almeida for providing the required means at the laboratory;

- To Prof. Miguel Ayala Botto from IST, for his guidance, support and invaluable advices in this subject when the author attended to the course of Advanced Control Systems;
- To Prof. Relógio Ribeiro from IST and Eng. Toco Emílio from LNEC, for their kind help and advices in developing the experimental model;
- To his colleague Eng. Alexandre Freitas, from LNEC, who kindly develop and design the experimental model used in this work, and with who he had interesting and fructuous discussions;
- To Doctor Álvaro Silva Ribeiro, Eng. Luís Martins, Eng. José Louro, Mr. Alexandre Pinheiro, Mr. António Pais, Mr. José Barreiros, Mr. Paulo Marques and Mr. Ricardo Mendes for providing the resources and helping with the instruments calibration, at LNEC;
- To his colleague Doctor Maria João Falcão and Doctor Cristina Oliveira for their kind guidance and support on this subject;
- To his colleagues Eng. João Reis, Eng. Gustavo Coelho and Mr. Iúri Martins from LNEC for their concern, support and companionship;
- To his colleague Eng. Luis Pinto from LNEC, for his kind support, professionalism and availability in helping the author during the experimental campaign;
- To Prof. Nuno Maia from IST, for his interest in this subject, support and advices;
- To Mr. Rogério Pereira, Mr. Joaquim Moura, Mr. Paulo Pires, Mr. Arménio Silva, Mr. Cláudio Neves and Mr. Eduardo Fernandes from LNEC, for their assistance in constructing the experimental model, technical support and companionship;
- To the administrative staff from LNEC and IST, Mrs. Francelina Lopes, Mrs. Rute Silva, Mrs. Elvira Silva and Mrs. Carla Leitão;
- To several colleagues whose names are not listed, which provided assistance one way or another, the author feels very much indebted;
- To all my friends and specially my family, I would like to thank wholeheartedly for their companionship, concern, support, assistance and never-ending encouragement.

Fernando Virgílio Pires de Oliveira

Table of Contents

Resumo.....i
Abstract.....iii
Acknowledgements.....v
Table of Contents.....vii
List of Figures.....ix
List of Tables.....xv
List of Abbreviations.....xix
List of Symbols.....xxi
Publications.....xxv
Chapter 1 - Introduction.....1
1.1 Motivation.....2
1.2 Objective.....4
1.3 Outline of the Dissertation.....6
Chapter 2 - State-of-the-Art.....9
2.1 Historic Evolution.....10
2.2 Seismic Risk.....12
2.3 Earthquakes.....13
2.3.1 Earthquake: a natural disaster.....13
2.3.2 Seismic Action.....15
2.3.3 The Seismic Action for the Portuguese Territory.....16
2.3.4 The Seismic Action and Structures Natural Frequencies.....18
2.4 Seismic Safety.....20
2.4.1 Seismic Safety Enhancement using Resistance Capacity.....21
2.4.2 Seismic Safety Enhancement using Protection Systems.....22
2.5 Semi-Active Control.....28
2.6 Hybrid Base-Isolated Structures With SA Devices.....30
2.7 Base-isolated Structures.....32
2.7.1 Structural Models.....32
2.7.2 Damping Models.....33
2.7.3 State-Space model.....34
2.8 Semi-active devices.....35
2.8.1 Devices Formulation.....35
2.8.2 Fluid Viscous Dampers.....35
2.8.3 Magneto-rheological Dampers.....42
2.9 Control Strategies.....61
2.9.1 Problem Formulation.....61
2.9.2 Classical Control.....64
2.9.3 Optimal Control.....65
2.9.4 Lyapunov based methods.....69
2.9.5 Modulated Homogeneous Friction.....70
2.9.6 Force Derivative Feedback.....71
2.9.7 Sliding Mode Control.....71
2.9.8 Quantitative Feedback Theory.....72
2.9.9 Backstepping control.....72

2.9.10 Fuzzy Logic....73
2.9.11 Neural Network....73
2.9.12 Clipped control....74
2.10 Final Remarks....77
Chapter 3 - Semi-Active Control Strategies....79
3.1 Problem Description....80
3.1.1 Structural Models....80
3.1.2 Passive Device Formulation....82
3.1.3 SA device Formulation....82
3.1.4 Earthquake Ground Motions....83
3.1.5 Evaluation Criteria....85
3.2 Original Structure and Passive Control....85
3.3 Semi-active Control....88
3.3.1 Lyapunov Based Control....90
3.3.2 Nonlinear Feedback Control....91
3.3.3 Sliding Mode Control....95
3.3.4 Modulated Homogeneous Friction Control....97
3.3.5 Integral Control....99
3.3.6 Optimal Control....104
3.3.7 Model Predictive Control....108
3.3.8 Force-tracking schemes: adjusting damping rules....119
3.4 SDOF Model: Comparison of results....120
3.5 MDOF Model Numerical Evaluation....121
3.6 Final Remarks....126
Chapter 4 - Experimental Studies on Semi-Active Control....129
4.1 Experimental Test Set-up....130
4.1.1 LNEC uniaxial shaking table....131
4.1.2 Measurement and Control Chain....134
4.1.3 Two degree-of-freedom mechanical model....147
4.1.4 SA device....153
4.1.5 Experimental Campaign....161
4.2 Numerical Simulations and Tuning....163
4.2.1 Original Structure....164
4.2.2 Passive control....164
4.2.3 Semi-active control....164
4.2.4 Summary of results in numerical simulations....168
4.3 Experimental Trial....170
4.3.1 Original Structure....171
4.3.2 Passive control....171
4.3.3 Semi-active control....172
4.3.4 Summary of results in experimental trials....173
4.4 Comparison of Numerical and Experimental Results....176
4.4.1 Time domain....176
4.4.2 Frequency domain....177
4.5 Final Remarks....181
Chapter 5 - Conclusions and Future Work....183
5.1 Conclusions....184
5.2 Future Work....186
References....187
Annex....201

List of Figures

Chapter 1 - Introduction

Figure 1.1 - Dynamic protection systems applications (from Oliveira 2009).....2

Figure 1.2 - Tokyo National Museum of Emerging Science and Innovation and 30-t MR fluid damper (from *Spencer Jr. 2008*).....3

Chapter 2 - State-of-the-Art

Figure 2.1 - Left: View of Lisbon during the 1755 earthquake (original engraving in Museu da Cidade, Lisbon); Right: Gaiola Pombalina construction (from http://www.lnec.pt).....10

Figure 2.2 - Tectonic plates near Portugal (left). Active and possible active faults in Portugal.....14

Figure 2.3 - Seismic zones for the Portuguese territory according to the Eurocodigo8 2010.....17

Figure 2.4 - General form of the elastic response spectra (acceleration) according to the Eurocodigo8 2010.....18

Figure 2.5 - Typical response spectra and building structures fundamental frequencies (adapted form *Lopes 2008*).....19

Figure 2.6 - Comparison between earthquakes frequency content (acceleration magnitude spectra) and the range of fundamental frequencies in building structures.....19

Figure 2.7 - Structural protective systems.....22

Figure 2.8 - Up: Schematic view of a fixed and base isolated structure. Bottom: Base-isolated viaduct.....23

Figure 2.9 - Structure with passive energy dissipation devices.....24

Figure 2.10 - Generic structure with a semi-active control system: system implementation (left); block diagram (right).....26

Figure 2.11 - Generic structure employing an active control system: system implementation (left); block diagram (right).....27

Figure 2.12 - Semi-active control devices implementations in buildings: Bracing System type; Dispersed Devices type; and Base Isolation type.....30

Figure 2.13 - Semi-active control devices implementations in cable stayed bridges.....30

Figure 2.14 - Base isolated building employing a semi-active fluid viscous damper.....32

Figure 2.15 - Semi-active device: fluid viscous damper (FVD).....35

Figure 2.16 - Semi-active devices. Left: Device used by *Kawashima et al. 1992(b)*. Right: Modified passive device used by *Symans & Constantinou 1995*.....36

Figure 2.17 - Semi-active Hydraulic Dampers installed at the Kajima Shizuoka Building (*Kurata et al. 1999*).....38

Figure 2.18 - Damper device and installation by *Kurino et al. 2004*.....39

Figure 2.19 - Bingham mechanical model: viscous damping c_v and a frictional force f_f.....40

Figure 2.20 - Simulation results obtained with Bingham model for a sinusoidal input displacement at 1 Hz with: c_v=2,36 kN s/m and c_v=44,11 kN s/m; and f_f= 0 N.....41

Figure 2.21 - Maxwell model with friction: viscous damping c_v, a stiffness element k_m and a frictional force f_f.....41

Figure 2.22 - Force velocity transfer function (left). Simulation results obtained with the Maxwell model for a sinusoidal input displacement at 1 Hz with: c_v=cmin=2,36 kN s/m and c_v=cmax=44,11 kN s/m; T_d=0,006 s; and f_f= 0 N (right).....42

Figure 2.23 - Typical commercial linear MR damper (from *Dyke 1996*).....43

Figure 2.24 - Rheological fluids: chain-like structure formation under applied field.....44

Figure 2.25 - Typical MR fluids behaviour. Left: shear stress τ vs. shear strain γ for H_1>H_2 magnetic fields (static); Middle: shear stress τ vs. shear rate for H_1>H_2 magnetic fields; Right: yield stress τ_y vs. magnetic field and magnetic flux density (*B*) vs. magnetic field intensity (*H*)....45

Figure 2.26 - Herschel-Bulkley model (with m=0,9; 1 and 1,1) response to an input sinusoidal displacement....46

Figure 2.27 - Rheological fluids modes of operation: flow mode, shear mode and squeeze mode. 46

Figure 2.28 - MR dampers (low forces) for linear displacements....47

Figure 2.29 - Large-scale MR dampers for linear displacements....48

Figure 2.30 - Typical Force-Velocity plots for MR dampers under sinusoidal input: Left- curve evidencing several phenomena; Right-curve showing the damper equivalent damping coefficient evaluated using the dissipated energy criteria for two different input voltages (or currents)....51

Figure 2.31 - Block diagram of the system MR device with current driver....51

Figure 2.32 - Bingham mechanical model: viscous damper c_0, a frictional force ff and an offset f_0. 52

Figure 2.33 - Bi-viscous model (with f_f=750 N, c_0=5 kN s/m, c_1=90 kN s/m and f_0=0 N) response to an input sinusoidal displacement (10 mm at 2,5 Hz)....53

Figure 2.34 - Bi-viscous model with hysteresis. Force-velocity plot parameters description....53

Figure 2.35 - Extended Bingham mechanical model....53

Figure 2.36 - Extended Bingham model response to an input sinusoidal displacement (5 mm at 2,5 Hz) for two cases: 1) with f_f=750 N, c_0=5 kN s/m, k_1=50 kN/m, k_1=1300 kN s/m, k_2=20 kN/mm and f_0=0 N; 2) with f_f=785 N, c_0=5,2 kN s/m, k_1=50 kN/m, c_1=100 kN s/m, k_2=100 kN/mm and f_0=0 N....54

Figure 2.37 - Bouc-Wen model (with α=0,0028; *k*=88,25 kN/m; *D*=1; *A*=120, β=106 m^{-2}, γ=106 m^{-2} and n=2) response to an input sinusoidal displacement (10 mm at 2,5 Hz)....55

Figure 2.38 - Bouc-Wen plus viscous model representation....56

Figure 2.39 - Bouc-Wen plus viscous model (with c_0=5 kN s/m, k_0=2,5 kN/m, A=120, β=106 m^{-2}, γ=106 m^{-2}, k_z=88 kN/m, n=2 and x_0=38 mm) response to an input sinusoidal displacement (10 mm at 2,5 Hz)....56

Figure 2.40 - Phenomenological Bouc-Wen model representation (*Spencer Jr. et al. 1997(a)*)....57

Figure 2.41 - Phenomenological Bouc-Wen model (with c_0=5,3 kN s/m, c_1=93 kN s/m, k_0=1,4 kN/m, k_1=0,54 kN/m, *A*=207, β=2x106 m^{-2}, γ=2x106 m^{-2}, k_z=96,3 kN/m, n=2 and x_0=189 mm) response to an input sinusoidal displacement (10 mm at 2,5 Hz)....57

Figure 2.42 - Phenomenological Bouc-Wen model representation (*Yang 2001*)....58

Figure 2.43 - Bouc-Wen plus viscous model with Stribck effect (with c_0=5 kN s/m, k_0=2,5 kN/m, *A*=120, β=106 m^{-2}, γ=106 m^{-2}, k_z=88 kN/m, n=2, x_0=38 mm, ω_0=50 rad/s and ξ_0=0,5) response to an input sinusoidal displacement (10 mm at 2,5 Hz)....58

Figure 2.44 - Dahl model (with σ_0=1,5x10^4 kN/m; λ_0=670 N) response to an input sinusoidal displacement (10 mm at 2,5 Hz)....59

Figure 2.45 - Dahl plus viscous model (with c_0=5 kN s/m; k_w=670 N; ρ=2,24x104 m^{-1}) response to an input sinusoidal displacement (10 mm at 2,5 Hz)....60

Figure 2.46 - General semi-active control loop....62

Figure 2.47 - Basic control action with a clipped algorithm in the semi-active control loop: i) switch (sw) off – model-based feed-forward force tracking scheme; ii) switch (sw) on – force feedback. 64

Figure 2.48 - LQG with clipped control....67

Figure 2.49 - Clipped control in the control loop....75

Figure 2.50 - Clipped Control algorithm graphical representation....75

Figure 2.51 - Modified Clipped Control law graphical representation (*Jung et al. 2006*).....76

Chapter 3 - Semi-Active Control Strategies

Figure 3.1 - SDOF model schematic representation.....81

Figure 3.2 - General form of the elastic response spectra for horizontal ground motions and the values used to define the type 1.1 and type 2.1 spectra.....84

Figure 3.3 - Input ground motions considered. Left: one of ten artificial accelerograms; Middle: frequency spectra of 10 accelerograms; Right: response spectra of 10 accelerograms.....84

Figure 3.4 - Peak responses of the SDOF model (f_b=0,25 Hz; ξ_b=0,1) with a passive damper vs. device damping when subjected to 10 input type 1 accelerograms, for two velocity exponents α. 86

Figure 3.5 - Damping coefficients for the minimum mean of peak acceleration vs. SDOF system natural frequencies for α=0,15 (left) and α=1 (right).....87

Figure 3.6 - Time histories of the SDOF model (f_b=0,25 Hz; ξ_b=0,1) subjected to one Type 1 accelerogram: original system and with passive system for α=0,15.....88

Figure 3.7 - SA control general loop.....88

Figure 3.8 - Left: Force tracking scheme block diagram: switch (sw) off – model-based feed-forward force tracking scheme; switch (sw) on – force feedback. Right: Closed-loop system for controller design: plant with a controller in the feedback path.....89

Figure 3.9 - Time histories of the SDOF model (f_b=0,25 Hz; ξ_b=0,1) subjected to one Type 1 accelerogram: original system and with SA system manipulated by a DBB controller.....91

Figure 3.10 - Block diagram of the closed-loop system: structure employing an SA device (non-linear system) controlled by an output feedback control strategy (regulation).....91

Figure 3.11 - Peak responses of the SDOF model (f_b=0,25 Hz; ξ_b=0,1) with an SA device plus NOFC vs. controller gain when subjected to 10 input type 1 accelerograms.....94

Figure 3.12 - Time histories of the SDOF model (f_b=0,25 Hz; ξ_b=0,1) subjected to one Type 1 accelerogram: original system and with SA system manipulated by a NOFC controller.....95

Figure 3.13 Left - Peak responses of the SDOF model (f_b=0,25 Hz; ξ_b=0,1) with an SA device plus SMC vs. controller gain when subjected to 10 input type 1 accelerograms. Right - SMC controller gains selected for each SDOF system natural frequency.....97

Figure 3.14 - Time histories for the SDOF model (f_b=0,25 Hz; ξ_b=0,1) subjected to one Type 1 accelerogram: original (no devices), best passive and SA with SMC strategy.....97

Figure 3.15 Left - Peak responses of the SDOF model (f_b=0,25 Hz; ξ_b=0,1) with an SA device plus MHF vs. controller gain when subjected to 10 input type 1 accelerograms. Right - MHF controller gains selected for each SDOF system natural frequency.....98

Figure 3.16 - Time histories of the SDOF model (f_b=0,25 Hz; ξ_b=0,1) subjected to one Type 1 accelerogram system with SA system manipulated by the: original MHF controller (left); MHF and VD algorithm (right).....99

Figure 3.17 - Closed loop system with an Integral controller: Root Locus (left); and the transfer functions Bode diagram for different values of gain compared with the passive case (right).....101

Figure 3.18 Left - Peak responses of the SDOF model (f_b=0,25 Hz; ξ_b=0,1) with an SA device plus Integral control law vs. controller gain when subjected to 10 input type 1 accelerograms. Right - Integral controller gain (closed-loop damping ratio ξ) selected for each system natural frequency. 102

Figure 3.19 - Time histories for the SDOF model (f_b=0,25 Hz; ξ_b=0,1) subjected to one Type 1 accelerogram: original (no devices), best passive and SA with IVD strategy.....103

Figure 3.20 - SDOF structural systems frequency response functions: original (no devices), passive and SA with I VD and I COO.....104

Figure 3.21 - Root Locus of the SDOF closed loop system with weights on the relative displacement, relative velocity and absolute acceleration with constant weight on the input.....106

Figure 3.22 - Bode diagram of the SDOF closed loop system with weights $q_1<q_2$ compared with the original and passive systems.....106

Figure 3.23 - Peak responses of the SDOF model (f_b=0,25 Hz; ξ_b=0,1) with an SA device plus LQR controller vs. output weight q (with input weight r=1 s/kg) subjected to 10 input type 1 accelerograms.....107

Figure 3.24 - Peak responses of the SDOF model (f_b=0,25 Hz; ξ_b=0,1) with an SA device plus LQR controller vs. output acceleration weight q and different input weights r under 10 type 1 accelerograms.....107

Figure 3.25 - LQR controller output weights q function of SDOF system natural frequency.....108

Figure 3.26 - Block diagram of the closed-loop system: structure employing an SA device controlled by an MPC control strategy and an algorithm.....108

Figure 3.27 - Left: SDOF system mean peak responses (f_b=0,25 Hz and ξ_b=0,1 for MPCVD with HC=1 and r=1 s^2/kg) evolutions with control interval T_s and prediction horizon HP, when subjected to Type 1 seismic actions (10 accelerograms). Right: ratios vs. control interval T_s (relative to T_s=5 ms) for HP=50.....115

Figure 3.28 - Left: SDOF system responses (peak values) evolution with acceleration weight (f_b=0,25 Hz and ξ_b=0,1 for MPCVD with T_s=5 ms, HP=50, HC=1, r=1 s^2/kg), when subjected to type 1 seismic actions (10 input time accelerograms). Right: Time histories of system responses and inputs for the minimum acceleration weight for one input accelerogram.....116

Figure 3.29 - SDOF system eigenvalues moduli (maximum values) evolution with acceleration weight (f_b=0,25 Hz and ξ_b=0,1 for MPC VD with T_s=5 ms, HP=50, HC=1, r=1 s^2/kg).....117

Figure 3.30 - SDOF system responses (mean peak values) evolution with prediction horizon for different natural frequencies (f_b=0,25 to 1,00 Hz and ξ_b=0,1 with T_s=5 ms, HC=1, r=1 s^2/kg), when subjected to type 1 seismic actions (10 input time accel.): left - for MPCVD; right - for MPCCOO. 118

Figure 3.31 - MPC controller output weights function of SDOF system natural frequency.....119

Figure 3.32 - 10-storey base-isolated building, equivalent model and modal characteristics.....122

Figure 3.33 - Responses of the 10-storey base-isolated building to 10 type 1 and type 2 seismic actions.....124

Figure 3.34 - Time histories of base and top floor relative displacements and accelerations, input damping and force for the MDOF model subjected to one type 1 accelerogram.....126

Chapter 4 - Experimental Studies on Semi-Active Control

Figure 4.1 - Schematic representation of the experimental model for test in the shaking table.. 130

Figure 4.2 - LNEC Uniaxial Shaking Table experimental installation: shaking table with a 6 t mass on the platform, machine room and operation room.....131

Figure 4.3 - Shaking table control loop (system and MB HSA104 servo controller) during normal system operation (CAL switch set to OPER).....132

Figure 4.4 - Shaking table time response to a 2 mm square wave.....133

Figure 4.5 - Synthesized reference input signal in terms of displacement and acceleration (left) and the shaking table transfer function for different magnitudes of the input signal (right).....134

Figure 4.6 - Measurement and control chain.....135

Figure 4.7 - Force transducer 5 calibration set-up (left) and assembly on the testing machine (right).....141

Figure 4.8 - Displacement transducer calibration set-up (left) and transducer assembly (right)..142

Figure 4.9 - Shaking table (actuator) displacement transducer calibration set-up.....143

Figure 4.10 - Accelerometers measurement chain calibration set-up.....145
Figure 4.11 - Mini shaking table transfer function.....146
Figure 4.12 - Accelerometers 0, 1 & 2 measurement chain transfer functions.....147
Figure 4.13 - MDOF model and 2DOF model matching.....149
Figure 4.14 - Experimental model on the shaking table: perspective, top view and MR damper detail.....151
Figure 4.15 - Input signal to characterize the physical model (measured at unity scale factor). Displacement and acceleration series (left) and power spectral density in velocity (right).....151
Figure 4.16 - FRFs (A_i/A_g and A_s/A_g) for different input signal magnitudes.....152
Figure 4.17 - Comparison between the experimental FRFs and the regenerated ones at the maximum input signal magnitude (unitary scale factor).....152
Figure 4.18 - Modal parameters (natural frequencies and damping ratios) and spatial model parameters evolution with the magnitude of the input signal, obtained from the experimental data. 153
Figure 4.19 - LORD MR damper model RD-8041-1 with a current controller RD-3002-03.....154
Figure 4.20 - Relationship between the input voltage and electrical circuit current. Static and quasi-static tests.....154
Figure 4.21 - Current controller response to a square wave input (left) and the frequency response function (right).....155
Figure 4.22 - MR damper test set-up.....156
Figure 4.23 - MR damper transient response test under triangle-wave displacement and square-wave input voltage.....157
Figure 4.24 - MR damper time constant results: force response data and model adjustment (left); time constant T_d values (right).....157
Figure 4.25 - MR damper response under a sinusoidal input displacement and varying input voltage.....158
Figure 4.26 - Block diagram of the MR damper.....161
Figure 4.27 - Comparison between the MR damper force and the force evaluated by the Modified Bouc-Wen model, under a triangular wave displacement and a square wave input voltage.....161
Figure 4.28 - Time histories and response spectra of earthquake records: El Centro Newhall, Rinaldi and Sylmar (California, US); Erzinkan (Turkey), Jiji (Taiwan) and Kobe (Japan).....162
Figure 4.29 - Peak responses evolution of the 2DOF model with the MR damper in passive mode, vs. damper input voltage for all the input ground motions, in numerical simulations.....164
Figure 4.30 - SA control loop used in the numerical simulations.....165
Figure 4.31 - Evolution of peak responses with the controller gain for the 2DOF model with an MR device manipulated by MHF strategy, for all the input ground motions considered.....166
Figure 4.32 - Evolution of peak responses with the controller gain for the 2DOF model with an MR device manipulated by ICOO strategy, for all the input ground motions considered.....166
Figure 4.33 - Evolution of peak responses with the controller gain for the 2DOF model with an MR device manipulated by LQRCOO strategy, for all the input ground motions considered.....167
Figure 4.34 - Evolution of peak responses with the controller gain for the 2DOF model with an MR device manipulated by MPCCOO strategy, for all the input ground motions considered.....167
Figure 4.35 - Evolution of peak responses with the controller gain for the 2DOF model with an MR device manipulated by LQR2COO strategy, for all the input ground motions considered.....167
Figure 4.36 - Peak responses evolution of the 2DOF model with the MR damper in passive mode, vs. damper input voltage for all the input ground motions, in experimental trial.....171

Figure 4.37 - Comparison between the experimental FRFs for the original structure and passive solutions, obtained using the artificial accelerograms as input.....172

Figure 4.38 - Comparison between the experimental FRFs for the original structure and the SA solutions, obtained using the artificial accelerograms as input.....173

Figure 4.39 - Time histories (relative displacements, accelerations and force), of the 2DOF model in the original, Pass1, ICOO and LQR2COO cases, subjected to Kobe (NS) earthquake record, during the experimental test.....176

Figure 4.40 - Comparison between the numerical and experimental FRFs for the Original structure, obtained using the artificial accelerograms as input.....179

Figure 4.41 - Comparison between the numerical and experimental FRFs for the Pass1 case, obtained using the artificial accelerograms as input.....179

Figure 4.42 - Comparison between the numerical and experimental FRFs for the ICOO case, obtained using the artificial accelerograms as input.....180

Figure 4.43 - Comparison between the numerical and experimental FRFs for the LQR2COO case, obtained using the artificial accelerograms as input.....180

Annex

Figure A1 - Comparison between the numerical and experimental FRFs for the Original structure, obtained using the artificial accelerograms as input.....228

Figure A2 - Comparison between the numerical and experimental FRFs for the Pass0 case, obtained using the artificial accelerograms as input.....229

Figure A3 - Comparison between the numerical and experimental FRFs for the Pass1 case, obtained using the artificial accelerograms as input.....229

Figure A4 - Comparison between the numerical and experimental FRFs for the Pass5 case, obtained using the artificial accelerograms as input.....230

Figure A5 - Comparison between the numerical and experimental FRFs for the DBB case, obtained using the artificial accelerograms as input.....230

Figure A6 - Comparison between the numerical and experimental FRFs for the MED case, obtained using the artificial accelerograms as input.....231

Figure A7 - Comparison between the numerical and experimental FRFs for the MHF case, obtained using the artificial accelerograms as input.....231

Figure A8 - Comparison between the numerical and experimental FRFs for the ICOO case, obtained using the artificial accelerograms as input.....232

Figure A9 - Comparison between the numerical and experimental FRFs for the LQRCOO case, obtained using the artificial accelerograms as input.....232

Figure A10 - Comparison between the numerical and experimental FRFs for the MPCCOO case, obtained using the artificial accelerograms as input.....233

Figure A11 - Comparison between the numerical and experimental FRFs for the LQR2COO case, obtained using the artificial accelerograms as input.....233

List of Tables

Chapter 2 - State-of-the-Art

Table 2.1 - Base Isolation devices (*Lopes 2008*).....24

Table 2.2 - Passive Energy Dissipation devices.....25

Table 2.3 - MR fluid characteristics from Lord Corporation and Liquid Research Limited.....45

Chapter 3 - Semi-Active Control Strategies

Table 3.1 - Structural responses evaluation criteria.....85

Table 3.2 - SDOF original structure mean peak responses.....86

Table 3.3 - SDOF structure with passive devices responses (ratios) for different natural frequencies and velocity exponents.....87

Table 3.4 - Ratios of mean of peak responses for the SDOF structure with additional systems. 120

Table 3.5. MDOF system responses. Comparisons with the original structure.....125

Chapter 4 - Experimental Studies on Semi-active Control

Table 4.1. Quantities associated with the developed model, its correspondence with the sensor (measurement) or signal (generation) and with 2DOF mechanical model variables 131

Table 4.2 - Shaking table set-up parameters: servo controller and hydraulic system.....133

Table 4.3. Data acquisition and control system characteristics.....135

Table 4.4. Sensors and command signals description main characteristics.....135

Table 4.5. Signal conditioner: boards description and correspondence to dSPACE DS2003 136

Table 4.6. Uncertainty balance for force transducer 5 (range ±3,6 kN) with measurement chain. 141

Table 4.7. Uncertainty balance for displacement transducer 7 (range ±60 mm) and associated measurement chain.....142

Table 4.8. Uncertainty balance for displacement transducer 8 (range ±15 mm) and associated measurement chain.....143

Table 4.9. Uncertainty balance for displacement transducer 9 (range ±68 mm) and associated measurement chain.....144

Table 4.10. Uncertainty balance for the mini shaking table displacement transducer (range ±5 mm) and associated measurement chain.....146

Table 4.11 - Summary table of measurement and control chain parameters.....147

Table 4.12. 2DOF model mechanical springs: geometry and results of experimental characterization.....150

Table 4.13 - 2DOF model: summary of characteristics and frequencies calculated from individual characteristics using the model equations.....150

Table 4.14 - MR damper static test results and model parametrization.....156

Table 4.15 - MR damper stationary test results and models parametrization. Curves for different peak velocity values (or sine excitation freq. from 0,25 Hz to 1,75 Hz at 12,5 mm of mag.).....160

Table 4.16 - Scale factors applied to the input ground motions.....163

Table 4.17 - Structural responses evaluation criteria on the 2DOF model responses analysis…163

Table 4.18 - Controllers tuning parameters obtained from the numerical simulations and considered also in the experimental implementation.....166

Table 4.19 - Summary of average ratios (Rao) and number of best cases (#best) under type 1 seismic actions, in numerical simulations.....168

Table 4.20 - Summary of average ratios (Rao) and number of best cases (#best) under type 2 seismic actions, in numerical simulations....169
Table 4.21 - Summary of average ratios (Rao) and number of best cases (#best) under earthquake records, in numerical simulations....169
Table 4.22 - Number of best cases (#best) for each solution, in numerical simulations....170
Table 4.23 - Summary of average ratios (Rao) and number of best cases (#best) under type 1 seismic actions, in experimental trials....174
Table 4.24 - Summary of average ratios (Rao) and number of best cases (#best) under type 2 seismic actions, in experimental trials....174
Table 4.25 - Summary of average ratios (Rao) and number of best cases (#best) under earthquake records, in experimental trials....175
Table 4.26 - Number of best cases (#best) for each solution, in experimental trials....175
Table 4.27 - Comparison of the number of best cases (#best) for each solution, in numerical simulations (red) and in experimental trials (green)....177
Table 4.28 - Identified natural frequencies and damping ratios obtained from the numerical (num) and experimental (exp) and the correspondent error (e) in percentage for the main solutions...178

Annex

Table A1 - Original structure evaluation criteria with type 1 and 2 input ground motions, in numerical simulations....203
Table A2 - Original structure evaluation criteria with earthquake records, in numerical simulat..203
Table A3 - Evaluation criteria with Accelerogram 1 under type 1 and 2 input ground motions, in numerical simulations....204
Table A4 - Evaluation criteria with Accelerogram 2 under type 1 and 2 ground motions, in numerical simulations....204
Table A5 - Evaluation criteria with Accelerogram 3 under type 1 and 2 input ground motions, in numerical simulations....205
Table A6 - Evaluation criteria with Accelerogram 4 under type 1 and 2 ground motions, in numerical simulations....205
Table A7 - Evaluation criteria with Accelerogram 5 under type 1 and 2 input ground motions, in numerical simulations....206
Table A8 - Evaluation criteria with Accelerogram 6 under type 1 and 2 ground motions, in numerical simulations....206
Table A9 - Evaluation criteria with Accelerogram 7 under type 1 and 2 input ground motions, in numerical simulations....207
Table A10 - Evaluation criteria with Accelerogram 8 under type 1 and 2 ground motions, in numerical simulations....207
Table A11 - Evaluation criteria with Accelerogram 9 under type 1 and 2 input ground motions, in numerical simulations....208
Table A12 - Evaluation criteria with Accelerogram 10 under type 1 and 2 ground motions, in numerical simulations....208
Table A13 - Evaluation criteria with El Centro earthquake, in numerical simulations....209
Table A14 - Evaluation criteria with Newhall earthquake, in numerical simulations....209
Table A15 - Evaluation criteria with Rinaldi earthquake, in numerical simulations....210
Table A16 - Evaluation criteria with Sylmar earthquake, in numerical simulations....210
Table A17 - Evaluation criteria with Erzikan earthquake, in numerical simulations....211
Table A18 - Evaluation criteria with Jiji earthquake, in numerical simulations....211

Table A19 - Evaluation criteria with Kobe earthquake, in numerical simulations.....212
Table A20 - Summary of average ratios (Rao) and number of best cases (#best) under type 1 seismic actions, in numerical simulations.....212
Table A21 - Summary of average ratios (Rao) and number of best cases (#best) under type 2 seismic actions, in numerical simulations.....213
Table A22 - Summary of average ratios (Rao) and number of best cases (#best) under earthquake records, in numerical simulations.....213
Table A23 - Number of best cases (#best) for each solution, in numerical simulations.....214
Table A24 - Original structure evaluation criteria with type 1 and 2 input ground motions, in experimental trials.....216
Table A25 - Original structure evaluation criteria with earthquake records, in experimental trials. 216
Table A26 - Evaluation criteria with Accelerogram 1 under type 1 and 2 input ground motions, in experimental trials.....217
Table A27 - Evaluation criteria with Accelerogram 2 under type 1 and 2 ground motions, in experimental trials.....217
Table A28 - Evaluation criteria with Accelerogram 3 under type 1 and 2 input ground motions, in experimental trials.....218
Table A29 - Evaluation criteria with Accelerogram 4 under type 1 and 2 ground motions, in experimental trials.....218
Table A30 - Evaluation criteria with Accelerogram 5 under type 1 and 2 input ground motions, in experimental trials.....219
Table A31 - Evaluation criteria with Accelerogram 6 under type 1 and 2 ground motions, in experimental trials.....219
Table A32 - Evaluation criteria with Accelerogram 7 under type 1 and 2 input ground motions, in experimental trials.....220
Table A33 - Evaluation criteria with Accelerogram 8 under type 1 and 2 ground motions, in experimental trials.....220
Table A34 - Evaluation criteria with Accelerogram 9 under type 1 and 2 input ground motions, in experimental trials.....221
Table A35 - Evaluation criteria with Accelerogram 10 under type 1 and 2 ground motions, in experimental trials.....221
Table A36 - Evaluation criteria with El Centro earthquake, in experimental trials.....222
Table A37 - Evaluation criteria with Newhall earthquake, in experimental trials.....222
Table A38 - Evaluation criteria with Rinaldi earthquake, in experimental trials.....223
Table A39 - Evaluation criteria with Sylmar earthquake, in experimental trials.....223
Table A40 - Evaluation criteria with Erzikan earthquake, in experimental trials.....224
Table A41 - Evaluation criteria with Jiji earthquake, in experimental trials.....224
Table A42 - Evaluation criteria with Kobe earthquake, in experimental trials.....225
Table A43 - Summary of average ratios (Rao) and number of best cases (#best) under type 1 seismic actions, in experimental trials.....225
Table A44 - Summary of average ratios (Rao) and number of best cases (#best) under type 2 seismic actions, in experimental trials.....226
Table A45 - Summary of average ratios (Rao) and number of best cases (#best) under earthquake records, in experimental trials.....226
Table A46 - Number of best cases (#best) for each solution, in experimental trials.....227

List of Abbreviations

2DOF	Two Degree-Of-Freedom
AMD	Active Mass Damper
ANN; NN	Artificial Neural Network or Neural Network
ARE	Algebraic *Riccati* Equation
COO	Clipped On-Off algorithm
DBB	Decentralized Bang-Bang
DOF	Degree-of-freedom
ER	Electro-Rheological
FVD	Fluid Viscous Damper
FPS	Friction Pendulum System
FRF	Frequency Response Function
FS, FSR	Full Scale Range
GR law	Gutenberg–Richter law
H_2	System norm - 2 norm
H_∞	System norm - infinity norm
HMD; ATMD	Hybrid Mass Damper (HMD) and also called Active Tuned Mass Damper (ATMD)
I, IVD, ICOO	Integral Controller, I controller with VD and COO algorithms
INV-MR	Inverse model of the MR damper
IP	Identify Parameters
ITAE	Integral of Time multiplied Absolute Error criterion
LQG	Linear Quadratic Gaussian
LQG/H_2	Linear Quadratic Gaussian synthesis using the H_2 norm criteria
LQR, LQRVD, LQRCOO, LQR2COO	Linear Quadratic Regulator, LQR with with VD and COO algorithms, and LQR with the COO algorithm considering the full model of the 2DOF system
LTI	Linear Time Invariant
LVDT	Linear Variable Differential Transformer
MDOF	Multi Degree-Of-Freedom
MHF, MHFVD, MHFCOO	Modulated Homogeneous Friction: original, with VD algorithm and with COO algorithm

MIMO	Multiple Input Multiple Output
MPC, MPCVD, MPCCOO	Model Predictive Control, MPC with VD and COO algorithms
MR	Magneto-Rheological
MSE	Mean Square Error
NDOF	N Degree-Of-Freedom
NMP	Non-Minimum-Phase
NN	Neural Network
NNPC	Neural Network Predictive Control
NOFC	Nonlinear Output Feedback Controller
OO	On-Off algorithm
PI	Proportional plus Integral control
PID	Proportional-Integral-Derivative control
QFT	Quantitative Feedback Theory
RMS	Root Mean Square
SA	Semi-active
SA-NC	Semi-Active Neuro-Controller
SDOF	Single Degree-Of-Freedom
SHD	Semi-active Hydraulic Damper
SISO	Single Input Single Output
SMA	Shape Memory Alloys
SMC	Sliding Mode Control
TLCD	Tuned Liquid Column Damper
TLD	Tuned Liquid Damper
TMD	Tuned Mass Damper
VD	Variable Damping algorithm
VE	Viscoelastic
ZOH	Zero-order Hold

List of Symbols

Symbols

0	Zero vector/matrix
1	Unitary column vector
#best	Number of best cases for a specific solution: see table 4.17
a, a_g	Acceleration and ground acceleration
a_g, a_{gr}	Design peak ground acceleration and Reference peak ground acceleration, $a_g=\gamma_I \cdot a_{gR}$ (response spectra definition)
$\boldsymbol{A}$	State (or system) matrix (state-space representation)
$\boldsymbol{B}$	Input vector (state-space representation)
c, $\boldsymbol{C}$	Viscous damping and viscous damping matrix
$\boldsymbol{C}_o$, $\boldsymbol{C}_s$	Controllability matrix (output and state)
$\boldsymbol{C}_y$	Output matrix (state-space representation)
$\boldsymbol{D}_y$	Direct feedthrough matrix (state-space representation)
E	Exposition
E_x	Energy of type x: total (' ') or other forms ('x')
$\boldsymbol{E}$	Input disturbance vector (state-space representation)
f_x	Frequency of vibration (for a specific case or mode 'x'), $f=1/T$
f_y, $\boldsymbol{f}_y$	Input force and input force vector (for a specific case or device 'y')
g	Controller gain (I, MHF and Force Derivative controllers)
$\boldsymbol{G}$	Input force location vector
H	Hazard
i	Imaginary unit: $i^2=-1$
I	Electric current
I	Identity matrix
J	Cost function or performance index
k, $\boldsymbol{K}$	SDOF stiffness and MDOF stiffness matrix
$\boldsymbol{K}_c$	Optimal controller gain
$\boldsymbol{K}_o$	Observer controller gain
k_p, k_i	Proportional and Integral controller gain (PI control)

m, $\boldsymbol{M}$	SDOF mass and MDOF mass matrix
MM	Modified Mercalli scale
MMS or M_w	Moment Magnitude Scale
M_L	Ritcher scale or Local Magnitude scale
M_0	Seismic moment
M*x*	Mean of peak responses of *x* from 10 accelerograms of the same type as input
$\boldsymbol{P}$, $\boldsymbol{S}$	Solution of ARE for the optimal controller and observer
p_1, p_n	Annual probability of an earthquake occurring, (p_1=1/T_r) and the probability of being exceeded in *n* years
P*f*/W	Peak force over the structure weight
P*x*	Peak responses of *x* for one accelerogram
q, $\boldsymbol{Q}$, $\mathcal{Q}$	Weighting parameter and weighting matrices, on state(s) or output(s) (controller synthesis, LQR and MPC)
r, $\boldsymbol{R}$, $\mathcal{R}$	Weighting parameter and weighting matrices on input(s) (controller synthesis, LQR and MPC)
R	Seismic risk
$\mathbb{R}$, $\mathbb{R}^+$, $\mathbb{R}^n$	Real number, positive real number and the n-dimensional real space
Rao	Average ratio of output variables ratios (for RP*x* or RR*x*)
RMS*x*	Root Mean Square of x
RMS*f*/W	RMS force over the structure weight
RP*x*	Ratio of peak responses of *x* for a specific solution, passive or semi-active, relative to the peak responses of *x* for the original structure
RR*x*	Ratio of RMS value of *x* for a specific solution, passive or semi-active, relative to the RMS value of *x* for the original structure
R*x*	Ratio of mean peak responses of *x* for a specific solution, passive or semi-active, relative to the same values for the original structure
$r(x,y)$	Coefficient of correlation between *x* and *y*
s	Laplace variable (complex number): $s=\sigma+i\cdot\omega$, with real numbers σ and $\cdot\omega$
S	Soil parameter (response spectra definition)
$S_e(T)$	Elastic response spectra, function of the period of vibration T
S_q	Standard quantity measurement
T	Period of vibration, T=1/f
T_B, T_C, T_D,	Periods for response spectra definition

T_d	SA device time constant
T_r	Return period of an earthquake (T_r=1/p_1)
T_s	Discretization period or control interval (MPC controller)
u_{SA}	Generic SA device input variable, bounded by $u_{SA,min} \leq u_{SA} \leq u_{SA,max}$
$u(x)$	Uncertainty associated with quantity x
U, U_p	Expanded uncertainty and expanded uncertainty at p confidence interval
v	Velocity
V_x	Electric voltage (for a specific case 'x')
V	Vulnerability
$V(\boldsymbol{z})$	Lyapunov function of the states $\boldsymbol{z}$
x, $\boldsymbol{x}$	Displacement and displacement vector
$x_g, \ddot{x}_g$	Input ground motion displacement and acceleration
$\boldsymbol{y}$	Output vector
$\boldsymbol{z}$	State vector
α	Velocity exponent of FVD dampers
γ_I	Coefficient of importance (response spectra definition)
γ	Shear strain
η	Damping correction factor (response spectra definition)
ξ	Viscous damping factor
τ	Shear stress
ω	Angular frequency ω=2π/T

Functions & Operators

cov($\boldsymbol{x}$,$\boldsymbol{y}$)	Covariance: cov($\boldsymbol{x}$,$\boldsymbol{y}$)=E[$\boldsymbol{x}\cdot\boldsymbol{y}^T$]-E[$\boldsymbol{x}$]·E[$\boldsymbol{y}$]
e	Euler's number, e=2,718281828
E[x], E[$\boldsymbol{x}$]	Expected value or mean value of x, and mean values of vector $\boldsymbol{x}$
exp(x) or e^x	Exponential function of argument x
$f(\boldsymbol{x})$, $\boldsymbol{f}(\boldsymbol{x})$	General function of arguments $\boldsymbol{x}$
fr(·)	First Row of a vector/matrix
H[x]	Heaviside step function or unit step function
ln(x)	Natural logarithm function of argument x (base e)

log(x)	Decimal logarithm (base 10)
$L_f^k \boldsymbol{h}(\boldsymbol{z}_c)$	Lie derivative of order k, is the k derivative of $\boldsymbol{h}(\boldsymbol{z}_c)$ along $\boldsymbol{f}(\boldsymbol{z}_c)$
max($\boldsymbol{x}$)	Maximum of $\boldsymbol{x}$
min($\boldsymbol{x}$)	Minimum of $\boldsymbol{x}$
sgn(x)	Sign function
var($\boldsymbol{x}$)	Variance: $\mathrm{var}(\boldsymbol{x})=E[\boldsymbol{x}\cdot\boldsymbol{x}^T]-(E[\boldsymbol{x}])^2$
$\boldsymbol{w}\sim(\boldsymbol{x},\boldsymbol{y})$	Process noise with mean $\boldsymbol{x}$ and covariance $\boldsymbol{y}$
$\boldsymbol{x}^T$	Transpose of $\boldsymbol{x}$
$\bar{\boldsymbol{x}}$	Mean value of $\boldsymbol{x}$
$\lvert\boldsymbol{x}\rvert$ or abs($\boldsymbol{x}$)	Absolute value of $\boldsymbol{x}$
$\lVert\boldsymbol{x}\rVert_p$	p-norm: vector norm (p=2, Eucledian norm, or $p=\infty$, max. norm) or signal norm (p=2, quadratic norm, or $p=\infty$, peak value in time)
$\lVert\boldsymbol{x}\rVert_P^2$	Quadratic form or the square weight norm of vector $\boldsymbol{x}$ with a symmetric matrix P
$\dot{x}, \ddot{x}$ or dx/dt, d^2x/dt^2	First and second time derivatives of a generic variable x
σ_x	Standard deviation of x: $\sigma_x=\sqrt{\mathrm{var}(x)}$
$\partial h/\partial x$	Partial derivative of function h with respect to x
$\nabla h(\boldsymbol{x})$	Gradient of $h(\boldsymbol{x})$
$\int h(x)\ dx$	Integral of $h(\boldsymbol{x})$
$\sqrt{x}$	Square-root of x

Publications

List of author's publications directly related with the research work developed in this thesis.

Scientific Journals

Oliveira F., Botto M., Morais P. and Suleman A. *Semi-active control of base-isolated buildings with semi-active dampers using an integral control law*. Journal of Structural Engineering. Under revision.

Oliveira F., Morais P. and Suleman A. *Experimental evaluation of Semi-Active Control Strategies for Base Isolated Buildings*. Earthquake Engineering & Engineering Vibration. Submitted.

Oliveira F., Morais P. and Suleman A. *A Comparative Study of Semi-Active Control Strategies for Base Isolated Buildings*. Earthquake Engineering & Engineering Vibration 14(3): 487-502, September 2015. DOI:10.1007/s11803-015-0039-9.

Oliveira F., Morais P. and Suleman A. *Predictive Control for Earthquake Response Mitigation of Buildings Using Semi-active Fluid Dampers*. Shock and Vibration Journal Volume 2014, Article ID 670683 (14 pages), July 2014. http://dx.doi.org/10.1155/2014/670683.

National Publications

Oliveira F., Morais P. and Suleman A. *Sistemas semi-ativos para a mitigação de vibrações em edifícios com isolamento de base sujeitos a ações sísmicas*. Construção Magazine nº62 - O Laboratório Nacional de Engenharia Civil, Julho/Agosto 2014.

Conference Proceedings

Oliveira F., Morais P. and Suleman A. *Semi-active control of base-isolated structures*. Procedia Engineering Volume 114:401-409, 2015. ICSI2015 – 1st International Conference on Structural Integrity, Madeira Island, Portugal, 1st to 4th September 2015. doi:10.1016/j.proeng.2015.08.085.

Oliveira F., Morais P. and Suleman A. *Semi-Active control using an output non-linear feedback strategy*. EURODYN2014 – IX international Conference on Structural Dynamics, Porto, Portugal, 30th June to 2nd July 2014.

Oliveira F., Morais P. and Suleman A. *Predictive Control for Earthquake Response Mitigation of Buildings Using Semi-active Fluid Dampers*. ICEDyn2013 – International Conference on Structural Engineering Dynamics, Sesimbra, Portugal, June 17-19, 2013.

Oliveira F., Morais P. and Suleman A. Semi-active control of a fluid viscous damper for vibration mitigation. 15th World Conference of Earthquake Engineering. Lisbon, 24 to 28 September, 2012.

Oliveira F., Botto M., A. Suleman and P. Morais, *Semi-Active Viscous Damper for Controlling Civil Engineering Structures Subjected to Earthquakes*. 10th Portuguese Conference on Automatic Control, Funchal, Portugal, 16-18 July, 2012. **Awarded at the conference as the Best industrial paper**.

Oliveira, F., Morais, P and Suleman, A. *Sistemas Semi-ativos na proteção sísmica de estruturas*. Jornadas de Investigação e Inovação LNEC – Cidades e Desenvolvimento, LNEC, Lisboa, 18 a 20 de Junho de 2012.

Morais P. J. G., **Oliveira F. V. P.**, Falcão, M. J., Campos Costa, A. *Sistema Mecânico para Simulação Física do Comportamento Dinâmico de Estruturas*. CNME2010 – Congresso Nacional de Mecânica Experimental, Guimarães – 21 a 23 de Abril de 2010.

Chapter 1

Introduction

Summary

This study entitled *Semi-active systems for structural vibration mitigation* follows the development of a research done in semi-active control of civil engineering structures subjected to earthquake loads aiming to address structural vibration control using adequate control strategies developed for this purpose. This introductory chapter outlines the research motivation, the problem statement, the objectives and the relevance of this study.

1.1 Motivation

Natural disasters like earthquakes or strong winds have shown to be the most catastrophic events causing loss of life and property damage, leading to economic and human losses. These natural events show how humanity and its works are vulnerable to the forces of nature. Other actions such as traffic-induced vibrations can also affect human comfort or can damage structures. Structures subjected to these kind of events may not only became uncomfortable for people but also very dangerous in case of collapse. Moreover, structures like buildings are being constructed in modern cities according to several restrictions. One of those restrictions is the limited availability of terrain which lead to the development of higher and slender structures. These aspects in conjunction with the current trend to create sustainable buildings has led the construction community to develop and implement innovative solutions for those structures to resist loads (*Soong & Dargush 1997*) - figure 1.1.

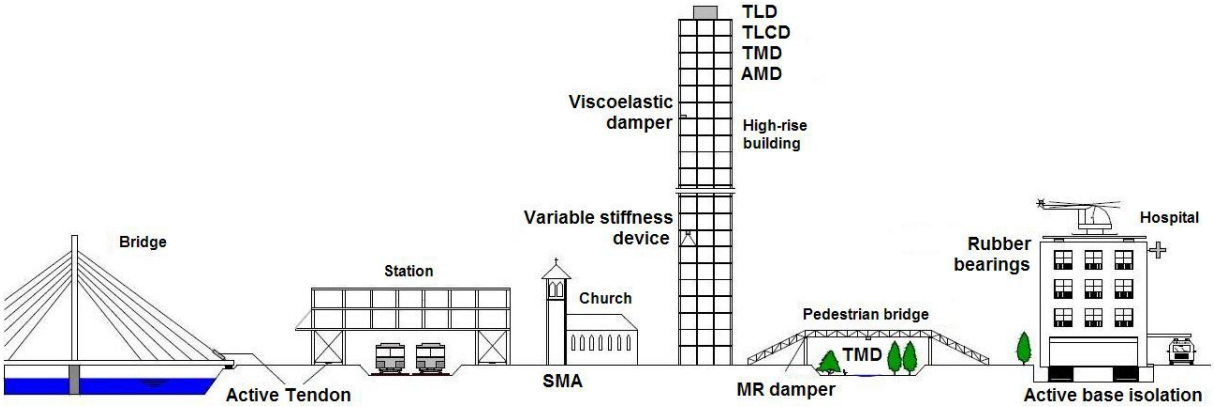

Figure 1.1 - Dynamic protection systems applications (from *Oliveira 2009*).

The traditional design methods for earthquake resistance of structures allow the occurrence of damage by using the inelastic deformation capacity of some elements. This kind of approach could be problematic for structures that should be operational during and after the occurrence of those events, like the ones that are vital for civil protection: hospitals; energy power supply; communication centres; civil protection and fire station buildings; are notable examples. Thus, energy dissipation devices have been proposed as an alternative way to improve structures resistance to earthquakes and also for other dynamic loads such as wind and traffic-induced vibrations. The idea is that part of the input load energy is dissipated by those devices. In general terms, it is intended that structures equipped with protection systems can reduce the structural responses (relative displacements and accelerations). Initial solutions comprised the installation of passive devices but due to limited performance, active systems had gained more acceptance. However, the higher performance of active systems is achieved at a much higher system complexity and higher energy requirements. Hybrid solutions combining active and passive devices were also proposed as a better way to improve structures performance. Recent solutions based on the principle that it is possible

to adjust the characteristics of passive devices in real-time and the associated advantages regarding lower power requirements led to the research and development of energy dissipation systems employing semi-active devices (*Symans & Constantinou 1999; Soong & Spencer Jr. 2002; Chu et al. 2005; Casciati et al. 2012*).

Semi-active devices such as variable Fluid Viscous Dampers (FVD) or Magneto-Rheological (MR) dampers can be used to control structures dynamic behaviour with lower power requirements. Several applications employing these type of devices can now be found more frequently (*Symans & Constantinou 1999; Soong & Spencer Jr. 2002*). See an example of an MR damper application in figure 1.2. In recent years MR dampers have been considered for use in semi-active systems. This type of damper offer some advantages when compared to others: higher damping forces with lower power requirements and a more compact geometry. However, the nonlinear behaviour makes the mathematical modelling a challenge.

Figure 1.2 - Tokyo National Museum of Emerging Science and Innovation and 30-t MR fluid damper (from *Spencer Jr. 2008*).

The integration of these devices in structures for controlling the seismic responses using the adaptability they provide is also a complex control problem to solve. Even if both structure and device are described by linear models the resultant model is a nonlinear system (structure plus device) with bounded inputs. Moreover, the resulting hybrid system, structure plus semi-active device, is affected by time delays due to measurement process, computation of control variable and device dynamics. It is also expected that the whole model parameters have associated uncertainties resulting from the adopted model and measurement uncertainties. Adding up to all of these issues the whole systems is subjected to unknown disturbances, the seismic action. The control problem can be stated as:

$$\begin{aligned} \dot{\boldsymbol{z}} &= f_1\left(\boldsymbol{z}, \ddot{x}_g, \boldsymbol{f}_{SA}\right) \\ \boldsymbol{f}_{SA} &= f_2\left(\boldsymbol{z}, \boldsymbol{u}_{SA}\right), \ \boldsymbol{u}_{SA,min} \leq \boldsymbol{u}_{SA} \leq \boldsymbol{u}_{SA,max} \end{aligned} \tag{1.1}$$

where: $\boldsymbol{z}$ is the state vector; $\ddot{x}_g$ is the input disturbance (earthquake); $\boldsymbol{f}_{SA}$ is the vector of generated forces by semi-active devices; $\boldsymbol{u}_{SA}$ are the input variables to the dampers whose

values are bounded $\boldsymbol{u}_{SA,min} \leq \boldsymbol{u}_{SA} \leq \boldsymbol{u}_{SA,max}$. Although the time variable is not explicitly shown in the equation, all the terms are time dependent. Functions $f_1(\cdot)$ and $f_2(\cdot)$ are also dependent of model parameters which are usually time-invariant and thus take constant values. The control problem can be stated as: *find the inputs to the devices (control signals) such that optimize the whole system performance, i.e. conducting to small displacements and small accelerations in the structure.*

A common approach for controller design of hybrid systems consisting of structural systems with semi-active devices, is to assume the device as an active one and then use clipped algorithms to command the device. This approach is described in the literature as a force tracking scheme. Thus, some of the issues described above are not directly accounted in the controller design which could compromise the system performance.

Recently a specific type of hybrid system has been studied. It consists on a base-isolated structure equipped with semi-active devices installed at the base level (*Luo et al. 2001; Gavin & Aldemir 2005*; *Komatsu et al. 2007*; *Bahar et al. 2010*) to reduce the isolation displacement. It is referred that under near-field seismic actions, base-isolated structures could face large displacements at the base due to pulse-like ground motions which make them vulnerable to structural damage (*Kelly 1999*). Thus, damping systems which can reduce base isolator displacements without increasing superstructure response, for both near- and far-field ground motions, have been required (*Gavin & Aldemir 2005*).

To solve the issues described above advanced methodologies are needed. With this in mind, this research aimed precisely to cope with some of these issues taking into account the control objectives. Some controllers were implemented and tuned taking into account the disturbance characteristics, namely by using the seismicity of the site where the structure is to be constructed. Control laws were formulated taking into account the device characteristics on the device formulation and considering also the unknown disturbance in the formulation of the control law. Moreover, it was given emphasis to control laws formulated and implemented in such a way that only a few measurements are required, namely those at the base level.

1.2 Objective

The objective of this thesis was to address the structural vibration control of civil engineering structures subjected to earthquakes using semi-active systems. Emphasis was given to the modelling and design of control strategies to mitigate the vibrations induced in the structure by the input ground motions.

A comprehensive study of semi-active devices namely FVD with adjustable characteristics and MR devices was performed. The goal was to find reliable mathematical models to

describe its mechanical behaviour and that may be suitable for control design.

Typical structures, namely those of main importance were taken into account for implementation of semi-active systems. Mathematical models describing the dynamic behaviour of those structures were used in the analysis of the applicability of semi-active systems.

Several control strategies were identified and systematised for use in this context. Other control strategies from other fields were implemented in this type of control problems in order to account the complexities associated with the device and with the structure, like non-linearities and measurement limitations, and with the unknown disturbances (seismic action).

The performance of the structure equipped with semi-active systems was evaluated by means of numerical simulations and experimental tests comparing the results with the uncontrolled structure and with the structure equipped with an optimized passive solution.

The study is entitled *Semi-active systems for structural vibration mitigation* and falls within the mechanical engineering domain and embraces other areas of knowledge like: modal analysis; control systems; structural dynamics; smart structures; instrumentation; and rheology. It should be noted that this study add values and knowledge to applications in the civil engineering domain and namely on the earthquake engineering field. This study aims at contributing to:

- the development and implementation of several semi-active control strategies whose performance is evaluated in the context of base-isolation systems, being the best one identified through numerical and experimental analysis, and proposed for this kind of applications;
- the analysis of classical control strategies already used in other contexts and its implementation in this area: integral control law; optimal control law; modulated homogeneous friction; maximum energy dissipation algorithm;
- the development of semi-active control strategies that takes into account the device characteristics in the controller formulation, namely the force tracking scheme using a model predictive controller and a nonlinear output feedback strategy that accounts for the device formulation in the definition of the control law;
- the understanding of the influence of the controller tuning on the whole structural system performance, which reinforces that the controller parameters should be identified according to a methodology which relies on numerical simulations considering a set of representative ground motions (based on the seismicity of the site) and the structural model.

The importance of these goals, both for the industrial and academic communities, should be stressed out.

First, the development of semi-active control strategies that take into account the device characteristics is still a challenge due to the nonlinearities of the devices in the formulation. In this work, contributions are given in this direction. A predictive controller that takes into account the device dynamics in the controller internal model is proposed. However this strategy still needs an algorithm to adjust the control variable inside the working regime. Nonlinear procedures are also used to formulate the control law. A formulation taking into account the device mathematical model is derived using an output linearization. A dedicated algorithm is used to adjust the control variable. Beyond those, the sliding mode control strategy is also considered.

Secondly, this work also gives a contribution to the research community by comparison of the structural performance of the system with different control strategies with the uncontrolled one and with the one equipped with optimized passive solutions. The comparison is made through numerical simulations and experimental tests, and identifies the best solution which can be applied in base isolation applications. A methodology relying on numerical simulations considering a set of representative ground motions and the structural model was found to be useful in identifying the controller parameters and should be followed when tuning the controller.

Finally, due to the type of applications considered, base-isolated structures, only measurements at the base could be used. Thus, collocated control is used which facilitates the development of technological solutions. Those devices can be as compact as the common passive systems. A damper having embedded sensors, hardware, software and power supply (batteries), would confer the capacity of working autonomously and provide better performance than the passive one.

1.3 Outline of the Dissertation

Taking into account the main objectives mentioned above the thesis structure follows the development of the investigation done in semi-active control of civil engineering structures subjected to earthquake loads. This work is structured in five chapters, including this one, **Chapter 1**: *Introduction*, where the theme is introduced justifying the importance and motivation of this study in the engineering domain and particularly in the vibration control field with applications for the seismic engineering field.

In order to accomplish the objectives a review of the main topics related with semi-active control of civil engineering structures when subjected to input disturbances is presented in **Chapter 2**: *State-of-the-art*. It starts with an introduction to the earthquake engineering field

covering some historical facts and the main topics contributing to the seismic risk, followed by a characterization of the seismicity and the description of the seismic action for the Portuguese territory. The main approaches contributing to the seismic safety and reducing the vulnerability are described, namely those related with protective systems: passive, semi-active, active and hybrid control systems. Special emphasis is given to semi-active control of civil engineering structures and in particular to hybrid base-isolated structures. The common approaches considered for solving this type of problems are introduced and the structural models, devices models and control strategies are reviewed. Some of the most relevant developments and applications are also described and summarized.

The problem of reducing earthquake induced vibrations of civil engineering structures using semi-active systems is explored in **Chapter 3**: *Semi-active Control - Theoretical developments and numerical simulations* -. The semi-active active control problem is defined taking into account a general mass-lumped model for the structure and the Maxwell model as a general way to model the transient and stationary regime of SA devices. Several force tracking schemes already used in other areas based on the integral control law, on the optimal control law and on the modulated homogeneous friction algorithm as controllers, and on algorithms as adjusting rules, are described. A Lyapunov controller is also described for this purpose. Three control methods are also described and formulated: i) a force-tracking scheme based on the model predictive controller; ii) a nonlinear output feedback controller; iii) and a sliding mode control approach. A preliminary numerical study on a single degree of freedom (SDOF) mechanical model was performed to analyse the applicability of these strategies in structures, and the results are presented and discussed. Then, a more realistic model, a typical 10-storey base-isolated building is described and considered for performance evaluation, being the results of numerical simulations presented and discussed. The methodology proposed to tune the controller using the system model and a set of ground motions is also described. A comparison of results with the original (uncontrolled) structure and with the structure equipped with passive devices is analysed and discussed.

The validation of the semi-active control techniques analysed is performed through numerical simulations and experimental tests, which is described in **Chapter 4**: *Experimental Studies on Semi-active Control - Numerical and experimental validation of semi-active control strategies* -. For this purpose, a physical model representative of the phenomenon under study comprising a two degree-of-freedom mechanical model with magneto-rheological dampers, the measurement chain comprising the sensors and the data acquisition system, and the controller architecture comprising the hardware and software, are defined, described and the results of the mechanical and metrological characterization are presented. The models are described and its parametrization is explained and discussed. The experimental

tests of the mechanical model performed on a shaking table using different input ground motions are described and the results for each case (uncontrolled, passive and semi-active cases) are presented and discussed. The results of numerical simulations for the same cases using the adopted models is presented, discussed and compared with the experimental test results, for validation of the control strategies.

The level reached and the limitations of this work is presented and discussed in **Chapter 5**: *Conclusions*. It is made a reference to main original contributions and conclusions of this work, highlighting the importance of this research and mentioning future work to be developed.

Chapter 2

State-of-the-art

Summary

This chapter is devoted to a detailed description of the main topics related with semi-active control of civil engineering structures when subjected to input disturbances like earthquakes. Although the focus is on semi-active control, the chapter begins with brief introduction to earthquake engineering and then introduces and describes the main aspects contributing to the seismic risk: seismicity, vulnerability and exposition. The seismicity concept is introduced and the seismic action is defined in terms of response spectra. The vulnerability topic is also covered and the main approaches contributing to the seismic safety are described. Special emphasis is given to semi-active control and in particular to hybrid base-isolated structures with semi-active devices. Fluid viscous dampers and magneto-rheological dampers are the most common type of devices in civil engineering applications and a detailed description is made. The mathematical models of building structures, the devices models and control strategies are reviewed and presented. Alongside the most relevant developments and applications of semi-active control systems are also described and summarized.

2.1 Historic Evolution

Records of efforts to construct earthquake resistant structures can be found in many countries for a long time. In Portugal, for example, there are accounts of structures similar to the ones used to reconstruct Lisbon after the 1755 earthquake (estimated magnitude: 8,5 to 9 MMS) being tested using military forces to input the load during tests. The type of construction used to reconstruct Lisbon consisted in structural systems made of wood filled with masonry elements and plastered in the end, was called *Gaiola Pombalina* (see figure 2.1). The name is due to the main involvement and contribution of the Kingdom Secretary of State (Prime-Minister) Marquês de Pombal in the reconstruction of the city. This type of construction conferred and is still conferring good resistance to horizontal forces like the ones produced by earthquakes. Despite this, it was only in the first half of the XX century that Earthquake engineering was established as a science field (*Lopes 2008*).

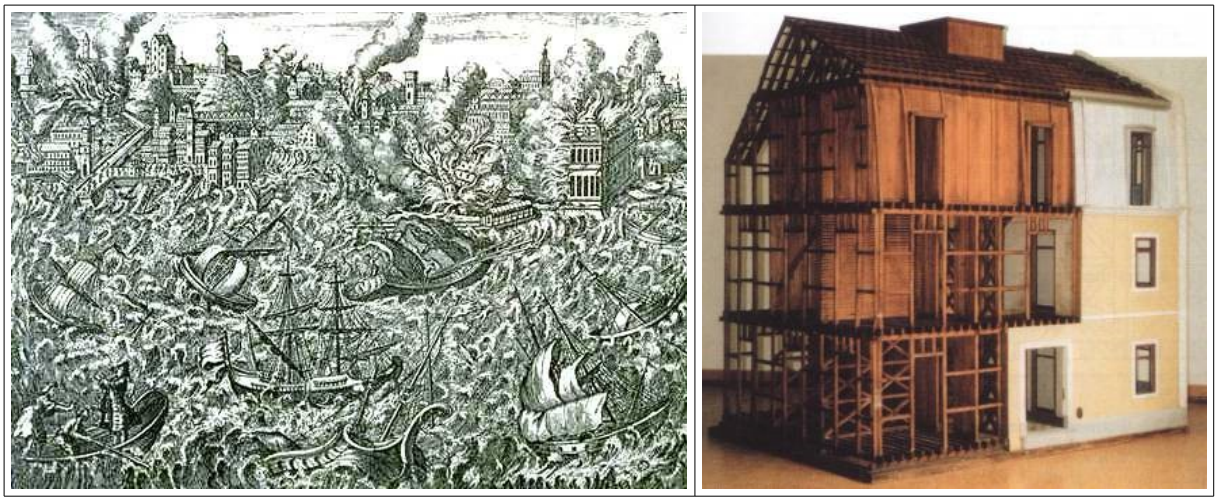

Figure 2.1 - Left: View of Lisbon during the 1755 earthquake (original engraving in Museu da Cidade, Lisbon); Right: *Gaiola Pombalina* construction (from http://www.lnec.pt).

The Earthquake Engineering is the scientific field concerned with the protection of society, the natural and the man-made environment from earthquakes by limiting the seismic risk to socio-economically acceptable levels. The main objectives are (*Lopes 2008*):

- foresee the potential consequences of strong earthquakes on urban areas and civil infrastructures;
- design, construct and maintain structures to perform at earthquake exposure up to the expectations and in compliance with building codes.

The first institutions dedicated to the study of seismic phenomena and its consequences were founded in the late of the 19th century in Japan. It was at that time, after the Yokohama (Japan) earthquake (1880) that Professor John Milne, Sir James Alfred Ewing and Thomas Gray, British scientist working in Japan, found the Seismological Society of Japan. John Milne was a British geologist and mining engineering working at the Imperial College of

Engineering in Tokyo at that time, to which was attributed the invention of the seismograph. He also proposed the first base isolation system for structures subjected to earthquakes, by demonstrating that a wood house over ball bearings could be isolated from earthquakes (*Housner et al. 1997)*. In the seismic isolation branch several solutions were patented until the end of the sixties, although there are no references of any applications of those proposed solutions. The first application of this type of solution was made at a primary school building in Macedónia in 1969, using elastomeric bearings to separate the substructure from the superstructure. After that, the use of base isolation systems started to be implemented in several buildings all over the world (*Moreira de Andrade 2007*).

Several progresses were made since the beginning of the 20th century due to experimental studies. The first shaking table was developed by F. J. Rogers in 1906 to study soil behaviour when subjected to seismic loads. However it was only after the twenties that several shaking tables were developed in Japan and in the United States, allowing the study of structures dynamic behaviour.

At that time only reduced models (scaled) were possible to test under several limitations. It was only after the developments in computer science that new shaking tables with large capacities of control were developed, like the one developed in 1972 in Berkeley at the Earthquake Engineering Research Centre (http://peer.berkeley.edu/).

In what seismic safety is concerned, several measures were unfortunately only taken after the occurrence of those events. It was after the devastating earthquake of Messina (Italy) in 1908, that a commission of technicians from the governmental entities formulate and define the recommendations for structures to resist horizontal to loads. Later on, in Japan was introduced the seismic coefficient to design earthquake resistant structures that contributed for the establishment of codes. Similar rules were introduced in the United States during the thirties, where for the first time were obtained earthquake records from a seismograph network installed years before. These results allowed for the adjustment of the peak acceleration values established in the codes. Later on (1941), George Housner established the response spectra concept, a criteria still used in current codes, based on the results of earthquake records.

During the thirties important criteria for earthquake classification was introduced: the Mercalli Modified Earthquake Scale (intensity scale which is a measure of the energy released, that quantifies the effects of an earthquake on earth's surface); and the Richter Scale (that is a magnitude scale that quantifies the energy contained in an earthquake).

Portugal also followed the evolution in this domain. Júlio Ferry Borges was one of the most important specialists in seismic engineering and was involved in the development of the

modern codes for earthquake resistant structures. The codes have been following the recommendations made in several reports of international institutions of seismic engineering. In recent years, LNEC (Laboratório Nacional de Engenharia Civil) coordinated the technical commission responsible for elaborating and implementing the Eurocode 8 in Portugal, that is now the current code in use for designing structures in seismic zones (http:/www.lnec.pt).

On the other hand, in recent years a different philosophy has been proposed and consequently implemented in civil engineering structures for structural response mitigation under wind and seismic loads. The idea is that part of the input energy (from wind or earthquake) is absorbed by additional structural devices installed on the structure. These devices can be classified according to the source of energy used to operate as: passive; semi-active; active; and hybrid. Passive energy dissipation systems were the first to be proposed for mitigation of earthquake induced vibrations. First, were the metallic dampers to be developed during the seventies; then the friction, viscous and tuned liquid dampers, during the eighties; and recently were also proposed viscoelastic dampers (*Soong & Dargush 1997*). In the end of the eighties and during the nineties several applications of semi-active, active and hybrid systems have been considered and implemented, specially in Japan (*Soong & Spencer Jr. 2002*).

2.2 Seismic Risk

Natural phenomena like earthquakes often produce adverse effects that can be minimized if an effective risk management strategy is implemented. The risk may defined as the result of the estimation involving an uncertain danger that may result in undesired consequences for people, property and environment. It takes into account the occurrence probability and the consequences. Seismic risk (or earthquake risk) may be defined as the potential economic, social and environmental consequences of hazardous events that may occur in a specified period of time. Seismic risk refers to the expected losses to a given 'elements at risk', over a specified future time period (*LESSLOSS 2007*). The risk at a specific site is measured by the element losses in that region as consequence of the earthquake, and/or by the probability of those consequences occur during a specified exposure time. Buildings, cities, countries, the population, the infra-structures and equipments, the economic activities and others, are some examples of elements at risk (*Sousa 2006*). The principal factors that affect the seismic risk are the hazard, the vulnerability and the exposition:

$$R = f(H, V, E) \tag{2.1}$$

Hazard (*H*) is the probability of occurrence of an earthquake of a certain severity, within a specific period of time, at a given location or in a given area. Vulnerability (*V*) is related with the damage that a particular element or set of elements may suffer as a consequence of an

earthquake. Finally, the exposition (*E*) is the value of the elements exposed to the earthquake. According to the way in which the element at risk is defined, the risk may be measured in terms of expected economic loss, or in terms of numbers of lives lost or the extent of physical damage to property, where appropriate measures of damage are available (*LESSLOSS 2007, Sousa 2006*).

The evaluation of seismic risk is used to classify potential consequence of earthquake events all around the world. The variation of any of those parameters has direct influence on the seismic risk. As an example, it is expected that a specific site subjected to strong earthquakes but sparsely populated has a small seismic risk. Moreover, two different sites with the same population subjected to similar earthquake severities, have much higher risk as more vulnerable are their structures. In order to mitigate the seismic risk of a specific site without moving people or property (thus maintaining the same hazard and exposition) the vulnerability must be reduced, and thus improvements in seismic safety are required (*Cansado Carvalho 2001, Sousa 2006*).

Referring to the particular case of Portugal, recent works showed that: a moderate hazard associated with higher magnitude events with large occurrence periods (*Carvalho 2007*) is verified; the vulnerability is high due to insufficient structural earthquake resistance in general; and consequently a higher seismic risk is verified in some sites (*Cansado Carvalho 2001*). *Sousa 2006* showed that Beja, Faro, Lisbon, Santarém and Setúbal counties have the highest seismic risk, being Lisbon county the one with highest risk. It is shown also that economical losses result mainly from small intensity earthquakes than from those that contribute to the human losses. The region of Lisboa and Vale do Tejo is also the one showing major losses, both human and economical. The metropolitan area of Lisbon in particular is the one that contributes more due to the highest exposition values. For the Lisbon county, a hypothetical case was simulated assuming that if buildings were constructed with the actual regulation codes the economical losses could be reduced in 88 % compared to the existing situation. As a result of the LESSLOSS project, mitigation actions consisting in strengthening buildings could lead to reductions in destroyed and damaged buildings as in the number of deaths up to 78 % (*LESSLOSS 2007*). This results show how important is the vulnerability in reducing the seismic risk.

2.3 Earthquakes

2.3.1 Earthquake: a natural disaster

The explanations for the origin of earthquakes are very old. In the ancient Greece the problem was discussed and the origin was attributed to the winds or seas inside the earth. Aristotle developed a vulcanist model where the fire inside the earth played an important role in the origin of seismic vibrations. On the other hand, the Neptunists associated the

earthquake origins to the collapse of underground caves dig by ancient oceans. However, it was just recently (XX century) with the advent of the plate tectonics that rational explanations were accepted by the scientific community. This theory was formulated in 1912 by the German Alfred Wegener but only gained acceptance with the observations of the ocean floor made by the British Fred Vine and Drummond Matthews in 1963 (*Lopes 2008*).

The plate tectonic states that Earth's lithosphere (crust and portion of the upper mantle: 40 to 280 km thick) is broken into plates that move over the asthenosphere, with a relative motion in the boundaries that forces the occurrence of earthquakes. When the earthquake is generated in the plates boundaries it is called interplate earthquake. However, sometimes geological faults in plates are reactivated due to the induced stress at the plates boundaries which leads to the occurrence of earthquakes at those faults, this ones designated as intraplate earthquakes. Portugal has been affected by interplate earthquakes generated at the Açores-Gibraltar fault (that separates the Eurasian plate and the African plate) and by intraplate earthquakes generated at the active faults in the territory (see figure 2.2).

Figure 2.2 - Tectonic plates near Portugal (left). Active and possible active faults in Portugal.

When the Earth's equilibrium state is disturbed at the fault (the hypocentre), the accumulated elastic energy is released leading to the propagation of seismic waves: Primary waves (P-waves) which are the faster ones; Secondary waves (S-waves) which are the second ones to be captured by the seismographs; and surface waves, the Rayleigh and Love waves which occur at the lithosphere and are slower than the others. The radiated energy is related with the moment magnitude scale (MMS or M_w) which is nowadays the scale used to measure the size of earthquakes. This one is dependent of the seismic moment (M_0) which is a measure of the energy released during the earthquake. The MMS scale succeeded the Richter magnitude scale (or local magnitude scale M_L) which is function of the motion

measured by the seismometer and the distance between the seismic station and the hypocentre. The effects of an earthquake at a specific site are then measured by another scale, the Modified Mercalli scale (MM), which measures the intensity of an earthquake. The seismic action intensity is thus evaluated by comparing the effects (observation of damages and data gathered from people) with the intensity tables of the scale. Relationships between magnitude and intensity scales can also be found in the literature.

2.3.2 Seismic Action

The seismicity (seismic activity) of an area is characterized by the number of earthquakes of a certain magnitude occurred in a specific period of time. In order to characterize the seismicity at a specific site, the historic seismicity, the instrumental seismicity and the geological evidence must be considered. Moreover, the territory is divided in seismic source zones which define the geographical variation of earthquake activity. The analysis of the seismicity lead to the establishment of laws (usually empirical) to describe several phenomena: i) the relationship between the magnitude and the total number of earthquakes, in any given region, in a specific time period, of at least that magnitude is described by the Gutenberg-Richter law (GR law), given as $\log N = a - b \cdot M$, where N as the number of earthquakes with magnitude equal or superior to M and, a and b are constants defined in the catalogue of earthquakes; ii) the seismic waves lose energy as it propagates through the earth and their attenuation is characterized by specific laws too; iii) finally, the seismic waves are also modified by local effects, the last 30 m of the lithosphere (bed-rock) (*Lopes 2008*).

In this context the return period T_r concept is always adopted. It is a statistical measure typically based on historical data denoting the average recurrence interval of an earthquake with a certain magnitude over an extended period of time. Assuming a constant annual probability of an earthquake occurring, its value is given by the inverse of the return period, as the probability $p_1 = 1/T_r$. This quantity reflects the number of occurrences per year, given by $p_1 = N_s/N_y$, number of occurrences N_s over the number years N_y. The probability of being exceeded in n years, is obtained by $p_n = p_{n-1} + p_1 \cdot [1 - p_{n-1}]$ which is equivalent to using the Poisson model, $p_n = 1 - \exp(-p_1 \cdot n)$. Thus, the return period is related with the probability of occurrence in n years by $T_r = -n/\ln(1 - p_n)$. For the return period expressed in the Portuguese code (*Eurocodigo8 2010*), T_r=475 years (or p_{50}= 10%), only the historical seismicity can be considered. Although this information is very useful to evaluate the seismicity, it is qualitative and could be insufficient to characterize the seismic action. For this purpose the instrumental seismicity is more straightforward, since allows the quantification of the movement. However, in Portugal records are only available after 1902 which justifies the use of other tool, like mathematical modelling of the seismic source. *Carvalho 2007* developed and applied the stochastic finite-fault modelling with identified parameters, which were regionally evaluated,

for estimation of Portuguese ground motion earthquakes.

The seismic action is thus dependent of several factors like the generation, the propagation and the local effects, which determine its amplitude and frequency content. The ground motion resulting at a specific site is characterized by non-stationary stochastic processes whose amplitude and frequency content change during the occurrence of the earthquake (*Carvalho 2007*). The seismic action ground motion can then be obtained from:

- the available records from past earthquakes;
- the response spectra established or stipulated by the codes, in which the generated accelerogram must match the correspondent spectra;
- the results of well established mathematical models of the source, namely when no records from the instrumental seismicity are available; at a specific local the seismic action is modified by accounting for the source, propagation and local effects.

2.3.3 The Seismic Action for the Portuguese Territory

The establishment of seismic codes for Portugal dates in 1958 with the Regulamento de Segurança das Construções Contra Sismos (RSCCS) document (*RSCCS 1958*). After that some revisions and complements were made and the Regulamento de Segurança e Acções (*RSA 1983*) code was implemented. Actually the *Eurocodigo8 2010* is in place for designing structures for earthquake resistance. Two types of seismic actions are considered for the Portuguese territory:

- type 1: far field and interplate seismic action generated at the Açores-Gibraltar fault, which is considered for the Mainland Portugal and Madeira; longer duration earthquakes rich in the lower frequencies with magnitudes above or equal to 5,5;
- type 2: near field and intraplate seismic action considered for the Mainland Portugal and Açores; short duration earthquakes rich in the higher frequencies with magnitudes bellow to 5,5.

The zones specified by the code are defined accordingly as in figure 2.3.

As stated before the return period of the reference seismic action is T_r=475 years (or a probability of being exceeded in 50 years p_{50}=10 %). Under different return periods (or probabilities) the reference seismic action is corrected using an importance factor γ_I: i) seismic action with different return period T_{rN}, $\gamma_I \sim (T_r/T_{rN})^{-1/k}$; ii) seismic action with a probability of being exceeded p_l in l years equal to the reference seismic action probability of being exceeded p_n in n years, $\gamma_I \sim (n/l)^{-1/k}$; iii) seismic action with a probability of being exceeded p_{nN} in n years different from the reference seismic action probability of being exceeded p_n in the same n years, $\gamma_I \sim (p_{nN}/p_n)^{-1/k}$. These expressions are result of the assumed relationship for the

annual probability of occurrence, $p_1 \sim k_0 \cdot a_{gR}^{-k}$; where k is a parameter dependent of the seismicity, a_{gR} is the reference ground motion acceleration (soil type A) and k_0 is a constant. k=1,5 for type 1 seismic actions, k=2,5 for type 2 seismic actions in Mainland Portugal and, k=3,6 for type 2 seismic actions in Azores are the values of that parameter for the Portuguese territory. The importance factor γ_I is also considered in definition of the seismic action according to the importance of the structure under analysis. For an importance factor γ_I=1, the ultimate limit state verification considers a design seismic action equivalent to the reference seismic action. Under the serviceability limit state verification the return period of the design seismic action is T_r=95 years (or p_{10}=10 %). The code refers that the ultimate and serviceability limit state verification seismic actions have the same spectral configuration (response spectra) but a reduction coefficient is considered for the second one.

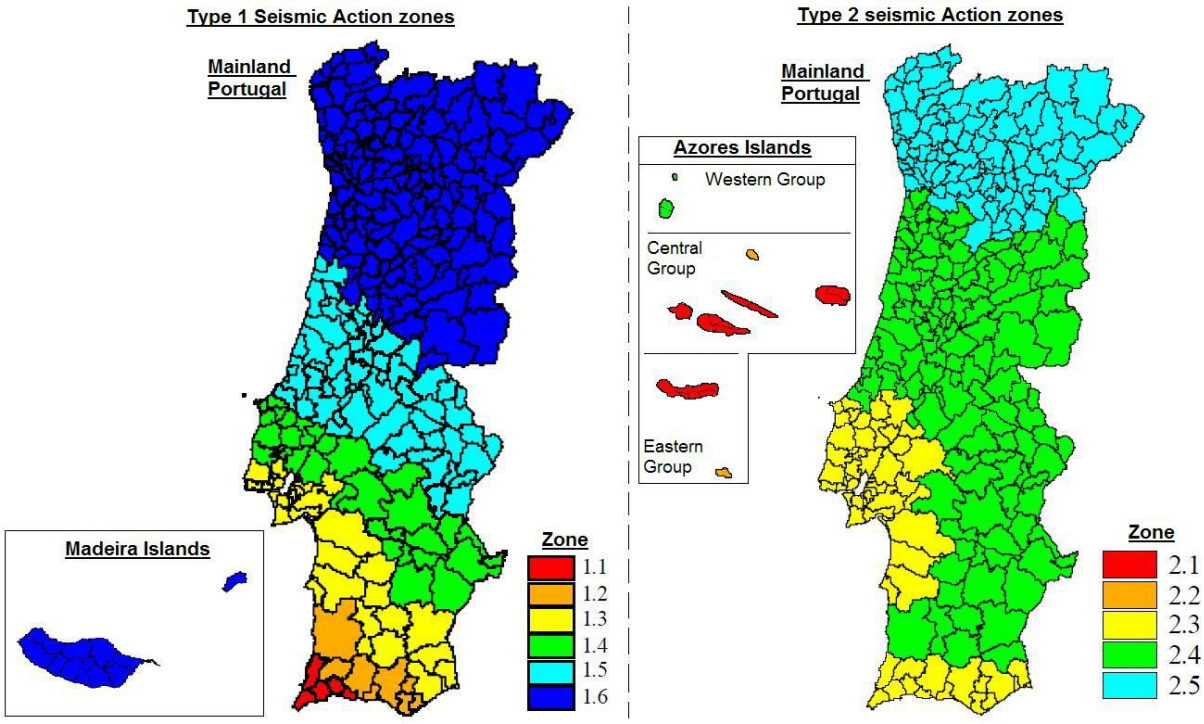

Figure 2.3 - Seismic zones for the Portuguese territory according to the *Eurocodigo8 2010*.

For each zone, type of action and soil type an elastic response spectra is defined. See general form in figure 2.4. These spectra is a smooth response spectra resulting from the statistical analysis of a set of accelerograms representative of a specific site. It represents the structure response (representative peak values) function of the vibration period taking into account a specific structural damping (usually ξ=5 %). The response can be given in terms of displacement, velocity or acceleration, which are related each other by the angular frequency $\omega=2\pi/T$. For the general spectra in figure 2.4 the *Eurocodigo8 2010* defines the parameters: $S_e(T)$ is the elastic response spectra (in terms of acceleration); T is the vibration period of a linear single degree of freedom system; $a_g=\gamma_I \cdot a_{gR}$ is the design ground

acceleration which is dependent of the reference ground motion acceleration (soil type A) a_{gR} and an importance factor γ_I (that characterizes the structure importance or the seismic action return period); T_B and T_C are the limits of the constant spectral acceleration branch; T_D is the value defining the beginning of the constant displacement branch; S is a soil parameter; η=[10/(5+ξ)]$^{1/2}$ is a damping correction factor (η=1 for ξ=5 %); k_e=2,5 for horizontal component of the seismic action and k_e=3 for the vertical component; under the vertical component S=1 and a_g is substituted by the correspondent vertical component a_{vg} leading to the vertical elastic response spectra $S_{ve}(T)$. To account the non-elastic behaviour another spectra including the behaviour factor is defined in the code.

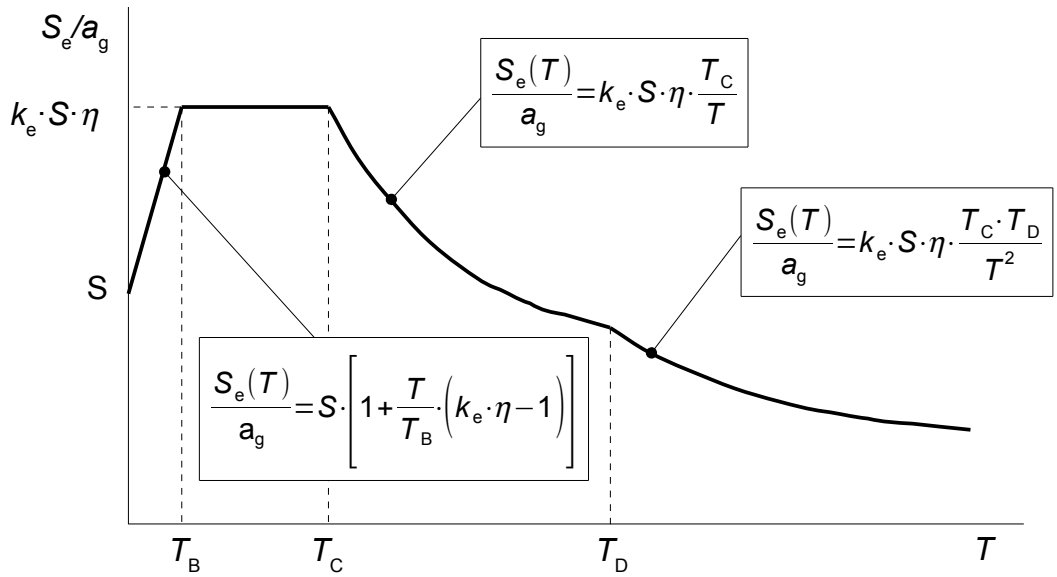

Figure 2.4 - General form of the elastic response spectra (acceleration) according to the *Eurocodigo8 2010*.

The response spectra is very useful for design purposes since easily the designer can extract the peak acceleration values taking into account the structural period of vibration under analysis. Moreover, accelerograms for the site under consideration can be synthesized to match the correspondent spectra. The code stipulates the use of at least 3 accelerogroms per direction in the design procedure.

2.3.4 The Seismic Action and Structures Natural Frequencies

In general the seismic events can be characterized by amplitude Fourier spectra with a band of interest between 0,1 Hz and 20 Hz. Being characterized as stationary or non-stationary processes the frequency content resides in that band but the frequency components are considered constant or variable with time, respectively. However, in general the process is always considered stationary.

On the other hand it is known that fixed base structures fundamental frequency is dependent of its height. Lower fundamental frequencies are associated to tall structures like high-rise

buildings and towers, and thus higher fundamental frequencies correspond to low buildings (*Tilly 1986*). Empirical laws to estimate structures fundamental frequency from its hight or from its number of floors have been obtained from experimental tests made on different structures, which were then included on the design codes for guidance, like the *RSA 1983* and recently on *Eurocodigo8 2010*. In order to move away structures fundamental frequency from the seismic input action frequency content and bring it to the magnitude increase part of the spectra where the input energy is lower, base-isolated systems are being developed and implemented in buildings, namely in those of higher important classes: hospitals; energy power stations; communication centres; civil protection and fire station buildings, and others. Care must be taken however when using this technology with soft soils since the structural responses can be amplified (*Moreira de Andrade 2007, Lopes 2008*). Figure 2.5 compares two response spectra with the typical natural frequency of building structures.

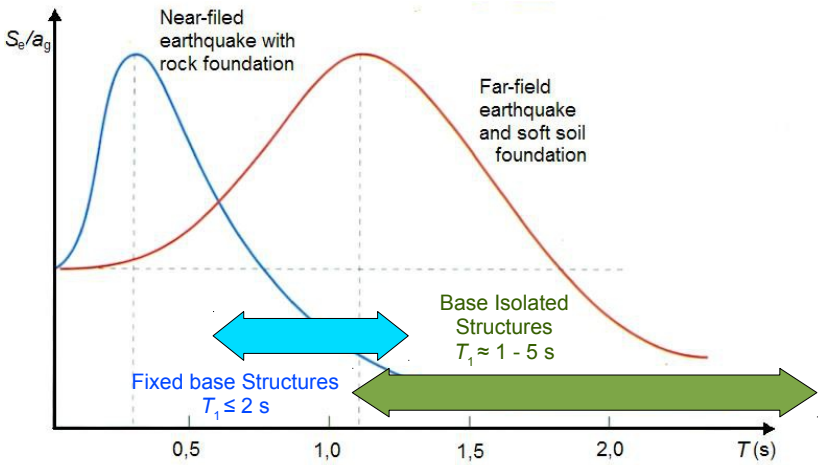

Figure 2.5 - Typical response spectra and building structures fundamental frequencies (adapted form *Lopes 2008*).

In order to compare the general seismic input action frequency content with the range of fundamental frequencies found in civil engineering structures, figure 2.6 shows a schematic drawing comparing the data.

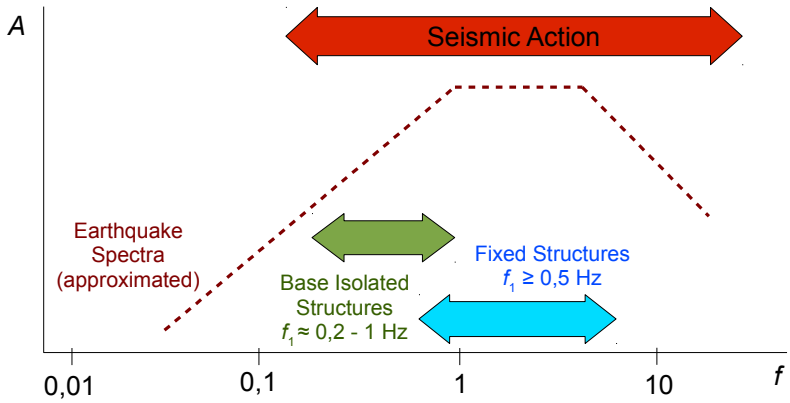

Figure 2.6 - Comparison between earthquakes frequency content (acceleration magnitude spectra) and the range of fundamental frequencies in building structures.

2.4 Seismic Safety

The effects of earthquakes have direct influence on the population, on buildings, on structures and infrastructures, and have also an indirect influence on tourism and economy. According to statistics earthquakes are one of the most destructive natural catastrophes in the world and some authors refer that earthquakes effects have a natural tendency to increase due to the growth of population in urban areas which led also to a rapid increase of low quality construction to house them (*Lopes 2008*).

The loss of human lives and the enormous costs associated with large earthquakes have instigated the evolution of seismic safety enhancement to prevent their negative effects on society. Techniques for protection of structures against seismic events have been developed through times. The current earthquake codes use the resistance capacity of structures allowing some inelastic deformations when subjected to strong earthquakes. By providing sufficient strength and ductility, structures should be able to dissipate the dynamic input energy of the earthquake (*Soong & Dargush 1997*).

However, the conventional techniques provide no protection to the building contents or to secondary structural features like sensitive equipment in hospitals and human heritage in museums (*LESSLOSS 2007*). As a result new innovative systems have been developed in order to improve the structures dynamic behaviour. These protective systems allow for a higher energy dissipation and decrease the structure internal forces and moments.

The energy dissipation can be analysed by considering the following time-dependent conservation of energy relationship (*Soong & Dargush 1997*, *Symans & Constantinou 1998*):

$$E = E_k + E_s + E_h + E_d \tag{2.2}$$

where: E is the absolute energy input from the earthquake, which represents the work done by the total base shear force at the foundation on the ground displacement and account for the effect of the inertia forces on the structure; E_k is the absolute kinetic energy; E_s is the elastic (recoverable) strain energy (potential energy); E_h is the irrecoverable energy dissipated by the structural system through inelastic or other forms of action (inherent structural system damping, plastic strain energy, or broadly speaking, viscous and hysteretic damping mechanisms); and E_d is the energy dissipated by supplemental damping systems. Under the conventional technique approach the term E_d=0 and the structural performance is accomplished by the occurrence of inelastic deformations which contributes to increase E_h. With the inclusion of additional energy dissipation systems in the structure, the term E_d is present and accounts for the major portion of the energy that is absorbed during the earthquake and its presence affects the other terms in equation (2.2).

2.4.1 Seismic Safety Enhancement using Resistance Capacity

Earthquake actions were at the beginning treated as idealized static loads of suitable magnitude that must be resisted by the structure. Using this approach structures were designed to resist against small earthquakes in the elastic regime, while for moderate or severe seismic events, structures were permitted to become damaged but not to collapse. This philosophy was the basis for a number of codes since the twentieth century (*Soong & Dargush 1997*).

The current code for designing structures against seismic events implemented in Portugal is the *Eurocodigo8 2010*. Its purpose is that during a seismic event human lives are protected, damage is limited and important structures for civil protection remain operational. The National Authorities have established criteria for different types of buildings and other civil engineering works on the basis of the consequences of failure which lead to verify the following requirements:

- *no collapse requirement* which is associated with the ultimate limit state verification: under a rare seismic event the structure shall be designed and constructed to withstand the seismic action without local or global collapse to protect human lives, thus retaining its structural integrity and the residual load bearing capacity during and after the seismic event; assumes that structural damages could be significant but the structure should not collapse;
- *damage limitation requirement* associated with serviceability limit state verification: the structure should be designed and constructed to withstand a frequent seismic action (thus, having a larger probability of occurrence), without the occurrence of damage and the associated limitations of use; the main goal is damage limitation in order to rapidly repair the structure in an economical way; (*Eurocodigo8 2010*).

The design criteria presented in the code assumes the possibility of occurrence of important damages, either in structural or non-structural elements, so that the structure absorbs the input energy. Then, detailing rules of structural members and nodes and the appropriate structural configuration for specific zones are prescribed. The designed structure has to comprise enough resistance, ductility, stiffness and inelastic deformation capacity in order to meet the performance requirements and compliance criteria. During a large earthquake certain parts of the structure will experience inelastic deformations with a stable hysteretic loop that allows for the dissipation of the seismic energy. Although some damages such as cracking of the concrete or steel yielding could occur, the structure should not collapse for the seismic action considered (*Lopes 2008*).

Eurocode 8 also covers the design of seismically isolated structures in which the isolating

system located between the base of the structure (superstructure) and the foundation (substructure) is designed in order to reduce the seismic response. This can be obtained by increasing the fundamental period of the isolated structure, by modifying the fundamental mode shape, by increasing damping or by the combination of these last two characteristics (*Eurocodigo8 2010*).

2.4.2 Seismic Safety Enhancement using Protection Systems

Several protection systems for enhancing structural functionality and safety against natural and man-made hazards have been developed, with particular emphasis for mitigation of wind and seismic response of buildings and bridges. Those systems can be classified into (figure 2.7): passive systems; semi-active systems; active systems; and hybrid systems (*Soong & Dargush 1997; Symans & Constantinou 1999; Soong & Spencer Jr. 2002; Chu et al. 2005; Lopes 2008*).

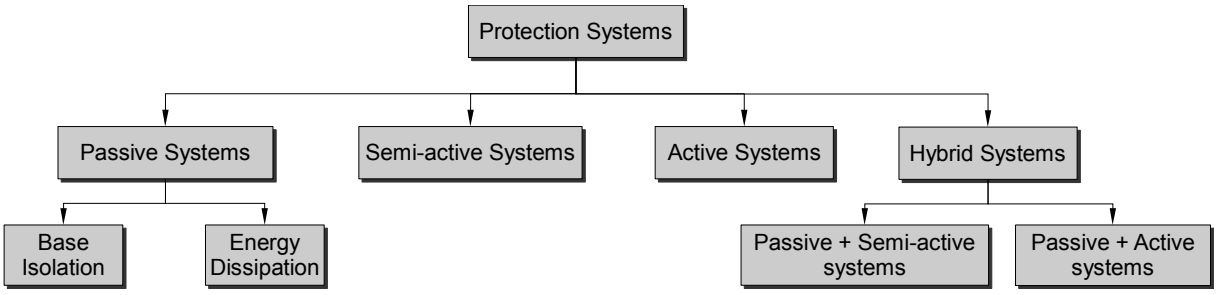

Figure 2.7 - Structural protective systems.

Base isolation use bearings installed between the base of the structure (superstructure) and the foundation soil (substructure) providing a discontinuity surface on the horizontal plane by means of material flexibility and damping. Passive energy dissipation systems comprise a range of materials and devices placed at specific points on the structure for enhancing damping, stiffness, and strength. Semi-active and active systems use force devices and sensors attached at specific points in the structure together with controllers to enhance its structural behaviour for improving safety. The difference between semi-active and active systems relies on the working principle. Semi-active systems use force devices comprising small power sources to change its mechanical properties in order to modify the behaviour of the structural system. Semi-active systems can be seen as controllable passive devices. On the other hand, active systems comprise force devices that need considerable power sources to input energy into the structure in order to improve its dynamic behaviour. Finally, hybrid systems are referred as a combination of passive and semi-active systems or passive and active systems. Here passive systems encompass also the base isolation systems.

Base Isolation

The purpose of base isolation is to relieve the connections between the structures base and the foundation soil on the horizontal plane. Base isolation systems have their roots in the

concept that if the structure could be suspended in thin air, then no damage caused by ground motion would occur. A base isolated structure becomes more flexible in the horizontal direction since its fundamental frequency is reduced and the capacity of filtering the excitation components close to the fundamental frequency of the structure increase. A base isolated structure is usually supported by a series of bearings or sliders placed between the structure and its foundation, in case of a building structure, or between the deck and the pier cap, in case of bridges and viaducts (figure 2.8).

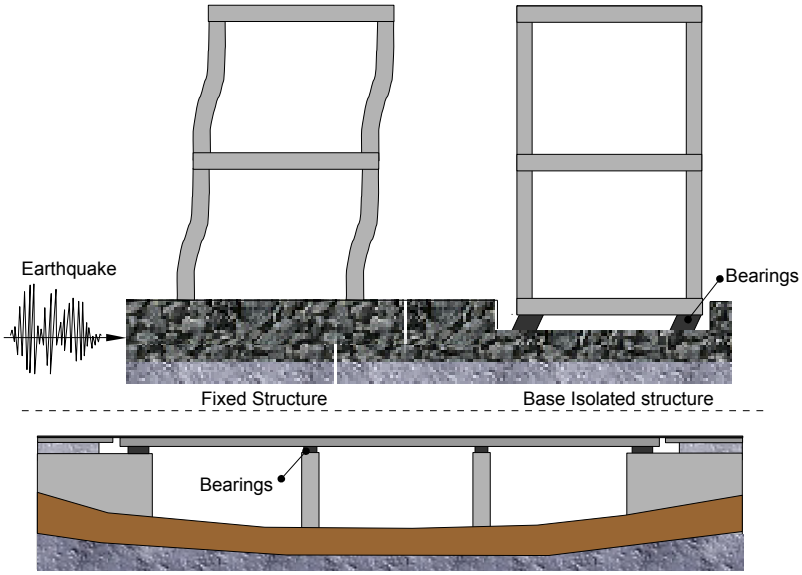

Figure 2.8 - Up: Schematic view of a fixed and base isolated structure. Bottom: Base-isolated viaduct.

Those bearings are usually stiff in the vertical direction to support the structure weight and flexible enough in the horizontal direction to reduce the fundamental frequency of the structure. Some damping is added depending on the type of bearing implemented. There are already several types of base isolation devices. Manufacturers like Aseismic Devices Co. (http:///www.adc21.com), FIP Industriale (http://www.fip-group.it/fip_ind_eng) and Maurer Söhne Group (http://www.maurer-soehne.com) have available several types of devices for different applications. The most common used for seismic isolation are summarized in table 2.1.

Base isolation is now considered a more mature technology with a wider range of applications (*Moreira de Andrade 2007*). In Portugal those devices have been applied in bridges and recently in important buildings too. An example of application of elastomeric bearings can be seen in Salgueiro Maia bridge in Santarém (*Azevedo & Guerreiro 2007*). In what concerns to building structures, Hospital da Luz in Lisboa was designed and built with base isolation devices to prevent the disruption of medical cares strongly needed during and after an earthquake (*Guerreiro et al. 2005*).

Base Isolation devices		
type	description	device example
Elastomeric Bearings	Support bearings composed of a vulcanized rubber block, reinforced with steel plates, referred as steel shims fitted on bottom and top with steel plates;	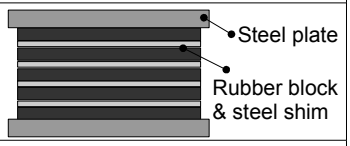
Lead Rubber Bearings	Laminated rubber with a lead core to increase the energy dissipation, fitted on bottom and top with steel plates;	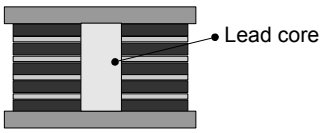
Sliding Friction pendulum	Concave sliding surface with minimum potential energy in the centre (equilibrium point), with low friction, where the period of the isolation system is determined by the radius of curvature of the concave surface;	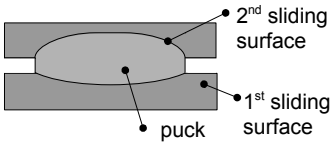

Table 2.1 - Base Isolation devices (*Lopes 2008*).

Passive Energy Dissipation

The main goal of this technology when incorporated into a structure is to absorb portion of the input energy and thereby reduce the energy dissipation on the primary structural members. The devices and materials used with this technology aim for enhancing damping, stiffness and strength, and are effective for seismic and wind induced vibrations mitigation. Figure 2.9 shows the typical applications of these devices in buildings: by using bracing systems with damping devices linking adjacent floors for reduction of inter-story driftf; by using tuned systems installed at specific points to absorb the energy at the tuned frequency.

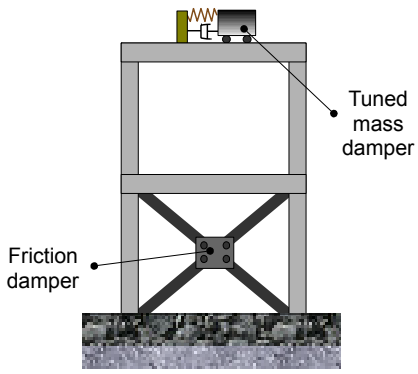

Figure 2.9 - Structure with passive energy dissipation devices.

In *Soong & Dargush 1997* a great review of this technology is presented including the basic concepts, theory, practical considerations and structural applications. Other selected references concerning with this subject are: *Sadek et al. 1996*, *Soong & Spencer Jr. 2002 and Towashiraporn et al. 2002*. Aseismic Devices Co. (http:///www.adc21.com), FIP Industriale (http://www.fip-group.it/fip_ind_eng) and Maurer Söhne Group (http://www.maurer-soehne.com) are also the companies that have been developing and commercialising this type of devices. Table 2.2 describes the type of passive energy dissipation systems available.

Passive Energy Dissipation devices		
Metallic dampers	Specially designed geometries (usually triangular or X shapes) that dissipate energy through inelastic deformation of metals (usually mild steel); these devices are used in conjunction with bracing systems connecting consecutive floors;	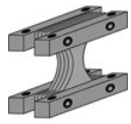
Friction dampers	These devices use the mechanism of solid friction, which is developed between two solid bodies sliding relative to one another in order to provide the desired energy dissipation; usually implemented in X bracing systems and having slip joints with friction pads;	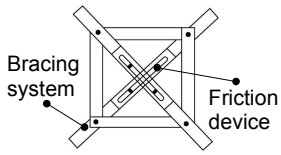
Viscoelastic dampers	Viscoelastic (VE) dampers consist in VE layers (copolymers or glassy substances) bonded with steel plates; when implemented in the structure, the vibration energy is dissipated through shear deformation;	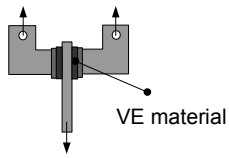
Fluid Viscous dampers (FVD)	Usually consist of a piston within a damper housing filled with oil or a compound of silicone, where the piston may contain a number of small orifices that dissipate energy when it moves and forces the fluid passing from one side to the other side of the chamber; another type is the viscous wall, which consists of a plate moving in a thin steel case filled with a highly viscous fluid;	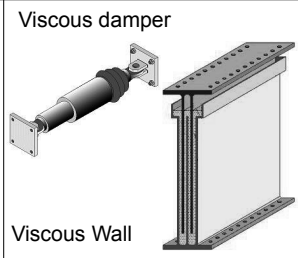
Tuned Mass Dampers (TMD)	Consist of one degree of freedom oscillator attached and tuned to one resonance frequency of the structure (usually the fundamental), in order to reduce the vibrations associated to that vibration mode;	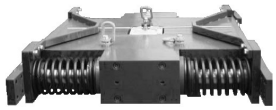
Tuned Liquid Dampers (TLD) and Tuned Liquid Column Dampers (TLCD)	Consist of additional devices (reservoirs) filled with liquids (usually water) where its behaviour (liquid motion) is tuned to one resonance frequency of the structure (usually the fundamental); the devices are attached at specific points in the structure in order to reduce the vibrations associated to that mode;	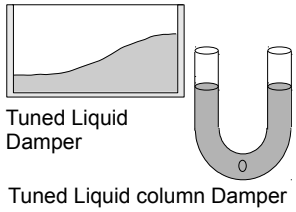
Shape Memory Alloys (SMA)	The superelasticity property of the alloy (usually Ni-Ti alloy) is exploited so that for low-level vibrations the SMA device grants a stiff connection while for a medium intensity earthquake the transmitted stress induces a martensite transformation, increasing the damping capabilities of the device;	SMA are usually bars available for structural applications;

Table 2.2 - Passive Energy Dissipation devices.

Semi-active systems

Semi-active systems are control systems that use adjustable passive devices (semi-active devices) to regulate the behaviour of the main structure when subjected to input disturbances from earthquake or wind actions. The structure employs several devices and sensors dispersed over the structure to input the forces and measure structural responses. Figure 2.10 shows an example of a generic structure employing a semi-active system. The

measured forces or responses are used by the controller to adjust the signal (control variable) that changes the mechanical properties of the device. The control forces developed by semi-active devices are dependent of the adjusted control variable and of the structural motion experienced.

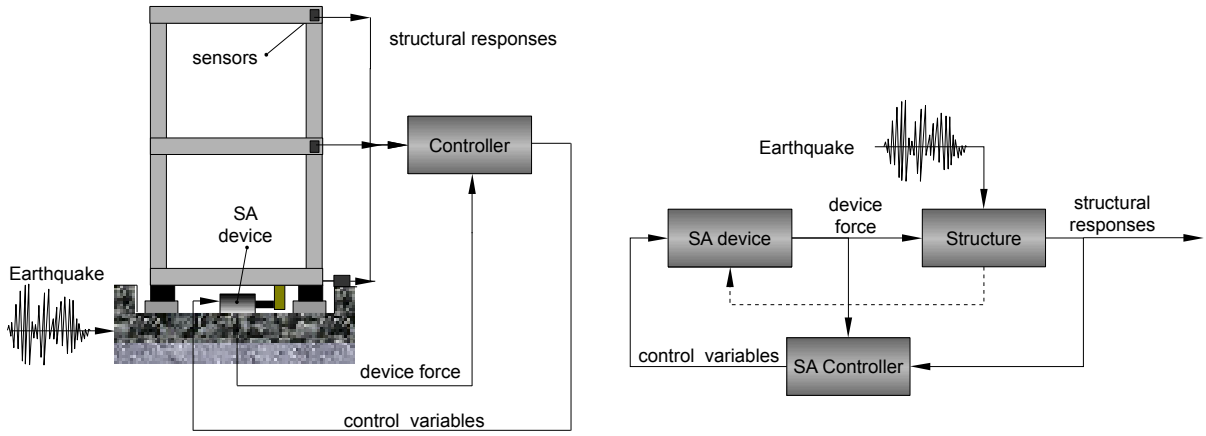

Figure 2.10 - Generic structure with a semi-active control system: system implementation (left); block diagram (right).

This type of control system works with a small power supply to energize all the components that comprise the electrical circuit: controller, sensors and devices. With regard to the devices, variable stiffness, fluid viscous dampers (FVD), electro-rheological (ER) dampers and magnetorheological (MR) dampers, friction dampers, semi-active tuned mass dampers and semi-active tuned liquid dampers, are examples of researched and available technologies. Review papers on this subject can be found in: *Spencer Jr. & Sain 1997*, *Spencer Jr. & Soong 1999, Symans & Constantinou 1999, Soong & Spencer Jr. 2002* and more recently in *Casciati et al. 2012*. Due to the non-linear behaviour of the devices, a number of control strategies and algorithms have been adopted for semi-active systems. *Dyke & Spencer 1997* and *Jansen & Dyke 2000* describe the first proposed control algorithms, namely: control based on the Lyapunov stability theory; bang-bang; modulated homogeneous friction; and clipped optimal control. Recently, more complex algorithms have been proposed, which are based on: robust control (*Mejía 2005*); fuzzy logic (*Shook et al. 2007*); and neural networks (*Bani-Hani & Sheban 2006*).

Active systems

Active systems are control systems that make use of force devices (electrohydraulic or electromechanical) installed at specific points in the structure, which together with sensors and controllers regulate the main structure behaviour subjected to input disturbances from earthquakes and or wind. Contrary to semi-active systems, these one need considerable power sources to input energy into the structure in order to modify its dynamic behaviour. Figure 2.11 shows an example of a structure equipped with an active system, namely

employing an active mass damper and active cable devices. Active systems use feedback from sensors signals to generate the control signals for the active devices at the controller which calculate the control forces. Large power sources are required to energize the devices power system.

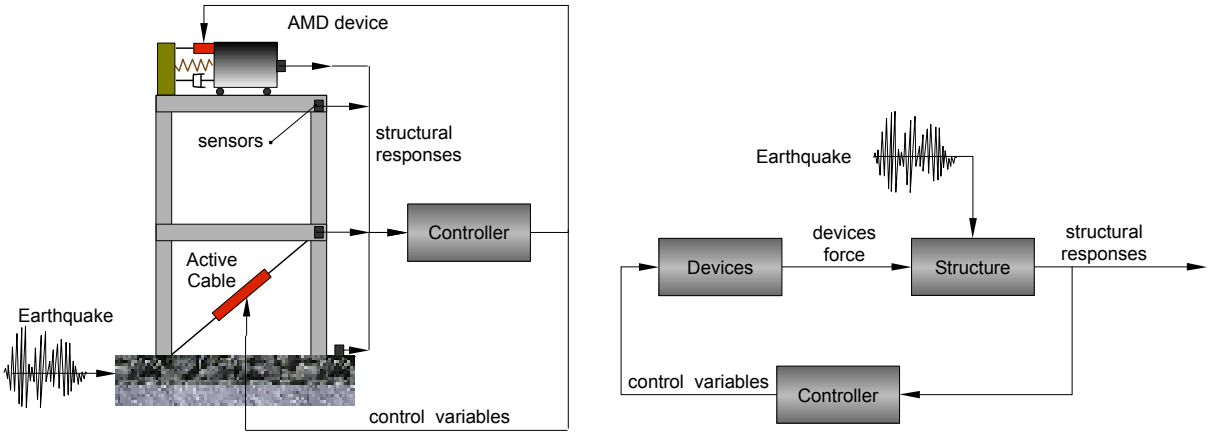

Figure 2.11 - Generic structure employing an active control system: system implementation (left); block diagram (right).

During the last 30 years several types of devices have been developed for reducing wind and earthquake induced vibrations. Reviews of the subject can be found in *Soong & Spencer Jr. 2002, Chu et al. 2005* and recently in *Casciati et al. 2012*. Some of the technologies available can be described according to the following groups:

- **Active Mass Damper (AMD)**: also known as active mass driver, this device is constituted by a mass connected to the structure through a spring, a damper and an actuator; the system regulates the movement of the mass, provides restoring force and damping to the structure;
- **Active Cables**: also called active tendons, these devices consist of cables connected to actuators that input control forces in the structure; typical applications can be found in buildings where active cables are connected diagonally between floors;
- **Active Bracing**: used specially for building applications, it consists of a set of metallic bars forming an inverted V shape (a bracing system), connected to an actuator that input the forces in the bracing system, increasing the structural system performance.

In order to control these devices different strategies have been proposed: linear quadratic regulator (LQR); linear quadratic Gaussian (LQG); predictive control; modal control; sliding mode control; H_2 and H_∞ control (*Inaudi et al. 1992*, *Dyke et al. 1994, Loh et al. 1999*).

Applications of this type of devices for seismic hazard mitigation can also be found in *Soong & Spencer Jr. 2002, Ikeda 2009* and *Casciati et al. 2012*.

Hybrid systems

Hybrid systems are a combination of passive and active or semi-active control systems. The idea behind this type of protection systems is that portion of the control objective is accomplished by the passive system and then less active control effort is needed. Less power resources are then needed to operate the system. For this reason hybrid systems are continuously being developed with different combinations of devices. Reviews of the subject and applications can be found in *Soong & Spencer Jr. 2002, Chu et al. 2005* and recently in *Casciati et al. 2012*. The typical hybrid systems found in literature are:

- **Active Base Isolation**: consists of a base isolation system combined with actively controlled actuators;
- **Semi-Active Base Isolation**: consists of a base isolation system combined with semi-active devices;
- **Hybrid Mass Damper (HMD)**: also called active tuned mass damper (ATMD), this device consists of a tuned mass damper (TMD) combined with an active mass damper (AMD).

2.5 Semi-Active Control

A semi-active control system may be defined as a system which typically requires a small external power source for operation (e.g. a battery) and is provided with devices that use the motion of the structure to develop dissipative forces which can be adjusted by modifying its properties in real time, according to the prescribed control objectives (*Symans & Constantinou 1999*). Semi-active devices are referred as controllable passive devices that allow for the adjustment of mechanical properties. There is no input of mechanical energy into the controlled structural system (i.e., including the structure and control devices) which makes the whole system intrinsically stable from the dynamic point of view. One advantage of this type of devices is attributed to the fact that they offer the adaptability of active control devices without requiring the associated large power sources (*Dyke 1996, Dyke et al. 1996(a), Dyke et al. 1996(b), Jansen & Dyke 2000*). Most of them only need a few watts of power to change the dynamic characteristics of the device and can dissipate a small amount of energy even if the power fails. Semi-active devices generally operate with a battery (its own power source), which make them autonomous and independent of the main power source of the structure that could fail during an earthquake event (*Spencer Jr. & Sain 1997*).

The first semi-active control systems were proposed in the 1920s when patents were issued for shock absorbers. The working principle was based on elastically supported masses to activate hydraulic valves or even through the use of electrical contacts and a solenoid valve to direct the fluid flow. *Karnopp et al. 1974* mention in his work some doubts about the

successful implementation of early studies since most of the devices were inherently nonlinear and no tools were available for analysing and understanding the dynamic response of SA systems at that time.

Afterwards, the semi-active concept was successfully applied to a broad class of vehicle vibration isolation problems, ranging from tractors and other farm vehicles, to high-speed ground transportation vehicles. *Hrovat et al. 1983* proposed the first application of semi-active structural control for systems subjected to environmental loads. In his work a semi-active tuned mass damper was proposed to reduce wind induced motion of tall buildings. The semi-active device proposed in that study is a damper consisting of a piston-cylinder combination supplemented by a control valve assembly, which can be seen as the predecessor of the variable orifice damper. During the 1990s, a large amount of research was done in semi-active technologies in other fields of engineering, specially concerning applications for automotive vibration control and vibration isolation (*Symans & Constantinou 1999*).

Since then, the interest on semi-active control for structural applications has been gaining acceptance, specially in the field of civil engineering. The implementation of semi-active devices in structures can be made in different ways. In building structures, for example, three different basic configurations can be found as figure 2.12 shows (*Jansen 2000*):

- **Bracing System type**: the devices are usually used with bracing systems to connect adjacent floors;
- **Dispersed Devices type**: different devices types are placed at specific points on the structure; these devices are usually semi-active tuned mass dampers and semi-active tuned liquid dampers;
- **Base Isolation type**: also referred as hybrid base-isolation system type, it consists in using bearings between the structure and foundation (base isolation) in conjunction with semi-active devices installed at the base level.

In bridges and viaducts bearings are used to connect the columns and abutments to the deck, and semi-active devices can be installed between the abutment and the deck in order to mitigate longitudinal vibrations (*Loh et al. 2003*, *Jung et al. 2003*). Other implementation of these devices in bridges is devoted to mitigate wind induced cables vibration of cable-stayed bridges (*Christenson 2001*), where a few applications can now be found, namely on Sutong Bridge in China and Eilandbrug Kampen Bridge in Netherlands (http://www.maurer-soehne.com). The implementation of SA devices to mitigate the longitudinal bridge deck vibrations was studied and proposed by *Oliveira 2003* and *Oliveira 2009*. See an example of implementation of these devices in figure 2.13.

A survey of supplemental energy dissipation devices and its applications focussing on semi-active devices can be found in the work of *Soong & Spencer Jr. 2002*. Recently, *Ikeda 2009* also published a lot of work where are described applications and verification methods for active and semi-active control of buildings in Japan.

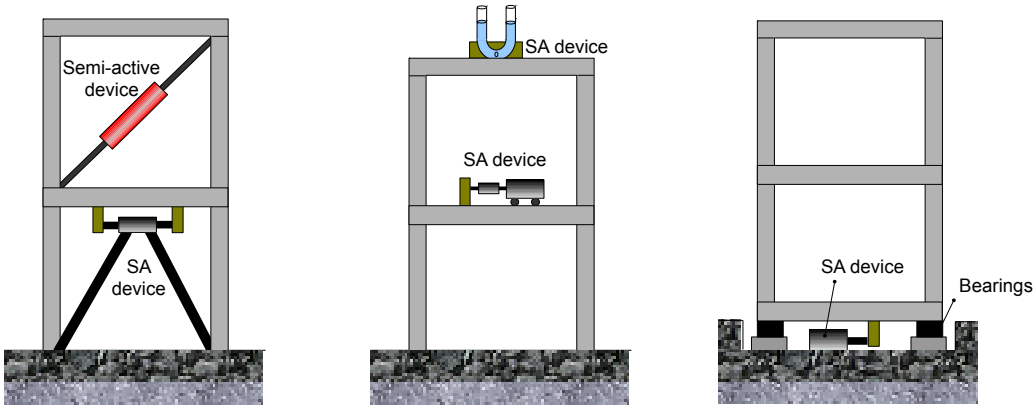

Bracing System type Dispersed Devices Base Isolation type

Figure 2.12 - Semi-active control devices implementations in buildings: Bracing System type; Dispersed Devices type; and Base Isolation type.

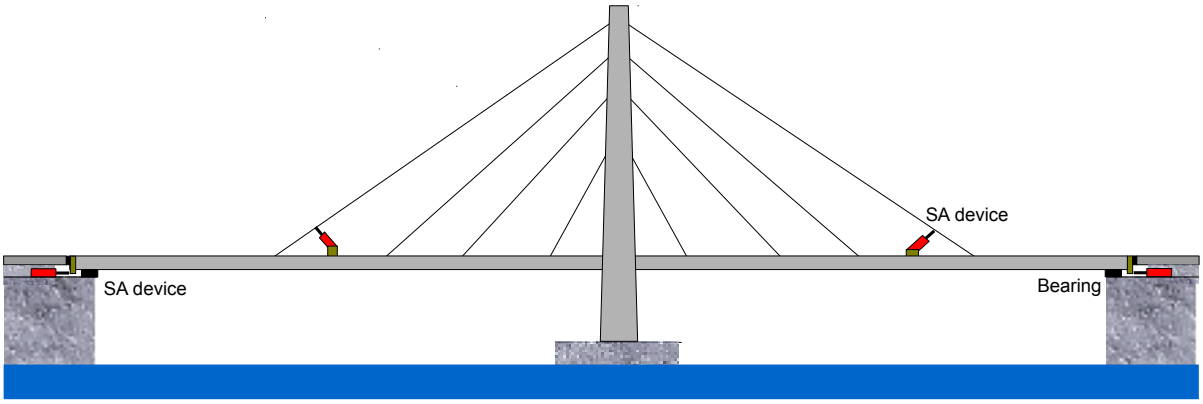

Figure 2.13 - Semi-active control devices implementations in cable stayed bridges.

In the following sub-chapters the most recent applications of SA systems in structures will be discussed: i) base isolation type; ii) device technologies used for this purpose, like fluid dampers and MR dampers; iii) and a review of the control strategies and algorithms used.

2.6 Hybrid Base-Isolated Structures With SA Devices

The base-isolation concept, i.e. a superstructure (main structure) constructed over a base floor which in turn is supported by bearings connected to the foundations, was proposed 100 years ago (*Chopra 1995*) but only in the end of the eighties has been considered as an earthquake-resistant design strategy (*Kelly 1999*). This approach is used for reducing the transmission of seismic forces and energy to the structure and is now prescribed in most codes for designing structures against seismic events. The main goal of base isolation is to decouple the structure (superstructure) from the foundation so that it behaves like a rigid body with reduced inter-storey drifts, as stipulated in structural safety guidelines, and

reduced absolute accelerations as related to comfort and equipment safety. The basic concept of base isolation is: i) to increase the natural period of the structure far enough from the expected predominant earthquake periods at the installation sites; ii) that the fundamental period of the fixed-based structure (without base isolation) is much shorter than the isolated structure natural period, such that the higher modes, which contribute to the floor accelerations and inter-storey drifts, have very small participation factors. Under these conditions, base isolation systems can be a better option (*Chopra 1995*). However, two important aspects have to be taken into account when designing this type of structures: i) the base-isolation system must be well tuned taking into account the expected characteristics of the seismic excitations; ii) large isolation displacements could occur, specially at near fault locations where large pulse-like ground motions are generated (*Luo et al. 2001*). To reduce those displacements supplementary devices are often prescribed but it is found that under those circumstances structural inter-storey drifts and absolute accelerations can increase (*Kelly 1999*). Thus, damping systems which can reduce base isolator displacements without increasing superstructure response, for both near and far-field ground motions, are therefore desirable (*Gavin & Aldemir 2005*).

One way to achieve this goal is by introducing controllable devices on structures and the semi-active control technique has received much attention in recent years (*Symans & Constantinou 1999; Soong & Spencer Jr. 2002; Chu et al. 2005; Casciati et al. 2012*). Hybrid systems comprising base-isolated structures with semi-active systems have been studied and proposed as an alternative to base isolation with passive systems (*Luo et al. 2001; Gavin & Aldemir 2005; Komatsu et al. 2007; Bahar et al. 2010*). Semi-active systems comprise several devices and sensors dispersed over the structure. Magneto-rheological (MR) and fluid viscous dampers (FVD) are typical examples of semi-active devices (*Soong & Spencer Jr. 2002*). Semi-active fluid dampers (oil dampers) are still the most common solution today when large forces are needed and are the primary solution considered for practical applications in Japan (*Ikeda 2009*).

This hybrid system concept consisting of base-isolated structures with semi-active system devices installed at the base level is now being investigated for earthquake induced vibrations reduction. A schematic view of a hybrid base-isolated building is found in figure 2.14.

The following sections describe the mathematical models considered for the base-isolated structures and for the devices and the recent control strategies considered in this type of problems.

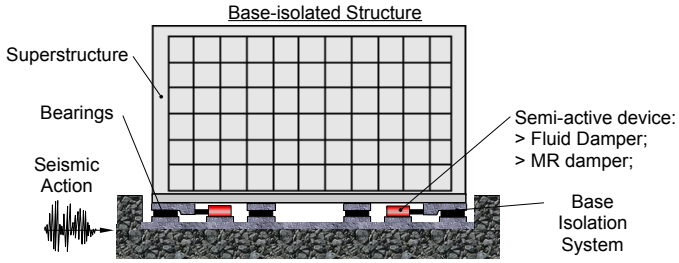

Figure 2.14 - Base isolated building employing a semi-active fluid viscous damper.

2.7 Base-isolated Structures

2.7.1 Structural Models

A satisfactory approach usually considered in the building modelling is considering the linear time-invariant system theory (LTI) such that: i) each floor has very high stiffness where the mass is concentrated; ii) the connections between floors are massless elements where the stiffness and damping are concentrated. In base-isolated structures the superstructure is constructed over a base floor which in turn is supported by bearings. Different types of bearings can be found (friction pendulum, lead rubber bearings or elastomeric bearings) each one characterized by a specific non-linear model, although in certain cases linear approximations can be used, specially for the first type of device. Figure 2.14 depicts the hybrid system: base isolated structure with semi-active devices at the base level. Under these circumstances the model of this system is described by the following equations:

$$\begin{gathered} m_b \cdot \ddot{x}_{0g} = -m_b \cdot \ddot{x}_g - \boldsymbol{\Phi}_{bi} - \boldsymbol{f}_{ad} + f_{c10} \\ \boldsymbol{M}_s \cdot \ddot{\boldsymbol{x}}_{srg} + \boldsymbol{C}_s \cdot \dot{\boldsymbol{x}}_{srg} + \boldsymbol{K}_s \cdot \boldsymbol{x}_{srg} = -\boldsymbol{M}_s \cdot \boldsymbol{1} \cdot \ddot{x}_g + f_{c1} \\ \text{with} \\ f_{c10} = c_1 \cdot \left(\dot{x}_{1g} - \dot{x}_{0g} \right) + k_1 \cdot \left(x_{1g} - x_{0g} \right) \\ f_{c1} = s_1 \cdot \left(c_1 \cdot \dot{x}_{0g} + k_1 \cdot x_{0g} \right), s_1 = \{1 \; 0 \; \ldots \; 0\}^T \end{gathered} \tag{2.3}$$

where: m_b is the mass of the base floor; $\boldsymbol{\Phi}_{bi}$ describes the bearings behaviour; $\boldsymbol{f}_{ad}$ describes the behaviour of additional devices at the base level; f_{c10} is the coupling force between the base and the superstructure; f_{c1} is a force component that results from the decoupling; $\boldsymbol{M}_s$, $\boldsymbol{C}_s$ and $\boldsymbol{K}_s$ are the superstructure mass, damping and stiffness matrices; x_{og} and x_{1g} are the base and first floor relative displacements to the ground; $\boldsymbol{x}_{srg}=\{x_{1g} \; x_{2g} \; \ldots \; x_{ng}\}^T$ is the vector of superstructure relative displacements to the ground floor (at each floor); and $\ddot{x}_g$ is the input ground motion (acceleration).

For base isolation design it is common to consider a linear model at the initial design phase to analyse the system dynamics and in the final design phase include the non-linearities of the devices (*Chopra 1995*). For bearings design they are assumed as linear elastic and viscous damping elements:

$$\boldsymbol{\Phi}_{bi} = c_b \cdot \dot{x}_{0g} + k_b \cdot x_{0g} \tag{2.4}$$

where: c_b and k_b are the damping and stiffness properties of the bearings. Under these circumstances, the model in equation (2.3) can be reduced to a single equation that represents the key responses of civil engineering structures by its mass $\boldsymbol{M}$, stiffness $\boldsymbol{K}$ and damping $\boldsymbol{C}$ matrices, which take into account the characteristics of the base isolation system, the linear model in (2.4), and the m forces $\boldsymbol{f}=\boldsymbol{f}_{ad}$ developed by additional devices:

$$\boldsymbol{M}\cdot\ddot{\boldsymbol{x}}_{rg}+\boldsymbol{C}\cdot\dot{\boldsymbol{x}}_{rg}+\boldsymbol{K}\cdot\boldsymbol{x}_{rg}=-\boldsymbol{M}\cdot\boldsymbol{1}\cdot\ddot{x}_g+\boldsymbol{G}\cdot\boldsymbol{f} \tag{2.5}$$

This equation describes the mechanical behaviour of a n degree of freedom model (base plus n-1 floors) where: $\boldsymbol{1}$ is a unitary column vector; $\boldsymbol{G}$ is the matrix that defines the input forces location; and $\boldsymbol{x}_{rg}=\{x_{0g}\ \boldsymbol{x}_{srg}^T\}^T$ is the vector of relative displacements to the ground. For a unidirectional analysis problem only one force will be developed (m=1) and thus will be $\boldsymbol{G}_{nx1}=[-1\ 0\ \ldots\ 0]^T$.

Equation (2.5) expresses a force equilibrium between the inertia forces, dissipation forces and elastic forces with the external forces. It is an equilibrium dynamic relationship used to describe continuous non-homogeneous structures resulting from the discretization of structures characteristics, which are in general distributed, using a convenient number of coordinates to completely describe its dynamics (*Maia et al. 1998*).

2.7.2 Damping Models

The dissipation forces considered in equation (2.5) are usually of the viscous type (proportional to velocity). In fact energy dissipation in civil engineering structures can result from several mechanisms at the same time: thermal effects of repeated elastic straining of the material; internal friction effects when a solid is deformed; friction at steel connections; opening and closing of microcracks in concrete; friction between the structure and nonstructural elements such as partition walls; and structure-soil interaction. Due to the difficulties in modelling each one of these damping mechanisms, the viscous damping is used as an idealized equivalent manner to describe all the damping mechanisms presented in structures (*Chopra 1995*). This idealized manner is also mathematically convenient to solve the equations of motion (*Maia et al. 1997*). Thus, the damping coefficient is selected so that the vibration energy dissipated is equivalent to the energy dissipated in all mechanisms. If the damping is amplitude dependent an adequate deformation amplitude has to be considered for using the equivalent viscous damping. Non-viscous damping models have been considered in structural dynamics too. The hysteretic, solid or structural damping, is an alternative model that describes better the load/deflection hysteresis of materials and the dissipated energy is frequency independent. In contrast with the viscous model, this one is proportional to displacement but still in phase with velocity. As the hysteretic model is proportional to displacement and the viscous model is proportional to its derivative, a general

model based on the theory of fractional derivatives (non-integer order derivatives) was proposed by *Maia et al. 1998* to describe the damping of linear systems.

Recalling equation (2.5), the damping matrix $\boldsymbol{C}$ can be proportional (classical damping) or non-proportional (nonclassical). Although the superstructure damping matrix $\boldsymbol{C}_s$ can be classical, the whole structure damping matrix $\boldsymbol{C}$ is nonclassical since base-isolated structures consist of two parts (base-isolation system and the superstructure) with significantly different levels of damping. Other civil engineering examples of nonclassical damping matrices are the structure-soil system or a concrete dam with water impounded behind the dam. In such cases the damping matrix is constructed by assembling the matrices of the subsystems, each one constructed using the classical approaches. Two formulations are commonly used for the classical damping approach: *Rayleigh* damping and *Caughey* damping (*Chopra 1995*). *Rayleigh* damping is a linear combination of stiffness and mass matrices:

$$\boldsymbol{C}_s = \alpha \cdot \boldsymbol{M}_s + \beta \cdot \boldsymbol{K}_s \tag{2.6}$$

where α and β are constants. It can be evaluated by considering the modal damping of one or two system modes. When this model is considered a damping distribution similar to mass and stiffness distribution is being assumed which is in fact a plausible hypothesis for structures made of homogeneous material without any other damping mechanisms. The other classical model, *Caughey* damping, has a damping matrix of the following form:

$$\boldsymbol{C}_s = \boldsymbol{M}_s \cdot \sum_{i=0}^{n-1} \alpha_i \cdot \left(\boldsymbol{M}_s^{-1} \cdot \boldsymbol{K}_s\right)^i \tag{2.7}$$

where α_i are constants that can be evaluated using the modal damping ratios of the structure obtained experimentally.

2.7.3 State-Space model

The equation of motion in (2.3) can be written in the state space form as:

$$\dot{\boldsymbol{z}} = f\left(\boldsymbol{z}, \ddot{x}_g, \boldsymbol{f}_{ad}\right) \quad , \quad f\left(\boldsymbol{z}, \ddot{x}_g, \boldsymbol{f}_{ad}\right) = \begin{cases} \dot{x}_{0g} \\ \dot{\boldsymbol{X}}_{srg} \\ -\ddot{x}_g - \boldsymbol{\Phi}_{bi}/m_b - \boldsymbol{f}_{ad}/m_b + f_{c10}/m_b \\ -\boldsymbol{M}_s^{-1} \cdot \boldsymbol{C}_s \cdot \dot{\boldsymbol{x}}_{srg} - \boldsymbol{M}_s^{-1} \cdot \boldsymbol{K}_s \cdot \boldsymbol{x}_{srg} - \boldsymbol{1} \cdot \ddot{x}_g + \boldsymbol{M}_s^{-1} \cdot f_{c1} \end{cases} \tag{2.8}$$

where: $\boldsymbol{z} = \left\{\boldsymbol{x}_{rg}\, \dot{\boldsymbol{x}}_{rg}\right\}^T$ is the state vector. In the linear case, the state-space form of (2.5) is given by:

$$\begin{matrix} \dot{\boldsymbol{z}} = \boldsymbol{A} \cdot \boldsymbol{z} + \boldsymbol{B} \cdot \boldsymbol{f} + \boldsymbol{E} \cdot \ddot{x}_g \\ \boldsymbol{y} = \boldsymbol{C}_y \cdot \boldsymbol{z} + \boldsymbol{D}_y \cdot \boldsymbol{f} \end{matrix} \quad , \quad \boldsymbol{A} = \begin{bmatrix} \boldsymbol{0} & \boldsymbol{I} \\ -\boldsymbol{M}^{-1} \cdot \boldsymbol{K} & -\boldsymbol{M}^{-1} \cdot \boldsymbol{C} \end{bmatrix}, \ \boldsymbol{B} = \begin{Bmatrix} \boldsymbol{0} \\ \boldsymbol{M}^{-1} \cdot \boldsymbol{G} \end{Bmatrix}, \ \boldsymbol{E} = \begin{Bmatrix} \boldsymbol{0} \\ -\boldsymbol{1} \end{Bmatrix} \tag{2.9}$$

where: $\boldsymbol{y}$ is the output vector; $\boldsymbol{A}$ is the state matrix; $\boldsymbol{B}$ and $\boldsymbol{E}$ are input vectors; $\boldsymbol{C}_y$ is the output matrix; $\boldsymbol{D}_y$ is the feedthrough vector; $\boldsymbol{0}$ and $\boldsymbol{I}$ are a null and identity matrices respectively. With

$\boldsymbol{C}_y=\boldsymbol{A}$ and $\boldsymbol{D}_y=\boldsymbol{B}$ the outputs quantities will be the relative velocities and absolute accelerations.

2.8 Semi-active devices

2.8.1 Devices Formulation

A detailed description of the most common devices used in semi-active control of civil engineering structures is presented. The focus is on fluid viscous dampers and magneto-rheological devices. Applications of these devices in real structures are also referred. However, the core of this subsection is on the mathematical models used to evaluate the device force given the input motion (the state $\boldsymbol{z}$, or a function of the states) and the control variable u_{SA}:

$$f_{SA}=f\left(\boldsymbol{z},u_{SA}\right),\ u_{SA,min}\leq u_{SA}\leq u_{SA,max} \tag{2.10}$$

2.8.2 Fluid Viscous Dampers

One of the devices considered in semi-active control is the variable fluid viscous damper (FVD) - figure 2.15. Typically it mainly consists of a hydraulic cylinder with a piston head connected to the piston rod which is guided by the cylinder heads. The two chambers are connected by the annular passage between the cylinder and the piston head and by a hydraulic link. One valve is placed in the hydraulic link to control part of the flow from one chamber to the other. The fluid is usually oil or silicone and the control valves may be solenoid valve type for on–off control or servovalves for continuous control. As the piston rod is in motion, a pressure differential across the piston head is created which develops a damping force in the damper rod. The damping force can be changed by controlling the amount of fluid that passes through the valve. Although the mechanical behaviour of the device is non-linear, under certain conditions it is possible to achieve an almost linear model. Depending on the type of valve, the resisting force and thus the damping coefficient can be changed continuously or in two or three stages, in the range of admissible damping values.

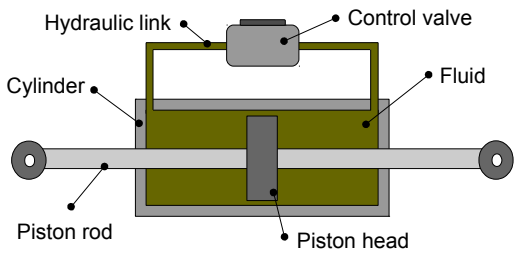

Figure 2.15 - Semi-active device: fluid viscous damper (FVD).

<u>Fluids</u>

The fluids used in the development of the fluid viscous damper devices are usually oils. Since higher damping forces are needed, silicon oils are always considered in this type of applications. The behaviour of these fluids in shear is Newtonian and described by the following relationship:

$$\tau=\eta\cdot\dot{\gamma} \tag{2.11}$$

where: τ is the shear stress; $\dot{\gamma}$ is the shear rate; and η is the dynamic viscosity. The fluids used for these type of devices usually are characterized by higher viscosities (typically of the order of 100 cSt).

Fluid damper devices

The use of variable-damping devices in structures was introduced by *Feng & Shinozuka 1993* (earlier in conference *Feng & Shinozuka 1990*) for controlling the motion of bridges experiencing seismic motion. A bang-bang (on-off) control and an instantaneous optimal control algorithms were developed to control the damping coefficient. A fluid damper for continuous control using a servovalve was described later by *Kawashima et al. 1992(a)*. During that time, a comparative study between active, semi-active and passive fluid dampers with continuous control, bang-bang control strategies and fixed damping respectively was made by *Shinozuka et al. 1992*. The performance evaluation of each device was carried on a quarter length scale bridge model and experimental tests were conducted on a shaking table. The semi-active device performed better than passive but similar to the active one. Analytical and experimental studies of semi-active fluid dampers for controlling highway bridges was conducted by *Kawashima et al. 1992(b)*. The device is shown in figure 2.16 (left) and comprised two servovalves which independently controlled the fluid flow for relative motions of the piston in both directions. The device had an output force of about 200 kN, a stroke of ±13 cm, a length of about 1,2 m and the power required for valve operation was 50 W. *Kawashima & Unjoh 1993* performed shaking table tests on a reduced-scale seismically isolated single-span bridge and a simple heuristic control algorithm was developed for that purpose. Large reductions in deck displacement and acceleration were found but according to these researchers the reductions were associated with the higher effective damping of the controlled structure.

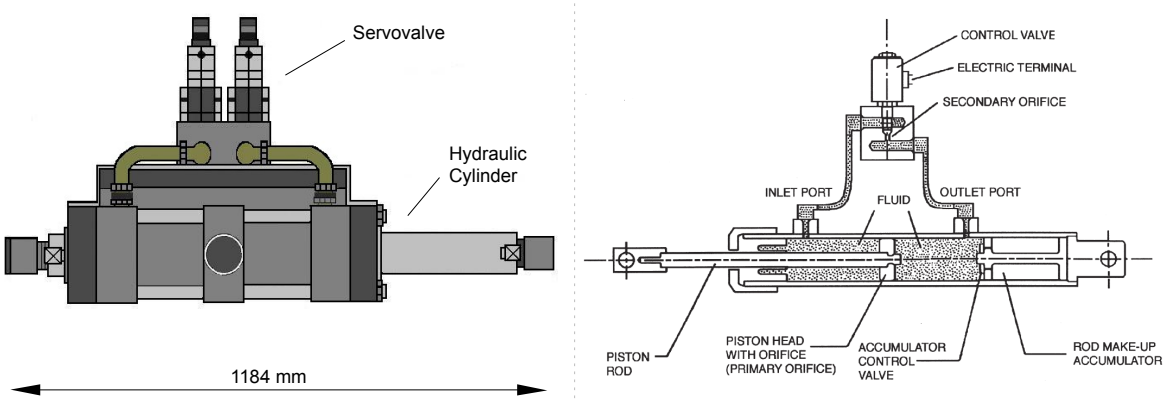

Figure 2.16 - Semi-active devices. Left: Device used by *Kawashima et al. 1992(b).* Right: Modified passive device used by *Symans & Constantinou 1995*.

Patten et al. 1994 conducted an experimental study on this type of devices and developed a mathematical model to describe the device behaviour. The damper comprised a balanced

piston rod and an external control valve containing an orifice which was controlled by a small electric motor which took about 10 ms to go from a fully-open valve configuration to a full-closed valve configuration. The devices were evaluated on a 3-storey scaled steel structure and large reductions were found in comparison with the uncontrolled case.

Based on the design of a passive fluid damping devices *Symans et al. 1994* developed a semi-active versions for seismic application. The dampers are of by-pass type as the one in figure 2.16 (right): a two-stage damper controlled by a solenoid valve; and a variable fluid damper controlled by a servovalve. The dampers characteristics were ±75 mm of stroke, an output force of 8,9 kN and the power required to operate them was about 55 W and 3,5 W respectively. A mathematical model based on fluid mechanics principles and a simplified fluid viscous dashpot model were proposed to describe the dynamic behaviour of the semi-active fluid dampers. Several tests considering different control algorithms and input ground motions were performed. The results of an extensive analytical and experimental study performed by *Symans & Constantinou 1995* were presented later on. *Symans & Constantinou 1997* summarize the result of the study and referred: significant reductions (peak responses) can be obtained with the structural systems employing the semi-active devices when compared with the original structure (without any control device), despite those reductions were similar to the ones obtained with the passive control system with higher damping. However, this study was limited to structural systems with fundamental periods of 0,36 s and 0,56 s.

At that time other researchers were working in this area. Experimental tests with a similar semi-active fluid damper having an external bypass loop containing a flow control valve were conducted by *Kurata et al. 1994*. The damper had a stroke of ±50 mm, a rated output force of about 20 kN and the flow control valve required only 30 W of power for operation. The effectiveness of this device was evaluated on a 3-storey structure using a bracing system configuration, and an optimal control algorithm was used to synthesize the controller. The structure was tested in a uni-axial shaking table and good reductions in peak accelerations and top displacement were found. *Kurata et al. 1999* reported the first application of a semi-active hydraulic damper (SHD) system in a 5-storey building (Shizuoka City, Japan) – see figure 2.17. The device was able to provide a maximum damping force of 1000 kN with only an electric power of 70 W. This system comprised several bracing systems with semi-active fluid dampers installed between adjacent floors. The controller for the SHD was designed to minimize the building response and a relative velocity feedback law based on the Linear Quadratic Regulator (LQR) was adopted. They confirmed the performance of the implemented system through a simulation analysis and a dynamic loading test on the SHD.

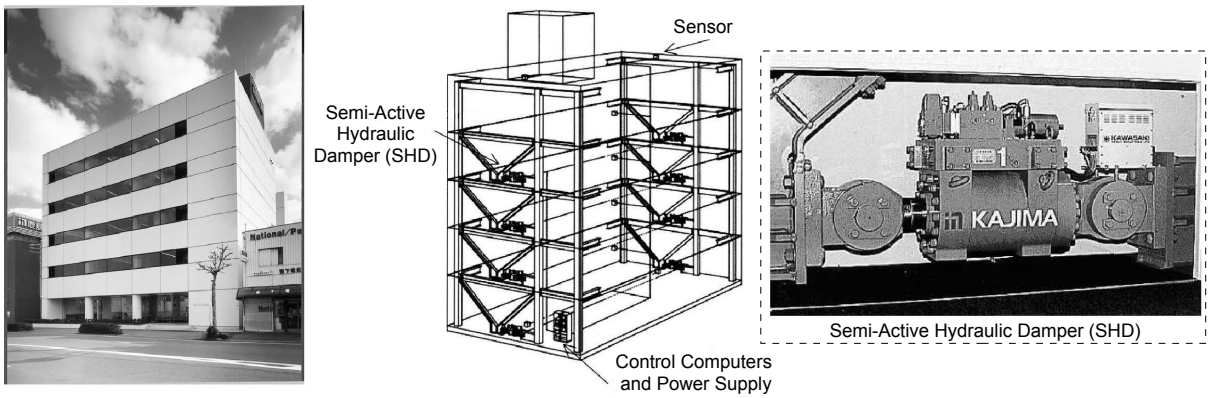

Figure 2.17 - Semi-active Hydraulic Dampers installed at the Kajima Shizuoka Building (*Kurata et al. 1999*).

In research project financed by the European Union, *Occhiuzzi & Serino (1) 2003* developed a semi-active device by adapting servovalves to a commercial passive device. This semi-active prototype was combined with a set of flexible plates which constitutes the semi-active assembly to install on the structure. Sine sweep and earthquake excitation tests were performed on a SDOF steel frame building equipped with two identical semi-active assemblies. *Occhiuzzi & Serino (2) 2003* showed that with an on-off algorithm and compensating time delays using a sine-fit prediction method, reductions in displacement response when compared to that obtained in a passive configuration, were found. In terms of acceleration the results are comparable to the passive case and better than that of the original frame.

A semi-active oil damper that can change its damping coefficient between the maximum and minimum values using a solenoid valve (on-off type) equipped with the necessary control equipment (sensors and a controller) was proposed by *Kurino et al. 2002*. This semi-active device system was successfully installed in several buildings, and better performance than that of the passive case were found (*Mori et al. 2002; Kurino et al. 2003*). Concerned with the power supply of these type of devices, *Kurino et al. 2004* developed a self powered device which uses the oil pressure balance between the chambers to control the valve opening that links both chambers. This 'passive' hydraulic damper equivalent to a semi-active damper was verified through numerical simulations on an MDOF building model where the effectiveness of this approach was confirmed (see figure 2.18). Full scale dampers (maximum forces of 2,1 MN) of this type have been developed and experimental test show that this solution can absorb much more vibration energy than conventional dampers. The damper is being currently implemented and 15 high-rise buildings in Japan have already adopted this solution (*Kurino et al. 2009*).

Several applications of semi-active control variable damping systems are now found (*Ikeda 2009*). As stated before, the first semi-active damper system was implemented in an office

building of five stories and a basement, located in Shizuoka City, Japan, for seismic response reduction (*Kurata et al. 1999*). An application related with vibration control of bridge structures is found in a highway I-35 bridge in Oklahoma for controlling traffic-induced vibrations. Semi-active variable orifice fluid dampers and stiffness devices have been used in several applications (*Symans & Constantinou 1999*). The first semi-active base-isolated structure was finished in 2000: the House of Creation and Imagination of Keio University (Yokohama). The semi-active base isolation system consisted of laminated rubber bearings with 8 hydraulic oil dampers whose damping coefficient can be set in five stages (*Ikeda 2009*). Another application was made later (2005) in the 11-storey of Keio University building - Mita South Building. The base isolation system comprises laminated rubber bearings and 10 hydraulic dampers in each direction that can be set to two values of damping. The control laws are based on the bilinear optimal control theory and on the sliding mode control theory (*Komatsu et al. 2007*).

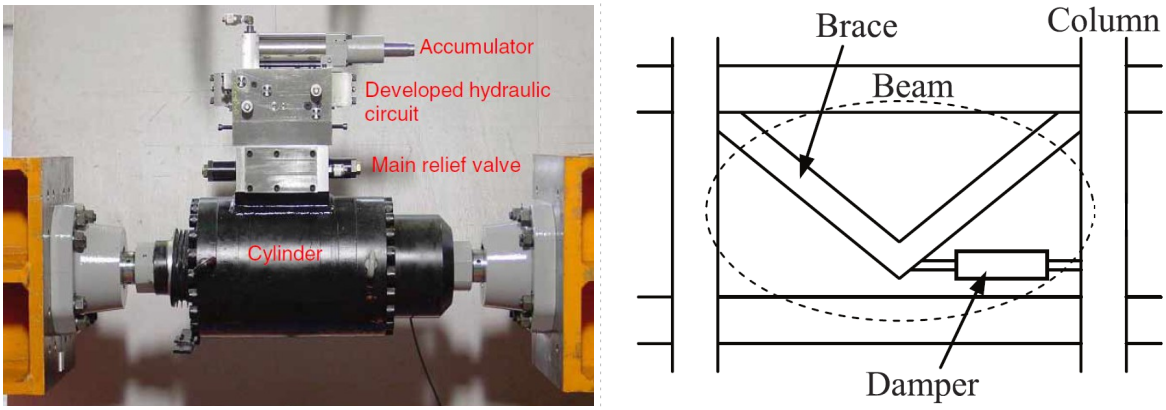

Figure 2.18 - Damper device and installation by *Kurino et al. 2004*.

Models for Fluid damper devices

It is well known from the fluid mechanics that when the fluid flows through a simple orifice the differential pressure varies with the squared of fluid velocity - Bernoulli's equation. The resultant hydraulic component developed using this principle varies its output force with respect to the square law, and is called hydraulic damping element. When researchers decided to develop fluid dampers the first problem to be solved was to work on a damper design that would provide an output more in keeping with systems theory (linear) than with the principle of the simple hydraulic flows. The result of research projects where several damper internal constructions were evaluated made it possible to achieve (or almost) the desired linear output form (*Taylor 1999*). For example, the damper piston head orifices are now designed in such a way that the fluid flow is altered according to the fluid speed, resulting in a force output that is essentially proportional to the relative velocity between the piston head and damper housing. These conditions are achieved with high viscosity fluids,

small gaps and long flow passages. Such orifices are known as fluidic control orifices; fluidic resulting from concatenation of fluid and logic, i.e. logical operations using fluids (*Soong & Dargush 1997; Symans & Constantinou 1998*). The result of several investigations in this domain made available today dampers with different velocity exponents, described by the following mathematical relationship (*Symans & Constantinou 1998; Taylor 1999; Castellano et al. 2004*):

$$f_p = c_p \cdot |\dot{x}_r|^{\alpha} \cdot \mathrm{sgn}(\dot{x}_r) \tag{2.12}$$

where: f_p is the damper force; c_p is the damping coefficient; $\dot{x}_r$ is the relative velocity between the piston rod and the cylinder case; and α is the velocity exponent. Typical values of the velocity exponent for seismic applications are α<1. Recent technological developments made available devices with velocity exponents α=0,15 (*Castellano et al. 2004*). Bridge applications in low activity seismic zones have often utilized an exponent of 2. Wind damping applications presently are most popular with exponents in the range of 0,5 to 1 (*Taylor 1999*). *Symans & Constantinou 1998* examined the energy dissipation of a generalised fluid damper and showed that as lower is the velocity exponent of the damper more is the dissipation of energy.

For semi-active fluid dampers, unitary velocity exponents were also prescribed. These dampers are in general manufactured to follow a linear force-velocity relationship. The analytical models to describe the mechanical behaviour of semi-active fluid viscous dampers are thus based on linear or bi-linear force-velocity relationships. To account the device dynamics, those models are always complemented by a first order dynamic system model which results in the well known Maxwell model.

1) Dashpot and Bingham model

The simplest model to characterize the mechanical behaviour of the device is the classical linear viscous dashpot model (force proportional to velocity). However, even very low, friction will be present between the moving pieces of the device. For example, the type of device as the one shown in figure 2.15 has the piston rod in contact with the cylinder heads with mechanical gaskets between them, like o-rings, to create a seal and reduce the friction.

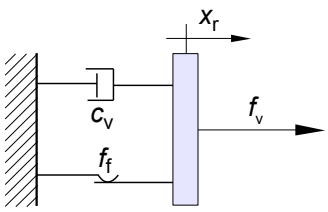

Figure 2.19 - Bingham mechanical model: viscous damping c_v and a frictional force f_f.

So, the mechanical model that describes both viscous and frictional forces consists of a dashpot in parallel with a friction element (figure 2.19). Figure 2.20 shows the behaviour of this model for a sinusoidal input considering f_f =0.

The Bingham model is described by the following equation:

$$f_v = c_v \cdot \dot{x}_r + f_f \cdot \mathrm{sgn}(\dot{x}_r), \quad c_{min} \le c_v \le c_{max} \tag{2.13}$$

where: c_v is the viscous damping that can be changed between c_{min}, with the control valve fully open, and c_{max}, with the control valve fully closed; f_f is the frictional force which is usually of minor significance. The relationship between the control valve input (command voltage) and damping is dependent of the valve type. It is assumed that this relationship is unitary.

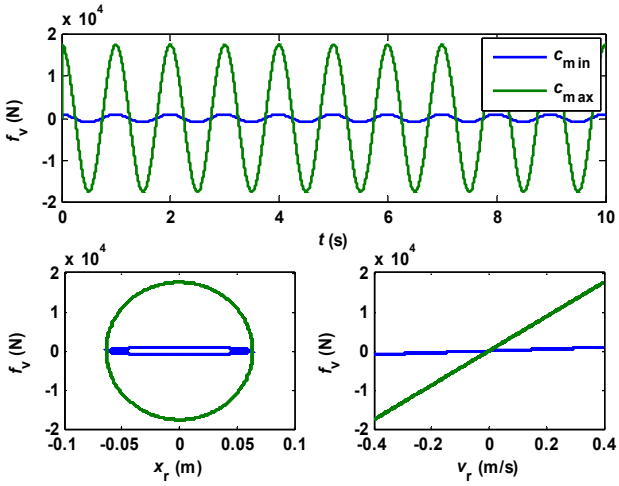

Figure 2.20 - Simulation results obtained with Bingham model for a sinusoidal input displacement at 1 Hz with: c_v=2,36 kN s/m and c_v=44,11 kN s/m; and f_f= 0 N.

2) Maxwell model with friction

A more elaborated model which includes a stiffness element due to the fluid compressibility (and other elastic elements present in de device, like an accumulator for example) or the dynamics of the device (by the time lag representing the response of the semi-active device) is the Maxwell model. This model is thus frequency dependent due to this viscoelastic effect. The model is extended to include also the frictional effects. Figure 2.21 shows a schematic representation of this model. The model is described by the following equation:

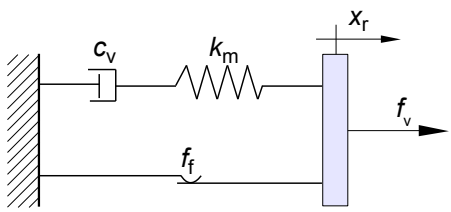

Figure 2.21 - Maxwell model with friction: viscous damping c_v, a stiffness element k_m and a frictional force f_f.

$$f_v + T_d \dot{f}_v = c_v \cdot \dot{x}_r + f_f \cdot \mathrm{sgn}(\dot{x}_r), \quad c_{min} \le c_v \le c_{max} \tag{2.14}$$

where: c_v is the viscous damping that can be changed between c_{min} and c_{max}; $T_d = c_v/k_m$ is the relaxation time or time lag, representing the response of the semi-active device (namely fluid compressibility and valve dynamics); f_f is the frictional force which is usually of minor significance.

The inverse of the relaxation time is the corner frequency that represents the frequency value at which damping begins to decay (in the present case at -20 dB/dec) – see figure 2.22 left. Here again it is assumed a transfer function with a unitary gain in the frequency range of interest for the control valve. The behaviour of this model for a sinusoidal input is shown also

in figure 2.22 right. It can be seen the contribution of the relaxation time for the hysteresis loop visible in the force velocity plot. This is the common model considered to describe the mechanical behaviour of semi-active fluid viscous damper (*Symans & Constantinou 1995; Komatsu et al. 2007*).

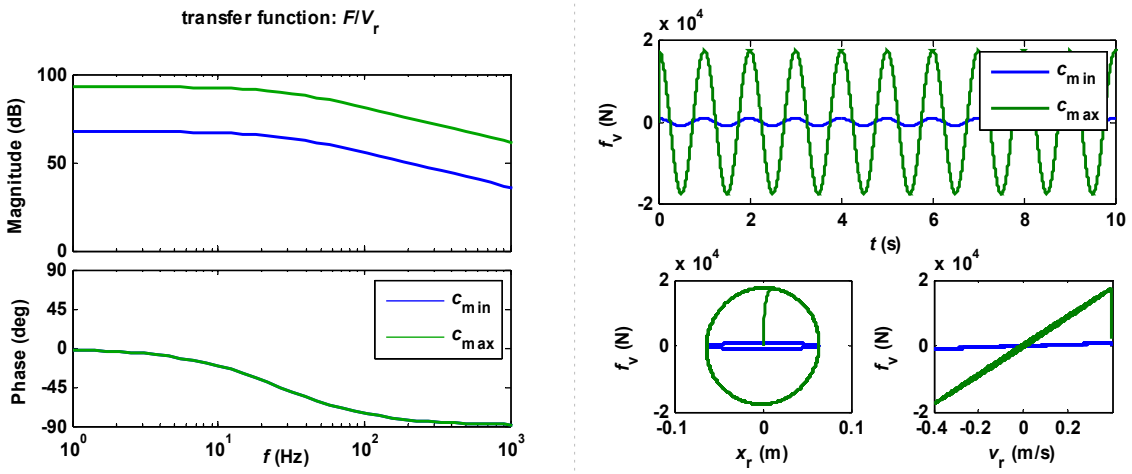

Figure 2.22 - Force velocity transfer function (left). Simulation results obtained with the Maxwell model for a sinusoidal input displacement at 1 Hz with: c_v=c_{min}=2,36 kN s/m and c_v=c_{max}=44,11 kN s/m; T_d=0,006 s; and f_f= 0 N (right).

3) Other models

Mechanical based models were also developed to describe the mechanical behaviour of the viscous fluid damper device. *Symans & Constantinou 1995* developed a general model to describe the dynamic behaviour of semi-active fluid dampers using the principles of fluid mechanics. This dynamic model accounts for the fluid compressibility and the losses in the circuit (piston head and control valve). Due to the special design of the orifices in the piston head a linear relationship was used to model the energy loss in the piston head. Conversely, the control valve energy loss was model by the orifice flow relation (nonlinear model: pressure drop proportional to the square of velocity). Model equations were established using the fluid formulation (Newtonian model) and the fluid equations of motion (momentum equations). The fluid motion for a specific device can be derived (velocity profile, pressure gradient and force) which establishes the device model. For this model the force-velocity relationship of the damper changes from a linear relation to a nonlinear one as the valve opens. Although this model predicts adequately the mechanical behaviour of the damper it is more complex than the previous ones and does not account for dynamic characteristics of the control valve. In fact, those authors used the Maxwell model in their studies.

In certain applications the damping coefficient c_v follows a bi-linear law dependent of velocity. An example of devices following this law can be found in *Komatsu et al. 2007*.

2.8.3 Magneto-rheological Dampers

The other type of semi-active device used in semi-active control is the Magneto-rheological

(MR) damper type (figure 2.23).

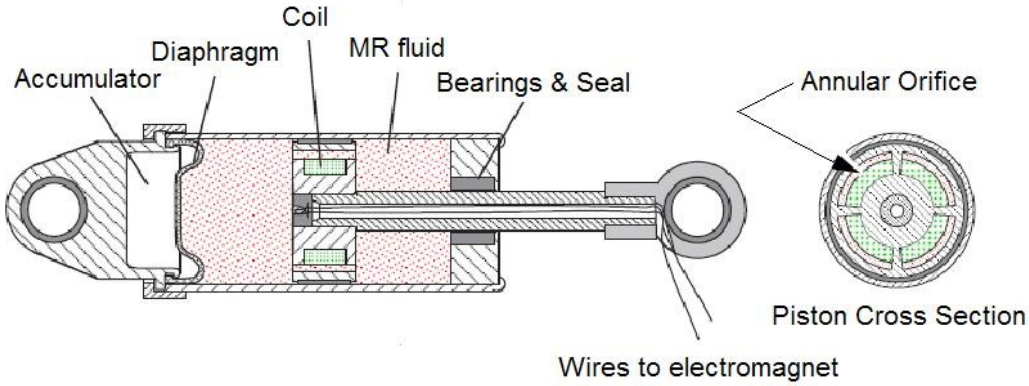

Figure 2.23 - Typical commercial linear MR damper (from *Dyke 1996*).

MR dampers are devices with a special design filled with MR fluids in the interior that make use of the MR effect to develop forces when a relative movement is applied between the device ends. The force can be modified by applying a magnetic field perpendicular to the direction of fluid flow. A common type MR device is the linear displacement damper that consists of a cylinder with a piston head inside connected to the piston rod, which separates it in the two chambers, filled with a MR fluid. By moving the piston rod the fluid is forced to flow from one chamber to the other through special orifices (depending on the type of device) where the magnetic field can be applied perpendicular to the direction of fluid flow, resulting from the applied current through electromagnetic coils. The magnetic field (or current) aligns the magnetic particles of the MR fluid which modifies the flow characteristics and thus the mechanical properties of the device (hysteresis loop).

MR fluids

The discovery and development of MR fluids can be credited to Jacob Rabinow, patented at the US National Bureau of Standards in the late 1940s, for application in a clutch (*Rabinow 1948a; Rabinow 1948b; Rabinow 1951*). Motivated by the work of Rabinow several types of magnetic fluid clutches using magnetizable fluid for power transmission were patented during the following years. The study and development of rheological devices only revived in the 1980s but manly devoted to ER fluids. During the 1990s MR fluids attracted the scientific community due to its advantageous characteristics over the ER fluids. *Carlson and Chrzan 1994* patented MR dampers with different embodiments and improved characteristics which could reach about 500 lbs (226,8 kg) of peak force. Later on, several MR fluid devices were produced and commercialized by Lord Corporation under the Rheonetic™ branch: linear dampers; rotary brakes; vibration dampers (*Carlson et al. 1996*). Lord Corporation (http:/www.lord.com) and Liquid Research Limited (http://www.liquidsresearch.com) are two companies that develop, manufacture and deliver ferrofluids. The first one also develops and

commercialize several types of devices and solutions for different purposes.

MR fluids typically consist of micron sized, magnetically polarizable particles dispersed in a carrier medium such as mineral or silicone oil, or even water. When the magnetic field is applied, those particles acquire dipole moment aligned with the external field which force the particles to form linear chains (see figure 2.24). The rheology of the fluid is reversible almost instantaneously, changing from a free-flowing liquid to a semi-solid with controllable yield strength. Transition to rheological equilibrium can be achieved in a few milliseconds allowing the construction of devices with a high bandwidth. A variety of proper additives (dispersants, friction modifiers, anti-wear agents, etc.) similar to those found in commercial lubricants are commonly added to discourage gravitational settling and promote particle suspension, enhance lubricity, modify viscosity and inhibit wear to improve seal and bearing life (*Spencer Jr. et al. 1997(b); Yang 2001*). However the addition of suspension agents in conjunction with changes in the magnetic particle microstructure contributes for the shear thinning effect verified in some MR fluids (*Jolly et al. 1999*). MR fluid strength depends on the square of the saturation magnetization of the suspended particles and the key to achieve a strong MR fluid is to choose a particle with a large saturation magnetization. The best available particles for this purpose are alloys of iron and cobalt. Very high cost make them prohibitive for practical applications. Thus, particles of pure iron are commonly used. Typically MR fluids yield strength can reach 50-100 kPa when subjected to 150-400 kA/m magnetic fields (value limited by magnetic saturation of the particles). These fluids can operate within a wide range of temperatures (-40 to 150 ºC) with slightly variations on the yield strength, can be operated with common power sources (12-24 V at 1 A power supply) and have a small response time (order of ms) (*Soong & Dargush 1997; Preumont 2002*). Some properties of the fluids commercially available are presented in table 2.3. The typical constitutive behaviour of MR fluids in shear is shown in figure 2.25. It can be seen the separation between the pre- and post-yield regions, where a linear behaviour is found in the first one and a non-Newtonion behaviour in the second one. The shear thinning effect observed in MR fluids is identified by the non-linear stress-strain rate plot due to the viscosity reduction for higher strain rates. Finally, it is clear the yield strength limitation by the magnetic flux density.

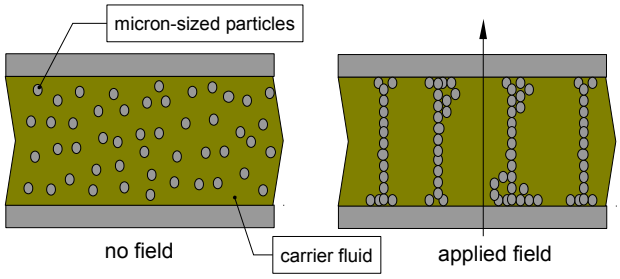

Figure 2.24 - Rheological fluids: chain-like structure formation under applied field.

In order to describe the fluid behaviour several non-linear models have been proposed: Bingham model (*Phillips 1969*; *Jolly et al. 1999*); and the Herschel-Bulkley model (*Wang & Gordaninejad 1999; Yang 2001*).

Supplier	Lord Corporation			Liquid Research	
Property/Fluid	MRF-122EG	MRF-132DG	MRF-140CG	MRHCCS4-A	MRHCCS4-B
Carrier fluid	Hydrocarbon	Hydrocarbon	Hydrocarbon	Hydrocarbon	Hydrocarbon
Op. Temp. (ºC)	-40 to 130	-40 to 130	-40 to 130	-40 to 140	-40 to 140
Density (g/cm^3)	2,32 to 2,44	2,98 to 3,18	3,54 to 3,74	2,49	3,08
Colour	Dark grey	Dark grey	Dark grey	grey	grey
Particles (solids)	Iron (1-20 µm)	Iron (1-20 µm)	Iron (1-20 µm)	n/a	n/a
Weight Perc. Solids (%)	72	81	85	70	80
Viscosity (Pa s), under no field at 40 ºC, 500-800 1/s	0,07±0,02	0,09±0,015	0,28±0,07	n/a	n/a
Shear stress (kPa) -no field, 100 /s, 40 ºC -no field,1000 /s, 40 ºC -under field	 0,022 0,075 28 (400 kA/m)	 0,02 0,11 49 (300 kA/m)	 0,05 0,32 60 (200 kA/m)	 0,01 0,15 -	 0,012 0,200 -
Flash point (ºC)	>150	>150	>150	> 190	>190

Table 2.3 - MR fluid characteristics from Lord Corporation and Liquid Research Limited.

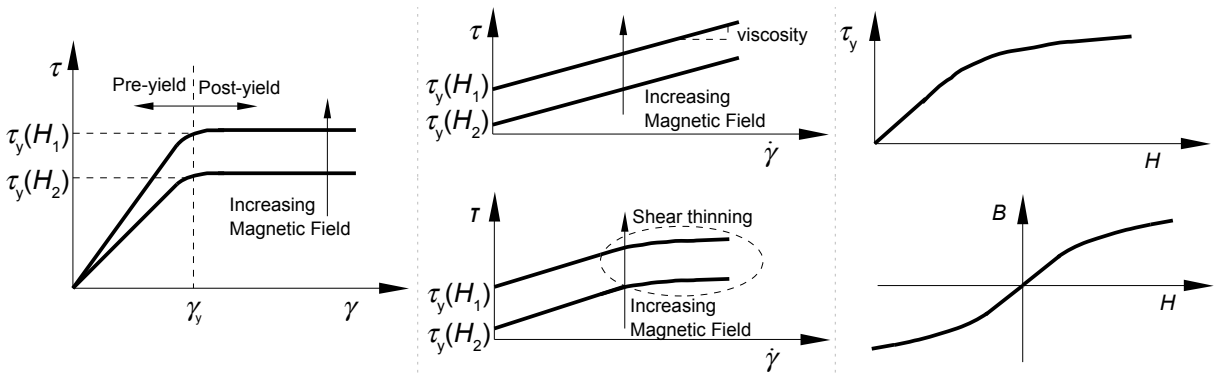

Figure 2.25 - Typical MR fluids behaviour. Left: shear stress τ vs. shear strain γ for H_1>H_2 magnetic fields (static); Middle: shear stress τ vs. shear rate $\dot{\gamma}$ for H_1>H_2 magnetic fields; Right: yield stress τ_y vs. magnetic field and magnetic flux density (B) vs. magnetic field intensity (H).

The Bingham model for MR fluids includes a magnetic field dependent rigid and perfectly plastic element connected in parallel with a Newtonian viscosity element. This stress strain relationship is valid above the yield stress:

$$\tau = \tau_y(H) \cdot \mathrm{sgn}(\dot{\gamma}) + \eta \cdot \dot{\gamma} \tag{2.15}$$

where: τ is the shear stress, $\tau_y(H)$ is the yield stress dependent of the magnetic filed H; $\dot{\gamma}$ is the shear rate; and η is the dynamic viscosity. Below the yield stress (at strains below 10^{-3}) the fluid behaves viscoelastically:

$$\tau = G \cdot \gamma, \text{for } \tau < \tau_y(H) \tag{2.16}$$

where: G is the shear modulus (modulus of rigidity).

Since MR fluids can exhibit shear thinning effect, an alternative to the Bingham model is the

Herschel-Bulkley model:

$$\tau = \left(\tau_y(H) + K \cdot |\dot{\gamma}|^{1/m}\right) \cdot \mathrm{sgn}(\dot{\gamma}) \tag{2.17}$$

where: K and m are the fluid parameters; the shear thinning effect is obtained for m>1 while the shear thickening effect is obtained for m<1; for m=1 the model reduces to the Bingham plastic model. A comparison of results between models is found in figure 2.26.

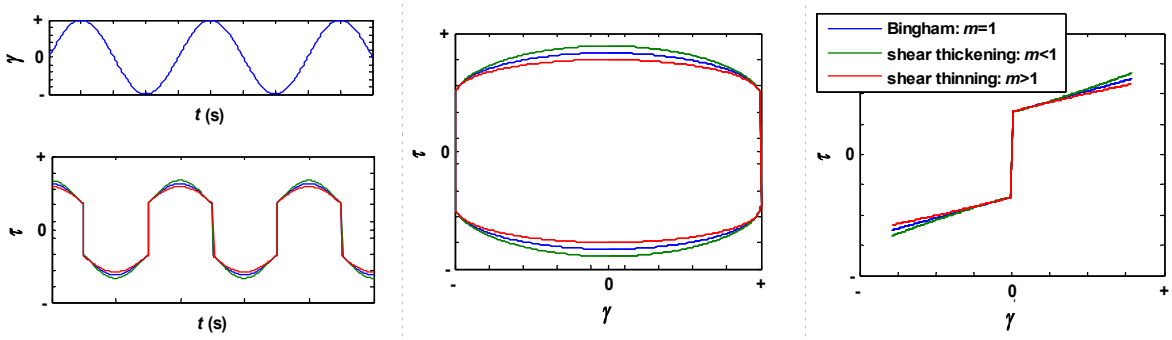

Figure 2.26 - Herschel-Bulkley model (with m=0,9; 1 and 1,1) response to an input sinusoidal displacement.

To use the MR effect specific devices are developed which can operated in different ways depending on the specific application. MR devices filled with MR fluids can be operated in three different modes: valve mode (or flow mode); shear mode; and squeeze mode; see figure 2.27 (*Soong & Dargush 1997; Preumont 2002*).

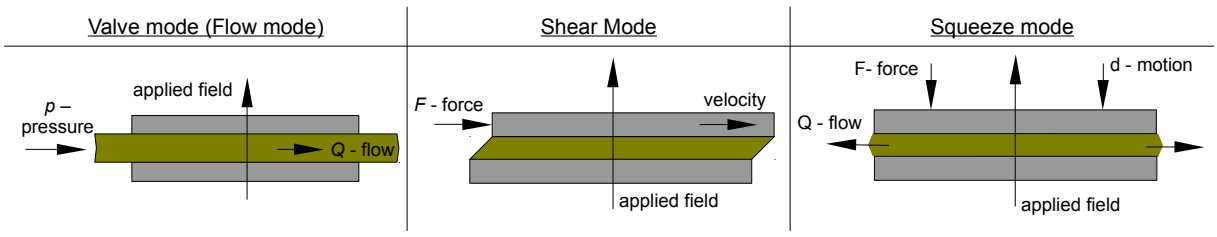

Figure 2.27 - Rheological fluids modes of operation: flow mode, shear mode and squeeze mode.

In the valve mode electrodes or poles are fixed and the applied field between them is used to align the micron-sized particles of the fluid that will adjust the fluid flow pressure gradient. Applications of this mode can be found in normal operating mode of dampers and shock absorbers. In the shear mode electrodes or poles are moving relative to each other and as the field is applied the fluid yield stress increases changing the electrodes relative movement. Types of shear mode devices include clutches and brakes (*Carlson et al. 1996; Jolly et al. 1999*). The third mode of operation is the squeeze mode and occurs when the electrodes or poles move toward each other in the direction of the applied field, squeezing out the fluid. The damping effect can be modified by changing the applied field which is useful for vibration motion control. This type of operation is most suitable for applications involving the control of small movements (order of mm) with large forces. The squeeze mode has been used only for research purposes, specially in vibration control of rotors (*Wang et al.*

2005(b)).

MR devices

MR devices have been developed for semi-active control in many areas (http:/www.lord.com). Examples can be found in: automotive suspensions where several studies have been made (*Goncalves 2001; Sassi et al. 2005*) and recently that technology resulted in applications for automotive and military vehicles suspensions; seat suspensions (*De Man et al. 2005*); steer-by-wire devices; clutches; aircraft landing gears; dampers for structural seismic protection; (*Dyke 1996; Symans & Constantinou 1999*). Linear dampers are one of the most common used MR devices. Some MR devices of this type are used for investigation purposes and others for actual applications. Some of manufactures of this type of devices are Lord Corporation (http://www.lord.com) and Sanwa Tekki Corporation (http://www.tekki.co.jp). Several small force capacity prototypes have been developed; see figure 2.28.

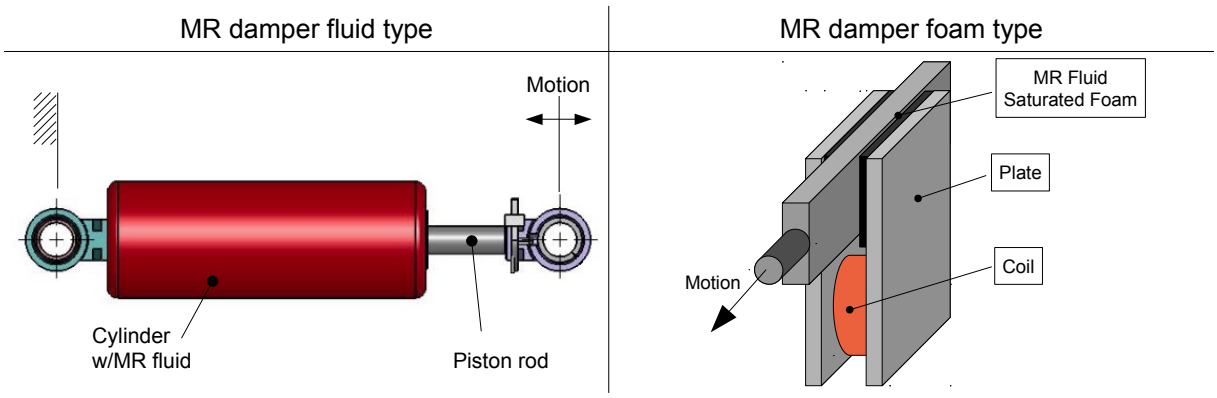

Figure 2.28 - MR dampers (low forces) for linear displacements.

A prototype of a MR damper having a stroke of ±2,5 cm and a force capacity of 3 kN was developed by Lord Corp (*Dyke 1996*). It consists of a fixed orifice damper filled with a MR fluid as shown in figures 2.23 and 2.28 (left).The fluid valve is contained within the damper piston and consists of an annular flow channel subjected to a magnetic field applied radially and perpendicular to the direction of fluid flow, resulting from the applied current (0 to 1 A) through the electromagnetic coils. The peak power required for operation of the damper is less than 10 W. Similar to this one, Lord Corp. has available dampers suitable for industrial applications. RD-8040-1 and RD-8041-1 are short and long stroke (55 and 74 mm) MR dampers respectively with a force capacity up to 3 kN (peak to peak) that work with common power sources (12 VDC, 1 A). Another type of devices with less capacity devoted for other applications and used also for research purposes is the MR damper foam type - figure 2.28 right. *Yi et al. 1999* refer a study where multiple MR dampers were used for control a seismically excited structure. The device consists of two steel parallel plates with a thin foam saturated with MR fluid between them and an electromagnet consisting of a coil at one end.

The force generated by the device can reach 29 N and the stroke is at least 10 mm. Similar devices were used by *Mejía 2005* and *Zapateiro 2009* for earthquake response reduction on scaled porch structures.

Large-scale MR dampers have also been developed for real-scale applications (figure 2.29).

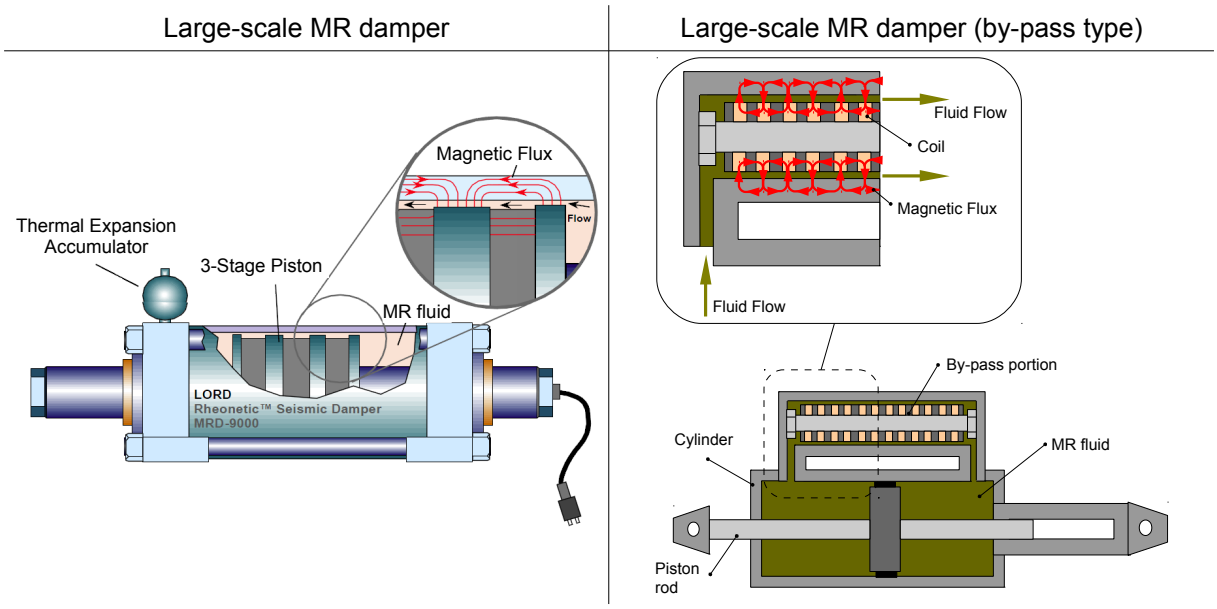

Figure 2.29 - Large-scale MR dampers for linear displacements.

A large-scale MR damper was developed and described by *Spencer Jr. et al. 1997(b)* for seismic response control – figure 2.29 left. The damper consists of a cylindrical housing, that is part of the magnetic circuit, with a concentric double ended piston and three sections employing electromagnetic coils. The effective fluid orifice is the entire annular space between the piston outside diameter and the inside of the damper cylinder housing that results in four effective valve regions. The damper is provided with a small pressurized accumulator to accommodate thermal expansion of the fluid. The device has a rated force output of 200 kN, a stroke of 8 cm, a maximum power requirement of about 22 W, a viscosity of 0,6 Pa·s, a maximum yield stress of 50 kPa, a length of about 1 m and weighs about 2,5 kN. A bypass-type of MR fluid dampers were described by *Sunakoda et al. 2000* and *Fujitani et al. 2000* for mitigation of earthquake or wind induced vibrations - figure 2.29 right. In this type of dampers the fluid flows from a high pressure chamber to a low pressure chamber in the valve mode through a bypass outside of the main cylinder. The device was designed so that the annular gap between the outside of the magnetic pole and the inside of the bypass cylinder will experience a magnetic field perpendicular to the fluid flow. Those authors refer the development of a 2, 20 and 200 kN MR dampers. The last damper is referred as large-scale device for vibration control of full-scale building structures. These type of devices are now available from Sanwa Tekki Corporation. Later on, *Hitchcock et al. 2002* developed a similar MR damper capable of developing 2,5 kN of maximum force at a velocity of 2 cm/s

with a current of 2 A. The maximum stroke of the damper is 2 inch (5,08 cm). The implementation of MR devices usually require pre-analysis of its effectiveness for use in specific applications. Practical hints to develop MR fluid devices were provided by *Carlson 2005* (see also *Carlson et al. 1996*, *Jolly et al. 1999* and *Yang 2001*). An overview of the properties of a range of MR fluids is detailed and a set of empirical equations used to develop and optimize the design of MR fluid devices that allow for the simultaneous optimization of all geometric, fluid and electrical parameters is presented too. *Yang et al. 2008* also described, analysed and provided recommendations for design and fabrication of MR dampers. Design procedures for active, semi-active and passive control systems were also described in detail by *Jinping & Hui 2009*.

In what concerns to full-scale implementations, MR dampers were installed for the first time in 2001 on the Nihon-Kagaku-Miraikan, the Tokyo National Museum of Emerging Science and Innovation, with two 30 t MR fluid dampers installed between the third and fifth floors. Sanwa Tekki Corp. design and built the dampers using Lord Corporation MR fluid (*Spencer Jr. 2008*). According to *Ikeda 2009* MR dampers in these applications have small contributions for the protection of structures against earthquakes. Concerning to base isolated structures, a 40 t MR damper was installed in a residential building in Japan along with laminated rubber bearings, lead dampers and oil dampers (see *Spencer & Nagarajaiah 2003*). Other applications of MR dampers in civil engineering structures can be found in cable-stayed bridges to mitigate wind induced vibrations. The Dongting Lake Bridge in Hunan, China, constitutes the first full-scale implementation of MR dampers for bridge structures. In this application, two MR dampers were installed per cable constituting a total of 312 MR dampers. On other bridges the same principle was applied by the Maurer Söhne Group (http://www.maurer-soehne.com), namely on Sutong Bridge in China and Eilandbrug Kampen Bridge in Netherlands.

Models for MR devices

The models for MR devices can be characterized: i) according to the properties they must represent, models can be categorized as *quasi-static* and *dynamic models*; ii) according to the modelling method adopted, models can be categorized as *parametric* and *non-parametric*.

Quasi-static models have been mainly developed for design purposes of MR devices and revealed to be useful mainly in the design phase. Model equations can be established using the fluid formulation (Bingham model, Herschel-Bulkley model or other) under a specific operational mode (valve, shear or squeeze mode) depending on the device design. From the fluid equations of motion (momentum equations) the fluid motion for a specific device can be

derived (velocity profile, pressure gradient and force) which establishes the device quasi-static model. Several quasi-static models have been developed (see *Yang 2001*), however this type of models do not capture the non-linear behaviour of the devices, especially the force-velocity relationship *Wang & Liao 2011*.

To describe the non-linear mechanical behaviour of these devices, modelling based on the laws of physics is complex, and models that combine physical understanding of the device along with the black-box description have been considered. Thus, several parametric and non-parametric models have been proposed and considered for MR modelling. Non-parametric models, include: polynomial models; multifunction models; black-box models; query-based models; neural network models; fuzzy-logic models; wavelet models; and Ridgenet models. In what concerns to parametric models, different approaches have been considered to model devices behaviour: Bingham models; Bi-viscous models; Viscoelastic-plastic models; Stiffness-viscosity-elasto-slide model; Bouc-Wen models; Lu-Gre hysteresis operated-based models; Hyperbolic tangent models; Sigmoid function-based models; Equivalent models; and Phase transition models. A review paper on MR parametric models by *Wang & Liao 2011* was recently published where they made available the state-of-the-art on parametric dynamic modelling as well as the review on identification and validation techniques. In the following sections some models of reference considered to describe mechanical behaviour of the devices will be presented.

The models used to describe the mechanical behaviour of MR dampers should accurately model the experimental observed phenomena in order to take full advantage of the controllable features of the devices. Some of those phenomena are shown in figure 2.30 and described as:

i) *hysteresis*: due to the nature of the device, hysteresis loops are found in dampers behaviour, whose are dependent of the applied current (or Voltage) and input movement (amplitude and frequency); the hysteresis loop has two distinct domains, a pre- and post-yield regions; the first one exhibits a strong hysteresis typical of a viscoelastic material, while the second one is plastic with a nonzero yield force; this yield force is also function of the applied current; the damper damping coefficient can be estimated as the mean slope of the hysteresis loop; non-symetric hysteresis can be found in some dampers, specially in those having an accumulator which introduces a force offset;

ii) *roll-off*: this phenomena occurs for small velocities and is a rapid and smooth transition between the post-yield branch of the force-velocity curve and zero velocity as the velocity decreases in modulus, where the curve has a non-linear relationship;

according to *Spencer Jr. et al. 1997(a)* this phenomena is due due to bleed or blow-by of fluid between the piston and the cylinder;

iii) *force overshot or Stribeck effect*: when the velocity changes in sign force overshoots are observed due to the inertial effects of the damper (piston rod), which is more pronounced in large-scale dampers (*Yang 2001*); in rotational MR dampers this phenomena was also observed and referred as the Stribeck effect (*Weber 2013*);

iv) *controllability* and other *non-linearities*: in certain cases MR dampers can only reach a stable force after some cycles when exposed to sinusoidal inputs, which is the result of damper static friction; the yield force of the damper as well as the peak force increase with the applied current; the displacement amplitude as well as the frequency of the excitation modifies the non-linear force-velocity relationship behaviour; thus, when controlling these devices the non-linearities should be accounted.

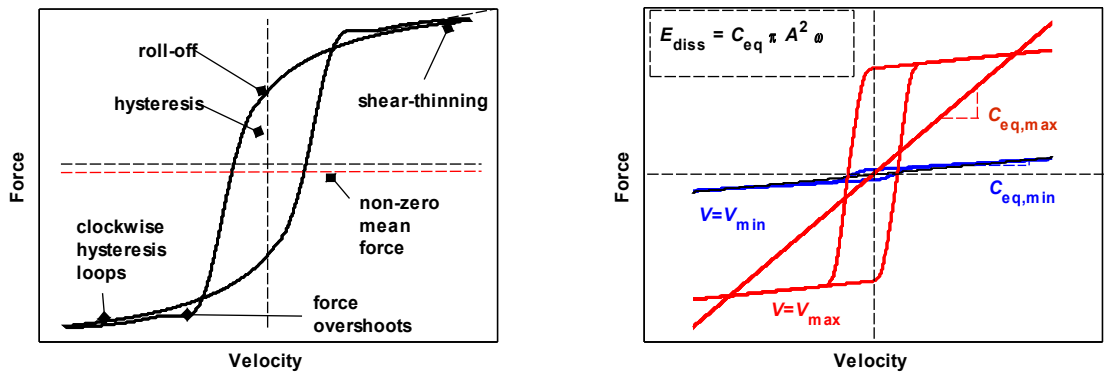

Figure 2.30 - Typical Force-Velocity plots for MR dampers under sinusoidal input: Left- curve evidencing several phenomena; Right-curve showing the damper equivalent damping coefficient evaluated using the dissipated energy criteria for two different input voltages (or currents).

Device damping force is dependent of the magnetic field (applied voltage or current) and excitation, including stroke and frequency. The models that will be presented next are used to describe MR dampers behaviour when the magnetic field is held constant, and thus those models must be complemented in order to include the influence of the fluctuating magnetic field. Moreover, MR damper dynamics as well as the response of the current driver must also be taken into account. The block diagram for the MR damper under variable input voltage or current is presented in figure 2.31.

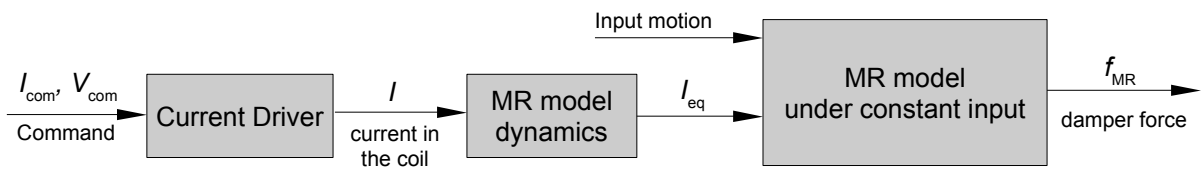

Figure 2.31 - Block diagram of the system MR device with current driver.

1) Bingham Model

The Bingham model is the simplest model to describe the mechanical behaviour of the MR devices. It is based on the Bingham plastic model, in which a body behaves solid until a minimum yield stress, and then a linear relationship between the stress and the rate of deformation. It consists of: a Coulomb element, described by a frictional force f_f which defines the device yield force dependence of the magnetic field; with a viscous damper described by its damping coefficient c_0 in parallel; and an offset f_0 due to the presence of an accumulator in some devices. The force developed is given by equation (2.18), where the frictional force changes with the magnetic field.

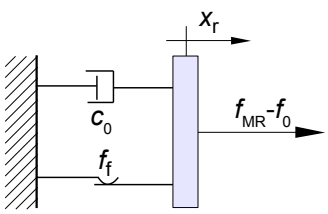

Figure 2.32 - Bingham mechanical model: viscous damper c_0, a frictional force f_f and an offset f_0.

$$f_{MR}=c_0\cdot\dot{x}_r+f_f\cdot\mathrm{sgn}(\dot{x}_r)+f_0,\quad f_{min}\leq f_f\leq f_{max} \tag{2.18}$$

where $\dot{x}_r$ is the device piston velocity. The model response behaviour to a sinusoidal input is identical to the one found in figure 2.26 (blue curve). Although this model has long been used to describe the mechanical behaviour of MR and ER devices, it does not reproduce well the hysteretic behaviour of the devices. To characterize the dynamic behaviour of the damper, the following parameters must be identified: IP=[c_0, f_0, f_f].

2) Bi-Viscous Models

An extension of the Bingham model is the bi-viscous model which considers a linear model described by a viscous behaviour in the pre-yield region. The model is given by:

$$f_{MR}-f_0=\begin{cases} c_1\cdot\dot{x}_r, & |\dot{x}_r|\leq v_f \\ c_0\cdot\dot{x}_r+f_f\cdot\mathrm{sgn}(\dot{x}_r), & |\dot{x}_r|>v_f \end{cases} \quad \text{with: } v_f=\frac{f_f}{c_1-c_0} \tag{2.19}$$

where: c_1 and c_0 are the pre- and post-yielding damping coefficients respectively; f_f is the yield force and v_f the correspondent velocity; and an offset f_0 due to the presence of an accumulator on some devices. An example of the model response to a sinusoidal input is given in figure 2.33. The model parameters needed to characterize the model are: IP=[c_0, c_1, f_0, f_f].

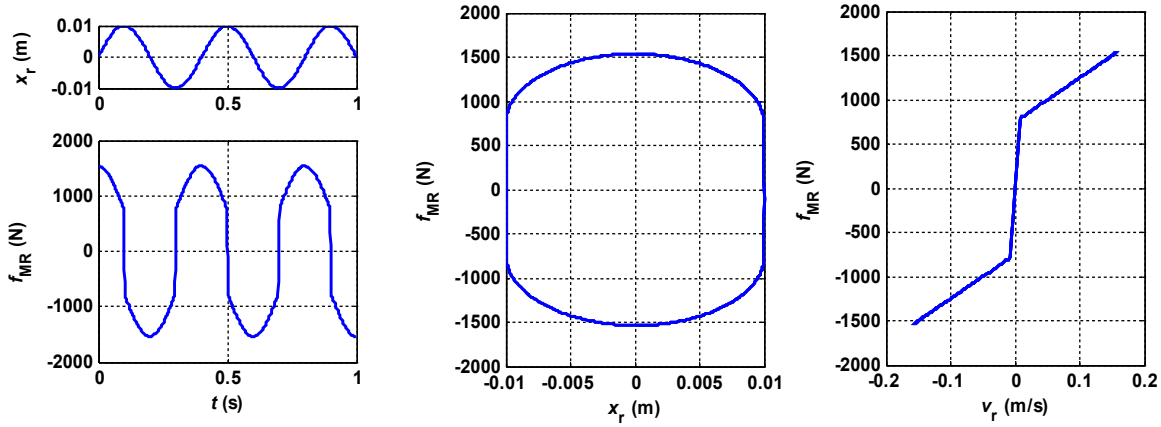

Figure 2.33 - Bi-viscous model (with f_f=750 N, c_0=5 kN s/m, c_1=90 kN s/m and f_0=0 N) response to an input sinusoidal displacement (10 mm at 2,5 Hz).

A version of this model including the hysteretic phenomena found in MR dampers was proposed by *Wereley et al. 1998*. The model is described by the following expressions (equation (2.20)) according to figure 2.34. The force-displacement plot is similar to the bi-viscous model but in this case the force-velocity plot exhibits hysteresis.

$$f_{MR}-f_0=\begin{cases} c_0\cdot\dot{x}_r-f_f, & \dot{x}_r\le v_1\wedge\ddot{x}_r>0 \\ c_1\cdot(\dot{x}_r-v_0), & -v_1\le\dot{x}_r\le v_2\wedge\ddot{x}_r>0 \\ c_0\cdot\dot{x}_r+f_f, & v_2\le\dot{x}_r\wedge\ddot{x}_r>0 \\ c_0\cdot\dot{x}_r+f_f, & v_1\le\dot{x}_r\wedge\ddot{x}_r<0 \\ c_1\cdot(\dot{x}_r+v_0), & -v_2\le\dot{x}_r\le v_1\wedge\ddot{x}_r<0 \\ c_0\cdot\dot{x}_r-f_f, & \dot{x}_r\le -v_2\wedge\ddot{x}_r<0 \end{cases} \qquad (2.20)$$

$$\text{with } v_1=\frac{f_f-c_1\cdot v_0}{c_1-c_0},\quad v_2=\frac{f_f+c_1\cdot v_0}{c_1-c_0}$$

In order to characterize the dynamic behaviour of the damper, the following parameters must be identified: IP=[c_0, c_1, v_0 f_0, f_f].

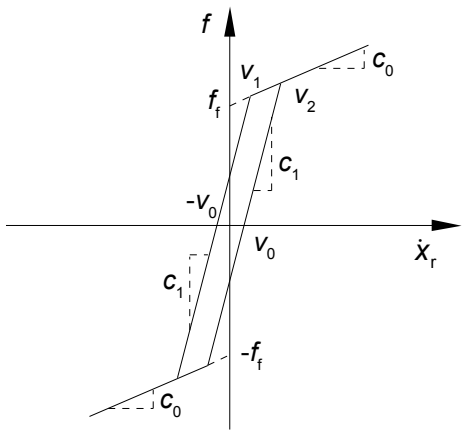

Figure 2.34 - Bi-viscous model with hysteresis. Force-velocity plot parameters description.

3) Extended Bingham Model

An extension to the Bingham model to describe the behaviour of electro-rheological devices was proposed by *Gamota & Filisko 1991*. The model consists of the Bingham model (i.e., a frictional element in parallel with a dashpot) in series with a linear viscoelastic solid model (two springs and a damping coefficient) – see figure 2.35.

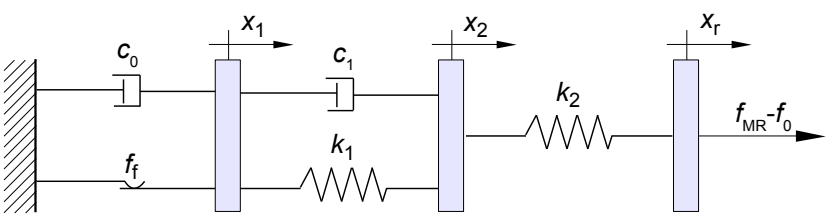

Figure 2.35 - Extended Bingham mechanical model.

This model has the ability to describe hysteresis phenomena and is described by:

$$f_{MR}-f_0=\begin{cases} c_0\cdot\dot{x}_1+f_f\cdot\mathrm{sgn}(\dot{x}_1) \\ k_1\cdot(x_2-x_1)+c_1\cdot(\dot{x}_2-\dot{x}_1) \quad |f_{MR}|>f_f \\ k_2\cdot(x_r-x_2) \\ \cdots\cdots\cdots\cdots\cdots\cdots\cdots\cdots\cdots\cdots \\ k_1\cdot(x_2-x_1)+c_1\cdot\dot{x}_2 \quad |f_{MR}|\leq f_f \\ k_2\cdot(x_r-x_2) \end{cases} \tag{2.21}$$

An example of model behaviour is presented in figure 2.36. This model can predict well the force-displacement and the force-velocity behaviour of MR dampers and even the roll-off phenomena. However, for small values of c_1, the equations are extremely stiff which sometimes constitutes a difficulty in solving it numerically. Figure 2.36 shows a comparison of results provided by this model to a sinusoidal input for two different roll-off modelling. The parameters needed to characterize the mechanical behaviour are: IP=[k_1, k_2, c_0, c_1, f_0, f_f].

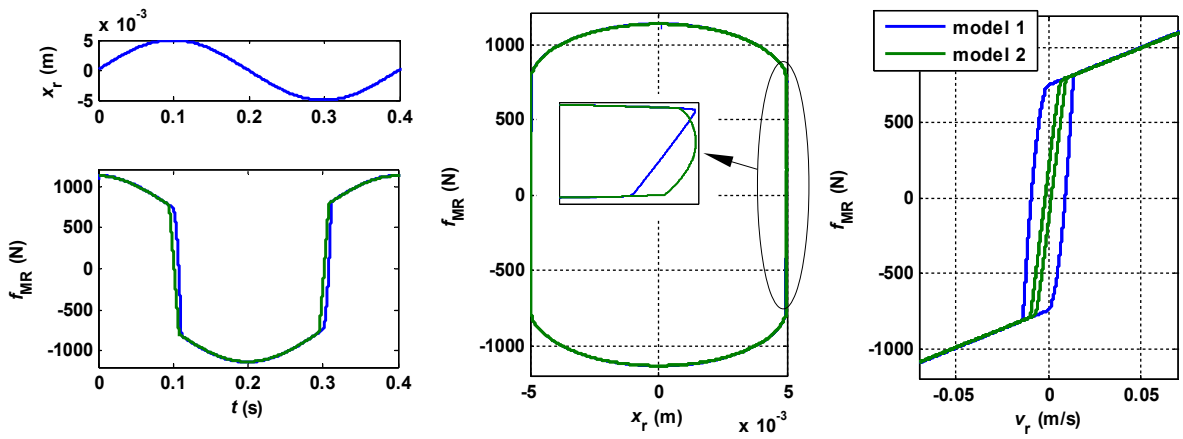

Figure 2.36 - Extended Bingham model response to an input sinusoidal displacement (5 mm at 2,5 Hz) for two cases: 1) with f_f=750 N, c_0=5 kN s/m, k_1=50 kN/m, c_1=1300 kN s/m, k_2=20 kN/mm and f_0=0 N; 2) with f_f=785 N, c_0=5,2 kN s/m, k_1=50 kN/m, c_1=100 kN s/m, k_2=100 kN/mm and f_0=0 N.

4) Bouc-Wen model

The hysteresis model of Bouc was modified by Wen and is one of the mathematical models used to describe the hysteretic behaviour (*Wen 1976*). This Bouc-Wen model represents the true hysteresis in the form:

$$\begin{aligned} \Phi_{BW}&=\alpha\cdot k\cdot x_r+(1-\alpha)\cdot D\cdot k\cdot z \\ \dot{z}&=D^{-1}\cdot\left[A\cdot\dot{x}_r-\beta\cdot|\dot{x}_r|\cdot|z|^{n-1}\cdot z-\gamma\cdot\dot{x}_r\cdot|z|^n\right] \end{aligned} \tag{2.22}$$

This model was developed in the context of mechanical systems in which Φ_{BW} is the restoring force, x_r is the displacement, z is the an auxiliary variable used to define the hysteresis loop in conjunction with the constants η, A, β and γ. These ones control the shape and size of the hysteresis loop. The conditions $\eta\geq1$, $D>0$, $k>0$ and $0<\alpha<1$ must be satisfied. The first term $\alpha\cdot k\cdot x$ defines the linear elastic component of the model and the second one $(1-\alpha)\cdot D\cdot k\cdot z$

defines the purely hysteretic component. Parameter α defines the post-yield stiffness ratio and D is the yield constant displacement. The response of this model to a sinusoidal input is presented in figure 2.37.

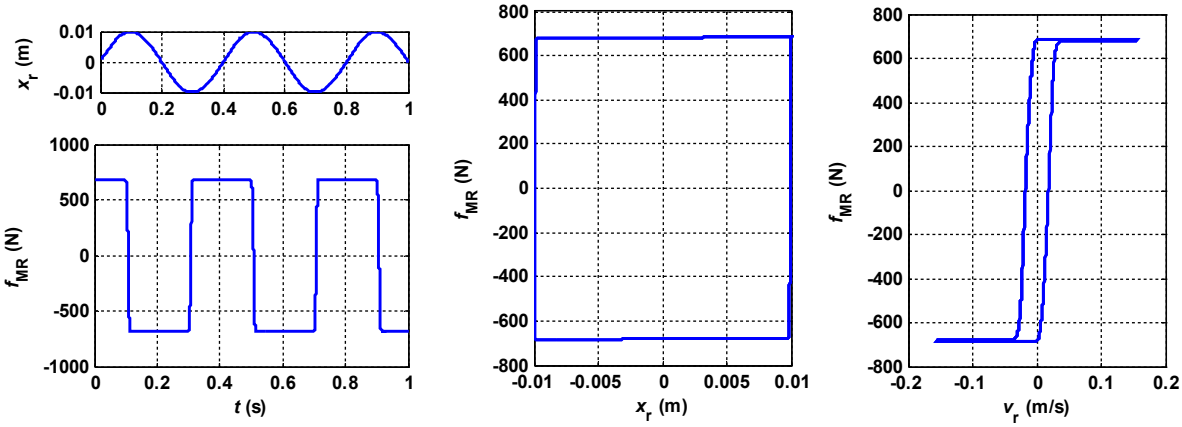

Figure 2.37 - Bouc-Wen model (with α=0,0028; k=88,25 kN/m; D=1; A=120, β=10^6 m^{-2}, γ=10^6 m^{-2} and n=2) response to an input sinusoidal displacement (10 mm at 2,5 Hz).

A normalized version of this model was proposed by *Ikhouane & Rodellar 2005(i)* which uses a fewer number of parameter to describe the mechanical behaviour. They made an analytical study of this model and characterize the model limit cycle analytically which was useful to derive a parameter identification method, this one described in *Ikhouane & Rodellar 2005(ii)*. The influence of this model parameters on the hysteresis loop was made later on by *Ikhouane et al. 2007*. This normalized version has a new internal dynamic variable $w=z/z_0$ which lies in the range $w\in\{-1,1\}$ and has the following form:

$$\begin{aligned}&\Phi_{BW}=k_x\cdot x_r+k_w\cdot w\\&\dot{w}=\rho\cdot\left[\dot{x}_r-\sigma\cdot|\dot{x}_r|\cdot w\cdot|w|^{n-1}+(\sigma-1)\cdot\dot{x}_r\cdot|w|^n\right]\\&\text{with}: k_x=\alpha\cdot k;\ k_w=(1-\alpha)\cdot D\cdot k\cdot z_0;\ \rho=\frac{A}{D\cdot z_0};\ \sigma=\frac{\beta}{\beta+\gamma};\ z_0=\sqrt[n]{\frac{A}{\beta+\gamma}}\end{aligned} \tag{2.23}$$

with: k_x>0, k_w>0, ρ>0 and σ≥0. The results provided with this model (figure 2.37) have a post-yield constant force which does not represent well the mechanical behaviour of MR dampers. Thus, an additional velocity dependent term is needed. The linear elastic term ($k_x\cdot x_r$) is then augmented or substituted by a linear viscous term dependent of the relative velocity ($c_0\dot{x}_r$) in order to adequate the model for MR modelling.

A Bouc-Wen plus viscous model was proposed by *Spencer Jr. et al. 1997(a)* to describe the mechanical behaviour of MR dampers. It consists of a damper in parallel with the Bouc-Wen model. The model is schematically depicted in figure 2.38 and is described by the following equations:

$$f_{MR}=c_0\cdot\dot{x}_r+k_0\cdot(x_r-x_0)+k_z\cdot z$$
$$\dot{z}=A\cdot\dot{x}_r-\beta\cdot|\dot{x}_r|\cdot z\cdot|z|^{n-1}-\gamma\cdot\dot{x}_r|z|^n \qquad (2.24)$$

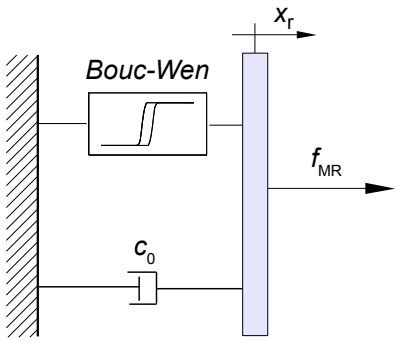

Figure 2.38 - Bouc-Wen plus viscous model representation.

The linear component of this model has two contributions: one from the original Bouc-Wen model, resulting from the spring element with $k_0=\alpha\cdot k$; and an additional one resulting from the damper,·with damping c_0. The hysteretic component results only from the Bouc-Wen model where $k_z=(1-\alpha)\cdot D\cdot k$. The yield constant is in this case D=1. Parameters A, β, γ and n define the shape of the hysteresis loop through the evolutionary variable z. The initial force f_0 present in some dampers is incorporated in the model by an initial deformation x_0 ($f_0=-k_0\cdot x_0$) The normalized version of this model consists in the normalized version of the Bouc-Wen model (equation (2.23), with $k_w=z_0\cdot k_z$) plus the viscous term $c_0\dot{x}_r$contribution. A typical behaviour due to an input sinusoidal deformation is shown in figure 2.39.

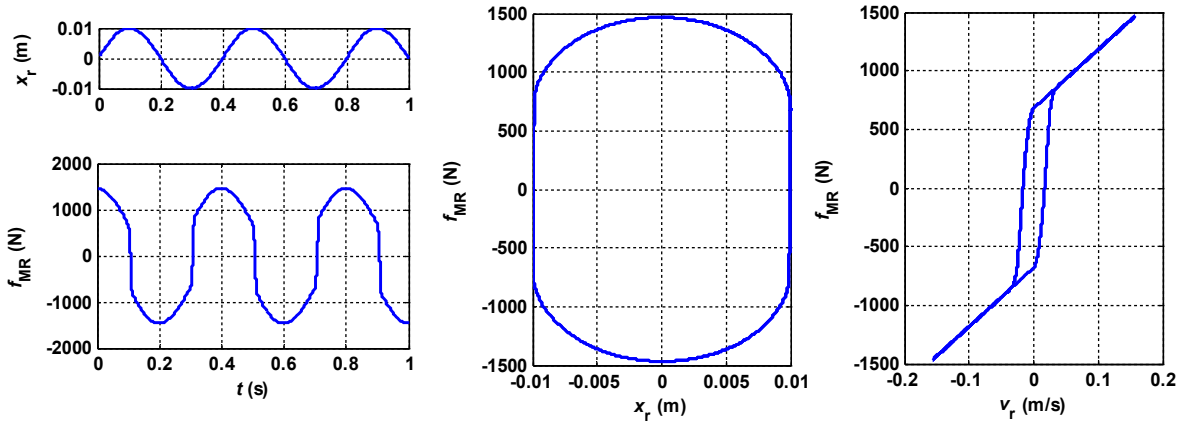

Figure 2.39 - Bouc-Wen plus viscous model (with c_0=5 kN s/m, k_0=2,5 kN/m, A=120, β=10^6 m^{-2}, γ=10^6 m^{-2}, k_z=88 kN/m, n=2 and x_0=38 mm) response to an input sinusoidal displacement (10 mm at 2,5 Hz).

In order to characterize the dynamic behaviour of the damper, the following parameters must be identified: IP=[k_0, k_z, c_0, A, β, γ, n x_0].

After testing MR dampers, analysing the data and parametrize the Bouc-Wen model - equation (2.24) - *Spencer Jr. et al. 1997(a)* verified that it predicts well the force-displacement behaviour and possesses a force-velocity behaviour that is more close to experimental data. However the nonlinear force-velocity response of the Bouc-Wen model does not roll-off in the region where the acceleration and velocity have opposite signs and the magnitude of the velocities are small. To overcome this problem a modified version of Bouc-Wen model was proposed (figure 2.40) which include two additional elements: a damping coefficient c_1 that affects the force roll-off at lower velocities and a stiffness

coefficient k_1. The model is described by:

$$f_{MR}=\begin{cases} c_0\cdot(\dot{x}_r-\dot{y})+k_0\cdot(x_r-y)+k_1\cdot(x_r-x_0)+k_z\cdot z \\ c_1\cdot\dot{y}+k_1\cdot(x_r-x_0) \end{cases}$$
$$\dot{z}=A\cdot(\dot{x}_r-\dot{y})-\beta\cdot|\dot{x}_r-\dot{y}|\cdot z\cdot|z|^{n-1}-\gamma\cdot(\dot{x}_r-\dot{y})|z|^n \qquad (2.25)$$

Figure 2.41 shows the typical behaviour provided by this model to a sinusoidal input where it is evident the roll-off phenomena in the force-velocity plot. The following parameters must be identified to characterize the mechanical behaviour of MR dampers:

IP=[k_0, k_1, k_z, c_0, c_1, A, β, γ, n x_0].

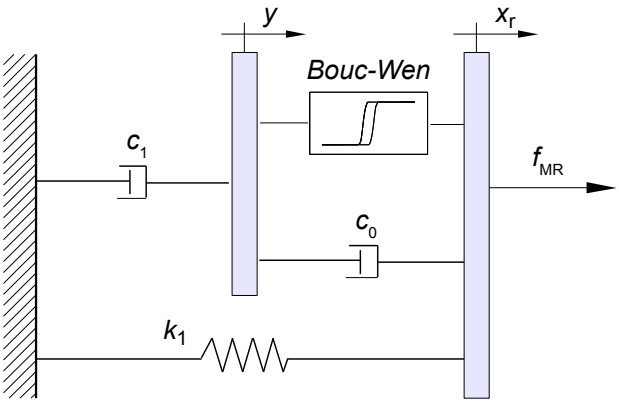

Figure 2.40 - Phenomenological Bouc-Wen model representation (*Spencer Jr. et al. 1997(a)*).

A normalized version of this model can also be obtained in the same way. Defining a new internal dynamic variable $w=z/z_0$ which lies in the range $w\in\{-1,1\}$, after substituting and manipulating the expressions in equation (2.25) leads to:

$$f_{MR}=\begin{cases} c_0\cdot(\dot{x}_r-\dot{y})+k_0\cdot(x_r-y)+k_1\cdot(x_r-x_0)+k_w\cdot w \\ c_1\cdot\dot{y}+k_1\cdot(x_r-x_0) \end{cases}$$
$$\dot{w}=\rho\cdot\left[(\dot{x}_r-\dot{y})-\sigma\cdot|\dot{x}_r-\dot{y}|\cdot w\cdot|w|^{n-1}+(\sigma-1)\cdot(\dot{x}_r-\dot{y})\cdot|w|^n\right] \qquad (2.26)$$
$$\text{with: } k_w=k_z\cdot z_0;\ \rho=\frac{A}{z_0};\ \sigma=\frac{\beta}{\beta+\gamma};\ z_0=\sqrt[n]{\frac{A}{\beta+\gamma}}$$

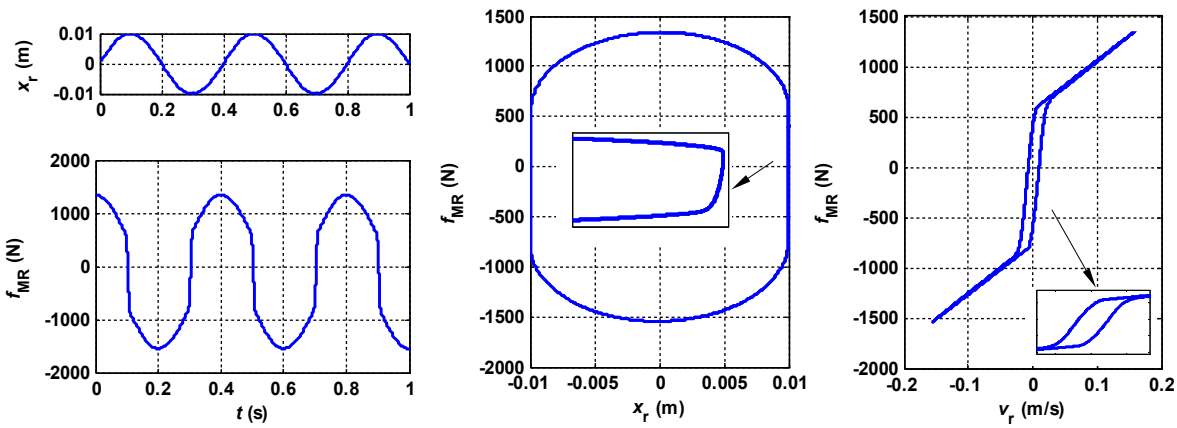

Figure 2.41 - Phenomenological Bouc-Wen model (with c_0=5,3 kN s/m, c_1=93 kN s/m, k_0=1,4 kN/m, k_1=0,54 kN/m, A=207, β=2x10^6 m^{-2}, γ=2x10^6 m^{-2}, k_z=96,3 kN/m, n=2 and x_0=189 mm) response to an input sinusoidal displacement (10 mm at 2,5 Hz).

When dealing with large-scale MR dampers other phenomena were identified in the experimental data. In addition to the roll-off phenomena, MR fluid stiction and inertial effects, force overshoots, clockwise hysteresis loops in the velocity extremes and shear thinning

were found in the force-velocity plots. To overcome these problems *Yang 2001* studied several models and proposed a Bouc-Wen model based on the phenomenological model in figure 2.42. The model is composed by the classical Bouc-Wen model in parallel with a dashpot element with a velocity dependent damping coefficient attached to a rigid mass. The mass element accommodates the inertial effects and the clock wise hysteresis loops in the velocity extremes and the velocity dependent damping element contributes to model the shear thinning effect and roll-off. This model has the following formulation:

$$\begin{aligned} &f_{MR}=c(\dot{x}_r)\cdot\dot{x}_r+k_0\cdot(x_r-x_0)+k_z\cdot z+m\cdot\ddot{x}_r \\ &\dot{z}=A\cdot\dot{x}_r-\beta\cdot|\dot{x}_r|\cdot z\cdot|z|^{n-1}-\gamma\cdot\dot{x}_r|z|^n \\ &\text{with}: c(\dot{x}_r)=a_1\cdot\exp(-a_2|\dot{x}_r|)^p \end{aligned} \tag{2.27}$$

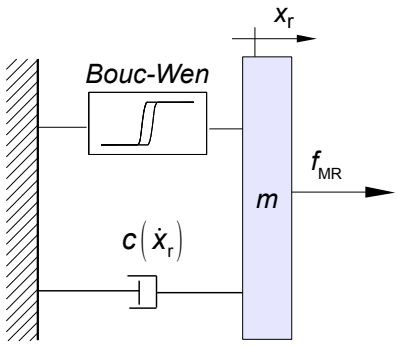

Figure 2.42 - Phenomenological Bouc-Wen model representation (*Yang 2001*).

Parameters a_1, a_2 and p are positive constants, having p<1 in order to model the shear-thinning effect in the post-yield region.

Another way to model the force overshoot was proposed by *Weber 2013.* A Bouc-Wen model complemented by a second order dynamic model was used to describe that phenomena due to the Stribeck effect. The model is described by the following equations:

$$\begin{aligned} &f_{MR}=c_0\cdot\dot{x}_r+k_0\cdot(x_r-x_0)+k_z\cdot z^s \\ &\ddot{z}^s+2\cdot\xi_0\cdot\omega_0\cdot\dot{z}^s+\omega_0^2=\omega_0^2\cdot z \\ &\dot{z}=A\cdot\dot{x}_r-\beta\cdot|\dot{x}_r|\cdot z\cdot|z|^{n-1}-\gamma\cdot\dot{x}_r|z|^n \end{aligned} \tag{2.28}$$

where z^s denotes an internal variable that includes the Stribeck effect, which is related with z by a second order dynamic model having a natural frequency ω_0 and damping ratio ξ_0. The typical behaviour provided by this model is found in figure 2.43.

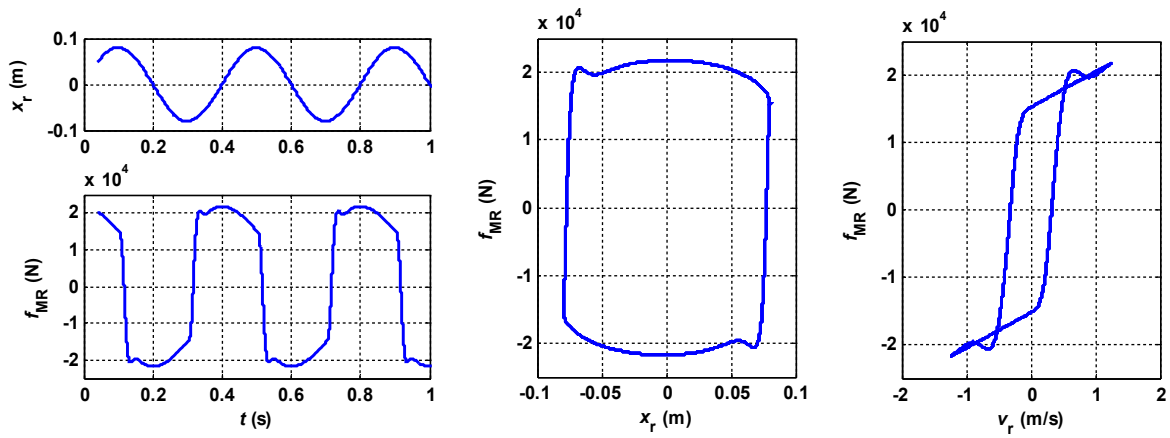

Figure 2.43 - Bouc-Wen plus viscous model with Stribck effect (with c_0=5 kN s/m, k_0=2,5 kN/m, A=120, β=10^6 m^{-2}, γ=10^6 m^{-2}, k_z=88 kN/m, n=2, x_0=38 mm, ω_0=50 rad/s and ξ_0=0,5) response to an input sinusoidal displacement (10 mm at 2,5 Hz).

With the exception of the force overshoot, the behaviour is similar to the one of the Bouc-Wen model plus a viscous element -see figure 2.39. In addition to the parameters to describe the Bouc-Wen model plus viscous model, two additional parameters are required to characterize the dynamic behaviour of the damper, and thus: IP=[k_0, k_z, c_0, A, β, γ, n, x_0, ω_0, ζ_0,].

5) Dahl models

Another model that has been used to describe the MR mechanical behaviour are the Dahal's family models. The Dahl model was originally proposed by *Dahl 1968* to describe the sliding and rolling friction phenomena of dynamic systems. The equations are given by:

$$\begin{aligned} \Phi_D &= \sigma_0 \cdot z \\ \dot{z} &= \dot{x}_r - \frac{\sigma_0}{\lambda_0} z \cdot |\dot{x}_r| \end{aligned} \tag{2.29}$$

where: Φ_D is the restoring force; x_r is the displacement; σ_0 and λ_0 are constants; and z is internal dynamic variable. This model is a particular case of the Bouc-Wen model (equation (2.22)) with: α=0; k=σ_0; β=σ_0/λ_0; γ=0; D=1; A=1; and n=1. In the same way, the normalized version is a particular case of equation (2.23) with: k_x=0; σ=1; n=1; z_0=λ_0/σ_0; k_w=λ_0; and ρ=σ_0/λ_0.

$$\begin{aligned} \Phi_D &= k_w \cdot w \\ \dot{w} &= \rho \cdot \left(\dot{x}_r - |\dot{x}_r| \cdot w \right) \end{aligned} \tag{2.30}$$

An example of the results provided with this model to a sinusoidal input can be found in figure 2.44.

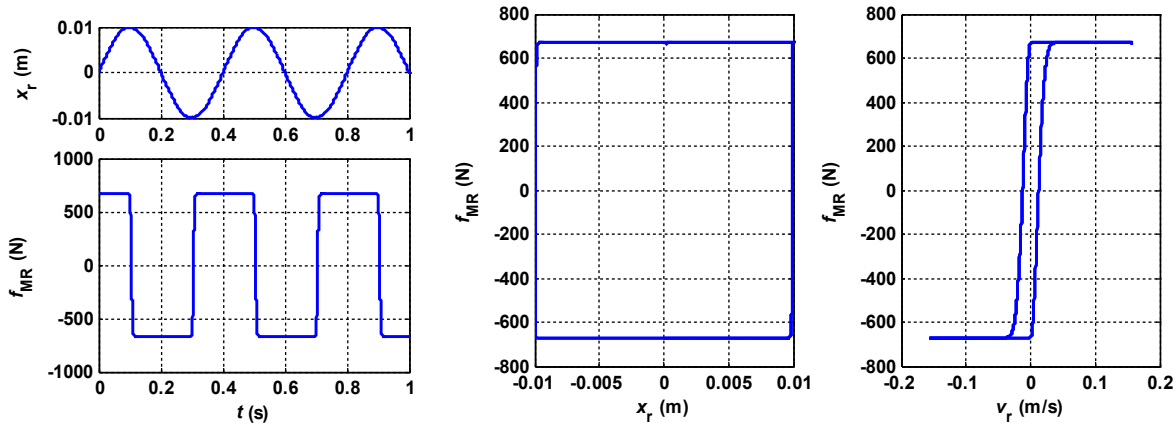

Figure 2.44 - Dahl model (with σ_0=1,5x10^4 kN/m; λ_0=670 N) response to an input sinusoidal displacement (10 mm at 2,5 Hz).

As for the Bouc-Wen model an additional velocity dependent term is needed to describe the mechanical behaviour of MR dampers. The viscous plus dry-friction (Dahl) model was proposed by *Ikhouane & Dyke 2007* to describe the mechanical behaviour of shear mode

MR dampers. This model was later on used by *Rodríguez et al. 2009* to describe the behaviour of large-scale MR dampers and compared with the Bouc-Wen model, where this last one showed to better fit experimental data. The model is also referred as the viscous Dahl model and is described by the following equations (in the normalized form):

$$\begin{aligned} f_{MR} &= c_0 \cdot \dot{x}_r + k_w \cdot w \\ \dot{w} &= \rho \cdot \left(\dot{x}_r - |\dot{x}_r| \cdot w \right) \end{aligned} \tag{2.31}$$

Figure 2.45 shows an example of this model response to a sinusoidal input. It can be seen that the results are very similar to the Bouc-Wen plus viscous model ones. The following parameters are needed to characterize the model: IP=[c_0, k_w, ρ].

A more general model can include a force offset and/or a displacement dependent term to account for example the influence of an accumulator in a single ended damper. Thus the device force is described by:

$$f_{MR} = c_0 \cdot \dot{x}_r + k_0 \cdot x_r + k_z \cdot z + f_0 \tag{2.32}$$

where: the term $k_0 \cdot x_r$. accounts for the accumulator stiffness; and f_0 describes the force offset that could be alternatively included in the model as an initial deformation by taking $f_0 = -k_0 \cdot x_0$. To characterize the model two additional parameters must be identified and thus IP=[k_0, c_0, f_0, k_w, ρ].

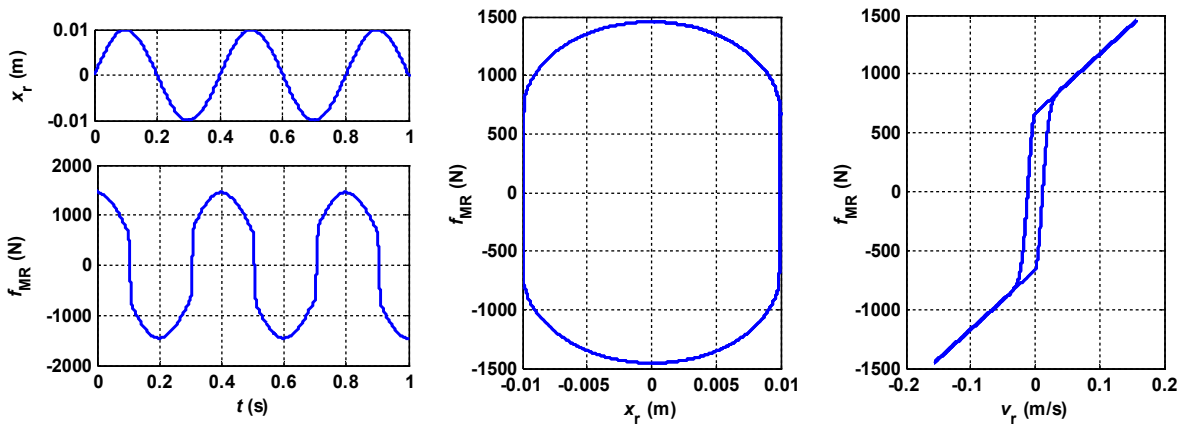

Figure 2.45 - Dahl plus viscous model (with c_0=5 kN s/m; k_w=670 N; ρ =2,24x10^4 m^{-1}) response to an input sinusoidal displacement (10 mm at 2,5 Hz).

Model Extension

Depending on the type of input considered, current or voltage, some model parameters will be dependent of these quantities. Empirical relationships (usually polynomial) are then used to describe those parameters as function of the input (voltage or current). For example *Spencer Jr. et al. 1997(a)* used first order polynomials to describe the voltage dependence of Bouc-Wen model parameters A, c_1 and c_0. When modelling large-scale MR dampers, *Yang 2001* used third order polynomials.

Current Driver

The command current (or voltage) should be developed quickly in the electromagnetic coil of the MR damper in order to minimize delays. To achieve quick changes in the coil current a pulse width modulation (PWM) servo amplifier is commonly used as a current driver. This solution was analysed and proposed by *Yang 2001* in detriment of a voltage driver power supply. In that study a second order system was used to describe the transfer function of the current driver, which mainly incorporates a PWM servo amplifier with a PI controller:

$$G(s)=\frac{c\cdot s+d}{s^2+a\cdot s+b} \tag{2.33}$$

where: s is the Laplace variable; a, b c and d are constants. This model can be identified using an input (voltage or current) band-limited Gaussian white noise and measuring the current developed in the damper coil (*Chae et al. 2013(II)*).

MR damper dynamics

A first order dynamic system model has been usually considered to describe the damper dynamics involved with the response time of the device in reaching the steady-state condition (*Dyke 1996; Yang 2001*). In terms of currents the model is given by:

$$\frac{d\,I_{eq}}{dt}=\eta\cdot(I-I_{eq}) \tag{2.34}$$

where: η (inverse of the time constant) reflects the response time of the MR damper, I is the current generated by the current driver input voltage and I_{eq} is the equivalent current that inputs in the MR damper model (at constant current). A theoretical basis that justifies the validity of this model was presented by *Chae et al. 2013(II)*. It is based on the total magnetic flux around the annular gap (between the cylinder housing and piston) resulting from the magnetic flux on the eletromagnetic coil and the formation of an eddy currents in the damper cylinder housing and piston.

2.9 Control Strategies

2.9.1 Problem Formulation

Having a structural system (as described previously in section 2.7), employing semi-active devices (as the ones described in section 2.8) and subjected to input disturbances (the earthquake, see section 2.3), the control theory should answer to the following question: *what should be the input to the device (control signal) that maximizes the performance (small displacements and small accelerations in the structure)*?

Describing the problem in terms of block diagrams, a block defined as the controller which computes the appropriate control signal using a set of system responses and/or inputs is required. The vibration mitigation problem is a regulation control problem with zero reference.

A general closed-loop used in semi-active control is depicted in figure 2.46.

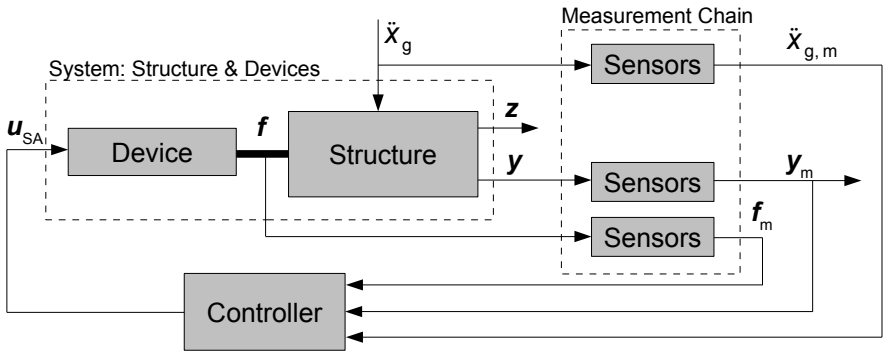

Figure 2.46 - General semi-active control loop.

The system to be controlled consists of a structure employing semi-active devices which is disturbed by an input ground motion (the earthquake) $\ddot{x}_g$ and dissipative forces $\boldsymbol{f}$ are generated by those devices due to its motion and modified through the command $\boldsymbol{u}_{SA}$. This control variable is generated by the controller taking into account the measurements of the disturbances $\ddot{x}_{g,m}$, the measured input forces $\boldsymbol{f}_m$ and output responses $\boldsymbol{y}_m$ such that the responses $\boldsymbol{z}$ or $\boldsymbol{y}_m$ provide good performances. A distinction is made between the real quantity and the measured one (subscript m) due to the influence of the measurement chain (sensors, signal conditioners, acquisition and processing system and others) which should be close to an ideal sub-system, i.e. having a transfer function with unitary gain and in phase in the frequency range of interest. For convenience this assumption will be considered generally in the following chapters. Figure 2.46 represents itself the common approaches considered in semi-active control:

1. **feedback control schemes**: only the signals from sensors (force and/or responses, thus no feed-forward from ground motion) are used to compute the control variable; the corrective control variables are function of the outputs whose are result of input effects (*DiStefano III et al. 1967*);
2. **feedback plus feedforward control schemes**: in addition to the signals from sensors the input ground motion measurements can be used to compute the control variables too; the idea is to anticipate the effects of the disturbances and cancel them out by suitable control actions; feedforward is used to remove most of the effect of the measured disturbance while feedback removes the remaining as well as dealing with unmeasured disturbances (*Maciejowski 2002*).

The synthesis of the controller requires a model (mathematical or physical) of the system. Even when both structure and device are described by linear models, a nonlinear dynamic system (structure plus device) with bounded inputs is obtained. The whole system is of the

form (state-space equation):

$$\dot{\boldsymbol{z}}_c = \boldsymbol{f}_c\left(\boldsymbol{z}_c, \ddot{x}_g, \boldsymbol{u}_{SA}\right),\ \boldsymbol{u}_{SA,min} \leq \boldsymbol{u}_{SA} \leq \boldsymbol{u}_{SA,max} \tag{2.35}$$

where: $\boldsymbol{f}_c$ are nonlinear functions of the states $\boldsymbol{z}_c$, input disturbance $\ddot{x}_g$ (ground motion) and control variables $\boldsymbol{u}_{SA}$ (input for the device that forces it to change its behaviour during motion); $\boldsymbol{z}_c$ is the augmented state-vector that includes the states of the structure and of the device. The resulting system in equation (2.35) is a non-linear system with bounded inputs. The goal is to find the control variable (inside the admissible region) that minimizes the structural accelerations and relative displacements.

To tackle this kind of problems several different ways can be addressed. The analysis and design of nonlinear systems can be made using a set of available procedures which are known as nonlinear control. Nonlinear control in general intends to derive feedback control laws that force the closed-loop to follow the intended specifications. A lot of methods have been used in semi-active control: Lyapunov based methods; sliding mode control; intelligent paradigms, like neural networks or fuzzy-logic; and force-tracking. This last one in particular has been successfully applied in semi-active control and comprises different control schemes.

As stated before, to implement a specific control approach a number of variables are required to compute the control variable. In certain circumstances some of those variables could not be accessible due to certain limitations. Thus, it is necessary to reconstruct those variables using the available ones. In those situations an observer can be designed if the system is observable. This one consists in a model of the system and a gain which are used to reconstruct the variables from the available measurements. The Kalman filter technique has been used extensively in several domains (*Lewis 1986*) and in particular in semi-active control. The controller block in figure 2.46 has then embedded an observer that estimates the unmeasured variables needed to compute the control variable.

Force tracking as the name indicates means that the device force has to follow a reference force. In these schemes the controller block is split in two parts linked in series: a first one that computes the desired control force based on the feedback signals; and a second one, referred as SA algorithm, that computes the control variable based on the desired force and/or on the device force (measured or computed). It should be noted that semi-active devices are dissipative and thus does not have the ability to inject energy in the system, which means that do not always follow the desired force. Nevertheless this approach has shown good results. In the first part the desired force is computed using any linear or non-linear control strategy, like the classical PID controller, optimal control theory, or other. From here, the straightforward way would be considering the inverse model of the device to

compute the control variable online. This approach is also classified as *model-based feed-forward force tracking scheme*. The advantage of this approach is that no force measurements are needed. However, nor always is possible to invert the model and approximations using empirical rules are considered. Thus, if force measurements are considered, the control variable can be computed using those measurements and the desired force. This approach is classified as *nonlinear force tracking scheme based on force feedback* (or simply *force feedback*) and also known as *clipped control*. Usually bang-bang control laws are used. An approach that considers both previous schemes has also been used for this purpose. This one is denominated as *combined feedforward feedback force tracking scheme*.

The following subsections will describe more deeply some of this control schemes which have been considered for semi-active control.

2.9.2 Classical Control

The basic control actions used in industrial automatic controllers are used to compute the control signal for reducing the deviation between the output and the reference. The control action is defined according to the manner the control signal is computed: i) two position control or on-off control; and the PID (proportional-integral-derivative) controller in general (*Ogata 1970*). For the purpose of semi-active control the integral (I) and the proportional plus integral (PI) control actions with feedback from the acceleration have been considered in conjunction with SA control algorithms according to the block diagram in figure 2.47.

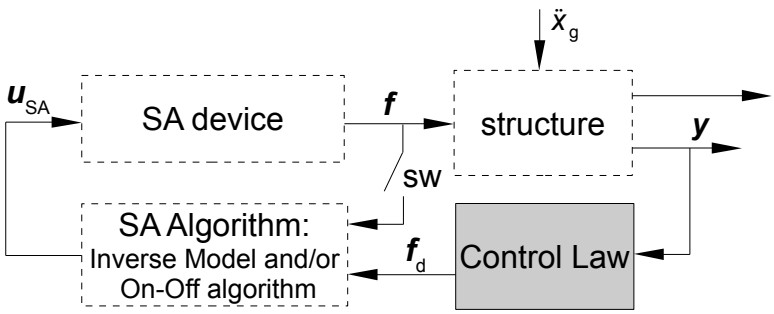

Figure 2.47 - Basic control action with a clipped algorithm in the semi-active control loop: i) switch (sw) off – model-based feed-forward force tracking scheme; ii) switch (sw) on – force feedback.

Assuming a SISO case (single-input single output), the general case for a PI control law to implement in the loop is given by:

$$f_{d,i} = -k_p \cdot \ddot{x}_i - k_i \int_0^{\tau} \ddot{x}_i \; d\tau = -k_p \cdot \ddot{x}_i - k_i \cdot \dot{x}_i \qquad (2.36)$$

where: k_p and k_i are the proportional and integral controller gains respectively; $\ddot{x}_i$ and $\dot{x}_i$ are the absolute acceleration and velocity at ith floor. The controller gains can be designed taking into account the objectives by different procedures or methods.

The integral controller computes a control signal that is proportional to the sum of the instantaneous error over time which contributes to eliminate the steady-state error or offset. Although in many industrial processes the integral action is used in conjunction with the proportional and with the proportional plus derivative control actions (*Ogata 1970*), in the field of vibration isolation it has been used solely or with the proportional term. When used solely it is well known as the sky-hook damper. It consists in including a force generating element in the isolation interface and a sensor at the receiving end of the transmission path, which using an integral control law computes the desired control action. This allows to combine -40 dB/decade attenuation rate at high frequency with critical damping (no overshoot) (*Preumont 2002*). The proportional term increases the sensitivity but will retain the steady-state error. Care must be taken in the design in order to avoid unstable controllers which affect the performance of the whole system.

The integral control law in conjunction with the inverse model of the device was proposed by *Symans & Constantinou 1995* as a force tracking scheme for controlling structural responses of one and two DOF systems employing SA fluid dampers when subjected to earthquake motions. Compared to the best passive case no improvements were found. However this study was limited to structural systems with fundamental periods of 0,36 s and 0,56 s. More recently *Aguirre et al. 2011* proposed a PI controller with a clipped algorithm for controlling MR dampers behaviour installed in structures to reduce earthquake responses. Through numerical simulations they found a comparable performance to other control strategies.

Semi-active systems have also been considered in solving vibration isolation problems. *Liu et al. 2005* studied the vibration isolation characteristics of one degree of freedom system employing a semi-active device with four established control strategies based on sky-hook control and balance control. The results showed that semi-active system can always provide better isolation at higher frequencies than a conventional passive one.

2.9.3 Optimal Control

Optimal control theory is a mathematical optimization method for deriving control laws. It was developed to solve more complex problems in the field of control theory with more demanding performance and objectives for the control system. Optimal control deals with the problem of finding a control law for a given system such that a certain optimality criterion is achieved. This criterion is described by mathematical expressions in terms of the control variables, called cost functions or performance indices, that are optimized (usually minimized). The problem is usually formulated given: i) the system state equation and output equation; ii) the control vector; the constraints of the problem; the performance index; and the system parameters (*Ogata 1970*). For the particular case of linear systems and considering the quadratic integral cost functional as the performance index the problem is

called Linear Quadratic Regulator (LQR):

$$J=\int_0^{\infty} L(\boldsymbol{z},\boldsymbol{f}_{\mathrm{d}})\,dt \tag{2.37}$$

$L(\boldsymbol{z},\ \boldsymbol{f}_{\mathrm{d}})$ is a quadratic integrand function of the states (or outputs) and desired input. It is considered the steady-state case (infinite upper limit in the integral of 2.37) and time-invariant regulator problem (time-invariant system in equation 2.9). A general quadratic function that weights the outputs $\boldsymbol{y}$ and the inputs $\boldsymbol{f}_{\mathrm{d}}$, is given by:

$$\begin{aligned} L(\boldsymbol{z},\boldsymbol{f}_{\mathrm{d}}) &= \boldsymbol{y}^{\mathrm{T}}\cdot\boldsymbol{Q}_{\mathrm{y}}\cdot\boldsymbol{y}+\boldsymbol{f}_{\mathrm{d}}{}^{\mathrm{T}}\cdot\boldsymbol{R}_{\mathrm{f}}\cdot\boldsymbol{f}_{\mathrm{d}} \\ &= \boldsymbol{z}^{\mathrm{T}}\cdot\boldsymbol{Q}\cdot\boldsymbol{z}+\boldsymbol{f}_{\mathrm{d}}{}^{\mathrm{T}}\cdot\boldsymbol{R}\cdot\boldsymbol{f}_{\mathrm{d}}+2\cdot\boldsymbol{z}^{\mathrm{T}}\cdot\boldsymbol{N}\cdot\boldsymbol{f}_{\mathrm{d}} \\ \text{with}: \boldsymbol{Q} &= \boldsymbol{C}_{\mathrm{y}}^{\mathrm{T}}\cdot\boldsymbol{Q}_{\mathrm{y}}\cdot\boldsymbol{C}_{\mathrm{y}},\ \ \boldsymbol{R}=\boldsymbol{R}_{\mathrm{f}}+\boldsymbol{D}_{\mathrm{y}}^{\mathrm{T}}\cdot\boldsymbol{Q}_{\mathrm{y}}\cdot\boldsymbol{D}_{\mathrm{y}},\ \ \boldsymbol{N}=\boldsymbol{C}_{\mathrm{y}}^{\mathrm{T}}\cdot\boldsymbol{Q}_{\mathrm{y}}\cdot\boldsymbol{D}_{\mathrm{y}} \end{aligned} \tag{2.38}$$

where: $\boldsymbol{Q}_{\mathrm{y}}$ is a semi-positive definite matrix that weights the outputs and $\boldsymbol{R}_{\mathrm{f}}$ is a positive definite matrix that weights the desired inputs. The performance index of (2.37) has cross product terms when expressed in terms of the states and inputs due to the direct feedthrough term (through matrix $\boldsymbol{D}_{\mathrm{y}}$) of the system (see equation 2.9). The solution of the deterministic problem, i.e. assuming a null disturbance $\ddot{x}_{\mathrm{g}}$, will yield linear control laws (time invariant and steady-state) function of the states (*Anderson & Moore 1989*):

$$\boldsymbol{f}_{\mathrm{d}}=-\boldsymbol{K}_{\mathrm{c}}\cdot\boldsymbol{z},\ \ \boldsymbol{K}_{\mathrm{c}}=\boldsymbol{R}^{-1}\cdot\left[\boldsymbol{B}^{\mathrm{T}}\cdot\boldsymbol{P}+\boldsymbol{N}^{\mathrm{T}}\right] \tag{2.39}$$

where $\boldsymbol{K}_{\mathrm{c}}$ is the gain matrix and $\boldsymbol{P}$ is the solution of the adequate *algebraic Riccati equation* (ARE):

$$\boldsymbol{P}\cdot\boldsymbol{A}+\boldsymbol{A}^{T}\cdot\boldsymbol{P}-(\boldsymbol{P}\cdot\boldsymbol{B}+\boldsymbol{N})\cdot\boldsymbol{R}^{-1}\cdot(\boldsymbol{B}^{\mathrm{T}}\cdot\boldsymbol{P}+\boldsymbol{N}^{\mathrm{T}})+\boldsymbol{Q}=\boldsymbol{0} \tag{2.40}$$

with $\boldsymbol{Q}$, $\boldsymbol{R}$ and $\boldsymbol{N}$ defined according to (2.38). Choosing adequate values for weights $\boldsymbol{Q}_{\mathrm{y}}$ and $\boldsymbol{R}_{\mathrm{f}}$ will lead to the gain matrix $\boldsymbol{K}_{\mathrm{c}}$.

In seismic engineering the system under study is subjected to an input ground motion $\ddot{x}_{\mathrm{g}}$ with stochastic characteristics and thus this problem has to be solved in the stochastic environment, stochastic LQR, which has the same solution of the deterministic case if the input ground motion is assumed to be white noise. A shaping filter could be used to model the ground excitation characteristics, like the Kanai-Tajimi shaping filter (*Wang 2006*), the pulse filter (*Agrawal & Zhou 2004*) or other filter that best model the earthquake characteristics. The shaping filter can be given by:

$$\begin{aligned} \dot{\boldsymbol{z}}_{\mathrm{f}} &= \boldsymbol{A}_{\mathrm{f}}\cdot\boldsymbol{z}_{\mathrm{f}}+\boldsymbol{B}_{\mathrm{f}}\cdot w \\ \ddot{x}_{\mathrm{g}} &= \boldsymbol{C}_{\mathrm{f}}\cdot\boldsymbol{z}_{\mathrm{f}} \end{aligned} \tag{2.41}$$

where: w is a white noise excitation; $\boldsymbol{z}_{\mathrm{f}}$ are the states of the shaping filter which is described by state matrix $\boldsymbol{A}_{\mathrm{f}}$, input vector $\boldsymbol{B}_{\mathrm{f}}$ and output vector $\boldsymbol{C}_{\mathrm{f}}$; $\ddot{x}_{\mathrm{g}}$ is the ground motion (earthquake)

affecting the structure. Combining equations (2.9) and (2.41), the augmented model has $\boldsymbol{z}_a=\{\boldsymbol{z}\ \boldsymbol{z}_f\}^T$ as the state vector and is given by:

$$\begin{matrix}\dot{\boldsymbol{z}}_a=\boldsymbol{A}_a\cdot\boldsymbol{z}_a+\boldsymbol{B}_a\cdot\boldsymbol{f}_d+\boldsymbol{E}_a\cdot w\\ \boldsymbol{y}=\boldsymbol{C}_a\cdot\boldsymbol{z}_a+\boldsymbol{D}_y\cdot\boldsymbol{f}_d\end{matrix},\quad \boldsymbol{A}_a=\begin{bmatrix}\boldsymbol{A} & \boldsymbol{E}\cdot\boldsymbol{C}_f\\ \boldsymbol{0} & \boldsymbol{A}_f\end{bmatrix},\ \boldsymbol{B}_a=\begin{Bmatrix}\boldsymbol{B}\\ \boldsymbol{0}\end{Bmatrix},\ \boldsymbol{E}_a=\begin{Bmatrix}\boldsymbol{0}\\ \boldsymbol{B}_f\end{Bmatrix},\ \boldsymbol{C}_a=[\boldsymbol{C}_y\ \ 0] \tag{2.42}$$

In these circumstances the augmented system in (2.42) should be considered instead of the structure model in (2.9) and the shaping filter parameters should be identified for the ground motions considered. However, due to the nature of earthquake ground motions it could be difficult to identify a filter that model the earthquake characteristics. However it is usually assumed that the input ground motion is a white noise disturbance $w=\ddot{x}_g$. In the description of this strategy the structure model of equation (2.9) will be considered in the formulation instead of the augmented model in equation (2.42).

Moreover, if only a few measurements are available, the states have to be estimated and an estimator (observer) must be designed. Thus, when the system is affected by Gaussian white noise processes (disturbances and measurement noise) the so-called Linear Quadratic Gaussian (LQG) problem is formulated for this purpose. The LQG controller is then a combination of a Kalman filter (state estimator) with a Linear Quadratic Regulator (LQR) which can be designed independently according to the *separation principle* (*Skogestad & Postlethwaite 1996; Preumont 2002*). The LQG is then implemented with a clipped control algorithm for semi-active control as illustrated in figure 2.48. In this situation, the resulting controller is referred as clipped optimal control (*Dyke 1996*).

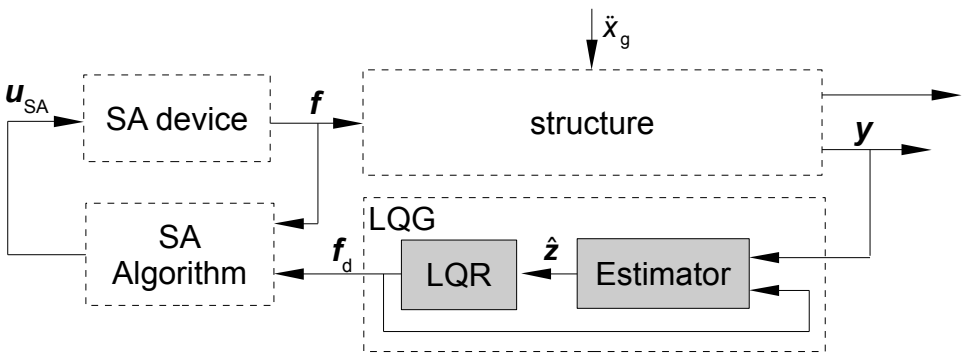

Figure 2.48 - LQG with clipped control.

In this case the control law of (2.39) will be function of the estimated state $\hat{\boldsymbol{z}}$ instead of the true state $\boldsymbol{z}$. The Kalman filter has a structure similar to the system (structure) with feedback from the measurement output $\boldsymbol{y}$:

$$\dot{\hat{\boldsymbol{z}}}=\boldsymbol{A}\cdot\hat{\boldsymbol{z}}+\boldsymbol{B}\cdot\boldsymbol{f}_d+\boldsymbol{K}_o\cdot(\boldsymbol{y}-\boldsymbol{C}_y\cdot\hat{\boldsymbol{z}}) \tag{2.43}$$

where $\boldsymbol{K}_o$ is the estimator gain matrix. The closed loop equation of the LQG problem with the estimator is given by:

$$\begin{Bmatrix} \dot{\boldsymbol{z}} \\ \dot{\boldsymbol{e}} \end{Bmatrix} = \begin{bmatrix} \boldsymbol{A}-\boldsymbol{B}\boldsymbol{K}_{\mathrm{c}} & \boldsymbol{B}\boldsymbol{K}_{\mathrm{c}} \\ \boldsymbol{0} & \boldsymbol{A}-\boldsymbol{K}_{\mathrm{o}}\boldsymbol{C}_{\mathrm{y}} \end{bmatrix} \begin{Bmatrix} \boldsymbol{z} \\ \boldsymbol{e} \end{Bmatrix} + \begin{bmatrix} \boldsymbol{E} & \boldsymbol{0} \\ \boldsymbol{E} & -\boldsymbol{K}_{\mathrm{o}} \end{bmatrix} \begin{Bmatrix} w \\ \boldsymbol{v} \end{Bmatrix} \tag{2.44}$$

where: $\boldsymbol{e}=z-\hat{z}$ is the estimation error; $w=\ddot{x}_{\mathrm{g}}$ is the process noise; and $\boldsymbol{v}$ is measurement noise. Assuming that both are white noise processes with zero mean, E[w]=0 and E[$\boldsymbol{v}$]=**0**, and covariances E[$w \cdot w^{\mathrm{T}}$]=w_0, E[$\boldsymbol{v} \cdot \boldsymbol{v}^{\mathrm{T}}$]=$\boldsymbol{V}$ and E[$w \cdot \boldsymbol{v}^{\mathrm{T}}$]=**0**, the steady-state gain matrix that minimizes the cost function is given by (*Lewis 1986*):

$$\boldsymbol{K}_{\mathrm{o}}=\boldsymbol{S} \cdot \boldsymbol{C}_{\mathrm{y}}^{\mathrm{T}} \cdot \boldsymbol{V}^{-1} \tag{2.45}$$

where $\boldsymbol{S}$ is the solution of the Riccati equation:

$$\boldsymbol{A} \cdot \boldsymbol{S}+\boldsymbol{S} \cdot \boldsymbol{A}^{\mathrm{T}}+w_0 \cdot \boldsymbol{E} \cdot \boldsymbol{E}^{\mathrm{T}}-\boldsymbol{S} \cdot \boldsymbol{C}_{\mathrm{y}}^{\mathrm{T}} \cdot \boldsymbol{V}^{-1} \cdot \boldsymbol{C}_{\mathrm{y}} \cdot \boldsymbol{S}=\boldsymbol{0} \tag{2.46}$$

The Kalman filter is designed assuming that statistical information about the disturbances w_0 and noise $\boldsymbol{v}$ are available. However, the designer can adjust the correspondent covariance matrices (w_0 and $\boldsymbol{V}$) to achieve a good compromise in estimating the state vector and control aggressiveness. If such information is not available the estimator can be designed using other techniques, like pole-placement for example, choosing the estimator poles to be a factor of 2 to 6 faster than the controller poles (*Franklin et al. 1998*).

Thus, the LQG is a dynamic system having as input the measurement $\boldsymbol{y}$ and output the desired force $\boldsymbol{f}_{\mathrm{d}}$ given by:

$$\begin{aligned} \dot{\hat{\boldsymbol{z}}} &= (\boldsymbol{A}-\boldsymbol{B} \cdot \boldsymbol{K}_{\mathrm{c}}-\boldsymbol{K}_{\mathrm{o}} \cdot \boldsymbol{C}_{\mathrm{y}}) \cdot \hat{\boldsymbol{z}}+\boldsymbol{K}_{\mathrm{o}} \cdot \boldsymbol{y} \\ \boldsymbol{f}_{\mathrm{d}} &= -\boldsymbol{K}_{\mathrm{c}} \cdot \hat{\boldsymbol{z}} \end{aligned} \tag{2.47}$$

which in terms of transfer function, the transfer matrix of the regulator $\boldsymbol{K}_{\mathrm{LQG}}$ is given by:

$$\boldsymbol{F}_{\mathrm{d}}=\boldsymbol{K}_{\mathrm{LQG}} \cdot \boldsymbol{Y}, \text{ with: } \boldsymbol{K}_{\mathrm{LQG}}=-\boldsymbol{K}_{\mathrm{c}} \cdot \left[s \cdot \mathbf{I}-\boldsymbol{A}+\boldsymbol{B} \cdot \boldsymbol{K}_{\mathrm{c}}+\boldsymbol{K}_{\mathrm{o}} \cdot \boldsymbol{C}\right]^{-1} \cdot \boldsymbol{K}_{\mathrm{o}} \tag{2.48}$$

where: $\boldsymbol{F}_{\mathrm{d}}$ and $\boldsymbol{Y}$ are Laplace transform of $\boldsymbol{f}_{\mathrm{d}}$ and $\boldsymbol{y}$ respectively; and s is the Laplace variable.

It is shown in *Skogestad & Postlethwaite 1996* that the H_2 optimization control problem which involves the minimization of the lower *linear fractional transformation* norm to derive the controller $\boldsymbol{K}$ (feedback from output) is equivalent to the LQG problem described above to determine $\boldsymbol{K}_{\mathrm{LQG}}$.

The LQR and LQG formulations presented above have been used for semi-active control in force tracking schemes. A force feedback scheme using the LQR in conjunction with the inverse model of the device was proposed by *Symans & Constantinou 1995* for one and two DOF structural systems employing semi-active fluid viscous dampers. Despite the results were not convincing about this solution, *Sadek & Mohraz 1998* made a parametric study covering a wide range of system natural frequencies and control criteria (different matrices weights) which showed the potential of this strategy for low frequency structural systems.

The LQG/H2 control was first proposed by *Dyke 1996* to derive the desired force for use in conjunction with a clipped control algorithm for semi-active control of structures employing MR dampers, as in the loop of figure 2.48. Following this work, *Dyke & Spencer 1996, Yi et al. 1999, Jansen & Dyke 2000* and *Yi et al. 2001* explored the use of this strategy with more dampers. *Christenson 2001* studied in his thesis the coupled building problem using semi-active devices. The clipped-optimal H2/LQG control was proposed as a semi-active control strategy for coupled building and the results of numerical simulations showed that semi-active strategy provides better performance than the passive one. The application of this strategy to the study of asymmetric buildings under torsional motions due earthquake ground motions was investigated by *Yoshida 2003*. MR devices were used for this purpose and the clipped optimal control and a modified version were used. Both numerical and experimental studies were conducted and the results showed that the performance of a semi-active controller using MR dampers was significantly better than using passive control (*Yoshida et al. 2003*). The strategy was also verified numerically in full scale asymmetric buildings: a nine story building and a L-shaped 8-story building (*Yoshida & Dyke 2005*); and in asymmetric structures with different mass distributions per floor (*Gattulli et al. 2008*). In base isolated structures *Yoshioka et al. 2002* and *Ramallo et al. 2002* implemented the clipped optimal control strategy for controlling the behaviour of MR devices installed at the base level, for response reduction due to earthquakes when subjected to far-field and near-field earthquake excitations. In the same subject *Shook et al. 2007* considered a similar strategy under the possibility of using a variable gain controller. The clipped optimal control strategy is accepted nowadays and is being also considered for comparison with more recent control strategies (*Wang 2006, Lee et al. 2008, K-Karamodin and H-Kazemi 2010*).

2.9.4 Lyapunov based methods

Feedback control laws can be established using the Lyapunov stability theory. This approach requires the definition of a Lyapunov function (system function) denoted as $V(\boldsymbol{z})$, which must be a positive definite function of the states ($\boldsymbol{z}$) of the system (see general models in section 2.7). Typically these functions are quadratic functions of the system variables (or states):

$$V(\boldsymbol{z}) = \sum_{j} \boldsymbol{v}_j^T \boldsymbol{P} \boldsymbol{v}_j \tag{2.49}$$

where $\boldsymbol{v}_j$ are vectors of variables (related with the states $\boldsymbol{z}$) and $\boldsymbol{P}$ is a positive definite matrix (that results from the system function or is defined). Assuming that the origin is a stable equilibrium point, according to Lyapunov stability theory (second method), if the rate of change of the Lyapunov function $\dot{V}(\boldsymbol{z})$ is negative semi-definite, then the origin is stable in the sense of Lyapunov. Thus, in developing the control law, the goal is to choose input control variables for each device that will result in $\dot{V}(\boldsymbol{z})$ as negative as possible. Several

control laws have been established using the Lyapunov stability theory and in general those laws result in Heaviside step functions family:

$$u_{SA,i} = u_{SA,max} \cdot H\left[f_L(\boldsymbol{z}, \boldsymbol{f})\right],\ u_{SA,min} \leq u_{SA} \leq u_{SA,max} \tag{2.50}$$

where $f_L(\boldsymbol{z}, \boldsymbol{f})$ is a unidimensional function of the states and inputs.

An infinite number of Lyapunov functions may be selected which may result in a variety of control laws. Some of the proposed laws are: Bang-Bang control (also defined as control based on Lyapunov stability theory) which considers a quadratic system function; Decentralized Bang-Bang control which considers the total vibratory energy as the system function; and the Maximum Energy Dissipation which considers the relative vibratory energy of the structure as the system function. *Dyke & Spencer 1997* and *Jansen & Dyke 2000* considered these strategies for vibration control of porch structures prototypes using MR dampers. Significant reductions in terms of relative displacements and accelerations were obtained when compared to the uncontrolled case, although in some cases the passive case surpasses these semi-active ones. An analytical study covering both damping and stiffness changes using the Lyapunov stability theory to derive the control law was carried out by *Luo et al. 2001*. They proposed the adjustment of both damping and stiffness of the base and first floor of base-isolated structures. A numerical example of a 10-storey base-isolated structure was considered and reductions of base displacements and inter-storey drifts were found to be better than the passive case.

2.9.5 Modulated Homogeneous Friction

A force tracking scheme used with variable friction devices was adapted for use with MR dampers by *Dyke & Spencer 1997*. Originally proposed by *Inaudi 1997*, this strategy was considered due the strong similarities between the behaviour of variable friction devices and MR dampers. It consists in a control law to derive the desired force and a clipped algorithm to define the device control variable. In this approach, the control law is given by:

$$\begin{gathered} f_d = -g \cdot \left|P\left[\Delta(t)\right]\right| \\ P\left[\Delta(t)\right] = \Delta(t-s),\ s = \left\{\min x \geq 0 : \dot{\Delta}(t-x) = 0\right\} \end{gathered} \tag{2.51}$$

where g is a proportional gain to be defined and $\Delta(t\text{-}s)$ is the most recent local extrema in the deformation. The clipped control algorithm adopted is:

$$u_{SA} = u_{SA,max} \cdot H\left[f_d - |f|\right],\ u_{SA,min} \leq u_{SA} \leq u_{SA,max} \tag{2.52}$$

In the works of *Dyke & Spencer 1997* and *Jansen & Dyke 2000* this scheme was considered for reducing earthquake induced vibrations of structural models employing MR dampers. Smaller relative displacements were obtained than the best passive case although a small increase in the accelerations was verified.

2.9.6 Force Derivative Feedback

Force-feedback control received great attention in the active cable control of cable-stayed bridges where the concept of integral force feedback was introduced. The same approach was considered in active vibration isolation as an alternative way of the acceleration feedback controller. The resulting control law for feedback is given by the integral of the transmitted force (*Preumont 2002*). In semi-active control a feedback control law given by the derivative of the MR passive device force is considered to evaluate the desired force:

$$f_{\mathrm{d}} = -g \cdot \dot{f}_{MR,s} \tag{2.53}$$

where g is a positive constant gain. This control law in conjunction with a force tracking scheme based on the inverse model of the MR device was proposed by *Rodríguez et al. 2012* for seismic protection of base-isolated buildings. To implement this strategy a pair of MR dampers installed in parallel are needed: one working in passive mode with a force transducer in series, which will be used as sensor $f_{\mathrm{MR,s}}$; and another working semi-actively that tries to follow the desired force of (2.53) by modifying the control variable (electric current) according to the tracking scheme. The proposed strategy was considered for evaluation in a benchmark base-isolated structure. Reductions in relative displacements without increasing the accelerations were found.

2.9.7 Sliding Mode Control

Sliding mode control (SMC) is a robust nonlinear control strategy that forces the system to reach a sliding surface in a finite time and remain there by switching the control structure. The basic idea is to design a variable structure control law that restricts the evolution of the system states to a required dynamic, usually denominated by the switching surface or sliding surface. The main advantages of this method are: i) able to deal with uncertainties, modelling errors and disturbances; ii) the dynamic behaviour of the system is simplified by the dynamic defined by the sliding surface; iii) has the ability to specify the closed-loop desired performance through the sliding surface dynamics. One referred disadvantage is that the higher commutation frequency between the control laws could excite the non modelled modes and increase the model errors which could also destabilize the system. The method requires the design of a sliding surface and a switched feedback control law to make the state trajectory to reach the surface and to maintain in it afterwards until slide back to the origin (*Utkin 1992; Khalil 2002*).

This type of controller was evaluated numerically by *Cho 2004* in building structures and bridges employing MR dampers and was also compared with other control algorithms. *Moon et al. 2003* also tested this type of controller on a bridge benchmark structure employing MR dampers. *Qing et al. 2003* synthesized a variable structure controller (sliding mode controller)

based on the 'reaching law' method to evaluate its efficiency on semi-active MR dampers in reducing structural vibrations induced by earthquakes. This strategy was also considered by *Komatsu et al. 2007* for controlling a base-isolated building employing semi-active fluid viscous dampers in Japan and better performances in terms of acceleration for the same level of displacements were obtained when compared with the passive case.

2.9.8 Quantitative Feedback Theory

Quantitative feedback theory (QFT) is a frequency domain technique to achieve a desired robust design over a specified region of the system uncertainty. QFT is based in the fact that feedback is needed in control because of plant uncertainties, parameters and/or disturbances, which lead to exceeding the acceptable system performance uncertainty. QFT has been developed for: highly uncertain linear time invariant (LTI) SISO (single input single output) and MIMO (multiple input multiple output) systems; nonlinear and time-varying SISO and MIMO plants and for plants with distributed control inputs and sensors; single and multiple-loop dithered non-linear (adaptive) systems with LTI plants and for a special class of non-linear compensation; non-minimum-phase (NMP) MIMO plants, plants with both zeros and poles in the right half-plane and LTI plants with incidental hard non-linearities such as saturation (*Horowitz 2001*).

This control technique was considered for vibration control of structures and in particular structures employing MR dampers by *Villamizar et al. 2004*. The control strategy followed the force tracking scheme in which a QFT controller plus a clipped control algorithm were considered and thus the MR model was not considered for controller design. Numerical simulations and experimental tests on reduced models showed the advantages of applying this technique on real structures (*Mejía 2005*). A step forward was done by *Zapateiro 2009* and *Zapateiro et al. 2010* who introduce the device dynamics in the formulation by treating the nonlinear terms of the device as uncertainties leading to a controller design with plant uncertainties.

2.9.9 Backstepping control

Backstepping is a design procedure developed for a special class of nonlinear dynamic systems and which interlaces the choice of a Lyapunov function with the design of feedback control laws. It consists in breaking the design problem for the full system into a sequence of design problems for lower order subsystems, and in the final a feedback design is achieved. Backstepping can solve stabilization, tracking and robust control problems (*Khalil 2002*).

This control strategy was considered by *Mejía 2005* in a 10-storey base isolated numerical example and experimentally on a 6 storey model with MR dampers, showing better reductions than the passive case. *Luo et al. 2006, Zapateiro 2009* and also *Zapateiro et al. 2010* considered the backstepping control strategy to control the force of a MR damper in the

same structural models but their formulation was improved in terms of robustness by applying adaptation laws to the structural uncertain parameters of the system.

2.9.10 Fuzzy Logic

Intelligent paradigms like fuzzy logic have been also considered to control semi-active devices installed in structural systems. Fuzzy logic was originally introduced in the 1960s with the proposal for the fuzzy set theory and has been applied in many fields. It is based on the human logic used for the resolution of common problems and resulted from the fact that humans usually have to deal with undefined or non-existent information. In the field of control engineering the idea is to develop a controller using a set of rules to deal with the feedback information in order to define the control input.

This strategy was studied by *Loh et al. 2003* to control MR dampers installed on a bridge and the results of numerical simulations showed that the established control algorithm is useful in reducing displacement and acceleration responses. *Kim et al. 2006* used neuro-fuzzy models to describe the dynamic behaviour of a base isolation system consisting of a single degree of freedom system supported in a friction pendulum system (FPS) with MR dampers. A fuzzy logic controller to modulate the voltage of the MR damper was developed using the absolute acceleration and relative displacement as inputs. Through numerical simulations and experimental tests they showed that the proposed semi-active system perform better than the passive cases. *Shook et al. 2007* also considered fuzzy logic for controlling MR dampers installed in a base isolated system and good performance was found specially when the structure is subjected to earthquakes with large accelerations.

2.9.11 Neural Network

Another intelligent paradigm considered for control purposes is the neural network mathematical structure. Neural networks (NN) have their origins in the way how human brain works and consist in a finite number of neurons organized through a finite number of layers, interconnected, that relate the inputs with the outputs. Each neuron is a processing unit that evaluates an output based on the inputs from the outputs of lower layer neurons. Several weighing coefficients are used in these relationships, which are afterwards adjusted during the training phase using experimental data. A cost function is used as criteria to evaluate the neural network performance. When used for control purposes this cost function is always quadratic and function of the states.

The neural network approach for structural vibration control was first proposed by *Ghaboussi & Joghataie 1995* and *Chen et al. 1995*. Afterwards it has been considered for semi-active control by several researchers. *Bani-Hani & Sheban 2006* proposed a semi-active neuro-controller (SANC) to modulate the MR damper input voltage in order to mitigate structural vibrations. The SANC was trained using an inverse neural network model (INV-MR) that

replicates the inverse dynamics of the MR damper and a linear quadratic Gaussian (LQG) algorithm. The INV-MR was developed using the analytical Bouc-Wen model of the MR damper and was used to determine the control voltage in order to replicate the desired force estimated by the LQG. The strategy was evaluated on a 6 degree-of-freedom base isolated structure. Better performances than the passive case were found for a wide range of input ground motions. A similar approach was used later on by *K-Karamodin and H-Kazemi 2010*. In this study the researchers used a neural network predictive control algorithm (NNPC) to determine the required voltage for the MR damper to replicate the control force estimated by LQG controller. The LQG and NNPC system were then used to train a semi-active neuro-controller (SANC). With this approach the control voltage is evaluated directly at a lower computational cost. NNPC consists of a neural network model of MR damper (NNMR) with predictive capabilities which is trained using a modified Bouc-Wen model. The algorithm was simulated using on 3-story full-scale nonlinear building excited at the base. The results showed that SANC performed better than other tested controllers (passive and clipped optimal control) and is able to deal with moderate and severe seismic events.

A force tracking scheme using a neurocontroller and a clipped algorithm was proposed by *Lee et al. 2006.* The neurocontroller was evaluated using a training algorithm based on a cost function and sensitivity evaluation algorithm. This concept was applied to a benchmark building with a linear elastomeric isolation system and the results of numerical simulations showed that the proposed scheme can reduce the floor acceleration, base shear and building corner drift with a slight increase of base displacement.

Shook et al. 2007 proposed a NEURO–MR controller consisting of a simplified Bouc–Wen model and a neural-network for vibration mitigation of a base isolated structure employing MR dampers. The responses of the structure and command voltage for the MR damper from the previous three time steps are selected as the input nodes of the NEURO–MR network and the output is the optimal MR damper voltage signal. This approach was found to be effective in minimizing the acceleration of the superstructure that was subject to moderate excitations.

2.9.12 Clipped control

This section describes some algorithms used in force feedback tracking schemes that must be implemented in conjunction with a control strategy, as those described previously. It can be used with any type of semi-active device since no model of the device is needed for implementation. The controller is designed to compute the desired control force and the algorithm (clipped control) makes the device to replicate the desired force (see figure 2.49). This strategy was first proposed by *Dyke 1996* (see also *Dyke et al. 1996(a), Dyke et al. 1996(b), Spencer Jr. et al. 1996*) with an LQG/H2 control strategy to compute the desire

force and a clipped algorithm to select the command signal of a single MR damper in a structural system. *Dyke & Spencer 1996* extended the control algorithm for controlling multiple MR devices and a numerical study demonstrating the efficacy of the control algorithm was presented. *Yi et al. 1999, Jansen & Dyke 2000* and *Yi et al. 2001* verified the performance of this algorithm numerically and experimentally on a six storey porch structure. This strategy has been common in semi-active control and several clipped control algorithms and modifications have been applied in control loops.

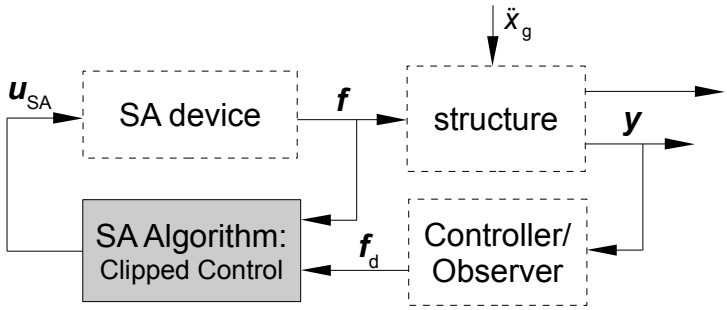

Figure 2.49 - Clipped control in the control loop.

Original Clipped Control Algorithm

This algorithm is based on the two-position or on-off control action (*Ogata 1970*) where the control law is dependent on the actuating error signal (difference between the desired and the device force). The control variable should be selected by the following procedure: if the ith damper device is providing the desired force (f=f_d), the control variable damper should remain at the present level; on the other hand, if the magnitude of the force produced by the damper is smaller than the magnitude of the desired force and the two forces have the same sign, the control variable is increased to the maximum level u_{max}, so as to increase the force produced by the damper to track the desired one. Otherwise, the control variable is set to the minimum value u_{min}. This algorithm is graphically represented in figure 2.50, where u_c takes the maximum value u_{max}, and can be stated as (*Dyke 1996*):

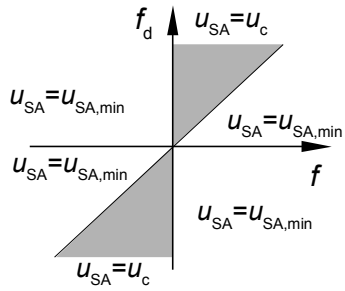

Figure 2.50 - Clipped Control algorithm graphical representation.

$$u_{SA}=u_{SA,max}\cdot \mathrm{H}[(f_d-f)f],\ u_{SA,min}\leq u_{SA}\leq u_{SA,max} \tag{2.54}$$

To avoid abrupt transitions between the minimum and maximum values a continuous version of this law is stated as (*Preumont 2002*):

$$u_{SA}=\mathrm{sat}_p\left[u_{SA,min}+g\left(|f_d|-|f|\right)\right]\cdot \mathrm{H}[f_d\cdot f],\ u_{SA,min}\leq u_{SA}\leq u_{SA,max}$$
$$\text{with: } \mathrm{sat}_p(x)=\begin{cases} u_{SA,min}, & \text{for } x\leq u_{SA,min} \\ x, & \text{for } u_{SA,min}\leq x\leq u_{SA,max} \\ u_{SA,max}, & \text{for } x>u_{SA,max} \end{cases} \tag{2.55}$$

where: $u_{SA,min}$ is a bias input that aims to increase the working band; g is a proportional gain. Taking $u_{SA,min}$=0 and g very large, the on-off version of the algorithm is obtained (equation 2.54).

Modified Versions

In some situations when the dominant frequencies of the system under control are low, large changes in the forces applied to the structure may result in high local acceleration values. *Yoshida & Dyke 2004* proposed a modification of the original clipped control algorithm to reduce this effect consisting in continuously changing the control variable. Thus, u_c is determined using a linear relationship with a slope μ obtained as the relationship between $u_{SA,max}$ and f_{max}. When the desired force is larger than the maximum force that the device can produce, the maximum voltage is applied. This modified clipped-optimal control algorithm is graphically represented in figure 2.50 and is given by:

$$u_{SA}=u_c\cdot \mathrm{H}\left[(f_d-f)f\right],\ u_{SA,min}\leq u_{SA}\leq u_{SA,max}$$
$$\text{with: } u_c=\begin{cases}\mu\cdot f_d & \text{for } |f_d|\leq f_{max}\\ u_{SA,max} & \text{for } |f_d|>f_{max}\end{cases};\quad \mu=\frac{u_{SA,max}}{f_{max}} \tag{2.56}$$

With this modification, *Yoshida & Dyke 2004* showed that is possible to reduce the peak accelerations significantly.

The previous modified clipped control algorithms could reduce the peak accelerations significantly but this modification from the original clipped control algorithm might increase the peak drifts slightly. Another modified version of this algorithm to solve this issue was proposed by *Jung et al. 2006*. They suggested that the region of graph where the device is activated should be divided as graphically represented in figure 2.51 and expressed by the following equation:

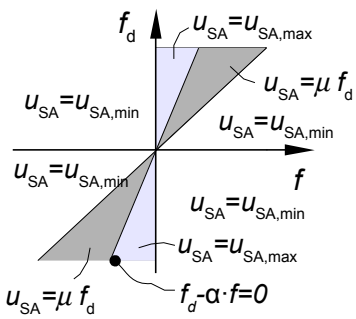

Figure 2.51 - Modified Clipped Control law graphical representation (*Jung et al. 2006*).

$$u_{SA}=u_c\cdot \mathrm{H}\left[(f_d-f)f\right],\ u_{SA,min}\leq u_{SA}\leq u_{SA,max}$$
$$\text{with: } u_c=\begin{cases}\mu\cdot f_d & \text{for } |f|\leq|f_d|<\alpha|f|\\ u_{SA,max} & \text{for } |f_d|\geq\alpha|f|\end{cases};\quad \mu=\frac{u_{SA,max}}{f_{max}};\quad \alpha>1 \tag{2.57}$$

where α is the coefficient to be properly selected. In their work, *Jung et al. 2006* proposed α=2 and the results obtained showed that this modified version of the clipped control algorithm performs slightly better than the others.

Other version of the algorithm was proposed by *Aguirre et al. 2011* which is described by:

$$u_{SA}=\mathrm{h}\left[(f_d-f)f\right],\ 0\le u_{SA}\le u_{SA,max}$$
$$\text{with}:\ \mathrm{h}(x)=\begin{cases}0 & \text{for } x\le 0\\ k_u\cdot x & \text{for } 0\le x\le u_{SA,max}/\mathrm{k}_u\\ u_{SA,max} & \text{for } x\ge u_{SA,max}/\mathrm{k}_u\end{cases} \tag{2.58}$$

where: k_u is a design parameter. In their case k_u=1 was chosen. This algorithm is similar to the one of *Preumont 2002* (equation 2.55) when $u_{SA,min}$=0 and k_u=1.

2.10 Final Remarks

Semi-active control has been considered for vibration mitigation of civil engineering structures when subjected to earthquake loads, thus contributing to vulnerability reductions and consequently to the seismic risk reduction. In solving semi-active control problems, the resulting system is always nonlinear, is subjected to unknown disturbances (earthquake motion) and has bounded input control variables. Control strategies that can handle with all these system characteristics are thus desired. However, due to the difficulties in dealing with all those aspects, the problem is always solved considering several assumptions to use a set of procedures to tackle each sub-problem separately. This chapter showed a review of the topics associated with semi-active systems for vibration mitigation of earthquake induced responses in civil engineering structures.

Chapter 3

Semi-Active Control Strategies

- Theoretical basis and numerical simulations -

Summary

In this chapter control strategies are explored to manipulate semi-active devices for reducing structural responses of base-isolated buildings. Nine force tracking schemes, a Lyapunov based control law, a nonlinear output feedback control strategy and the sliding mode control strategy are described and formulated to solve this type of problems. The modulated homogeneous friction, the integral controller, the linear quadratic regulator and the model predictive controller are considered to derive a desired force on force tracking schemes. The algorithms considered to “clip” the control variable are: the inverse model of the damper and on-off algorithms. For analysis of those strategies mathematical models representative of the base-isolated structures and of the devices are considered. A single degree of freedom (SDOF) mechanical model is first adopted to analyse the applicability of these strategies in structures. A more realistic model, a typical 10-storey base-isolated building (multi degree of freedom model - MDOF) is then considered for performance evaluation. The Maxwell model is adopted as a general way to model the transient and stationary regime of SA devices. Several earthquake ground motions (near- and far-field) for the Portuguese territory have been considered in the analysis. A methodology to tune the controller using the system model and the seismicity of the site is considered as adequate. Comparisons with the original structure and with the structure employing optimized passive devices are made. Using the SDOF structural model it is shown that the proposed strategies are adequate for lower fundamental frequency structures and thus for base-isolated buildings. This is also verified on the MDOF structural model The results show that base-isolated structures employing SA systems can outperform the original structure as well as the one with the best passive solution.

3.1 Problem Description

Hybrid base-isolated buildings consist of a superstructure constructed over a base floor. The superstructure is supported by bearings with devices (passive or semi-active) installed at the base level. This solution is currently being considered to reduce relative displacements and maintain or reduce the responses at the superstructure. In this work semi-active devices with variable damping characteristics are proposed as a better solution for this purpose. Different control strategies to manipulate the devices are proposed, described and verified numerically using the Matlab/Simulink environment. A fixed time step of 1 ms was used. The proposed solutions are compared with the original structure (no devices) and with the structure employing passive devices. Several parameters are considered for performance evaluation, namely peak responses. Furthermore, input ground motions for the Portuguese territory from Eurocode 8 are used as input disturbances in the mathematical models. The following mathematical models are considered:

1. Structural Models: lumped-mass models (spatial models) described by mass, stiffness and damping properties;
2. Passive device: a power velocity law was considered to describe the force-velocity relationship of typical fluid viscous dampers;
3. Semi-active (SA) devices: the Maxwell model with a variable damping device and a fixed time constant is used to model a generic dissipative device.

3.1.1 Structural Models

The structural models considered here for base-isolated structures are linear time and invariant (LTI) systems. Recalling the formulation in section 2.7, the system of equations is given by (equation 2.5):

$$\boldsymbol{M}\cdot\ddot{\boldsymbol{x}}_{rg}+\boldsymbol{C}\cdot\dot{\boldsymbol{x}}_{rg}+\boldsymbol{K}\cdot\boldsymbol{x}_{rg}=-\boldsymbol{M}\cdot\boldsymbol{1}\cdot\ddot{x}_g+\boldsymbol{G}\cdot f_{ad} \tag{3.1}$$

where: $\boldsymbol{x}_{rg}$ is the vector of relative displacements at each floor (degree-of-freedom) to the ground, with the respective time derivatives, relative velocity and relative acceleration; f_{ad} describes the forces developed by additional devices at the base level; $\ddot{x}_g$ is the input ground motion (acceleration); $\boldsymbol{1}$ is a unitary column vector; $\boldsymbol{G}$=[-1 0…0]^T is the matrix that defines the input forces location which in this case is at the base; $\boldsymbol{M}$, $\boldsymbol{C}$ and $\boldsymbol{K}$ are the mass, damping and stiffness matrices respectively. The model is described in the state-space form by (equation 2.9):

$$\begin{matrix}\dot{\boldsymbol{z}}=\boldsymbol{A}\cdot\boldsymbol{z}+\boldsymbol{B}\cdot f_{ad}+\boldsymbol{E}\cdot\ddot{x}_g\\ \boldsymbol{y}=\boldsymbol{C}_y\cdot\boldsymbol{z}+\boldsymbol{D}_y\cdot f_{ad}\end{matrix},\quad \boldsymbol{A}=\begin{bmatrix}\boldsymbol{0} & \boldsymbol{I}\\ -\boldsymbol{M}^{-1}\cdot\boldsymbol{K} & -\boldsymbol{M}^{-1}\cdot\boldsymbol{C}\end{bmatrix},\ \boldsymbol{B}=\begin{Bmatrix}\boldsymbol{0}\\ \boldsymbol{M}^{-1}\cdot\boldsymbol{G}\end{Bmatrix},\ \boldsymbol{E}=\begin{Bmatrix}\boldsymbol{0}\\ -\boldsymbol{1}\end{Bmatrix} \tag{3.2}$$

where: $\boldsymbol{z}$ is the state vector; $\boldsymbol{y}$ is the output vector; $\boldsymbol{A}$ is the state matrix; $\boldsymbol{B}$ and $\boldsymbol{E}$ are input

vectors; $\boldsymbol{C}_y$ is the output matrix; $\boldsymbol{D}_y$ is the feedthrough vector; **0** and **I** are null and identity matrices respectively. With $\boldsymbol{C}_y=\boldsymbol{A}$ and $\boldsymbol{D}_y=\boldsymbol{B}$ the outputs quantities will be the relative velocities and absolute accelerations.

Common base isolation systems are designed to have natural frequencies bellow 1 Hz and damping ratios around 0,1. SDOF mathematical models with natural frequencies ranging between 0,25 and 1 Hz with a damping ratio of 0,1 and a mass of m=5750 kg were first considered to analyse the applicability of these strategies.

SDOF model

The SDOF model in building modelling is a mathematical idealization of the structure which represents some key response characteristics of the building behaviour (*Soong & Dargush 1997*) - figure 3.1. It can be used to model the behaviour of the first mode of vibration of the structure. In practical terms this model can represent the behaviour of base isolated structures (e.g. building supported by bearings) where the superstructure is considered as a rigid body. The simplest way to model a base-isolation system is to consider a linear elastic and viscous damping elements ($\boldsymbol{K}=k_b$ and $\boldsymbol{C}=c_b$) and the rigid mass that represents the whole mass of the superstructure ($\boldsymbol{M}=m$). A device is connected to this mass which develops a force f_{ad} and an input ground motion x_g excites the model. Equation (3.1) is reduced to the following equation:

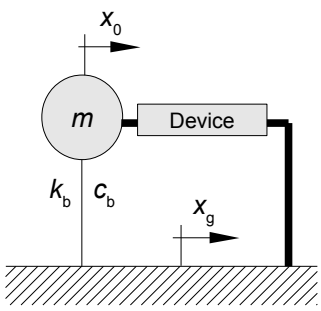

Figure 3.1 - SDOF model schematic representation.

$$m\cdot\ddot{x}_{0g}+c_b\cdot\dot{x}_{0g}+k_b\cdot x_{0g}=-m\cdot\ddot{x}_g-f_{ad} \tag{3.3}$$

where $x_{0g}=x_0-x_g$ is the relative displacement to the ground, with the respective time derivatives, relative velocity and relative acceleration. The state-space equation of the model is given by:

$$\begin{matrix}\dot{\boldsymbol{z}}=\boldsymbol{A}\cdot\boldsymbol{z}+\boldsymbol{B}\cdot f_{ad}+\boldsymbol{E}\cdot\ddot{x}_g\\ \boldsymbol{y}=\boldsymbol{C}_y\cdot\boldsymbol{z}+\boldsymbol{D}_y\cdot f_{ad}\end{matrix},\quad \boldsymbol{A}=\begin{bmatrix}0 & 1\\ -k_b/m & -c_b/m\end{bmatrix},\ \boldsymbol{B}=\begin{Bmatrix}0\\ -1/m\end{Bmatrix},\ \boldsymbol{E}=\begin{Bmatrix}0\\ -1\end{Bmatrix} \tag{3.4}$$

where: $\boldsymbol{z}=\{x_{0g}\ \dot{x}_{0g}\}^T$ is the state vector; and $\boldsymbol{C}_y$ and $\boldsymbol{D}_y$ are defined according to the quantities for output $\boldsymbol{y}$. The roots of the characteristic equation of (3.3) or the eigenvalues of $\boldsymbol{A}$ in (3.4), also denominated as the poles of the SDOF system, are given by:

$$\begin{aligned}s_{1,2}&=-\frac{c_b}{2\cdot m}\mp\sqrt{\left(\frac{c_b}{2\cdot m}\right)^2-\frac{k_b}{m}}\\ &=-\omega_b\cdot\xi_b\mp\omega_b\sqrt{\xi_b^2-1}\end{aligned} \tag{3.5}$$

whose modal properties (natural frequency and damping ratio) are given by:

$$f_b=\frac{\omega_b}{2\cdot\pi},\quad \omega_b=\sqrt{\frac{k_b}{m}},\quad \xi_b=\frac{c_b}{2\cdot m\cdot\omega_b};\tag{3.6}$$

Physical systems, i.e. with constants m, k_b, c_b, f_b, $\xi_b \in \mathbb{R}^+$, are always stable (the roots given by (3.5) have always negative real parts) and are also output (absolute base acceleration, with $\boldsymbol{C}$=[-k_b/m -c_b/m] and $\boldsymbol{D}$=-1/m) and state (relative displacement and velocity) controllable since the correspondent controllability matrices $\boldsymbol{C}_o$ and $\boldsymbol{C}_s$ have full rank (*Ogata 1970*):

$$\boldsymbol{C}_o=[\boldsymbol{C}\cdot\boldsymbol{B}\ \ \boldsymbol{C}\cdot\boldsymbol{A}\cdot\boldsymbol{B}\ \ \boldsymbol{D}];\ \ \boldsymbol{C}_s=[\boldsymbol{B}\ \ \boldsymbol{A}\cdot\boldsymbol{B}]\tag{3.7}$$

3.1.2 Passive Device Formulation

One way to dissipate the seismic energy is by including additional passive dissipation energy systems. In this work, the focus was put on fluid viscous damper type as elements of additional energy dissipation systems. This strategy was used to verify the effectiveness of the proposed semi-active control strategies. The passive fluid viscous damper has the following constitutive law:

$$f_p=c_p\cdot|\dot{x}_r|^{\alpha}\cdot\mathrm{sgn}(\dot{x}_r)\tag{3.8}$$

where: c_p is the damping coefficient, α is the velocity exponent; $\dot{x}_r=\dot{x}_{0g}$ is the relative velocity between the cylinder case and the piston head of the damper that is $\dot{x}_{0g}$ when associated to the structural models; and f_p is the force developed by the passive device, which is accounted in the models described previously as f_{ad}=f_p. Typical values for the velocity exponent for seismic applications are α<1. Recent technological developments made available devices with velocity exponents α=0,15 (*Castellano et al. 2004*). Notice that for α=1 the model reduces to the classical dashpot model. In this work we will consider devices with exponents less or equal to one ($\alpha\leq$1) and damping coefficients that lead to the whole system (structure plus passive device) best performance.

3.1.3 SA device Formulation

The semi-active (SA) device considered in this chapter is intended to be representative of general energy dissipation devices, like the fluid viscous dampers or the magneto-rheological devices described in the previous chapter. As any system, these devices are represented by a transient and a stationary regime. The first one is related with device time response, the time to develop the device force (stationary regime) after the command to change its characteristics. It is related with each component that is part of the device, for example: current controller, electrovalves, device, etc. This time response, also referred as the total time delay, can be described as the sum of pure time delays (or dead time) and lag (or phase delay), which are also designated as static and dynamic response time respectively (*Symans & Constantinou 1995*).Time delays can change during operation (as the control variable

increases or decreases) and an average time delay considering both operation processes is usually taken. In this work the device total time response (or delay) is accounted as lag and a first order dynamic system is considered for the device response. In what concerns to the stationary regime each type of device is represented by a specific model (see previous chapter, p.ex. FVD dampers or MR dampers), which describes the energy dissipated by the device. To describe these phenomena the classical dashpot model with an equivalent damping value is considered in this chapter. Thus, taking both regimes into account the device model results in the classical Maxwell model:

$$f_{SA} + T_d \dot{f}_{SA} = c_v \cdot \dot{x}_r, \quad c_{min} \leq c_v \leq c_{max} \tag{3.9}$$

where: c_v is the viscous damping that can be changed between c_{min} and c_{max}; T_d is the relaxation time or time lag, representing the response of the semi-active device; f_{SA} is the device force which is accounted in the models described previously as f_{ad}=f_{SA}; and $\dot{x}_r = \dot{x}_{0g}$ is the relative velocity between the cylinder case and the piston head of the damper.

The type of device and the available solutions will determine the values of the time constant T_d and of the range of variable damping coefficients [c_{min}, c_{max}], which by themselves have influence on the whole system performance. In previous works several values have been considered. *Sadek & Mohraz 1998* considered a damping ratio between 5 % and 40 % (of the structure first mode of vibration). *Gavin & Aldemir 2005* referred damping ratio ranges between 6 % and 54 % or even between 9 % and 87 %. Other experiments performed referred values that can manipulate the first mode damping ratio between 5 % and 16 %, approximately (*Symans & Constantinou 1995*, *Komatsu et al. 2007*). In this work a range of damping between 5 % and 45 % of the critical damping is considered based on the results of a preliminary study where it was found that higher damping values for c_{max} do not provide significantly performance improvements. Concerning to the time constant, previous experimental works referred time constants around T_d=50 ms for the SA fluid dampers (*Symans & Constantinou 1995*, *Komatsu et al. 2007*) and around T_d=6 ms for MR devices (*Dyke & Spencer 1997*). A time constant T_d=50 ms was considered in this work.

3.1.4 Earthquake Ground Motions

The input actions considered in this chapter are representative of two different types of ground motions for the Portuguese territory: near and far field. Artificial accelerograms were generated using the response spectrums provided in the Eurocode 8 for Portugal (*Eurocodigo8 2010*) for Type 1 (far field) seismic action and Type 2 (near field) seismic action. Ten accelerograms were generated for each spectrum of the horizontal component of the seismic action. The accelerograms were generated under the following assumptions:

- for zone 1, which corresponds to a reference peak ground acceleration of a_{gR}=2,5

m/s^2; other zones would lead to inferior values of the reference ground acceleration;

- for soil type D, which is the one that leads to the highest response spectra acceleration response, soil parameters are S=1,35 for type one seismic action and S=1,8 for type two seismic action; S=1,5 was considered for both seismic actions;
- a class II importance was considered for which a correspondent importance factor γ_I=1 is used to multiply the seismic action; this unitary importance factor corresponds to T_r=475 years of return period for the design seismic action; if other return period was considered the correspondent importance factor should be taken into account according to the seismic action type (see *Eurocodigo8 2010*), which ranges from 0,65 to 1,95 for type one seismic actions and from 0,75 to 1,5 for type two seismic actions for return periods from 283 to 1303 years for the design seismic action;
- the structural damping is assumed to be ξ=5 % which corresponds to a damping correction factor η=1 in the definition of the response spectra; higher damping coefficients lead to inferior damping correction factors, given as $\eta=[10/(5+\xi)]^{1/2}$.

The values used to define the response spectra are presented in figure 3.2.

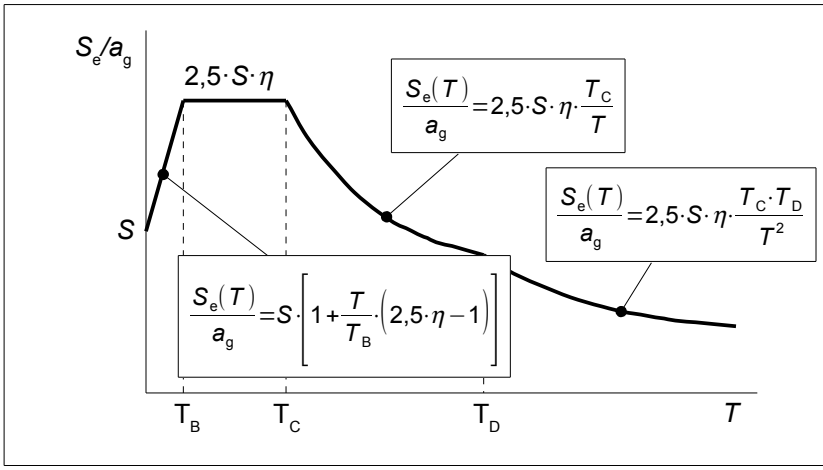

Param.	Type 1	Type 2
a_{gR} (m/s^2)	2,5	2,5
γ_I	1	
$a_g=\gamma_I\cdot a_{gR}$ (m/s^2)	2,5	2,5
S	1,5	1,5
η	1	1
T_B (s)	0,1	0,1
T_C (s)	0,8	0,3
T_D (s)	2,0	2,0

Figure 3.2 - General form of the elastic response spectra for horizontal ground motions and the values used to define the type 1.1 and type 2.1 spectra.

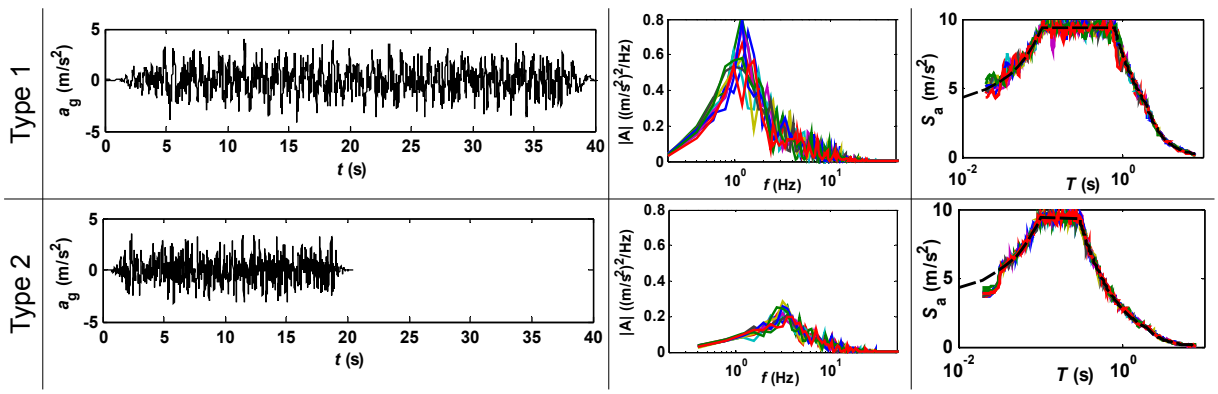

Figure 3.3 - Input ground motions considered. Left: one of ten artificial accelerograms; Middle: frequency spectra of 10 accelerograms; Right: response spectra of 10 accelerograms.

One example of the generated artificial accelerograms, the power spectral density of each one and the resulting response spectrums are presented in figure 3.3. It is shown that the generated accelerograms match the Eurocode National Annex. It can be seen also that type 1 input action has a longer duration, is richer in the lower frequencies (or higher periods) and has higher amplitudes.

3.1.5 Evaluation Criteria

In order to analyse the performance of the structural systems under study, the time responses in terms of relative displacements, absolute accelerations, device force and base shear force resulting from each accelerogram as input were used to extract the peak values. Using the peak values from the 10 responses, the mean value is evaluated and used as a representative value of the system response for each type of seismic action. The systems being analysed are the original structure (structural model only), the structure employing passive devices (with fixed damping value) and the structure employing the SA devices. The ratios of mean peak responses in relation to the original structure ones are used to evaluate the structure performance with additional systems. Ratios higher than 1 indicate that the response of the structure with additional systems is bigger than that of the original structure. Good performance is thus associated with smaller ratios. Table 3.1 summarizes the structural responses evaluation criteria considered herein.

Parameter	Description
x	Specific time response x: x_{ig} - relative displacement of floor i to the ground; a_i - absolute acceleration of floor i; f - device force; V – base shear force;
Px	Peak responses of x for one accelerogram;
Mx	Mean of peak responses of x from 10 accelerograms of the same type as input;
Rx	Ratio of mean of peak responses of x for a specific solution, passive or semi-active, relative to the mean of peak responses of x for the original structure, from 10 accelerograms of the same type as input;

Table 3.1 - Structural responses evaluation criteria.

3.2 Original Structure and Passive Control

To verify the effectiveness of the proposed semi-active control strategies the original structure, without any additional system, and the original structure employing passive fluid dampers were considered for comparison purposes. The original structures (section 3.1.1) considered here are linear and time invariant dynamic systems subjected to input disturbances without any additional input force. Conversely the original structure employing passive devices results in a nonlinear time invariant dynamic system subjected to input disturbances, described by the following nonlinear equation of motion:

$$\boldsymbol{M}\cdot\ddot{\boldsymbol{x}}_{rg}+\boldsymbol{C}\cdot\dot{\boldsymbol{x}}_{rg}+\boldsymbol{K}\cdot\boldsymbol{x}_{rg}-\boldsymbol{G}\cdot c_p\cdot|\dot{x}_{0g}|^{\alpha}\cdot\mathrm{sgn}(\dot{x}_{0g})=-\boldsymbol{M}\cdot\boldsymbol{1}\cdot\ddot{x}_g \qquad (3.10)$$

SDOF model analysis

The results of the original structure in terms of mean peak responses for different natural frequencies subjected to type 1 and 2 seismic actions are shown in 3.2. An example of the time responses is found in figure 3.6.

	Type 1 seismic action responses							Type 2 seismic action responses						
f_b (Hz)	0,25	0,37	0,50	0,62	0,75	0,87	1,00	0,25	0,37	0,50	0,62	0,75	0,87	1,00
Mx_{0g} (m)	0,293	0,278	0,266	0,222	0,187	0,155	0,131	0,113	0,109	0,104	0,0845	0,0704	0,0602	0,0516
Ma_0 (m/s^2)	0,765	1,554	2,694	3,457	4,253	4,742	5,298	0,300	0,623	1,062	0,62	1,618	1,848	2,088

Table 3.2 - SDOF original structure mean peak responses.

The passive system was also considered for comparison with the semi-active systems under study. The best damping coefficient for each structural system subjected to each type of seismic action was determined. For each damping constant the system responses were obtained and the peak responses considering each input accelerogram were determined. Figure 3.4 shows typical responses evolutions with the damping coefficient for two different velocity exponents (α=0,15 and α=1) – see section 2.8.2, Models for Fluid damper devices. The results show that increasing damping the relative displacements can be reduced, however at the expense of increasing the absolute accelerations. Higher reductions on relative displacements can even be obtained with small velocity exponents and higher damping values, but higher accelerations are also obtained.

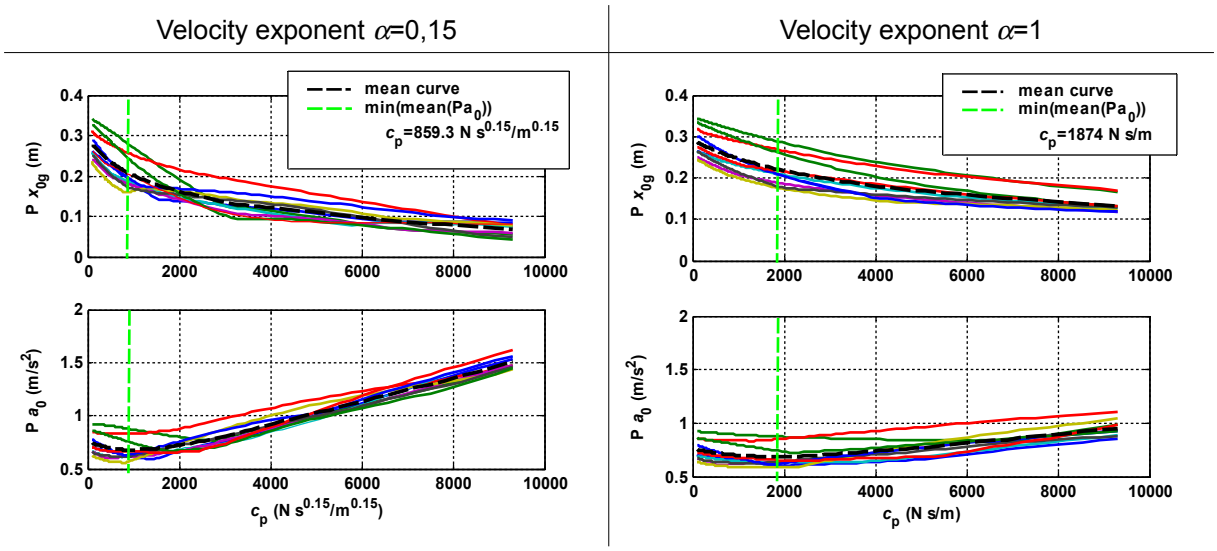

Figure 3.4 - Peak responses of the SDOF model (f_b=0,25 Hz; ξ_b=0,1) with a passive damper vs. device damping when subjected to 10 input type 1 accelerograms, for two velocity exponents α.

In order to minimize the relative displacements with small impact on the accelerations, the damping value that minimizes the acceleration was the criteria chosen to select the passive system. The average curve of the responses to 10 accelerograms was then evaluated and

the minimum value of the peak acceleration curve for the range of damping considered was used to identify the best damping coefficient. This procedure was applied to several system natural frequencies and for each seismic action type. Different velocity exponents were considered for the passive device law and the lower exponent was found to be the one that best minimizes better both relative displacements and accelerations (see table 3.3).

Type 1 seismic action														
	Rx_{0g}							Ra_0						
f_b(Hz)	0,25	0,37	0,50	0,62	0,75	0,87	1,00	0,25	0,37	0,50	0,62	0,75	0,87	1,00
α=0,15	**0,71**	**0,49**	**0,30**	**0,23**	**0,23**	**0,21**	**0,18**	**0,89**	**0,74**	**0,61**	**0,56**	**0,52**	**0,51**	**0,49**
α=0,5	0,71	0,51	0,39	0,29	0,29	0,27	0,25	0,89	0,74	0,62	0,60	0,56	0,55	0,53
α=1	0,75	0,58	0,45	0,39	0,38	0,38	0,34	0,90	0,77	0,63	0,62	0,59	0,59	0,57
Type 2 seismic action														
α=0,15	0,86	**0,55**	**0,44**	**0,42**	**0,43**	**0,49**	**0,41**	**0,97**	**0,81**	**0,69**	**0,70**	**0,67**	**0,68**	**0,70**
α=0,5	**0,83**	0,59	0,50	0,40	0,46	0,51	0,47	0,97	0,82	0,71	0,72	0,68	0,68	0,70
α=1	0,85	0,64	0,53	0,54	0,54	0,54	0,51	0,97	0,84	0,75	0,75	0,72	0,69	0,70

Table 3.3 - SDOF structure with passive devices responses (ratios) for different natural frequencies and velocity exponents.

The values of the damping for the passive devices with α=0,15 and α=1 can be observed in figure 3.5. An increasing tendency for damping as the system natural frequency increases can be detected. It is also clear that the optimized damping values differ from distinct seismic actions, meaning that different damping values should be defined for each input type.

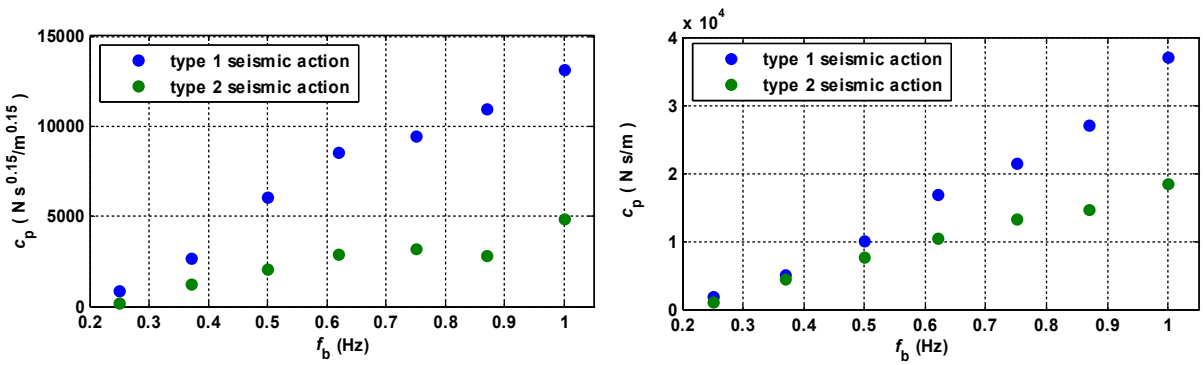

Figure 3.5 - Damping coefficients for the minimum mean of peak acceleration vs. SDOF system natural frequencies for α=0,15 (left) and α=1 (right).

For evaluation of the effectiveness of the proposed SA systems the best passive system is considered for comparison and thus passive devices with α=0,15 and the optimized damping values are used (figure 3.5). An example comparing the time responses of the original system with the passive for one input accelerogram is presented in figure 3.6.

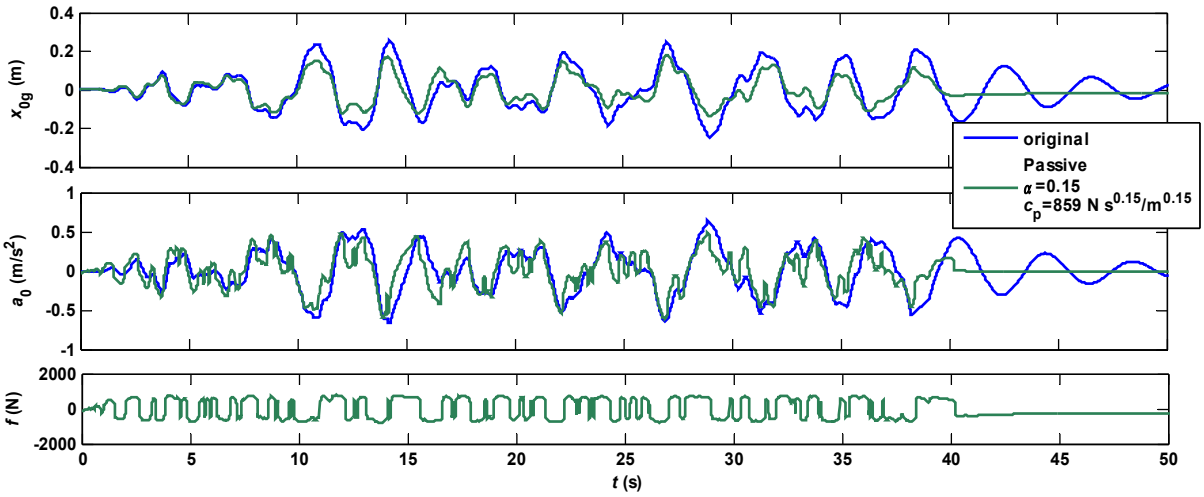

Figure 3.6 - Time histories of the SDOF model (f_b=0,25 Hz; ξ_b=0,1) subjected to one Type 1 accelerogram: original system and with passive system for α=0,15.

3.3 Semi-active Control

The control problem to solve can be stated by using the structure model and the device model, which results in a new state-space system. This system has an augmented state-vector $\boldsymbol{z}_c=\{\boldsymbol{z}\ ,\ f_{SA}\}^T$, the ground motion $\ddot{x}_g$ as an input disturbance, and the device damping coefficient c_v as the control variable. The model and the corresponding matrices are given by:

$$\begin{aligned}\dot{\boldsymbol{z}}_c&=\boldsymbol{A}_c\cdot\boldsymbol{z}_c+\boldsymbol{g}(\boldsymbol{z}_c)\cdot c_v+\boldsymbol{E}_c\cdot\ddot{x}_g\\ \boldsymbol{y}&=\boldsymbol{C}_c\cdot\boldsymbol{z}_c\end{aligned}\quad,\quad \boldsymbol{A}_c=\begin{bmatrix}\boldsymbol{A} & \boldsymbol{B}\\ 0 & -1/T_d\end{bmatrix},\boldsymbol{g}(\boldsymbol{z}_c)=\begin{Bmatrix}\boldsymbol{0}\\ \dot{x}_r/T_d\end{Bmatrix},\boldsymbol{E}_c=\begin{Bmatrix}\boldsymbol{E}\\ 0\end{Bmatrix}\qquad(3.11)$$

where: $\boldsymbol{A}_c$, $\boldsymbol{E}_c$ and $\boldsymbol{C}_c$ are the new system matrices; $\boldsymbol{g}(\boldsymbol{z}_c)$ is the input vector dependent on the states, namely relative velocity.

The system in equation (3.11) is a non-linear system with a bounded input damping ($c_{min}<c_v<c_{vmax}$). The goal is to find the damping coefficient (inside the admissible region) that minimizes the structural accelerations and relative displacements. Using the available information from measurements, different control approaches will be derived to compute the damping coefficient. The control loop of this problem is depicted in figure 3.7.

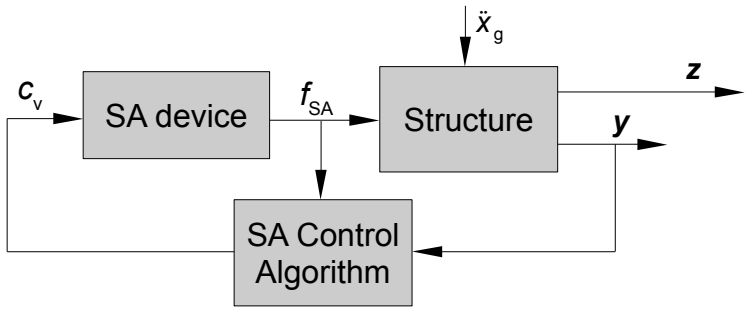

Figure 3.7 - SA control general loop.

For implementation of the control strategies and establishment of the control laws, the single degree-of-freedom SDOF approach of the structural model in (3.1) described in section 3.1.1

was considered. This approach results from the fact that base-isolated structures first vibration mode (pole nearest the imaginary axis) will dominate the transient response behaviour (the ratios of the poles real part exceed five and there are no zeros nearby), and thus are called dominant poles (*Ogata 1970*). Moreover, it is well accepted that the movement of the superstructure can be considered similar to the one of a rigid body when a base isolation system is used since the interaction forces (damping and elastic forces developed between the base and first floor) will be small in comparison with the rest of the forces acting on the base (*Luo et al. 2001*; *Rodríguez et al. 2012*).

In this work, a Lyapunov based method (also designated as Decentralized Bang-Bang control - DBB), a nonlinear output feedback control approach (NOFC), the sliding mode control strategy (SMC) and nine force tracking schemes are considered to tackle this problem. Force tracking schemes use a control law to derive the desired force and a damping adaptation rule (algorithm) to find the device damping coefficient (figure 3.8 - left).

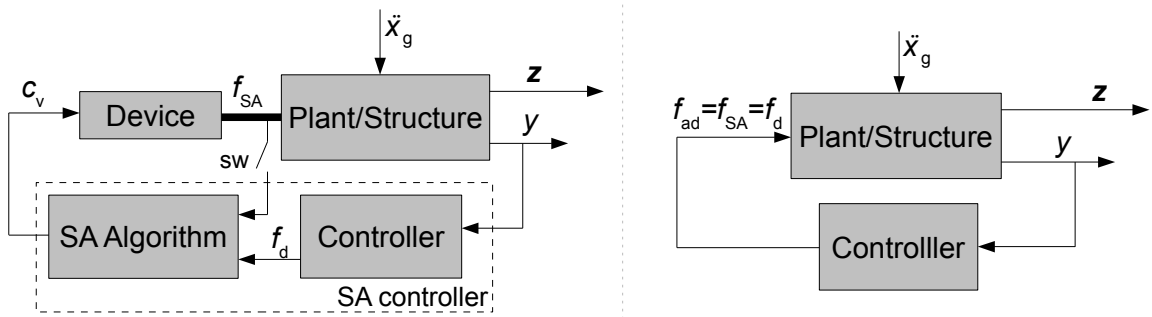

Figure 3.8 - Left: Force tracking scheme block diagram: switch (sw) off – model-based feed-forward force tracking scheme; switch (sw) on – force feedback. Right: Closed-loop system for controller design: plant with a controller in the feedback path.

Modulated Homogeneous Friction (MHF) with an on-off adaptation rule is one of the force tracking schemes. The Integral control law (I), the Linear Quadratic Regulator (LQR) and a Model Predictive Control strategy (MPC) are three linear controllers that are used in conjunction with a variable damping algorithm (VD) or a clipped on-off algorithm (COO), resulting on the six force tracking schemes combinations: IVD; ICOO; LQRVD; LQRCOO; MPCVD; and MPCCOO. The closed-loop diagram of the linear counterpart (figure 3.8 - right) can be used for controller design. The MHF force tracking scheme was also used in conjunction with those algorithms resulting in: MHFVD and MHFCOO.

In general, SA control laws are dependent on a design parameter that should be selected appropriately. This parameter should be selected such that the closed-loop system is stable. Moreover, since this parameter could have influence on the closed-loop system performance a representative sample of input ground motions (accelerograms) of the site were the structure is to be installed are considered for use in numerical simulations of the structural model to select the parameter that minimizes the mean peak acceleration responses.

3.3.1 Lyapunov Based Control

Control Law Formulation

This algorithm can be established using the Lyapunov stability theory. Considering the total vibratory energy in the structure (kinetic plus potential energy) as the Lyapunov function $V(\boldsymbol{z})$ the algorithm is defined as the Decentralized Bang-Bang control (DBB) (*Dyke & Spencer 1997*, *Jansen & Dyke 2000*) and used here for semi-active control of base-isolated structures. For the system in equation (3.1) $V(\boldsymbol{z})$ is given by:

$$V(\boldsymbol{z})=\frac{1}{2}\boldsymbol{x}_{\mathrm{rg}}^{\mathrm{T}}\cdot\boldsymbol{K}\cdot\boldsymbol{x}_{\mathrm{rg}}+\frac{1}{2}\left(\dot{\boldsymbol{x}}_{\mathrm{rg}}+\boldsymbol{1}\cdot\dot{x}_{\mathrm{g}}\right)^{\mathrm{T}}\cdot\boldsymbol{M}\cdot\left(\dot{\boldsymbol{x}}_{\mathrm{rg}}+\boldsymbol{1}\cdot\dot{x}_{g}\right) \tag{3.12}$$

which is proven to be a positive definite function of the states $\boldsymbol{z}$ and thus a Lyapunov function. The rate of change (with respect to time) of $V(\boldsymbol{z})$ is given by:

$$\dot{V}(\boldsymbol{z})=\boldsymbol{x}_{\mathrm{rg}}^{\mathrm{T}}\cdot\boldsymbol{K}\cdot\dot{\boldsymbol{x}}_{\mathrm{rg}}+\left(\dot{\boldsymbol{x}}_{\mathrm{rg}}+\boldsymbol{1}\cdot\dot{x}_{\mathrm{g}}\right)^{\mathrm{T}}\cdot\left(-\boldsymbol{C}\cdot\dot{\boldsymbol{x}}_{\mathrm{rg}}-\boldsymbol{K}\cdot\boldsymbol{x}_{\mathrm{rg}}+\boldsymbol{G}\cdot f_{\mathrm{ad}}\right) \tag{3.13}$$

Then, the only way to modify the rate of change of the Lyapunov function is through the last term which contains the force vector. To make as large and negative as possible the device damping should follow the following control law:

$$c_{\mathrm{v}}=c_{\mathrm{max}}\,\mathrm{H}\left[-\left(\dot{\boldsymbol{x}}_{\mathrm{rg}}+\boldsymbol{1}\cdot\dot{x}_{\mathrm{g}}\right)^{\mathrm{T}}\cdot\mathbf{G}\cdot f_{\mathrm{ad}}\right],\ c_{\mathrm{min}}\leq c_{\mathrm{v}}\leq c_{\mathrm{max}} \tag{3.14}$$

where: $\mathrm{H}[\cdot]$ is the Heaviside step function; Equation (3.14) can be simplified for each direction in:

$$c_{\mathrm{v}}=c_{\mathrm{max}}\,\mathrm{H}\left[\dot{x}_{0}\cdot f_{\mathrm{SA}}\right],\ c_{\mathrm{min}}\leq c_{\mathrm{v}}\leq c_{max} \tag{3.15}$$

The control law requires the measurement of absolute velocity and applied force.

If the relative vibratory energy of the structure is used as the Lyapunov function $V(\boldsymbol{z})$, the algorithm is defined as the Maximum Energy Dissipation (MED) (*Dyke & Spencer 1997*, *Jansen & Dyke 2000*):

$$V(\boldsymbol{z})=\frac{1}{2}\boldsymbol{x}_{\mathrm{rg}}^{\mathrm{T}}\cdot\boldsymbol{K}\cdot\boldsymbol{x}_{\mathrm{rg}}+\frac{1}{2}\dot{\boldsymbol{x}}_{\mathrm{rg}}^{\mathrm{T}}\cdot\boldsymbol{M}\cdot\dot{\boldsymbol{x}}_{\mathrm{rg}} \tag{3.16}$$

The control law is given by:

$$c_{\mathrm{v}}=c_{\mathrm{max}}\,\mathrm{H}\left[\dot{x}_{0\mathrm{g}}\cdot f_{\mathrm{SA}}\right],\ c_{\mathrm{min}}\leq c_{\mathrm{v}}\leq c_{max} \tag{3.17}$$

For this particular case, where the device formulation is given by equation (3.9), equation (3.17) will always result in the device maximum damping value (c_{max}), thus the name of the algorithm (MED). This solution is not the type of solution one is looking for, since as was found this one reduces well the relative displacement but at the expense of increasing the acceleration (see figure 3.4).

SDOF model analysis

The results of the original structure employing an SA device manipulated by a DBB controller can be found in table 3.4. It is found that this controller is effective in reducing the relative displacements for lower natural frequency systems (f_b≤0,37 Hz for type 1 seismic actions and f_b≤0,50 Hz for type 2 seismic actions) but not good in reducing the absolute accelerations, which surpass the acceleration values of the original structure for f_b=0,25 Hz. This observation can be found in one example of the time responses, input damping and force for one accelerogram, as depicted in figure 3.9.

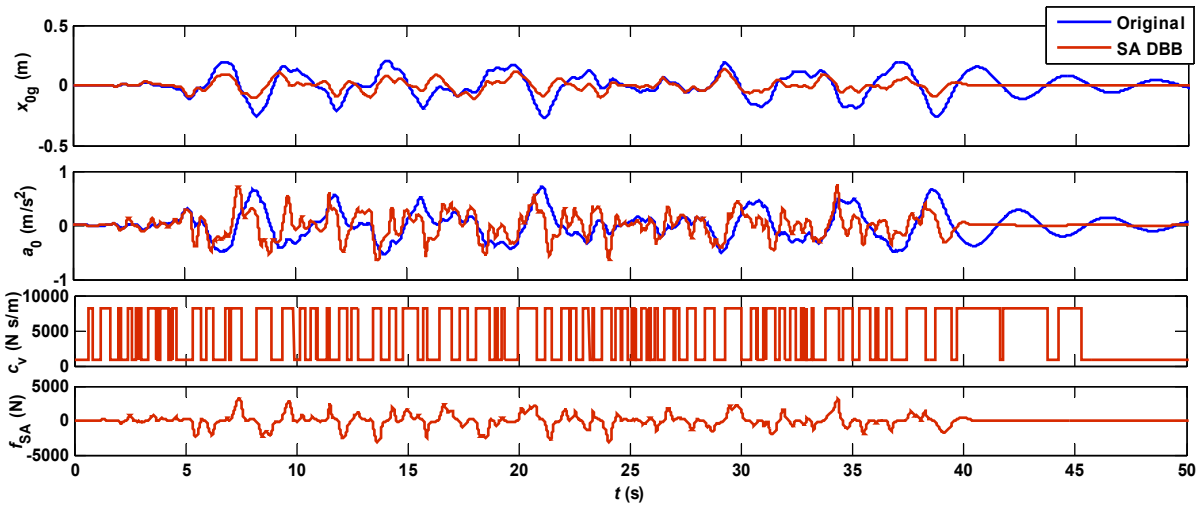

Figure 3.9 - Time histories of the SDOF model (f_b=0,25 Hz; ξ_b=0,1) subjected to one Type 1 accelerogram: original system and with SA system manipulated by a DBB controller.

3.3.2 Nonlinear Feedback Control

Nonlinear Feedback is a procedure for synthesis of feedback control laws for nonlinear control systems. This approach involves a transformation of a nonlinear system into a linear and controllable one which can then be controlled using linear control strategies. Two variants can be found depending on the variables for feedback: i) *state feedback control*, if the states are available; ii) *output feedback control*, if only some variables are accessible for output, which sometimes are intended to follow a reference function, *output tracking*; (*Isidori 1995*). In this section we will consider the *output feedback control* to find the desired damping coefficient (control input) of the nonlinear system described previously (see equation (3.11)). The closed-loop system is shown in figure 3.10.

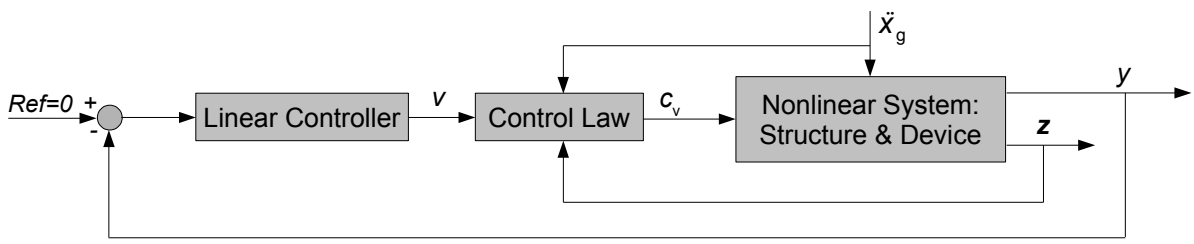

Figure 3.10 - Block diagram of the closed-loop system: structure employing an SA device (non-linear system) controlled by an output feedback control strategy (regulation).

Nonlinear Output Feedback Controller Formulation

Consider the following SISO nonlinear system:

$$\begin{aligned}\dot{\boldsymbol{z}}_c &= \boldsymbol{f}(\boldsymbol{z}_c)+\boldsymbol{g}(\boldsymbol{z}_c)\cdot u+\boldsymbol{p}(\boldsymbol{z}_c)\cdot w\\ y &= h(\boldsymbol{z}_c)\end{aligned} \tag{3.18}$$

where: $\boldsymbol{z}_c$ is the state vector assumed to belong to the set $U\in\mathbb{R}^n$; u is the input with $u\in\mathbb{R}$; w is an input disturbance with $w\in\mathbb{R}$; y is the output with $y\in\mathbb{R}$; $\boldsymbol{f}(\boldsymbol{z}_c)$, $\boldsymbol{g}(\boldsymbol{z}_c)$ and $\boldsymbol{p}(\boldsymbol{z}_c)$ are $\mathbb{R}^n$ mappings defined in the open set U, and are smooth in their arguments ($\boldsymbol{z}_c$); $h(\boldsymbol{z}_c)$ is a $\mathbb{R}$ mapping also defined in U and smooth in $\boldsymbol{z}_c$.

The system is said to have a relative degree r at $\boldsymbol{z}_{c|0}$ if:

1) $L_g\, L_f^k \boldsymbol{h}(\boldsymbol{z}_c)=0$, for all $\boldsymbol{z}_{c|0}$ in the neighbourhood of $\boldsymbol{z}_{c|0}$ and $k<r-1$;

2) $L_g\, L_f^{r-1} \boldsymbol{h}(\boldsymbol{z}_{c|0})\neq 0$.

where: $L_f^k \boldsymbol{h}(\boldsymbol{z}_c)=L_f\left[L_f^{k-1}\boldsymbol{h}(\boldsymbol{z}_c)\right]\cdot\boldsymbol{f}(\boldsymbol{z}_c)$, is the k derivative of $\boldsymbol{h}(\boldsymbol{z}_c)$ along $\boldsymbol{f}(\boldsymbol{z}_c)$, Lie derivative, with $L_f \boldsymbol{h}(\boldsymbol{z}_c)=\nabla \boldsymbol{h}(\boldsymbol{z}_c)\cdot\boldsymbol{f}(\boldsymbol{z}_c)$ and $L_f^0 \boldsymbol{h}(\boldsymbol{z}_c)=\boldsymbol{h}(\boldsymbol{z}_c)$.

There may be points where the relative degree cannot be defined, which occur when the first function of the following sequence is not identically zero in the neighbourhood of $\boldsymbol{z}_{c|0}$ but it is zero at $\boldsymbol{z}_c=\boldsymbol{z}_{c|0}$: $\left\{L_g \boldsymbol{h}(\boldsymbol{z}_c),\ L_g\, L_f \boldsymbol{h}(\boldsymbol{z}_c),\ \ldots,\ L_g\, L_f^k \boldsymbol{h}(\boldsymbol{z}_c)\right\}$. However, the relative degree can be defined in an open and dense subset of the set U where the system is defined.

The relative degree r can also be defined as the number of times one has to differentiate (time derivative) the output y such that u appears explicitly. Thus, the k time derivative of y is:

- $y^{(k)}=L_f^k \boldsymbol{h}(\boldsymbol{z}_c)+L_g\, L_f^{k-1}\boldsymbol{h}(\boldsymbol{z}_c)\cdot u+L_p\, L_f^{k-1}\boldsymbol{h}(\boldsymbol{z}_c)\cdot w$, with $L_g\, L_f^{k-1}\boldsymbol{h}(\boldsymbol{z}_c)=0$ for k-1<r-1, and $L_p\, L_f^{k-1}\boldsymbol{h}(\boldsymbol{z}_c)=0$ for $0\leq k-1\leq r-1$.

Considering the system described by equation (3.18) and assuming that disturbance w is available for measurement then a control law can be established as:

$$u=a(\boldsymbol{z}_c)+b(\boldsymbol{z}_c)\cdot v+c(\boldsymbol{z}_c)\cdot w \tag{3.19}$$

with: $a(\boldsymbol{z}_c)=\dfrac{-L_f^r \boldsymbol{h}(\boldsymbol{z}_c)}{L_g\, L_f^{r-1}\boldsymbol{h}(\boldsymbol{z}_c)}$; $b(\boldsymbol{z}_c)=\dfrac{1}{L_g\, L_f^{r-1}\boldsymbol{h}(\boldsymbol{z}_c)}$; $c(\boldsymbol{z}_c)=\dfrac{-L_p\, L_f^{r-1}\boldsymbol{h}(\boldsymbol{z}_c)}{L_g\, L_f^{r-1}\boldsymbol{h}(\boldsymbol{z}_c)}$; and v is the external reference for input resulting from the linear controller.

A linear control law that solves the problem of regulating the output (zero reference) is given:

$$v=-\sum_{i=0}^{r-1} k_i\cdot y^{(i)} \tag{3.20}$$

where: k_i are the controller constants; and $y^{(i)}$ is the i derivative of the output y. As stated

before, the r time derivative of the output is:

$$y^{(r)}=\mathrm{L}_f^r \boldsymbol{h}(\boldsymbol{x})+\mathrm{L}_g\,\mathrm{L}_f^{r-1}\boldsymbol{h}(\boldsymbol{x})\cdot u+\mathrm{L}_p\,\mathrm{L}_f^{r-1}\boldsymbol{h}(\boldsymbol{x})\cdot w=v \tag{3.21}$$

Then, substituting (3.20) in (3.21) results in the following characteristic equation:

$$y^{(r)}+k_{r-1}\cdot y^{(r-1)}+\ldots+k_0\cdot y=0 \tag{3.22}$$

whose parameters k_i should be chosen so that the roots lie in the left half plane, in order to achieve convergence to zero as time goes to infinity.

Finally, the design of the control law should keep the variables that represent the system internal behaviour bounded.

<u>Hybrid Base-Isolated Building Controller Formulation</u>

For the nonlinear system described in (3.11) with the assumption of the SDOF model approach for the structural model, a control law is established using the described formulation. Thus:

- $\boldsymbol{f}(\boldsymbol{z}_c)=\boldsymbol{A}_c\cdot\boldsymbol{z}_c=\begin{bmatrix}0 & 1 & 0\\ -k_b/m & -c_b/m & -1/m\\ 0 & 0 & -1/T_d\end{bmatrix}\cdot\boldsymbol{z}_c;\ \ \boldsymbol{g}(\boldsymbol{z}_c)=\begin{bmatrix}0\\0\\ \dot{x}_{0g}/T_d\end{bmatrix};\ \ \boldsymbol{p}(\boldsymbol{z}_c)=\begin{bmatrix}0\\-1\\0\end{bmatrix};$
- $\boldsymbol{h}(\boldsymbol{z}_c)=\begin{bmatrix}-k_b/m & -c_b/m & -1/m\end{bmatrix}\cdot\boldsymbol{z}_c;$
- and the disturbance is $w=\ddot{x}_g$.

The relative degree is then found after differentiating the output r=1 times. It can be seen that the relative degree is defined at any point if $\dot{x}_{0g}\neq 0$. To accomplish this requirement a small modification is performed in the last entry of the input vector $\boldsymbol{g}(\boldsymbol{z}_c)$ without modifying considerably the solution:

$$\boldsymbol{g}(\boldsymbol{z}_c)=\begin{bmatrix}0 & 0 & \dot{x}_{0g}/T_d+\varepsilon_a\cdot\mathrm{sgn}(\dot{x}_{0g}/T_d+\varepsilon_a)\end{bmatrix}^{\mathrm{T}}=\begin{bmatrix}0 & 0 & D\end{bmatrix}^{\mathrm{T}} \tag{3.23}$$

where ε_a is a small constant. Each term resulting from (3.21) is given by:

$$\begin{aligned}
&\mathrm{L}_f\boldsymbol{h}(\boldsymbol{z}_c)=\frac{k_b\cdot c_b}{m^2}\cdot x_{0g}+\left[\left(\frac{c_b}{m}\right)^2-\frac{k_b}{m}\right]\cdot\dot{x}_{0g}+\left[\frac{c_b}{m^2}+\frac{1}{T_d\cdot m}\right]\cdot f_{SA}\\
&\mathrm{L}_g\,\mathrm{L}_f^0\boldsymbol{h}(\boldsymbol{z}_c)=\mathrm{L}_g\boldsymbol{h}(\boldsymbol{z}_c)=-\frac{D}{m}\\
&\mathrm{L}_p\,\mathrm{L}_f^0\boldsymbol{h}(\boldsymbol{z}_c)=\mathrm{L}_p\boldsymbol{h}(\boldsymbol{z}_c)=\frac{c_b}{m}
\end{aligned} \tag{3.24}$$

Finally, the terms of the control law in (3.19) are given by:

$$\boldsymbol{a}(\boldsymbol{z}_c)=\frac{k_b\cdot c_b}{m}\frac{x_{0g}}{D}+\left(\frac{c_b^2}{m}-k_b\right)\frac{\dot{x}_{0g}}{D}+\left(\frac{c_b}{m}+\frac{1}{T_D}\right)\frac{f_{SA}}{D};\ \ \boldsymbol{b}(\boldsymbol{z}_c)=-\frac{m}{D};\ \ \boldsymbol{c}(\boldsymbol{z}_c)=\frac{c_b}{D} \tag{3.25}$$

In the control law (3.19) u is used instead of c_v because the first one can take values outside the range of admissible damping values of the device. Thus an adjusting rule to 'clip' the damping values provided by equation (3.19) is considered:

$$c_v = \begin{cases} c_{min}, & u < c_{min} \\ u, & c_{min} \le u \le c_{max} \\ c_{max}, & u > c_{max} \end{cases} \tag{3.26}$$

The following linear control law obtained from equation (3.20) was considered for the reference input:

$$v = -k_0 \cdot y \tag{3.27}$$

Substituting this result in the correspondent output equation obtained from (3.21), the following characteristic equation is achieved:

$$\dot{y} + k_0 \cdot y = 0 \tag{3.28}$$

It can be seen that any value with k_0>0 put the roots in the left half plane, leading to an exponential decay as time goes to infinity.

The derived control law should keep the variables that represent the system internal behaviour bounded. From equation (2.24) it is stated that the input damping for the system is bounded $c_{min} \le c_v \le c_{max}$ and thus the input damping just modifies the dissipative force and has no authority to destabilize the system. The closed loop system is then always asymptotically stable.

SDOF model analysis

The small constant ε_a=10^{-4} m/s^2 was taken in the numerical simulations without modifying considerably the solution. Numerical simulations were performed to analyse the influence of the controller gain k_0 on the peak responses. An example of a typical evolution of the peak responses for 10 input accelerograms is found in 3.11. It is found that higher gains always conduct to smaller responses. In that range of gains the responses are insensitive to the gain value. Taking into account all the different system natural frequencies and type of seismic actions a controller gain k_0=1000 s^{-1}

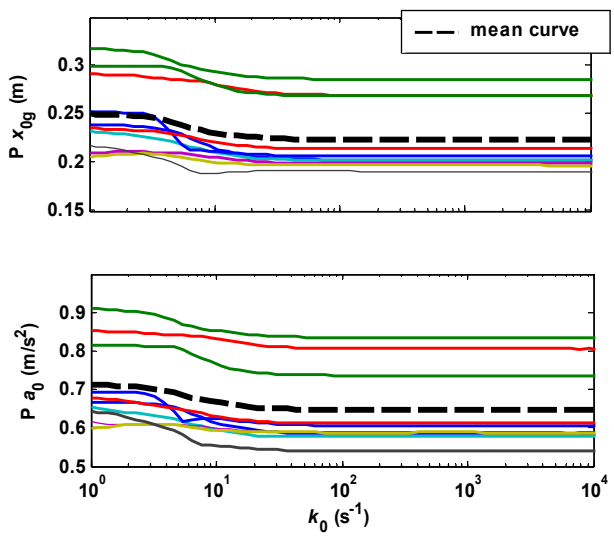

Figure 3.11 - Peak responses of the SDOF model (f_b=0,25 Hz; ξ_b=0,1) with an SA device plus NOFC vs. controller gain when subjected to 10 input type 1 accelerograms.

was chosen. The results provided by this strategy using the identified linear controller gains can be found in table 3.4. It is show that this control strategy (NOFC) provide better results than the original system for any case, and better in terms of accelerations than the passive system for lower natural frequency systems (f_b≤0,37 Hz). An example of the time responses, input damping and force for one accelerogram is depicted in figure 3.12. Notice the continuous variation of the input damping between the range of admissible values.

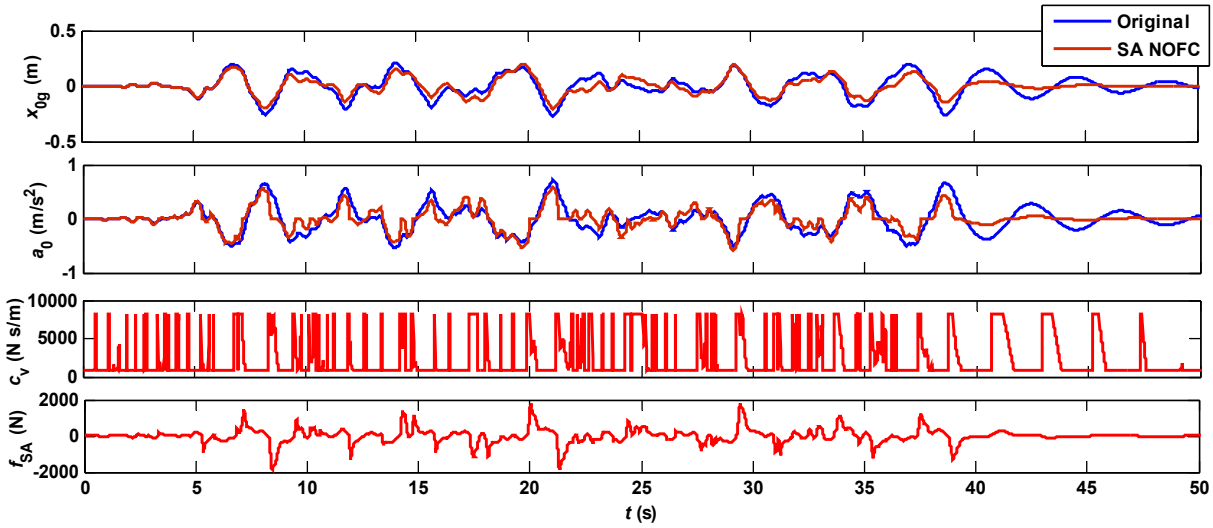

Figure 3.12 - Time histories of the SDOF model (f_b=0,25 Hz; ξ_b=0,1) subjected to one Type 1 accelerogram: original system and with SA system manipulated by a NOFC controller.

3.3.3 Sliding Mode Control

Sliding mode control (SMC) is also a nonlinear control strategy that forces the system to reach a sliding surface (or switching surface) in a finite time and remains there by switching the control structure. Thus, the system dynamics will be similar to the dynamics of the sliding surface. The three steps to design the controller are:

1. Definition of the sliding surface $s(\boldsymbol{z}_c)$ with the intended dynamics:

$$s(\boldsymbol{z}_c)=0 \tag{3.29}$$

2. Ensure that the system states reach the sliding surface, which can be verified through:

$$\begin{aligned} V(\boldsymbol{z}_c)&=\frac{1}{2}s^2(\boldsymbol{z}_c)>0,\ \text{ i.e., } \textit{positive definite} \\ \dot{V}(\boldsymbol{z}_c)&=s(\boldsymbol{z}_c)\cdot\dot{s}(\boldsymbol{z}_c)<0,\ \text{ i.e., } \textit{negative definite} \end{aligned} \tag{3.30}$$

3. Ensure that the system states remain on the sliding surface; a control law consisting of an equivalent component and a nonlinear component ensures that the system states reach the sliding surface in finite time and remain there despite the modelling errors, disturbances and imperfections:

$$\begin{aligned} &u = u_{eq} + u_N \\ &\text{with:} \\ &u_{eq} = \frac{-L_f s(\boldsymbol{z}_c)}{L_g s(\boldsymbol{z}_c)} \\ &u_N,\ \text{on-off rule} \end{aligned} \tag{3.31}$$

Hybrid Base-Isolated Building SMC Controller Formulation

For the nonlinear system described in (3.11) with the assumption of the SDOF model approach for the structural model, the following sliding surface $s(\boldsymbol{z}_c)$ is considered:

$$s(\boldsymbol{z}_c) = \gamma \cdot x_{0g} + \beta \cdot \dot{x}_{0g} + f_{SA} \tag{3.32}$$

where γ and β are positive real constants. In order to ensure the convergence of the states, $V(\boldsymbol{z}_c)$ and $\dot{V}(\boldsymbol{z}_c)$ are given by:

$$\begin{aligned} &V(\boldsymbol{z}_c) = \boldsymbol{z}_c^T \cdot \boldsymbol{P} \cdot \boldsymbol{z}_c,\ \boldsymbol{P} = \frac{1}{2}\begin{bmatrix} \gamma^2 & \gamma\cdot\beta & \gamma \\ \gamma\cdot\beta & \beta^2 & \beta \\ \gamma & \beta & 1 \end{bmatrix} \geq 0 \\ &\dot{V}(\boldsymbol{z}_c) = -\boldsymbol{z}_c^T \cdot \boldsymbol{Q} \cdot \boldsymbol{z}_c,\ \boldsymbol{Q} = -(\boldsymbol{A}_c^T \cdot \boldsymbol{P} + \boldsymbol{P} \cdot \boldsymbol{A}_c) \geq 0 \end{aligned} \tag{3.33}$$

In equation (3.33) the positive definiteness of $\boldsymbol{P}$ and $\boldsymbol{Q}$ matrices is only reached for certain γ and β values. The control law is given by the sum of an equivalent component, obtained from equation (3.31), and a nonlinear component, given by:

$$\begin{aligned} &u = u_{eq} + u_N \\ &\text{with:} \\ &u_{eq} = -\gamma \cdot T_d + \frac{\beta \cdot T_d \cdot c_b}{m} + \frac{\beta \cdot T_d \cdot k_b}{m}\frac{x_{0g}}{\dot{x}_{0g}} + \frac{\beta \cdot T_d \cdot c_b}{m}\frac{f_{SA}}{\dot{x}_{0g}} + \frac{f_{SA}}{\dot{x}_{0g}} \\ &u_N = -\rho \cdot \mathrm{sgn}(s(\boldsymbol{z}_c)) \end{aligned} \tag{3.34}$$

where ρ is a positive real constant. The constants γ and β that lead to the system best performance were obtained through numerical simulations using representative accelerograms. In order to avoid a division by zero, the relative velocity is considered a small constant ε=10^{-4} m/s when $|\dot{x}_{0r}| \leq \varepsilon$.

The SMC law should keep the variables that represent the system internal behaviour bounded, and thus the adjusting rule of equation (3.26) is used to 'clip' the damping values. Under these circumstances the closed loop system is always asymptotically stable.

SDOF model analysis

Numerical simulations were performed to analyse the influence of constants γ and β in the peak responses. Good results were found with γ=β. An example of a typical evolution of the peak responses for 10 input accelerograms can be found in figure 3.13-left. Using the minimum acceleration as criteria to select the parameters, a reduction in the relative

displacement is also achieved. Under these circumstances the parameters for the systems under study were obtained and are depicted in figure 3.13-right. The results provided by this strategy with the identified γ and β parameters can be found in table 3.4. It is show that this control strategy (SMC) provide better results than the original system for any case, and better in terms of accelerations than the passive system with f_b≤0,62 Hz and f_b≤1 Hz for type 1 and type 2 seismic actions respectively. An example of the time responses, input damping and force for one accelerogram can be observed in figure 3.14.

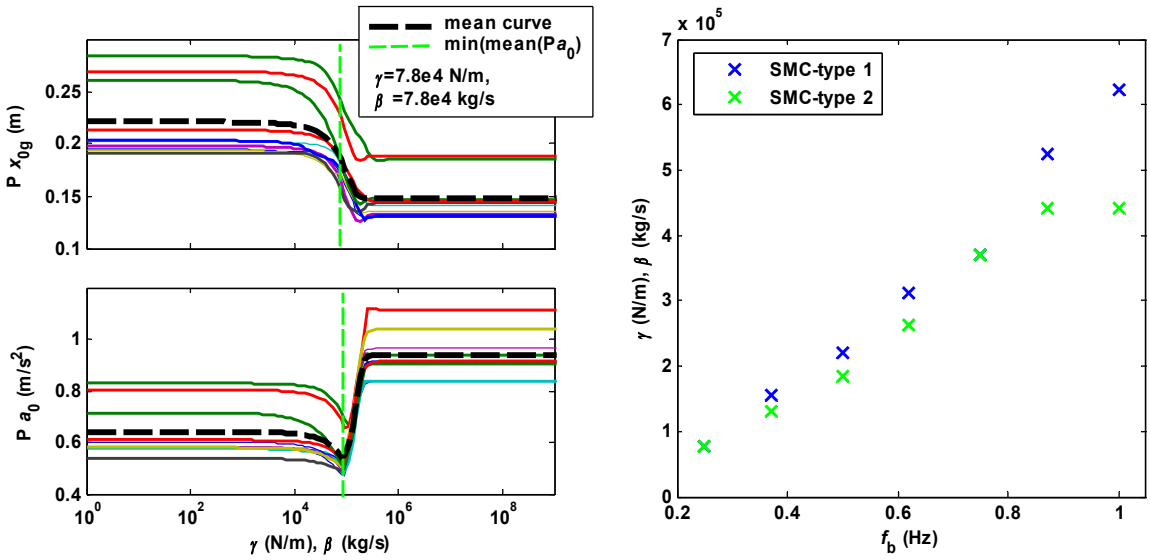

Figure 3.13 Left - Peak responses of the SDOF model (f_b=0,25 Hz; ξ_b=0,1) with an SA device plus SMC vs. controller gain when subjected to 10 input type 1 accelerograms. Right - SMC controller gains selected for each SDOF system natural frequency.

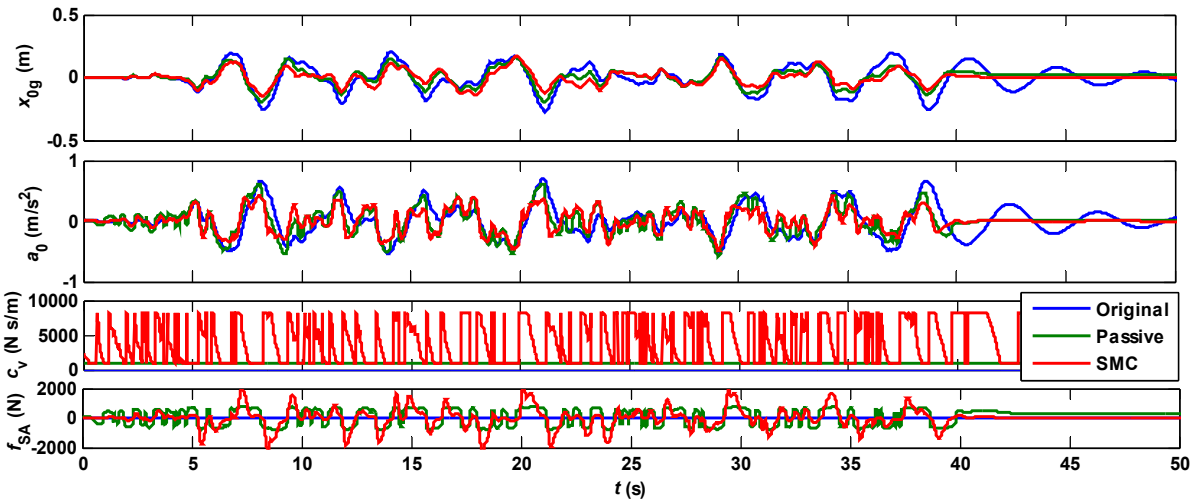

Figure 3.14 - Time histories for the SDOF model (f_b=0.25 Hz; ξ_b=0,1) subjected to one Type 1 accelerogram: original (no devices), best passive and SA with SMC strategy.

3.3.4 Modulated Homogeneous Friction Control

Control Law Formulation

The modulated homogeneous friction (MHF) force tracking scheme proposed by *Inaudi 1997*

was considered in these studies for semi-active control of base-isolated structures. The block diagram of the force tracking scheme has the structure shown in figure 3.8 (left) with force feedback path from the force measurements of the device. Recalling to section 2.9.5, the control law used to derive the desired force is given by:

$$f_d = -g \cdot \left| P\left[\Delta(t)\right] \right| \qquad P\left[\Delta(t)\right] = \Delta(t-s),\ s = \left\{ \min x \geq 0 : \dot{\Delta}(t-x) = 0 \right\} \tag{3.35}$$

where: g is a proportional gain to be defined; and $\Delta(t\text{-}s)$ is the most recent local extrema in the base deformation x_{0g}. In accordance to the original MHF force tracking scheme, the following clipped control algorithm is considered:

$$c_v = c_{max} \cdot \mathrm{H}\left[f_d - |f_{SA}|\right],\ c_{min} \leq c_v \leq c_{max} \tag{3.36}$$

The base floor relative displacement and the device force are needed for implementation of this control strategy. This strategy is also dependent of the selected gain for the controller. The variable damping algorithm and the clipped on-off algorithm in section 3.3.8 were also considered with this strategy.

SDOF model analysis

Numerical simulations were performed to analyse the influence of the controller gain g on the peak responses. A typical evolution of the peak responses for 10 input accelerograms can be found in figure 3.15 (left).

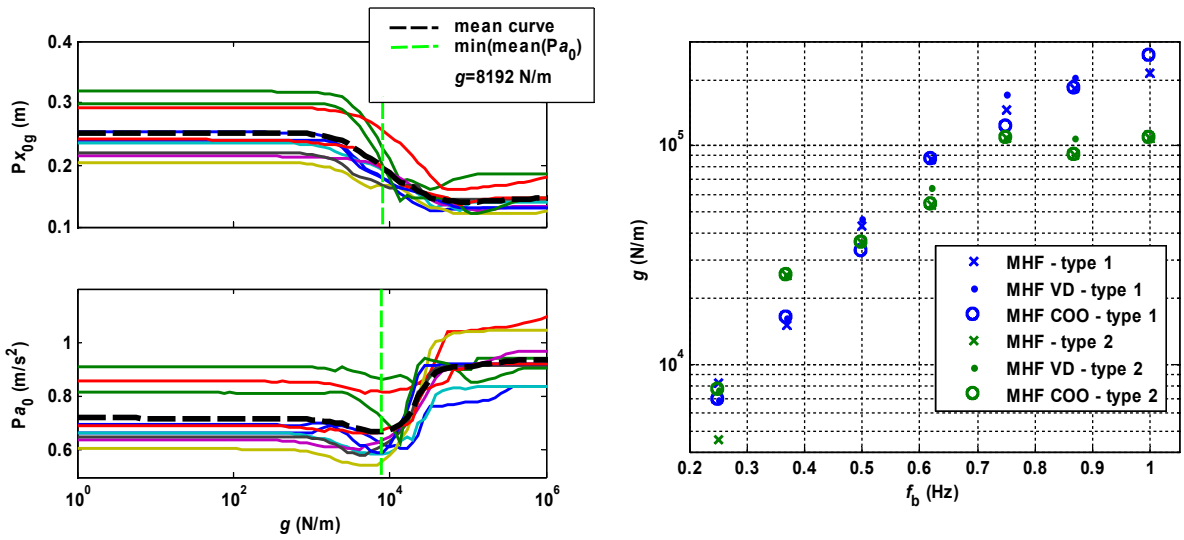

Figure 3.15 Left - Peak responses of the SDOF model (f_b=0,25 Hz; ξ_b=0,1) with an SA device plus MHF vs. controller gain when subjected to 10 input type 1 accelerograms. Right - MHF controller gains selected for each SDOF system natural frequency.

The minimum value of the mean peak responses of the acceleration was used to identify the controller gain g. The values obtained for each system natural frequency are found in the same figure (figure 3.15 right). An increasing tendency of the controller gain as the system natural frequency increases is observed. It is also observed a dependence of the gain value

with the type of seismic action and with the type of algorithm that is more expressive for higher natural frequency systems. For lower natural frequency systems the dependence has small impact on the system response if any value in range defined by both values is considered for the controller design.

The results of numerical simulations provided by this strategy using the identified controller gains can be found in table 3.4. It is found that all these strategies lead to better performance than the original system and the results provided by different algorithms are very similar. With this controller the SDOF model perform better than the passive case for lower natural frequencies (f_b=0,25 Hz). It performs better than NOFC in terms of relative displacements for the whole range of natural frequencies and in terms of accelerations only for f_b≥0,5 Hz. An example of the time response is shown in figure 3.16. In both force tracking schemes it is evident how the device force tries to follow the desired force of the controller by changing the damping coefficient: the original MHF with an on-off algorithm and the VD varies the damping in between the damping limits.

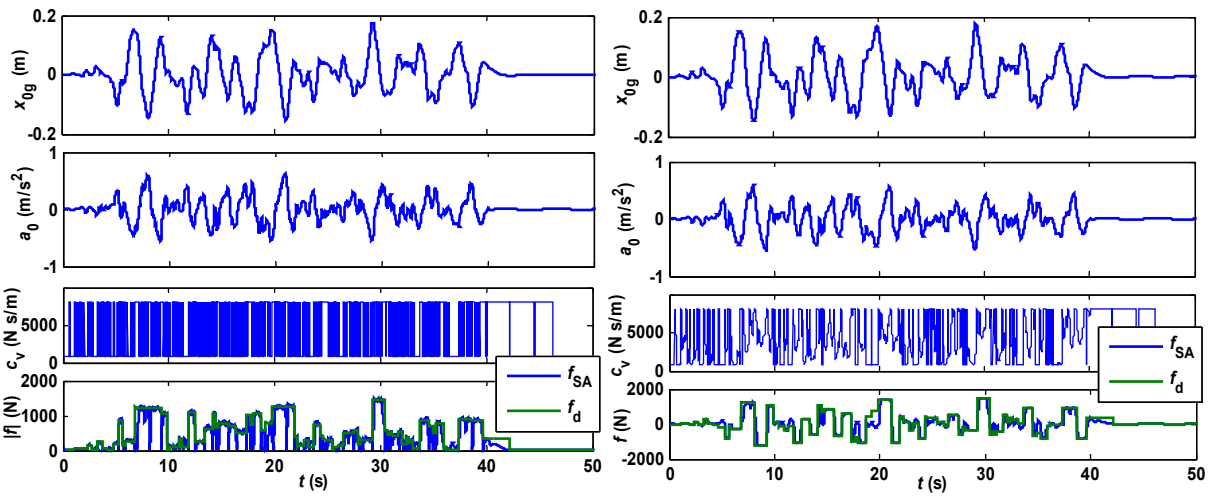

Figure 3.16 - Time histories of the SDOF model (f_b=0,25 Hz; ξ_b=0,1) subjected to one Type 1 accelerogram system with SA system manipulated by the: original MHF controller (left); MHF and VD algorithm (right).

3.3.5 Integral Control

The integral controller alone, for instance in the well known example of the sky-hook damper (or absolute velocity feedback) is used in a force tracking scheme to derive the desired force.

Controller Formulation

The output of the controller or the desired force f_d is given as:

$$f_d = g \int_0^{\tau} \ddot{x}_0 \, d\tau = g \cdot \dot{x}_0 \tag{3.37}$$

where: g is the controller gain; $\ddot{x}_0$ and $\dot{x}_0$ are the absolute acceleration and velocity at the

base floor respectively. Notice that there is no minus sign in the equation since it was already included in the system model through vector ***G***. The closed-loop diagram in figure 3.8 (right) can be used for controller design. Its transfer function can be derived from the system model in equation (3.1). By applying the Laplace transform to the equation in terms of absolute coordinates the following transfer functions result is achieved:

$$A_0 = P_d \cdot A_g + s^2 P \cdot F_{ad}, \quad \begin{array}{l} P_d = \dfrac{c_b \cdot s + k_b}{m \cdot s^2 + c_b \cdot s + k_b} \\ P = \dfrac{-1}{m \cdot s^2 + c_b \cdot s + k_b} \end{array} \tag{3.38}$$

where: A_0, A_g and F_{ad} are the Laplace transforms of $\ddot{\boldsymbol{x}}_0$, $\ddot{x}_g$ and f_{ad}; P and P_d are plant model and disturbance model respectively; s is the complex variable. Substituting F_{ad} by the Laplace transform of equation (3.37), F_{ad}=g/$s \cdot A_0$, the closed-loop transfer function P_{CL} is obtained:

$$A_0 = P_{CL} \cdot A_g, \quad \begin{array}{l} P_{CL} = S \cdot P_d, \quad S = \dfrac{1}{1 + g/s \cdot P} = \dfrac{m \cdot s^2 + c_b \cdot s + k_b}{m \cdot s^2 + (c_b + g) \cdot s + k_b} \\ P_{CL} = \dfrac{c_b \cdot s + k_b}{m \cdot s^2 + (c_b + g) \cdot s + k_b} = \dfrac{2 \cdot \xi_b \cdot \omega_b \cdot s + \omega_b^2}{s^2 + 2 \cdot (\xi_b + \xi_a) \cdot \omega_b \cdot s + \omega_b^2} \end{array} \tag{3.39}$$

where: S is the sensitivity function. The controller gain should then be chosen to accomplish the control objectives (reduce accelerations and relative displacements) under the range of stable solutions (P_{CL} is stable).

<u>Controller Design</u>

The stability of the linear closed-loop system can be determined by the location of the poles in the s plane. Stability is guaranteed if all the poles lie in the left-half s plane. Therefore, to guarantee fast, well damped transient response characteristics, the poles should have a damping ratio ξ>0,4 and the system must exhibit a settling time t_s<4/($\xi \cdot \omega_d$), where ω_d is the undamped natural frequency and $\xi = \xi_b + \xi_a$ is the intended damping ratio for the closed-loop system (*Ogata 1970*). $\xi_a = g/(2 \cdot m \cdot \omega_d)$ is the damping ratio provided by the integral controller.

In order to evaluate the control system performance the transient response is commonly used. The response of a control system often exhibits damped oscillations before reaching the steady-state. Thus fast responses with low overshoot and small offset are always preferable to be achieved, which may be obtained if the system damping ratio is in the interval 0,5≤ξ≤0,8. The analysis of several performance indices, like the ITAE (Integral of Time multiplied Absolute Error criterion) indicates that second order systems with ξ=0,7 corresponds to the optimal or near optimal value for the performance index (*Ogata 1970*). The performance can also be specified in terms of frequency response of the transfer

function. In terms of stability one should look for values of the controller gain that are able to locate the closed-loop system poles in the left-half plane. The system under study is always stable for any value of the gain, since the poles, roots of the denominator of P_{CL} in equation (3.39), are always on the left-half plane. It is also stated that the maximum peak of the sensitivity function is $\|S\|_\infty \leq 2$ (*Skogestad & Postlethwaite 1996*). This is always verified for the current system since the magnitude of the sensitivity function is bounded by $\xi_b/\xi \leq \|S\|_\infty \leq 1$. Moreover, the design of active systems with an integral control action consists of choosing the controller gain that locates the system poles at the real axis (critical damping ξ=1) (*Preumont 2002*). The controller gain for a specific system damping ratio ξ is given by:

$$g = 2 \cdot m \cdot \omega_b \cdot (\xi - \xi_b) \tag{3.40}$$

Having the structure characterized by its mass *m*, natural frequency ω_b and damping ratio ξ_b, and defining the intended system damping ξ it is possible to design the controller gain *g*. As stated before this control strategy reduces the resonance peak keeping the attenuation rate in higher frequency. Figure 3.17 shows the root locus of the closed-loop system as the open-loop gain *g* changes (left), and the transfer functions Bode diagram for different values of the gain *g* (right). The root locus has the shape of a linear viscous damping system (for damping increase). In the frequency domain the increase of damping provided by the integral control law does not influence the acceleration higher frequency attenuation, although it amplifies the lower frequency components of the relative displacement.

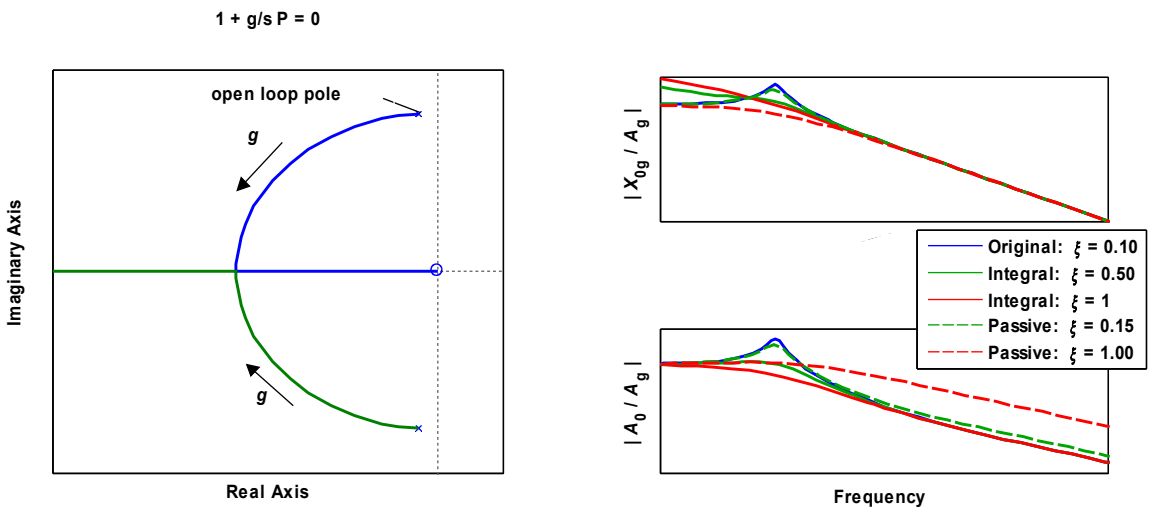

Figure 3.17 - Closed loop system with an Integral controller: Root Locus (left); and the transfer functions Bode diagram for different values of gain compared with the passive case (right).

Some hints to derive the controller gain as a function of the system desired damping ratio were referred previously, mostly agreeing that the desired damping should be specified in a

broad range of values: 0,4≤ξ≤1. For the controller design we will consider a representative sample of input ground motions (accelerograms) of the site were the structure is to be installed and select the gain (or damping) that minimizes the mean peak acceleration responses. It will be shown that the optimal value to use with semi-active viscous fluid dampers for vibration mitigation of structures subjected to earthquake loads is dependent on the structure natural frequency and is always lower than the critical damping.

Adjusting Damping Rules

The VD and COO algorithms in section 3.3.8 were considered for use with this controller.

SDOF model analysis

Numerical simulations were performed on this system with different controller gains to identify the best controller gain for each strategy. An example of a typical evolution of the peak responses of the 10 input accelerograms with the controller gain is found in 3.18 (right). With the minimum of mean peak responses as the criterion to identify the controller gain, the values for each type of seismic action and algorithm were identified. The correspondent system damping ratios ξ were obtained and the results are depicted also in figure 3.18 (right). Similar values are found independent of the seismic action and algorithm. The damping ratios lie between 40 and 90 % approximately and have a decreasing tendency with the system natural frequency. Although different values of damping ratio are found for the same system natural frequencies (different algorithms and input action type), small impact on the system response is observed if any value in that range is considered for the controller design.

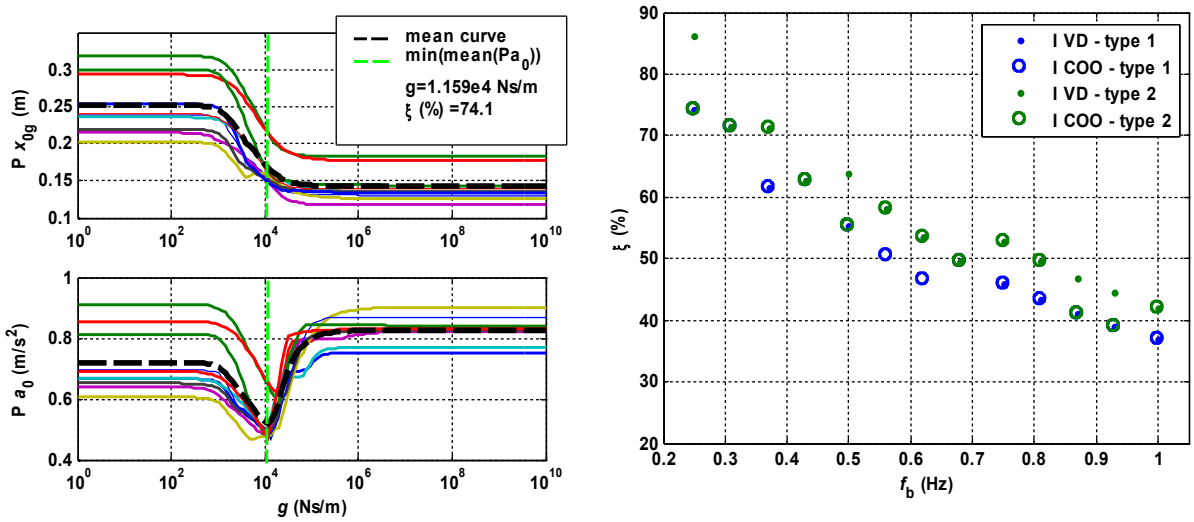

Figure 3.18 Left - Peak responses of the SDOF model (f_b=0,25 Hz; ξ_b=0,1) with an SA device plus Integral control law vs. controller gain when subjected to 10 input type 1 accelerograms. Right - Integral controller gain (closed-loop damping ratio ξ) selected for each system natural frequency.

The results of numerical simulations provided by these tracking schemes using the identified

controller gains can be found in table 3.4. Similar results are found with both tracking schemes and better performance than the original system. Comparing with the passive solution better results are found in terms of accelerations for structural systems with f_b≤0,50 Hz for type 1 seismic actions and f_b≤1,00 Hz for type 2 seismic actions. An example of the time responses compared with the ones provided by the original and passive cases is found in figure 3.19.

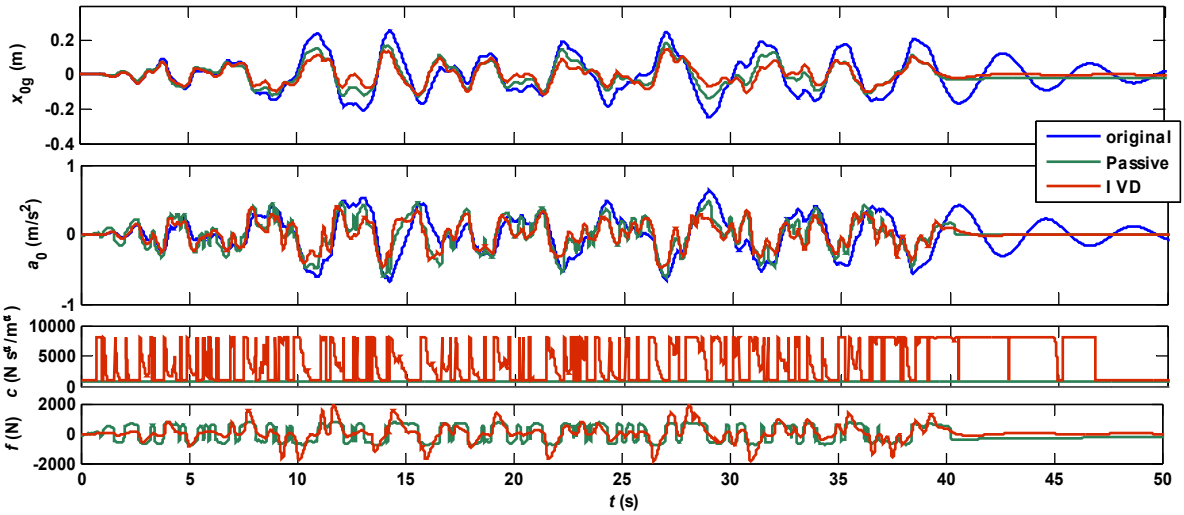

Figure 3.19 - Time histories for the SDOF model (f_b=0.25 Hz; ξ_b=0,1) subjected to one Type 1 accelerogram: original (no devices), best passive and SA with IVD strategy.

A frequency domain analysis was also performed. The frequency response functions (FRF) were obtained using a band limited white-noise excitation (Gaussian noise filtered by a low-pass filter at 50 Hz). Two FRFs for two different systems (f_b=0,25 Hz and f_b=1 Hz with ξ_b=0,1) are represented in figure 3.20. In general both passive and SA solutions increase the structural damping as can be seen by the reduction in the resonance peaks. However, SA systems can reduce the resonance peak without increasing significantly the roll-off, meaning that the SA control strategy follows in part the control law (integral control action, see Bode plot in figure 3.17 (right)). In fact it is impossible for the SA system to be able to follow the integral control action due to the nature of the correspondent device, which cannot add energy to the system, but instead it can only dissipate it. It can be seen that lower fundamental frequency systems have the resonance peak close to the magnitude increase part of the input action (compare with figure 3.3). This means that system responses to seismic actions are more attenuated under these circumstances than with higher fundamental frequency systems. It can be seen that SA systems in particular attenuate more the acceleration response than passive ones. This is due to the fact that an increase of damping with a passive system leads to a lower decay rate after the resonance peak. The performance gains are even more obvious for input actions with higher frequency

components, i.e. type 2 seismic actions. In these cases, SA peak acceleration responses are improved for a higher range of systems fundamental frequencies as mentioned previously and observed in table 3.4. In this situation the resonance peak of the system is closer to the higher magnitude components of the input action and therefore the SA system acceleration reductions are similar or superior to the passive system ones. Comparing the SA system acceleration FRFs with the original structure ones, a higher reduction of the resonance peak is achieved with the former, although the original structure rolls-off better after the cross over frequency and up to 20 Hz approximately. In terms of relative displacements, bigger attenuations are found for the passive system with higher fundamental frequencies, meaning that relative displacements are more reduced with a passive system.

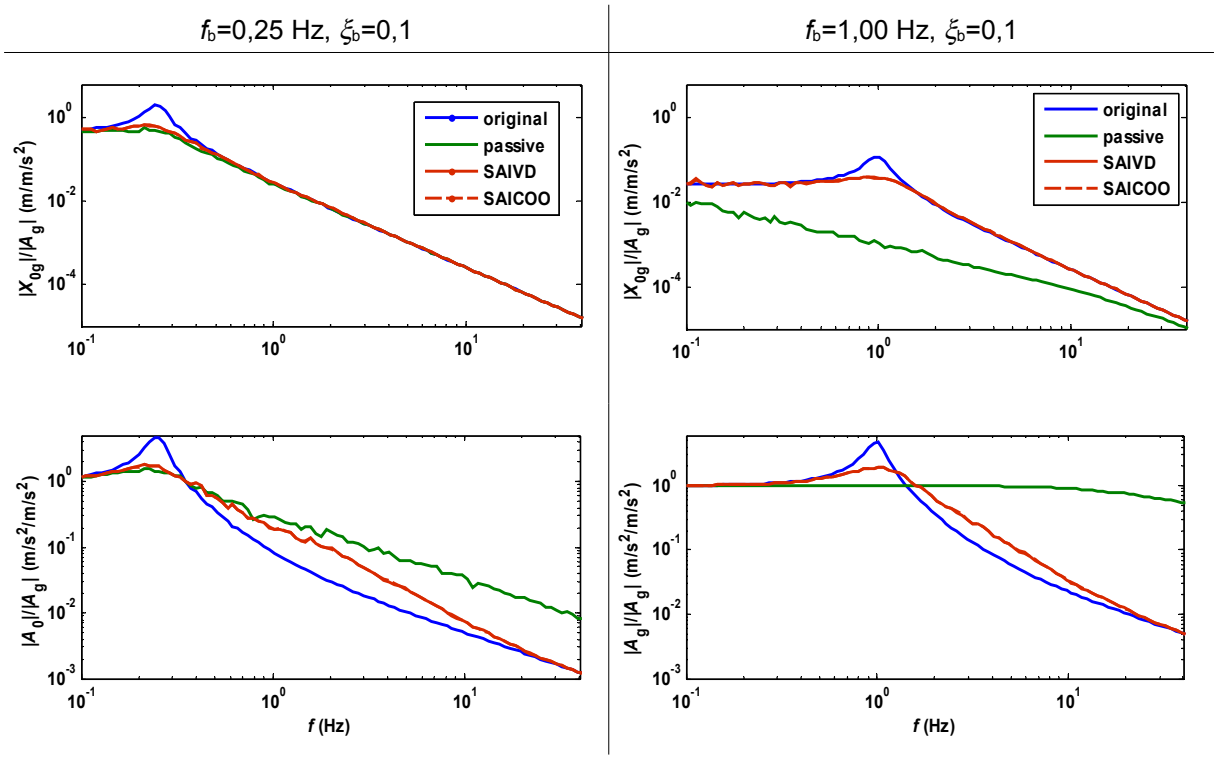

Figure 3.20 - SDOF structural systems frequency response functions: original (no devices), passive and SA with I VD and I COO.

3.3.6 Optimal Control

The so-called linear quadratic regulator (LQR) was considered to derive the desired force for the SA algorithm. This controller computes a control signal that is proportional to states of the system, that should be available or can be reconstructed. Assuming that the system is subjected to white noise excitation $w=\ddot{x}_g$ with zero mean E[w]=0 and known variance E[$w \cdot w^T$]=w_0, the performance index that weights the output y and the input desired force f_d is given by (see section 2.9.3):

$$J=\lim_{\tau\to\infty}\frac{1}{\tau}\mathrm{E}\left\{\int_0^{\tau} q\cdot y^2+r\cdot f_d^2 \;\; \mathrm{d}t\right\} \tag{3.41}$$

where: q and r are the weighting values on the output and input respectively; and E[·] is the expectation operator. The output considered to derive the controller gain can be any variable available from measurement: relative displacement; relative velocity; or the absolute acceleration. The solution of this problem will lead to a linear control law function of the states $\boldsymbol{z}$, which is found considering the time invariant and steady-state solution given by a constant gain matrix $\boldsymbol{K}_c$. The solution was presented previously in equation (2.39):

$$f_d = -\boldsymbol{K}_c \cdot \boldsymbol{z}, \quad \boldsymbol{K}_c = \boldsymbol{R}^{-1} \cdot \left[\boldsymbol{B}^T \cdot \boldsymbol{P} + \boldsymbol{N}^T\right] \tag{3.42}$$

where $\boldsymbol{P}$ is the solution of the adequate *algebraic Riccati equation* (ARE), equation (2.40):

$$\boldsymbol{P} \cdot \boldsymbol{A} + \boldsymbol{A}^T \cdot \boldsymbol{P} - (\boldsymbol{P} \cdot \boldsymbol{B} + \mathbf{N}) \cdot \boldsymbol{R}^{-1} \cdot (\boldsymbol{B}^T \cdot \boldsymbol{P} + \boldsymbol{N}^T) + \boldsymbol{Q} = \mathbf{0} \tag{3.43}$$

Matrices $\boldsymbol{Q}$, $\boldsymbol{R}$ and $\boldsymbol{N}$ are defined according to (2.38), and recalled here:

$$\begin{aligned} \boldsymbol{Q} &= q \cdot \boldsymbol{C}_y^T \cdot \boldsymbol{C}_y \\ \boldsymbol{R} &= r + q \cdot \boldsymbol{D}_y^T \cdot \boldsymbol{D}_y \\ \boldsymbol{N} &= q \cdot \boldsymbol{C}_y^T \cdot \boldsymbol{D}_y \end{aligned} \tag{3.44}$$

Adequate controller solutions should be stable in closed-loop (linear counterpart, considering $f_{SA}=f_d$). Substituting equation (3.42) in (3.2), the closed-loop system is found:

$$\dot{\boldsymbol{z}} = (\boldsymbol{A} - \boldsymbol{B} \cdot \boldsymbol{K}_c) \cdot \boldsymbol{z} + \boldsymbol{E} \cdot \ddot{x}_g \tag{3.45}$$

Thus, controller gains $\boldsymbol{K}_c$ should be chosen such that the dynamic matrix ($\boldsymbol{A}$-$\boldsymbol{B} \cdot \boldsymbol{K}_c$) eigenvalues have negative real part.

With the presented formulation a preliminary analysis was made in order to identify the weights that are more beneficial for the system response. Numerical simulations were performed considering a representative sample of input ground motions (accelerograms) in order to identify the value that minimizes the mean peak acceleration responses.

Adjusting Damping Rules

The VD and COO algorithms in section 3.3.8 were also considered here.

SDOF model analysis

Numerical simulations were performed considering weights on different variables: i) relative displacement, thus $\boldsymbol{C}_y$=[1 0] and $\boldsymbol{D}_y$=0; ii) relative velocity, thus $\boldsymbol{C}_y$=[0 1] and $\boldsymbol{D}_y$=0; and absolute acceleration, thus $\boldsymbol{C}_y$=[$-k_b/m$ $-c_b/m$] and $\boldsymbol{D}_y$=$-1/m$. The resulting closed-loop systems for varying output weight q for any of these cases is always stable as can be observed on the root locus in figure 3.21. The input weight r has no influence on the root-locus form however it changes the aspect ratio. In order to achieve the same closed-loop system poles with a different input weight, a higher r forces the output weight q to be higher too. The root-locus shows that weighting the: i) relative displacement, increases the closed-loop natural

frequency and the closed-loop damping ratio up to a constant value; ii) relative velocity, the shape is similar to the one of a linear viscous damping system (for damping increase); iii) absolute acceleration, for lower gains the root-locus shape is similar to the one weighting the relative velocity, and for higher gains is similar to the one weighting the relative displacement. The Bode diagram for two different weights $q_1<q_2$ can be found in figure 3.22. As the frequency response provided by the integral control law, the LQR controller synthesis weighting on the relative velocity provides similar frequency response characteristics: resonance peak reduction keeping the roll-off on the acceleration. However, it must be emphasized that this solution is a state (relative displacement and relative velocity) feedback controller and the integral controller is an absolute velocity feedback controller. The controllers with weights on the relative displacement and absolute acceleration introduce a different static gain on the response, but both keep the roll-off on the acceleration, which does not happen with the passive solution.

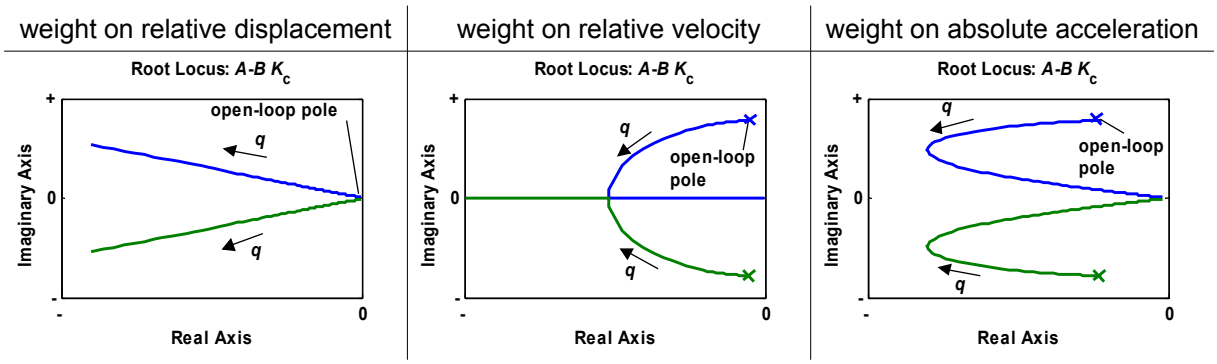

Figure 3.21 - Root Locus of the SDOF closed loop system with weights on the relative displacement, relative velocity and absolute acceleration with constant weight on the input.

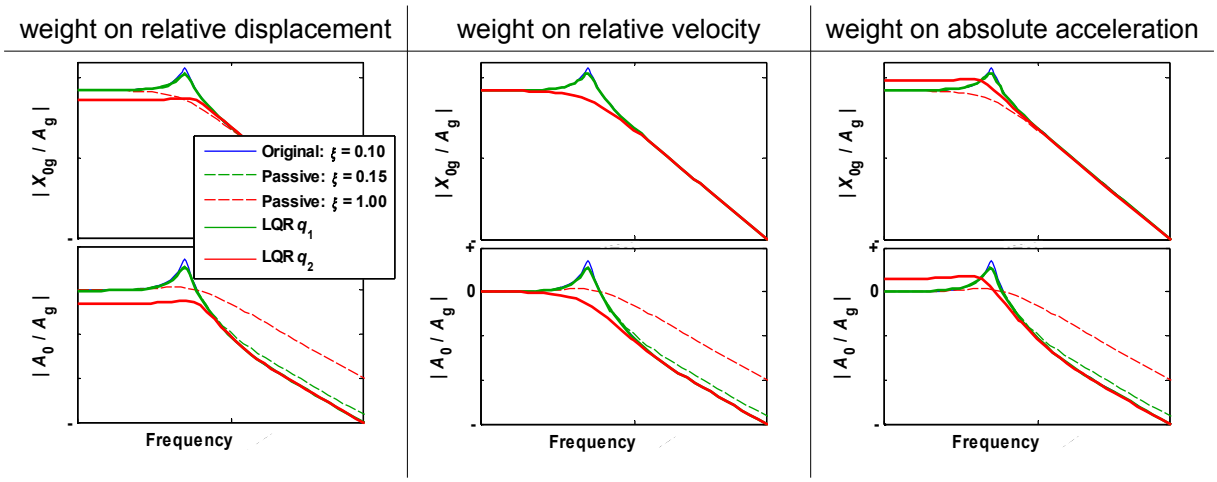

Figure 3.22 - Bode diagram of the SDOF closed loop system with weights $q_1<q_2$ compared with the original and passive systems.

In order to analyse the influence of each weight on the system performance numerical simulations were performed using the described earthquake ground motions. The results in figure 3.23 are typical evolutions of the peak responses with the output weight. Comparing

the results provided by each case it was found that weighting the absolute acceleration always provides better performance (reduction of relative displacements and acceleration). The results show also that increasing the relative displacement or relative velocity weight always leads to higher accelerations. The influence of the input weight on the responses is depicted in figure 3.24. It is found a translation of the curves to the higher output weights as the input weight is increased, which is in accordance to the results found from the analysis of the root-locus. Thus, in the LQR controller synthesis an input weight r=1 was always considered and the output variable to weight was the absolute acceleration. In fact, previous studies have already showed that acceleration is more straightforward and convenient to measure than the relative displacement and relative velocity which define the states of the system (*Dyke et al. 1996(c)*).

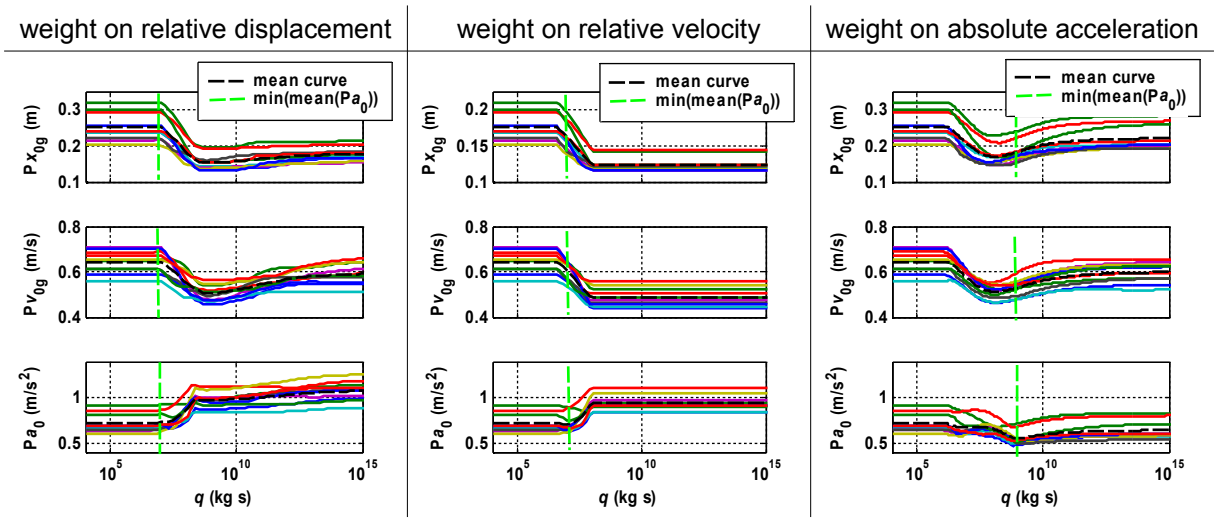

Figure 3.23 - Peak responses of the SDOF model (f_b=0,25 Hz; ξ_b=0,1) with an SA device plus LQR controller vs. output weight q (with input weight r=1 s/kg) subjected to 10 input type 1 accelerograms.

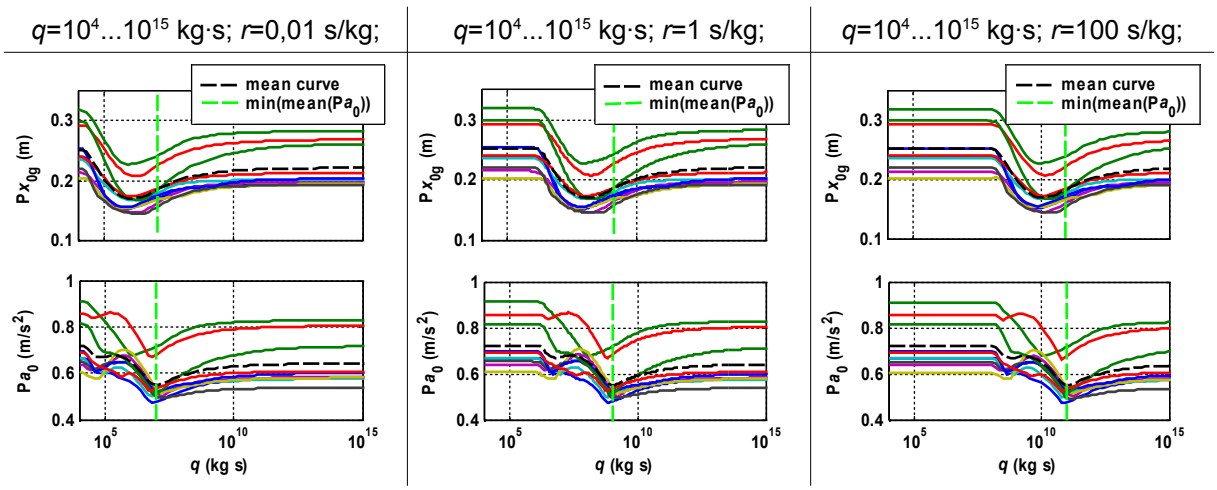

Figure 3.24 - Peak responses of the SDOF model (f_b=0,25 Hz; ξ_b=0,1) with an SA device plus LQR controller vs. output acceleration weight q and different input weights r under 10 type 1 accelerograms.

Using the minimum of mean peak responses as the criterion to identify the output weight q to design the controller gain vector $\boldsymbol{K}_c$, the values were identified and the results are found in

figure 3.25.

As for the damping ratio in the integral control law, different values of output weight are found for the same system natural frequencies. Notice that higher weighting values are obtained for type 2 seismic actions and for VD algorithms, but small impact on the system response is observed if any value in that range is considered for the controller design. Responses provided by this force tracking schemes using the identified output weights can be found in table 3.4. it was found that: both force tracking schemes: provide similar results (VD and COO algorithms); perform better than the original system and better than the passive one in terms of accelerations for structural systems with f_b≤0,62 Hz for type 1 seismic actions and f_b≤1,00 Hz for type 2 seismic actions; have slightly inferior performance than the integral law force tracking schemes in terms of both relative displacements and accelerations.

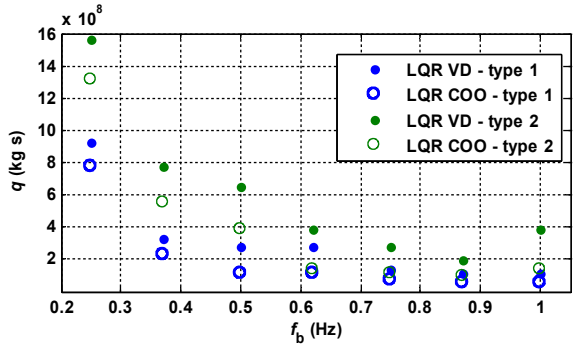

Figure 3.25 - LQR controller output weights q function of SDOF system natural frequency.

3.3.7 Model Predictive Control

A predictive control strategy was also considered to derive the desired force (figure 3.26).

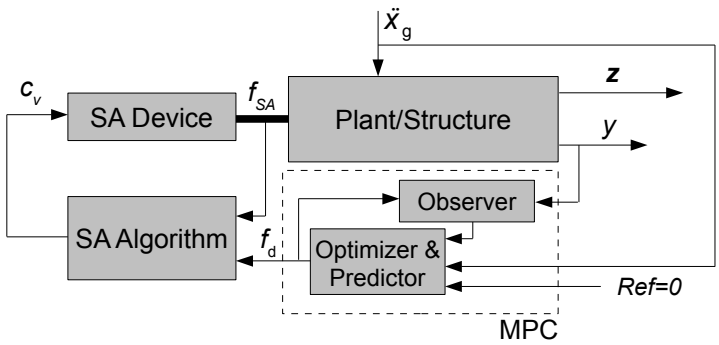

Figure 3.26 - Block diagram of the closed-loop system: structure employing an SA device controlled by an MPC control strategy and an algorithm.

The idea behind this controller consists in predicting future outputs from actual measurements and past inputs using the system model (predictor), compare those outputs with the reference output (base floor acceleration) values, which is set to zero, and determine input trajectories that result from the solution of an optimization problem (optimizer). Only the first input is applied to the plant, and then the whole cycle of measurement, prediction and input calculation is repeated in the next sampling interval (receding horizon). Since the states

are not always available, this strategy can use an observer to estimate the states (observer).

Controller Formulation

The prediction model of the MPC block is a linear model of the plant. From the continuous model, a discrete time version can be obtained by taking T_s as the discretization period. T_s in this context is also denominated the control interval, time between consecutive time instants. The discrete-time model resulting from the continuous one in equation (3.2) is given by:

$$\boldsymbol{z}(k+1)=\boldsymbol{A}_d\cdot\boldsymbol{z}(k)+\boldsymbol{B}_d\cdot f_{SA}(k)+\boldsymbol{E}_d\cdot a_g(k) \tag{3.46}$$

where: k is the time step resulting from the discretization process ($k=t/T_s$); $\boldsymbol{E}_d=\boldsymbol{E}$; and the transition matrix $\boldsymbol{A}_d$ and the input matrix $\boldsymbol{B}_d$ are dependent on the discretization method considered (rectangular approximation, zero-order hold (ZOH), or other).

The prediction model used in the controller formulation considers input delays resulting from the input action f_{SA} generated by the device due to the device time response (described by T_d). Thus, the formulation takes into account that the desired force f_d computed at time t-T_d will result in a force f_{SA} applied by the device on the structure at time t. Since the controller is formulated in discrete-time domain, the following relationship holds:

$$f_{SA}(k)=f_d(k-d) \tag{3.47}$$

Measurement delays are assumed to be small when compared to the input delays and thus are not considered in the formulation. It is also assumed that the controller computes the input during the control interval T_s (or sampling period). Under these assumptions, the structural model described by equation (3.2) for the SDOF case with input time delays, results in the following discrete-time domain controller internal model (n_a=2+d states, one input, one disturbance and one controlled outputs):

$$\begin{aligned}\boldsymbol{z}_a(k+1)&=\boldsymbol{A}_a\cdot\boldsymbol{z}_a(k)+\boldsymbol{B}_a\cdot f_d(k)+\boldsymbol{E}_a\cdot a_g(k)\\ y(k)&=\boldsymbol{C}_a\cdot\boldsymbol{z}_a(k)\end{aligned} \tag{3.48}$$

where $\boldsymbol{z}_a$(k) is the augmented state vector and $\boldsymbol{A}_a$, $\boldsymbol{B}_a$, $\boldsymbol{E}_a$ and $\boldsymbol{C}_a$ are given by:

$$\begin{gathered}\boldsymbol{z}_a(\mathrm{k})=\left\{\boldsymbol{z}(\mathrm{k})^T,\ \boldsymbol{f}_u(\mathrm{k})^T\right\}^T\\ \boldsymbol{A}_a=\begin{bmatrix}\boldsymbol{A}_d & \boldsymbol{B}_d\cdot\boldsymbol{C}_u\\ \boldsymbol{0} & \boldsymbol{A}_u\end{bmatrix},\ \boldsymbol{B}_a=\begin{bmatrix}\boldsymbol{0}\\ \boldsymbol{B}_u\end{bmatrix},\ \boldsymbol{E}_a=\begin{bmatrix}\boldsymbol{E}_d\\ \boldsymbol{0}\end{bmatrix},\ \boldsymbol{C}_a=\begin{bmatrix}\boldsymbol{C}_d & \boldsymbol{0}\end{bmatrix},\end{gathered} \tag{3.49}$$

where:

$$\begin{gathered}\boldsymbol{f}_u(\mathrm{k})=\left\{f_d(\mathrm{k-d}),\dots,f_d(\mathrm{k-1})\right\}^T\\ \boldsymbol{A}_u=\begin{bmatrix}0&1&0&\dots&0\\0&0&1&\dots&0\\0&0&0&\ddots&\vdots\\0&0&0&\dots&1\\0&0&0&\dots&0\end{bmatrix},\ \boldsymbol{B}_u=\begin{bmatrix}0\\0\\\vdots\\0\\1\end{bmatrix},\ \boldsymbol{C}_u=\begin{bmatrix}1\\0\\\vdots\\0\\0\end{bmatrix}^T\end{gathered} \tag{3.50}$$

Using this model to predict the behaviour of the system for a specific prediction horizon (HP steps) and considering that the input force remains constant after a specific control horizon (HC steps), then the output predictions are obtained using equation (3.48):

$$\hat{\boldsymbol{z}}_{\mathrm{a}}(k+j|k)=\boldsymbol{A}_{\mathrm{a}}\cdot\hat{\boldsymbol{z}}_{\mathrm{a}}(k+j-1|k)+\boldsymbol{B}_{\mathrm{a}}\cdot\hat{f}_{\mathrm{d}}(k+j-1|k)+ \\ +\boldsymbol{E}_{\mathrm{a}}\cdot a_{\mathrm{g}}(k+j-1),\ \text{for } j=1\ldots\mathrm{HP} \tag{3.51}$$

The model in equation (3.51) starts from the value of the state at instant *k*:

$$\hat{\boldsymbol{z}}_{a}(k|k)=\hat{\boldsymbol{z}}_{a}(k) \tag{3.52}$$

Some terms in the equation have a hat over the variable which means that some of them could not be available at that time instant. The state vector is one of the variables that could not be available if the states are not measured and thus an observer has to be used to estimate them. We will discuss the observer design later. The control force is not available either at the time when one computes the predictions, one just knows the forces at previous instants. It is common then to assume that inputs change up to times *k*+HC-1 and remain constant after that:

$$\hat{f}_{\mathrm{d}}(k+j|k)=\hat{f}_{\mathrm{d}}(k+HC-1|k),\ \text{for } j=\mathrm{HC}\ldots\mathrm{HP}-1 \tag{3.53}$$

Thus, as stated before, the control inputs up to *k*+HC-1 are solution of the optimization problem but only the first one will be used as input. Writing the equations in terms of the input moves, one gets:

$$\Delta\hat{f}_{\mathrm{d}}(k+j|k)=\hat{f}_{\mathrm{d}}(k+j|k)-\hat{f}_{\mathrm{d}}(k+j-1|k),\ \text{for } j=0\ldots\mathrm{HC}-1 \tag{3.54}$$

Assuming that at time *k* one already knows *f*(k-1) and after iterating the model up to *j*=HP, one gets (*Maciejowski 2002*):

$$\boldsymbol{Z}(k)=\mathcal{A}\cdot\hat{z}_{a}(k)+\mathcal{B}\cdot f_{\mathrm{d}}(k-1)+\mathcal{H}\cdot\Delta\boldsymbol{F}_{\mathrm{d}}(k)+\mathcal{E}\cdot\boldsymbol{A}_{\mathrm{g}}(k) \tag{3.55}$$

where:

- $\boldsymbol{Z}(k)=\left\{\hat{\boldsymbol{z}}(k+1|k)^{\mathrm{T}},\ \ldots,\hat{\boldsymbol{z}}(k+\mathrm{HP}|k)^{\mathrm{T}}\right\}^{\mathrm{T}}$ is the vector (dimension n_a·HPx1) with each state vector predictions at instant *k* for instant *k*+1 to *k*+HP;
- $\hat{\boldsymbol{z}}_{\mathrm{a}}(\mathrm{k})$ is the estimated state vector (dimension n_ax1) at instant *k* (when the full state vector is not available);
- *f*(*k*-1) is the force at instant *k*-1 (scalar);
- $\Delta\boldsymbol{F}_{\mathrm{d}}(k)=\left\{\Delta f_{\mathrm{d}}(k|k)^{\mathrm{T}},\ \ldots,\Delta f_{\mathrm{d}}(k+\mathrm{HC}\text{-}1|k)^{\mathrm{T}})\right\}^{\mathrm{T}}$ is the vector (dimension HCx1) of future force input moves, $\Delta f_{\mathrm{d}}(\mathrm{k})=f_{\mathrm{d}}(\mathrm{k})-f_{\mathrm{d}}(\mathrm{k-1})$;
- $\boldsymbol{A}_{\mathrm{g}}(k)=\left\{a_{\mathrm{g}}(k),\hat{a}_{\mathrm{g}}(k|k),\ \ldots,\hat{a}_{g}(k+\mathrm{HP}\text{-}1|k))\right\}^{\mathrm{T}}$ is the vector of measured (actual)

and future disturbances (dimension HPx1); for the future disturbances it is common practice to assume constant and equal to the last measured value $a_g(k)$, thus $\boldsymbol{A}_g(k)=\mathbf{1}\cdot a_g(k)$.

The matrices $\mathcal{A}$ (dimension $n_a\cdot$HPxn_a), $\mathcal{B}$ (dimension $n_a\cdot$HPx1), $\mathcal{H}$ (dimension $n_a\cdot$HPxHC) and $\mathcal{E}$ (dimension $n_a\cdot$HPxHP) are given by:

$$\mathcal{A}=\begin{bmatrix}\boldsymbol{A}_a\\ \vdots\\ \boldsymbol{A}_a^{HC}\\ \boldsymbol{A}_a^{HC+1}\\ \vdots\\ \boldsymbol{A}_a^{HP}\end{bmatrix},\ \mathcal{E}=\begin{bmatrix}\boldsymbol{E}_a & \mathbf{0} & \cdots & \mathbf{0}\\ \boldsymbol{A}_a\cdot\boldsymbol{E}_a & \boldsymbol{E}_a & \cdots & \mathbf{0}\\ \vdots & \vdots & \ddots & \vdots\\ \boldsymbol{A}_a^{HP-1}\cdot\boldsymbol{E}_a & \boldsymbol{A}_a^{HP-2}\cdot\boldsymbol{E}_a & \cdots & \boldsymbol{E}_a\end{bmatrix},$$

$$\mathcal{B}=\begin{bmatrix}\boldsymbol{B}_a\\ \vdots\\ \sum_{j=0}^{j=HC-1}\boldsymbol{A}_a^j\cdot\boldsymbol{B}_a\\ \sum_{j=0}^{j=HC}\boldsymbol{A}_a^j\cdot\boldsymbol{B}_a\\ \vdots\\ \sum_{j=0}^{j=HP-1}\boldsymbol{A}_a^j\cdot\boldsymbol{B}_a\end{bmatrix},\ \mathcal{H}=\begin{bmatrix}\boldsymbol{B}_a & \cdots & \mathbf{0}\\ \vdots & \ddots & \vdots\\ \sum_{j=0}^{j=HC-1}\boldsymbol{A}_a^j\cdot\boldsymbol{B}_a & \cdots & \boldsymbol{B}_a\\ \sum_{j=0}^{j=HC}\boldsymbol{A}_a^j\cdot\boldsymbol{B}_a & \cdots & \boldsymbol{A}_a\cdot\boldsymbol{B}_a+\boldsymbol{B}_a\\ \vdots & \ddots & \vdots\\ \sum_{j=0}^{j=HP-1}\boldsymbol{A}_a^i\cdot\boldsymbol{B}_a & \cdots & \sum_{j=0}^{j=HP-HC}\boldsymbol{A}_a^j\cdot\boldsymbol{B}_a\end{bmatrix} \tag{3.56}$$

The output predictions from k+1 to k+HP can be obtained using the output equation of the model - last expression of equation (3.48) - which leads to:

$$\begin{aligned}&\boldsymbol{Y}(k)=\mathcal{C}_a\cdot\boldsymbol{Z}(k)\Leftrightarrow\\ &\boldsymbol{Y}(k)=\boldsymbol{\Psi}\cdot\hat{\boldsymbol{z}}_a(k)+\boldsymbol{T}\cdot f_d(k-1)+\boldsymbol{\Theta}\cdot\Delta\boldsymbol{F}_d(k)+\boldsymbol{\Xi}\cdot\boldsymbol{A}_g(k)\end{aligned} \tag{3.57}$$

Where each term in the equation is given by:

- $\boldsymbol{Y}(k)=\left\{\hat{y}(k+1|k)^T,\ \ldots,\ \hat{y}(k+HP|k)^T\right\}^T$ is the vector of output predictions at instant k for instant k+1 to k+HP (dimension HPx1);
- $\mathcal{C}_a=\mathrm{diag}([\boldsymbol{C}_a,\cdots,\boldsymbol{C}_a])$ is the composed output matrix (block diagonal) for k+1 to k+HP instants (dimension HPx$n_a\cdot$HP);
- and the matrices are given by $\boldsymbol{\Psi}=\mathcal{C}_a\cdot\mathcal{A}$ (dimension HPxn_a), $\boldsymbol{T}=\mathcal{C}_a\cdot\mathcal{B}$ (dimension HPx1) $\boldsymbol{\Theta}=\mathcal{C}_a\cdot\mathcal{H}$ (dimension HPxHC) and $\boldsymbol{\Xi}=\mathcal{C}_a\cdot\mathcal{E}$ (dimension HPxHP).

The optimal input force moves can be obtained as the solution of an unconstrained optimization problem (minimization) with the following cost function that weights the outputs and the input moves over the prediction horizon and control horizon:

$$V(k)=\sum_{i=1}^{HP}\|\hat{y}(k+i|k)\|_q^2+\sum_{i=0}^{HC-1}\|\Delta\hat{f}_d(k+i|k)\|_r^2=\|\boldsymbol{Y}(k)\|_{\mathcal{Q}}^2+\|\Delta\boldsymbol{F}_d(k)\|_{\mathcal{R}}^2 \quad (3.58)$$

where:

- $\|\boldsymbol{x}\|_{\boldsymbol{P}}^2=\boldsymbol{x}^{\mathbf{T}}\cdot\boldsymbol{P}\cdot\boldsymbol{x}$ is a quadratic form or the square weighted norm (with $\boldsymbol{P}$ weight);
- q (scalar) and r (scalar) are the weighting values on the output and input respectively;
- $\mathcal{Q}$ (dimension HPxHP) and $\mathcal{R}$ (dimension HCxHC) are the composed weighting matrices (block diagonal) with q and r weighting values for each instant k in the diagonal.

Defining the tracking error between the future target trajectory and the free response of the system (the response that would occur over the prediction horizon if no input changes were made, $\Delta\boldsymbol{F}_d=\mathbf{0}$), and considering the future target trajectory equal to zero, regulation problem, then the tracking error at instant k over the prediction horizon is given by:

$$\boldsymbol{E}(k)=-\boldsymbol{Y}(k)=-\boldsymbol{\Psi}\cdot\hat{\boldsymbol{z}}_a(k)-\boldsymbol{T}\cdot f(k-1)-\boldsymbol{\Xi}\cdot\boldsymbol{A}_g(k) \quad (3.59)$$

Substituting (3.59) in (3.58) one gets:

$$\begin{aligned}V(k)&=\|\boldsymbol{\Theta}\cdot\Delta\boldsymbol{F}_d(k)-\boldsymbol{E}(k)\|_{\mathcal{Q}}^2+\|\Delta\boldsymbol{F}_d(k)\|_{\mathcal{R}}^2\\&=\boldsymbol{E}(k)^{\mathrm{T}}\cdot\mathcal{Q}\cdot\boldsymbol{E}(k)-2\Delta\boldsymbol{F}_d(k)^{\mathrm{T}}\cdot\boldsymbol{\Theta}^{\mathbf{T}}\cdot\mathcal{Q}\cdot\boldsymbol{E}(k)+\Delta\boldsymbol{F}_d(k)^{\mathrm{T}}\cdot\left[\boldsymbol{\Theta}^{\mathbf{T}}\cdot\mathcal{Q}\cdot\boldsymbol{\Theta}+\mathcal{R}\right]\cdot\Delta\boldsymbol{F}_d(k)\\&=\mathcal{C}_{\text{term}}-\Delta\boldsymbol{F}_d(k)^{\mathrm{T}}\cdot\mathcal{G}_{\text{term}}+\Delta\boldsymbol{F}_d(k)^{\mathrm{T}}\cdot\mathcal{H}_{\text{term}}\cdot\Delta\boldsymbol{F}_d(k)\end{aligned} \quad (3.60)$$

where:

- $\mathcal{C}_{\text{term}}=\boldsymbol{E}(k)^{\mathrm{T}}\cdot\mathcal{Q}\cdot\boldsymbol{E}(k)$; $\mathcal{G}_{\text{term}}=2\cdot\boldsymbol{\Theta}^{\mathbf{T}}\cdot\mathcal{Q}\cdot\boldsymbol{E}(k)$; $\mathcal{H}_{\text{term}}=\boldsymbol{\Theta}^{\mathbf{T}}\cdot\mathcal{Q}\cdot\boldsymbol{\Theta}+\mathcal{R}$;

The optimal input move can be obtained by finding the gradient of the cost function and set it to zero:

$$\nabla_{\Delta\boldsymbol{F}_d(\mathrm{k})}V(k)=-\mathcal{G}_{\text{term}}+2\cdot\mathcal{H}_{\text{term}}\cdot\Delta\boldsymbol{F}_d(k)=0 \quad (3.61)$$

And thus, the sequence of optimal input moves is given by:

$$\Delta\boldsymbol{F}_d(\mathrm{k})=\frac{1}{2}\mathcal{H}_{\text{term}}^{-1}\cdot\mathcal{G}_{\text{term}} \quad (3.62)$$

In order to guarantee the minimum solution the second derivative, or the Hessian matrix of V, should be positive definite. The Hessian matrix is given by:

$$\frac{\partial^2 V(k)}{\partial\Delta\boldsymbol{F}(\mathrm{k})^2}=2\cdot\mathcal{H}_{\text{term}}=2\cdot\left[\boldsymbol{\Theta}^{\mathbf{T}}\cdot\mathcal{Q}\cdot\boldsymbol{\Theta}+\mathcal{R}\right] \quad (3.63)$$

The sufficient conditions to guarantee the minimum are that one weighting matrix ($\mathcal{Q}$ or $\mathcal{R}$) is positive definite and the other is semi-positive definite.

The first term of $\Delta\boldsymbol{F}_d(\mathrm{k})$ is the optimal input move for the plant and the corresponding optimal

force can be obtained summing the previous instant force, from equation (3.54).

In order to avoid the inversion of $\mathcal{H}_{\text{term}}$ in computing equation (3.62), the optimal solution should be obtained in a different way. The cost function in equation (3.60) can be written as a square length of a vector $\boldsymbol{V}_{\text{v}}$ as in the following expression (*Maciejowski 2002*):

$$V(k)=\left\|\boldsymbol{V}_{\text{v}}(k)\right\|^2, \text{with } \boldsymbol{V}_{\text{v}}(k)=\begin{bmatrix}\boldsymbol{S}_{\mathcal{Q}}\cdot\left(\boldsymbol{\Theta}\cdot\Delta\boldsymbol{F}_{\text{d}}(k)-\boldsymbol{E}(k)\right)\\ \boldsymbol{S}_{\mathcal{R}}\cdot\Delta\boldsymbol{F}_{\text{d}}(k)\end{bmatrix} \tag{3.64}$$

where: $\boldsymbol{S}_{\mathcal{Q}}$ and $\boldsymbol{S}_{\mathcal{R}}$ are the square-roots of $\mathcal{Q}$ and $\mathcal{R}$ respectively, with $\boldsymbol{S}_{\mathcal{R}}^{\text{T}}\cdot\boldsymbol{S}_{\mathcal{R}}=\mathcal{R}$, $\boldsymbol{S}_{\mathcal{Q}}^{\text{T}}\cdot\boldsymbol{S}_{\mathcal{Q}}=\mathcal{Q}$. The minimum length of vector $\boldsymbol{V}_{\text{v}}(k)$ minimizes the cost function $V(k)$ and thus, gives the optimal input moves $\Delta\boldsymbol{F}(\text{k})$. Again, finding the gradient of $V(k)$ in equation (3.64) leads to the following least-squares problem:

$$\begin{bmatrix}\boldsymbol{S}_{\mathcal{Q}}\cdot\boldsymbol{\Theta}\\ \boldsymbol{S}_{\mathcal{R}}\end{bmatrix}\cdot\Delta\boldsymbol{F}_{\text{d}}(\text{k})=\begin{bmatrix}\boldsymbol{S}_{\mathcal{Q}}\cdot\boldsymbol{E}(\text{k})\\ \boldsymbol{0}\end{bmatrix} \tag{3.65}$$

which is a better way for computational implementation.

Observer Design

If one cannot have access to the full state vector an observer has to be used to estimate the state vector. The observer is a copy of the plant model with feedback from measured plant outputs and observer outputs through a gain matrix to correct the state estimate. Since the systems is always subjected to process and measurement noise, the observer is designed using the Kalman filter technique (*Lewis 1986*). The system model in equation (3.48) is augmented with a measurement noise term which is modelled as Gaussian white-noise process. For this purpose the input ground motion is assumed to be process noise with Gaussian characteristics. Thus, both noises are described by zero mean and variance w_0 and v_0 respectively. The augmented model is:

$$\begin{aligned}&\boldsymbol{z}_{\text{a}}(k+1)=\boldsymbol{A}_{\text{a}}\cdot\boldsymbol{z}_{\text{a}}(k)+\boldsymbol{B}_{\text{a}}\cdot f_{\text{d}}(k)+\boldsymbol{E}_{\text{a}}\cdot a_{\text{g}}(k)\\ &y(k)=\boldsymbol{C}_{\text{a}}\cdot\boldsymbol{z}_{\text{a}}(k)+v(k)\\ &\quad\text{with } a_{\text{g}}(k)\sim(0,w_0),\ \ v(k)\sim(0,v_0)\end{aligned} \tag{3.66}$$

The equations of the observer are given by:

$$\begin{aligned}&\hat{\boldsymbol{z}}_{\text{a}}(k+1|k)=\boldsymbol{A}_{\text{a}}\cdot\hat{\boldsymbol{z}}_{\text{a}}(k|k)+\boldsymbol{B}_{\text{a}}\cdot f_{\text{d}}(k)\\ &\hat{y}(k|k-1)=\boldsymbol{C}_{\text{a}}\cdot\hat{\boldsymbol{z}}_{\text{a}}(k|k-1)\\ &\hat{\boldsymbol{z}}_{\text{a}}(k|k)=\hat{\boldsymbol{z}}_{\text{a}}(k|k-1)+\boldsymbol{K}_{\text{o}}\cdot\left[y(k)-\hat{y}(k|k-1)\right]\end{aligned} \tag{3.67}$$

where: $\boldsymbol{K}_{\text{o}}$ is the *Kalman* gain. The first two expressions reflect the effect of system dynamics in the estimation. The first one in particular defines *a priori* estimate (before including the measurement $y(k)$), the state time update, which provides a prediction of the state. The third equation defines *a*n *posteriori* estimate that reflects the effect of system measurement, the

measurement update, and provides a correction based on the measurement update. Manipulating the expressions of equation (3.67), the *Kalman* filter is given by:

$$\begin{aligned}
&\hat{\boldsymbol{z}}_{\mathrm{a}}(k+1|k)=\boldsymbol{A}_{\mathrm{a}}\left(\mathbf{I}-\boldsymbol{K}_{\mathrm{o}}\cdot\boldsymbol{C}_{\mathrm{a}}\right)\cdot\hat{\boldsymbol{z}}_{\mathrm{a}}(k|k-1)+\boldsymbol{B}_{\mathrm{a}}\cdot f_{\mathrm{d}}(k)+\boldsymbol{A}_{\mathrm{a}}\cdot\boldsymbol{K}_{\mathrm{o}}\cdot\boldsymbol{y}(k)\\
&\boldsymbol{K}_{\mathrm{o}}=\boldsymbol{P}_{\mathrm{o}}\cdot\boldsymbol{C}_{\mathrm{a}}^{\mathrm{T}}\cdot\left[v_{\mathrm{o}}+\boldsymbol{C}_{\mathrm{a}}\cdot\boldsymbol{P}_{\mathrm{o}}\cdot\boldsymbol{C}_{\mathrm{a}}^{\mathrm{T}}\right]^{-1}\\
&\boldsymbol{P}_{\mathrm{o}}=\boldsymbol{E}_{\mathrm{a}}\cdot w_{\mathrm{o}}\cdot\boldsymbol{E}_{\mathrm{a}}^{\mathrm{T}}+\boldsymbol{A}_{\mathrm{a}}\cdot\boldsymbol{P}_{\mathrm{o}}\cdot\boldsymbol{A}_{\mathrm{a}}^{\mathrm{T}}-\boldsymbol{A}_{\mathrm{a}}\cdot\boldsymbol{P}_{\mathrm{o}}\cdot\boldsymbol{C}_{\mathrm{a}}^{\mathrm{T}}\left[v_{\mathrm{o}}+\boldsymbol{C}_{\mathrm{a}}\cdot\boldsymbol{P}_{\mathrm{o}}\cdot\boldsymbol{C}_{\mathrm{a}}^{\mathrm{T}}\right]^{-1}\cdot\boldsymbol{C}_{\mathrm{a}}\cdot\boldsymbol{P}_{\mathrm{o}}\cdot\boldsymbol{A}_{\mathrm{a}}^{\mathrm{T}}
\end{aligned} \tag{3.68}$$

The formulation of equation (3.68) gives the expressions for the *Kalman* filter with a stationary gain. The *Kalman* gain $\boldsymbol{K}_{\mathrm{o}}$ is obtained after solving the *Riccati* equation with adequate covariance matrices. As stated in *Maciejowski 2002*, unitary variances (w_0 and v_0) are a compromise between observer response in estimating the state vector and control aggressiveness. It would be preferable a deadbeat observer but it will always lead to aggressive control actions which can compromise the overall performance of the system.

Stability

Although the SA closed-loop system (figure 3.26) is always stable, since the SA device is dissipative and can not add energy to the system, the closed-loop system of the linear counterpart (loop without SA algorithm and SA device) could be unstable under certain conditions. The implemented MPC controller with this characteristics computes desired forces f_{d} that go to infinity, which leads to an SA system with less performance. The designed MPC controller should then be stable in closed-loop (linear counterpart). Lets then analyse the closed-loop system of the linear counterpart. The input move $\Delta f_{\mathrm{d}}(\mathrm{k})$ resulting from the optimization problem, which will be used to compute the desired force is the first term of $\Delta\boldsymbol{F}_{\mathrm{d}}(\mathrm{k})$, and can be expressed as:

$$\Delta f_{\mathrm{d}}(\mathrm{k})=\boldsymbol{C}_1\cdot\hat{\boldsymbol{z}}_{\mathrm{a}}(\mathrm{k}|\mathrm{k})+C_2\cdot f_{\mathrm{d}}(\mathrm{k}-1)+C_3\cdot a_{\mathrm{g}}(\mathrm{k}) \tag{3.69}$$

where constants $\boldsymbol{C}_1$, C_2 and C_3 are the first entries of the correspondent parcels, given by:

- $\boldsymbol{C}_1=\mathrm{fr}\left(-\boldsymbol{T}_{\mathrm{term}}\cdot\boldsymbol{\Psi}\right)$; $C_2=\mathrm{fr}\left(-\boldsymbol{T}_{\mathrm{term}}\cdot\boldsymbol{T}\right)$; $C_3=\mathrm{fr}\left(-\boldsymbol{T}_{\mathrm{term}}\cdot\boldsymbol{\Xi}\cdot\mathbf{1}\right)$;

where: fr(x) is the first row of vector x; $\boldsymbol{T}_{\mathrm{term}}=\left(\boldsymbol{\Theta}^{\mathrm{T}}\cdot\mathcal{Q}\cdot\boldsymbol{\Theta}+\mathcal{R}\right)^{-1}\cdot\boldsymbol{\Theta}^{\mathrm{T}}\cdot\mathcal{Q}$. Using equations (3.69) and (3.54) to compute the desired force f_{d}, and substituting it on the system and observer expressions - equations (3.66) and (3.67) - the closed-loop system (linear counterpart) is:

$$\begin{aligned}
&\begin{bmatrix}\boldsymbol{z}_{\mathrm{a}}(k+1)\\ \hat{\boldsymbol{z}}_{\mathrm{a}}(k+1|k)\end{bmatrix}=\\
&=\begin{bmatrix}\boldsymbol{A}_{\mathrm{a}}+\boldsymbol{B}_{\mathrm{a}}\cdot\left(\boldsymbol{C}_1\cdot\boldsymbol{K}_{\mathrm{o}}\cdot\boldsymbol{C}_{\mathrm{a}}+(C_2+1)\cdot\mathbf{M}_{01}\right) & \boldsymbol{B}_{\mathrm{a}}\cdot\boldsymbol{C}_1\cdot(\mathbf{I}-\boldsymbol{K}_{\mathrm{o}}\cdot\boldsymbol{C}_{\mathrm{a}})\\ \boldsymbol{A}_{\mathrm{a}}\cdot\boldsymbol{K}_{\mathrm{o}}\cdot\boldsymbol{C}_{\mathrm{a}}+\boldsymbol{B}_{\mathrm{a}}\cdot\left(\boldsymbol{C}_1\cdot\boldsymbol{K}_{\mathrm{o}}\cdot\boldsymbol{C}_{\mathrm{a}}+(C_2+1)\cdot\mathbf{M}_{01}\right) & \left(\boldsymbol{A}_{\mathrm{a}}+\boldsymbol{B}_{\mathrm{a}}\cdot\boldsymbol{C}_1\right)\cdot(\mathbf{I}-\boldsymbol{K}_{\mathrm{o}}\cdot\boldsymbol{C}_{\mathrm{a}})\end{bmatrix}\cdot\begin{bmatrix}\boldsymbol{z}_{\mathrm{a}}(k)\\ \hat{\boldsymbol{z}}_{\mathrm{a}}(k|k-1)\end{bmatrix}+\\
&\qquad+\begin{bmatrix}\boldsymbol{E}_{\mathrm{a}}+\boldsymbol{B}_{\mathrm{a}}\cdot C_3\\ \boldsymbol{B}_{\mathrm{a}}\cdot C_3\end{bmatrix}\cdot a_{\mathrm{g}}(k)
\end{aligned} \tag{3.70}$$

where: **I** is the identity matrix; and $\mathbf{M}_{01}$ is the matrix that satisfies $f_d(k-1)=\mathbf{M}_{01}\cdot\mathbf{z}_a(k)$. Stability is achieved with the dynamic matrix eigenvalues of equation (3.70) inside the unit circle.

Adjusting Damping Rules

The VD and COO algorithms in section 3.3.8 were also considered with this strategy.

SDOF model analysis

The predictive controller described above has several adjustable parameters: weights (output weight q and input move weight r), horizons (HP and HC), control interval (T_s) and observer dynamics (described by variances w_0 and v_0). For nonlinear problems tuning these parameters is a question of applying a set of 'rules of thumb' based on experience gained from simulations (*Maciejowski 2002*). Adequate values for those parameters in this kind of problems were found considering the minimum of mean peak acceleration as criteria. Taking into account the results obtained in the LQR controller analysis, acceleration feedback is considered which is in fact the only variable weighted for the purpose of MPC controller synthesis. The observer was designed with a Kalman filter with unitary variance matrices (w_0=1 m/s^2 and v_0=1 m/s^2). The control interval (or sampling period) should be adequate to capture the system dynamics. Its value is delimited by the time taken to solve the optimization problem and by the inverse of the Nyquist frequency, obtained from the smallest time constant of the system. It should also be small enough so that the control input (desired force or damping) responds quickly to the output changes. An example of the influence of this parameter on the system's performance (mean peak responses) is shown in figure 3.27.

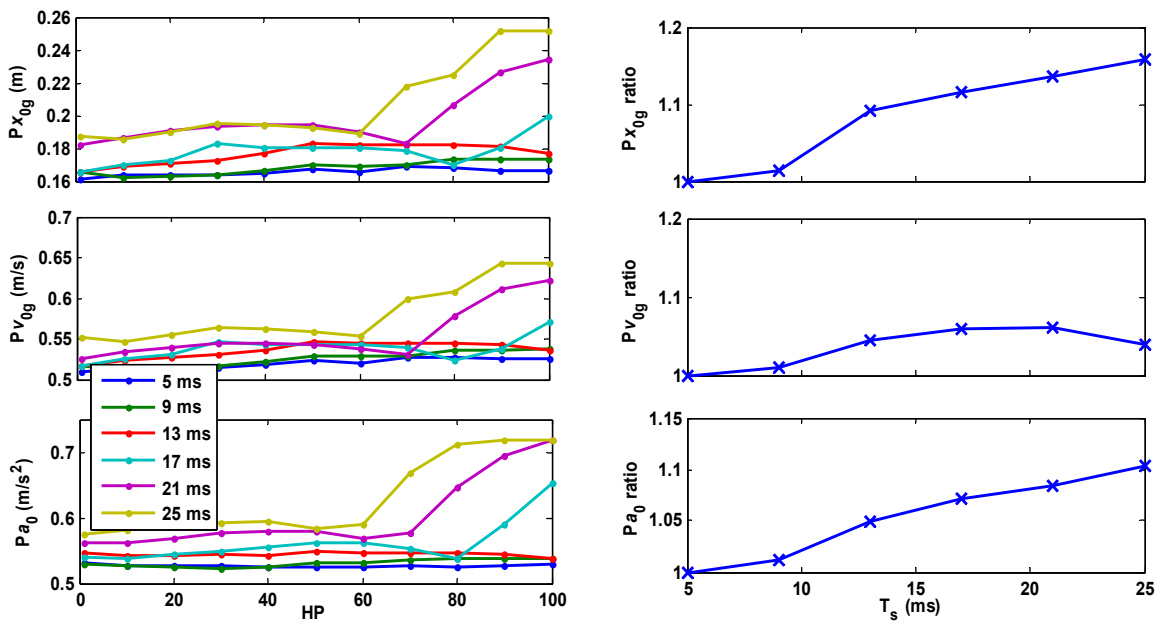

Figure 3.27 - Left: SDOF system mean peak responses (f_b=0,25 Hz and ξ_b=0,1 for MPCVD with HC=1 and r=1 s^2/kg) evolutions with control interval T_s and prediction horizon HP, when subjected to Type 1 seismic actions (10 accelerograms). Right: ratios vs. control interval T_s (relative to T_s=5 ms) for HP=50.

A comparison of results with different values of control interval and prediction horizons is presented. It is shown that higher control intervals lead to poor performance (increases in relative displacements and absolute accelerations). Higher control intervals also have a negative impact on the evolution of responses with the prediction horizon. As the control interval increases the range of prediction horizons that lead to good performances gets smaller (see figure 3.27 left), and thus as the control interval increases smaller prediction horizons should be considered to achieve good performance. A control interval (or sampling time) of T_s=5 ms was considered in this work.

The influence of weights and horizons on the response was analysed through a parametric study. Each structural system with an SA device was subjected to the set of accelerograms for each seismic action type (type 1 and 2) and the mean peak values were evaluated. Applying this procedure for different weights and horizons, combinations of these parameters that lead to the best system response (minimum acceleration) were found. Figure 3.28 (left) shows the typical evolution of system responses with the controller acceleration weight q for each input accelerogram.

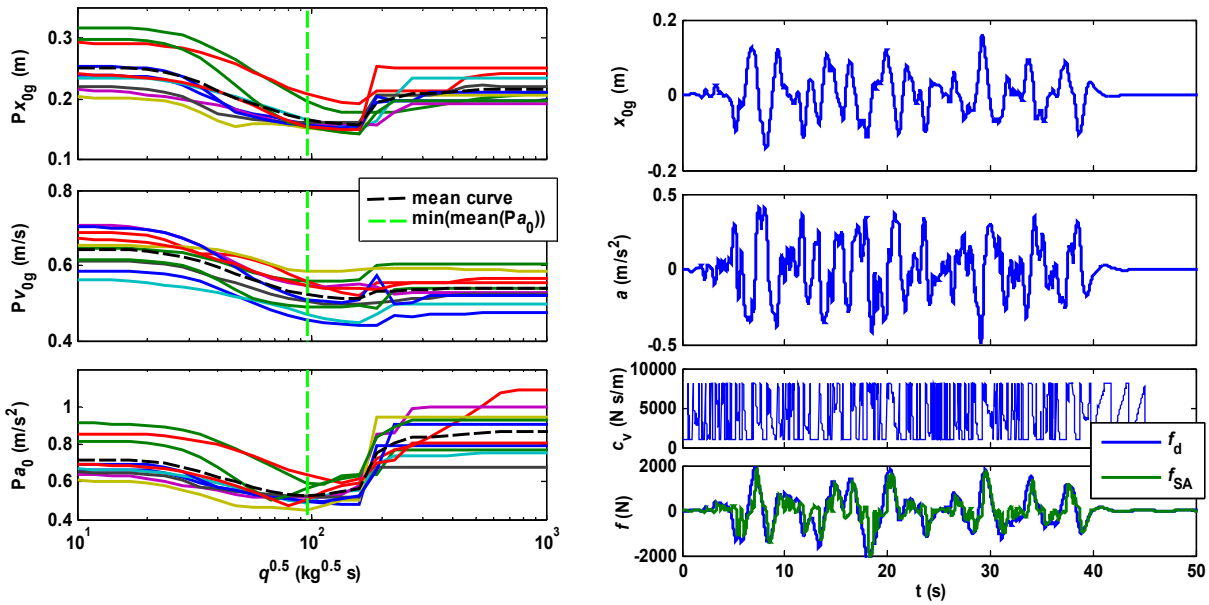

Figure 3.28 - Left: SDOF system responses (peak values) evolution with acceleration weight (f_b=0,25 Hz and ξ_b=0,1 for MPCVD with T_s=5 ms, HP=50, HC=1, r=1 s^2/kg), when subjected to type 1 seismic actions (10 input time accelerograms). Right: Time histories of system responses and inputs for the minimum acceleration weight for one input accelerogram.

Using the minimum of mean peak acceleration as the criteria to design the controller, reductions in relative displacement and velocity are also achieved, which leads also to reductions in base shear forces too. Higher values for this weighting parameter lead to poor performances in terms of relative displacement and acceleration. In fact, for higher acceleration weights the closed-loop system becomes unstable and the desired force resulting from the controller goes to infinity which leads a poor performance SA system. It

can be seen on figure 3.28 (right) the responses of system when subjected to one input accelerogram evidencing that the minimum acceleration weight leads the device force to follow almost the desired force resulting from the controller.

In order to identify the range of parameter values that lead to stable systems, the maximum moduli of the eigenvalues of the closed-loop system is considered. Stable systems have their eigenvalues inside the unit circle and thus their moduli must be less than one. For the example considered in figure 3.28, the evolution of system poles with the acceleration weight q is found in figure 3.29. For this example, stable systems are obtained with acceleration weights less than $q^{0,5}$<150 (approximately). An interesting result of this plot is that the minimum of the maximum eigenvalues moduli corresponds to an acceleration weight close to the acceleration weight that minimizes the acceleration response. In fact this correspondence was verified for all the other cases analysed in this work. Thus, a preliminary criteria for designing MPC controllers for use with SA devices can be the closed-loop eigenvalues moduli, which beyond the information of system's stability can also give information about the MPC candidate parameters. Afterwards a verification can be performed on the system model using the seismicity of site where the structure will be installed.

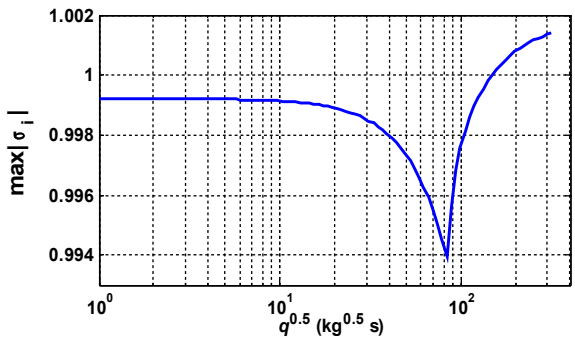

Figure 3.29 - SDOF system eigenvalues moduli (maximum values) evolution with acceleration weight (f_b=0,25 Hz and ξ_b=0,1 for MPC VD with T_s=5 ms, HP=50, HC=1, r=1 s^2/kg).

As for the LQR controller, it was found that an increase on the input move weight (r) moves those curves (evolution response curves) to the right, meaning that the acceleration weight that minimizes the acceleration response increases too. In fact, increasing the input move weight relative to the weights on the outputs has the effect of reducing the control activity (*Maciejowski 2002*) – see cost function in equation (3.58). In the present study a unitary value in the input move weight was considered.

After finding the minimum of each mean peak acceleration curve and the correspondent weights, the evolution of responses with prediction horizon was identified. In general the results show an almost constant evolution of the responses with the prediction horizon HP up to a certain value dependent of the system natural frequency and control interval, from which

the responses increases (poor performances). Figure 3.30 shows an example of those evolutions for different system natural frequencies subjected to type 1 seismic actions with both VD and COO algorithms. Similar evolutions were obtained with type 2 seismic actions. It is shown that higher system natural frequencies reduce that constant evolution range. Thus, prediction horizons inferior to 70 are found to be adequate for the cases under study. In fact, having found no significant influence of the prediction horizon on the results in that range, the smallest value is desired in order to reduce the order (matrices dimension) of the optimization problem. However, since the internal model has input delays to account the device time response, one should assure that HP>*d*. In the present study the instant delays are *d*=10 and thus the prediction horizon was set to HP=50.

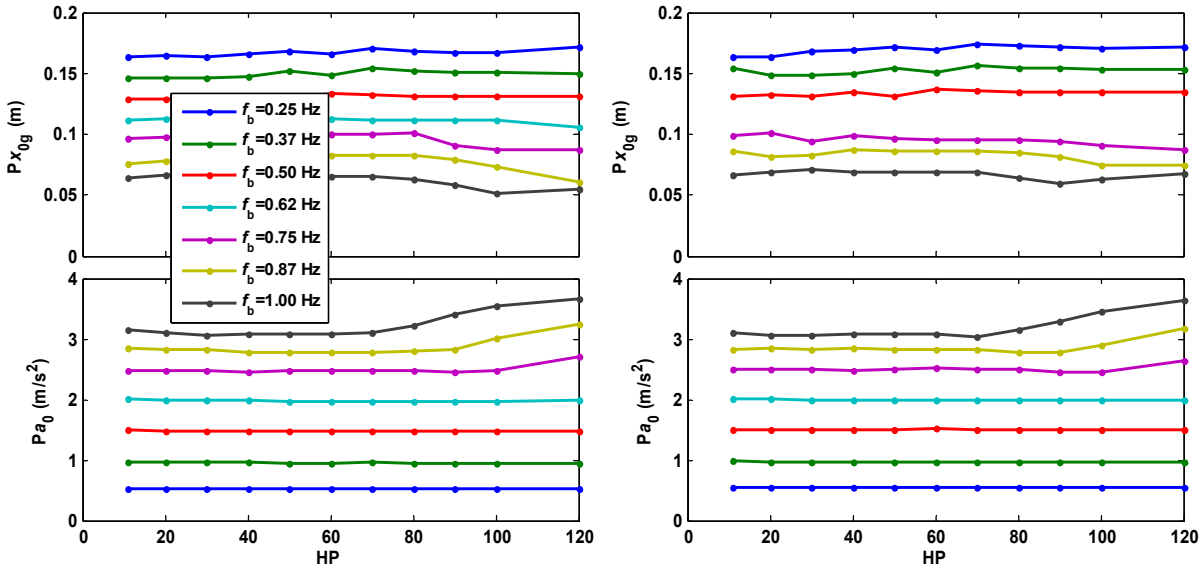

Figure 3.30 - SDOF system responses (mean peak values) evolution with prediction horizon for different natural frequencies (f_b=0,25 to 1,00 Hz and ξ_b=0,1 with T_s=5 ms, HC=1, r=1 s^2/kg), when subjected to type 1 seismic actions (10 input time accel.): left - for MPCVD; right - for MPCCOO.

In what concerns to the influence of the control horizon HC in the results, no evidence of improvements where found with HC>1, and thus the unitary value was considered in the subsequent analysis.

The resulting acceleration weights obtained for the range of natural frequencies considered (f_b=0,25 to 1,00 Hz and ξ_b=0,1) in this study and with the previous identified controller parameters (T_s=5 ms, d=10, HP=50, HC=1, r=1 s^2/kg, w_0=1 m/s^2 and v_0=1 m/s^2) are depicted in figure 3.31. Contrary to the LQR controller, the MPC output weight has an increasing tendency with the system natural frequency. These output weights are less sensitive to the seismic action type and control algorithm for the same system natural frequency. The responses provided by these tracking schemes with the identified output weights can be found in table 3.4. The results show that these force tracking schemes: also perform better than the passive one in terms of accelerations for structural systems structural systems with

f_b≤0,50 Hz for type 1 seismic actions and f_b≤1,00 Hz for type 2 seismic actions; are also better than the LQR ones; have slightly inferior performance than the integral law force tracking schemes in terms of both relative displacements and accelerations; both algorithms provide almost similar results (VD and COO).

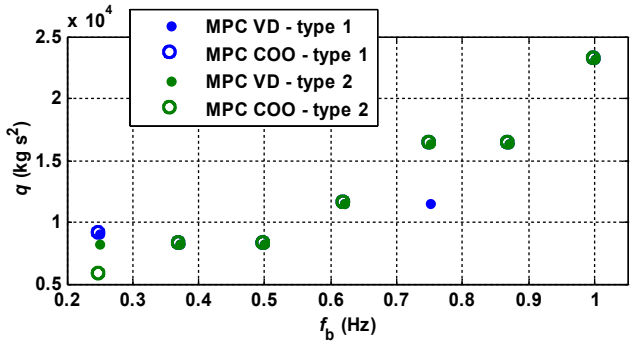

Figure 3.31 - MPC controller output weights function of SDOF system natural frequency.

3.3.8 Force-tracking schemes: adjusting damping rules

A change on the device characteristic is only able to modify the force magnitude but not its sign. Thus, the semi-active fluid damper can only reproduce dissipative forces and then it cannot always follow the force derived by the controller f_d. Within the force tracking scheme considered for semi-active control, two different rules (algorithms) were used to derive the damping coefficient using the desired force information: i) Variable Damping algorithm (VD); ii) Clipped On-Off control (COO).

The **variable damping (VD)** control algorithm is implemented in line with a controller which results in a model-based feed-forward force tracking scheme. It consists in changing the damper coefficient according to the desired force using the device mathematical model and taking into account the device physical limits. Using the device model, equation (3.9), the damping is derived by inverting the equation:

$$c_v = \frac{f_d + T_d \dot{f}_d}{\dot{x}_{r0}}, \quad c_{min} \le c_v \le c_{max} \tag{3.71}$$

This algorithm uses the desired force f_d and its derivative (which is numerically computed) and the relative velocity $\dot{x}_{0r}$ (of the base isolation system mass to the ground) to compute the damping. In order to avoid a division by zero, the relative velocity is considered a small constant ε=10^{-4} m/s when $|\dot{x}_{0r}| \le \varepsilon$. To implement this algorithm the device should be able to change the damping continuously between the minimum and maximum value.

The **clipped on-off algorithm (COO)** is implemented in line with a controller which results in a force feedback tracking scheme. It has been already referred in section 2.9.12, equation (2.54), and is considered here for semi-active control. The idea is that the maximum damping should only be applied if the device force modulus is less than the desired force modulus

and, both have the same sign. The control law that describes this algorithm is the following:

$$c_v = c_{max} \cdot H\left[(f_d - f_{SA}) \cdot f_{SA}\right],\ c_{min} \leq c_v \leq c_{max} \tag{3.72}$$

This algorithm is adequate for use with solenoid valves which only deal with on-off control. However, a force measurement is also needed for implementation.

3.4 SDOF Model: Comparison of results

Having analysed each control method separately for the SDOF model considering the input ground motions of the Portuguese seismic actions, the results obtained are presented in table 3.4.

Type 1 seismic action														
	Rx_{0g}							Ra_0						
f_b(Hz)	0,25	0,37	0,50	0,62	0,75	0,87	1,00	0,25	0,37	0,50	0,62	0,75	0,87	1,00
Passive	0,71	0,49	0,30	0,23	0,23	0,21	0,18	0,89	0,74	0,61	0,56	0,52	0,51	0,49
DBB	**0,49**	**0,46**	0,40	0,40	0,41	0,42	0,41	1,09	0,82	0,71	0,69	0,66	0,67	0,66
NOFC	0,76	0,69	0,67	0,69	0,70	0,71	0,70	**0,85**	**0,74**	0,71	0,73	0,73	0,74	0,73
SMC	**0,63**	0,55	0,49	0,48	0,50	0,50	0,50	**0,71**	**0,61**	**0,54**	**0,54**	0,54	0,56	0,56
MHF	**0,67**	0,59	0,47	0,45	0,43	0,44	0,45	**0,87**	0,77	0,68	0,68	0,66	0,66	0,65
MHFVD	**0,69**	0,58	0,47	0,45	0,42	0,44	0,40	**0,86**	0,77	0,69	0,69	0,67	0,67	0,66
MHFCOO	**0,69**	0,58	0,50	0,45	0,44	0,44	0,44	**0,86**	0,78	0,69	0,69	0,67	0,68	0,68
IVD	**0,58**	0,54	0,48	0,48	0,49	0,51	0,51	**0,68**	**0,60**	**0,53**	**0,55**	0,56	0,57	0,57
ICOO	**0,58**	0,54	0,48	0,50	0,50	0,52	0,52	**0,68**	**0,60**	**0,53**	**0,54**	0,56	0,57	0,56
LQRVD	**0,62**	0,56	0,50	0,51	0,52	0,54	0,54	**0,72**	**0,62**	**0,55**	**0,56**	0,56	0,58	0,58
LQRCOO	**0,64**	0,56	0,50	0,51	0,54	0,56	0,56	**0,73**	**0,62**	**0,55**	**0,56**	0,57	0,59	0,59
MPCVD	**0,57**	0,54	0,50	0,51	0,54	0,53	0,50	**0,69**	**0,61**	**0,55**	0,57	0,58	0,59	0,58
MPCCOO	**0,58**	0,54	0,51	0,52	0,51	0,56	0,53	**0,71**	**0,63**	**0,56**	0,58	0,59	0,60	0,58
Type 2 seismic action														
Passive	0,86	0,55	0,44	0,42	0,43	0,49	0,41	0,97	0,81	0,69	0,70	0,67	0,68	0,70
DBB	**0,52**	**0,47**	**0,42**	0,45	0,47	0,47	0,48	1,21	0,95	0,81	0,82	0,80	0,81	0,84
NOFC	**0,78**	0,73	0,68	0,74	0,74	0,73	0,71	**0,90**	**0,79**	0,73	0,79	0,78	0,78	0,76
SMC	**0,63**	0,58	0,54	0,56	0,56	0,56	0,58	**0,76**	**0,65**	**0,60**	**0,62**	**0,63**	**0,64**	**0,66**
MHF	**0,67**	0,59	0,54	0,57	0,53	0,59	0,62	**0,96**	0,82	0,73	0,76	0,74	0,76	0,77
MHF VD	**0,69**	0,58	0,54	0,55	0,54	0,59	0,63	**0,89**	**0,81**	0,73	0,77	0,75	0,76	0,79
MHFCOO	**0,69**	0,59	0,54	0,57	0,54	0,59	0,63	**0,91**	0,82	0,73	0,76	0,75	0,76	0,79
IVD	**0,59**	**0,53**	0,48	0,53	0,55	0,57	0,59	**0,73**	**0,62**	**0,58**	**0,63**	**0,62**	**0,64**	**0,68**
ICOO	**0,60**	**0,54**	0,50	0,54	0,55	0,58	0,58	**0,74**	**0,63**	**0,57**	**0,61**	**0,61**	**0,63**	**0,65**
LQRVD	**0,64**	0,59	0,55	0,57	0,59	0,58	0,59	**0,77**	**0,66**	**0,60**	**0,64**	**0,65**	**0,65**	**0,66**
LQRCOO	**0,65**	0,60	0,55	0,57	0,59	0,59	0,59	**0,79**	**0,67**	**0,60**	**0,65**	**0,65**	**0,64**	**0,65**
MPCVD	**0,58**	**0,55**	0,51	0,55	0,55	0,59	0,60	**0,75**	**0,65**	**0,58**	**0,64**	**0,64**	**0,65**	**0,68**
MPCCOO	**0,62**	0,57	0,53	0,56	0,57	0,60	0,61	**0,78**	**0,67**	**0,60**	**0,65**	**0,63**	**0,66**	**0,68**

Table 3.4 - Ratios of mean of peak responses for the SDOF structure with additional systems.

Relative displacements and absolute accelerations values (mean peak values) are shown in terms of ratios relative to the original structure responses for comparison. Ratios higher than 1 indicate that the response of the structure with devices is bigger than that of the original

structure. Moreover, values in bold correspond to solutions that perform better than the passive one (ratios inferior than those of the passive solution) and those underlined refer to solutions with less performance than the original structure (ratios higher than one).

The results show that, except DBB for f_b=0,25 Hz, all solutions (passive and semi-active) lead to better performances than the original system. DBB controller showed to be best solution in terms of relative displacements for lower natural frequency systems (f_b≤0,37 Hz for type 1 seismic actions and f_b≤0,50 Hz for type 2 seismic actions), but with highest accelerations solution too. In terms of accelerations SA solutions that perform better than the passive case are: i) NOFC for structural systems with f_b≤0,37 Hz; ii) MHF with the correspondent algorithms, for structural systems with f_b=0,25 Hz; iii) SMC, integral control, LQR and MPC with the correspondent algorithms for structural systems with f_b≤0,50 Hz for type 1 seismic actions and f_b≤1,00 Hz for type 2 seismic actions. This is in fact the range of frequencies of typical base-isolated structures. The results show that force tracking schemes are the best in reducing the accelerations and at the same time can reduce the relative displacements better than the original structure. Moreover, force tracking schemes with an integral controller showed to be the best ones. Those SA systems with an integral controller (IVD and ICOO) can provide reductions in relative displacements (between 40 % to 50 % approximately) when compared to the original structure and provide the minor acceleration responses (f_b≤0,62 Hz for type 1 seismic actions and f_b≤1,00 Hz for type 2 seismic actions). Although the MPC controller uses a more elaborate formulation with an embedded model of the system, it provides almost similar performance than the integral controller one. It was found also that different control algorithms (VD and COO) provide similar results.

3.5 MDOF Model Numerical Evaluation

A ten-storey base isolated structure depicted in figure 3.32 was considered to evaluate the effectiveness of the presented strategies in reducing the structural responses.

MDOF model

The superstructure dynamic characteristics considered in this example were estimated taking into account the empirical law for typical dual frame-wall structures provided by the Portuguese Safety Code (*RSA 1983*):

$$f_{s1}=\frac{16}{n},\quad \omega_{s1}=2\,\pi\, f_{s1} \tag{3.73}$$

where n is the total number of floors. The superstructure fundamental frequency is f_{s1}=1,6 Hz (n=10), and is assumed to have damping ratio of ξ_1=5 %. Each floor has a mass of m_f=10^5 kg. The stiffness and damping matrices were determined considering a constant stiffness between floors and a stiffness proportional damping matrix ($\boldsymbol{C}_s$=$a_0\cdot\boldsymbol{K}_s$). The resultant

stiffness and damping coefficients between floors are k_f=452,43 kN/mm and c_f=1,51 kN s/mm. The proportional coefficient (a_0=0,0033 s) was chosen to fit the first mode damping ratio. The superstructure is supported on a base isolation system with mass $m_b=1{,}4\cdot m_f$ and laminated rubber bearings made of natural rubber. An equivalent linear elastic and viscous model is assumed to model the bearing elements. Considering a target frequency of f_b=0,4 Hz and an equivalent damping ratio of ξ_b=10 % for the base isolation system (building assumed to be rigid), the base isolation stiffness k_b and damping coefficient c_b can be estimated assuming that the superstructure stiffness is much superior than base isolation system stiffness, thus:

$$f_b=\frac{1}{2\cdot\pi}\sqrt{\frac{k_b}{m_b+n\cdot m_f}},\quad \xi_b=\frac{c_b}{2\cdot(m_b+n\cdot m_f)\cdot\xi_b}; \tag{3.74}$$

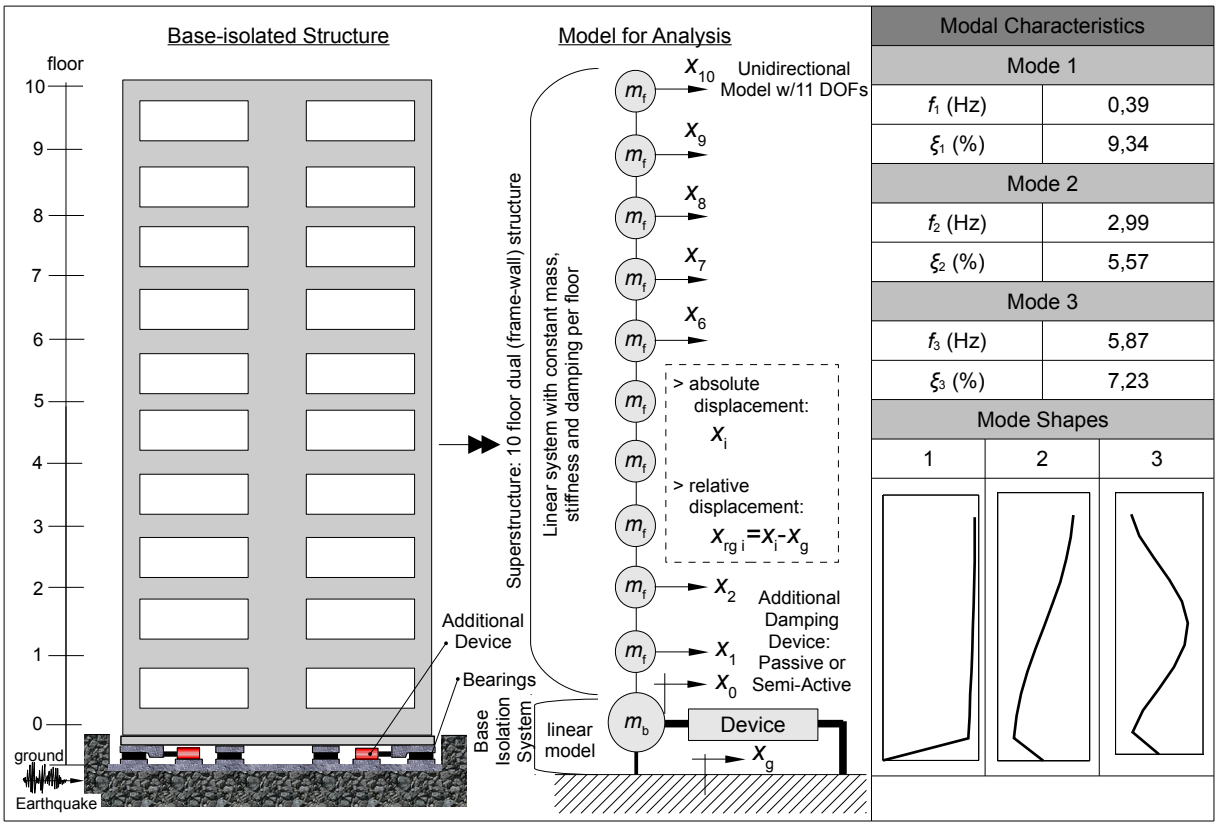

Figure 3.32 - 10-storey base-isolated building, equivalent model and modal characteristics.

The values obtained are then: k_b=7,20 kN/mm and c_b=0,57 kN s/mm. Both base-isolation system and superstructure are coupled and the base-isolated system model is achieved as in figure 3.32. The first three modes modal characteristics are presented in the same figure. The results show that the first mode (isolation mode) has a natural frequency very close to the target frequency due to the small superstructure flexibility, since this one remains almost rigid and the base isolation system undergoes the main deformation. The other modes (structural modes) involve deformation of both isolation system and superstructure and, their

frequencies are increased with the inclusion of the isolation system. In terms of damping, the first and second modes damping remain similar to the uncoupled systems but the higher modes are dampened due to the assumed damping model (stiffness proportional).

Additional devices are installed at the base level connecting the ground to the base isolation system which develop a force f_{ad}. The ground motion x_g inputs the earthquake energy into the model. The equation of motion of the system including the base isolation system is given by equation (3.1) with: $\boldsymbol{G}$=[-1 0 … 0]^T; and $\boldsymbol{x}_{rg}=\{x_{0g}\ \ x_{1g}\ \ ...\ \ x_{10g}\}^T$ is the vector of relative displacements to the ground, $x_{ig}=x_i-x_g$ with i=0,1...10, and the respective time derivatives, relative velocity and relative acceleration; the mass, damping and stiffness matrices are respectively given by:

$$\boldsymbol{M}=\mathrm{diag}\left(m_b\ \ m_1\ \ \ldots\ \ m_{10}\right)$$

$$\boldsymbol{K}=\begin{bmatrix} k_b+k_f & -k_f & \boldsymbol{0} \\ -k_f & & \\ \boldsymbol{0} & & \boldsymbol{K_s} \end{bmatrix},\ \boldsymbol{K_s}=\begin{bmatrix} 2\cdot k_f & -k_f & 0 & \cdots & 0 \\ -k_f & 2\cdot k_f & -k_f & 0 & \vdots \\ 0 & \ddots & \ddots & \ddots & 0 \\ \vdots & 0 & -k_f & 2\cdot k_f & -k_f \\ 0 & \cdots & 0 & -k_f & k_f \end{bmatrix} \tag{3.75}$$

$$\boldsymbol{C}=\begin{bmatrix} c_b+c_f & -c_f & \boldsymbol{0} \\ -c_f & & \\ \boldsymbol{0} & & \boldsymbol{C_s} \end{bmatrix},\ \boldsymbol{C_s}=a_0\cdot\boldsymbol{K}_s=\begin{bmatrix} 2\cdot k_f & -c_f & 0 & \cdots & 0 \\ -c_f & 2\cdot c_f & -c_f & 0 & \vdots \\ 0 & \ddots & \ddots & \ddots & 0 \\ \vdots & 0 & -c_f & 2\cdot c_f & -c_f \\ 0 & \cdots & 0 & -c_f & c_f \end{bmatrix}$$

The model described in the state-space form is given by equation (3.2) with $\boldsymbol{z}=\left\{\boldsymbol{x}_{rg}\,\dot{\boldsymbol{x}}_{rg}\right\}^T$ as the state vector; and $\boldsymbol{C}_y$ and $\boldsymbol{D}_y$ are defined according to the quantities for output $\boldsymbol{y}$.

Apart from the original structure, two passive systems (with constant damping and velocity exponent α=1) were considered for comparison with the SA systems: Passive C_{id} with the device having a damping coefficient c_{id}=1,1 kN s/mm (additional damping of ξ_{id}=0,19), which is the damping that leads the structure to a relative displacement similar to the structure employing the best SA system (with IVD controller); and Passive C_{max} with the device having the maximum damping considered for the SA device, c_{max}=2,58 kN s/mm (additional damping of ξ_{max}=0,45). Additional damping referred in terms of damping ratio is relative to the isolation critical damping, $c_c=2\cdot m\cdot\omega_b$, where $\omega_b=2\cdot\pi\cdot f_b$ and $m=m_b+n\cdot m_f$ are the angular frequency the total mass of the structure.

SA devices with the same characteristics of those in previous examples were taken into account: time constant T_d=0,05 s; and additional damping varying between $0{,}05\leq\xi_{SA}\leq0{,}45$. Using the same procedure to tune the controllers as for the SDOF model, the following values were obtained for each control strategy: g=2x10^6 N/m for MHF; k_0=1000 s^{-1} for NOFC;

γ=2x10^6 N/m and β=2x10^6 kg/s for SMC; g=1,5 kN s/mm for IVD and ICOO; q=5,1x10^{11} kg·s for LQRVD and q=2,5x10^{11} kg·s for LQRCOO, both with r=1 s/kg; and q=10^8 kg·s^2, r=1 s^2/kg, HP=50, T_s=5 ms d=10 for MPCVD and MPCCOO. Notice that different values are considered for the LQR controller. Different output weighting values were found with the algorithms considered and with the seismic action type considered. A compromise was assumed when using the same weight for different seismic actions type. A better performance would be obtained if four weighting values were used (one for each combination of algorithm and seismic action).

MDOF model analysis

The performance for each structural system (MDOF model alone and with additional systems) was evaluated through numerical simulations considering both seismic actions type. The results obtained in terms of mean peak responses of the relative displacements and accelerations along structure floor can be found in figure 3.33. The ratios of the mean peak responses and base shear force M*V* in relation to the original structure responses as well as the ratio of the mean peak device force in relation to the structure weight M*f*/W are presented in table 3.5.

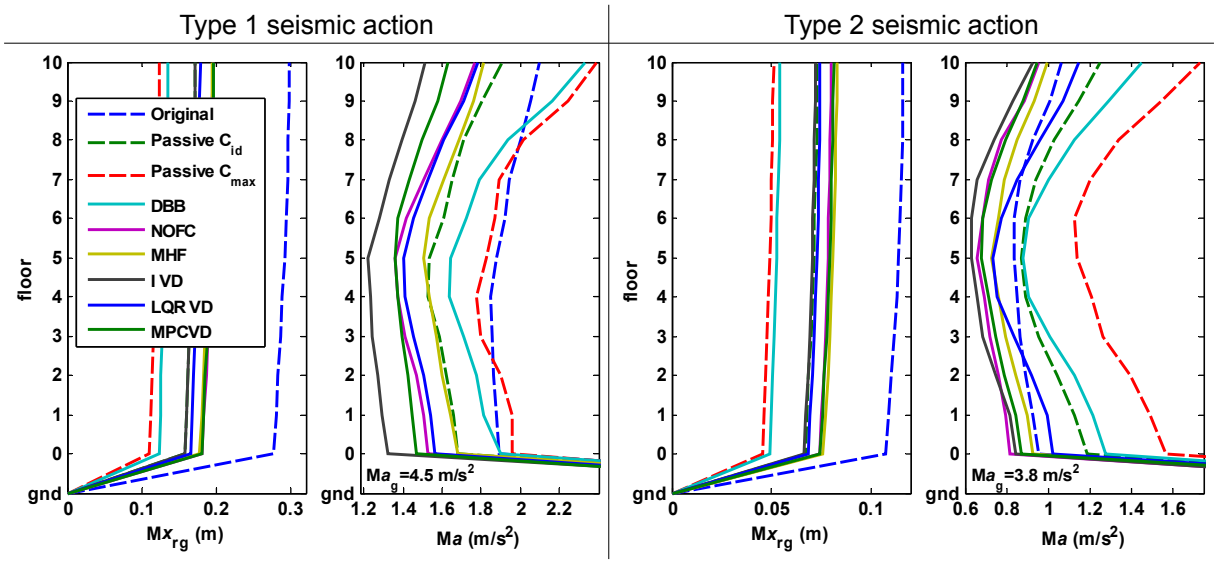

Figure 3.33 - Responses of the 10-storey base-isolated building to 10 type 1 and type 2 seismic actions.

All solutions reduce the structure relative displacements being the maximum damping passive C_{max} case the best one for this quantity. However an increase in the acceleration responses is observed, namely for type 2 seismic actions, where the highest amplifications are verified. The SA solution with a DBB control strategy almost reach the same level of displacements than the Passive C_{max}, with lower accelerations, but higher than the original structure ones in the higher floors for type 1 seismic actions and in all floors with type 2 seismic actions. The other SA strategies perform better than the passive ones in terms of

accelerations and at the same time providing better reductions than the original structure ones in terms of relative displacements. However, the SA system with an optimal controller (LQR) subjected to type 2 seismic actions has inferior performance in terms of accelerations than the original structure. In fact this controller was tuned considering both seismic actions type and thus better results would be found if the controller was tuned for each seismic action separately. The Passive C_{id} case, which is the one having relative displacements similar to the those with an IVD controller, shows inferior performance in terms of absolute accelerations when compared to that one. As for the SDOF systems the best SA system is the IVD. More elaborate strategies, like NOFC, SMC or even the MPC controllers, do not perform better than IVD. MHF force tracking schemes showed also better performance than the Passive C_{id} in terms of acceleration but with inferior performance than this one in terms of relative displacements. It is verified also that force tracking schemes with variable damping algorithms (VD) usually provide better performance than those with on-off algorithms (namely COO). SA systems also perform better than the passive ones in terms of base shear forces transmitted to the structure, since part of the seismic force is dissipated by the devices. For the same reason, force tracking schemes with an integral controller provide better than the other strategies. It is shown that SA device control forces (mean peak values) are always below 10 % of the structure weight.

	Type 1 seismic action						Type 2 seismic action					
	Mx_{0g} (m)	Mx_{10g} (m)	Ma_0 (m/s^2)	Ma_{10} (m/s^2)	MV (kN)		Mx_{0g} (m)	Mx_{10g} (m)	Ma_0 (m/s^2)	Ma_{10} (m/s^2)	MV (kN)	
Original	0,276	0,298	1,894	2,095	2050		0,108	0,116	0,957	1,065	818	
	Rx_{0g}	Rx_{10g}	Ra_0	Ra_{10}	RV	Mf/W	Rx_{0g}	Rx_{10g}	Ra_0	Ra_{10}	RV	Mf/W
Passive C_{id}	0,57	0,58	0,89	0,91	0,74	0,06	0,62	0,63	1,24	1,18	0,80	0,02
Passive C_{max}	0,4	0,41	1,03	1,14	0,78	0,10	**0,42**	**0,44**	1,64	1,63	0,93	0,05
DBB	**0,46**	**0,47**	1,33	1,36	0,85	**0,04**	**0,44**	**0,45**	**1,00**	**1,11**	**0,76**	0,10
NOFC	0,66	0,66	**0,81**	**0,84**	**0,70**	0,09	0,69	0,69	**0,86**	**0,90**	**0,75**	0,03
SMC	**0,63**	**0,63**	**0,75**	**0,77**	**0,68**	**0,05**	0,71	0,72	**0,89**	**0,88**	**0,77**	**0,02**
MHF	0,64	0,65	0,93	**0,89**	0,79	0,03	0,70	0,70	**1,07**	**1,00**	0,84	**0,01**
MHFVD	0,64	0,65	**0,89**	**0,87**	0,80	0,03	0,71	0,71	**0,97**	**0,94**	0,84	**0,01**
MHFCOO	0,64	0,65	0,91	**0,89**	0,80	0,03	0,70	0,71	**1,02**	**0,96**	0,84	**0,02**
IVD	**0,57**	**0,58**	**0,70**	**0,72**	**0,62**	**0,05**	**0,62**	**0,62**	**0,88**	**0,87**	**0,68**	**0,02**
ICOO	0,58	**0,58**	**0,75**	**0,74**	**0,63**	**0,05**	**0,62**	**0,62**	**1,00**	**0,95**	**0,68**	**0,02**
LQRVD	0,60	0,60	**0,83**	**0,85**	**0,70**	**0,05**	0,64	0,64	**1,07**	**1,07**	**0,75**	**0,02**
LQRCOO	0,67	0,67	**0,88**	**0,86**	**0,73**	**0,04**	0,70	0,71	**1,13**	**1,06**	**0,78**	**0,02**
MPCVD	0,65	0,66	**0,77**	**0,78**	**0,70**	**0,04**	0,69	0,70	**0,91**	**0,89**	**0,75**	**0,02**
MPCCOO	0,66	0,66	**0,81**	**0,81**	**0,71**	**0,04**	0,69	0,70	**0,98**	**0,93**	**0,75**	**0,02**

Table 3.5. MDOF system responses. Comparisons with the original structure.

The control effectiveness of SA systems can be observed in figure 3.34 where the time responses at the base, upper floor and the inputs (damping coefficient and force) for one

input accelerogram of the original system, with Passive C_{id} and with IVD systems is shown. Reductions on the relative displacements around 40 % and accelerations between 12 % and 30 % relative to the original structure, and improvements in the absolute accelerations between 20 % and 30 % when compared to the Passive C_{id} case are found for the best SA solution (IVD).

The results obtained with the MDOF model showed also that changing damping in real time with an adequate control strategy can improve the structural system performance by reducing both relative displacements and absolute accelerations.

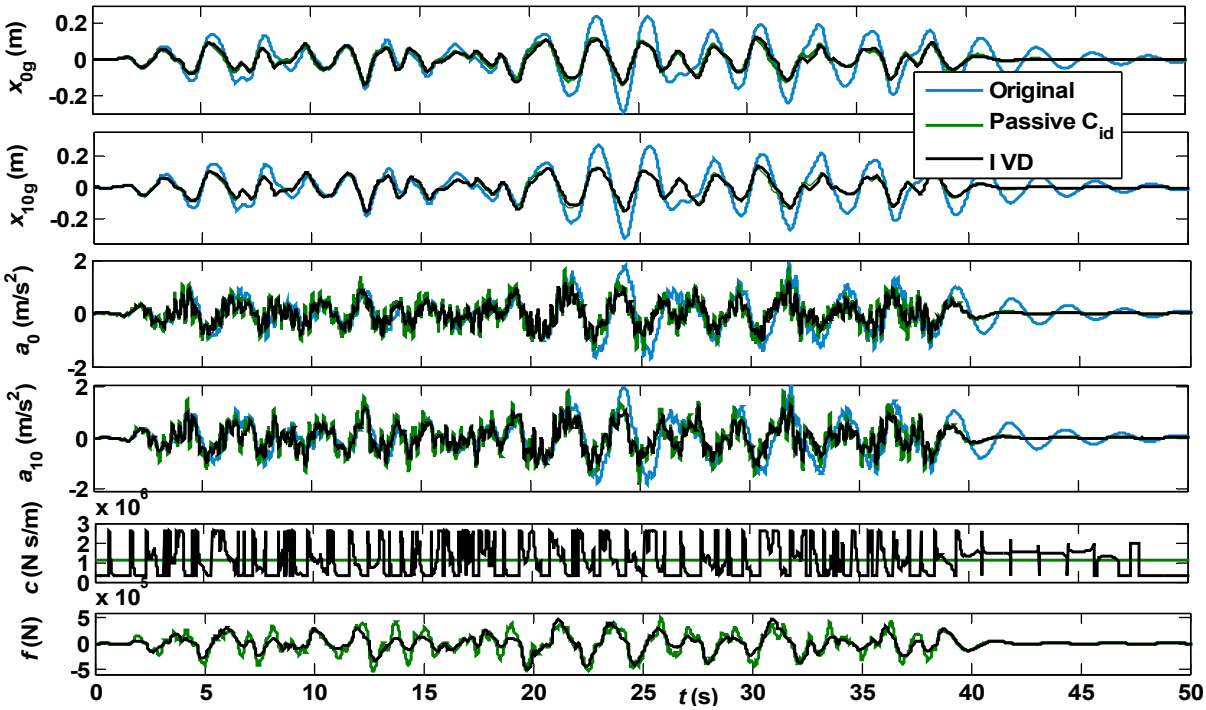

Figure 3.34 - Time histories of base and top floor relative displacements and accelerations, input damping and force for the MDOF model subjected to one type 1 accelerogram.

3.6 Final Remarks

In this chapter several control strategies were analysed to derive semi-active devices installed at the foundation level of base-isolated structures. The overall objective of the study was to evaluate the effectiveness of several control strategies in reducing the responses of base-isolated structures when subjected to earthquake loads. Nonlinear control laws and force tracking schemes were analysed. Force tracking schemes with a modulated homogeneous friction controller, an integral controller, an optimal controller and a model predictive controller were used in conjunction with different adjusting damping rules. Numerical simulations on a SDOF model and on a MDOF model were performed using a set of 10 accelerograms of type 1 and type 2 of the Portuguese seismic actions (total of 20).

The SDOF model was considered in first place to provide an insight to the hybrid base

isolated structures concept. A procedure to design the controller based on numerical simulations using the minimum acceleration criteria was used. Typical natural frequencies of base-isolated structures were considered for the SDOF model and the IVD showed to be the best SA control strategy, being the ICOO, SMC and MPC strategies the following ones in providing good performance. IVD outperforms the original structure and the structural system with passive devices for natural frequencies bellow 0,6 Hz subjected to type 1 and type 2 artificial accelerograms generated for the Portuguese territory. The output feedback controller NOFC showed to be effective in terms of accelerations on the SDOF model only for lower natural frequency systems, but with slightly higher relative displacements. MHF controllers showed to be better than NOFC in terms of relative displacements and in terms of accelerations for higher natural frequency systems. The LQR controllers showed to be the force tracking controllers with inferior performance (slightly inferior than the MPC ones). The results show also that VD and COO algorithms provide similar performance for the SDOF model, although the VD is slightly better.

A MDOF model representative of a ten-storey base-isolated structure was used to verify the effectiveness of the proposed control strategies. With the exception of DBB controller, all strategies can reduce the relative displacements of the original structure and at the same time improve the accelerations responses better than the passive cases. As for the SDOF model the IVD control strategy showed to be the best SA control strategy and ICOO the second best one for type 1 seismic actions. For type 2 seismic actions MPCVD is the second best one control strategy in terms of accelerations. The NOFC strategy is in general better than LQR and MHF force tracking schemes in terms of accelerations but not in terms of relative displacements. It is found that the LQR force tracking schemes show the lowest performance in terms of accelerations for type 2 seismic actions, resulting from the fact that its design is highly dependent on the seismic action type and algorithm.

In general it was found that it is possible to improve the behaviour of base-isolated structures with SA systems, being the IVD strategy the best one and thus the one to be chosen for this purpose. It was shown that the controller gain has a large influence in the systems performance and thus, its design should be thoroughly analysed. It is recommended to identify the controller gain using a model of the structure subjected to a set of representative ground motions of the site and select the value that minimizes the peak accelerations.

Chapter 4

Experimental Studies on Semi-active Control

- Numerical and experimental validation of semi-active control strategies -

Summary

In this chapter a numerical and experimental analysis of semi-active (SA) control strategies for controlling seismic-excited structures is performed. The chapter starts with the description of the physical model developed consisting of a two degree-of-freedom (2DOF) mechanical model with a magneto-rheological (MR) damper. The measurement chain comprising the sensors and the data acquisition system, as well as the controller architecture comprising the hardware and software, are also described and characterized accordingly. Each component of the model is characterized through experimental tests and the candidate models are presented and parametrized using the measured data. Linear elastic and viscous models are used to describe the mechanical behaviour of the 2DOF mechanical system, while the Bouc-Wen family models are used to describe the behaviour of the MR damper. Seven SA control strategies were implemented for numerical and experimental evaluation whose controllers were tuned using the system model and the ground motions. The artificial accelerograms for the Portuguese territory as well as several earthquake records were considered in the analysis. Comparisons with the original structure and with the passive cases are performed in time and frequency domain. The results reveal that the response of the structure is effectively mitigated by all of the analysed control methods but achieving different levels of performance. It is shown that SA systems can outperform the original structure as well as the one using the best passive solution in most of the strategies. The integral control law leads to the best performance only when collocated control is considered. If more information (responses) of the structure is available for control, the linear quadratic regulator technique shows to perform even better.

4.1 Experimental Test Set-up

The validation of the SA strategies presented in the last chapter was verified through experimental tests on the LNEC uniaxial shaking table using a 2DOF mechanical model representative of the physical phenomenon under study. Associated to the physical model were the semi-active devices, the sensors and signal conditioners, the data acquisition and controller unit. Figure 4.1 shows a schematic view of the developed experimental model.

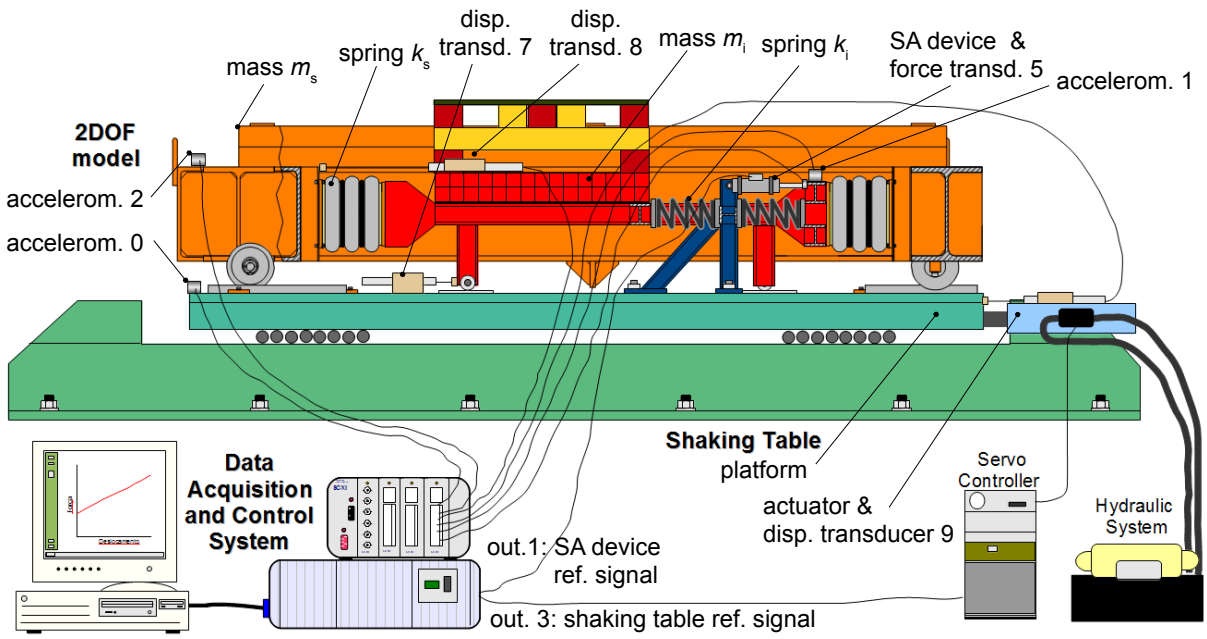

Figure 4.1 - Schematic representation of the experimental model for test in the shaking table.

The 2DOF model was idealized with two springs having a total stiffness k_i that link the ground to mass m_i, and two other springs with a total stiffness k_s that link the mass m_i to mass m_s. The masses are supported by roller bearings over the shaking table platform. The system damping will result from the damping associated with this mechanism that shall be mainly due to the rolling friction. An additional device, an SA device of MR damper type, is attached between the ground and mass m_i to increase the system damping. This device is operated by the data acquisition and control system using the information provided by the sensors signals (1 force transducer, 3 accelerometers and 3 displacement transducers). The reference signal for the shaking table is also defined on the data acquisition and control system. This equipment allows also the implementation of the control strategies and the measurement of the intended quantities. Table 4.1 summarizes the measured and generated quantities associated with the experimental model as well as its upper bound values considered for the equipment and sensors selection.

All the tasks performed for the development and installation of the physical model will be described in the following sub-sections.

Measured Quantities			
Quantity	Sensor nº	Model Variable	Expected Range
Shaking Table platform acceleration	accelerometer 0	$\ddot{x}_g$	±2 m/s^2
Base floor (mass m_i) acceleration	accelerometer 1	$\ddot{x}_i$	±2 m/s^2
Upper floor (mass m_s) acceleration	accelerometer 2	$\ddot{x}_s$	±2 m/s^2
SA device force	force transducer 5	f	±1,5 kN
Shaking Table displacement	displacement transducer 9	x_g	±85 mm
Base floor (mass m_i) relative displacement to the ground (Shaking Table platform)	displacement transducer 7	$x_{ig}=x_i-x_g$	±60 mm
Upper floor (mass m_s) relative displacement to the base floor (mass m_i)	displacement transducer 8	$x_{si}=x_s-x_i$	±10 mm
Generated Quantities			
Quantity	Signal	Model Variable	Expected Range
Shaking Table platform reference signal	output 3	$X_{g,ref}$	±85 mm
SA device reference signal	output 1	u_{SA}	0-5 V

Table 4.1. Quantities associated with the developed model, its correspondence with the sensor (measurement) or signal (generation) and with 2DOF mechanical model variables (see section 4.1.3).

4.1.1 LNEC uniaxial shaking table

Equipment Description

The uniaxial shaking table consists of a steel platform able to receive models up to 6 tons with dimensions of 3x2 m^2 in plant. The platform slides over several bearings mounted on the main structure. A hydraulic actuator linked between the main structure and the platform is used to input the displacement time histories. The actuator is able to provide 220 kN of force within 170 mm of stroke. A hydraulic oil circuit regulated by a servovalve which is operated by a servo-controller is used to supply the actuator. One displacement transducer is incorporated in the actuator to measure the platform position and used as the feedback signal in the control loop. The servo-controller and associated hardware to operate the equipment are installed on a cabinet located at the operation room. Signals for input in the shaking table are connected to the cabinet, which can be generated on a signal generator or on a computer. Figure 4.2 depicts some views of this experimental installation.

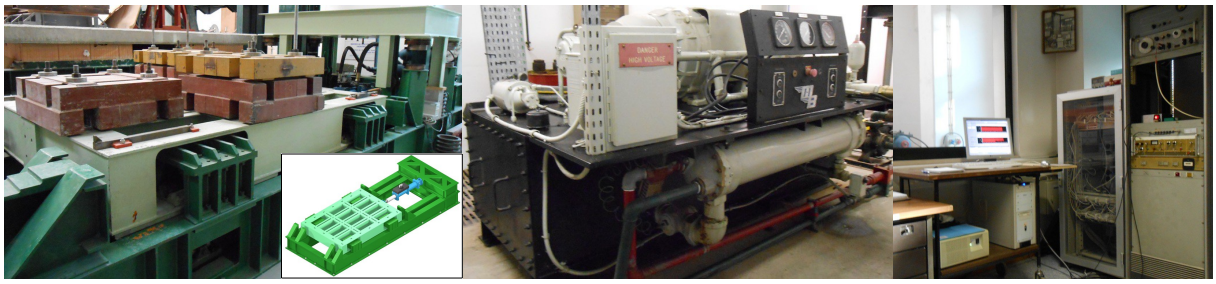

Figure 4.2 - LNEC Uniaxial Shaking Table experimental installation: shaking table with a 6 t mass on the platform, machine room and operation room.

This installation is located on the Ferry Borges's building at LNEC campus. A detailed description of this experimental installation can be found in the LNEC website (www.lnec.pt/organizacao/de/nesde/puniaxial) and in *Bairrão & Duque 1998*.

The shaking table movement is manipulated by an electronic amplifier (MB electronics – HSA104 Servo Controller) that computes the driver signal for the servo valve using the feedback signal from the displacement transducer (installed inside the actuator) and an input desired reference signal. The simplified control loop (closed-loop system) including the electronic amplifier and the model on the shaking table is shown in figure 4.3.

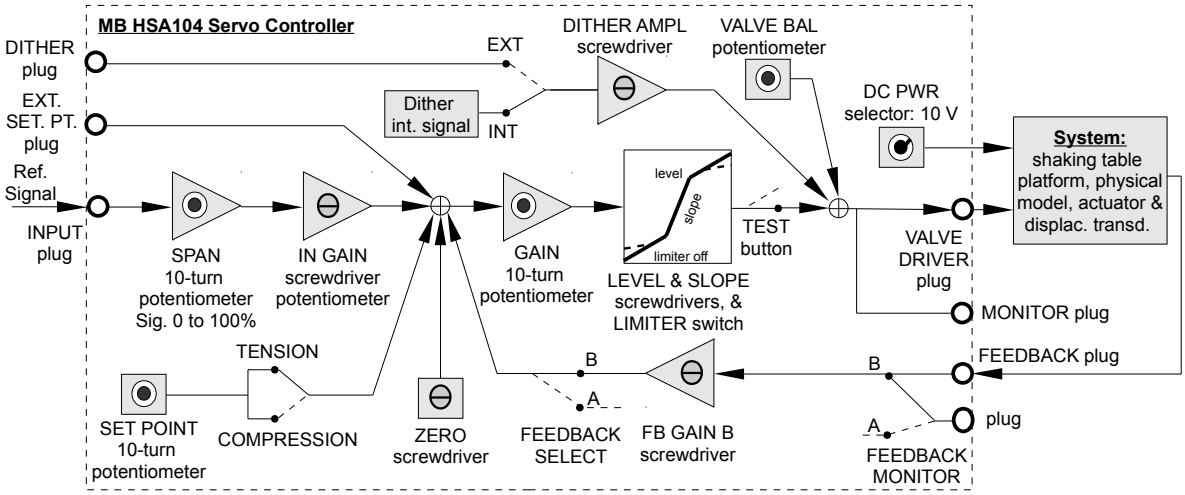

Figure 4.3 - Shaking table control loop (system and MB HSA104 servo controller) during normal system operation (CAL switch set to OPER).

The servo controller has several parameters that allows the adjustment of the static gain and of the controller proportional gain. In this application (displacement control), only feedback B channel is used. The controls used and adjusted in the experimental studies are presented in table 4.2.

Equipment Set-up

The adjustment of the servo controller parameters are intended to achieve an adequate closed-loop system performance.

The static gain (relationship between the shaking table displacement and output 3 reference signal) was set to be close to 1 cm/V (thus, ±8,5 V for the ±85 mm). 'FB Gain B' and 'In Gain' screwdrivers were adjusted to obtain approximately that relationship using the displacement measurements and the input voltage on the system. In parallel with the displacement transducer calibration this value was evaluated using a standard displacement measurements (see section 4.1.2) at the same step tests, as 0,9913 cm/V.

The proportional gain was adjusted online with a 6 t rigid mass on the shaking table platform, using a square wave with 2 mm of magnitude. To goal was to achieve a fast response with

small overshoots (less than 20%) and good tacking (*Skogestad & Postlethwaite 1996*). The controller proportional gain was set to k_p=0,98 which leads to the system time response shown in figure 4.4. Thus, the following time domain performance indices were found: rise time t_r=60 ms; settling time t_s=150 ms (5% criteria); overshoot M_p=7 % (at 143 ms).

HSA104 Servo Controller					
Button/Plug	Value	Button/Plug	Value	Button/Plug	Value
CAL	Oper	IN GAIN	Adjusted	VAL BAL	-
DC PWR	10	GAIN	0,98	DITHER	INT
FEEDBACK SELECT	B	SET POINT	0,82		AMP Adjusted
FEEDBACK MONITOR	B		TENSION	TEST	-
SPAN	0 to 100%	LIMITER	OFF	MONITOR BNC	Output Signal
BNC Plug	Feedback Signal	STABILITY LEVEL	Adjusted		
FB GAIN A	Not used	STABILITY SLOPE	Adjusted		
FB GAIN B	Adjusted	POWER	ON		
TARE	Not used	ZERO	Adjusted		
Analog Meter: 8 signals for visualization/monitor: Input, Transducer Power Supply, Output, Feedback, Driver, Dither and Auxiliary		EXT. SET. PT.	not used	Power	115 V
		MONITOR	not used	INPUT PLUG	Input signal
		VALVE DRIVER PLUG	signal for servovalve	FEEDBACK (bottom right plug)	Disp. Transd. signal
		DITHER PLUG	Not used	VALVE FB	not used
Hydraulic System					
System and Ready On buttons powered		Main pressure, p_{main}	1200 psi	Return pressure, p_{return}	150 psi

Table 4.2 - Shaking table set-up parameters: servo controller and hydraulic system.

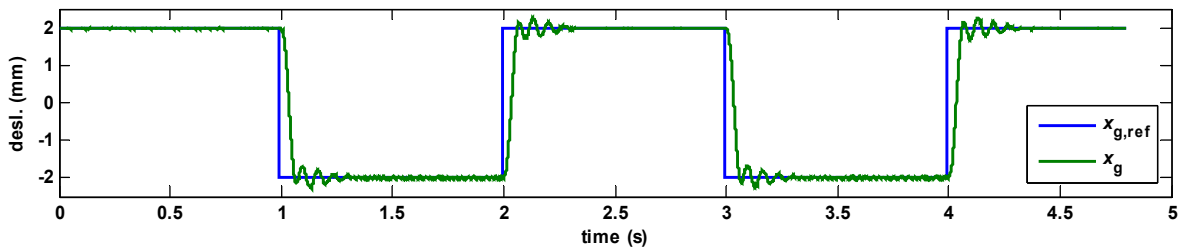

Figure 4.4 - Shaking table time response to a 2 mm square wave.

After tuning the parameters the closed-loop performance was characterized in the frequency domain. A white noise spectra passed through a higher-pass filter at 0,3 Hz was used to synthesize the acceleration input time signal with 100 s of duration, and considered to characterize the shaking table dynamically. The correspondent displacement signal to input on the system was obtained by integration of the acceleration twice. Then, the shaking table transfer function between the output and the reference displacement was obtained for different amplitudes of the input signal: reference input signals with 21, 40 and 81 mm of

peak displacement (see figure 4.5). The shaking table dynamic range varies between 5,5 Hz and 14,5 Hz for higher amplitudes and lower amplitudes respectively.

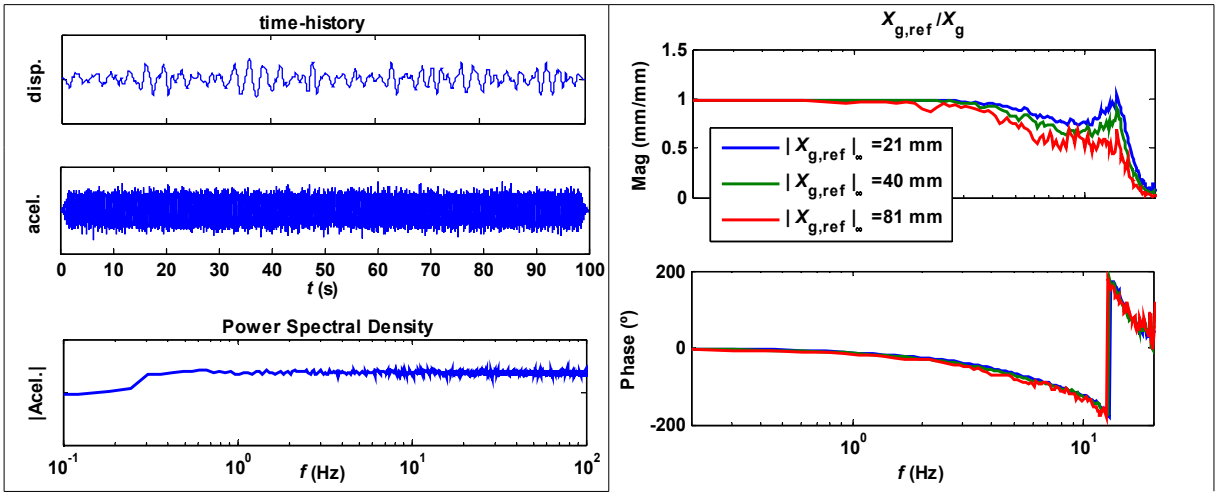

Figure 4.5 - Synthesized reference input signal in terms of displacement and acceleration (left) and the shaking table transfer function for different magnitudes of the input signal (right).

4.1.2 Measurement and Control Chain

Equipment Description

In order to perform the experience several equipments and instruments were needed for measurement of the intended quantities and command the signal for the device. Moreover, the command signal for the shaking table is also taken into account in the definition of the measurement and control system units. In this work a data acquisition and control system based on dSPACE solution was used. It consists of one computer referred as the host PC, and a data acquisition and controller unit referred as the expansion box which is an autonomous computer to run the experiences in real time. A signal conditioner unit was developed at LNEC (Centro de Instrumentação Cientifica) to supply the sensors and adjust its signals to the expansion box characteristics. The quantities for measurement are displacements, accelerations and force. The system also defines the command signals to the shaking table and to the SA device. To run an experience an application (for control or only for measurement) is created in the Matlab/Simulink and downloaded to the expansion box. The application is configured on the computer using the dSPACE ControlDesk software. During the experience the expansion box runs autonomously and in real time, and the data can be visualized in the computer. Figure 4.6 depicts the measurement and control chain and tables 4.3, 4.4 and 4.5 describe the main characteristics of each component. The selection of this equipment and in particular the sensors, resulted from preliminary numerical simulations on the developed 2DOF mechanical model (see section 4.1.3), resulting on the expected values in table 4.1. A sampling period of 0,2 ms (or sampling frequency of 5 kHz), which is more than twice the boards low-pass filters cut-off frequency, was used to avoid aliasing.

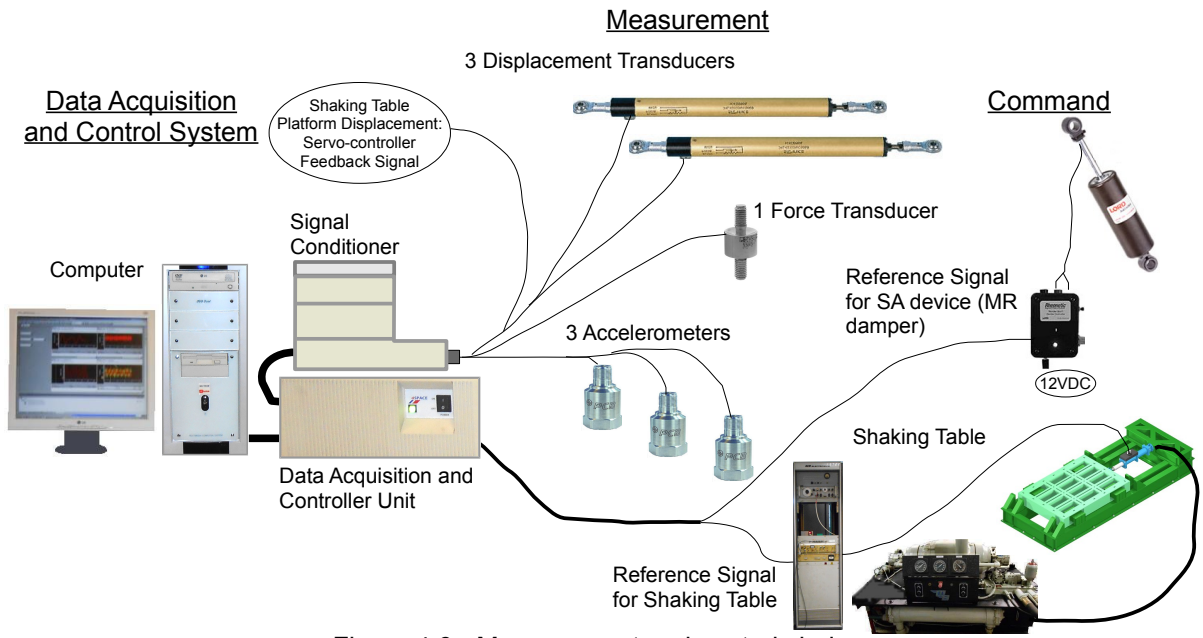

Figure 4.6 - Measurement and control chain.

Component	Characteristics
Computer (host PC)	>Pentium 4 at 3,2 GHz, 2 GB RAM, with Microsoft Windows XP Professional v2002 sp3 >dSPACE DS817 link board (PC): for connection with the expansion box via proprietary cross-over cable >Software: Matlab/Simulink 2010 sp2; dSPACE Control Desk Generation 7.4
Data Acquisition and Controller Unit (expansion box)	>dSPACE PX10 expansion box: for installation of the host PC boards >dSPACE DS814 link board (box): for connection with the host PC via proprietary cross-over cable >dSPACE DS1006 processor board >dSPACE DS2003 multi-channel A/D board: with 32 channels, 4 to 16 bits of resolution (programmable) and ±5 V or ±10 V output range (programmable) with 5 mA output current >dSPACE DS2003 multi-channel D/A board: with 32 channels, 14 bits resolution and ±5 V or ±10 V output range (programmable) with 5 mA output current

Table 4.3. Data acquisition and control system characteristics.

Sensor	Qt.	Manufacturer/model	Range	Sensibility	Electrical characteristics
Accelerometer	3	PCB 393B12	0,5 g	10 V/g	Power Supply: 24 V, 4 mA
Force Transducer	1	HBM U9B	5 kN	1 mV/V	Power Supply: 0,5 to 12 V
Displacement Transducer	2	Sifernice 34L8D103W03263D	200 mm	50 Ω/mm	
	1	Shaking Table Displacement Transducer: Servo-controller Feedback signal	200 mm	Obs.: associated to the shaking table control system.	
Command Signal	Qt	Description			Range
Ground	1	reference signal for the Shaking table movement			± 10 V
MR damper	1	reference signal for the MR damper controller kit			0 to 5 V

Table 4.4. Sensors and command signals description main characteristics.

Slot/ board	Quantity	Electrical sig. denomination	Pin nº DS2003 board	Characteristics
0	Acceleration	Acel0	1	>Gain selector: 1, 2, 4, 8, 16 >Offset adjustment >Low-pass filter at 125Hz
1		Acel1	3	
2		Acel2	5	
3				
4				
5	Force	ExcF0	13	>Gain selector: range values from 1 to 1,5x10^5 >Offset adjustment >Low-pass filter at 1750Hz of 2nd or 4th order >Excitation signal: 5 VDC or 10 VDC
		SignIF0	15	
6		ExcF1	17	
		SignIF1	19	
7	Displacement	ExcD1	21	>Gain selector: range values from 1 to 1,5x10^5 >Offset adjustment >Low-pass filter at 1700Hz of 2nd or 4th order >Excitation signal: 5 VDC or 10 VDC
		SignID1	23	
8		ExcD2	25	
		SignID2	27	
9	V	SgnAux	31	>Gain selector: range values from 1 to 1,5x10^5 >Low-pass filter at 1700Hz of 2nd or 4th order

Table 4.5. Signal conditioner: boards description and correspondence to dSPACE DS2003 board.

Measurement Chain Characterization

The measurement chain for each measured variable consisting of the sensor, signal conditioner and data acquisition was calibrated using the LNEC's laboratory traceable reference standards. The main objective is to establish a relationship between the values provided by the measurement chain equipment and the values provided by the reference standard. The first one provides the values in terms of electrical voltage and the second in terms of the physical quantity: length, acceleration and force. Both length and force measurement chains were calibrated in static conditions. The acceleration measurement chains were calibrated in dynamic conditions.

Length and Force measurement chain calibration

In order to assure measurement quality within the modern metrology probabilistic approach, the evaluation of measurement uncertainty and traceability was performed according to the *Guide to the Uncertainty in Measurement* (*BIPM et al. 2008*). The calibration procedures developed at Metrological Quality Division (NQM) of LNEC which are based in national and international standards were taken into consideration in the calibration process. The calibration procedure used here is intended to evaluate the measurement uncertainty taking into account the sources of uncertainty resulting from the mathematical model parameters, model deviations, reversibility, repeatability, measurements and the uncertainties associated with the reference standard measurements.

The adopted calibration procedure consists in the following steps:

1. **Tests:** measurement tests consisting of n_r repetitions of n step tests (at least 10), starting at the zero step, going to other steps in the measurement range always in the same direction up to the extreme, inverting beyond the extreme and finishing at zero; at each step one sample was obtained with the reference standard and n_s samples were obtained with the measurement chain; for each step an average and the standard deviation are evaluated from the n_s samples obtained with the measurement chain and used as representative values of the sample;
2. **Adopted model:** for each repetition the linear model relating the standard quantity measurements S_q with the measured input voltage V_i (voltage supply to the sensor) and the measured output voltage V_o (voltage resulting from the sensor stimulus) of the measurement chain, was adopted (*Ribeiro & Martins 2009*):

$$S_q = a + b \cdot \frac{V_o}{V_i} \tag{4.1}$$

the model parameters (a, b) as well as the correlation coefficient $r(S_q, V_o/V_i)$ were estimated for each repetition and an average of those n_r values is calculated as representative of the model parameters; the law of propagation of uncertainty is obtained from (*BIPM et al. 2008*):

$$\begin{aligned} u^2(S_q) &= \sum u_i^2(S_q) \\ u_i^2(S_q) &= c_i^2 \cdot u^2(x_i), \quad \text{for } i = j \\ u_i^2(S_q) &= 2 \cdot c_i \cdot c_j \cdot u(x_i) \cdot u(x_j) \cdot r(x_i, x_j), \quad \text{for } i \neq j \end{aligned} \tag{4.2}$$

where: $u(S_q)$ is the combined standard uncertainty which is the sum of each term $u_i(S_q)$; $c_i = \partial S_q / \partial x_i$ are the sensitivity coefficients; and r is the coefficient of correlation; for the adopted model $y = f(x_i)$ in equation (4.1), $y = S_q$ and $x_i = \{a, b, V_o, V_i\}$, $u(S_q)$ is:

$$\begin{aligned} u^2(S_q) = & \left(\frac{\partial S_q}{\partial a}\right)^2 \cdot u^2(a) + \left(\frac{\partial S_q}{\partial b}\right)^2 \cdot u^2(b) + \left(\frac{\partial S_q}{\partial V_o}\right)^2 \cdot u^2(V_o) + \left(\frac{\partial S_q}{\partial V_i}\right)^2 \cdot u^2(V_i) \\ & + 2 \frac{\partial S_q}{\partial a} \frac{\partial S_q}{\partial b} \cdot u(a) \cdot u(b) \cdot r(a, b) + 2 \frac{\partial S_q}{\partial V_o} \frac{\partial S_q}{\partial V_i} \cdot u(V_o) \cdot u(V_i) \cdot r(V_o, V_i) \\ & + u^2(S_q)_{lin} + u^2(S_q)_{rev} + u^2(S_q)_{rep} + + u^2(S_q)_{ref} \end{aligned} \tag{4.3}$$

where: $u(S_q)_{lin}$, $u(S_q)_{rev}$, $u(S_q)_{rep}$ and $u(S_q)_{ref}$ are the standard uncertainties associated with the linearity, reversibility, repeatability and with the reference standard measurements respectively; the other terms $u(\cdot)$ are standard uncertainties of the correspondent variables; the law of propagation of uncertainty assumes that there are no correlations between the quantities and the parameters and thus $r(a, V_o)=0$, $r(a, V_i)=0$, $r(b, V_o)=0$ and $r(b, V_i)=0$;

using the adopted model (equation 4.1) and the standard quantity measurements (mean values), the calibration error (residual) $e=S_q-a-b\cdot V_o/V_i$ for each step is calculated; the variance and covariance components associated with the model parameters for each repetition are calculated as:

$$\mathrm{var}(a)=\sigma_e^2\left[\frac{1}{n}+\frac{\overline{V_o/V_i}}{\sum_{j=1}^{n}\left[\left(V_o/V_i\right)_j-\overline{V_o/V_i}\right]^2}\right],\quad \mathrm{var}(b)=\frac{\sigma_e^2}{\sum_{j=1}^{n}\left[\left(V_o/V_i\right)_j-\overline{V_o/V_i}\right]^2}$$
$$\mathrm{cov}(a,b)=\frac{-\sigma_e^2\cdot\overline{V_o/V_i}}{\sum_{j=1}^{n}\left[\left(V_o/V_i\right)_j-\overline{V_o/V_i}\right]^2},\quad r(a,b)=\frac{\mathrm{cov}(a,b)}{\sqrt{\mathrm{var}(a)}\sqrt{\mathrm{var}(b)}},\quad \sigma_e^2=\frac{1}{n-2}\sum_{j=1}^{n}e_j^2 \tag{4.4}$$

where n is the number of steps (samples), $\overline{V_o/V_i}$ is the average of V_o/V_i for the n steps, and σ_e^2 is the variance estimator of the residuals e; its square root is the standard deviation σ_e, which is evaluated for each repetition and the average value is calculated and used as representative value of the distribution; similarly, the standard deviations $\sigma_a=\sqrt{\mathrm{var}(a)}$ and $\sigma_b=\sqrt{\mathrm{var}(b)}$ are also calculated, and the maximum values are used as an upper bound for the n_r repetitions; finally, the standard uncertainty of measurement u is evaluated as a type A uncertainty, given by:

$$u(a)=\frac{\max(\sigma_a)}{\sqrt{n_r}},\quad u(b)=\frac{\max(\sigma_b)}{\sqrt{n_r}},\quad u(S_q)_{lin}=\frac{\overline{\sigma_e}}{\sqrt{n_r}} \tag{4.5}$$

moreover, the minimum value of the coefficient of correlation $r(a,b)$ for the n_r repetitions was used as representative value in the law of propagation of uncertainties;

3. **Reversibility:** for each repetition the reversibility errors where evaluated at each step as the deviation between the two values obtained with the measurement chain V_o/V_i, as referred in point 2, being one obtained in one direction and the other after inverting the direction of step application, during the calibration tests; after converting the values to the physical quantity being analysed (with the model b value) the maximum and minimum reversibility errors considering all steps and repetitions are calculated to evaluate this uncertainty component contribution, considering a uniform distribution (type B uncertainty):

$$u(S_q)_{rev}=\frac{\max(e_{rev})-\min(e_{rev})}{\sqrt{12}} \tag{4.6}$$

4. **Repeatability:** using the values obtained with the measurement chain V_o/V_i, as referred in point 2, and converting those values to the physical quantity being

analysed (with the model *b* value) the dispersion at each step for the n_r repetitions is evaluated by the sample standard deviation σ_{rep}; the maximum value for the sample standard deviation is taken and the standard uncertainty of measurement for this component is evaluated by the standard deviation of the mean (type A uncertainty):

$$u(S_q)_{rep}=\frac{\max(\sigma_{rep})}{\sqrt{n}} \tag{4.7}$$

5. **Voltage measurement:** both excitation signal for the sensor V_i and the output voltage V_o resulting from the sensor stimulus are measured with the data acquisition and control system; in this category the resolution, the gain error, the offset error and the measurement stability were considered; concerning to the first one, the uncertainty is evaluated using the equipment *resolution* in volts and considering a uniform distribution (type B uncertainty), being the resolution calculated as half of the minimum measurement interval, thus:

$$u(V)_{res}=\frac{0{,}5\cdot V_{res}}{\sqrt{3}} \tag{4.8}$$

in what concerns to the *gain error* and *offset error* components, the values specified by the equipment manufacturer are assumed to be expanded uncertainties $U_{95\%}$ that are converted to standard uncertainty *u* using a factor of 2 (effective degrees of freedom>50), thus:

$$u(V)=U(V)/2 \tag{4.9}$$

for the present case, the equipment manufacturer (dSPACE) specifies for the DS2003 multi-channel A/D board a resolution up to 16 bit, a measurement range up to ±10 V, a gain error of 0,2 %FSR (full scale range) and an offset error of ±2,5 mV, which leads to $u(V)_{res}$=0,088 mV, $u(V)_{gain}$=20 mV (at most) and $u(V)_{offset}$=2,5 mV; finally the uncertainty component of *stability* $u(V)_{stability}$ was evaluated by finding the maximum standard deviation of the n_s measurements for all steps and all repetitions; the resulting standard uncertainty is evaluated combining the four components by summing the variances:

$$u(V)=\sqrt{u(V)_{res}^2+u(V)_{gain}^2+u(V)_{offset}^2+u(V)_{stability}^2} \tag{4.10}$$

in the evaluation of the uncertainty gain component the maximum measured voltage (in some cases ±5 V) is considered instead of the equipment full range; moreover for each repetition the coefficient of correlation $r(V_o,V_i)$ is calculated as:

$$r(V_i,V_o)=\frac{\mathrm{cov}(V_i,V_o)}{u(V_i)\cdot u(V_o)},\quad \mathrm{cov}(V_i,V_o)=\frac{1}{n(n-1)}\sum_{j=1}^{n}\left[\left(V_{i,j}-\overline{V}_i\right)\cdot\left(V_{o,j}-\overline{V}_o\right)\right] \tag{4.11}$$

the maximum value of $r(V_o,V_i)$ for the n_r repetitions is taken as an upper bound for calculation of the combined standard uncertainty;

6. **Standard Measurement:** the standard measurement provided by the reference standard are traceable to national standards; the uncertainty measurement associated with the reference standard and the associated measurement chain is provided by the expanded uncertainty at 95 % confidence interval $U_{95\%}$, which is converted to the standard uncertainty as in equation (4.9), $u_{standard}=U_{95\%}/2$;
7. **Expanded uncertainty:** the expanded uncertainty U is usually evaluated by the following expression (*BIPM et al. 2008*):

$$U_p(S_q)=\pm t_p \cdot u(S_q) \tag{4.12}$$

where t_p is the t-factor obtained such that the fraction of the confidence interval p of the t distribution is encompassed by the interval $[-t_p, +t_p]$ and $u(S_q)$ is the combined uncertainty obtained with law of propagation of uncertainty in equation (4.3); a confidence interval p=95 % is usually considered; the t-factor t_p is also function of the effective number of degrees of freedom ν_{eff};, which is evaluated from:

$$\upsilon_{eff}=\frac{u^4(S_q)}{\sum_{i=1}^{N}\frac{u_i^4(S_q)}{\upsilon_i}} \tag{4.13}$$

where: $u_i(S_q)$ is the contribution of each component to the combined uncertainty (equation 4.2); and ν_i are the correspondent degrees of freedom, which are given by the number of terms in a sum minus the number of constraints on the terms of the sum; thus, for parameters a, b and linearity contributions $\nu=n_r-1$; for the input and output measurement voltage as well as for the standard measurement $\nu=50$; for the reversibility $\nu=(n+1)-1$; for the repeatability $\nu=(2\cdot n+1)-1$; and for the correlated quantities $\nu=(2\cdot n+1)-2$.

Concerning to the force transducer 5 and the associated measurement chain, a 2550 gain was defined in the signal conditioner board and the input range ±10 V with 16 bit of resolution was selected in the correspondent channels of the data acquisition system. The calibration tests were performed at LNEC (UMA – Unidade de Metrologia Aplicada) using the universal testing machine EQ07 to apply the force steps with the standard sensor and the force transducer 5 connected in series with the machine ends. The standards used were: the EQ92 force transducer and the reading unit EQ94 for traction; and the EQ03 force transducer and the reading unit EQ94 for compression. The equipment maximum standard uncertainty $U_{95\%}$ is 0,324% and 0,225% of the measurement range respectively. Two

repetitions of [0;0,4;...,3,2;3,6;0] kN step tests and two repetitions of [0;0,4;...;3,2;3,6;3,6;3,2;...;0] kN were considered for both traction and compression. Figure 4.7 shows the set-up used.

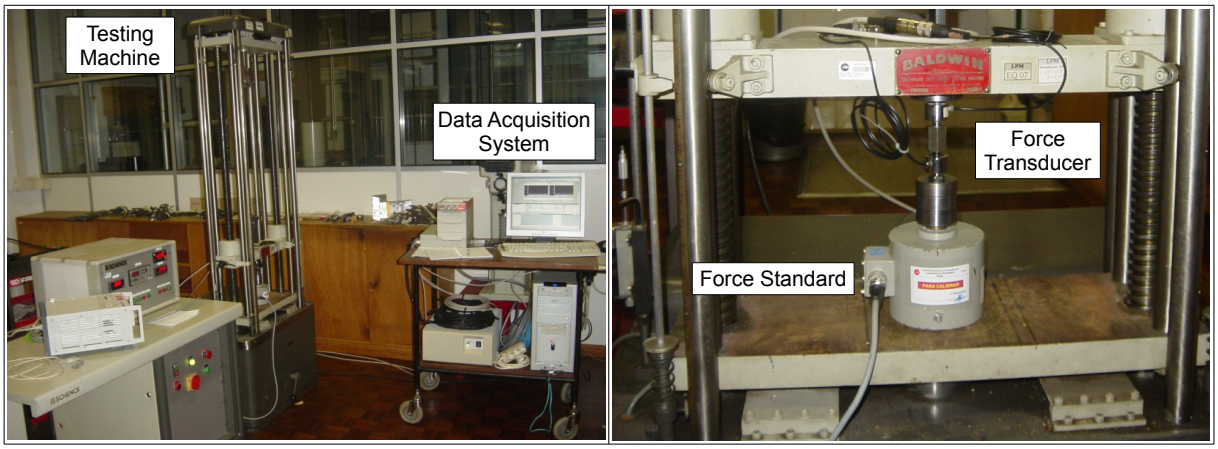

Figure 4.7 - Force transducer 5 calibration set-up (left) and assembly on the testing machine (right).

Applying the described calibration procedure the results of the estimates and uncertainties are reported in table 4.6. The major contribution to the combined uncertainty is due to the voltage measurements and standard measurements. Nevertheless, the obtained expanded uncertainty is around $U_{95\%}$=22 N (0,62 %FS).

Uncertainty Source	Estimate $\bar{x}_i$	Standard Uncertainty $u(x_i)$	Sensitivity Coefficients c_i	Coef. of Correlation $r(x_i,x_j)$	DOF ν_i	Contribution $u_i(S_q)$
Parameter *a*	0,0005 kN	0,0010 kN	1		3	0,001 kN (0,8%)
Parameter *b*	1,9302 kN/V/V	0,0010 kN/V/V	1,86 V/V		3	0,002 kN (2,4%)
Input Voltage V_i	5 V	0,0070 V	-0,7180 kN/V		50	0,005 kN (19,7%)
Output Voltage V_o	9,3 V	0,0099 V	0,3860 kN/V		50	0,004 kN (11,3%)
Linearity		0,0016 kN	1		3	0,002 kN (2,0%)
Reversibility		0,0008 kN	1		19	0,001 kN (0,5%)
Repeatability		0,0006 kN	1		39	0,001 kN (0,3%)
Standard Meas.	3,6 kN	0,0058 kN	1		50	0,006 kN (26,4%)
Correlation *a*-*b*	0,0005 kN 1,9302 kN/V/V	0,0010 kN 0,0010 kN/V/V	1 1,86 V/V	-0,0003	38	0,000 kN (0,0%)
Correlation V_i-V_o	5 V 9,3 V	0,0070 V 0,0099 V	-0,7180 kN/V 0,3860 kN/V	1,2293	38	0,007 kN (36,6%)
Combined Standard Uncertainty $u_i(S_q)$						0,011 kN (100%)
Effective DOF ν_{eff}						158
t-factor $t_{95\%}$						1,98
Expanded uncertainty $U_{95\%}$						0,022 kN (0,62 %FS)

Table 4.6. Uncertainty balance for force transducer 5 (range ±3,6 kN) with measurement chain.

In what concerns to the displacement transducers (nº 7 and 8) and the associated measurement chain, a gain 6 and 25 were chosen in the correspondent signal conditioner boards and an input range ±10 V with 16 bit of resolution was selected in the correspondent

channels of the data acquisition system. The calibration tests were performed at LNEC (UMA - Unidade de Metrologia Aplicada) using the Laser Beam length standard (Renishaw ML-10) installed in parallel with the transducer for calibration. The Laser Beam standard has a measurement range of 40 m, a resolution of 0,1 μm and a maximum standard uncertainty $U_{95\%}$=6,6 μm. Five repetitions of [0;+s;...;+l_r-s;+l_r;+l_r;+l_r-s;...;-l_r+s;-l_r;-l_r;-l_r+s;...;-s;0] were considered with l_r=60 mm and s=12 mm for displacement transducer 7 and l_r=15 mm and s=3 mm for displacement transducer 8. The set-up of the calibration is found in figure 4.8.

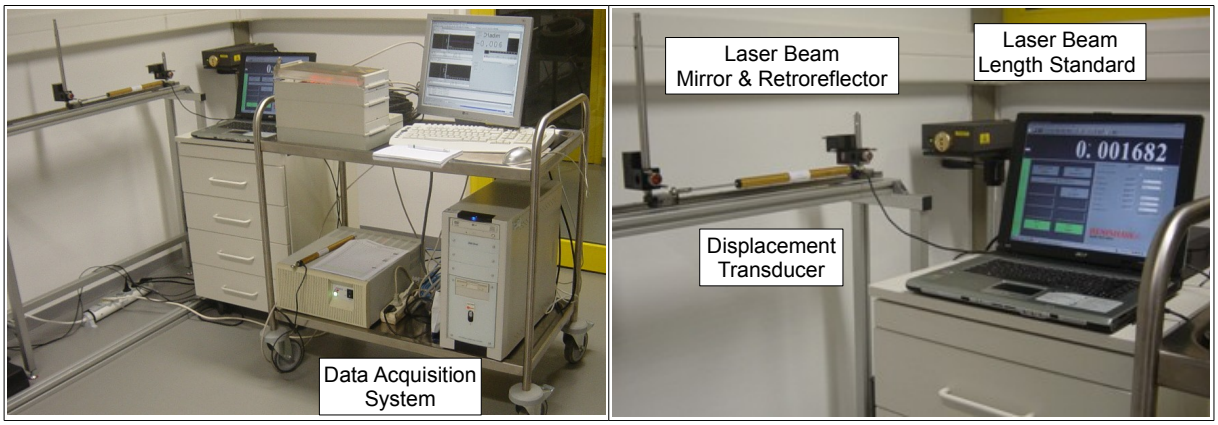

Figure 4.8 - Displacement transducer calibration set-up (left) and transducer assembly (right).

Applying the described calibration procedure the results of the estimates and uncertainties are presented in table 4.7 for displacement transducer 7 and in table 4.8 for displacement transducer 8 respectively.

Uncertainty Source	Estimate $\bar{x}_i$	Standard Uncertainty $u(x_i)$	Sensitivity Coefficients c_i	Coef. of Correlation $r(x_i,x_j)$	DOF ν_i	Contribution $u_i(S_q)$
Parameter a	-0,0930 mm	0,0051 mm	1		4	0,005 mm (0,1%)
Parameter b	33,3685 mm/V/V	0,0046 mm/V/V	1,8 V/V		4	0,008 mm (0,2%)
Input Voltage V_i	5 V	0,0077 V	-12,0127 mm/V		50	0,092 mm (27,2%)
Output Voltage V_o	9 V	0,0203 V	6,6737 mm/V		50	0,135 mm (58,5%)
Linearity	0 mm	0,0217 mm	1		4	0,022 mm (1,5%)
Reversibility	0 mm	0,0124 mm	1		11	0,012 mm (0,5%)
Repeatability	0 mm	0,0044 mm	1		22	0,004 mm (0,1%)
Standard Meas.	500 mm	0,0033 mm	1		50	0,003 mm (0,0%)
Correlation a-b	-0,0930 mm 33,3685 mm/V/V	0,0051 mm 0,0046 mm/V/V	1 1,8 V/V	-0,0032	21	0,001 mm (0,0%)
Correlation V_i-V_o	5 V 9 V	0,0077 V 0,0203 V	-12,0127 mm/V 6,6737 mm/V	0,1494	21	0,061 mm (11,9%)
Combined Standard Uncertainty $u_i(S_q)$					0,177 mm (100%)	
Effective DOF ν_{eff}					110	
t-factor $t_{95\%}$					1,98	
Expanded uncertainty $U_{95\%}$					0,351 mm (0,58 %FS)	

Table 4.7. Uncertainty balance for displacement transducer 7 (range ±60 mm) and associated measurement chain.

Uncertainty Source	Estimate $\bar{x}_i$	Standard Uncertainty $u(x_i)$	Sensitivity Coefficients c_i	Coef. of Correlation $r(x_i,x_j)$	DOF ν_i	Contribution $u_i(S_q)$
Parameter *a*	-0,0072 mm	0,0008 mm	1		4	0,001 mm (0,1%)
Parameter *b*	8,0013 mm/V/V	0,0007 mm/V/V	1,88 V/V		4	0,001 mm (0,2%)
Input Voltage V_i	5 V	0,0059 V	-3,0085 mm/V		50	0,018 mm (28,8%)
Output Voltage V_o	9,4 V	0,0103 V	1,6003 mm/V		50	0,016 mm (24,7%)
Linearity	0 mm	0,0038 mm	1		4	0,004 mm (1,3%)
Reversibility	0 mm	0,0120 mm	1		11	0,012 mm (13,2%)
Repeatability	0 mm	0,0021 mm	1		22	0,002 mm (0,4%)
Standard Meas.	500 mm	0,0033 mm	1		50	0,003 mm (1,0%)
Correlation *a*-*b*	-0,0072 mm 8,0013 mm/V/V	0,0008 mm 0,0007 mm/V/V	1 1,88 V/V	-0,0012	21	0,000 mm (0,0%)
Correlation V_i-V_o	5 V 9,4 V	0,0059 V 0,0103 V	-3,0085 mm/V 1,6003 mm/V	0,3041	21	0,018 mm (30,3%)
Combined Standard Uncertainty $u_i(S_q)$					0,033 mm (100%)	
Effective DOF ν_{eff}					112	
t-factor $t_{95\%}$					1,98	
Expanded uncertainty $U_{95\%}$					0,066 mm (0,44 %FS)	

Table 4.8. Uncertainty balance for displacement transducer 8 (range ±15 mm) and associated measurement chain.

Again, the major contributions to the uncertainty are due to the voltage measurements. As a final result, the obtained expanded uncertainty is around $U_{95\%}$=0,351 mm (0,58 %FS) for the first and $U_{95\%}$=0,066 mm (0,44 %FS) for the second one.

Finally, the shaking table displacement transducer (nº 9) and the associated measurement chain was subjected to the calibration tests on site (Ferry Borges's building) using the Laser Beam length standard (Renishaw ML-10) installed in parallel with the transducer for calibration (figure 4.9). A unitary gain was used in the signal conditioner board and an input range ±5 V with 16 bit of resolution was selected on the associated channel of the data acquisition system. The signal was read on the 'MONITOR' BNC plug bellow the Feedback switches on the servo controller.

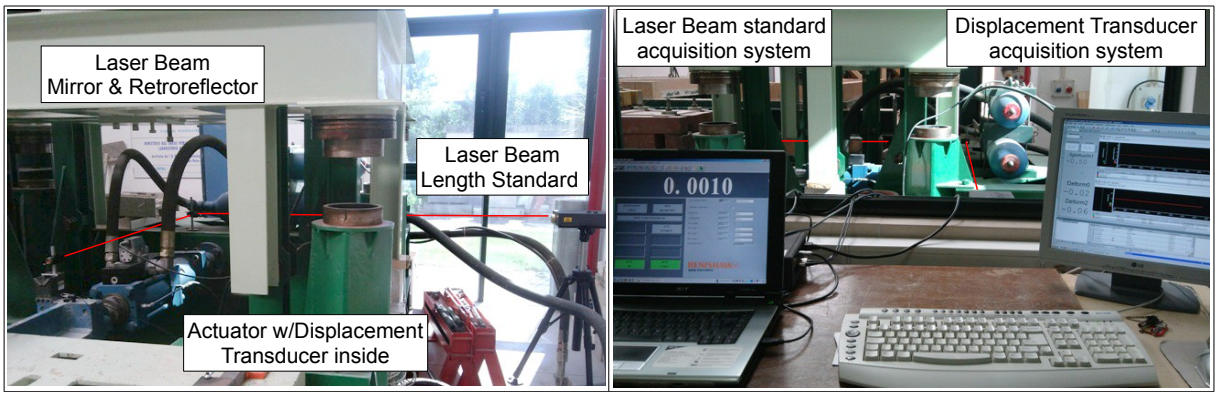

Figure 4.9 - Shaking table (actuator) displacement transducer calibration set-up.

Three repetitions of [0;+s;...;+l_r-s;+l_r;+l_r;+l_r-s;...;-l_r+s;-l_r;-l_r;-l_r+s;...;-s;0] were considered with l_r=68 mm and s=17 mm. In this case only the output sensor signal was accessible and thus the excitation voltage is not accounted as in the mathematical formulation (equation 4.1). The described calibration procedure was performed taking this aspect into account. The results of the estimates and the associated errors and uncertainties are presented in table 4.9. The major contributions to the uncertainty is due to the voltage measurements and linearity. As a result the obtained expanded uncertainty is around $U_{95\%}$=0,336 mm (0,39 %FS).

Uncertainty Source	Estimate $\bar{x}_i$	Standard Uncertainty $u(x_i)$	Sensitivity Coefficients c_i	Coef. of Correlation $r(x_i,x_j)$	DOF ν_i	Contribution $u_i(S_q)$
Parameter a	-14,6327 mm	0,0237 mm	1		2	0,024 mm (2,4%)
Parameter b	-29,5022 mm/V	0,0156 mm/V	2,8 V		2	0,044 mm (8,1%)
Output Voltage V_o	3,35 V	0,0036 V	-29,5022 mm/V		50	0,106 mm (47,7%)
Linearity	0 mm	0,0957 mm	1		2	0,096 mm (38,6%)
Reversibility	0 mm	0,0066 mm	1		11	0,007 mm (0,2%)
Repeatability	0 mm	0,0057 mm	1		22	0,006 mm (0,1%)
Standard Meas.	500 mm	0,0033 mm	1		50	0,003 mm (0,0%)
Correlation a-b	-14,6327 mm -29,5022 mm/V	0,0237 mm 0,0156 mm/V	1 2,8 V	0,3303	21	0,026 mm (2,9%)
Combined Standard Uncertainty $u_i(S_q)$					0,154 mm (100%)	
Effective DOF ν_{eff}					12	
t-factor $t_{95\%}$					2,18	
Expanded uncertainty $U_{95\%}$					0,336 mm (0,39 %FS)	

Table 4.9. Uncertainty balance for displacement transducer 9 (range ±68 mm) and associated measurement chain.

Acceleration measurement chain characterization

The metrological characterization of the accelerometers and the associated measurement chain was performed using the LNEC mini shaking table. This equipment consists of an electromagnetic shaker to input the motion to the platform, which rolls over the fixed body. The accelerometers for characterization are attached to the platform. This equipment has a displacement transducer (LVDT type) embedded used to measure the platform displacement which is the feedback signal of the control loop for regulation of the platform movement. This control loop makes use of an analogical PID controller implemented in a hardware box (see figure 4.10). The signal provided by the transducer was used to derive the platform displacement and also used as the reference signal to compute the frequency response functions between the accelerometers signals and the platform displacement. To goal is to identify the relationship between the electrical signal provided by the accelerometer and the shaking table platform acceleration which is computed by integrating twice the FRFs in terms of displacements.

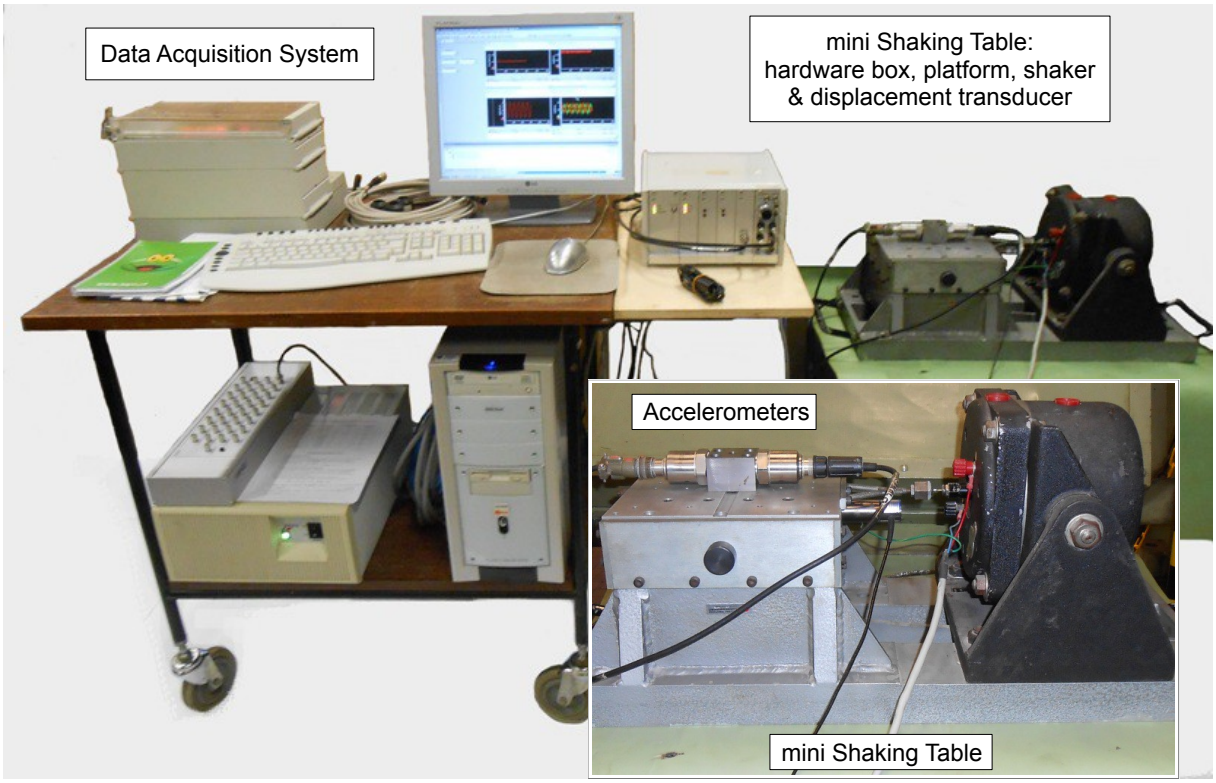

Figure 4.10 - Accelerometers measurement chain calibration set-up.

Before performing the accelerometers characterization, the mini Shaking Table was characterized using the same data acquisition system, through SgnAux signal used for displacement measurement: i) first, the transducer and the associated measurement chain were statically calibrated using the procedure described previously with the Laser Beam length standard (Renishaw ML-10) installed in parallel with the transducer; ii) then, the equipment was characterized dynamically in order to identify the dynamic range. Concerning to the transducer calibration, a unitary gain was used in the signal conditioner board and an input range ±10 V with 16 bit of resolution was selected on the associated channel of the data acquisition system. Three repetitions of $[0;+s;\ldots;+l_r-s;+l_r;+l_r;+l_r-s;\ldots;-l_r+s;-l_r;-l_r;-l_r+s;\ldots;-s;0]$ steps were considered with l_r=5 mm and s=1 mm, being the output voltage and the standard quantities measured at each step. Thus, the excitation voltage is not accounted as in the mathematical formulation (equation 4.1). Again, the described calibration procedure was performed taking this aspect in consideration. The results of the estimates and the associated errors and uncertainties are presented in table 4.10. It is observed that the major contributions to the uncertainty are due to the output voltage measurements and standard measurements, leading to an expanded uncertainty of $U_{95\%}$=0,012 mm (0,25 %FS).

The input time signal presented in figure 4.5 - left was also considered to characterize the mini shaking table dynamically. The mini shaking table transfer function between the output and the reference displacement was obtained (see figure 4.11). The shaking table dynamic

range is around 40 Hz which is adequate to characterize the accelerometers.

Uncertainty Source	Estimate $\bar{x}_i$	Standard Uncertainty $u(x_i)$	Sensitivity Coefficients c_i	Coef. of Correlation $r(x_i,x_j)$	DOF ν_i	Contribution $u_i(S_q)$
Parameter *a*	-0,0073 mm	0,0003 mm	1		2	0,000 mm (0,2%)
Parameter *b*	0,4908 mm/V	0,0000 mm/V	10 V		2	0,000 mm (0,5%)
Output Voltage V_o	10 V	0,0103 V	0,4908 mm/V		50	0,005 mm (66,5%)
Linearity	0 mm	0,0013 mm	1		2	0,001 mm (4,3%)
Reversibility	0 mm	0,0000 mm	1		11	0,000 mm (0,0%)
Repeatability	0 mm	0,0000 mm	1		22	0,000 mm (0,0%)
Standard Meas.	500 mm	0,0033 mm	1		50	0,003 mm (28,4%)
Correlation *a-b*	-0,0073 mm 0,4908 mm/V	0,0003 mm 0,0000 mm/V	1 10 V	-0,0019	21	0,000 mm (0,0%)
Combined Standard Uncertainty $u_i(S_q)$					0,006 mm (100%)	
Effective DOF ν_{eff}					87	
t-factor $t_{95\%}$					1,99	
Expanded uncertainty $U_{95\%}$					0,012 mm (0,25 %FS)	

Table 4.10. Uncertainty balance for the mini shaking table displacement transducer (range ±5 mm) and associated measurement chain.

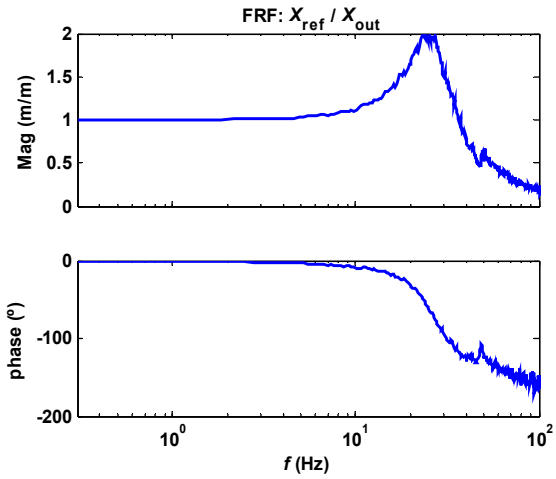

Figure 4.11 - Mini shaking table transfer function.

That input signal was later used to identify the accelerometers dynamic characteristics tested on the mini shaking table. Different amplitudes were used in the tests ranging from 35 mm/s^2 to 1 m/s^2 approximately. The transfer functions were evaluated for each accelerometer with the correspondent measurement (signal Acel0, Acel1 and Acel2) chain and can be found in figure 4.12. Lower magnitude input signals result in noisy FRFs. An average FRF was evaluated from the FRFs obtained with different magnitudes. It is found a dependence of the sensitivity with frequency. An average sensitivity value was calculated in the range of frequencies between 0,15 and 5 Hz.

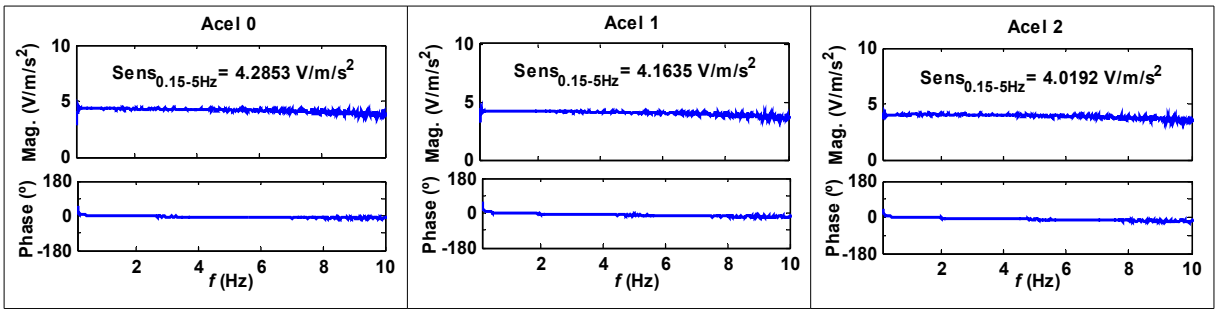

Figure 4.12 - Accelerometers 0, 1 & 2 measurement chain transfer functions.

Summary of measurement and control chain parameters

Table 4.11 summarizes the results of measurement and control chain characterization.

Measured Quantities							
Model Variable	Sensor	Elect. signal	Hardware LNEC	dSPACE DS2003	Measurement Chain Model	Range	$U_{95\%}$
$\ddot{x}_g$	PCB393B12 (AA 21)	Acel0	board 0, gain 2	pin 1, ±10V, 16bit	$\ddot{x}_g = \text{Acel0}/\text{Sens}_{0,15-5Hz}$ Sens^{-1}=0,2334 m/s^2/V	±2 m/s^2	-
$\ddot{x}_i$	PCB393B12 (AA 27)	Acel1	board 1, gain 2	pin 3, ±10V, 16bit	$\ddot{x}_i = \text{Acel1}/\text{Sens}_{0,15-5Hz}$ Sens^{-1}=0,2402 m/s^2/V	±2 m/s^2	-
$\ddot{x}_s$	PCB393B12 (AA 23)	Acel2	board 2, gain 2	pin 5, ±10V, 16bit	$\ddot{x}_s = \text{Acel2}/\text{Sens}_{0,15-5Hz}$ Sens^{-1}=0,2488 m/s^2/V	±2 m/s^2	-
f	HBM U9B	F0	board 5, gain 2550	pin 13, ±10V, 16bit	$f=a+b\cdot$F0/Exc0 a=0,0005 kN b=1,9302 kN/V/V	±3,6 kN	22 N (0,62%FS)
		Exc0		pin 15, ±10V, 16bit			
x_g	LVDT	SgnAux	board 9, gain 1	pin 31, ±5V, 16bit	$x_g=a+b\cdot$SgnAux a=-14,6327 mm b=-29,5022 mm/V	±85 mm (calib. in ±68 mm)	0,336 mm (0,39%FS)
$x_{ig}=x_i-x_g$	Sifernice 34L8D103W 03263D	ExcD1	board 7, gain 6	pin 21, ±10V, 16bit	$x_{ig}=a+b\cdot$SgnD1/ExcD1 a=-0,0930 mm b=33,3685 mm/V/V	±60 mm	0,351 mm (0,58%FS)
		SignD1		pin 23, ±10V, 16bit			
$x_{si}=x_s-x_i$	Sifernice 34L8D103W 03263D	ExcD2	board 8, gain 25	pin 25, ±10V, 16bit	$x_{si}=a+b\cdot$SgnD2/ExcD2 a=-0,0072 mm b=8,0013 mm/V/V	±15 mm	0,066 mm (0,44%FS)
		SignD2		pin 27, ±10V, 16bit			

Generated Quantities				
Model Variable	Elect. signal	DSPACE DS2103	Model	Range
$x_{g,ref}$	output3	pin 3, ±10V, 14bit	$x_{g,ref}=b\cdot$output3 b=9,913 mm/V	±85 mm
u_{SA}	output1	pin 1, ±5V, 14bit	u_{SA}=output1	0 to 5 V

Table 4.11 - Summary table of measurement and control chain parameters.

4.1.3 Two degree-of-freedom mechanical model

Description and Mathematical Model

The developed experimental model is a 2DOF mechanical model representative of typical

base isolated buildings excited by one dimensional earthquake loads. The equations of motion that describe the mechanical behaviour of the 2DOF structural system are given by equation (2.5). A damping matrix proportional to the mass is assumed since the developed physical model dissipative forces are mainly due to the rolling friction located at those DOFs. This fact was indeed confirmed during the identification process. The schematic representation of this system is in figure 4.13 (right) and its model is given by (spatial form):

$$\boldsymbol{M}\cdot\ddot{\boldsymbol{x}}_{\mathrm{rg}}+\boldsymbol{C}\cdot\dot{\boldsymbol{x}}_{\mathrm{rg}}+\boldsymbol{K}\cdot\boldsymbol{x}_{\mathrm{rg}}=-\boldsymbol{M}\cdot\boldsymbol{1}\cdot\ddot{x}_{\mathrm{g}}+\boldsymbol{G}\cdot f_{\mathrm{ad}}$$
$$\boldsymbol{M}=\begin{bmatrix} m_{\mathrm{i}} & 0 \\ 0 & m_{\mathrm{s}} \end{bmatrix},\ \boldsymbol{K}=\begin{bmatrix} k_{\mathrm{i}}+k_{\mathrm{s}} & -k_{\mathrm{s}} \\ -k_{\mathrm{s}} & k_{\mathrm{s}} \end{bmatrix},\ \boldsymbol{C}=\begin{bmatrix} c_{\mathrm{i}} & 0 \\ 0 & c_{\mathrm{s}} \end{bmatrix},\ \mathbf{G}=\begin{bmatrix} -1 \\ 0 \end{bmatrix} \tag{4.14}$$

where: m_{i} and m_{s}, k_{i} and k_{s}, c_{i} and c_{s}, are the mass, stiffness and damping respectively; f_{ad} is the force provided by an additional devices installed at the base; $\ddot{x}_{\mathrm{g}}$ is the input absolute acceleration at the base (ground); and $\boldsymbol{x}_{\mathrm{rg}}=\{x_{\mathrm{ig}}\ x_{\mathrm{sg}}\}^{\mathrm{T}}$ is the vector of relative displacements of the DOF to the ground: $x_{\mathrm{ig}}=x_{\mathrm{i}}-x_{\mathrm{g}}$; $x_{\mathrm{sg}}=x_{\mathrm{s}}-x_{\mathrm{g}}$. The system represented in state-space form is given as in equation (2.9) with the following matrices:

$$\dot{\boldsymbol{z}}=\boldsymbol{A}\cdot\boldsymbol{z}+\boldsymbol{B}\cdot f_{\mathrm{ad}}+\boldsymbol{E}\cdot\ddot{x}_{\mathrm{g}}$$
$$\boldsymbol{y}=\boldsymbol{C}_{\mathrm{y}}\cdot\boldsymbol{z}+\boldsymbol{D}_{\mathrm{y}}\cdot f_{\mathrm{ad}}$$
$$\boldsymbol{A}=\begin{bmatrix} \mathbf{0} & \mathbf{I} \\ -\boldsymbol{M}^{-1}\cdot\boldsymbol{K} & -\boldsymbol{M}^{-1}\cdot\boldsymbol{C} \end{bmatrix}=\begin{bmatrix} 0 & 0 & 1 & 0 \\ 0 & 0 & 0 & 1 \\ -\dfrac{k_{\mathrm{i}}+k_{\mathrm{s}}}{m_{\mathrm{i}}} & \dfrac{k_{\mathrm{s}}}{m_{\mathrm{i}}} & -\dfrac{c_{\mathrm{i}}}{m_{\mathrm{i}}} & 0 \\ \dfrac{k_{\mathrm{s}}}{m_{\mathrm{s}}} & -\dfrac{k_{\mathrm{s}}}{m_{\mathrm{s}}} & 0 & -\dfrac{c_{\mathrm{s}}}{m_{\mathrm{s}}} \end{bmatrix}, \tag{4.15}$$
$$\boldsymbol{B}=\begin{Bmatrix} \mathbf{0} \\ \boldsymbol{M}^{-1}\cdot\boldsymbol{G} \end{Bmatrix}=\begin{Bmatrix} 0 & 0 & -1/m_{\mathrm{i}} & 0 \end{Bmatrix}^{\mathrm{T}},\ \boldsymbol{E}=\begin{Bmatrix} \mathbf{0} \\ -\mathbf{1} \end{Bmatrix}=\begin{Bmatrix} 0 & 0 & -1 & -1 \end{Bmatrix}^{\mathrm{T}}$$

where: $\boldsymbol{z}=\{x_{\mathrm{ig}}\ x_{\mathrm{sg}}\ \dot{x}_{\mathrm{ig}}\ \dot{x}_{\mathrm{sg}}\}^{\mathrm{T}}$ is the state vector; $\boldsymbol{y}$ is the output vector defined according to the quantity required for output through the matrices $\boldsymbol{C}_{\mathrm{y}}$ and $\boldsymbol{D}_{\mathrm{y}}$. The correspondent characteristic equation is:

$$\begin{aligned}&(m_{\mathrm{i}}\ m_{\mathrm{s}})s^4+(m_{\mathrm{i}}\cdot c_{\mathrm{s}}+m_{\mathrm{s}}\cdot c_{\mathrm{i}})s^3+\\&+(m_{\mathrm{i}}\cdot k_{\mathrm{s}}+m_{\mathrm{s}}\cdot k_{\mathrm{i}}+m_{\mathrm{s}}\cdot k_{\mathrm{s}}+c_{\mathrm{i}}\cdot c_{\mathrm{s}})s^2+(c_{\mathrm{i}}\cdot k_{\mathrm{s}}+c_{\mathrm{s}}\cdot k_{\mathrm{i}}+c_{\mathrm{s}}\cdot k_{\mathrm{s}})s+k_{\mathrm{i}}\cdot k_{\mathrm{s}}=0\end{aligned} \tag{4.16}$$

Physical systems, i.e. constants m_{i}, m_{s}, c_{i}, c_{s}, k_{i}, k_{s},$\in\mathbb{R}^{+}$, are always stable (the roots given by (4.16) have always negative real parts). The undamped frequencies, i.e. taking c_{i}=0 and c_{s}=0, are obtained by solving the characteristic equation with $s=\mathrm{i}\cdot\omega$:

$$\omega_{1,2}^2=\frac{1}{2}\frac{m_{\mathrm{i}}\cdot k_{\mathrm{s}}+m_{\mathrm{s}}\cdot k_{\mathrm{i}}+m_{\mathrm{s}}\cdot k_{\mathrm{s}}}{m_{\mathrm{i}}\cdot m_{\mathrm{s}}}\mp\frac{1}{2}\sqrt{\left(\frac{m_{\mathrm{i}}\cdot k_{\mathrm{s}}+m_{\mathrm{s}}\cdot k_{\mathrm{i}}+m_{\mathrm{s}}\cdot k_{\mathrm{s}}}{m_{\mathrm{i}}\cdot m_{\mathrm{s}}}\right)^2-4\frac{k_{\mathrm{i}}\cdot k_{\mathrm{s}}}{m_{\mathrm{i}}\cdot m_{\mathrm{s}}}} \tag{4.17}$$

Taking as outputs the absolute acceleration at the base and at the top, thus

$\boldsymbol{C}_y=[\,-\boldsymbol{M}^{-1}\cdot\boldsymbol{K}\;-\boldsymbol{M}^{-1}\cdot\boldsymbol{C}\,]$ and $\boldsymbol{D}_y=\boldsymbol{M}^{-1}\cdot\boldsymbol{G}$, the system is said to be output and state (relative displacement and velocity) controllable since the correspondent controllability matrices $\boldsymbol{C}_o$ and $\boldsymbol{C}_s$ have full rank (*Ogata 1970*):

$$\boldsymbol{C}_o=[\boldsymbol{C}_y\cdot\boldsymbol{B}\;\;\boldsymbol{C}_y\cdot\boldsymbol{A}\cdot\boldsymbol{B}\;\;\boldsymbol{C}_y\cdot\boldsymbol{A}^2\cdot\boldsymbol{B}\;\;\boldsymbol{C}_y\cdot\boldsymbol{A}^3\cdot\boldsymbol{B}\;\;\boldsymbol{D}_y];\;\;\boldsymbol{C}_s=[\boldsymbol{B}\;\;\boldsymbol{A}\cdot\boldsymbol{B}\;\;\boldsymbol{A}^2\cdot\boldsymbol{B}\;\;\boldsymbol{A}^3\cdot\boldsymbol{B}] \quad (4.18)$$

Model Development

The model is intended to reproduce the characteristics of the base isolated building described in section 3.5: ten-storey base isolated structure. The 2DOF model was developed such that the first two modal characteristics (frequency and damping ratio) as well as the anti-resonance (fixed base frequency) were similar to the ones of the base isolated building (see figure 4.13).

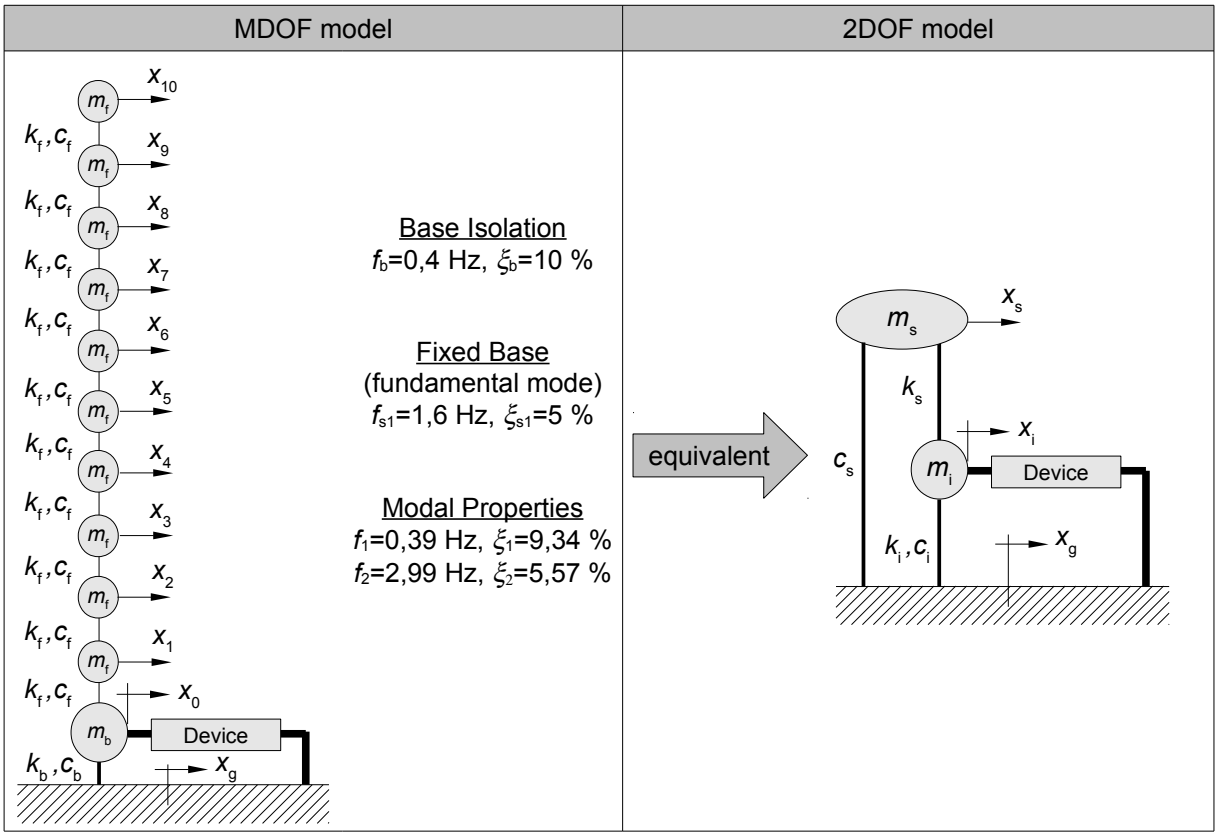

Figure 4.13 - MDOF model and 2DOF model matching.

Thus, the 2DOF model characteristics (mass and stiffness) were chosen such that the first two natural frequencies of the MDOF model match the 2DOF ones given by equation (4.17), and the building fixed base frequency (anti-resonance) match with the 2DOF model fixed base frequency ω_s. The rigid structure (index i) and fixed-base (index s) properties are given by:

$$\omega_i=\sqrt{\frac{k_s}{m_i+m_s}},\;\;\xi_i=\frac{c_i}{2\,(m_s+m_i)\,\omega_i};\;\omega_s=\sqrt{\frac{k_s}{m_s}},\;\;\xi_s=\frac{c_s}{2\,m_s\,\omega_s} \quad (4.19)$$

The stifness properties of the selected springs can be found in table 4.12. Two soft springs and two hard springs were tested in a universal testing machine at a velocity of 1mm/s where the force and displacement were measured using a laboratory traceable measurement chain. Soft springs were tested in compression (charge and uncharge) over a range of 190 mm and 3,5 kN. The same procedure was applied to the hard springs over a range of 90 mm and 19 kN. A linear model $f=k\cdot d$, force as the product of stiffness and displacement, was adjusted to the experimental data in the range slightly away from the zero force to avoid non-linearities due to the accommodation of spring ends to the machine seats. The corresponding values of stiffness k obtained from a linear regression as well as the coefficient of determination r^2 are presented in table 4.12.

	Geometry	Experimental data	Properties
soft spring	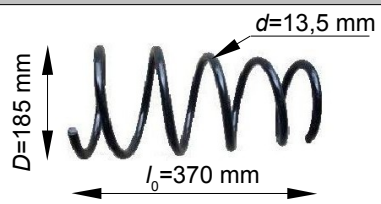	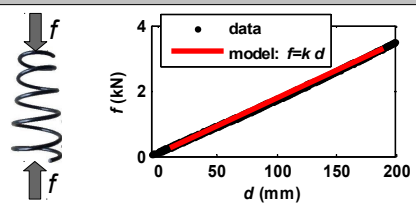	spring / k (N/mm) / r^2 (%): 1 / 17 / 99,9; 2 / 16,8 / 99,9; k_i / 33,8 / -
hard spring	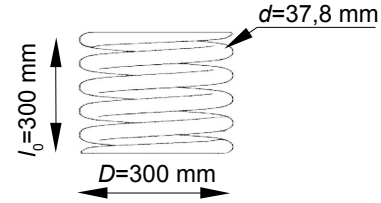	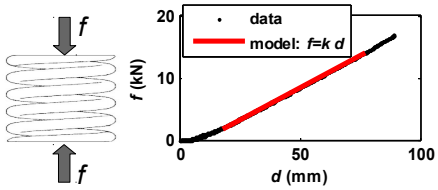	spring / k (N/mm) / r^2 (%): 1 / 201,1 / 99,8; 2 / 205,8 / 99,9; k_s / 406,9 / -

Table 4.12. 2DOF model mechanical springs: geometry and results of experimental characterization.

Taking into account that the idealized model has each pair of springs linked in parallel, the values for k_b and k_s are obtained by summing the correspondent stiffness values, as shown in table 4.12. The masses m_i and m_s were chosen taking into account the developed and designed mechanical system (figures 4.1 and 4.14) to fit as much as close the intended natural frequencies. Concerning to the structural damping, the resulting damping from the mechanism will be the only damping associated with the original structure (without devices) and thus no adjustment of damping was made. Table 4.13 summarizes the 2DOF model characteristics (mass and stiffness) as well as the undamped natural frequencies (for rigid structure f_i and fixed-base f_s) and modal frequencies, obtained with the assembly of components. It is observed that the values are close to the ones of the MDOF model.

Characteristics: mass and stiffness				Frequencies		
m_i (kg)	m_s (kg)	k_i (N/mm)	k_s (N/mm)	f_i (Hz)	f_s (Hz)	$f_{1,2}$ (Hz)
1790	3950	33,8	406,9	0,39	1,62	[0,38; 2,95]

Table 4.13 - 2DOF model: summary of characteristics and frequencies calculated from individual characteristics using the model equations.

Model Identification

The physical model was installed on the shaking table (figures 4.1 and 4.14), without the SA device, and was subjected to a campaign of tests in order to identify its modal properties.

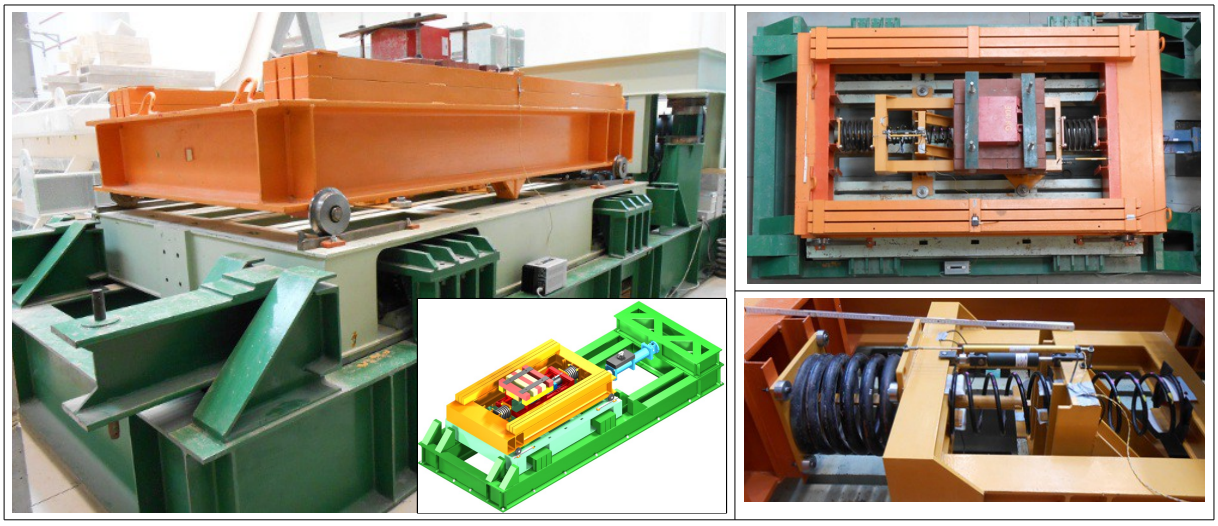

Figure 4.14 - Experimental model on the shaking table: perspective, top view and MR damper detail.

A white-noise signal of 360 s passed through a higher-pass filter at 0,2 Hz and integrated once was used as the reference displacement for the shaking table (figure 4.15). Five different magnitudes of this signal were considered in the tests, being that signal multiplied by the following scale factors: 0,6; 0,7; 0,8; 0,9; and 1,0. All the responses were measured as well as the input to the shaking table. From the time signals the FRFs were evaluated using the H1 estimator.

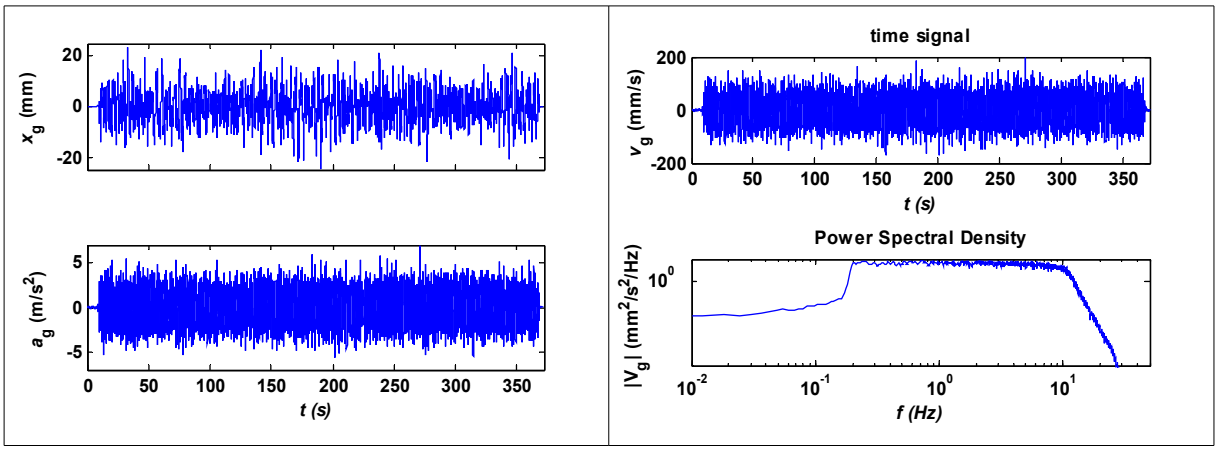

Figure 4.15 - Input signal to characterize the physical model (measured at unity scale factor). Displacement and acceleration series (left) and power spectral density in velocity (right).

Figure 4.16 shows the obtained FRFs. It is found a small dependence of the input magnitude on the system behaviour, namely on the natural frequencies and damping. In order to identify the system modal properties, the experimental model consisting on the frequency response functions in terms of accelerations and relative displacements to the ground (X_{ig}/A_g, X_{sg}/A_g, A_i/A_g, A_s/A_g), were used to identify the parameters of the continuous time model in equation

(4.15). The prediction-error minimization method available at Matlab was used for that purpose. In the identification process the model parameters m_i and m_s were assumed to be invariant and the other parameters, k_i, k_s, c_i and c_s were the selected unknown parameters in the identification process. A comparison between the experimental FRFs and the regenerated ones using the mathematical model with the identified parameters can be found in figure 4.17, for the maximum input signal magnitude. A good agreement is found between the experimental and the spatial model even for other input signal magnitudes.

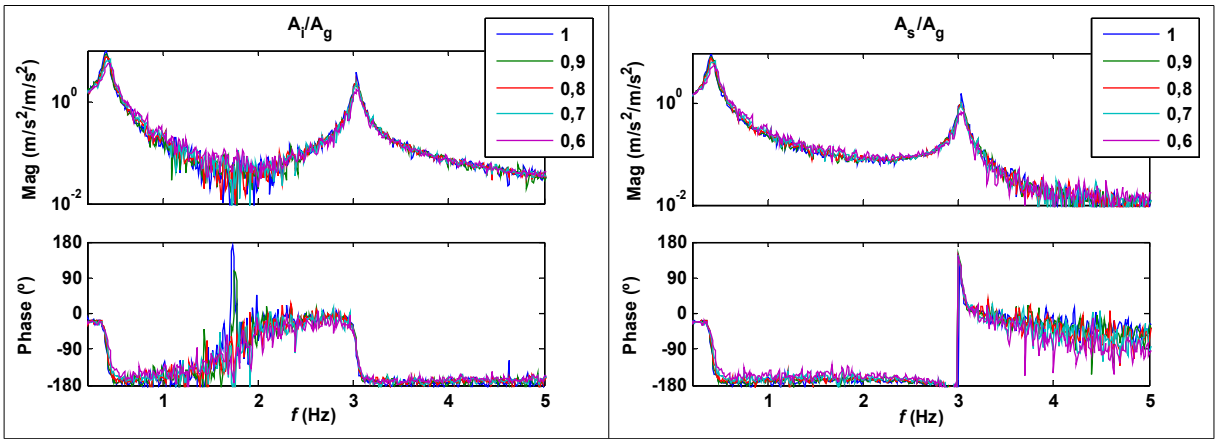

Figure 4.16 - FRFs (A_i/A_g and A_s/A_g) for different input signal magnitudes.

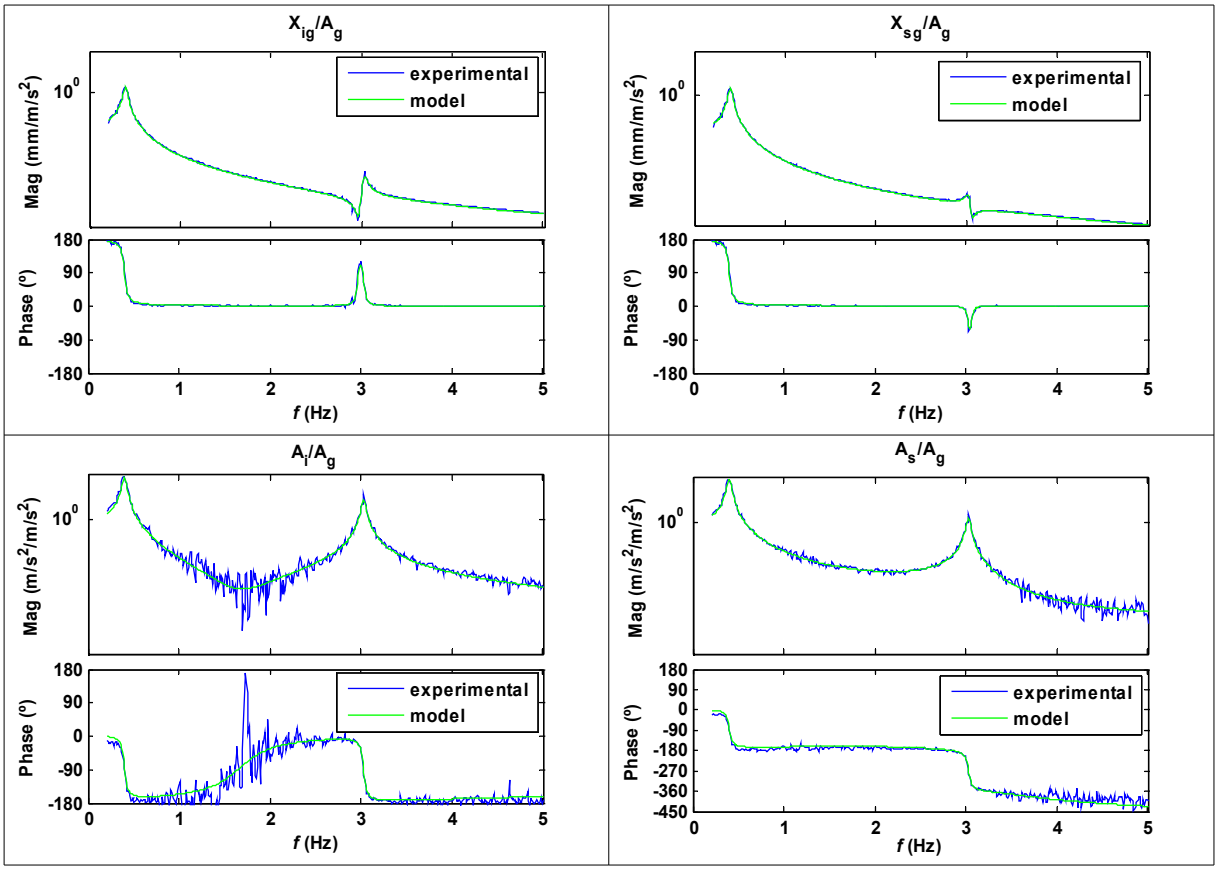

Figure 4.17 - Comparison between the experimental FRFs and the regenerated ones at the maximum input signal magnitude (unitary scale factor).

The evolution of the identified model parameters as well as the modal parameters with the magnitude of the input signal can be found in figure 4.18. It is observed a decreasing trend of the first modal frequency and both damping ratios as the input signal magnitude increases. This has direct effect on the spatial model parameters: a small decreasing in stiffness (k_i namely) and damping with the input signal magnitude. A *Rayleigh* damping model proportional to the mass matrix was found to describe well the dissipative mechanisms.

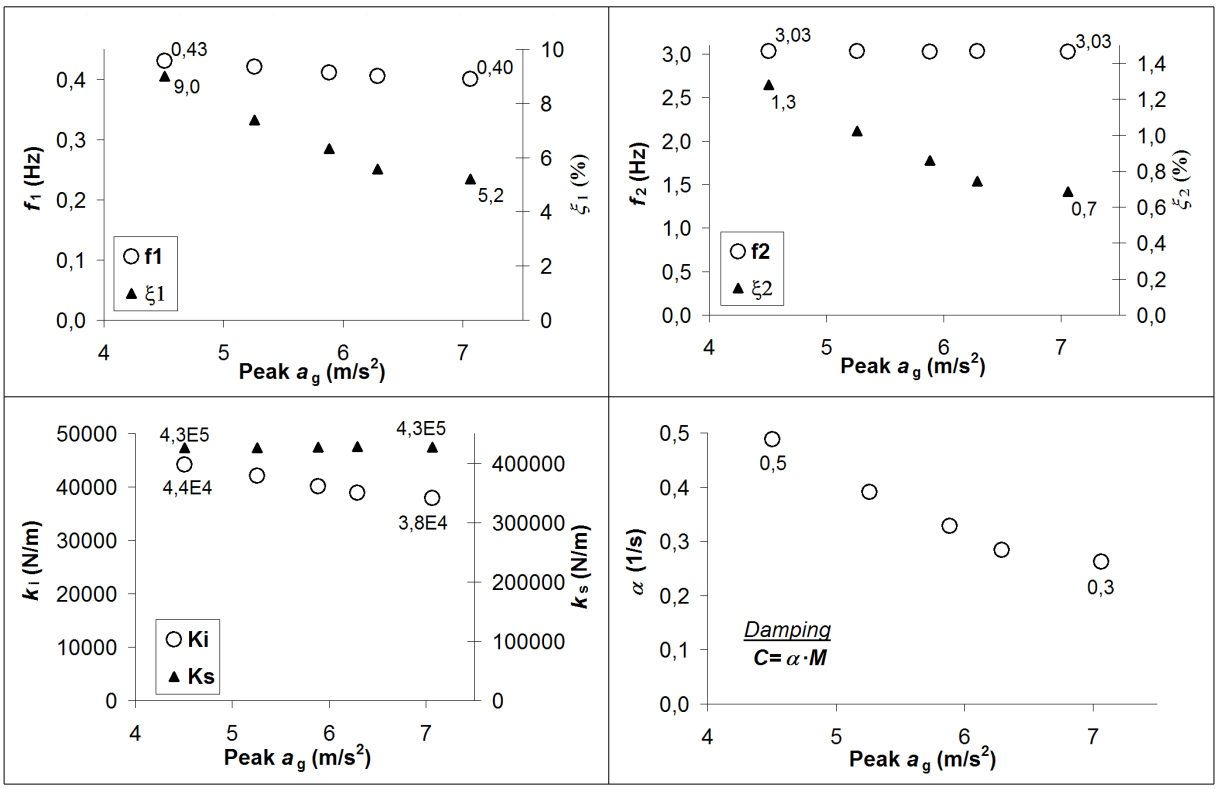

Figure 4.18 - Modal parameters (natural frequencies and damping ratios) and spatial model parameters evolution with the magnitude of the input signal, obtained from the experimental data.

4.1.4 SA device

Description

An MR damper model RD-8041-1 with a current controller RD-3002-03 manufactured by LORD Corporation (http://www.lord.com) was used as the SA device in this work. The damper has a stroke of 74 mm and can reach up to 1,5 kN at 0,2 m/s for a current in the coils around 2 A. The current controller uses the pulse width modulation (PWM) technique to control the current in the damper coil using an input voltage as reference. A power supply at constant voltage capable of producing at least 2 A of current was used. Figure 4.19 depicts the SA device. In order to characterize the mechanical behaviour of the assembly (damper plus current controller) several tests were performed.

Experimental Tests

Two type of tests were performed. The first one consisted of characterizing the current

controller behaviour with the damper attached but mechanically disconnected in order to identify the relationship between the input command voltage and the electric current on the damper electrical circuit. The second type of tests consisted in characterizing the whole SA device when subjected to mechanical work, like static tests, dynamic tests in stationary regime and dynamic tests in transient regime.

Figure 4.19 - LORD MR damper model RD-8041-1 with a current controller RD-3002-03.

Current Controller Characterization

In this test a known input current was injected in the damper electrical circuit and the electric current was measured. The electric current was obtained indirectly from the electrical voltage measured at the terminal of a proof resistor with R_p=68,8 mΩ connected in series. The input voltage and voltage measurement were performed with the data acquisition and control system described previously (section 4.1.2) using the output 1 channel to inject the electrical voltage and SgnAux channel to measure the electrical voltage at the resistor terminals. Eight repetitions (cycles) of steps and continuous input voltages were performed, starting at zero going to 5 V and returning to zero, being the correspondent output voltages measured. In figure 4.20 are presented the results of the tests where it is found a dead band from zero to up V_t≈0,6 V approximately, and then a linear relationship between both quantities.

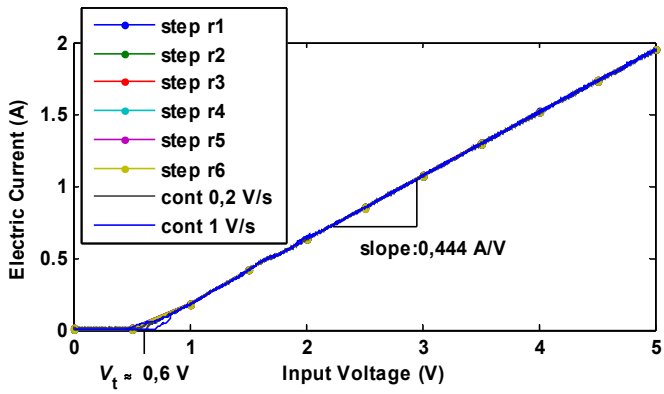

Figure 4.20 - Relationship between the input voltage and electrical circuit current. Static and quasi-static tests.

Moreover, the dynamic characteristics were evaluated considering a square wave and a

band-limited white noise as input signals. From the step response it was found that the current controller responds fast and without overshoot although slightly differences are found between the ascending and descending time responses. Figure 4.21-left depicts the current controller square wave (with 5 V of magnitude) response, which correspond to the following values in terms of time domain performance indices: i) ascending: rise time t_r=17 ms and settling time t_s=21 ms (5% criteria); ii) descending: rise time t_r=20 ms and settling time t_s=31 ms (5% criteria); iii) average: rise time t_r=19 ms and settling time t_s=26 ms.

The frequency response function was obtained using a band-limited (up to 500 Hz) white-noise signal with a mean value of 2,5 V, an RMS value of 0,39 V and a peak value of 2,3 V, in order to avoid crosses over the non-linearity below the transition voltage (V_t≈0,6 V). The FRF is depicted in figure 4.21-right, where a cut-off frequency f_c≈55 Hz is found.

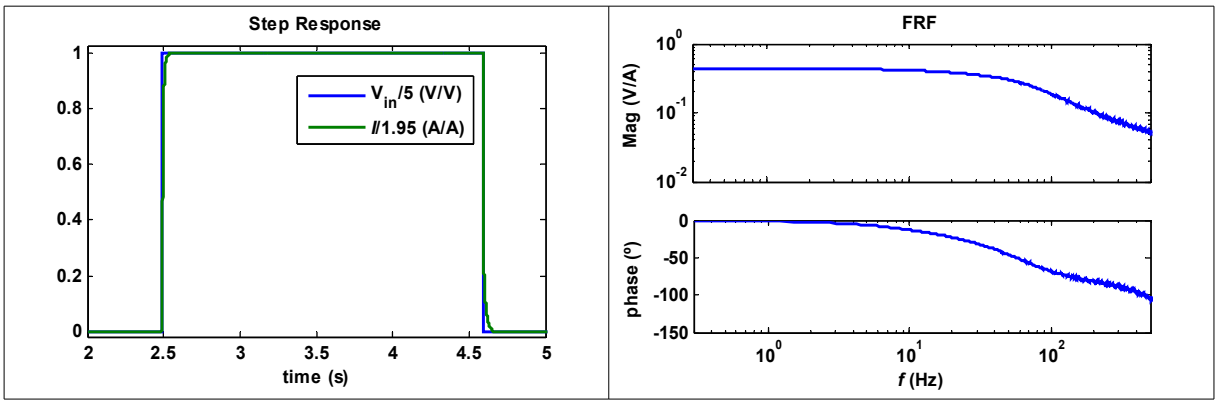

Figure 4.21 - Current controller response to a square wave input (left) and the frequency response function (right).

Damper Characterization

In order the characterize the whole damper mechanical behaviour different tests were performed: i) *static tests* at several displacement points; ii) *dynamic tests*, under a stationary regime in the whole displacement range, and under a transient regime. The tests were performed on a universal testing machine as depicted in figure 4.22. The damper was provided with the measurement chain previously calibrated, associated with the force (variable f) and displacement channels (variable x_{ig}).

The *static tests* are intended to identify the static components of the damper, that are described in terms of stiffness, offset force and frictional forces. The tests consisted in application of three displacement repetitions between -34 mm and 34 mm starting at zero, in steps of 8,5 mm. At each step a sample of 3 s from the displacement and force signals was collected and the correspondent mean values were used as representative values of each step. The obtained values are found in the graph of table 4.14.

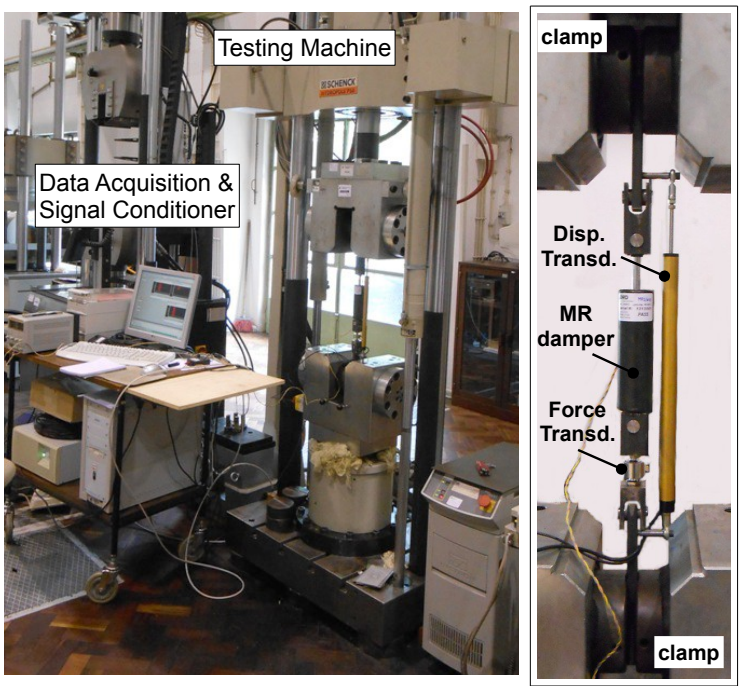

Figure 4.22 - MR damper test set-up.

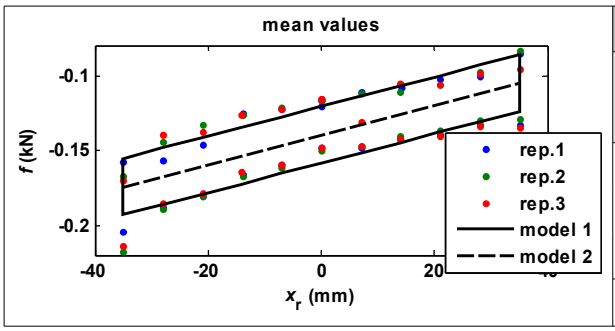

Model parameters and Mean Square Error		
parameter	values	
	model 1	model 2
f_0 (N)	-158,78	-139,831
f_f (N)	37,892	0
k_x (N/mm)	0,987	0,987
MSQ (N)	8,6 (0,6%FS)	20,3 (1,4%FS)

Table 4.14 - MR damper static test results and model parametrization.

The results show the three components referred previously (stiffness, offset force and frictional force) which can be described by the following model:

$$f = f_0 + f_f \cdot \mathrm{sgn}(v_r) + k_x \cdot x_r \tag{4.20}$$

where: f_0 and k_x are the offset force and stiffness due to the damper internal accumulator; f_f is the frictional force; f, v_r and x_r are the force, velocity and displacement at damper ends. The model parameters were adjusted to the data considering two approaches: i) model 1, where all parameters are taken into account; ii) model 2, by neglecting the non-linearity given by the frictional force, thus forcing f_f=0. Table 4.14 shows the results where mean square errors of 0,6% and 1,4% of the full damper force range were obtained with model 1 and 2 respectively.

Different *dynamic tests* were considered to identify the damper characteristics. The transient characteristics were identified from the experimental data obtained during dynamic tests using a triangle displacement signal and imposing a step voltage to the damper between inversions where an almost constant velocity is achieved. The tests were performed at

6,25 mm, 12,5 mm and 25 mm of wave amplitude, frequencies at 0,25 Hz to 0,75 Hz, and input steps from 0 V to 5 V and 5 V to 0 V. An example of the damper force response to these inputs can be found in figure 4.23.

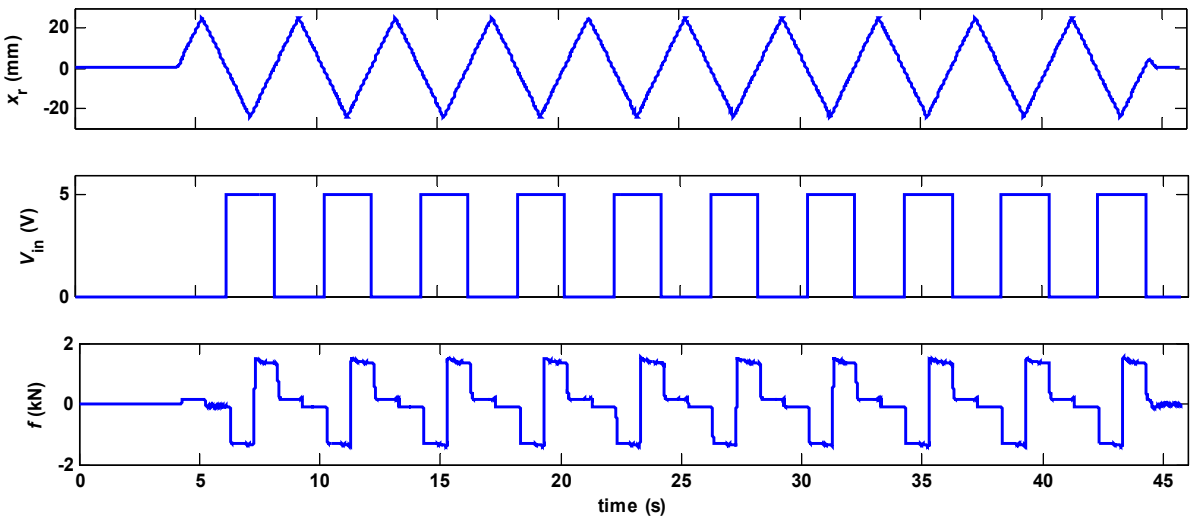

Figure 4.23 - MR damper transient response test under triangle-wave displacement and square-wave input voltage.

A first order dynamic system model was considered to describe the damper dynamics. At the constant velocity regime the force response to the step input can be described by:

$$f = f_{\text{step}} + C_{\text{step}} \cdot \left(1 - e^{t/Td}\right) \tag{4.21}$$

where: f_{step} and C_{step} define the initial condition and the step magnitude that can be evaluated from the initial and final points; $e^{t/Td}$ is the exponential of the time variable over the model time constant T_d, which one describes the damper time response characteristics. Adjusting this parameter to the experimental data using an optimization algorithm the time constant values for each test case were identified. For each test (as in figure 4.23) up to 10 time constant values were identified and an average was calculated as a representative value. Figure 4.24-left shows an example of the experimental data with the adjusted mathematical model to the data.

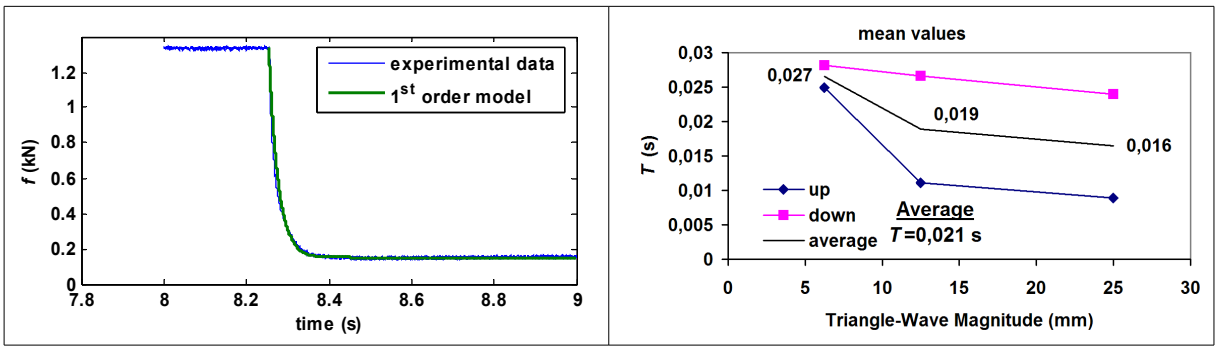

Figure 4.24 - MR damper time constant results: force response data and model adjustment (left); time constant T_d values (right).

The values obtained for the damper time constants show that the assembly is faster from 0 V to 5 V in reaching the stationary regime than the opposite. A little dependence on the magnitude of the wave is observed as shown in figure 4.24-right. The average time constant considering all the tests is found to be T_d=21 ms. An estimate of the damper response time is $4T_d$=84 ms which is the time needed to reach the 2% line of the final value (settling time, 2% criteria). Moreover, the damper was also subjected to dynamic tests under the stationary regime. 10 cycles of sinusoidal displacement waves were performed with: magnitude of 6,25 mm and frequencies from 0,25 Hz to 2 Hz; magnitude of 12,5 mm and frequencies from 0,25 Hz to 1,75 Hz; magnitude of 25 mm and frequencies from 0,25 Hz to 0,75 Hz. With these tests, peak velocities up to 140 mm/s approximately were covered. Input constant voltages from 0 V to 5 V were applied to the damper (current controller). An example of the damper response under a sinusoidal displacement input wave and varying the input voltage monotonically is shown in figure 4.25.

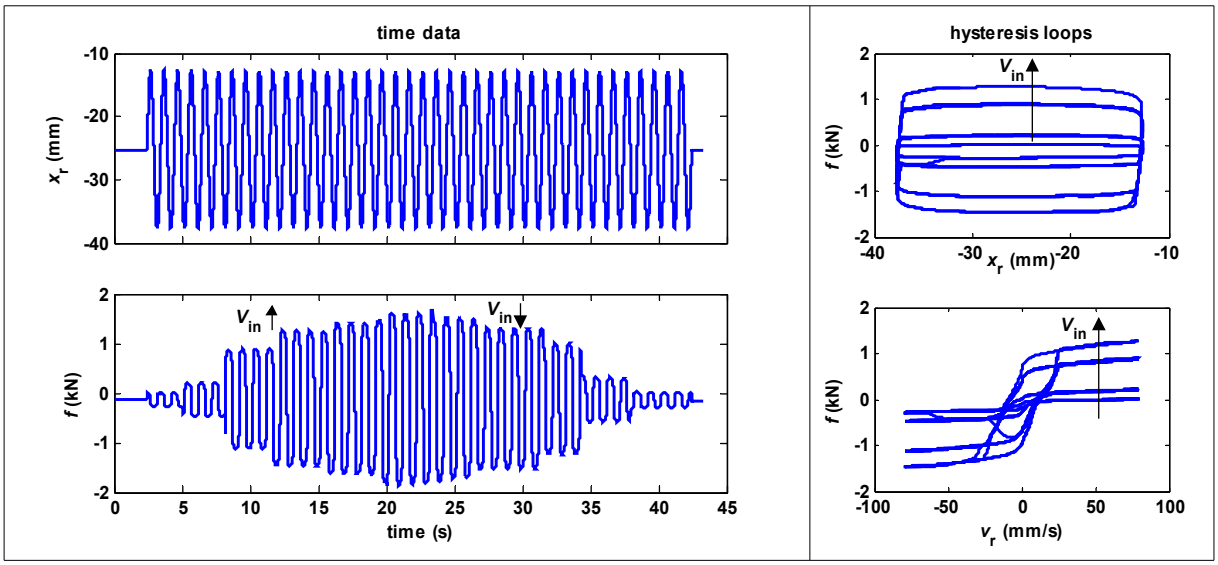

Figure 4.25 - MR damper response under a sinusoidal input displacement and varying input voltage.

To describe the damper behaviour three parametric models of the Bouc-Wen family were considered: i) Dahl model; ii) Bouc-Wen model; iii) and the Modified Bouc-Wen model. This models were already described in Chapter 2 section 2.8.3 and are recalled here again. The Bouc-Wen model with a viscous element in parallel is given by:

$$\begin{aligned} f &= f_0 + k_x \cdot x_r + c_0 \cdot \dot{x}_r + k_w \cdot w \\ \dot{w} &= \rho \cdot \left[\dot{x}_r - \sigma \cdot |\dot{x}_r| \cdot w \cdot |w|^{n-1} + (\sigma - 1) \cdot \dot{x}_r \cdot |w|^n \right] \end{aligned} \tag{4.22}$$

where: f_0 and k_x are the offset force and stiffness, already defined in the static model; c_0 is the post-yield damping coefficient; k_w is the yield force; ρ, σ and n are parameters used to model the hysteresis loop; $w \in [-1,1]$ is an internal variable (normalized) used to describe the force-

velocity hysteresis; notice that the frictional force is not accounted as in the static model since it is small when compared to the other contributions.

As stated before the Dahl model is a particular case of the Bouc-Wen model, by taking n=1 and σ=1.

Finally, the Modified Bouc-Wen model is given by:

$$f=\begin{cases} c_0\cdot(\dot{x}_r-\dot{y})+k_0\cdot(x_r-y)+k_1\cdot(x_r-x_0)+k_w\cdot w \\ c_1\cdot\dot{y}+k_1\cdot(x_r-x_0) \end{cases} \qquad (4.23)$$
$$\dot{w}=\rho\cdot\left[(\dot{x}_r-\dot{y})-\sigma\cdot|\dot{x}_r-\dot{y}|\cdot w\cdot|w|^{n-1}+(\sigma-1)\cdot(\dot{x}_r-\dot{y})\cdot|w|^n\right]$$

Compared to the Bouc-Wen model, there are now two stiffness components (k_0 and k_1), two viscous components (c_0 and c_1) and an additional variable (y) and its derivative. k_1 is the stiffness component k_x resulting from the static tests and k_0 is an additional stiffness component producing the same effect as k_1 in the hysteresis loop. c_0 is a post-yield damping coefficient and c_1 is a damping component that modifies the roll-off in the force-velocity curve. The remaining parameters have the same effect as in the Bouc-Wen model. Notice that an initial displacement x_0 replaces the initial force f_0, both related as f_0=-$k_1\cdot x_0$.

In order to identify the model parameters, an average cycle of the 9 intermediate cycles from the time data was used as input of an optimization algorithm. The optimization problem was formulated and a non-linear optimization algorithm, the interior point method, was used to identify the parameters for each configuration (frequency and input voltage). It must be referred that static stiffness parameters (k_x or k_1) was fixed in the optimization problem since it was already identified in the static tests. The offset force f_0 (or offset displacement x_0) was let free due to the fact that the test started in a different initial point (displacement). Moreover the exponent was restricted to the interval $n\in[1, 2]$. Initial estimates were given for the parameters, being some of them extracted from the experimental data (f_0 and c_0 namely). The results obtained are found in table 4.15 as well as the sum of the mean square error (MSE_{sum}) for all the tests, between the measured force and the predicted one by the model. It was found that parameters c_0, c_1, ρ and σ have a dependence on the peak velocity beyond the input voltage dependence. k_w is mainly dependent on the input voltage and the other parameters are also slightly dependent of both input voltage and peak velocity. The results show also that the modified Bouc-Wen model describes better the damper behaviour.

Finally, figure 4.26 shows the adopted block diagram with each model component used to describe the behaviour of the MR damper. The damper response time is included in the 'First Order Model' block, then the relationship between the Bouc-Wen family model parameters, input voltage and peak velocity is included in the 'Parameters Model' block, and finally the

Bouc-Wen family model in the correspondent block. In these studies the adopted model is thus Modified Bouc-Wen model with a set of tables having the data relating the model parameters with the input voltage and peak velocity (as in table 4.15) whose intermediate values are calculated using a linear interpolation. For implementation of the model the peak velocity is substituted by the absolute input velocity.

Dahl model	Bouc-Wen model	Modified Bouc-Wen model
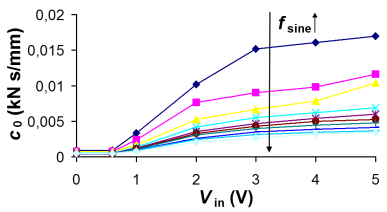	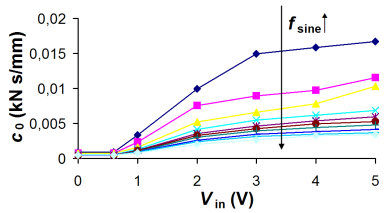	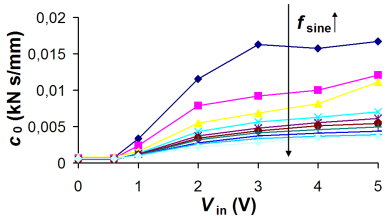
-	-	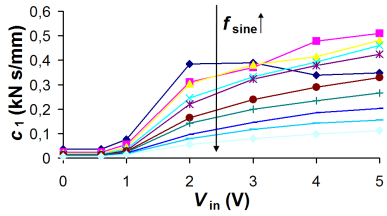
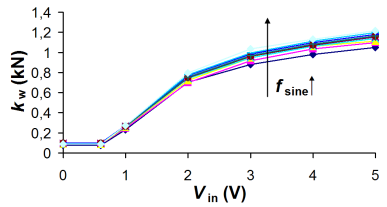	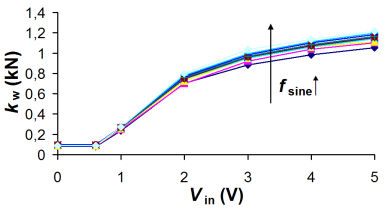	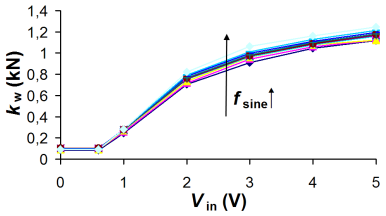
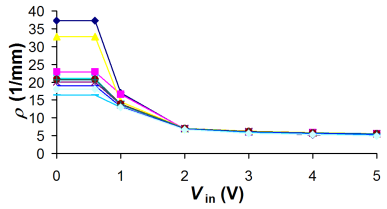	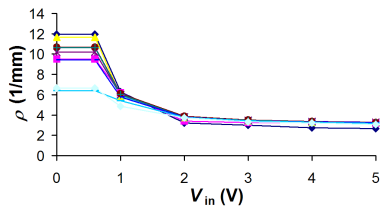	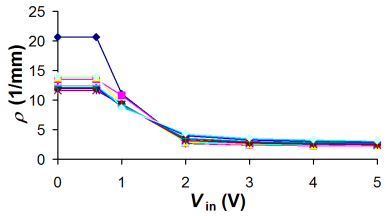
σ=1 (in the Bouc-Wen model formulation)	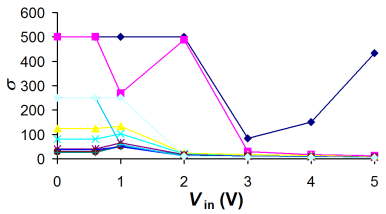	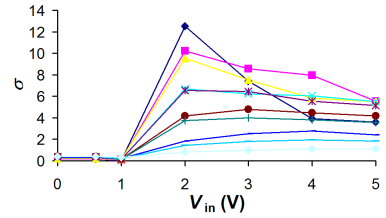
n=1 (Bouc-Wen model formul.) k_x=0,987 kN/m f_0=-0,132 kN	n=2 k_x=0,987 kN/m f_0=-0,132 kN	n=2 k_0=10^{-4} kN/m k_1=0,987 kN/m f_0=-0,132 kN
MSE_{sum}=0,026 kN	MSE_{sum}=0,017 kN	MSE_{sum}=0,007 kN

Table 4.15 - MR damper stationary test results and models parametrization. Curves for different peak velocity values (or sine excitation frequencies from 0,25 Hz to 1,75 Hz at 12,5 mm of magnitude).

An example showing a comparison of results between the measured force and the adopted

model force is shown in figure 4.27, where a good agreement between the data is observed.

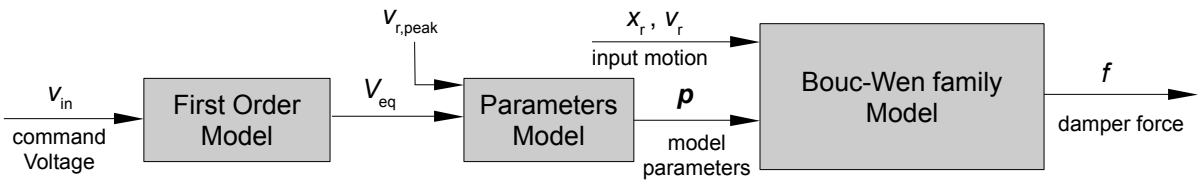

Figure 4.26 - Block diagram of the MR damper.

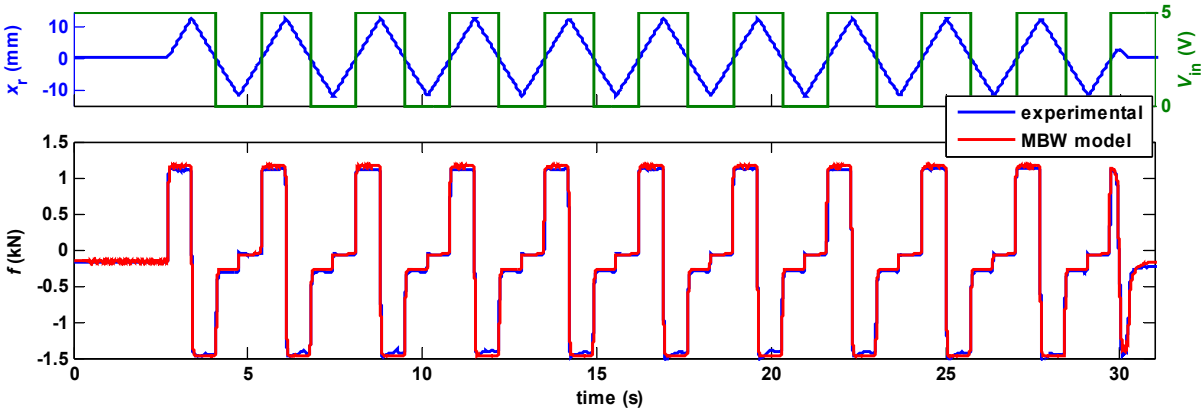

Figure 4.27 - Comparison between the MR damper force and the force evaluated by the Modified Bouc-Wen model, under a triangular wave displacement and a square wave input voltage.

4.1.5 Experimental Campaign

An experimental campaign was performed using the physical model described (2DOF model) consisting in applying several input signals on the shaking table platform, capture the time responses and evaluate the performance indices.

The physical model configurations tested were: i) the original structure (2DOF model only); ii) the structure with the MR damper in passive mode (under constant input voltage); iii) and the structure with the MR damper in semi-active mode, considering the most relevant strategy/algorithm described in the last chapter (see section 3.3).

In what concerns to the input ground motions, the artificial accelerograms generated for the Portuguese territory (type 1 and 2) described in section 3.1.4 were used for this context. Also a set of recorded earthquake ground motions described in *Narasimhan et al. 2006* were used: El Centro, Newhall, Rinaldi, Sylmar, Erzinkan, Jiji and Kobe records (see figure 4.28). In order to keep the input ground motions in the range of the shaking table displacements and MR damper stroke, scale factors were applied to the input signals. Table 4.16 lists the scale factors used.

The performance of 2DOF structural systems in different configurations (original, passive and semi-active) is evaluated by the evaluation criteria (performance indexes) described in table 4.17. Concerning to the ratios, values higher than 1 indicate that the response of the structure with an additional system is higher than that of the original one. Good performance is thus associated with smaller ratios.

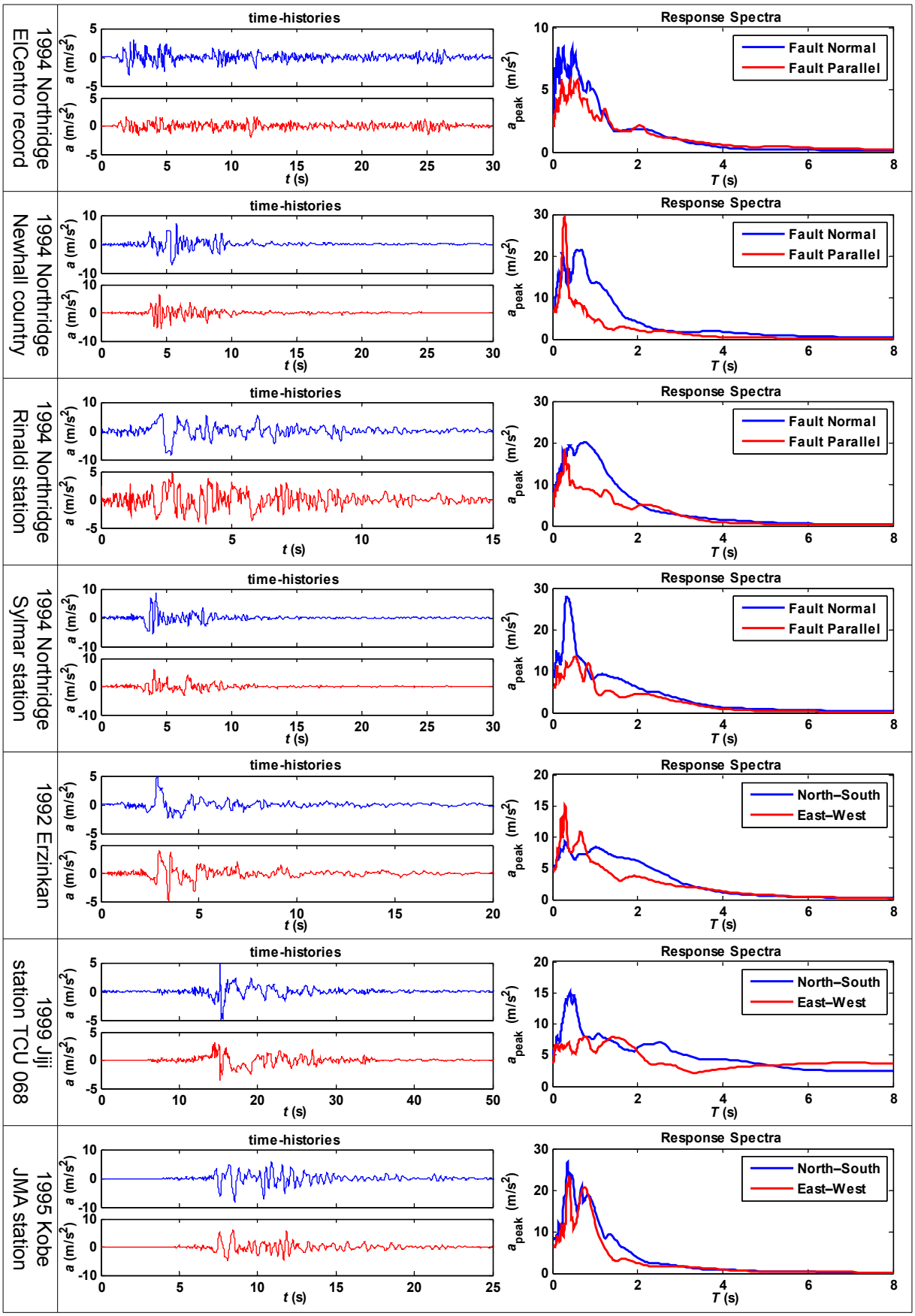

Figure 4.28 - Time histories and response spectra of earthquake records: El Centro Newhall, Rinaldi and Sylmar (California, US); Erzinkan (Turkey), Jiji (Taiwan) and Kobe (Japan).

Portuguese Artificial Accelerograms				Recorded Ground Motions		
Accelerogram	Type 1	Type 2		Earthquake	FN/NS	FP/EW
1	15 %	32 %		ElCentro	21 %	24 %
2	15 %	40 %		Newhall	9,5 %	19 %
3	15 %	40 %		Rinaldi	6,65 %	6,65 %
4	13,5 %	36 %		Sylmar	7,2 %	8 %
5	12 %	36 %		Erzikan	5,6 %	8 %
6	13,5 %	28 %		Jiji	5 %	5 %
7	13,5 %	32 %		Kobe	12,6 %	18 %
8	13,5 %	36 %				
9	13,5 %	40 %				
10	12 %	24 %				

Table 4.16 - Scale factors applied to the input ground motions.

Parameter	Description
x	Specific time variable *x*: relative displacements, accelerations or force;
P*x*	Peak value of *x;*
RMS*x*	Root Mean Square of x;
RP*x*	Ratio of peak responses of *x* for a specific solution, passive or semi-active, relative to the peak responses of *x* for the original structure;
RR*x*	Ratio of RMS value of *x* for a specific solution, passive or semi-active, relative to the RMS value of *x* for the original structure;
P*f*/W, RMS*f*/W	Peak force and RMS force over the structure weight;
Rao	Average ratio of output variables ratios (for RP*x* or RR*x*);
#best	Number of best cases for a specific solution (Passive or Semi-active) when compared with the other ones under study, in terms of Rao; the number of best cases have an associated suffix: 'a'-all the cases are considered; 'b'-the LQR2COO case is not taken in consideration; 'p'-only the passive cases are considered;

Table 4.17 - Structural responses evaluation criteria on the 2DOF model responses analysis.

As already mentioned numerical simulations are performed for tuning the SA controllers. Moreover the identification of the best passive case will be done in the same way. Thus, it will be shown first the results of numerical simulations, showing first the tuning process results, and then the results of the experimental campaign.

4.2 Numerical Simulations and Tuning

This task was carried out using the Matlab/Simulink environment where the simulations in time domain were performed using a fixed time step of 0,5 ms. Since a lot of data resulted from the simulations, even with the evaluation criteria parameters as time domain performances indexes, it will be presented in this section only the data concerning to the average ratio of output variables ratios (Rao). All the data can be found in annex A1.

4.2.1 Original Structure

The identified 2DOF model obtained with the input signal at maximum magnitude was considered in the numerical simulations: m_i=1790 kg, m_s=3950 kg, k_i=38 N/mm, k_s=430 N/mm and α=0,3 s^{-1}. This model was subjected to the described ground motions and the performance indexes were calculated. The results can be found in annex A1, tables A1 and A2.

4.2.2 Passive control

Considering the 2DOF model with the MR damper installed at the base in passive mode described by the model in figure 4.26 with the parameters of the Modified Bouc-Wen model in table 4.15, numerical simulations were performed on the model with different input voltages and taking into account the described input ground motions. Figure 4.29 shows the peak responses evolution with the input voltage on the damper. With the criteria of minimizing the upper mass (m_s) acceleration (peak response), which in this case is around 1 V of input voltage, one found reductions in the relative displacement at the base level with some improvements on top floor accelerations and structure relative displacement. The solutions with the minimum (0 V) and maximum (5 V) input voltages were also taken into account for comparison. Those solutions are described as Pass1, Pass0 and Pass5, and the results in terms of performance indexes are in the annex A1, tables A3 to A19.

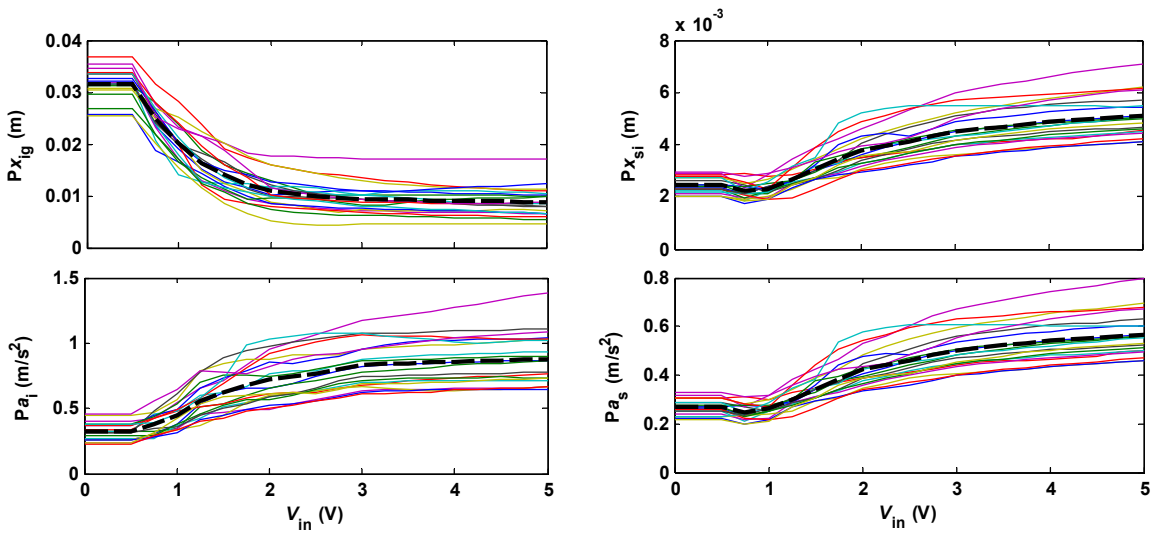

Figure 4.29 - Peak responses evolution of the 2DOF model with the MR damper in passive mode, vs. damper input voltage for all the input ground motions, in numerical simulations.

4.2.3 Semi-active control

The semi-active control algorithms considered here are: two Lyapunov based methods, namely the Decentralized Bang-Bang control – DBB and the Maximum Energy Dissipation algorithm – MED; six force tracking schemes, namely the Modulated Homogeneous Friction – MHF, the Integral control, two Linear Quadratic Regulator controllers and the Model Predictive Control plus a Clipped On-Off algorithm, referred as ICOO, LQRCOO, LQR2COO

and MPCCOO; all the schemes except the LQR2COO use the SDOF model of the structural system to synthesize the controller; for the LQR2COO the 2DOF model was used. Except this last one, the remaining semi-active control strategies have been already described in Chapter 3, section 3.3. The device force is in this case the MR device force and the control variable from the COO algorithm is the input voltage for the device. For the LQR2COO in particular, the desired force for the algorithm is obtained using the LQR strategy with full state feedback, in this case with the relative displacements and velocities to the ground, of both degrees of freedom.

On all the strategies used here the variables used for control are the relative displacements, velocities and accelerations. Both relative displacements and accelerations are measured. The velocities are obtained from the accelerations by integration in order to avoid noisy data.

Taking into account the particularities of the experimental task, the control loop was augmented to filter the noise always present in the variables used for control: i) displacement measurements are passed through a notch filter; ii) acceleration measurements are passed through a notch filter and a high-pass filter. The following loop (figure 4.30) was thus considered in the numerical simulations.

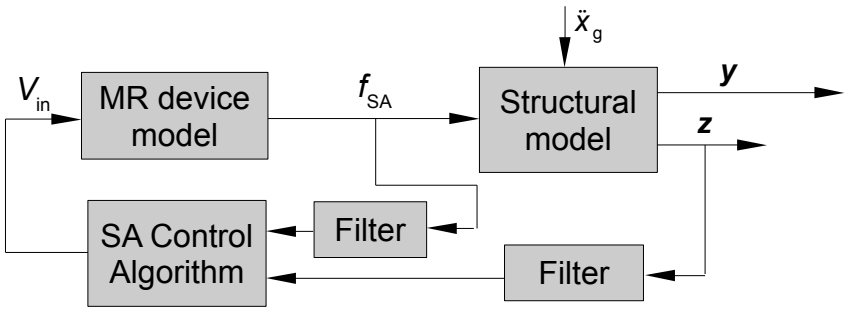

Figure 4.30 - SA control loop used in the numerical simulations.

The notch filter was tuned at 50 Hz to remove that component coming from electrical supply. A high-pass filter at 0,01 Hz was used to filter the low frequency components of the accelerometers (piezoelectric type) measurements that influence the integration process.

Tuning the Semi-Active Controllers

Most of the semi-active controllers used are parameters dependent (gain or weights) that need to be tuned. Numerical simulations were performed using the identified model and the specific semi-active control strategy according to the control loop of figure 4.30. For all the input ground motions the peak responses were identified and the mean peak response curve of the top mass (m_s) was used to identify the parameters. The evolution of the peak responses considering each strategy under study can be found on figures 4.31 to 4.35. Using the minimum of mean peak mass m_s acceleration as criteria, the controllers parameters were identified and the values are presented in table 4.18. These values were both considered in

the numerical and experimental evaluation of the proposed solutions.

strategy	MHF	ICOO	LQRCOO	MPCCOO	LQR2COO
parameters	g (N/m)	g (N/m)	q (kg s)/r (s/kg)	q (kg^{0,5} s)/r (s/kg^{0,5})	q (kg s)/r (s/kg)
value	13777	13777	2x10^7/1	1448/1	1,17x10^7/1

Table 4.18 - Controllers tuning parameters obtained from the numerical simulations and considered also in the experimental implementation.

Figures 4.31 to 4.35 show that with such criteria one can get reductions on the base floor relative displacement, the best reductions on the relative displacements between the two masses and on the top mass (m_s) acceleration, with small impact on the floor mass (m_i) acceleration, or in some cases even with good reductions.

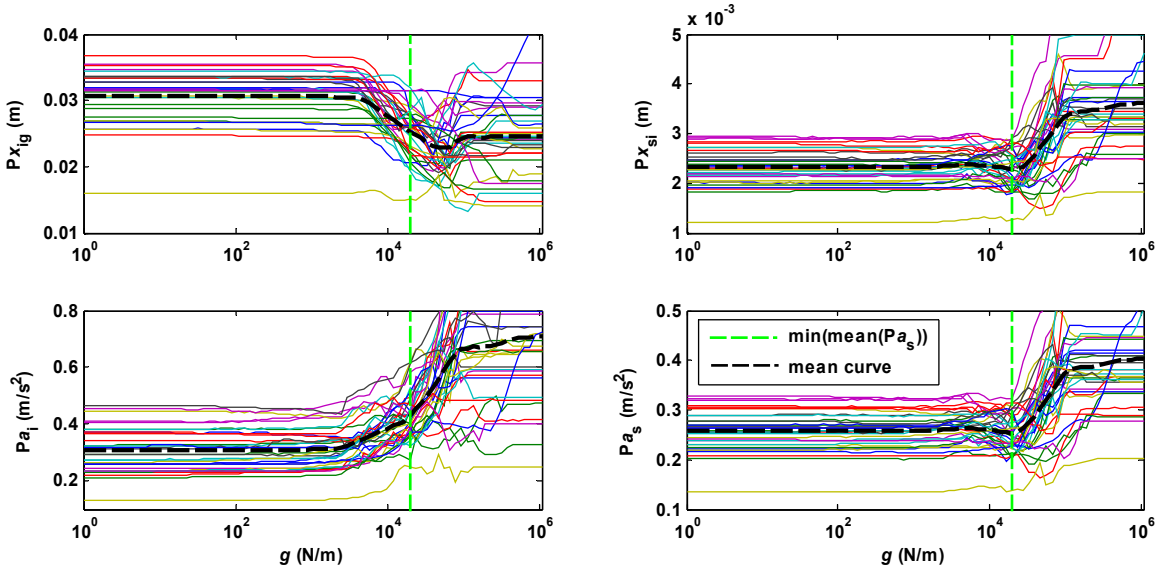

Figure 4.31 - Evolution of peak responses with the controller gain for the 2DOF model with an MR device manipulated by MHF strategy, for all the input ground motions considered.

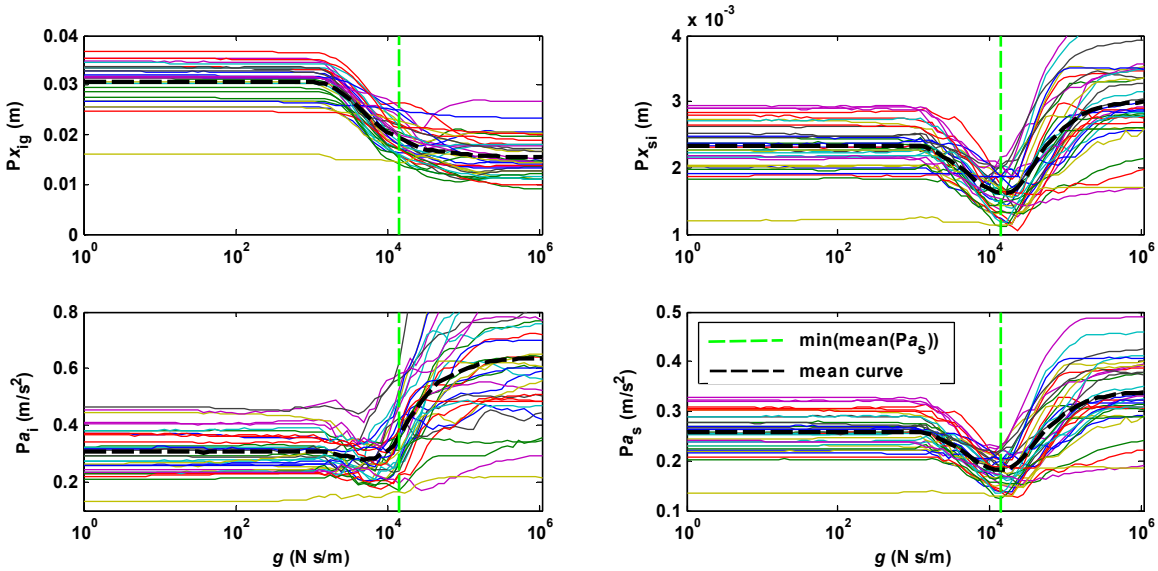

Figure 4.32 - Evolution of peak responses with the controller gain for the 2DOF model with an MR device manipulated by ICOO strategy, for all the input ground motions considered.

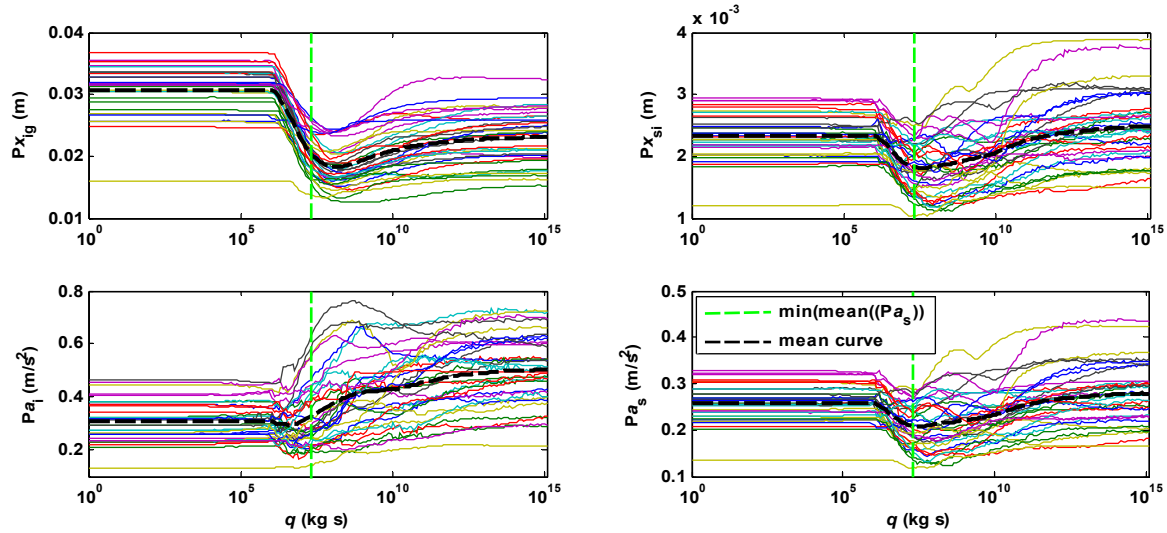

Figure 4.33 - Evolution of peak responses with the controller gain for the 2DOF model with an MR device manipulated by LQRCOO strategy, for all the input ground motions considered.

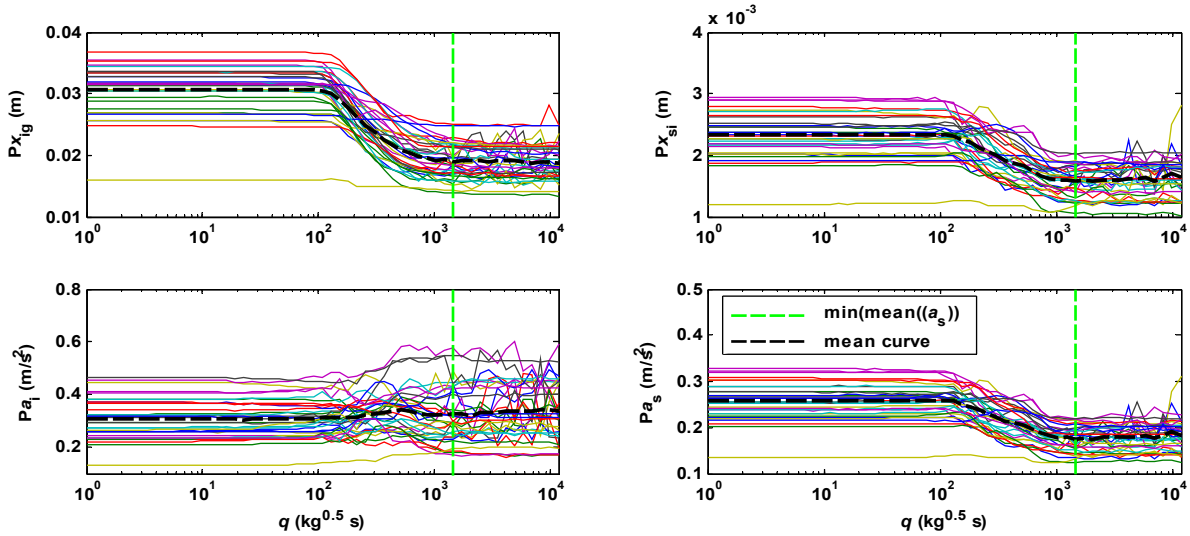

Figure 4.34 - Evolution of peak responses with the controller gain for the 2DOF model with an MR device manipulated by MPCCOO strategy, for all the input ground motions considered.

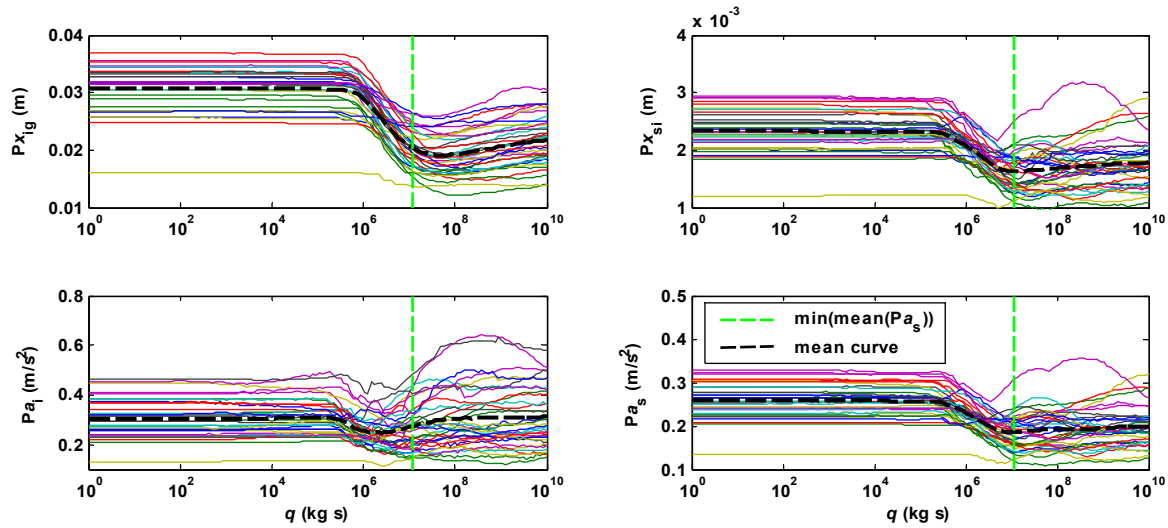

Figure 4.35 - Evolution of peak responses with the controller gain for the 2DOF model with an MR device manipulated by LQR2COO strategy, for all the input ground motions considered.

Notice that MED and DBB strategies does not have any parameter to be tuned and thus were not subjected to this process. The results in terms of performance indexes for the semi-active control can be found in annex A1, tables A3 to A19.

4.2.4 Summary of results in numerical simulations

Tables A3 to A19 show the results for the solutions under study compared with the original structure in terms of the evaluation criteria. Looking to those data it is observed that in general the passive solution with maximum input voltage Pass5, as well as the DBB and MED SA strategies lead to the highest reductions at the base relative displacement but at the expense of increasing the masses relative displacements and accelerations when compared to the original structure ones, as shown by the underlined values in the tables. On the other hand, the bold data on those tables show that in general the other SA strategies, i.e. MHF, ICOO, LQRCOO, MPCCOO and LQR2COO, perform better than the passive Pass1 case, and also better than the original structure one. Only a few cases show an inferior performance than the original structure, but in general better than the passive Pass1. This is observed in both peak and RMS values. In order to compare all the solutions under all input ground motions the average ratio 'Rao' was computed and used as a representative value of each solution performance. The results are also in annex A1 (tables A20 to A22) and presented in this section too, on tables 4.19 to 4.21. With this criteria the same observations can be drawn as can be seen by the underlined and bold data on the tables.

Type 1 - Peak values											
Case	Acc. 1	Acc. 2	Acc. 3	Acc. 4	Acc. 5	Acc. 6	Acc. 7	Acc. 8	Acc. 9	Acc. 10	#best
Pass0	**0,72**	0,75	**0,87**	0,79	0,75	**0,81**	0,96	0,74	0,82	0,83	3p
Pass1	0,75	0,69	0,92	0,77	0,71	0,82	0,85	0,70	0,81	0,77	7p
Pass5	1,48	1,37	1,31	1,43	1,34	1,40	1,60	1,29	1,47	1,42	
DBB	0,99	1,02	1,09	1,09	1,00	1,06	1,13	1,07	1,12	1,06	
MED	1,48	1,36	1,32	1,45	1,33	1,40	1,59	1,30	1,47	1,41	
MHF	0,84	0,83	0,94	0,80	0,74	0,87	1,07	0,77	0,82	0,85	
ICOO	**0,55**	**0,57**	**0,66**	**0,58**	**0,55**	**0,61**	**0,66**	**0,51**	**0,64**	**0,53**	4a/7b
LQRCOO	**0,56**	**0,60**	**0,60**	**0,54**	**0,61**	**0,63**	**0,67**	**0,53**	**0,59**	**0,57**	3b
MPCCOO	**0,68**	**0,64**	**0,85**	**0,68**	**0,61**	**0,71**	0,89	**0,60**	**0,76**	**0,67**	
LQR2COO	**0,47**	**0,63**	**0,59**	**0,48**	**0,55**	**0,63**	**0,60**	**0,48**	**0,52**	**0,53**	8a
Type 1 - RMS values											
Case	Acc. 1	Acc. 2	Acc. 3	Acc. 4	Acc. 5	Acc. 6	Acc. 7	Acc. 8	Acc. 9	Acc. 10	#best
Pass0	0,75	0,84	0,87	0,79	**0,90**	0,78	0,82	0,79	0,84	**0,85**	2p
Pass1	0,67	0,72	0,82	0,73	0,90	0,74	0,77	0,72	0,75	0,91	9p
Pass5	1,17	1,25	1,44	1,30	1,68	1,32	1,34	1,32	1,35	1,77	
DBB	0,80	0,85	0,95	0,90	1,13	0,88	0,91	0,89	0,90	1,15	
MED	1,18	1,26	1,44	1,31	1,68	1,33	1,35	1,33	1,36	1,78	
MHF	0,69	0,75	**0,78**	0,75	**0,89**	**0,71**	**0,76**	0,74	0,80	**0,87**	
ICOO	**0,50**	**0,53**	**0,62**	**0,54**	**0,66**	**0,54**	**0,56**	**0,54**	**0,57**	**0,64**	10a/10b
LQRCOO	**0,53**	**0,57**	**0,63**	**0,57**	**0,70**	**0,58**	**0,61**	**0,57**	**0,59**	**0,68**	
MPCCOO	**0,57**	**0,62**	**0,70**	**0,64**	**0,75**	**0,62**	**0,66**	**0,63**	**0,67**	**0,75**	
LQR2COO	**0,51**	**0,54**	**0,62**	**0,55**	**0,67**	**0,55**	**0,58**	**0,54**	**0,57**	**0,65**	3a

Table 4.19 - Summary of average ratios (Rao) and number of best cases (#best) under type 1 seismic actions, in numerical simulations.

Type 2 - Peak values											
Case	Acc. 1	Acc. 2	Acc. 3	Acc. 4	Acc. 5	Acc. 6	Acc. 7	Acc. 8	Acc. 9	Acc. 10	#best
Pass0	**0,81**	**0,83**	**0,67**	**0,76**	0,74	**0,76**	0,88	0,73	0,80	0,89	5p
Pass1	0,88	0,85	0,68	0,90	0,72	0,77	0,84	0,69	0,83	0,97	5p
Pass5	1,66	1,92	1,21	1,70	1,42	1,26	1,69	1,27	1,41	1,85	
DBB	1,24	1,12	0,86	1,26	1,10	0,87	1,05	1,05	1,05	1,26	
MED	1,67	1,91	1,21	1,71	1,44	1,26	1,69	1,27	1,42	1,85	
MHF	**0,80**	**0,76**	0,76	0,90	**0,72**	0,80	0,91	**0,69**	0,78	**0,87**	
ICOO	**0,81**	**0,66**	**0,52**	**0,77**	**0,59**	**0,51**	**0,68**	**0,55**	**0,69**	**0,73**	1a/10b
LQRCOO	**0,83**	**0,71**	**0,64**	**0,86**	**0,71**	**0,62**	**0,71**	**0,61**	**0,73**	**0,78**	
MPCCOO	**0,83**	**0,68**	**0,58**	**0,86**	**0,64**	**0,63**	**0,74**	**0,60**	**0,73**	**0,76**	
LQR2COO	**0,77**	**0,57**	**0,52**	**0,67**	**0,56**	**0,47**	**0,64**	**0,52**	**0,59**	**0,68**	10a
Type 2 - RMS values											
Case	Acc. 1	Acc. 2	Acc. 3	Acc. 4	Acc. 5	Acc. 6	Acc. 7	Acc. 8	Acc. 9	Acc. 10	#best
Pass0	0,84	**0,96**	0,87	**0,90**	0,88	**0,73**	**0,94**	0,83	0,98	**0,87**	5p
Pass1	0,81	0,97	0,81	0,92	0,80	0,79	1,06	0,74	0,96	0,99	5p
Pass5	1,55	1,79	1,39	1,62	1,55	1,48	2,07	1,41	1,53	2,00	
DBB	1,04	1,10	0,92	1,06	1,03	0,91	1,27	0,93	1,02	1,32	
MED	1,55	1,80	1,39	1,63	1,55	1,49	2,08	1,41	1,54	2,01	
MHF	**0,75**	**0,88**	0,84	**0,85**	**0,73**	**0,68**	**0,99**	0,75	**0,96**	**0,85**	
ICOO	**0,62**	**0,70**	**0,59**	**0,69**	**0,57**	**0,54**	**0,76**	**0,59**	**0,65**	**0,68**	5a/10b
LQRCOO	**0,73**	**0,82**	**0,73**	**0,79**	**0,70**	**0,66**	**0,87**	**0,67**	**0,80**	**0,81**	
MPCCOO	**0,71**	**0,80**	**0,73**	**0,77**	**0,65**	**0,66**	**0,86**	**0,67**	**0,85**	**0,75**	
LQR2COO	**0,63**	**0,69**	**0,63**	**0,68**	**0,61**	**0,52**	**0,79**	**0,58**	**0,63**	**0,72**	5a

Table 4.20 - Summary of average ratios (Rao) and number of best cases (#best) under type 2 seismic actions, in numerical simulations.

Peak val.	El Centro		Newhall		Rinaldi		Sylmar		Erzikan		Jiji		Kobe		
Case	FN	FP	FN	FP	FN	FP	FN	FP	NS	EW	NS	EW	NS	EW	#best
Pass0	0,88	0,93	**1,09**	**0,80**	**1,02**	0,79	**0,87**	0,80	0,87	**0,86**	0,80	**0,68**	**0,86**	**0,93**	8p
Pass1	0,82	0,96	1,23	0,80	1,27	0,59	0,91	0,75	0,82	0,93	0,71	0,75	1,04	1,02	6p
Pass5	1,59	1,84	2,48	1,43	2,50	1,28	1,17	1,58	1,22	1,48	0,78	1,02	2,32	2,00	
DBB	1,11	1,00	1,87	1,28	1,93	0,92	**0,87**	1,01	0,95	1,06	**0,66**	0,94	1,46	1,37	
MED	1,59	1,85	2,48	1,44	2,50	1,28	1,17	1,57	1,21	1,47	0,79	1,02	2,32	2,01	
MHF	0,95	1,20	1,37	0,83	1,34	0,82	0,92	0,85	0,97	1,05	0,82	0,88	**1,01**	**0,99**	
ICOO	**0,80**	**0,85**	**1,00**	**0,71**	**1,05**	**0,53**	**0,59**	**0,55**	**0,66**	**0,65**	**0,60**	**0,70**	**0,65**	**0,77**	3a/8b
LQRCOO	**0,67**	**0,81**	**0,91**	0,83	**1,01**	**0,53**	**0,72**	**0,57**	**0,65**	**0,69**	**0,67**	**0,64**	**0,89**	**0,82**	2a/7b
MPCCOO	0,87	1,07	**1,13**	**0,78**	**1,16**	**0,71**	**0,77**	**0,71**	**0,78**	**0,78**	0,75	**0,72**	**0,85**	**0,79**	
LQR2COO	**0,63**	**0,76**	**0,97**	**0,69**	**0,94**	**0,45**	**0,55**	**0,50**	**0,58**	**0,68**	**0,62**	**0,64**	**0,75**	**0,88**	9a
RMS val.	El Centro		Newhall		Rinaldi		Sylmar		Erzikan		Jiji		Kobe		
Case	FN	FP	FN	FP	FN	FP	FN	FP	NS	EW	NS	EW	NS	EW	#best
Pass0	0,85	0,92	**1,13**	0,86	1,00	0,81	0,87	0,83	0,87	0,76	0,69	0,77	**1,03**	**1,00**	3p
Pass1	0,84	0,91	1,28	0,68	0,98	0,58	0,61	0,62	0,64	0,63	0,44	0,67	1,22	1,01	11p/1b
Pass5	1,61	1,28	2,08	1,05	1,74	0,88	0,73	0,97	0,67	0,95	**0,41**	0,86	2,30	1,86	
DBB	1,13	0,94	1,51	0,77	1,12	**0,58**	**0,53**	**0,58**	**0,55**	0,64	**0,42**	0,95	1,47	1,33	
MED	1,61	1,29	2,09	1,06	1,74	0,89	0,73	0,98	0,67	0,96	**0,41**	0,86	2,31	1,87	
MHF	**0,79**	**0,90**	1,33	0,74	**0,95**	0,63	**0,57**	0,70	0,68	0,75	0,51	0,85	**1,08**	**0,98**	
ICOO	**0,64**	**0,67**	**0,98**	**0,53**	**0,82**	**0,46**	**0,44**	**0,46**	**0,50**	**0,51**	**0,38**	0,73	**0,84**	**0,76**	10a/13b
LQRCOO	**0,66**	**0,69**	**1,02**	**0,64**	**0,86**	**0,52**	**0,52**	**0,50**	**0,55**	**0,56**	**0,43**	0,68	**1,00**	**0,88**	
MPCCOO	**0,76**	**0,82**	**1,15**	**0,64**	**0,97**	**0,55**	**0,55**	**0,56**	**0,63**	0,65	**0,45**	0,76	**0,91**	**0,87**	
LQR2COO	**0,62**	**0,66**	**1,00**	**0,53**	**0,81**	**0,48**	**0,46**	**0,48**	**0,53**	**0,53**	**0,40**	**0,67**	**0,93**	**0,83**	5a

Table 4.21 - Summary of average ratios (Rao) and number of best cases (#best) under earthquake records, in numerical simulations.

From the average ratio 'Rao' the number of best cases for each solution was identified in each type of input ground motion. Table 4.22 (also table A23 in annex A1) summarizes the

results.

Peak values					
Case	Type 1	Type 2	Type 1&2	Earthquakes	All
Pass0	3p	5p	8p	8p	16p
Pass1	7p	5p	12p	6p	18p
Pass5					
DBB					
MED					
MHF					
ICOO	4a/7b	1a/10b	5a/17b	3a/8b	8a/25b
LQRCOO	3b		3b	2a/7b	2a/10b
MPCCOO					
LQR2COO	8a	10a	18a	9a	27a
RMS values					
Case	Type 1	Type 2	Type 1&2	Earthquakes	All
Pass0	2p	5p	7p	3p	10p
Pass1	9p	5p	14p	11p/1b	25p/1b
Pass5					
DBB					
MED					
MHF					
ICOO	10a/10b	5a/10b	15a/20b	10a/13b	25a/33b
LQRCOO					
MPCCOO					
LQR2COO	3a	5a	8a	5a	13a

Table 4.22 - Number of best cases (#best) for each solution, in numerical simulations.

From table 4.22 it is observed that taking into account only the passive cases, Pass1 has the major number of best cases (numbers ending in 'p'). Considering all the solutions, the results show that LQR2COO has the major number of best cases, in terms of peak values, being ICOO the following one (numbers ending in 'a'). However, looking in terms of RMS values ICOO has the major number of best cases. This result is even more evident if the LQR2COO strategy is not considered in the comparison (numbers ending in 'b'), which is the case when only collocated control is considered for comparison. The superiority of LQR2COO strategy over the ICOO one is achieved due to the better performance of the first one on the masses relative displacement and accelerations, and namely the base acceleration, although both have in general similar performance in terms of base relative displacements (see tables A3 to A19). Summing up, ICOO is better than the best passive (Pass1) and consequently better than the original structure, but performing slightly inferior than LQR2COO.

4.3 Experimental Trial

This task was carried out using the set-up already described in section 4.1 and also depicted in figure 4.1. As already mentioned a sampling period of 0,2 ms was used in the dSPACE system and thus both the control system and acquisition process worked at this rate. Since

the physical phenomenon under study has the highest frequency around 3 Hz, all the acquired data for post-processing was passed through a low-pass filter at 10 Hz and downsampled online with a factor of 25, resulting in a sampling period of 5 ms, which reduces considerably the amount of data acquired. This data was then used to determine the performance indexes described. As already mentioned in the numerical simulations section, a lot of data resulted, and thus only the data concerning to the average ratio of output variables ratios (Rao) will be presented here. All the other data can be found in annex A2.

4.3.1 Original Structure

The experimental 2DOF mechanical model was subjected to the scaled input ground motions and the resulting time responses were used to evaluate the performance indexes. The results can be found in annex A2, tables A24 and A25.

4.3.2 Passive control

The 2DOF model with the MR damper installed at the base was also tested under different input voltages for the several input ground motions considered. Figure 4.36 shows the ratios of peak responses evolution with the input voltage on the damper.

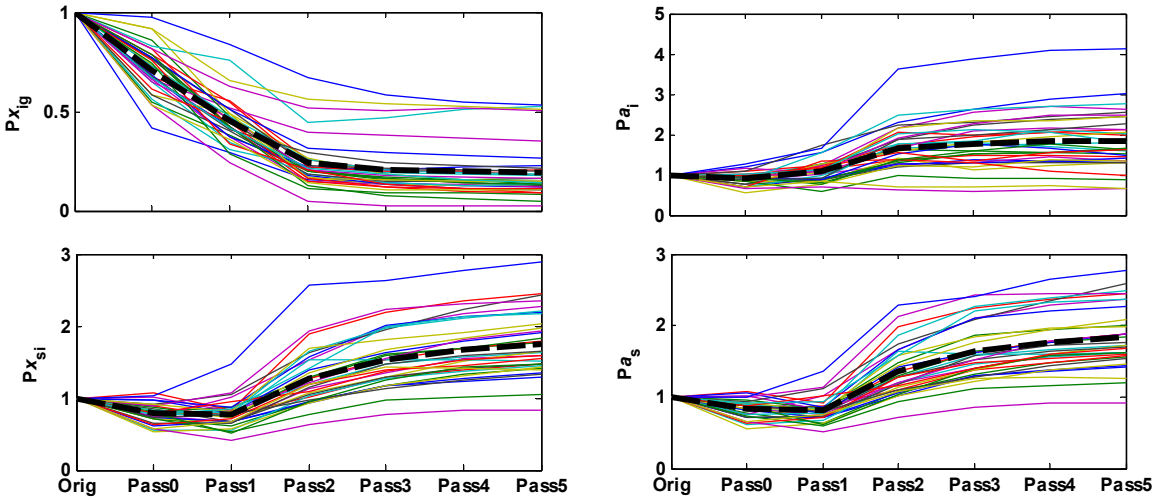

Figure 4.36 - Peak responses evolution of the 2DOF model with the MR damper in passive mode, vs. damper input voltage for all the input ground motions, in experimental trial.

A similar trend to the one obtained in the numerical simulations (figure 4.29) is observed. Moreover, with the criteria of minimizing the top floor m_s acceleration (peak response), the input voltage around 1 V is also identified.

The solutions with 0 V, 1 V and 5 V (Pass0, Pass1 and Pass5 respectively) were considered for comparison and the results in terms of performance indexes can be found in annex A2, tables A26 to A42.

A comparison of the passive cases in terms of FRFs is presented in figure 4.37. The FRFs were obtained from the collected time responses of the system using all the artificial accelerograms (10 type 1 & 10 type 2) as inputs. It is observed that as the input voltage

increases the resonance peaks are reduced, the base relative displacement is reduced, but on the other responses the magnitude is increased on the frequencies far from the resonance. It is also visible that above 2 V of input voltage the FRFs magnitude are highly dampened and those FRFs show almost similar responses.

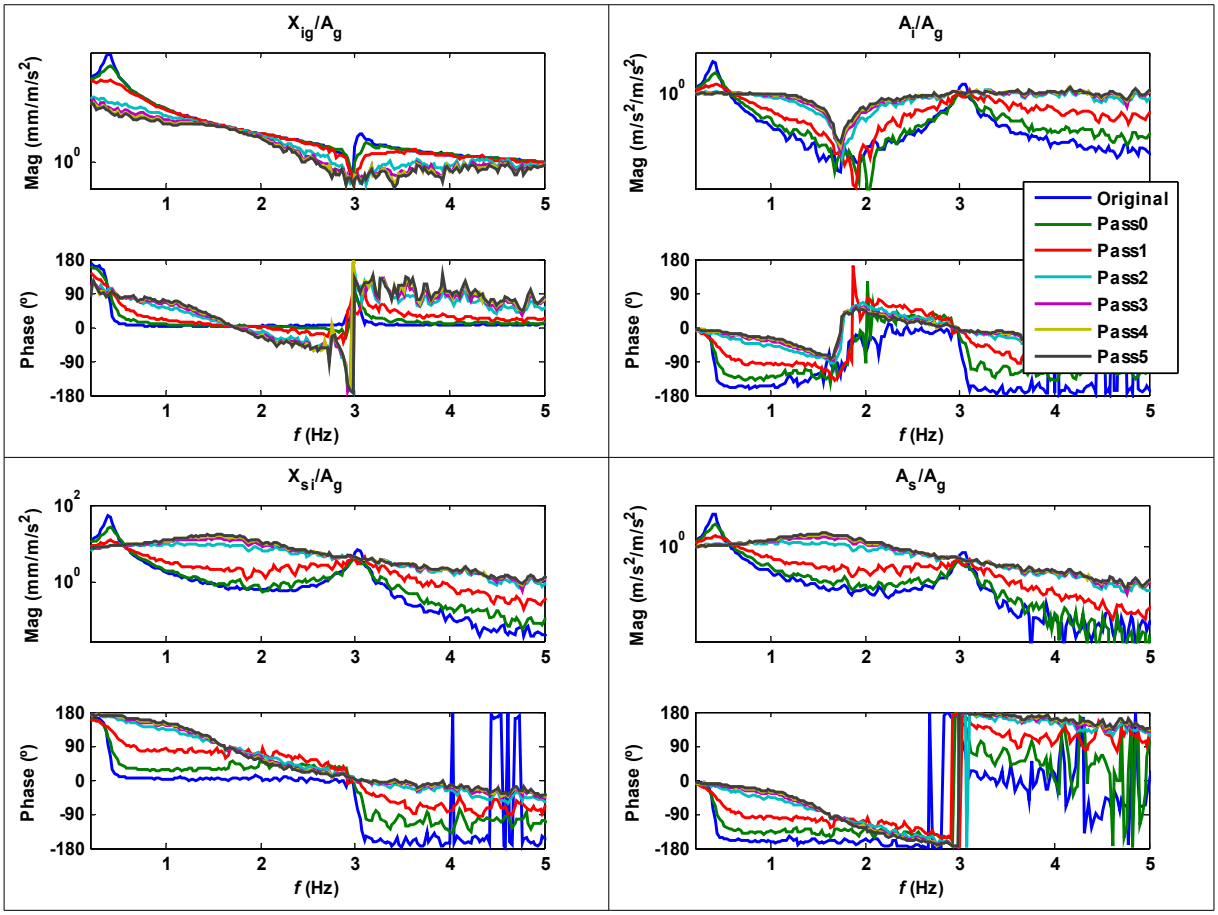

Figure 4.37 - Comparison between the experimental FRFs for the original structure and passive solutions, obtained using the artificial accelerograms as input.

4.3.3 Semi-active control

The semi-active control strategies under study, DBB, MED, MHF, ICOO, LQRCOO, MPCCOO and LQR2COO were implemented in a Simulink project with the associated filters and variables reconstruction (namely velocities) according to the control loop (figure 4.30) as described in the numerical simulations section of this chapter (section 4.2.3). Each project was compiled and a real time application was created for running in the dSPACE system. The identified tuned parameters presented in table 4.18 were used in the experimental trials. From the measured time data the performance indexes were calculated and the results are presented in annex A2, tables A26 to A42.

In terms of FRFs, figure 4.38 shows a comparison between the experimental FRFs of the original structural system with the SA solutions. It is observed that all the solutions reduce the relative displacement at the base being the DBB and MED cases the ones that reduce more

that response. On the other responses it is observed that the resonance peaks are dampened with all solutions. With DBB and MED case it is observed the major response increase in the responses away from the resonances, showing similarities with the passive case with higher input voltages. The other SA cases show in general similar evolutions with frequency but with slightly differences in the responses.

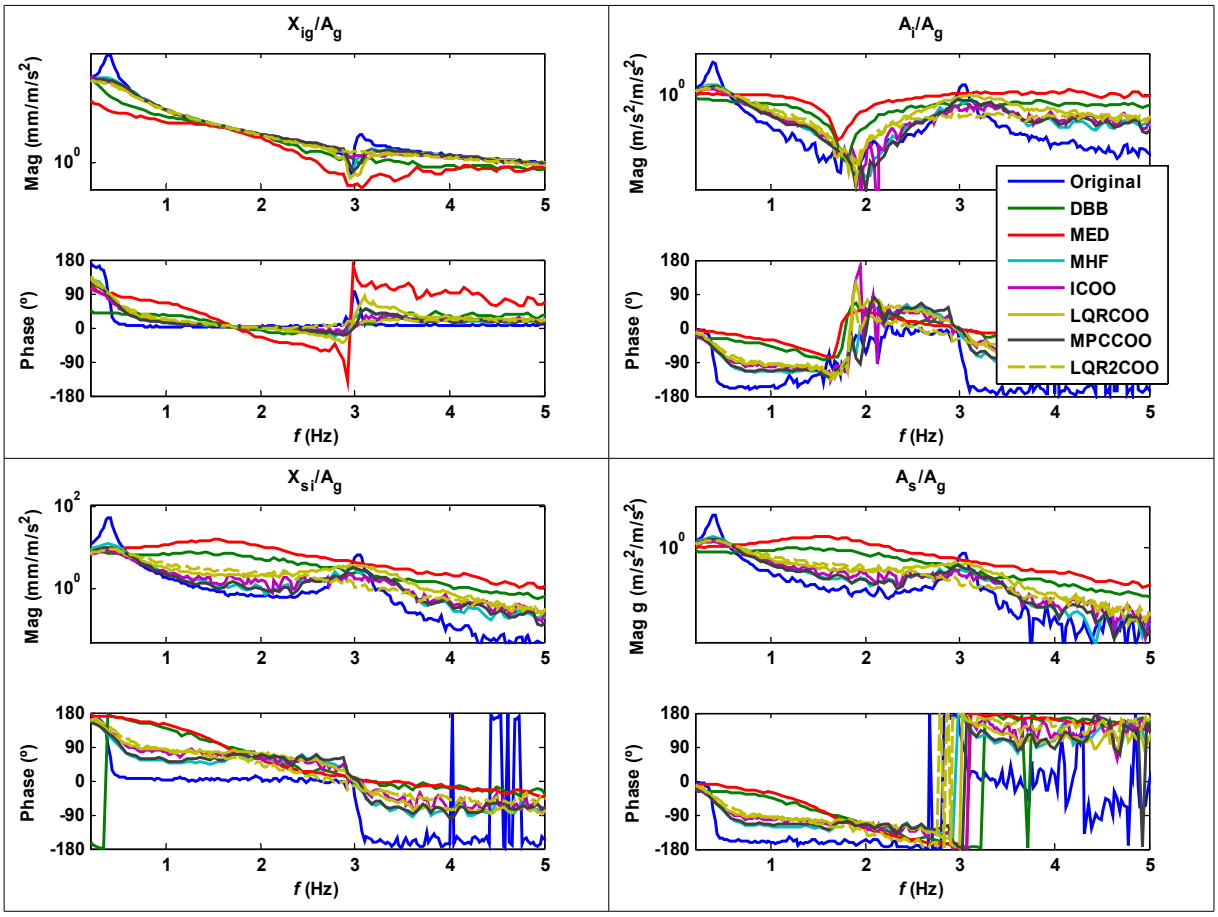

Figure 4.38 - Comparison between the experimental FRFs for the original structure and the SA solutions, obtained using the artificial accelerograms as input.

4.3.4 Summary of results in experimental trials

Tables A26 to A42 present the results for the solutions under study compared with the original case in terms of the evaluation criteria. As in the numerical simulations, similar achievements are reached in the experimental trials. In general: Pass5 as well as the DBB and MED SA strategies lead to the higher reductions at the base relative displacement but with highest increase on the masses relative displacements and accelerations; MHF, ICOO, LQRCOO, MPCCOO and LQR2COO, perform better than the passive Pass1 case, and also better than the original structure one; the same achievements are verified in terms of the average ratio 'Rao' – see tables 4.23 to 4.25 (or the annex A2, tables A43 to A45).

The number of best cases is summarized in table 4.26 (and also in table A46, annex A2).

Type 1 - Peak values											
Case	Acc. 1	Acc. 2	Acc. 3	Acc. 4	Acc. 5	Acc. 6	Acc. 7	Acc. 8	Acc. 9	Acc. 10	#best
Pass0	**0,62**	0,74	**0,81**	**0,78**	0,78	0,78	0,83	0,77	0,83	0,92	3p
Pass1	0,64	0,60	0,83	0,81	0,67	0,66	0,72	0,65	0,82	0,79	7p
Pass5	1,03	1,16	1,17	1,28	1,16	1,20	1,15	1,01	1,35	1,44	
DBB	0,79	0,88	0,95	0,93	0,92	0,91	0,96	0,79	1,15	1,21	
MED	0,99	1,07	1,13	1,25	1,12	1,08	1,16	0,94	1,25	1,40	
MHF	**0,64**	0,62	0,96	**0,69**	0,79	0,79	**0,71**	**0,59**	0,87	0,87	
ICOO	**0,47**	**0,50**	**0,64**	**0,50**	**0,52**	**0,55**	**0,52**	**0,45**	**0,57**	**0,57**	1a/6b
LQRCOO	**0,42**	**0,50**	**0,56**	**0,56**	**0,56**	**0,51**	**0,49**	**0,47**	**0,63**	**0,63**	5b
MPCCOO	**0,60**	**0,60**	**0,77**	**0,62**	**0,62**	**0,76**	**0,65**	**0,53**	**0,77**	**0,75**	
LQR2COO	**0,41**	**0,49**	**0,55**	**0,53**	**0,48**	**0,46**	**0,46**	**0,43**	**0,52**	**0,53**	9a
Type 1 - RMS values											
Case	Acc. 1	Acc. 2	Acc. 3	Acc. 4	Acc. 5	Acc. 6	Acc. 7	Acc. 8	Acc. 9	Acc. 10	#best
Pass0	0,52	0,71	0,81	0,59	0,82	0,65	0,68	0,73	0,77	**0,97**	1p
Pass1	0,46	0,57	0,72	0,58	0,81	0,60	0,62	0,63	0,67	0,98	9p
Pass5	0,87	1,02	1,27	1,05	1,48	1,10	1,08	1,13	1,25	1,95	
DBB	0,55	0,73	0,87	0,73	1,00	0,76	0,76	0,80	0,83	1,38	
MED	0,73	0,97	1,18	0,95	1,36	1,04	1,04	1,09	1,10	1,87	
MHF	**0,44**	0,58	**0,71**	**0,55**	**0,80**	0,61	**0,60**	**0,59**	**0,64**	**0,96**	
ICOO	**0,34**	**0,41**	**0,58**	**0,45**	**0,66**	**0,50**	**0,48**	**0,50**	**0,54**	**0,78**	7a/7b
LQRCOO	**0,33**	**0,47**	**0,58**	**0,47**	**0,64**	**0,52**	**0,47**	**0,51**	**0,54**	**0,80**	5a/5b
MPCCOO	**0,39**	**0,48**	**0,66**	**0,53**	**0,70**	**0,58**	**0,54**	**0,56**	**0,62**	**0,90**	
LQR2COO	**0,37**	**0,45**	**0,59**	**0,48**	**0,67**	**0,51**	**0,50**	**0,51**	**0,55**	**0,82**	

Table 4.23 - Summary of average ratios (Rao) and number of best cases (#best) under type 1 seismic actions, in experimental trials.

Type 2 - Peak values											
Case	Acc. 1	Acc. 2	Acc. 3	Acc. 4	Acc. 5	Acc. 6	Acc. 7	Acc. 8	Acc. 9	Acc. 10	#best
Pass0	**0,63**	**0,76**	**0,56**	**0,68**	0,95	0,90	0,98	0,78	0,96	0,86	4p
Pass1	0,66	0,94	0,60	0,75	0,86	0,72	0,89	0,76	0,80	0,83	6p
Pass5	1,25	1,91	1,10	1,49	1,76	1,39	1,81	1,33	1,53	1,56	
DBB	0,90	1,08	0,76	1,09	1,29	0,94	1,10	1,04	0,98	1,03	
MED	1,30	1,79	1,06	1,41	1,69	1,34	1,73	1,28	1,32	1,47	
MHF	**0,61**	**0,84**	0,64	**0,75**	0,92	**0,67**	**0,85**	**0,68**	0,85	0,84	
ICOO	**0,57**	**0,67**	**0,48**	**0,61**	**0,72**	**0,57**	**0,72**	**0,55**	**0,70**	**0,65**	3a/9b
LQRCOO	**0,65**	**0,78**	**0,56**	**0,66**	**0,73**	**0,65**	**0,72**	**0,63**	**0,78**	**0,71**	1a/1b
MPCCOO	**0,51**	**0,75**	**0,53**	**0,68**	0,87	**0,64**	**0,84**	**0,61**	**0,78**	**0,76**	1b
LQR2COO	**0,50**	**0,61**	**0,46**	**0,63**	**0,63**	**0,55**	**0,72**	**0,59**	**0,67**	**0,60**	8a
Type 2 - RMS values											
Case	Acc. 1	Acc. 2	Acc. 3	Acc. 4	Acc. 5	Acc. 6	Acc. 7	Acc. 8	Acc. 9	Acc. 10	#best
Pass0	0,67	**0,82**	0,66	0,72	0,83	**0,82**	**0,89**	0,76	0,96	**0,92**	4p
Pass1	0,64	0,86	0,62	0,67	0,75	0,88	0,96	0,69	0,80	0,97	6p
Pass5	1,33	1,56	1,16	1,38	1,52	1,76	2,07	1,34	1,53	2,12	
DBB	0,89	0,97	0,73	0,86	1,04	1,05	1,23	0,86	0,98	1,32	
MED	1,18	1,47	1,06	1,32	1,42	1,60	1,82	1,24	1,32	1,86	
MHF	**0,57**	**0,78**	0,66	**0,66**	**0,63**	**0,66**	**0,85**	**0,62**	0,85	**0,81**	
ICOO	**0,53**	**0,64**	**0,54**	**0,55**	**0,56**	**0,65**	**0,75**	**0,53**	**0,70**	**0,76**	6a/9b
LQRCOO	**0,61**	**0,74**	**0,58**	**0,61**	**0,63**	**0,75**	**0,83**	**0,60**	**0,78**	**0,78**	
MPCCOO	**0,54**	**0,68**	**0,57**	**0,54**	**0,59**	**0,67**	**0,80**	**0,55**	**0,78**	**0,82**	1b
LQR2COO	**0,50**	**0,65**	**0,52**	**0,50**	**0,57**	**0,66**	**0,75**	**0,54**	**0,67**	**0,83**	5a

Table 4.24 - Summary of average ratios (Rao) and number of best cases (#best) under type 2 seismic actions, in experimental trials.

Peak val.	El Centro		Newhall		Rinaldi		Sylmar		Erzikan		Jiji		Kobe		
Case	FN	FP	FN	FP	FN	FP	FN	FP	NS	EW	NS	EW	NS	EW	#best
Pass0	**0,92**	0,94	0,90	0,79	**1,07**	0,84	**0,81**	0,85	0,77	**0,68**	0,61	**0,62**	**0,86**	**0,92**	7p
Pass1	0,97	0,77	0,84	0,73	1,39	0,55	0,88	0,82	0,54	0,71	0,45	0,64	1,02	0,96	7p
Pass5	1,94	1,55	1,74	1,34	2,58	1,20	1,25	1,63	0,79	1,06	0,61	0,85	2,00	1,95	
DBB	1,22	0,99	1,35	1,07	1,76	0,86	**0,88**	1,12	0,74	0,94	**0,41**	0,84	1,52	1,23	
MED	1,76	1,36	1,69	1,29	2,59	1,07	1,15	1,51	0,79	1,03	0,55	0,85	1,96	1,92	
MHF	0,99	1,02	0,99	**0,70**	**1,29**	0,62	**0,79**	**0,82**	0,68	**0,67**	0,50	**0,61**	**0,93**	1,11	
ICOO	**0,80**	**0,68**	**0,73**	0,75	**1,05**	**0,52**	**0,54**	**0,65**	**0,52**	**0,54**	**0,41**	**0,60**	**0,65**	**0,69**	2a/4b
LQRCOO	**0,74**	**0,64**	**0,61**	**0,72**	**0,92**	**0,53**	**0,71**	**0,55**	**0,48**	**0,52**	**0,40**	**0,52**	**0,78**	**0,80**	3a/9b
MPCCOO	**0,92**	0,83	**0,82**	**0,67**	**1,17**	**0,54**	**0,79**	**0,69**	0,56	**0,61**	0,48	**0,61**	**0,77**	**0,91**	1b
LQR2COO	**0,66**	**0,64**	**0,62**	**0,64**	**0,92**	**0,45**	**0,50**	**0,56**	**0,42**	**0,44**	**0,34**	**0,50**	**0,74**	**0,80**	10a
RMS val.	El Centro		Newhall		Rinaldi		Sylmar		Erzikan		Jiji		Kobe		
Case	FN	FP	FN	FP	FN	FP	FN	FP	NS	EW	NS	EW	NS	EW	#best
Pass0	**0,81**	0,72	0,84	0,81	0,89	0,68	0,56	0,64	0,66	0,68	0,42	0,66	**0,87**	**0,89**	3p
Pass1	0,83	0,64	0,73	0,52	0,81	0,41	0,39	0,48	0,38	0,56	0,23	0,59	0,95	0,91	11p
Pass5	1,58	1,04	1,26	0,88	1,49	0,66	0,47	0,78	**0,38**	0,95	0,24	0,72	1,80	1,66	
DBB	1,08	0,72	0,90	0,63	0,88	0,52	**0,38**	**0,48**	**0,38**	0,65	**0,22**	0,76	1,21	1,09	
MED	1,42	0,95	1,16	0,84	1,43	0,61	0,45	0,72	**0,35**	0,92	**0,23**	0,68	1,68	1,58	
MHF	**0,76**	**0,62**	0,82	**0,51**	**0,75**	0,45	0,41	0,52	0,42	0,58	0,28	0,61	**0,82**	**0,91**	
ICOO	**0,65**	**0,53**	**0,59**	**0,42**	**0,71**	**0,36**	**0,28**	**0,38**	**0,33**	**0,46**	**0,22**	0,63	**0,70**	**0,65**	11a/13b
LQRCOO	**0,68**	**0,53**	**0,66**	**0,48**	**0,72**	**0,40**	**0,30**	**0,41**	**0,34**	**0,51**	0,24	**0,54**	**0,84**	**0,79**	2a/2b
MPCCOO	**0,78**	**0,60**	0,74	**0,47**	**0,66**	**0,41**	**0,37**	**0,48**	0,42	**0,53**	0,27	**0,59**	**0,78**	**0,83**	
LQR2COO	**0,71**	**0,55**	**0,63**	**0,42**	**0,70**	**0,40**	**0,28**	**0,46**	**0,34**	**0,45**	**0,22**	**0,55**	**0,78**	**0,75**	5a

Table 4.25 - Summary of average ratios (Rao) and number of best cases (#best) under earthquake records, in experimental trials.

Peak values					
Case	Type 1	Type 2	Type 1&2	Earthquakes	All
Pass0	3p	4p	7p	7p	14p
Pass1	7p	6p	13p	7p	20p
Pass5					
DBB					
MED					
MHF					
ICOO	1a/6b	3a/9b	4a/15b	2a/4b	6a/19b
LQRCOO	5b	1a/1b	1a/6b	3a/9b	4a/15b
MPCCOO		1b	1b	1b	2b
LQR2COO	9a	8a	17a	10a	27a
RMS values					
Case	Type 1	Type 2	Type 1&2	Earthquakes	All
Pass0	1p	4p	5p	3p	8p
Pass1	9p	6p	15p	11p	26p
Pass5					
DBB					
MED					
MHF					
ICOO	7a/7b	6a/9b	13a/16b	11a/13b	24a/29b
LQRCOO	5a/5b		5a/5b	2a/2b	7a/7b
MPCCOO		1b	1b		1b
LQR2COO		5a	5a	5a	10a

Table 4.26 - Number of best cases (#best) for each solution, in experimental trials.

As in the numerical simulations: Pass1 has the major number of best cases when only the

passive cases are analysed (numbers ending in 'p'); LQR2COO has the major number of best cases in terms of peak values, being ICOO the following one (numbers ending in 'a'); ICOO has the major number of best cases in terms of RMS values; ICOO has also the major number of best cases in terms of peak values and RMS values if only the collocated control strategies are considered (numbers ending in 'b').

An example of the time responses for one input ground motion comparing the original structure case, the passive one and the best SA strategies is presented in figure 4.39. The superiority of the SA strategies over the Pass1 case and consequently better than the original structure is evident shown in this example.

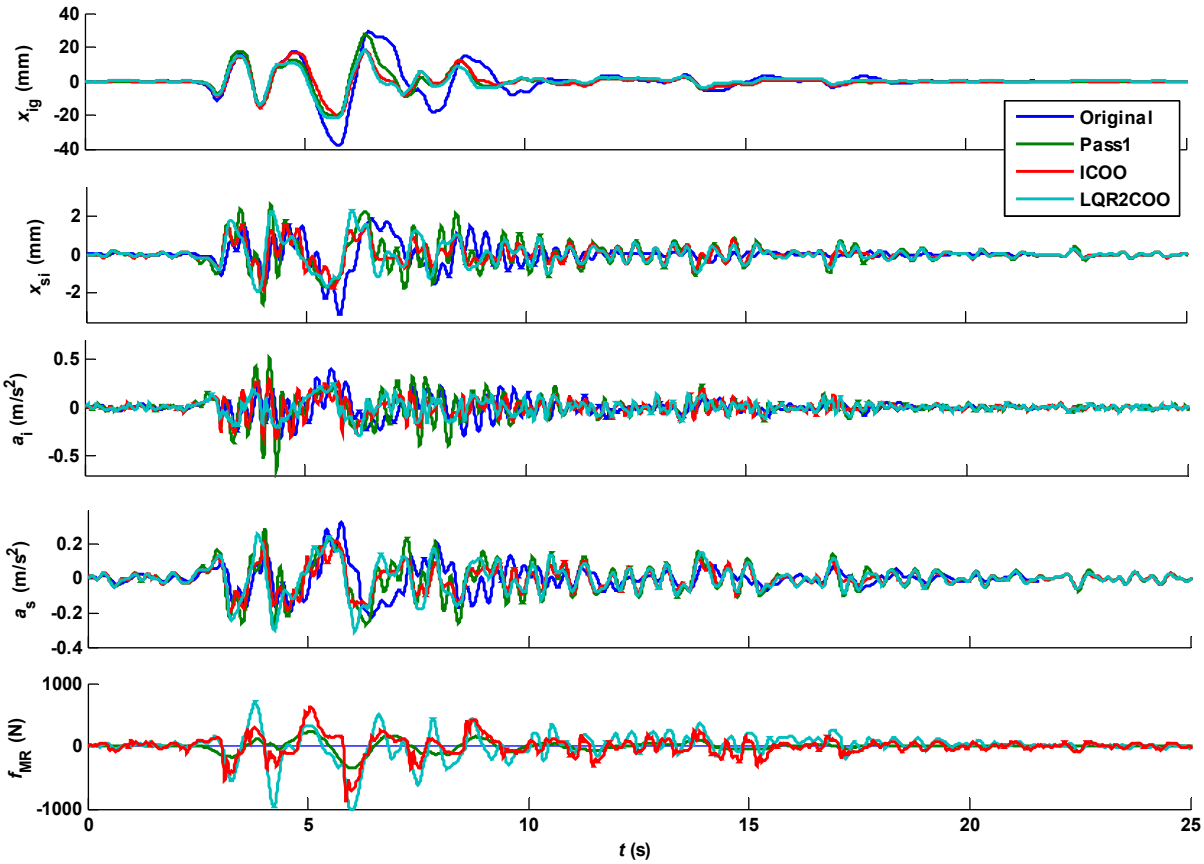

Figure 4.39 - Time histories (relative displacements, accelerations and force), of the 2DOF model in the original, Pass1, ICOO and LQR2COO cases, subjected to Kobe (NS) earthquake record, during the experimental test.

4.4 Comparison of Numerical and Experimental Results

4.4.1 Time domain

A qualitative comparison of the results obtained from both numerical and experimental results, in terms of the number of best cases, resulting from tables 4.22 and 4.26, is summarized in table 4.27. It is observed in general a similar trend in both numerical and experimental results. However, a slightly difference is observed in ICOO and LQRCOO solutions under different type of ground motions, for both numerical and experimental trials.

This result comes from the fact that with LQRCOO are found more best cases in the experimental trial than in the numerical simulations. This is more clear in terms of earthquake ground motions and in peak values. Thus, within this analysis it is found in general a good agreement between both numerical and experimental results, which indicates that the numerical model achieves the trends found with the physical model.

Peak values						
Case	Type 1&2		Earthquakes		All	
Pass0	8p	7p	8p	7p	16p	14p
Pass1	12p	13p	6p	7p	18p	20p
Pass5						
DBB						
MED						
MHF						
ICOO	5a/17b	4a/15b	3a/8b	2a/4b	8a/25b	6a/19b
LQRCOO	3b	1a/6b	2a/7b	3a/9b	2a/10b	4a/15b
MPCCOO		1b		1b		2b
LQR2COO	18a	17a	9a	10a	27a	27a
RMS values						
Case	Type 1&2		Earthquakes		All	
Pass0	7p	5p	3p	3p	10p	8p
Pass1	14p	15p	11p/1b	11p	25p/1b	26p
Pass5						
DBB						
MED						
MHF						
ICOO	15a/20b	13a/16b	10a/13b	11a/13b	25a/33b	24a/29b
LQRCOO		5a/5b		2a/2b		7a/7b
MPCCOO		1b				1b
LQR2COO	8a	5a	5a	5a	13a	10a

Table 4.27 - Comparison of the number of best cases (#best) for each solution, in numerical simulations (red) and in experimental trials (green).

An attempt to adjust the numerical and experimental time data was performed but due to the non-linearities of the physical model a satisfactory fit was not achieved. This can be attributed first to the non-linearities of the original structure, for which it was hard to identify a model to describe the dissipative forces, mainly due to rolling friction of the wheels. With the SA device installed, its non-linearity more influences the fit.

However, it must be emphasised that the main purpose of the numerical model is achieved since it shows a trend similar to the one of the experimental results in terms of the number of best cases.

4.4.2 Frequency domain

A comparison in the frequency domain was also performed. As already mentioned the FRFs were calculated using the collected time responses resulting from the input artificial accelerograms (10 type 1 and 10 type 2). A comparison between the FRFs obtained from the

numerical and experimental data for all the tested solutions can be found in annex A3, figures A1 to A11.

From the FRFs the natural frequencies and damping ratios were extracted using a prediction-error minimization method available at Matlab, to fit the FRF results to the ones of a state-space black-box model of 4th order (4 states). The resulting properties of this model are presented in table 4.28. For all the solutions, the relative errors in terms of the natural frequencies are bellow 8,5 % for the first mode, and bellow 1,8 % for the second mode of vibration, which is reasonable taking into account the differences in the numerical and experimental models already mentioned. Due to the uncertainties in identifying the damping, higher differences are found on the damping ratios errors, values that can reach 37 %.

case	Original			Pass0			Pass1			MHF		
	num	exp	e (%)	num	exp	e (%)	num	exp	e (%)	num	exp	e (%)
f_1 (Hz)	0,40	0,40	0,6	0,40	0,42	4,2	0,43	0,45	5,1	0,43	0,45	6,2
f_2 (Hz)	3,03	3,03	0,0	3,03	3,03	0,1	3,02	3,02	0,0	3,02	3,02	0,1
ξ_1 (%)	10,33	7,54	37,0	17,63	16,84	4,7	38,18	39,75	3,9	34,13	37,31	8,5
ξ_2 (%)	1,22	1,06	16,1	3,36	2,88	16,5	9,42	9,46	0,4	4,32	5,21	17,1
case	ICOO			LQRCOO			MPCCOO			LQR2COO		
	num	exp	e (%)	num	exp	e (%)	num	exp	e (%)	num	exp	e (%)
f_1 (Hz)	0,40	0,44	8,0	0,38	0,41	7,6	0,41	0,45	8,5	0,40	0,44	8,4
f_2 (Hz)	3,00	3,05	1,8	3,01	3,03	0,6	3,04	3,05	0,4	2,57	2,61	1,8
ξ_1 (%)	43,56	50,43	13,6	38,48	44,85	14,2	38,77	39,70	2,3	42,35	54,30	22,0
ξ_2 (%)	10,56	12,42	15,0	8,83	10,38	14,9	4,26	4,92	13,3	28,09	33,20	15,4

Table 4.28 - Identified natural frequencies and damping ratios obtained from the numerical (num) and experimental (exp) and the correspondent error (e) in percentage for the main solutions.

In figures 4.40 to 4.43 are presented some of the FRFs comparison, namely for the original structure, passive case Pass1 and the best SA cases, ICOO and LQR2COO. As stated before, all comparisons can be found in annex A3, figures A1 to A11.

From the comparison of the FRFs it was found a good agreement in general, with the best fit found for the original structure one. For the passive case, slightly differences are found on the relative displacement X_{si}/A_g and base acceleration A_i/A_g. For the SA cases, slightly differences are also found on the top acceleration A_s/A_g, and also a sub-estimate of the first mode of vibration magnitude for the relative displacements X_{ig}/A_g and X_{si}/A_g, and on the anti-resonance of A_i/A_g.

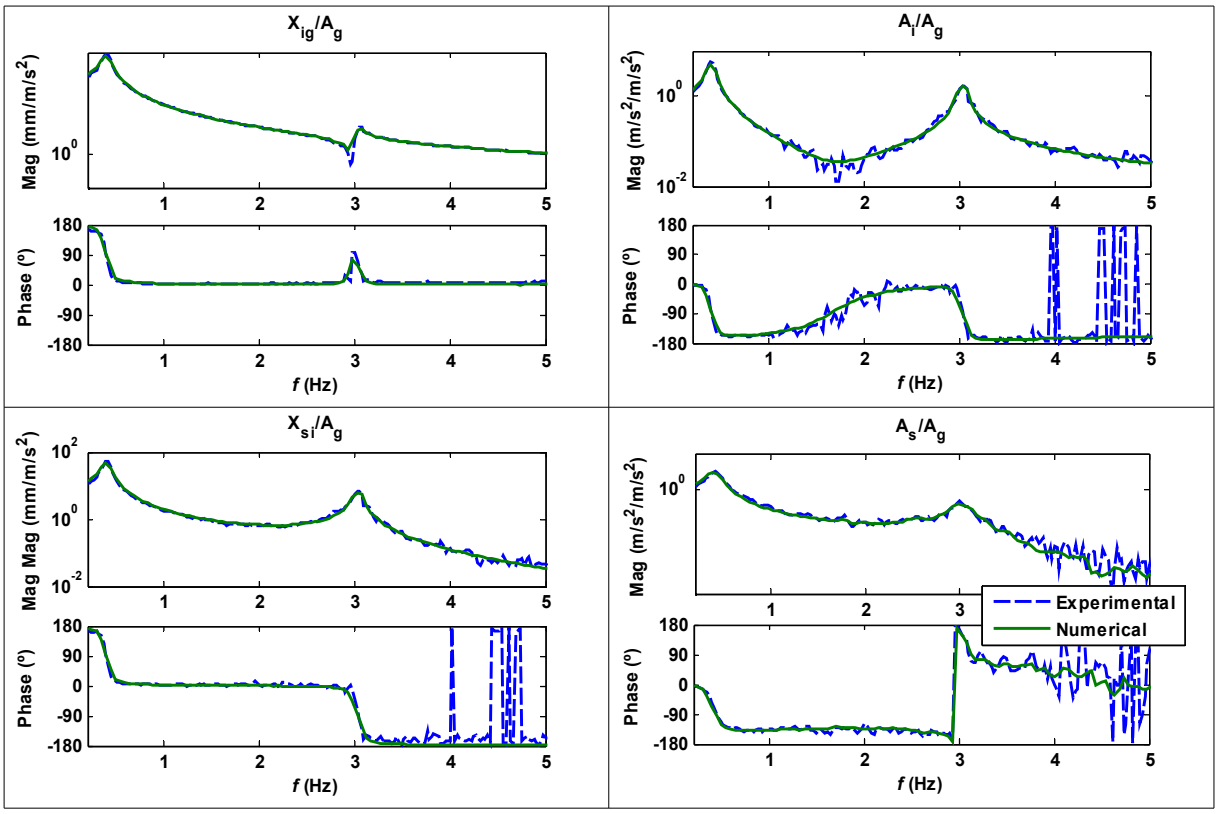

Figure 4.40 - Comparison between the numerical and experimental FRFs for the Original structure, obtained using the artificial accelerograms as input.

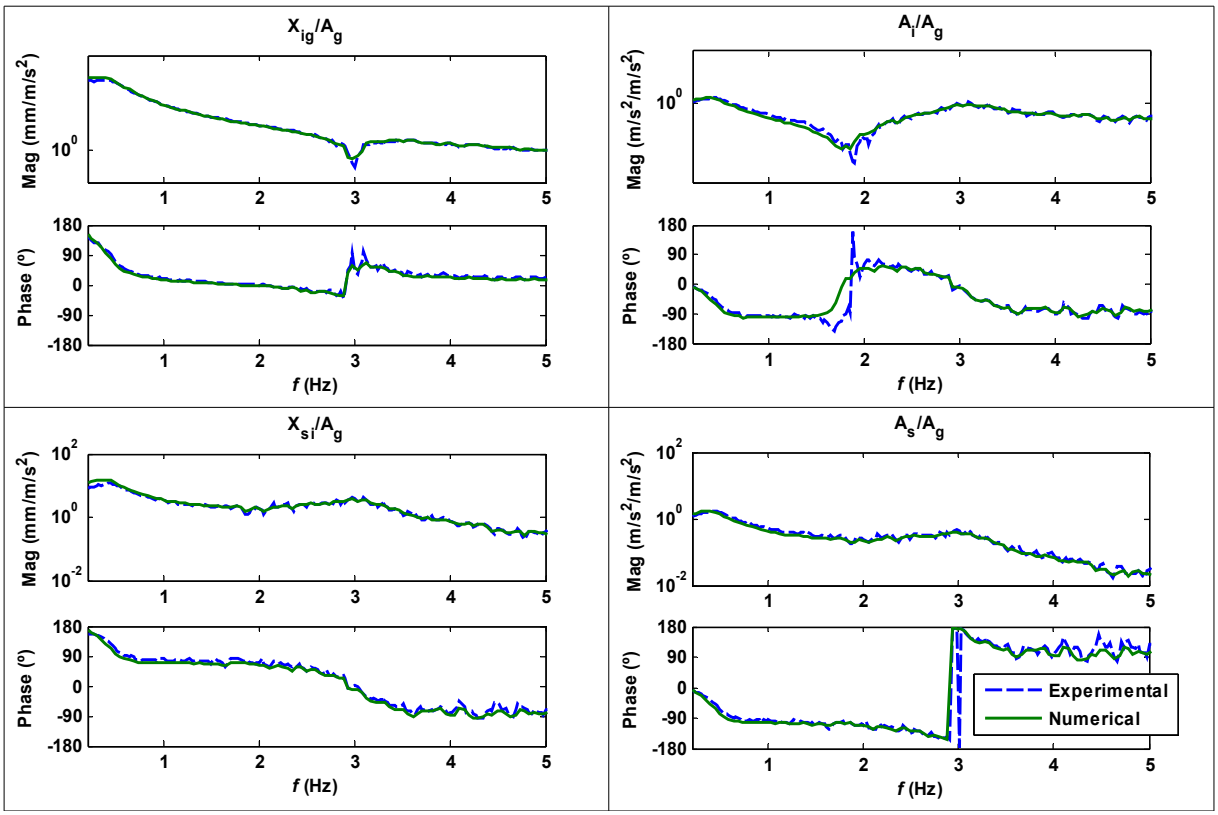

Figure 4.41 - Comparison between the numerical and experimental FRFs for the Pass1 case, obtained using the artificial accelerograms as input.

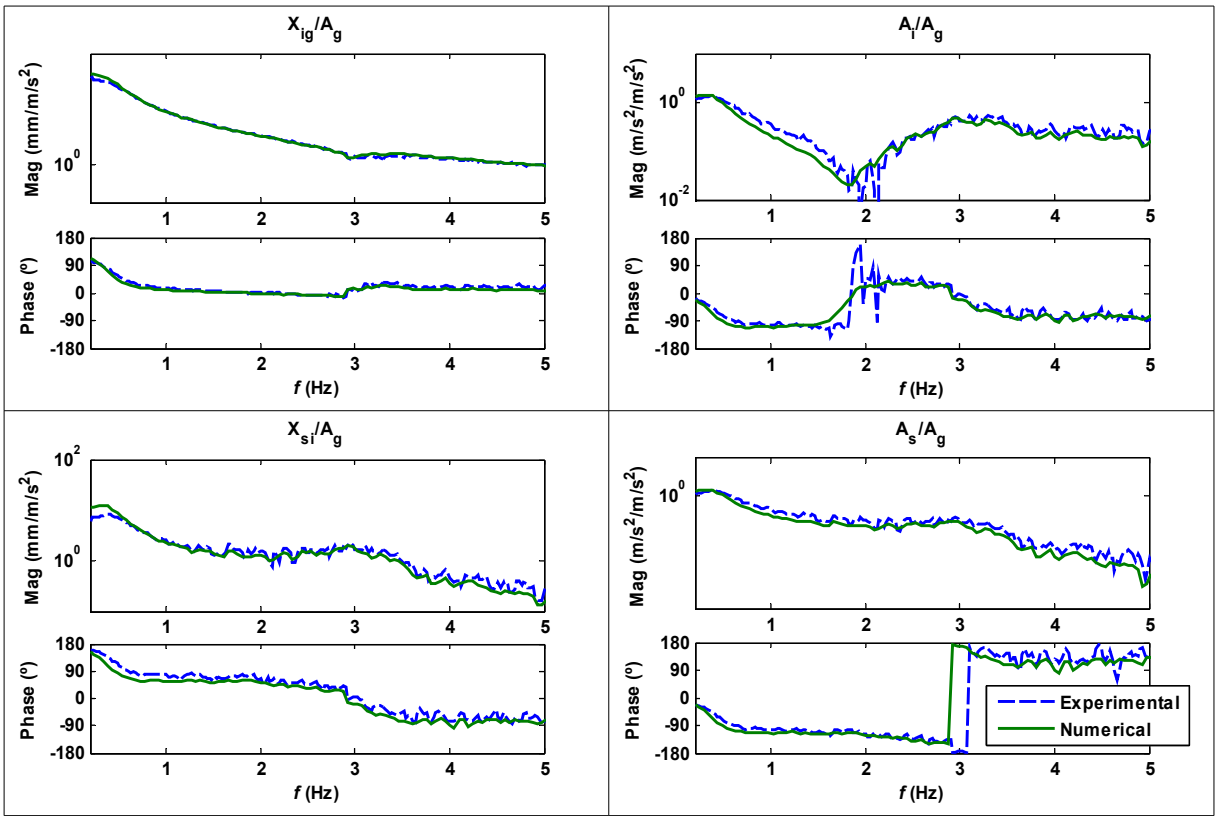

Figure 4.42 - Comparison between the numerical and experimental FRFs for the ICOO case, obtained using the artificial accelerograms as input.

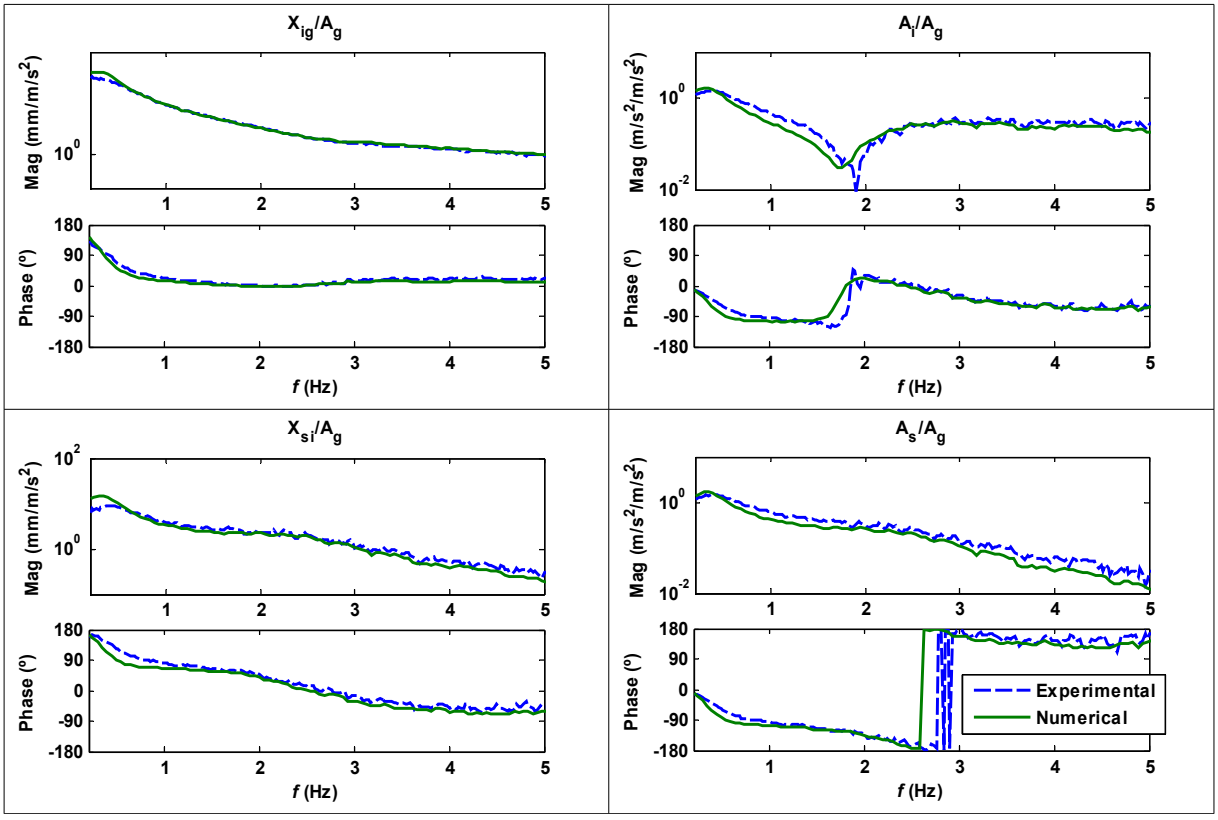

Figure 4.43 - Comparison between the numerical and experimental FRFs for the LQR2COO case, obtained using the artificial accelerograms as input.

4.5 Final Remarks

In this chapter several control strategies were considered for a comparative analytical and experimental study on a 2DOF mechanical model with an MR damper. The overall objective of the study was to validate experimentally the effectiveness of several control strategies in reducing the responses of base-isolated structures when subjected to earthquake loads.

Firstly, a 2DOF mechanical model representative of the phenomena under study as well as the experimental installation to perform the tests was described. The measurement and control chain used is thoroughly described and the metrological characterization and parametrization of the models is presented. The linear models used to describe each measurement chain quantity in the correspondent measurement range lead to an overall low uncertainty of measurement and thus validate the model for this purpose. Then, the development of the model, the mechanical characterization of its elements and the parametrization of the linear models are presented. The physical model without the MR device was tested on the shaking table and a linear continuous state-space model was used to describe its dynamic behaviour. The model was parametrized under different input ground motion magnitudes with good fittings in terms of FRFs. A small dependence of the model properties, namely the damping ratios, with the input ground motion magnitude is found. The MR damper was also subjected to several tests in order to characterize it: static and dynamic tests. A model structure consisting of a transient and stationary components is proposed. The first is described by a first order dynamic system while for the second a Bouc-Wen family model is used. The Modified Bouc-Wen model showed to be the most suitable in describing the mechanical behaviour of the damper.

Numerical simulations and experimental tests were performed with the model in different configurations and under different input ground motions in order to evaluate the performance of the SA control strategies. Seven SA controllers were evaluated: DBB, MED, MHF, ICOO, LQRCOO, MPCCOO and LQR2COO. In first place, numerical simulations were performed to tune the SA controllers for use in both numerical and experimental trials. From both numerical and experimental data analysis it was found that in general: Pass5 as well as the DBB and MED controllers lead to the higher reductions at the base relative displacement but with highest increase on the masses relative displacements and accelerations; MHF, ICOO, LQRCOO, MPCCOO and LQR2COO, perform better than the passive Pass1 case, and also better than the original structure. In terms of the best solutions, it was found that: Pass1 is the best passive case; LQR2COO is the best one in terms of peak values, being ICOO the following one; ICOO is the best in terms of RMS values; moreover, ICOO is also the best in terms of both peak values and RMS values if only collocated control strategies are considered for comparison.

Finally, the comparison of both numerical and experimental results showed that: a similar trend is found in both numerical and experimental results in terms of the number of best cases; in terms of FRFs it was found in general a good agreement although slightly differences are found on the magnitude of relative displacement and base acceleration; however in terms of natural frequencies both numerical and experimental results agree adequately.

In general it was found that it is possible to improve the behaviour of structures with SA systems, being the ICOO strategy the best one when collocated control is considered and LQR2COO the best one if other responses of the model are taken into consideration for control.

Chapter 5

Conclusions and Future Work

Summary

This last chapter presents the main conclusions of this work by describing the capabilities and limitations in using semi-active systems for vibration mitigation of base-isolated structures. A reference is made to main original contributions and conclusions, highlighting the importance of this research. Lastly, since no research work is ever finished or complete, suggestions for further research and work are given.

5.1 Conclusions

The purpose of this study was to develop knowledge on the design of semi-active control systems for vibration mitigation of base-isolated structures subjected to earthquake ground motions. The resulting control problem has specific attributes of relevance such as the nonlinearity of the whole system, time delays, model and measurement uncertainties, and unknown disturbances. The main contribution of this work was on the formulation and evaluation of several control strategies through numerical and experimental approaches. It was given special emphasis to collocated control due to the facility in developing a compact solution for application in real structures, with the same level of accessible installation as the passive solution. The semi-active strategy with an integral controller outperformed the other collocated control strategies, the passive case and the original structure one, with a straightforward implementation and design.

The control strategies explored in this work were Lyapunov based methods (Maximum Energy Dissipation algorithm - MED and Decentralized Bang-Bang control - DBB), feedback linearisation (Nonlinear Output Feedback Control - NOFC), Sliding Mode Control (SMC) and force tracking schemes based on the strategies Modulated Homogeneous Friction (MHF), Integral control law (I), Linear Quadratic Regulator (LQR) and Model Predictive Control strategy (MPC), and on the variable damping algorithm (VD) or a clipped on-off algorithm (COO). The contributions of this work can be summarized:

1. *the identification of a collocated control technique based on an integral control law and on the on-off algorithm, adequate for semi-active control of base isolated structures*; although this controller has been already used in the past for semi-active control, the results did not evidence improvements when compared with the passive solution, mainly due to the fact that it was implemented to rigid structures and the controller was not correctly tuned; in this work these issues have been overcome (see points 2 and 3);
2. *the design of semi-active controllers was proposed to be performed using a set of representative input ground motions*; with this approach a fine tuning can be performed although it requires a model of the system; a representative number of input ground motions must be considered, e.g. the ones representative of the site where the structure will be installed; using this analysis it is also possible to find how the controller tuning can influence the whole system performance;
3. *the confirmation of the applicability of semi-active control for base-isolated structures based on a parametric study made on SDOF systems with different natural frequencies covering the range of natural frequencies of interest, under a numerical*

analysis; this fact was indeed verified on a MDOF structural model representative of a typical base-isolated structure; the hybrid MDOF model manipulated by the controllers such as NOFC, SMC, MHFVD, IVD, ICOO, LQRVD, LQRCOO, MPCVD and MPCCOO, all shown a better performance than the best passive case on the peak responses at the superstructure level under artificial accelerograms as inputs;

4. *the formulation and implementation of semi-active control strategies whose performance have been evaluated in the context of base-isolation systems through numerical and experimental analysis*; from the comparison of results of both numerical and experimental results good agreement was found in the frequency domain; in the time domain, a similar trend in both numerical and experimental results in terms of the number of best cases was found; with the artificial accelerograms and the earthquake ground motions as inputs, SA controllers ICOO, LQRCOO, MPCCOO and LQR2COO all perform better than the best passive case in terms of the average ratio performance index and in almost cases in terms of accelerations and relative displacements;
5. *the semi-active control strategies that take into account the device characteristics in the controller formulation, namely the force tracking scheme using a model predictive controller, the nonlinear output feedback strategy that accounts for the device formulation in the definition of the control law, and the sliding mode control strategy, do not outperform the other strategies*; thus, it was shown that when the nonlinearities and the devices characteristics are taken into account in the formulation under the assumptions considered it is not advantageous to use these strategies; other strategies should be analysed for this purpose (see future work); the last two in particular were not formulated for implementation in the experimental trail due to the fact that some variables of the damper cannot be measured (internal variables);
6. *the passive case selected characterized by a higher reduction at the topmost mass acceleration shown a good compromise between the relative displacements and accelerations reductions and was used as a better solution for comparison with the SA controllers*; conversely, in other studies only the minimum and maximum damping solutions were used; with the approach considered here reductions in the relative displacements and accelerations are achieved, which are even better than the passive at minimum damping and consequently better than the original structure case;
7. *comparison of three Bouc-Wen family models in fitting to the experimental data, whose the modified version shown to better represent the dynamic behaviour of the*

damper; the developed models were complemented with a first order model to describe the transient regime and data matrices with the parameters dependent of input voltage and relative velocity; the dependence on velocity increased considerably the model effectiveness in reproducing the experimental data.

It should be noted that in the author's opinion this study add values and knowledge to applications in the civil engineering domain and namely on the earthquake engineering field. It is expected that this study creates impact among the researchers and designers in this field since this solution provides better performance than the actual passive solutions that are already being used.

5.2 Future Work

From the questions that were arisen during this work, there are some suggestions for future work that could be explored:

- analysis of the nonlinearity of the model on the results by performing the study under different scale factors on the input ground motions;
- evaluate the performance of the best strategies considering the two horizontal components of the input ground motion using two direction DOF models;
- analysis of other control strategies that take into account the nonlinearities in the controller formulation; it is the belief of the author that the system formulation included in the controller formulation will improve the system performance; although better fittings could be achieved with more complex models, the controller formulation is more difficult to tackle in these cases;
- identify the influence of the seismic action characteristics (response spectra type) on the controller design.

References

A

Agrawal & Zhou 2004
Agrawal A., Zhou X., *A novel active controller design based on H2/LQG algorithm with pulse filters*, Proc. 4th Int. Workshop on Structural Control and Health Monitoring, Columbia University, 2004.

Aguirre et al. 2011
Aguirre N., Ikhouane F., Rodellar J., *Proportional-plus-integral semiactive control using magnetorheological dampers*, Journal of Sound and Vibration 330(10):2185-2200, 2011.

Anderson & Moore 1989
Anderson B. D. O., Moore J. B., *Optimal Control: Linear Quadratic Methods*, Prentice-Hall, 1989.

Azevedo & Guerreiro 2007
Azevedo J., Guerreiro L., *Current Status of Seismic Isolation and Energy Dissipation R&D and Applications for Buildings, Bridges and Viaducts, in Portugal*, 10th World Conference on Seismic Isolation, Energy Dissipation and Active Vibrations Control of Structures, Istanbul, Turkey, 2007.

B

Bahar et al. 2010
Bahar A., Pozo F., Acho L., Rodellar J., Barbat A., *Hierarchical semi-active control of base-isolated structures using a new inverse model of magnetorheological dampers*, Computers and Structures 88(7-8):483–496, 2010.

Bairrão & Duque 1998
Bairrão R., Duque J., *Simulador Sísmico Unaxial-Descrição e Operação*, Relatório 94/98-C3ES/SES, Laboratório Nacional de Engenharia Civil (LNEC), 1998.

Bani-Hani & Sheban 2006
Bani-Hani K. A., Sheban M. A., *Semi-active neuro-control for base-isolation system using magnetorheological (MR) dampers*, Earthquake Engineering and Structural Dynamics 35(9):1119–1144, 2006.

BIPM et al. 2008
BIPM, IEC, IFCC, ILAC, ISO, IUPAC, IUPAP, OIML, *Evaluation of measurement data - Guide to the expression of uncertainty in measurement,* Joint Committee for Guides in Metrology, JCGM 100:2008, 2008.

Borutzky et al. 2002
Borutzky W., Barnard B. Thoma J., *An Orifice flow model for laminar and turbulent conditions,* Simulation Modelling Practice and Theory 10(3-4):141–152, 2002.

C

Cansado Carvalho 2001
Cansado Carvalho E., *Mitigação do Risco Sísimico em Portugal*, Redução da Vulnerabilidade Sísimica em Portugal, Encontro organizado pela SPES & GECoRPA na Ordem dos Engenheiros, Lisboa, Portugal, 2001.

Carlson 2005
Carlson J. D., *Magnetorheological fluids – Engineering applications today and tomorrow*, II ECCOMAS, Thematic Conference on Smart Structures and Materials, C.A. Mota Soares *et* al. (Eds.), Lisbon, Portugal, July 18-21, 2005.

Carlson and Chrzan 1994
Carlson J. D., Chrzan M. J., *Magnetorheological Fluid Dampers*, United States Patent nº 5277281, January 1994.

Carlson et al. 1996
Carlson, J. D., Catanzarite D. N., St Clair K. A., *Commercial Magneto- Rheological Fluid Devices*, Proceedings 5th Int. Conf. on ER Fluids, MR Suspensions and Associated Technology, W. Bullough Ed., World Scientific, Singapore, pp.20–28, 1996.

Carvalho 2007
Carvalho A., *Modelação da Acção Sísmica em Portugal*. PhD thesis. Instituto Superior Técnico, Universidade Técnica de Lisboa, 2007.

Casciati et al. 2012
Casciati F., Rodellar J., Yildirim U., *Active and semi-active control of structures–theory and applications: A review of recent advances*, Journal of Intelligent Material Systems and Structures 23(11):1181-1195, 2012.

Castellano et al. 2004
Castellano M. G., Colato G. P., Infanti S., *Use of viscous dampers and shock transmission units in the seismic protection of buildings*, Proceedings of the 13th world conference on earthquake engineering, paper 2172, Vancouver, B. C., Canada, August 1-6, 2004.

Chae et al. 2013(II)
Chae Y., Ricles J. M., Sause R., *Modelling of a large-scale magneto-rheological damper for seismic hazard mitigation. Part II: Semi-active mode*, Earthquake Engineering and Structural Dynamics 42(5):687-703, 2013.

Chen et al. 1995
Chen H. M., Tsai K. H., Qi G. Z., Yang J. C. S., Amini F., *Neural network for structural control*. Journal of Computing in Civil Engineering 9(2):168–176, 1995.

Cho 2004
Cho S., S*imple Control Algorithms for MR Dampers and Smart Passive Control System*, PhD Thesis, Korea Advanced Institute of Science and Technology, 2004.

Chopra 1995
Chopra A. K., *Dynamics of Structures: Theory and Applications to Earthquake Engineering (2nd edn)*, Prentice-Hall: New York, 1995.

Christenson 2001
Christenson R. E., *Semiactive Control of Civil Structures for Natural Hazard Mitigation: Analytical and Experimental Studies*, PhD Thesis, University of Notre Dame, Indiana, December 2001.

Chu et al. 2005
Chu S. Y., Soong T. T., Reinhorn A. M., *Active, Hybrid and Semi-Active Structural Control – A Design and Implementation Handbook*, John Wiley & Sons Ltd., 2005.

D

Dahl 1968
Dahl P. R., *A solid friction model - Technical Report TOR-158(3107-18)*, El-Secundo, CA: The Aerospace Corporation, 1968.

De Man et al. 2005
De Man P., Lemerle P., Mistrot P., Verschueren J-Ph., Preumont A., *An investigation of a semiactive suspension for a fork lift truck*, Vehicle System Dynamics 43(2):107–119, February 2005.

DiStefano III et al. 1967
DiStefano III J. J., Stubberud A. R., Williams I. J., *Feedback and Control Systems*, Schaum Publishing Co., New York, 1967.

Dyke 1996
Dyke S. J., *Acceleration Feedback Control Strategies for Active and Semi-Active Control Systems: Modeling, Algorithm Development and Experimental Verification*, PhD Thesis, University of Notre Dame, Indiana, July 1996.

Dyke & Spencer 1996
Dyke S. J., Spencer Jr. B. F., *Seismic response control using multiple magnetorheological dampers*, Proceedings of the 2nd International Workshop on Structural Control, Hong Kong, pp.163–173, 1996.

Dyke & Spencer 1997
Dyke, S. J., Spencer Jr. B. F., *A comparison of semiactive control strategies for the magnetorheological damper*, Proc. IASTED – International Conference on Intelligent Information Systems, pp.580–584, Bahamas, December 8–10, 1997.

Dyke et al. 1994
Dyke S. J., Spencer B. F., Quast P., Sain M. K., Kaspari D. C., Soong T. T., *Experimental Verification of Acceleration Feedback Control Strategies for an Active Tendon System*, Technical Report NCEER-94-0024, National Center for Earthquake Engineering Research, Buffalo, New York, August 1994.

Dyke et al. 1996(a)
Dyke S. J., Spencer Jr. B. F., Sain M. K., Carlson J. D., Modelling *and Control of Magnetorheological Dampers for Seismic Response Reduction,* Smart Materials and Structures 5(5):565–575, 1996.

Dyke et al. 1996(b)
Dyke S. J., Spencer Jr. B. F., Sain M. K., Carlson J. D., *Experimental Verification of Semi-Active Structural Control Strategies Using Acceleration Feedback*, Proceedings of the 3rd International Conference on Motion and Vibration Control, Vol.3, pp.291–296, Chiba, Japan, September 1996.

Dyke et al. 1996(c)
Dyke S. J., Spencer B. F., Quast P., Sain M. K., Kaspari D. C., Soong T. T., *Acceleration feedback control of MDOF structures*, Journal of Engineering Mechanics 122(9):907–917, 1996.

E

Eurocodigo8 2010
Eurocodigo8, *Projecto de Estruturas para Resistência aos Sismos – Parte1: Regras Gerais, Acções Símicas e Regras para Edifícios*, Instituto Português da Qualidade, NP EN 1998-1, 2010.

F

Feng & Shinozuka 1990
Feng Q., Shinozuka M., *Use of a variable damper for hybrid control of bridge response under earthquake*, Proceedings of U.S. National Workshop on Structural Control Research, USC Publications Nº CE-9013, 1990.

Feng & Shinozuka 1993
Feng Q., Shinozuka M., *Control of Seismic Response of Bridge Structures Using Variable Dampers*, Journal of Intelligent Material Systems and Structures 4(1):117-122, January 1993.

Franklin et al. 1998
Franklin G. F., Powell J. D., Workman M. L., *Digital Control of Dynamic Systems*, 3rd Edition, Addison Wesley Longman Inc., 1998.

Fujitani et al. 2000
Fujitani H., Sodeyama H., Hata K., Iwata N., Komatsu Y., Sunakoda K., Soda S., *Dynamic performance evaluation of 200 kN magneto-rheological damper*, Proceedings of the International Conference on Advances in Structural Dynamics, Vol.1, pp.319–326, Hong Kong, China, 2000.

G

Gamota & Filisko 1991
Gamota D. R., Filisko F. E., *Dynamic Mechanical Studies of Electrorheological Materials: Moderate Frequencies*, Journal of Rheology 35(3):399–425, 1991.

Gattulli et al. 2008
Gattulli V., Lepidi M., Potenza F., Carneiro R., *Semiactive Control Using MR Dampers of a Frame Structure under Seismic Excitation*, 2008 Seismic Engineering Conference Commemorating the 1908 Messina and Reggio Calabria Earthquake, Vol.1020, No.1, pp.153-161 AIP Publishing, 2008.

Gavin & Aldemir 2005
Gavin H. P., Aldemir U., *Optimal Control of Earthquake Response Using Semiactive Isolation*, Journal of Engineering Mechanics 131(8):769-776, 2005.

Ghaboussi & Joghataie 1995
Ghaboussi J., Joghataie A. *Active control of structure using neural networks*. Journal of Engineering Mechanics 121(4):555–567, 1995.

Goncalves 2001
Goncalves F. D., *Dynamic Analysis of Semi-Active Control Techniques for Vehicle Applications*, MSc Thesis, Faculty of the Virginia Polytechnic Institute and State University, Blacksburg, Virginia, 2001.

Guerreiro et al. 2005
Guerreiro L., Ferreira J., Colato G., Castellano G., Baldo P., *Base Isolation for Seismic Protection – The new hospital in Lisbon*, IABSE Symposium Report, Vol.90, No.2, pp.35-42, International Association for Bridge and Structural Engineering, 2005.

H

Hitchcock et al. 2002
Hitchcock G. H., Gordaninejad F., Wang X., *A New By-Pass, Fail-Safe, Magneto-Rheological Fluid Damper*, SPIE's, 9th Annual International Symposium on Smart Structures and Materials, pp. 345-351. International Society for Optics and Photonics, 2002.

Horowitz 2001
Horowitz I., *Survey of quantitative feedback theory (QFT)*, International Journal of Robust and Nonlinear Control 11(10):887:921, 2001.

Housner et al. 1997
Housner G. W., Bergman L. A., Caughey T. K., Chassiakos A. G., *Structural Control: Past, Present, and Future*, Journal of Engineering Mechanics 123(9):897-971, 1997.

Hrovat et al. 1983
Hrovat D., Barak P., Rabins M., *Semi-active versus passive or active tuned mass dampers for structural control*, Journal of Engineering Mechanics 109(3):691–705, 1983.

I

Ikeda 2009
Ikeda Y., *Active and semi-active vibration control of buildings in Japan - Practical applications and verification*, Structural Control and Health Monitoring 16(7-8):703–723, 2009.

Ikhouane & Dyke 2007
Ikhouane F., Dyke S. J., *Modeling and identification of a shear mode magnetorheological damper*, Smart Materials and Structures 16(3): 605–616, 2007.

Ikhouane & Rodellar 2005(i)
Ikhouane F., Rodellar J., *On the hysteretic Bouc–Wen model. Part 1: forced limit cycle characterization*, Nonlinear Dynamics 42(1):63–78, 2005.

Ikhouane & Rodellar 2005(ii)
Ikhouane F., Rodellar J., *On the hysteretic Bouc–Wen model. Part 2: Robust Parametric Identification*, Nonlinear Dynamics 42(1):79–95, 2005.

Ikhouane et al. 2007
Ikhouane F., Hurtado J. E., Rodellar J., *Variation of the hysteresis loop with the Bouc–Wen model parameters*, Nonlinear Dynamics 48(4):361–380, 2007.

Inaudi 1997
Inaudi J. A., *Modulated Homogeneous Friction: a semi-active damping strategy*, Earthquake Engineering and Structural Dynamics 26(3):361-376, 1997.

Inaudi et al. 1992
Inaudi J., López-Almansa F., Kelly J. M., Rodellar J., *Predictive control of base-isolated structures*, Earthquake Engineering & Structural Dynamics 21(6):471–482, 1992.

Isidori 1995
Isidori A., Nonlinear Control Systems (volume 1) – 3rd edition, Springer-Verlag, 1995.

J

Jansen 2000
Jansen L. M., *Response Modification of Buildings and Bridges: Comparative Studies in Seismic Control*, Sever Institute of Washington University, Saint Louis, Missouri, December, 2000.

Jansen & Dyke 2000
Jansen L. M., Dyke S. J., *Semi-Active Control Strategies for MR Dampers: A Comparative Study*, Journal of Engineering Mechanics 126(8):795–803, 2000.

Jinping & Hui 2009
Jinping O., Hui L., *Design approaches for active, semi-active and passive control systems based on analysis of characteristics of active control force*, Earthquake Engineering and Engineering Vibration 8(4):493-506, 2009.

Jolly et al. 1999
Jolly, M. R., Bender, J. W., Carlson, J. D., *Properties and Applications of Commercial Magnetorheological Fluids*, Journal of Intelligent Material Systems and Structures 10(1):5-13, January 1999.

Jung et al. 2003
Jung H., Spencer Jr. B. F., Lee I., *Control of Seismically Excited Cable-Stayed Bridge Employing Magnetorheological Fluid Dampers*, Journal of Structural Engineering 129(7):873-883, July 2003.

Jung et al. 2006
Jung H., Min Choi K., Spencer Jr. B. F., Lee I., A*pplication of some semi-active control algorithms to a smart base-isolated building employing MR dampers*, Structural Control Health Monitoring 13(2-3):693–704, 2006.

K

Karnopp et al. 1974
Karnopp D., Crosby M.J., Harwood R.A., *Vibration control using semi-active force generators*, Journal of Engineering for Industry 96(2):619–26, 1974.

Kawashima & Unjoh 1993
Kawashima K., Unjoh S., *Variable dampers and variable stiffness for seismic control of bridges*, Proceedings of International Workshop on Structural Control, pp.283–97, Honolulu, Hawaii, 5-7 August, 1993.

Kawashima et al. 1992(a)
Kawashima K., Unjoh S., Shimizu K., *Experiments on dynamics characteristics of variable damper*, Proceedings Japan National Symposium on Structural Response Control, 121, 1992.

Kawashima et al. 1992(b)
Kawashima K., Unjoh S., Iida H., Mukai H., *Effectiveness of the variable damper for reducing seismic response of highway bridges*, Proceedings of Second US–Japan Workshop on Earthquake Protective Systems for Bridges, PWRI, Tsukuba Science City, Japan, pp.479–493, 1992.

Kelly 1999
Kelly J. M., T*he Role of Damping in Seismic Isolation*, Earthquake Engineering and Structural Dynamics 28(1):3-20, 1999.

Khalil 2002
Khalil H. K., *Non-linear Systems (3rd edition)*, Prentice-Hall, Inc., 2002.

Kim et al. 2006
Kim H., Roschke P. N.,Lin P., Loh C., *Neuro-fuzzy model of hybrid semi-active base isolation system with FPS bearings and an MR damper*, Engineering Structures 28(7):947–958, 2006.

K-Karamodin and H-Kazemi 2010
K-Karamodin A., H-Kazemi H., *Semi-active control of structures using neuro-predictive algorithm for MR dampers*, Structural Control and Health Monitoring 278(10):1002–1020, 2008.

Komatsu et al. 2007
Komatsu H., Shinozaki Y., Sanui Y., Maseki R., Yoshida K., Kitagawa Y., Toyama J., Nagashima I., *A building with semi-active base isolation using sliding mode control*, Proceedings of SMSST'07, World Forum on Smart Materials and Smart Structures Technology, China, 2007.

Kurata et al. 1994
Kurata N., Kobori T., Takahahi M., Niwa N., Kurino H., *Shaking table experiment of active variable damping system*, Proceedings of First World Conference on Structural Control, Pasadena, CA, TP2, pp.108–117, 1994.

Kurata et al. 1999
Kurata N., Kobori T., Takahashi M., Niwa N., Midorikawa H., *Actual Seismic Response Control Building with Semi-Active Damper System*, Earthquake Engineering and Structural Dynamics 28(11):1427-1447, 1999.

Kurino et al. 2002
Kurino H., Yamada T., Tagami J. Shimizu K., *Semi-active structural control by switching oil damper with built-in controller*, Proceedings of the Third World Conference on Structural Control, Vol.3, pp.91-100, Como, Italy, 2002.

Kurino et al. 2003
Kurino H., Tagami J, Shimizu K., Kobori T., *Switching oil damper with built-in controller for structural control*, Journal of Structural Engineering 129(7): 895-904, 2003.

Kurino et al. 2004
Kurino H., Matsunaga Y., Yamada T., Tagami J., *High Performance Hydraulic Damper with Semi-active characteristics*, 13th World Conference on Earthquake Engineering, paper No.33, Vancouver, B.C., Canada, August 1-6, 2004.

Kurino et al. 2009
Kurino H., Orui S.,Shimizu K., *Structural Control by Innovative Oil Damper with Automatic On/Off Valve Operation*, Journal of Disaster Research 4(3):253-260, 2009.

L

Lee et al. 2006
Lee H., Yang G., Jung H., Spencer Jr. B. F., Lee I., *Semi-active neurocontrol of a base-isolated benchmark structure*, Structural Control and Health Monitoring 13(2-3):682–692, 2006.

Lee et al. 2008
Lee H., Jung H., Moon S., Lee S., Park E., Min K., *Experimental investigation of semiactive control systems based on MR dampers using full-scale steel frame building structure*, 15th International Congress on Sound and Vibration, pp. 299-306, Daejeon, Korea, 6-10 July 2008.

LESSLOSS 2007
LESSLOSS, *Risk Mitigation for Earthquakes and Landslides*, Report 2007/03, IUSS Press, Istituto Universitario di Studi Superiori, Pavia, Italia, 2007.

Lewis 1986
Lewis F. L., *Optimal Estimation: with an introduction to stochastic control theory*, John Willey & Sons, Inc., 1986.

Liu et al. 2005
Liu Y., Waters T. P., Brennan M. J., *A comparison of semi-active damping control strategies for vibration isolation of harmonic disturbances*, Journal of Sound and Vibration 280(1):21–39, 2005.

Loh et al. 2003
Loh C.,Wu L. Y., Lin P. Y., *Displacement control of isolated structures with semi-active control devices*, Journal of Structural Control 10(2): 77–100, 2003.

Loh et al. 1999
Loh C., Lin P., Chung N., *Experimental verification of building control using active bracing system*, Earthquake Engineering & Structural Dynamics 28(10):1099–1119, October 1999.

Lopes 2008
Lopes M., *Sismos e Edifícios*, 1ª edição, Edições Orion, 2008.

Luo et al. 2001
Luo N., Rodellar J., Vehí J., De la Sen M., *Composite semiactive control of a class of seismically excited structures*, Journal of the Franklin Institute 338(2):225–240, 2001.

Luo et al. 2006
Luo N., Villamizar R., Vehí J., Dyke S., *Semiactive backstepping control for vibration attenuation in structures equipped with magnetorheological actuators*, 2006 IEEE International Conference on Control Applications, pp.1091-1096, Munich, Germany, October 4-6, 2006.

M

Maciejowski 2002
Maciejowski, J.M., *Predictive control with constraints*, Pearson Education Limited, 2002.

Maia et al. 1997
Maia N., Silva J., He J., Lieven N., Lin R., Skingle G., To W., Urgueira A., *Theoretical and Experimental Modal Analysis*, Research Studies Press Ltd, England, 1997.

Maia et al. 1998
Maia N., Silva J., Ribeiro A., *On a General Model for Damping*, Journal of Sound and Vibration 218(5):749-767,1998.

Mejía 2005
Mejía R. V., *Robust Control of Systems Subjected to Uncertain Disturbances and Actuator Dynamics*, PhD Thesis, Universitat de Girona, Departament d'Electrònica, Informàtica I Automàtica, Giorgia, Spain, 2005.

Moon et al. 2003
Moon S. J., Bergman L. A., Voulgaris P. G., *Sliding Mode Control of Cable-Stayed Bridge Subjected to Seismic Excitation*, Journal of Engineering Mechanics 129(1):71-78, January 2003.

Moreira de Andrade 2007
Moreira de Andrade J. C. A., *Isolamento Sísmico de Base*, MSc Thesis, Instituto Superior Técnico, Universidade Técnica de Lisboa, Fevereiro de 2007.

Mori et al. 2002
Mori F., Sugiyama T., Suwa M., Kurino H., Fukushima I., *Application of semi-active switching oil damper to an actual 11-storey building*, Proceedings of the Third World Conference on Structural Control, Vol.2, pp.143-148, Como, Italy, 2002.

N

Narasimhan et al. 2006
Narasimhan S., Nagarajaiah S., Johnson E. A., Gavin H. P., *Smart base-isolated benchmark building. Part I: problem definition*, Structural Control and Health Monitoring 13:573–588, 2006.

O

Occhiuzzi & Serino (1) 2003
Occhiuzzi A., Serino G., *Semi-active Oleodynamic Damper for Earthquake Control. Part 1: design, manufacturing and experimental analysis of the device*, Bulletin of Earthquake Engineering 1(2):275–302, 2003.

Occhiuzzi & Serino (2) 2003
Occhiuzzi A., Serino G., *Semi-active Oleodynamic Damper for Earthquake Control. Part 2: Evaluation of Performance through Shaking Table Tests*, Bulletin of Earthquake Engineering 1(2):241-273, 2003.

Ogata 1970
Ogata K., *Modern Control Engineering*, Prentice Hall, Inc., 1970.

Oliveira 2003
Oliveira C., *Sistemas Semi-activos de Protecção Sísmica de Pontes*, MSc thesis, Instituto Superior Técnico, Lisboa, 2003.

Oliveira 2009
Oliveira C., *Dynamic Behaviour Analysis of Bridges with Adaptative Protection Systems*, PhD thesis, Instituto Superior Técnico, Lisboa, 2009.

P

Patten et al. 1994
Patten W. N., Kuo C. C., He Q., Liu L., Sack R. L., *Seismic structural control via hydraulic semi-active vibration dampers (SAVD)*, Proceedings of First World Conference on Structural Control, pp.83-89, Los Angeles, CA, 1994.

Phillips 1969
Phillips R. W., *Engineering Applications of Fluids with a Variable Yield Stress*, PhD Thesis, University of California, Berkeley, 1969.

Preumont 2002
Preumont André, *Vibration Control of Active Structures – An Introduction (2nd edition)*, Kluwer Academic Publishers, 2002.

Q

Qing et al. 2003
Qing S., Ling Z., Jinxiong Z., Qingxuan S., *Experimental study of the semi-active control of building structures using the shaking table*, Earthquake Engineering Structural Dynamics 32(15):2353–2376, 2003.

R

Rabinow 1948a
Rabinow J., *The magnetic fluid clutch*, AIEE Transactions 67(2):1308–1315, 1948.

Rabinow 1948b
Rabinow J., *Magnetic fluid clutch*, US National Bureau of Standards Technical News Bulletin 32(4):54–60, 1948.

Rabinow 1951
Rabinow J., *Magnetic fluid torque and force transmitting device*, US Patent Specification 2,575,360, 1951.

Ramallo et al. 2002
Ramallo J. C., Johnson E. A.,Spencer Jr. B. F., *"Smart" Base Isolation Systems*, Journal of Engineering Mechanics 128(10), October 2002.

RSCCS 1958
R.S.C.C.S., *Regulamento de Segurança das Construções contra os Sismos,* Decreto n.º 41658, de 31 de Maio de 1958. (in Portuguese).

Ribeiro & Martins 2009
Ribeiro A., Martins L., *Método de Confirmação Metrológica de Instrumentação Científica*, Informação Técnica Metrologia ITM 9, Laboratório Nacional de Engenharia Civil (LNEC), Lisboa, 2009.

Rodríguez et al. 2009
Rodríguez A., Iwata N.,Ikhouane F., Rodellar J., *Model Identification of large-scale magnetorheological fluid dampers*, Smart Materials and Structures 18(1):015010, 2009.

Rodríguez et al. 2012
Rodríguez A., Pozo F., Bahar A., Acho L., Vidal Y., Rodellar J., *Force-derivative feedback semi-active control of base-isolated buildings using large-scale MR fluid dampers*, Structural Control and Health Monitoring 19(1):120–145, 2012.

RSA 1983
R.S.A., *Regulamento de Segurança e Acções para Estruturas de Edifícios e Pontes*, Decreto- Lei nº 235/83, Imprensa Nacional – Casa da Moeda, E. P., Lisboa, Portugal, 1983. (in Portuguese).

S

Sadek et al. 1996
Sadek F., Mohraz B., Taylor A. W., Chung R. M., *Passive Energy Dissipation Devices for Seismic Applications*, NISTIR 5923, Building and Fire Research Laboratory, National Institute of Standards and Technology, Gaithersburg, Maryland, United States of America, 1996.

Sadek & Mohraz 1998
Sadek F., Mohraz B., *Semiactive control algorithms for structures with variable dampers*, Journal of Engineering Mechanics 124(9):981-990, 1998.

Sato et al. 1996
Sato T., Sato M., Tanaka S., Toki K., *Modelling of a variable damper and its application*, Proceedings of Second International Workshop on Structural Control, Hong Kong, 1996.

Sassi et al. 2005
Sassi S., Cherif K., Mezghani L., Thomas M., Kotrane A., *An innovative magnetorheological damper for automotive suspension: from design to experimental characterization*, Smart Materials and Structures 14(4):811–822, 2005.

Shinozuka et al. 1992
Shinozuka M., Constantinou M. C., Ghanem R., *Passive and active fluid dampers in structural applications*, Proc. US/China/Japan Workshop on structural control, pp.507-516, Shanghai, China, October 1992.

Skogestad & Postlethwaite 1996
Skogestad S., Postlethwaite I., *Multivariable Feedback Control – Analysis and Design*, John Wiley & Sons, 1996.

Shook et al. 2007
Shook D., Lin P., Lin T., Roschke P. N., *A comparative study in the semi-active control of isolated structures*, Smart Materials and Structures 16(4):1433–1446, 2007.

Soong & Dargush 1997
Soong T. T., Dargush G. F., *Passive Energy Dissipation Systems in Structural Engineering*, John Wiley & Sons Ltd., 1997.

Soong & Spencer Jr. 2002
Soong T. T., Spencer Jr. B. F., *Supplemental energy dissipation: state-of-the-art and state-of-thepractice*, Engineering Structures 24(3):243–259, 2002.

Sousa 2006
Sousa M. L., *Risco Sísmico em Portugal Continental*, PhD Thesis, Instituto Superior Técnico, Universidade Técnica de Lisboa, Lisboa, Portugal, 2006.

Spencer Jr. 2008
Spencer Jr. B. F., *Structural Control in Honor of Takuji Kobori*, The 14th World Conference on Earthquake Engineering, Beijing, China, October 12-17, 2008.

Spencer & Nagarajaiah 2003
Spencer Jr. B. F., Nagarajaiah S., State of the Art of Structural Control, Journal of Structural Engineering 129(7):845–856, 2003.

Spencer Jr. & Sain 1997
Spencer Jr. B. F., Sain M. K., *Controling Buildings - A new frontier in feedback*, special Issue of the IEEE Control Systems Magazine on Emerging Technology 17(6):19–35, December 1997.

Spencer Jr. & Soong 1999
Spencer Jr. B. F., Soong T. T., *New Applications and Development of Active, Semi-Active and Hybrid Control Techniques for Seismic and Non-Seismic Vibration in the USA*, Proceedings of International Post-SMiRT Conference Seminar on Seismic Isolation, Passive Energy Dissipation and Active Control of Vibration of Structures, pp.23-25, Cheju, Korea, August 23-25, 1999.

Spencer Jr. et al. 1996
Spencer Jr. B. F., Dyke S. J., Sain M. K., *Magnetorheological Dampers: A New Approach to Seismic Protection of Structures*, Proceedings of the 35th IEEE Conference on Decision and Control, Vol.1, pp.676-681, Kobe, Japan, December 1996.

Spencer Jr. et al. 1997(a)
Spencer Jr. B. F., Dyke S. J., Sain M. K., Carlson, J. D., *Phenomenological model for magnetorheological dampers*, Journal of Engineering Mechanics 123(3):230-238, 1997.

Spencer Jr. et al. 1997(b)
Spencer Jr. B. F., Carlson J. D., Sain M. K., Yang G., *On the Current Status of Magnetorheological Dampers: Seismic Protection of Full-Scale Structures*, Proceedings of the 1997 IEEE American Control Conference, Vol.1, pp.458-462, Albuquerque, New Mexico, June 1997.

Sunakoda et al. 2000
Sunakoda K., Sodeyama H., Iwata N., Fujitani H., Soda S., *Dynamic characteristics of magneto-rheological fluid damper*, Proceedings of SPIE Smart Structure and Materials Conference, Vol.3989, pp.194–203, Newport Beach, California, 2000.

Symans & Constantinou 1995
Symans M. D., Constantinou M. C., *Development and experimental study of semi-active fluid damping devices for seismic protection of structures*, Report No. NCEER 95-0011, National Center for Earthquake Engineering Research, Buffalo, NY, 1995.

Symans & Constantinou 1997
Symans M. D., Constantinou M. C., S*eismic testing of a building structure with semi-active fluid damper control system*, Earthquake Engineering and Structural Dynamics 26(7):759–777, 1997.

Symans & Constantinou 1998
Symans M. D., Constantinou M. C., *Passive Fluid Damping Systems for Seismic Energy Dissipation*, ISET Journal of Earthquake Technology 35(4):185-206, 1998.

Symans & Constantinou 1999
Symans M. D., Constantinou M. C., *Semi-active control systems for seismic protection of structures: a state-of-the-art review*, Engineering Structures 21(6):469–487, 1999.

Symans et al. 1994
Symans M. D., Constantinou M. C., Taylor D. P., Garnjost K. D., *Semi-active fluid viscous dampers for seismic response control*, First World Conference on Structural Control, pp.3–12, 1994.

T

Taylor 1999
Taylor D. P., *Buildings: Design for Damping*, (available online: http://taylordevices.com/Tech-Paper-archives/literature-pdf/56-BuildingsDesignforDamping.pdf) Taylor Devices Inc., North Tonawanda, NY, July 1999.

Tilly 1986
Tilly G. P., *Dynamic Behaviour of Concrete Structures*, Elsevier, 1986.

Towashiraporn et al. 2002
Towashiraporn P., Park J., Goodno B. J., Craig J. I., *Passive control methods for seismic response modification*, Progress in Structural Engineering Materials 4(1):74–86, 2002.

U

Utkin 1992
Utkin V. I., *Sliding modes in control and optimization*, Springer Verlag, 1992.

V

Villamizar et al. 2004
Villamizar R., Luo N., Vehí J., Rodellar J., *Active and semiactive QFT control for the structural vibration attenuation*, International Conference on Mechanical Vibration and Noise (MOVIC), St Louis, USA, August 8-11, 2004.

W

Wang 2006
Wang Y., *Control Strategies for 3D Smart Base Isolation Systems Using Modal and Nodal Approaches*, PhD Thesis, Sever Graduate School of Washington University, May 2006.

Wang & Gordaninejad 1999
Wang X., Gordaninejad F., *Flow analysis of field-controllable, electro- and magneto-rheological fluids using Herschel–Bulkley model*, Journal of Intelligent Materials Systems and Structures 10(8): 601–608, 1999.

Wang & Liao 2011
Wang D. H., Liao W. H., Magnetorheological fluid dampers: a review of parametric modelling Smart Materials and Structures 20(2):023001, 2011.

Wang et al. 2005(a)
Wang J. Y., Ni Y. Q., Ko J. M., Spencer Jr. B. F., *Magneto-rheological tuned liquid column dampers (MR-TLCDs) for vibration mitigation of tall buildings: modelling and analysis of open-loop control*, Computers and Structures 83(25):2023–2034, 2005.

Wang et al. 2005(b)
Wang J., Meng G., Feng N., Hahn E. J., *Dynamic performance and control of squeeze mode MR fluid damper–rotor system*, Smart Materials and Structures 14(4):529–539, 2005.

Weber 2013
Weber F., *Bouc-Wen model based real-time force tracking scheme for MR dampers*, Smart Materials and Structures 22(4):045012, 2013.

Wen 1976
Wen Y. K., *Method for random vibration of hysteretic systems*, Journal of Engineering Mechanics 102(2):249–263, 1976.

Wereley et al. 1998
Wereley N. M., Pang L. and Kamath G. M., *Idealized hysteresis modelling of electrorheological and magnetorheological dampers*, Journal of Intelligent Material, Systems and Structures 9(8):642–649, 1998.

White 1994
White F., *Fluid Mechanics - 3rd edition*, McGraw-Hill, 1994.

Y

Yang 2001
Yang G., *Large-Scale Magnetorheological Fluid Damper for Vibration Mitigation: Modelling, Testing and Control,* PhD Thesis, Department of Civil Engineering and Geological Sciences, Notre Dame, Indiana, 2001.

Yang et al. 2008
Yang L., Duan F., Eriksson A., *Analysis of the optimal design strategy of a magnetorheological smart structure*, Smart Materials and Structures 17(1):015047, 2008.

Yi et al. 1999
Yi F., Dyke S. J. Caicedo J. M., Carlson J. D., *Seismic response control using smart dampers, Proceedings of the IEEE American Control Conference*, Vol.2, pp.1022-1026, San Diego, 23–25 June, 1999.

Yi et al. 2001
Yi F., Dyke S. J., Caicedo J. M., Carlson J. D., *Experimental verification of multi-input seismic control strategies for smart dampers*, Journal of Engineering Mechanics 127(11):1152–1164, 2001.

Yoshida 2003
Yoshida O., *Torsionally Coupled Response Control of Earthquake Excited Asymetric Buildings: Development and Application of Effective Control Systems Using Smart Dampers*, PhD Thesis, Sever Institute of Washington University, May 2003.

Yoshida & Dyke 2004
Yoshida O., Dyke S. J., *Seismic Control of a Nonlinear Benchmark Building Using Smart Dampers*, Journal of Engineering Mechanics 130(4):386-392, 2004.

Yoshida & Dyke 2005
Yoshida O., Dyke S. J., *Response Control of Full-Scale Irregular Buildings Using Magnetorheological Dampers*, Journal of Structural Engineering 131(5):734-742, 2005.

Yoshioka et al. 2002
Yoshioka H., Ramallo J. C., Spencer Jr. B. F., *"Smart" Base Isolation Strategies Employing Magnetorheological Dampers*, Journal of Engineering Mechanics 128(5):540-551, 2002.

Yoshida et al. 2003
Yoshida O., Dyke S. J., Giacosa L. M., Truman K. Z., *Experimental Verification of Torsional Response Control of Asymmetric Buildings Using MR Dampers*, Earthquake engineering & Structural Dynamics 32(13):2085-2105, 2003.

Z

Zapateiro 2009
Zapateiro M., Semi-active control strategies for vibration mitigation in adaptronic systems equipped with MR dampers, PhD thesis, Universitat de Girona, Girona, Spain, 2009.

Zapateiro et al. 2010
Zapateiro M., Karimi H. R., Luo N., Spencer Jr. B. F., *Real-time hybrid testing of semiactive control strategies for vibration reduction in a structure with MR damper*, Structural Control and Health Monitoring 17(4):427–451, 2010.

Annex

The numerical and experimental study performed and presented in Chapter 4 was very extensive and a lot of data resulted from the analysis and processing of the results. The data was compacted in a suitable way and the relevant results were presented along the chapter. In the annex is left the whole data considered in the analysis.

The following sections are found:

- A1 Results of Numerical Simulations: shows the results in terms of performance indexes for all the considered input ground motions, under the numerical simulations performed with the mathematical models;
- A2 Results of the Experimental Campaign: shows the results in terms of performance indexes for all the considered input ground motions, under the experimental test performed on the physical model;
- A3 Comparison of Experimental and Numerical Results: shows a comparison in terms of frequency response functions obtained from the results of numerical and experimental tests.

A1 Results of Numerical Simulations

This section presents the results of the numerical simulations for the 2DOF model with different configurations in terms of the evaluation criteria described in table 4.17, when subjected to several inputs.

Those correspond to the: i) the original structure (2DOF model only); ii) the structure with the MR damper in passive mode with 0 V, 1 V and 5 V of input voltage, described as Pass0, Pass1 and Pass5 respectively; iii) and the structure with the MR damper in semi-active mode, considering several strategies/algorithms, such the Decentralized Bang-Bang control – DBB, the Maximum Energy Dissipation algorithm – MED, the Modulated Homogeneous Friction – MHF, the Integral control, two Linear Quadratic Regulator controllers and the Model Predictive Control plus a Clipped On-Off algorithm, referred as ICOO, LQRCOO, LQR2COO and MPCCOO respectively. All the schemes except the LQR2COO use the SDOF model of the structural system to synthesize the controller. For the LQR2COO the 2DOF model was used.

The input ground motions considered are described in section 4.1.5. 10 type 1 and 10 type 2 artificial accelerograms of the Portuguese territory were generated, and recorded ground motions were also used: El Centro (fault normal (FN) and fault parallel (FP) components), Newhall (FN and FP components), Rinaldi (FN and FP components), Sylmar (FN and FP components), Erzinkan (North–South (NS) and East–West (EW) components), Jiji (NS and EW components) and Kobe (NS and EW components) records.

Tables A1 and A2 show the results of the original structure in terms of peak and RMS values. Tables A3 to A19 presents the results of the passive and SA cases in terms of ratios. Ratios higher than one are underlined and those values with better results than (lower than) the best passive case (Pass1) are in bold. Finally, tables 20 to 22 summarized the data in terms of the average of response ratios (Rao) for identification of the best cases for each type of input ground motion. The number of best cases have an associated suffix: 'a'-when all the cases are considered; 'b'-when the LQR2COO case is not taken in consideration; 'p'-when only the passive cases are considered. For example, the result '2p' means that two best cases for the solution are found when only the passive cases are considered. Table A23 summarizes the number of best cases for each solution. In the identification of the best cases, values with identical ratios are accounted as best cases for the respective solutions.

Type	A1				A2			
Accel.	Px_{ig} (mm)	Px_{sg} (mm)	Pa_i (m/s^2)	Pa_s (m/s^2)	Px_{ig} (mm)	Px_{sg} (mm)	Pa_i (m/s^2)	Pa_s (m/s^2)
1	47,33	3,19	0,352	0,350	44,01	2,78	0,328	0,307
2	45,97	3,31	0,386	0,371	48,48	3,40	0,443	0,380
3	49,70	3,28	0,342	0,354	46,53	4,17	0,656	0,449
4	45,80	2,77	0,316	0,310	42,88	3,06	0,387	0,336
5	44,41	2,85	0,334	0,299	44,82	3,43	0,469	0,378
6	37,76	2,57	0,307	0,279	34,70	3,29	0,509	0,358
7	42,68	2,59	0,296	0,293	42,08	3,17	0,397	0,335
8	38,18	2,74	0,328	0,300	44,58	3,76	0,533	0,396
9	41,32	2,80	0,318	0,306	50,34	3,68	0,496	0,417
10	42,27	2,75	0,272	0,306	31,50	2,24	0,251	0,244
Accel.	RMSx_{ig} (mm)	RMSx_{sg} (mm)	RMSa_i (m/s^2)	RMSa_s (m/s^2)	RMSx_{ig} (mm)	RMSx_{sg} (mm)	RMSa_i (m/s^2)	RMSa_s (m/s^2)
1	17,25	1,07	0,113	0,117	14,65	0,93	0,105	0,101
2	15,99	1,01	0,114	0,111	14,78	0,94	0,107	0,103
3	14,13	0,88	0,091	0,096	14,09	1,06	0,177	0,115
4	13,73	0,85	0,089	0,093	15,36	0,96	0,106	0,106
5	11,21	0,70	0,076	0,077	14,21	0,95	0,130	0,104
6	12,90	0,80	0,085	0,088	12,57	0,86	0,124	0,094
7	13,64	0,85	0,090	0,093	9,95	0,68	0,098	0,075
8	12,66	0,80	0,089	0,087	14,42	1,03	0,160	0,112
9	14,07	0,87	0,091	0,096	16,51	1,07	0,130	0,117
10	9,60	0,60	0,065	0,066	7,80	0,55	0,084	0,060

Table A1 - Original structure evaluation criteria with type 1 and 2 input ground motions, in numerical simulations.

Type	FN/NS				FP/EW			
quake	Px_{ig} (mm)	Px_{sg} (mm)	Pa_i (m/s^2)	Pa_s (m/s^2)	Px_{ig} (mm)	Px_{sg} (mm)	Pa_i (m/s^2)	Pa_s (m/s^2)
ElCentro	42,72	2,78	0,301	0,297	38,47	2,58	0,311	0,274
Newhall	30,11	2,06	0,205	0,223	48,88	3,44	0,451	0,372
Rinaldi	30,27	2,03	0,202	0,222	40,41	2,53	0,270	0,271
Sylmar	46,45	3,05	0,378	0,343	42,04	2,62	0,291	0,278
Erzikan	34,61	2,13	0,222	0,236	31,28	2,13	0,250	0,239
Jiji	42,79	2,67	0,285	0,287	27,79	1,75	0,177	0,191
Kobe	40,54	2,74	0,313	0,288	41,15	3,05	0,389	0,330
quake	RMSx_{ig} (mm)	RMSx_{sg} (mm)	RMSa_i (m/s^2)	RMSa_s (m/s^2)	RMSx_{ig} (mm)	RMSx_{sg} (mm)	RMSa_i (m/s^2)	RMSa_s (m/s^2)
ElCentro	9,17	0,57	0,061	0,062	11,03	0,69	0,072	0,075
Newhall	5,99	0,38	0,039	0,041	13,72	0,88	0,106	0,096
Rinaldi	7,08	0,45	0,051	0,049	11,20	0,69	0,072	0,076
Sylmar	14,54	0,90	0,097	0,099	12,21	0,75	0,078	0,083
Erzikan	8,54	0,53	0,054	0,058	9,05	0,56	0,060	0,061
Jiji	14,75	0,91	0,094	0,099	7,33	0,45	0,047	0,049
Kobe	7,57	0,51	0,065	0,056	10,93	0,71	0,087	0,078

Table A2 - Original structure evaluation criteria with earthquake records, in numerical simulations.

Accel 1	Type 1						Type 2					
Case	RPx_{ig}	RPx_{sg}	RPa_i	RPa_s	Rao	Pf/W	RPx_{ig}	RPx_{sg}	RPa_i	RPa_s	Rao	Pf/W
Pass0	0,67	**0,73**	**0,74**	**0,75**	**0,72**	0,000	0,72	**0,78**	**0,98**	**0,75**	**0,81**	0,003
Pass1	0,40	0,76	1,07	0,77	0,75	0,003	0,41	0,79	1,47	0,85	0,88	0,006
Pass5	**0,21**	1,60	2,48	1,62	1,48	0,006	**0,15**	1,82	2,84	1,81	1,66	0,027
DBB	**0,31**	1,01	1,59	1,04	0,99	0,027	**0,22**	1,01	2,68	1,04	1,24	0,027
MED	**0,21**	1,60	2,46	1,62	1,48	0,027	**0,15**	1,84	2,86	1,82	1,67	0,027
MHF	0,50	**0,75**	1,37	**0,74**	0,84	0,027	0,56	**0,68**	**1,19**	**0,75**	**0,80**	0,011
ICOO	**0,37**	**0,47**	**0,86**	**0,48**	**0,55**	0,009	**0,38**	**0,71**	**1,45**	**0,70**	**0,81**	0,012
LQRCOO	0,42	**0,50**	**0,81**	**0,53**	**0,56**	0,012	0,46	**0,77**	**1,26**	**0,83**	**0,83**	0,011
MPCCOO	**0,40**	**0,63**	**1,05**	**0,65**	**0,68**	0,011	**0,39**	**0,74**	**1,47**	**0,72**	**0,83**	0,010
LQR2COO	0,41	**0,44**	**0,54**	**0,48**	**0,47**	0,011	0,46	**0,65**	**1,33**	**0,64**	**0,77**	0,012
Case	RRx_{ig}	RRx_{sg}	RRa_i	RRa_s	Rao	RMSf/W	RRx_{ig}	RRx_{sg}	RRa_i	RRa_s	Rao	RMSf/W
Pass0	0,70	0,74	**0,79**	0,76	0,75	0,000	0,75	0,83	**0,93**	0,85	0,84	0,002
Pass1	0,39	0,66	0,94	0,69	0,67	0,002	0,43	0,77	1,23	0,80	0,81	0,004
Pass5	**0,18**	1,57	1,34	1,59	1,17	0,004	**0,17**	1,94	2,13	1,95	1,55	0,014
DBB	**0,28**	0,87	1,17	0,89	0,80	0,014	**0,28**	1,03	1,81	1,05	1,04	0,008
MED	**0,19**	1,57	1,36	1,59	1,18	0,009	**0,17**	1,94	2,16	1,95	1,55	0,014
MHF	0,49	**0,63**	0,98	**0,66**	0,69	0,014	0,54	**0,69**	**1,03**	**0,72**	**0,75**	0,003
ICOO	0,40	**0,46**	**0,65**	**0,49**	**0,50**	0,003	0,45	**0,56**	**0,86**	**0,60**	**0,62**	0,003
LQRCOO	0,42	**0,51**	**0,66**	**0,55**	**0,53**	0,003	0,47	**0,68**	**1,07**	**0,72**	**0,73**	0,003
MPCCOO	0,42	**0,51**	**0,82**	**0,54**	**0,57**	0,003	0,48	**0,64**	**1,06**	**0,67**	**0,71**	0,003
LQR2COO	0,41	**0,52**	**0,56**	**0,56**	**0,51**	0,003	0,46	**0,63**	**0,76**	**0,66**	**0,63**	0,004

Table A3 - Evaluation criteria with Accelerogram 1 under type 1 and 2 input ground motions, in numerical simulations.

Accel 2	Type 1						Type 2					
Case	RPx_{ig}	RPx_{sg}	RPa_i	RPa_s	Rao	Pf/W	RPx_{ig}	RPx_{sg}	RPa_i	RPa_s	Rao	Pf/W
Pass0	0,68	0,74	**0,84**	0,73	0,75	0,003	0,73	0,85	**0,91**	**0,84**	**0,83**	0,003
Pass1	0,52	0,64	0,91	0,68	0,69	0,006	0,48	0,84	1,24	0,84	0,85	0,007
Pass5	**0,22**	1,51	2,25	1,51	1,37	0,027	**0,35**	2,09	3,13	2,09	1,92	0,029
DBB	**0,41**	1,04	1,58	1,05	1,02	0,027	**0,31**	1,06	2,07	1,05	1,12	0,027
MED	**0,22**	1,51	2,23	1,51	1,36	0,027	**0,35**	2,09	3,12	2,09	1,91	0,029
MHF	0,57	0,78	1,22	**0,75**	0,83	0,009	0,56	**0,66**	**1,18**	**0,66**	**0,76**	0,012
ICOO	**0,45**	**0,47**	**0,91**	**0,47**	**0,57**	0,016	**0,44**	**0,59**	**1,04**	**0,57**	**0,66**	0,015
LQRCOO	**0,44**	**0,61**	**0,75**	**0,61**	**0,60**	0,013	**0,47**	**0,67**	**1,01**	**0,71**	**0,71**	0,014
MPCCOO	**0,45**	**0,58**	0,92	**0,60**	**0,64**	0,013	**0,45**	**0,59**	**1,06**	**0,63**	**0,68**	0,012
LQR2COO	**0,45**	**0,64**	**0,80**	**0,63**	**0,63**	0,013	**0,48**	**0,54**	**0,71**	**0,56**	**0,57**	0,015
Case	RRx_{ig}	RRx_{sg}	RRa_i	RRa_s	Rao	RMSf/W	RRx_{ig}	RRx_{sg}	RRa_i	RRa_s	Rao	RMSf/W
Pass0	0,79	0,83	0,87	0,85	0,84	0,002	0,85	0,94	**1,09**	0,96	**0,96**	0,002
Pass1	0,47	0,71	0,95	0,75	0,72	0,004	0,54	0,90	1,51	0,93	0,97	0,004
Pass5	**0,20**	1,70	1,39	1,72	1,25	0,015	**0,31**	2,03	2,78	2,05	1,79	0,015
DBB	**0,32**	0,93	1,20	0,95	0,85	0,009	**0,40**	1,07	1,82	1,10	1,10	0,010
MED	**0,21**	1,70	1,40	1,72	1,26	0,015	**0,31**	2,03	2,81	2,05	1,80	0,015
MHF	0,55	**0,69**	1,04	**0,72**	0,75	0,003	0,62	**0,79**	**1,28**	**0,83**	**0,88**	0,003
ICOO	**0,45**	**0,49**	**0,63**	**0,54**	**0,53**	0,003	**0,53**	**0,62**	**0,98**	**0,66**	**0,70**	0,004
LQRCOO	**0,47**	**0,55**	**0,68**	**0,60**	**0,57**	0,004	**0,53**	**0,74**	**1,22**	**0,79**	**0,82**	0,004
MPCCOO	**0,47**	**0,56**	**0,86**	**0,60**	**0,62**	0,003	0,55	**0,70**	**1,20**	**0,74**	**0,80**	0,004
LQR2COO	**0,46**	**0,56**	**0,55**	**0,61**	**0,54**	0,004	**0,53**	**0,68**	**0,80**	**0,73**	**0,69**	0,004

Table A4 - Evaluation criteria with Accelerogram 2 under type 1 and 2 ground motions, in numerical simulations.

Accel 3	Type 1						Type 2					
Case	RPx_{ig}	RPx_{sg}	RPa_i	RPa_s	Rao	Pf/W	RPx_{ig}	RPx_{sg}	RPa_i	RPa_s	Rao	Pf/W
Pass0	0,74	0,86	**1,00**	0,86	**0,87**	0,003	0,66	0,65	**0,68**	**0,67**	**0,67**	0,003
Pass1	0,57	0,84	1,42	0,84	0,92	0,007	0,54	0,64	0,87	0,67	0,68	0,007
Pass5	**0,22**	1,39	2,23	1,42	1,31	0,027	**0,24**	1,49	1,57	1,56	1,21	0,027
DBB	**0,36**	1,06	1,84	1,10	1,09	0,027	**0,35**	0,85	1,36	0,88	0,86	0,027
MED	**0,22**	1,39	2,26	1,43	1,32	0,027	**0,24**	1,49	1,55	1,56	1,21	0,027
MHF	**0,56**	0,87	1,48	0,87	0,94	0,009	0,61	0,76	0,90	0,76	0,76	0,011
ICOO	**0,53**	**0,59**	**0,95**	**0,59**	**0,66**	0,016	**0,51**	**0,46**	**0,63**	**0,47**	**0,52**	0,014
LQRCOO	**0,47**	**0,54**	**0,81**	**0,57**	**0,60**	0,012	**0,48**	**0,60**	**0,85**	**0,64**	**0,64**	0,016
MPCCOO	**0,53**	**0,79**	**1,31**	**0,78**	**0,85**	0,013	**0,52**	**0,55**	**0,69**	**0,58**	**0,58**	0,012
LQR2COO	**0,49**	**0,53**	**0,81**	**0,54**	**0,59**	0,013	**0,50**	**0,47**	**0,62**	**0,49**	**0,52**	0,014
Case	RRx_{ig}	RRx_{sg}	RRa_i	RRa_s	Rao	RMSf/W	RRx_{ig}	RRx_{sg}	RRa_i	RRa_s	Rao	RMSf/W
Pass0	0,80	0,86	**0,94**	0,88	0,87	0,002	0,92	0,88	**0,76**	0,91	0,87	0,002
Pass1	0,50	0,78	1,17	0,82	0,82	0,004	0,63	0,83	0,92	0,87	0,81	0,004
Pass5	**0,23**	1,91	1,69	1,92	1,44	0,014	**0,30**	1,77	1,68	1,80	1,39	0,015
DBB	**0,34**	1,00	1,44	1,03	0,95	0,008	**0,38**	1,02	1,22	1,06	0,92	0,010
MED	**0,23**	1,91	1,70	1,92	1,44	0,014	**0,30**	1,77	1,70	1,79	1,39	0,015
MHF	0,58	**0,70**	**1,11**	**0,73**	**0,78**	0,003	**0,73**	**0,83**	**0,91**	**0,86**	0,84	0,004
ICOO	0,51	**0,56**	**0,81**	**0,60**	**0,62**	0,003	**0,58**	**0,57**	**0,57**	**0,62**	**0,59**	0,004
LQRCOO	0,52	**0,60**	**0,77**	**0,65**	**0,63**	0,003	**0,59**	**0,73**	**0,81**	**0,77**	**0,73**	0,004
MPCCOO	0,53	**0,61**	**0,99**	**0,65**	**0,70**	0,003	**0,61**	**0,72**	**0,84**	**0,75**	**0,73**	0,004
LQR2COO	**0,50**	**0,62**	**0,67**	**0,67**	**0,62**	0,004	**0,59**	**0,67**	**0,54**	**0,71**	**0,63**	0,004

Table A5 - Evaluation criteria with Accelerogram 3 under type 1 and 2 input ground motions, in numerical simulations.

Accel 4	Type 1						Type 2					
Case	RPx_{ig}	RPx_{sg}	RPa_i	RPa_s	Rao	Pf/W	RPx_{ig}	RPx_{sg}	RPa_i	RPa_s	Rao	Pf/W
Pass0	0,69	**0,80**	**0,87**	**0,81**	0,79	0,003	0,74	**0,74**	**0,81**	**0,75**	**0,76**	0,003
Pass1	0,31	0,80	1,18	0,81	0,77	0,006	0,46	0,78	1,59	0,78	0,90	0,007
Pass5	**0,23**	1,63	2,26	1,62	1,43	0,027	**0,18**	1,87	2,87	1,87	1,70	0,027
DBB	**0,25**	1,21	1,72	1,20	1,09	0,025	**0,38**	1,15	2,32	1,20	1,26	0,027
MED	**0,23**	1,64	2,27	1,64	1,45	0,027	**0,19**	1,86	2,90	1,87	1,71	0,027
MHF	**0,43**	0,81	1,17	**0,79**	**0,80**	0,008	0,64	0,82	**1,34**	0,80	0,90	0,010
ICOO	0,39	**0,54**	**0,85**	**0,55**	**0,58**	0,012	0,49	**0,58**	**1,43**	**0,58**	**0,77**	0,013
LQRCOO	0,38	**0,51**	**0,77**	**0,52**	**0,54**	0,011	0,48	**0,72**	**1,51**	**0,74**	**0,86**	0,014
MPCCOO	**0,40**	**0,66**	0,99	**0,67**	**0,68**	0,010	0,50	**0,72**	**1,50**	**0,73**	**0,86**	0,011
LQR2COO	**0,38**	**0,46**	**0,62**	**0,45**	**0,48**	0,012	0,48	**0,55**	**1,04**	**0,61**	**0,67**	0,014
Case	RRx_{ig}	RRx_{sg}	RRa_i	RRa_s	Rao	RMSf/W	RRx_{ig}	RRx_{sg}	RRa_i	RRa_s	Rao	RMSf/W
Pass0	0,71	0,78	**0,86**	0,80	0,79	0,002	0,81	0,88	**0,99**	0,90	**0,90**	0,002
Pass1	0,39	0,72	1,06	0,76	0,73	0,004	0,52	0,84	1,45	0,87	0,92	0,004
Pass5	**0,19**	1,76	1,51	1,76	1,30	0,012	**0,15**	1,85	2,64	1,86	1,62	0,014
DBB	**0,27**	0,97	1,35	0,99	0,90	0,008	**0,32**	1,01	1,87	1,04	1,06	0,009
MED	**0,19**	1,76	1,53	1,76	1,31	0,012	**0,15**	1,84	2,67	1,85	1,63	0,014
MHF	0,50	**0,68**	1,11	0,71	0,75	0,003	0,59	**0,76**	**1,27**	**0,79**	**0,85**	0,003
ICOO	0,43	**0,50**	**0,70**	**0,54**	**0,54**	0,003	**0,49**	**0,60**	**1,03**	**0,64**	**0,69**	0,004
LQRCOO	0,44	**0,55**	**0,70**	**0,59**	**0,57**	0,003	**0,50**	**0,72**	**1,20**	**0,75**	**0,79**	0,004
MPCCOO	0,45	**0,57**	**0,94**	**0,60**	**0,64**	0,003	**0,51**	**0,67**	**1,20**	**0,70**	**0,77**	0,003
LQR2COO	0,43	**0,56**	**0,60**	**0,60**	**0,55**	0,003	**0,49**	**0,66**	**0,87**	**0,70**	**0,68**	0,004

Table A6 - Evaluation criteria with Accelerogram 4 under type 1 and 2 ground motions, in numerical simulations.

Accel 5	Type 1						Type 2					
Case	RPx_{ig}	RPx_{sg}	RPa_i	RPa_s	Rao	Pf/W	RPx_{ig}	RPx_{sg}	RPa_i	RPa_s	Rao	Pf/W
Pass0	0,71	0,75	**0,73**	0,79	0,75	0,003	0,73	0,72	**0,79**	0,72	0,74	0,003
Pass1	0,39	0,68	1,03	0,74	0,71	0,006	0,45	0,67	1,05	0,71	0,72	0,007
Pass5	**0,15**	1,55	2,00	1,65	1,34	0,027	**0,27**	1,59	2,21	1,60	1,42	0,028
DBB	**0,30**	1,03	1,60	1,07	1,00	0,027	**0,45**	0,78	2,37	0,81	1,10	0,025
MED	**0,15**	1,56	1,98	1,66	1,33	0,027	**0,27**	1,59	2,27	1,60	1,44	0,028
MHF	0,50	**0,67**	1,09	0,70	0,74	0,008	0,53	**0,66**	**1,02**	**0,68**	**0,72**	0,011
ICOO	0,42	**0,49**	**0,74**	**0,53**	**0,55**	0,011	**0,42**	**0,53**	**0,91**	**0,52**	**0,59**	0,012
LQRCOO	0,41	**0,55**	**0,88**	**0,62**	**0,61**	0,010	0,48	**0,66**	**1,00**	**0,70**	**0,71**	0,013
MPCCOO	0,44	**0,57**	**0,84**	**0,61**	**0,61**	0,010	**0,45**	**0,59**	**0,93**	**0,61**	**0,64**	0,010
LQR2COO	0,42	**0,49**	**0,78**	**0,53**	**0,55**	0,011	0,47	**0,53**	**0,69**	**0,53**	**0,56**	0,011
Case	RRx_{ig}	RRx_{sg}	RRa_i	RRa_s	Rao	RMSf/W	RRx_{ig}	RRx_{sg}	RRa_i	RRa_s	Rao	RMSf/W
Pass0	0,82	**0,89**	**0,97**	**0,92**	**0,90**	0,001	0,84	0,89	**0,90**	0,91	0,88	0,002
Pass1	0,51	0,89	1,27	0,94	0,90	0,004	0,49	0,80	1,07	0,84	0,80	0,004
Pass5	**0,21**	2,34	1,82	2,35	1,68	0,014	**0,24**	1,94	2,05	1,96	1,55	0,015
DBB	**0,43**	1,19	1,69	1,22	1,13	0,008	**0,40**	1,03	1,64	1,06	1,03	0,009
MED	**0,21**	2,33	1,84	2,34	1,68	0,014	**0,24**	1,94	2,07	1,96	1,55	0,015
MHF	0,62	**0,81**	**1,27**	**0,84**	**0,89**	0,003	0,56	**0,70**	**0,93**	**0,74**	**0,73**	0,003
ICOO	0,54	**0,61**	**0,84**	**0,66**	**0,66**	0,003	**0,49**	**0,54**	**0,69**	**0,58**	**0,57**	0,004
LQRCOO	0,54	**0,67**	**0,86**	**0,73**	**0,70**	0,003	0,50	**0,67**	**0,89**	**0,72**	**0,70**	0,004
MPCCOO	0,56	**0,67**	**1,04**	**0,71**	**0,75**	0,003	0,51	**0,61**	**0,85**	**0,64**	**0,65**	0,003
LQR2COO	0,53	**0,69**	**0,72**	**0,74**	**0,67**	0,003	0,50	**0,63**	**0,62**	**0,67**	**0,61**	0,004

Table A7 - Evaluation criteria with Accelerogram 5 under type 1 and 2 input ground motions, in numerical simulations.

Accel 6	Type 1						Type 2					
Case	RPx_{ig}	RPx_{sg}	RPa_i	RPa_s	Rao	Pf/W	RPx_{ig}	RPx_{sg}	RPa_i	RPa_s	Rao	Pf/W
Pass0	0,80	**0,79**	**0,84**	**0,82**	**0,81**	0,003	0,77	**0,72**	**0,75**	0,78	**0,76**	0,003
Pass1	0,54	0,79	1,09	0,86	0,82	0,006	0,49	0,77	1,05	0,77	0,77	0,006
Pass5	**0,19**	1,60	2,17	1,63	1,40	0,027	**0,16**	1,54	1,78	1,57	1,26	0,027
DBB	**0,29**	1,02	1,86	1,05	1,06	0,025	**0,35**	0,81	1,50	0,81	0,87	0,025
MED	**0,19**	1,61	2,17	1,64	1,40	0,027	**0,16**	1,55	1,77	1,58	1,26	0,027
MHF	0,58	**0,78**	1,23	0,87	0,87	0,008	0,54	0,79	**1,04**	0,83	0,80	0,007
ICOO	**0,49**	**0,56**	**0,79**	**0,61**	**0,61**	0,010	**0,47**	**0,42**	**0,70**	**0,45**	**0,51**	0,010
LQRCOO	**0,50**	**0,58**	**0,81**	**0,64**	**0,63**	0,010	**0,48**	**0,62**	**0,70**	**0,66**	**0,62**	0,009
MPCCOO	**0,52**	**0,63**	**0,99**	**0,70**	**0,71**	0,010	0,51	**0,58**	**0,82**	**0,61**	**0,63**	0,009
LQR2COO	**0,50**	**0,55**	**0,89**	**0,60**	**0,63**	0,011	**0,47**	**0,42**	**0,54**	**0,45**	**0,47**	0,009
Case	RRx_{ig}	RRx_{sg}	RRa_i	RRa_s	Rao	RMSf/W	RRx_{ig}	RRx_{sg}	RRa_i	RRa_s	Rao	RMSf/W
Pass0	0,72	0,78	**0,83**	0,80	0,78	0,001	0,66	**0,73**	**0,79**	**0,74**	**0,73**	0,002
Pass1	0,43	0,73	1,03	0,77	0,74	0,004	0,37	0,81	1,15	0,84	0,79	0,004
Pass5	**0,16**	1,83	1,45	1,84	1,32	0,012	**0,14**	2,00	1,78	2,02	1,48	0,013
DBB	**0,30**	0,94	1,31	0,96	0,88	0,007	**0,32**	0,97	1,34	0,99	0,91	0,007
MED	**0,17**	1,83	1,47	1,84	1,33	0,012	**0,14**	2,00	1,80	2,02	1,49	0,013
MHF	0,52	**0,65**	**0,98**	**0,68**	**0,71**	0,003	0,49	**0,65**	**0,91**	**0,67**	**0,68**	0,003
ICOO	0,45	**0,49**	**0,67**	**0,53**	**0,54**	0,003	0,43	**0,50**	**0,68**	**0,54**	**0,54**	0,003
LQRCOO	0,46	**0,55**	**0,71**	**0,60**	**0,58**	0,003	0,43	**0,64**	**0,90**	**0,67**	**0,66**	0,003
MPCCOO	0,48	**0,55**	**0,86**	**0,59**	**0,62**	0,003	0,47	**0,61**	**0,92**	**0,64**	**0,66**	0,003
LQR2COO	0,45	**0,55**	**0,60**	**0,60**	**0,55**	0,003	0,40	**0,54**	**0,56**	**0,58**	**0,52**	0,003

Table A8 - Evaluation criteria with Accelerogram 6 under type 1 and 2 ground motions, in numerical simulations.

Accel 7	Type 1						Type 2					
Case	RPx_{ig}	RPx_{sg}	RPa_i	RPa_s	Rao	Pf/W	RPx_{ig}	RPx_{sg}	RPa_i	RPa_s	Rao	Pf/W
Pass0	0,78	1,01	**1,07**	0,99	0,96	0,003	0,80	0,88	**0,93**	0,92	0,88	0,003
Pass1	0,48	0,83	1,22	0,86	0,85	0,006	0,57	0,73	1,24	0,81	0,84	0,006
Pass5	**0,19**	1,80	2,62	1,78	1,60	0,027	**0,20**	1,94	2,59	2,02	1,69	0,027
DBB	**0,32**	1,23	1,76	1,22	1,13	0,027	**0,43**	0,93	1,86	0,98	1,05	0,027
MED	**0,18**	1,80	2,60	1,78	1,59	0,027	**0,21**	1,95	2,60	2,03	1,69	0,027
MHF	0,58	1,06	1,63	1,02	1,07	0,008	0,60	0,90	**1,21**	0,94	0,91	0,010
ICOO	0,49	**0,70**	**0,78**	**0,68**	**0,66**	0,012	**0,53**	**0,59**	**0,93**	**0,65**	**0,68**	0,013
LQRCOO	0,50	**0,66**	**0,89**	**0,63**	**0,67**	0,013	**0,50**	**0,63**	**1,00**	**0,71**	**0,71**	0,012
MPCCOO	0,52	0,89	1,27	0,87	0,89	0,010	**0,55**	**0,70**	**0,96**	**0,76**	**0,74**	0,011
LQR2COO	0,49	**0,56**	**0,78**	**0,55**	**0,60**	0,013	**0,48**	**0,57**	**0,86**	**0,63**	**0,64**	0,013
Case	RRx_{ig}	RRx_{sg}	RRa_i	RRa_s	Rao	RMSf/W	RRx_{ig}	RRx_{sg}	RRa_i	RRa_s	Rao	RMSf/W
Pass0	0,75	0,81	**0,89**	0,84	0,82	0,002	0,86	**0,94**	**1,00**	**0,97**	**0,94**	0,001
Pass1	0,44	0,76	1,08	0,80	0,77	0,004	0,59	1,07	1,47	1,11	1,06	0,004
Pass5	**0,17**	1,83	1,54	1,84	1,34	0,013	**0,25**	2,73	2,56	2,75	2,07	0,014
DBB	**0,28**	0,96	1,39	0,98	0,91	0,008	**0,50**	1,34	1,86	1,38	1,27	0,008
MED	**0,18**	1,83	1,56	1,84	1,35	0,013	**0,25**	2,72	2,59	2,75	2,08	0,014
MHF	0,53	**0,71**	**1,06**	**0,74**	**0,76**	0,003	**0,70**	**0,95**	**1,30**	**0,99**	**0,99**	0,003
ICOO	0,47	**0,51**	**0,71**	**0,56**	**0,56**	0,003	0,62	**0,71**	**0,93**	**0,76**	**0,76**	0,003
LQRCOO	0,48	**0,59**	**0,76**	**0,63**	**0,61**	0,003	0,61	**0,85**	**1,12**	**0,91**	**0,87**	0,003
MPCCOO	0,49	**0,59**	**0,92**	**0,62**	**0,66**	0,003	0,64	**0,81**	**1,13**	**0,85**	**0,86**	0,003
LQR2COO	0,46	**0,60**	**0,63**	**0,64**	**0,58**	0,003	0,60	**0,82**	**0,87**	**0,87**	**0,79**	0,004

Table A9 - Evaluation criteria with Accelerogram 7 under type 1 and 2 input ground motions, in numerical simulations.

Accel 8	Type 1						Type 2					
Case	RPx_{ig}	RPx_{sg}	RPa_i	RPa_s	Rao	Pf/W	RPx_{ig}	RPx_{sg}	RPa_i	RPa_s	Rao	Pf/W
Pass0	0,67	0,73	**0,80**	0,74	0,74	0,002	0,75	0,72	**0,72**	**0,73**	0,73	0,003
Pass1	0,43	0,69	0,97	0,73	0,70	0,006	0,48	0,69	0,86	0,73	0,69	0,006
Pass5	**0,18**	1,50	1,97	1,53	1,29	0,027	**0,19**	1,46	1,91	1,52	1,27	0,027
DBB	**0,34**	1,07	1,81	1,08	1,07	0,025	**0,41**	1,12	1,47	1,18	1,05	0,027
MED	**0,18**	1,51	1,97	1,53	1,30	0,027	**0,20**	1,46	1,91	1,52	1,27	0,027
MHF	0,50	0,71	1,13	**0,73**	0,77	0,007	0,57	0,61	0,90	**0,66**	**0,69**	0,012
ICOO	**0,43**	**0,47**	**0,67**	**0,47**	**0,51**	0,011	**0,44**	**0,44**	**0,85**	**0,46**	**0,55**	0,013
LQRCOO	0,44	**0,49**	**0,64**	**0,53**	**0,53**	0,011	**0,46**	**0,57**	**0,81**	**0,60**	**0,61**	0,012
MPCCOO	0,46	**0,53**	**0,86**	**0,55**	**0,60**	0,010	**0,47**	**0,55**	**0,78**	**0,58**	**0,60**	0,010
LQR2COO	0,45	**0,46**	**0,53**	**0,47**	**0,48**	0,011	**0,46**	**0,49**	**0,64**	**0,49**	**0,52**	0,013
Case	RRx_{ig}	RRx_{sg}	RRa_i	RRa_s	Rao	RMSf/W	RRx_{ig}	RRx_{sg}	RRa_i	RRa_s	Rao	RMSf/W
Pass0	0,73	0,79	**0,84**	0,81	0,79	0,002	0,83	0,84	**0,78**	0,86	0,83	0,002
Pass1	0,40	0,73	0,99	0,76	0,72	0,004	0,52	0,76	0,90	0,79	0,74	0,004
Pass5	**0,13**	1,88	1,39	1,89	1,32	0,013	**0,23**	1,85	1,69	1,87	1,41	0,015
DBB	**0,32**	0,99	1,26	1,01	0,89	0,007	**0,43**	1,03	1,22	1,06	0,93	0,010
MED	**0,14**	1,88	1,41	1,89	1,33	0,013	**0,23**	1,85	1,71	1,87	1,41	0,015
MHF	0,52	**0,68**	1,03	**0,71**	0,74	0,003	0,63	**0,74**	**0,86**	**0,77**	0,75	0,003
ICOO	0,44	**0,50**	**0,67**	**0,54**	**0,54**	0,003	**0,52**	**0,56**	**0,66**	**0,60**	**0,59**	0,004
LQRCOO	0,46	**0,55**	**0,68**	**0,59**	**0,57**	0,003	**0,52**	**0,66**	**0,80**	**0,70**	**0,67**	0,004
MPCCOO	0,47	**0,57**	**0,88**	**0,60**	**0,63**	0,003	0,54	**0,65**	**0,83**	**0,68**	**0,67**	0,003
LQR2COO	0,44	**0,56**	**0,56**	**0,60**	**0,54**	0,003	**0,51**	**0,62**	**0,55**	**0,66**	**0,58**	0,004

Table A10 - Evaluation criteria with Accelerogram 8 under type 1 and 2 ground motions, in numerical simulations.

Accel 9	Type 1						Type 2					
Case	RPx_{ig}	RPx_{sg}	RPa_i	RPa_s	Rao	Pf/W	RPx_{ig}	RPx_{sg}	RPa_i	RPa_s	Rao	Pf/W
Pass0	0,71	0,81	**0,92**	0,84	0,82	0,003	0,69	0,80	**0,91**	0,79	0,80	0,003
Pass1	0,40	0,80	1,19	0,83	0,81	0,006	0,45	0,79	1,31	0,76	0,83	0,007
Pass5	**0,24**	1,65	2,32	1,68	1,47	0,027	**0,17**	1,66	2,20	1,62	1,41	0,027
DBB	**0,35**	1,03	2,03	1,05	1,12	0,025	**0,35**	0,98	1,92	0,97	1,05	0,027
MED	**0,24**	1,65	2,30	1,68	1,47	0,027	**0,18**	1,66	2,24	1,61	1,42	0,027
MHF	0,49	**0,73**	1,30	**0,77**	0,82	0,008	0,53	**0,73**	**1,11**	**0,75**	0,78	0,011
ICOO	**0,39**	**0,61**	**0,96**	**0,61**	**0,64**	0,011	0,49	**0,57**	**1,14**	**0,55**	**0,69**	0,014
LQRCOO	**0,39**	**0,53**	**0,86**	**0,56**	**0,59**	0,011	0,49	**0,66**	**1,11**	**0,66**	**0,73**	0,013
MPCCOO	0,41	**0,67**	1,26	**0,70**	**0,76**	0,009	0,47	**0,66**	**1,16**	**0,63**	**0,73**	0,011
LQR2COO	**0,39**	**0,49**	**0,71**	**0,51**	**0,52**	0,010	0,49	**0,54**	**0,80**	**0,53**	**0,59**	0,013
Case	RRx_{ig}	RRx_{sg}	RRa_i	RRa_s	Rao	RMSf/W	RRx_{ig}	RRx_{sg}	RRa_i	RRa_s	Rao	RMSf/W
Pass0	0,76	0,82	**0,93**	0,85	0,84	0,002	0,84	0,95	**1,15**	0,96	0,98	0,002
Pass1	0,43	0,74	1,07	0,78	0,75	0,004	0,52	0,91	1,45	0,94	0,96	0,004
Pass5	**0,22**	1,83	1,53	1,83	1,35	0,014	**0,19**	1,85	2,24	1,86	1,53	0,016
DBB	**0,31**	0,94	1,38	0,96	0,90	0,008	**0,37**	1,05	1,61	1,07	1,02	0,010
MED	**0,23**	1,82	1,55	1,83	1,36	0,014	**0,19**	1,84	2,26	1,86	1,54	0,016
MHF	0,55	**0,72**	1,17	**0,75**	0,80	0,003	0,59	**0,88**	**1,45**	**0,90**	**0,96**	0,004
ICOO	0,46	**0,53**	**0,73**	**0,57**	**0,57**	0,003	**0,51**	**0,58**	**0,86**	**0,62**	**0,65**	0,004
LQRCOO	0,47	**0,57**	**0,73**	**0,61**	**0,59**	0,003	**0,51**	**0,75**	**1,16**	**0,79**	**0,80**	0,004
MPCCOO	0,48	**0,59**	**0,96**	**0,63**	**0,67**	0,003	0,54	**0,76**	**1,31**	**0,79**	**0,85**	0,004
LQR2COO	0,45	**0,58**	**0,63**	**0,63**	**0,57**	0,003	**0,49**	**0,64**	**0,72**	**0,68**	**0,63**	0,004

Table A11 - Evaluation criteria with Accelerogram 9 under type 1 and 2 input ground motions, in numerical simulations.

Accel 10	Type 1						Type 2					
Case	RPx_{ig}	RPx_{sg}	RPa_i	RPa_s	Rao	Pf/W	RPx_{ig}	RPx_{sg}	RPa_i	RPa_s	Rao	Pf/W
Pass0	0,79	0,84	**0,84**	0,84	0,83	0,003	0,81	0,90	**0,94**	0,90	0,89	0,003
Pass1	0,47	0,69	1,24	0,70	0,77	0,006	0,49	0,84	1,68	0,86	0,97	0,006
Pass5	**0,14**	1,53	2,45	1,53	1,42	0,027	**0,15**	2,16	2,91	2,17	1,85	0,027
DBB	**0,32**	1,07	1,76	1,07	1,06	0,027	**0,40**	1,13	2,34	1,16	1,26	0,024
MED	**0,15**	1,53	2,42	1,53	1,41	0,027	**0,15**	2,17	2,93	2,17	1,85	0,027
MHF	0,51	0,73	1,43	0,74	0,85	0,008	0,61	**0,78**	**1,31**	**0,77**	**0,87**	0,008
ICOO	**0,40**	**0,49**	**0,75**	**0,48**	**0,53**	0,011	0,56	**0,59**	**1,16**	**0,62**	**0,73**	0,011
LQRCOO	**0,44**	**0,53**	**0,74**	**0,55**	**0,57**	0,011	0,53	**0,67**	**1,22**	**0,71**	**0,78**	0,010
MPCCOO	**0,42**	**0,55**	**1,17**	**0,56**	**0,67**	0,009	0,58	**0,69**	**1,09**	**0,69**	**0,76**	0,009
LQR2COO	**0,43**	**0,49**	**0,68**	**0,52**	**0,53**	0,011	0,52	**0,56**	**1,05**	**0,60**	**0,68**	0,010
Case	RRx_{ig}	RRx_{sg}	RRa_i	RRa_s	Rao	RMSf/W	RRx_{ig}	RRx_{sg}	RRa_i	RRa_s	Rao	RMSf/W
Pass0	0,76	**0,84**	**0,93**	**0,87**	**0,85**	0,001	0,83	**0,88**	**0,85**	**0,91**	**0,87**	0,001
Pass1	0,46	0,91	1,32	0,95	0,91	0,004	0,53	1,05	1,29	1,09	0,99	0,004
Pass5	**0,22**	2,53	1,80	2,54	1,77	0,013	**0,17**	2,79	2,25	2,81	2,00	0,012
DBB	**0,45**	1,24	1,67	1,26	1,15	0,007	**0,52**	1,49	1,75	1,52	1,32	0,008
MED	**0,23**	2,53	1,82	2,54	1,78	0,013	**0,17**	2,78	2,28	2,80	2,01	0,012
MHF	0,59	**0,79**	**1,29**	**0,82**	**0,87**	0,002	0,69	**0,82**	**1,04**	**0,86**	**0,85**	0,002
ICOO	0,50	**0,59**	**0,84**	**0,64**	**0,64**	0,003	0,59	**0,65**	**0,80**	**0,70**	**0,68**	0,003
LQRCOO	0,53	**0,65**	**0,82**	**0,70**	**0,68**	0,003	0,61	**0,80**	**0,97**	**0,85**	**0,81**	0,003
MPCCOO	0,52	**0,67**	**1,12**	**0,71**	**0,75**	0,002	0,61	**0,72**	**0,91**	**0,76**	**0,75**	0,002
LQR2COO	0,52	**0,67**	**0,69**	**0,72**	**0,65**	0,003	0,59	**0,76**	**0,72**	**0,81**	**0,72**	0,003

Table A12 - Evaluation criteria with Accelerogram 10 under type 1 and 2 ground motions, in numerical simulations.

El Centro	FN						FP					
Case	RPx_{ig}	RPx_{sg}	RPa_i	RPa_s	Rao	Pf/W	RPx_{ig}	RPx_{sg}	RPa_i	RPa_s	Rao	Pf/W
Pass0	0,77	0,89	**0,97**	0,89	0,88	0,003	0,82	**0,92**	**1,03**	**0,96**	0,93	0,003
Pass1	0,50	0,79	1,12	0,87	0,82	0,006	0,58	0,94	1,35	0,98	0,96	0,006
Pass5	**0,22**	1,71	2,62	1,81	1,59	0,027	**0,29**	2,05	2,87	2,16	1,84	0,027
DBB	**0,29**	1,18	1,72	1,23	1,11	0,027	**0,36**	1,12	1,36	1,17	1,00	0,025
MED	**0,22**	1,72	2,61	1,81	1,59	0,027	**0,29**	2,05	2,88	2,17	1,85	0,027
MHF	0,56	0,81	1,51	0,92	0,95	0,008	0,78	1,15	1,70	1,18	1,20	0,010
ICOO	**0,41**	**0,70**	1,38	**0,71**	**0,80**	0,013	0,66	**0,76**	**1,21**	**0,77**	**0,85**	0,017
LQRCOO	**0,47**	**0,62**	**0,88**	**0,70**	**0,67**	0,011	0,68	**0,76**	**1,04**	**0,77**	**0,81**	0,012
MPCCOO	**0,49**	**0,74**	1,41	**0,84**	0,87	0,009	0,75	0,98	1,57	0,99	1,07	0,013
LQR2COO	**0,45**	**0,54**	**0,94**	**0,59**	**0,63**	0,012	0,69	**0,72**	**0,87**	**0,75**	**0,76**	0,014
Case	RRx_{ig}	RRx_{sg}	RRa_i	RRa_s	Rao	RMSf/W	RRx_{ig}	RRx_{sg}	RRa_i	RRa_s	Rao	RMSf/W
Pass0	0,75	**0,83**	**0,95**	**0,85**	0,85	0,001	0,83	0,90	1,02	0,92	0,92	0,001
Pass1	0,42	0,85	1,20	0,88	0,84	0,003	0,50	0,88	1,34	0,92	0,91	0,003
Pass5	**0,18**	2,25	1,73	2,26	1,61	0,010	**0,20**	1,73	1,47	1,74	1,28	0,009
DBB	0,47	1,26	1,53	1,28	1,13	0,007	**0,50**	0,96	1,32	0,97	0,94	0,007
MED	**0,19**	2,25	1,75	2,26	1,61	0,010	**0,20**	1,74	1,48	1,74	1,29	0,010
MHF	0,56	**0,71**	**1,15**	**0,74**	**0,79**	0,002	0,61	**0,83**	**1,31**	**0,86**	**0,90**	0,003
ICOO	0,49	**0,57**	**0,88**	**0,61**	**0,64**	0,002	0,52	**0,59**	**0,92**	**0,63**	**0,67**	0,003
LQRCOO	0,51	**0,62**	**0,83**	**0,67**	**0,66**	0,002	0,55	**0,65**	**0,88**	**0,69**	**0,69**	0,003
MPCCOO	0,54	**0,67**	**1,12**	**0,70**	**0,76**	0,002	0,60	**0,72**	**1,19**	**0,76**	**0,82**	0,003
LQR2COO	0,49	**0,63**	**0,69**	**0,68**	**0,62**	0,003	0,53	**0,66**	**0,76**	**0,70**	**0,66**	0,003

Table A13 - Evaluation criteria with El Centro earthquake, in numerical simulations.

Newhall	FN						FP					
Case	RPx_{ig}	RPx_{sg}	RPa_i	RPa_s	Rao	Pf/W	RPx_{ig}	RPx_{sg}	RPa_i	RPa_s	Rao	Pf/W
Pass0	0,89	**1,10**	**1,29**	**1,10**	**1,09**	0,003	0,69	**0,73**	**1,03**	**0,75**	**0,80**	0,003
Pass1	0,70	1,12	1,99	1,12	1,23	0,007	0,41	0,84	1,13	0,84	0,80	0,007
Pass5	**0,57**	2,42	4,39	2,52	2,48	0,029	**0,24**	1,37	2,70	1,40	1,43	0,027
DBB	**0,68**	1,58	3,52	1,71	1,87	0,028	**0,33**	1,15	2,48	1,15	1,28	0,025
MED	**0,58**	2,44	4,37	2,54	2,48	0,029	**0,24**	1,38	2,75	1,40	1,44	0,027
MHF	0,81	1,21	2,24	1,21	1,37	0,009	0,47	**0,76**	**1,31**	**0,77**	0,83	0,012
ICOO	0,77	**0,85**	**1,56**	**0,84**	**1,00**	0,015	0,46	**0,58**	**1,23**	**0,58**	**0,71**	0,015
LQRCOO	0,72	**0,86**	**1,20**	**0,87**	**0,91**	0,014	0,42	**0,75**	**1,40**	**0,76**	0,83	0,012
MPCCOO	0,81	**0,97**	**1,76**	**0,97**	**1,13**	0,011	0,48	**0,71**	**1,20**	**0,73**	**0,78**	0,010
LQR2COO	0,73	**0,84**	**1,36**	**0,96**	**0,97**	0,013	0,42	**0,61**	1,07	**0,65**	**0,69**	0,012
Case	RRx_{ig}	RRx_{sg}	RRa_i	RRa_s	Rao	RMSf/W	RRx_{ig}	RRx_{sg}	RRa_i	RRa_s	Rao	RMSf/W
Pass0	0,99	**1,10**	**1,31**	**1,13**	**1,13**	0,001	0,79	0,85	**0,94**	0,87	0,86	0,001
Pass1	0,73	1,23	1,87	1,29	1,28	0,003	0,42	0,67	0,95	0,69	0,68	0,003
Pass5	**0,37**	2,61	2,70	2,63	2,08	0,008	**0,14**	1,34	1,40	1,35	1,05	0,009
DBB	**0,67**	1,54	2,23	1,58	1,51	0,006	**0,28**	0,79	1,19	0,81	0,77	0,006
MED	**0,39**	2,62	2,72	2,64	2,09	0,008	**0,14**	1,34	1,40	1,35	1,06	0,009
MHF	0,89	**1,16**	2,04	**1,21**	1,33	0,002	0,53	0,71	1,00	**0,73**	0,74	0,003
ICOO	0,81	**0,88**	**1,29**	**0,95**	**0,98**	0,003	**0,41**	**0,48**	**0,71**	**0,51**	**0,53**	0,003
LQRCOO	0,82	**0,98**	**1,20**	**1,06**	**1,02**	0,002	0,45	**0,59**	**0,89**	**0,62**	**0,64**	0,003
MPCCOO	0,89	**1,01**	**1,62**	**1,07**	**1,15**	0,002	0,50	**0,59**	**0,86**	**0,61**	**0,64**	0,003
LQR2COO	0,80	**1,02**	**1,08**	**1,10**	**1,00**	0,003	0,45	**0,53**	**0,58**	**0,56**	**0,53**	0,003

Table A14 - Evaluation criteria with Newhall earthquake, in numerical simulations.

Rinaldi	FN						FP					
Case	RPx_{ig}	RPx_{sg}	RPa_i	RPa_s	Rao	Pf/W	RPx_{ig}	RPx_{sg}	RPa_i	RPa_s	Rao	Pf/W
Pass0	0,88	**0,94**	**1,28**	**0,97**	**1,02**	0,003	0,71	0,78	0,85	0,83	0,79	0,003
Pass1	0,79	1,26	1,71	1,33	1,27	0,007	0,36	0,56	0,85	0,60	0,59	0,006
Pass5	**0,58**	2,42	4,48	2,52	2,50	0,029	**0,12**	1,40	2,16	1,45	1,28	0,026
DBB	**0,77**	1,71	3,42	1,82	1,93	0,028	**0,27**	1,03	1,29	1,07	0,92	0,025
MED	**0,59**	2,41	4,48	2,52	2,50	0,029	**0,12**	1,40	2,15	1,45	1,28	0,026
MHF	0,86	**1,19**	2,08	**1,26**	1,34	0,010	0,49	0,82	1,14	0,84	0,82	0,008
ICOO	0,83	**0,92**	**1,50**	**0,93**	**1,05**	0,015	**0,36**	**0,46**	**0,82**	**0,48**	**0,53**	0,011
LQRCOO	**0,79**	**0,94**	**1,32**	**1,00**	**1,01**	0,016	0,39	**0,48**	**0,74**	**0,49**	**0,53**	0,010
MPCCOO	0,86	**0,97**	1,75	**1,05**	**1,16**	0,010	0,46	0,70	0,95	0,73	**0,71**	0,009
LQR2COO	0,80	**0,92**	**1,07**	**0,97**	**0,94**	0,016	0,38	**0,43**	**0,54**	**0,44**	**0,45**	0,010
Case	RRx_{ig}	RRx_{sg}	RRa_i	RRa_s	Rao	RMSf/W	RRx_{ig}	RRx_{sg}	RRa_i	RRa_s	Rao	RMSf/W
Pass0	0,95	**1,01**	**1,01**	**1,04**	1,00	0,001	0,76	0,80	0,84	0,82	0,81	0,001
Pass1	0,68	1,01	1,18	1,06	0,98	0,003	0,33	0,58	0,79	0,61	0,58	0,003
Pass5	**0,45**	2,12	2,26	2,15	1,74	0,008	**0,14**	1,19	1,03	1,19	0,88	0,007
DBB	**0,51**	1,13	1,64	1,18	1,12	0,005	**0,25**	0,59	0,86	0,61	**0,58**	0,004
MED	**0,47**	2,11	2,27	2,13	1,74	0,008	**0,15**	1,18	1,04	1,18	0,89	0,007
MHF	0,79	**0,90**	**1,17**	**0,96**	**0,95**	0,002	0,46	0,59	0,85	0,62	0,63	0,002
ICOO	0,69	**0,76**	**0,99**	**0,82**	**0,82**	0,002	0,39	**0,42**	**0,59**	**0,45**	**0,46**	0,002
LQRCOO	0,71	**0,84**	**0,99**	**0,91**	**0,86**	0,002	0,43	**0,49**	**0,65**	**0,52**	**0,52**	0,002
MPCCOO	0,85	**0,86**	1,23	**0,92**	**0,97**	0,003	0,47	**0,50**	**0,69**	**0,53**	**0,55**	0,002
LQR2COO	0,69	**0,83**	**0,81**	**0,90**	**0,81**	0,003	0,41	**0,47**	**0,53**	**0,51**	**0,48**	0,002

Table A15 - Evaluation criteria with Rinaldi earthquake, in numerical simulations.

Sylmar	FN						FP					
Case	RPx_{ig}	RPx_{sg}	RPa_i	RPa_s	Rao	Pf/W	RPx_{ig}	RPx_{sg}	RPa_i	RPa_s	Rao	Pf/W
Pass0	0,76	**0,87**	**0,96**	**0,88**	**0,87**	0,003	0,72	0,83	**0,80**	0,86	0,80	0,003
Pass1	0,58	0,96	1,13	0,96	0,91	0,007	0,45	0,72	1,03	0,79	0,75	0,006
Pass5	**0,13**	1,49	1,58	1,47	1,17	0,026	**0,21**	1,82	2,39	1,91	1,58	0,027
DBB	**0,43**	**0,88**	1,29	0,90	**0,87**	0,027	**0,26**	1,06	1,62	1,11	1,01	0,025
MED	**0,13**	1,48	1,59	1,46	1,17	0,026	**0,22**	1,82	2,36	1,90	1,57	0,027
MHF	**0,57**	**0,90**	1,28	**0,91**	0,92	0,009	0,54	**0,82**	1,23	**0,84**	0,85	0,008
ICOO	**0,47**	**0,54**	**0,78**	**0,55**	**0,59**	0,014	**0,40**	**0,47**	**0,85**	**0,49**	**0,55**	0,012
LQRCOO	**0,51**	**0,67**	**1,00**	**0,68**	**0,72**	0,012	**0,43**	**0,54**	**0,76**	**0,55**	**0,57**	0,012
MPCCOO	**0,57**	**0,76**	**0,99**	**0,77**	**0,77**	0,010	0,47	**0,72**	**0,94**	**0,74**	**0,71**	0,009
LQR2COO	**0,49**	**0,55**	**0,61**	**0,56**	**0,55**	0,012	**0,41**	**0,49**	**0,58**	**0,51**	**0,50**	0,012
Case	RRx_{ig}	RRx_{sg}	RRa_i	RRa_s	Rao	RMSf/W	RRx_{ig}	RRx_{sg}	RRa_i	RRa_s	Rao	RMSf/W
Pass0	0,83	0,87	0,90	0,88	0,87	0,001	0,77	0,82	0,87	0,84	0,83	0,001
Pass1	0,45	0,60	0,75	0,63	0,61	0,003	0,38	0,62	0,82	0,65	0,62	0,003
Pass5	**0,08**	0,97	0,88	0,97	0,73	0,007	**0,28**	1,32	0,95	1,32	0,97	0,008
DBB	**0,26**	**0,53**	0,78	0,55	**0,53**	0,005	**0,23**	0,62	0,83	0,63	**0,58**	0,005
MED	**0,08**	0,97	0,89	0,98	0,73	0,007	**0,30**	1,32	0,97	1,32	0,98	0,008
MHF	0,46	**0,54**	**0,71**	**0,57**	**0,57**	0,003	0,49	0,65	0,96	0,68	0,70	0,002
ICOO	**0,41**	**0,39**	**0,53**	**0,43**	**0,44**	0,003	**0,37**	**0,43**	**0,57**	**0,46**	**0,46**	0,002
LQRCOO	**0,44**	**0,49**	**0,64**	**0,52**	**0,52**	0,003	0,42	**0,48**	**0,59**	**0,51**	**0,50**	0,002
MPCCOO	0,47	**0,49**	**0,72**	**0,51**	**0,55**	0,003	0,47	**0,52**	**0,71**	**0,55**	**0,56**	0,002
LQR2COO	**0,42**	**0,46**	**0,48**	**0,49**	**0,46**	0,003	0,41	**0,48**	**0,51**	**0,51**	**0,48**	0,002

Table A16 - Evaluation criteria with Sylmar earthquake, in numerical simulations.

Erzikan	NS						EW					
Case	RPx_{ig}	RPx_{sg}	RPa_i	RPa_s	Rao	Pf/W	RPx_{ig}	RPx_{sg}	RPa_i	RPa_s	Rao	Pf/W
Pass0	0,79	0,86	**0,95**	0,86	0,87	0,003	0,79	0,88	**0,89**	0,87	**0,86**	0,002
Pass1	0,53	0,80	1,10	0,84	0,82	0,006	0,47	0,84	1,61	0,81	0,93	0,006
Pass5	**0,08**	1,47	1,89	1,46	1,22	0,026	**0,15**	1,74	2,33	1,72	1,48	0,026
DBB	**0,23**	1,03	1,48	1,04	0,95	0,022	**0,32**	0,98	1,94	0,98	1,06	0,023
MED	**0,08**	1,46	1,87	1,45	1,21	0,026	**0,15**	1,73	2,30	1,71	1,47	0,026
MHF	0,56	0,89	1,50	0,93	0,97	0,007	0,67	0,95	1,64	0,95	1,05	0,008
ICOO	**0,51**	**0,65**	**0,80**	**0,68**	**0,66**	0,011	0,58	**0,61**	**0,79**	**0,60**	**0,65**	0,012
LQRCOO	**0,52**	**0,62**	**0,85**	**0,60**	**0,65**	0,009	0,61	**0,65**	**0,84**	**0,67**	**0,69**	0,010
MPCCOO	0,55	**0,71**	1,16	**0,70**	**0,78**	0,009	0,68	**0,72**	**1,02**	**0,71**	**0,78**	0,010
LQR2COO	**0,50**	**0,56**	**0,68**	**0,57**	**0,58**	0,009	0,61	**0,65**	**0,83**	**0,65**	**0,68**	0,010
Case	RRx_{ig}	RRx_{sg}	RRa_i	RRa_s	Rao	RMSf/W	RRx_{ig}	RRx_{sg}	RRa_i	RRa_s	Rao	RMSf/W
Pass0	0,82	0,87	0,91	0,89	0,87	0,001	0,69	0,75	**0,82**	0,77	0,76	0,001
Pass1	0,45	0,64	0,79	0,67	0,64	0,002	0,37	0,63	0,87	0,66	0,63	0,003
Pass5	**0,08**	0,95	0,69	0,95	0,67	0,005	**0,11**	1,38	0,94	1,39	0,95	0,007
DBB	**0,23**	**0,60**	0,76	0,61	**0,55**	0,003	**0,35**	0,65	0,89	**0,66**	0,64	0,004
MED	**0,08**	0,95	0,69	0,95	0,67	0,005	**0,11**	1,39	0,94	1,39	0,96	0,007
MHF	0,52	**0,63**	0,91	**0,66**	0,68	0,002	0,54	0,69	1,06	0,71	0,75	0,002
ICOO	0,46	**0,45**	**0,59**	**0,49**	**0,50**	0,002	0,43	**0,48**	**0,62**	**0,51**	**0,51**	0,002
LQRCOO	0,49	**0,52**	**0,63**	**0,56**	**0,55**	0,002	0,50	**0,53**	**0,65**	**0,56**	**0,56**	0,002
MPCCOO	0,53	**0,56**	**0,82**	**0,59**	**0,63**	0,002	0,53	**0,59**	**0,86**	**0,62**	0,65	0,002
LQR2COO	0,47	**0,52**	**0,56**	**0,55**	**0,53**	0,002	0,47	**0,52**	**0,58**	**0,56**	**0,53**	0,002

Table A17 - Evaluation criteria with Erzikan earthquake, in numerical simulations.

Jiji	NS						EW					
Case	RPx_{ig}	RPx_{sg}	RPa_i	RPa_s	Rao	Pf/W	RPx_{ig}	RPx_{sg}	RPa_i	RPa_s	Rao	Pf/W
Pass0	0,74	0,82	**0,82**	0,84	0,80	0,003	0,57	**0,69**	**0,74**	**0,70**	**0,68**	0,002
Pass1	0,46	0,66	1,04	0,67	0,71	0,006	0,33	0,78	1,10	0,78	0,75	0,006
Pass5	**0,04**	1,11	**0,85**	1,13	0,78	0,025	**0,07**	1,49	1,02	1,49	1,02	0,024
DBB	**0,33**	**0,63**	**1,02**	**0,66**	**0,66**	0,021	0,49	0,98	1,33	0,98	0,94	0,021
MED	**0,05**	1,12	**0,86**	1,14	0,79	0,025	**0,07**	1,50	1,03	1,50	1,02	0,024
MHF	**0,58**	0,74	1,20	0,76	0,82	0,008	**0,54**	0,82	1,35	0,81	0,88	0,006
ICOO	0,48	**0,58**	**0,72**	**0,60**	**0,60**	0,015	**0,53**	**0,65**	**0,94**	**0,67**	**0,70**	0,013
LQRCOO	0,60	**0,64**	**0,78**	**0,66**	**0,67**	0,011	**0,49**	**0,61**	**0,83**	**0,64**	**0,64**	0,008
MPCCOO	0,58	0,71	0,97	**0,72**	0,75	0,011	**0,54**	**0,67**	**0,97**	**0,70**	**0,72**	0,009
LQR2COO	0,58	**0,64**	**0,61**	**0,67**	**0,62**	0,011	**0,50**	**0,63**	**0,81**	**0,64**	**0,64**	0,008
Case	RRx_{ig}	RRx_{sg}	RRa_i	RRa_s	Rao	RMSf/W	RRx_{ig}	RRx_{sg}	RRa_i	RRa_s	Rao	RMSf/W
Pass0	0,65	0,69	0,72	0,70	0,69	0,001	0,71	0,76	**0,81**	0,79	0,77	0,001
Pass1	0,30	0,45	0,55	0,47	0,44	0,003	0,38	0,74	0,82	0,76	0,67	0,003
Pass5	**0,03**	0,58	**0,43**	0,58	**0,41**	0,005	**0,07**	1,28	**0,81**	1,28	0,86	0,005
DBB	0,34	**0,42**	0,51	**0,43**	**0,42**	0,005	0,88	0,99	0,95	1,00	0,95	0,006
MED	**0,03**	0,59	**0,43**	0,59	**0,41**	0,005	**0,07**	1,29	**0,82**	1,28	0,86	0,005
MHF	0,41	0,48	0,67	0,50	0,51	0,002	0,68	0,79	1,10	0,81	0,85	0,002
ICOO	0,38	**0,34**	**0,43**	**0,37**	**0,38**	0,003	0,73	**0,68**	**0,79**	**0,71**	0,73	0,004
LQRCOO	0,41	**0,41**	**0,47**	**0,43**	**0,43**	0,002	0,64	**0,65**	**0,74**	**0,68**	0,68	0,002
MPCCOO	0,40	**0,41**	0,58	**0,43**	**0,45**	0,003	0,72	**0,69**	0,91	**0,72**	0,76	0,003
LQR2COO	0,38	**0,39**	**0,42**	**0,41**	**0,40**	0,002	0,64	**0,65**	**0,70**	**0,68**	**0,67**	0,002

Table A18 - Evaluation criteria with Jiji earthquake, in numerical simulations.

Kobe	NS						EW					
Case	RPx_{ig}	RPx_{sg}	RPa_i	RPa_s	Rao	Pf/W	RPx_{ig}	RPx_{sg}	RPa_i	RPa_s	Rao	Pf/W
Pass0	0,85	**0,83**	**0,89**	**0,89**	**0,86**	0,003	0,76	**0,95**	**1,05**	**0,97**	**0,93**	0,003
Pass1	0,61	0,89	1,67	0,99	1,04	0,007	0,62	1,10	1,22	1,13	1,02	0,007
Pass5	**0,47**	2,41	3,79	2,61	2,32	0,030	**0,49**	2,40	2,67	2,44	2,00	0,030
DBB	**0,44**	1,28	2,66	1,45	1,46	0,028	0,65	1,39	1,96	1,49	1,37	0,029
MED	**0,47**	2,41	3,78	2,61	2,32	0,030	**0,49**	2,42	2,68	2,46	2,01	0,030
MHF	0,67	0,91	1,50	**0,96**	**1,01**	0,010	0,72	**0,91**	1,40	**0,93**	**0,99**	0,011
ICOO	**0,57**	**0,58**	**0,80**	**0,64**	**0,65**	0,013	0,65	**0,68**	**1,08**	**0,70**	**0,77**	0,015
LQRCOO	**0,60**	**0,80**	**1,28**	**0,87**	**0,89**	0,017	0,63	**0,76**	**1,07**	**0,82**	**0,82**	0,016
MPCCOO	0,68	**0,79**	**1,07**	**0,85**	**0,85**	0,011	**0,71**	**0,73**	**0,90**	**0,80**	**0,79**	0,013
LQR2COO	**0,59**	**0,70**	**0,90**	**0,82**	**0,75**	0,016	0,64	**0,82**	**1,11**	**0,93**	**0,88**	0,017
Case	RRx_{ig}	RRx_{sg}	RRa_i	RRa_s	Rao	RMSf/W	RRx_{ig}	RRx_{sg}	RRa_i	RRa_s	Rao	RMSf/W
Pass0	0,99	**1,05**	**1,02**	**1,08**	**1,03**	0,001	0,91	**1,00**	**1,06**	**1,02**	**1,00**	0,001
Pass1	0,78	1,26	1,54	1,32	1,22	0,003	0,67	1,02	1,28	1,07	1,01	0,004
Pass5	**0,59**	2,97	2,65	3,00	2,30	0,012	**0,42**	2,33	2,33	2,36	1,86	0,013
DBB	**0,51**	1,71	1,90	1,77	1,47	0,008	**0,62**	1,44	1,78	1,48	1,33	0,009
MED	**0,60**	2,97	2,66	3,01	2,31	0,012	**0,42**	2,33	2,35	2,37	1,87	0,013
MHF	0,81	**1,04**	**1,36**	**1,10**	**1,08**	0,002	0,73	**0,93**	1,31	**0,97**	**0,98**	0,003
ICOO	**0,73**	**0,82**	**0,93**	**0,89**	**0,84**	0,002	**0,62**	**0,72**	**0,90**	**0,79**	**0,76**	0,003
LQRCOO	**0,73**	**1,03**	**1,11**	**1,12**	**1,00**	0,003	**0,66**	**0,89**	**1,02**	**0,96**	**0,88**	0,004
MPCCOO	0,79	**0,87**	**1,06**	**0,93**	**0,91**	0,002	0,71	**0,82**	**1,11**	**0,86**	**0,87**	0,003
LQR2COO	**0,71**	**1,03**	**0,86**	**1,11**	**0,93**	0,003	**0,64**	**0,88**	**0,86**	**0,95**	**0,83**	0,004

Table A19 - Evaluation criteria with Kobe earthquake, in numerical simulations.

Type 1 - Peak values											
Case	Acc. 1	Acc. 2	Acc. 3	Acc. 4	Acc. 5	Acc. 6	Acc. 7	Acc. 8	Acc. 9	Acc. 10	#best
Pass0	**0,72**	0,75	**0,87**	0,79	0,75	**0,81**	0,96	0,74	0,82	0,83	3p
Pass1	0,75	0,69	0,92	0,77	0,71	0,82	0,85	0,70	0,81	0,77	7p
Pass5	1,48	1,37	1,31	1,43	1,34	1,40	1,60	1,29	1,47	1,42	
DBB	0,99	1,02	1,09	1,09	1,00	1,06	1,13	1,07	1,12	1,06	
MED	1,48	1,36	1,32	1,45	1,33	1,40	1,59	1,30	1,47	1,41	
MHF	0,84	0,83	0,94	0,80	0,74	0,87	1,07	0,77	0,82	0,85	
ICOO	**0,55**	**0,57**	**0,66**	**0,58**	**0,55**	**0,61**	**0,66**	**0,51**	**0,64**	**0,53**	4a/7b
LQRCOO	**0,56**	**0,60**	**0,60**	**0,54**	**0,61**	**0,63**	**0,67**	**0,53**	**0,59**	**0,57**	3b
MPCCOO	**0,68**	**0,64**	**0,85**	**0,68**	**0,61**	**0,71**	0,89	**0,60**	**0,76**	**0,67**	
LQR2COO	**0,47**	**0,63**	**0,59**	**0,48**	**0,55**	**0,63**	**0,60**	**0,48**	**0,52**	**0,53**	8a
Type 1 - RMS values											
Case	Acc. 1	Acc. 2	Acc. 3	Acc. 4	Acc. 5	Acc. 6	Acc. 7	Acc. 8	Acc. 9	Acc. 10	#best
Pass0	0,75	0,84	0,87	0,79	**0,90**	0,78	0,82	0,79	0,84	**0,85**	2p
Pass1	0,67	0,72	0,82	0,73	0,90	0,74	0,77	0,72	0,75	0,91	9p
Pass5	1,17	1,25	1,44	1,30	1,68	1,32	1,34	1,32	1,35	1,77	
DBB	0,80	0,85	0,95	0,90	1,13	0,88	0,91	0,89	0,90	1,15	
MED	1,18	1,26	1,44	1,31	1,68	1,33	1,35	1,33	1,36	1,78	
MHF	0,69	0,75	**0,78**	0,75	**0,89**	**0,71**	**0,76**	0,74	0,80	**0,87**	
ICOO	**0,50**	**0,53**	**0,62**	**0,54**	**0,66**	**0,54**	**0,56**	**0,54**	**0,57**	**0,64**	10a/10b
LQRCOO	**0,53**	**0,57**	**0,63**	**0,57**	**0,70**	**0,58**	**0,61**	**0,57**	**0,59**	**0,68**	
MPCCOO	**0,57**	**0,62**	**0,70**	**0,64**	**0,75**	**0,62**	**0,66**	**0,63**	**0,67**	**0,75**	
LQR2COO	**0,51**	**0,54**	**0,62**	**0,55**	**0,67**	**0,55**	**0,58**	**0,54**	**0,57**	**0,65**	3a

Table A20 - Summary of average ratios (Rao) and number of best cases (#best) under type 1 seismic actions, in numerical simulations.

Type 2 - Peak values											
Case	Acc. 1	Acc. 2	Acc. 3	Acc. 4	Acc. 5	Acc. 6	Acc. 7	Acc. 8	Acc. 9	Acc. 10	#best
Pass0	**0,81**	**0,83**	**0,67**	**0,76**	0,74	**0,76**	0,88	0,73	0,80	0,89	5p
Pass1	0,88	0,85	0,68	0,90	0,72	0,77	0,84	0,69	0,83	0,97	5p
Pass5	1,66	1,92	1,21	1,70	1,42	1,26	1,69	1,27	1,41	1,85	
DBB	1,24	1,12	0,86	1,26	1,10	0,87	1,05	1,05	1,05	1,26	
MED	1,67	1,91	1,21	1,71	1,44	1,26	1,69	1,27	1,42	1,85	
MHF	**0,80**	**0,76**	0,76	0,90	**0,72**	0,80	0,91	**0,69**	0,78	**0,87**	
ICOO	**0,81**	**0,66**	**0,52**	**0,77**	**0,59**	**0,51**	**0,68**	**0,55**	**0,69**	**0,73**	1a/10b
LQRCOO	**0,83**	**0,71**	**0,64**	**0,86**	**0,71**	**0,62**	**0,71**	**0,61**	**0,73**	**0,78**	
MPCCOO	**0,83**	**0,68**	**0,58**	**0,86**	**0,64**	**0,63**	**0,74**	**0,60**	**0,73**	**0,76**	
LQR2COO	**0,77**	**0,57**	**0,52**	**0,67**	**0,56**	**0,47**	**0,64**	**0,52**	**0,59**	**0,68**	10a
Type 2 - RMS values											
Case	Acc. 1	Acc. 2	Acc. 3	Acc. 4	Acc. 5	Acc. 6	Acc. 7	Acc. 8	Acc. 9	Acc. 10	#best
Pass0	0,84	**0,96**	0,87	**0,90**	0,88	**0,73**	**0,94**	0,83	0,98	**0,87**	5p
Pass1	0,81	0,97	0,81	0,92	0,80	0,79	1,06	0,74	0,96	0,99	5p
Pass5	1,55	1,79	1,39	1,62	1,55	1,48	2,07	1,41	1,53	2,00	
DBB	1,04	1,10	0,92	1,06	1,03	0,91	1,27	0,93	1,02	1,32	
MED	1,55	1,80	1,39	1,63	1,55	1,49	2,08	1,41	1,54	2,01	
MHF	**0,75**	**0,88**	0,84	**0,85**	**0,73**	**0,68**	**0,99**	0,75	**0,96**	**0,85**	
ICOO	**0,62**	**0,70**	**0,59**	**0,69**	**0,57**	**0,54**	**0,76**	**0,59**	**0,65**	**0,68**	5a/10b
LQRCOO	**0,73**	**0,82**	**0,73**	**0,79**	**0,70**	**0,66**	**0,87**	**0,67**	**0,80**	**0,81**	
MPCCOO	**0,71**	**0,80**	**0,73**	**0,77**	**0,65**	**0,66**	**0,86**	**0,67**	**0,85**	**0,75**	
LQR2COO	**0,63**	**0,69**	**0,63**	**0,68**	**0,61**	**0,52**	**0,79**	**0,58**	**0,63**	**0,72**	5a

Table A21 - Summary of average ratios (Rao) and number of best cases (#best) under type 2 seismic actions, in numerical simulations.

Peak val.	El Centro		Newhall		Rinaldi		Sylmar		Erzikan		Jiji		Kobe		
Case	FN	FP	FN	FP	FN	FP	FN	FP	NS	EW	NS	EW	NS	EW	#best
Pass0	0,88	0,93	**1,09**	**0,80**	**1,02**	0,79	**0,87**	0,80	0,87	**0,86**	0,80	**0,68**	**0,86**	**0,93**	8p
Pass1	0,82	0,96	1,23	0,80	1,27	0,59	0,91	0,75	0,82	0,93	0,71	0,75	1,04	1,02	6p
Pass5	1,59	1,84	2,48	1,43	2,50	1,28	1,17	1,58	1,22	1,48	0,78	1,02	2,32	2,00	
DBB	1,11	1,00	1,87	1,28	1,93	0,92	**0,87**	1,01	0,95	1,06	**0,66**	0,94	1,46	1,37	
MED	1,59	1,85	2,48	1,44	2,50	1,28	1,17	1,57	1,21	1,47	0,79	1,02	2,32	2,01	
MHF	0,95	1,20	1,37	0,83	1,34	0,82	0,92	0,85	0,97	1,05	0,82	0,88	**1,01**	**0,99**	
ICOO	**0,80**	**0,85**	**1,00**	**0,71**	**1,05**	**0,53**	**0,59**	**0,55**	**0,66**	**0,65**	**0,60**	**0,70**	**0,65**	**0,77**	3a/8b
LQRCOO	**0,67**	**0,81**	**0,91**	0,83	**1,01**	**0,53**	**0,72**	**0,57**	**0,65**	**0,69**	**0,67**	**0,64**	**0,89**	**0,82**	2a/7b
MPCCOO	0,87	1,07	**1,13**	**0,78**	**1,16**	**0,71**	**0,77**	**0,71**	**0,78**	**0,78**	0,75	**0,72**	**0,85**	**0,79**	
LQR2COO	**0,63**	**0,76**	**0,97**	**0,69**	**0,94**	**0,45**	**0,55**	**0,50**	**0,58**	**0,68**	**0,62**	**0,64**	**0,75**	**0,88**	9a
RMS val.	El Centro		Newhall		Rinaldi		Sylmar		Erzikan		Jiji		Kobe		
Case	FN	FP	FN	FP	FN	FP	FN	FP	NS	EW	NS	EW	NS	EW	#best
Pass0	0,85	0,92	**1,13**	0,86	1,00	0,81	0,87	0,83	0,87	0,76	0,69	0,77	**1,03**	**1,00**	3p
Pass1	0,84	0,91	1,28	0,68	0,98	0,58	0,61	0,62	0,64	0,63	0,44	0,67	1,22	1,01	11p/1b
Pass5	1,61	1,28	2,08	1,05	1,74	0,88	0,73	0,97	0,67	0,95	**0,41**	0,86	2,30	1,86	
DBB	1,13	0,94	1,51	0,77	1,12	**0,58**	**0,53**	**0,58**	**0,55**	0,64	**0,42**	0,95	1,47	1,33	
MED	1,61	1,29	2,09	1,06	1,74	0,89	0,73	0,98	0,67	0,96	**0,41**	0,86	2,31	1,87	
MHF	**0,79**	**0,90**	1,33	0,74	**0,95**	0,63	**0,57**	0,70	0,68	0,75	0,51	0,85	**1,08**	**0,98**	
ICOO	**0,64**	**0,67**	**0,98**	**0,53**	**0,82**	**0,46**	**0,44**	**0,46**	**0,50**	**0,51**	**0,38**	0,73	**0,84**	**0,76**	10a/13b
LQRCOO	**0,66**	**0,69**	**1,02**	**0,64**	**0,86**	**0,52**	**0,52**	**0,50**	**0,55**	**0,56**	**0,43**	0,68	**1,00**	**0,88**	
MPCCOO	**0,76**	**0,82**	**1,15**	**0,64**	**0,97**	**0,55**	**0,55**	**0,56**	**0,63**	0,65	**0,45**	0,76	**0,91**	**0,87**	
LQR2COO	**0,62**	**0,66**	**1,00**	**0,53**	**0,81**	**0,48**	**0,46**	**0,48**	**0,53**	**0,53**	**0,40**	**0,67**	**0,93**	**0,83**	5a

Table A22 - Summary of average ratios (Rao) and number of best cases (#best) under earthquake records, in numerical simulations.

Peak values					
Case	Type 1	Type 2	Type 1&2	Earthquakes	All
Pass0	3p	5p	8p	8p	16p
Pass1	7p	5p	12p	6p	18p
Pass5					
DBB					
MED					
MHF					
ICOO	4a/7b	1a/10b	5a/17b	3a/8b	8a/25b
LQRCOO	3b		3b	2a/7b	2a/10b
MPCCOO					
LQR2COO	8a	10a	18a	9a	27a
RMS values					
Case	Type 1	Type 2	Type 1&2	Earthquakes	All
Pass0	2p	5p	7p	3p	10p
Pass1	9p	5p	14p	11p/1b	25p/1b
Pass5					
DBB					
MED					
MHF					
ICOO	10a/10b	5a/10b	15a/20b	10a/13b	25a/33b
LQRCOO					
MPCCOO					
LQR2COO	3a	5a	8a	5a	13a

Table A23 - Number of best cases (#best) for each solution, in numerical simulations.

A2 Results of the Experimental Campaign

This section presents the results of the experimental trials for the 2DOF model with different configurations in terms of the evaluation criteria described in table 4.17, when subjected to several inputs.

Those correspond to the: i) the original structure (2DOF model only); ii) the structure with the MR damper in passive mode with 0 V, 1 V and 5 V of input voltage, described as Pass0, Pass1 and Pass5 respectively; iii) and the structure with the MR damper in semi-active mode, considering several strategies/algorithms, such the Decentralized Bang-Bang control – DBB, the Maximum Energy Dissipation algorithm – MED, the Modulated Homogeneous Friction – MHF, the Integral control, two Linear Quadratic Regulator controllers and the Model Predictive Control plus a Clipped On-Off algorithm, referred as ICOO, LQRCOO, LQR2COO and MPCCOO respectively. All the schemes except the LQR2COO use the SDOF model of the structural system to synthesize the controller. For the LQR2COO the 2DOF model was used.

The input ground motions considered are described in section 4.1.5. 10 type 1 and 10 type 2 artificial accelerograms of the Portuguese territory were generated, and recorded ground motions were also used: El Centro (fault normal (FN) and fault parallel (FP) components), Newhall (FN and FP components), Rinaldi (FN and FP components), Sylmar (FN and FP components), Erzinkan (North–South (NS) and East–West (EW) components), Jiji (NS and EW components) and Kobe (NS and EW components) records.

Tables A24 and A25 show the results for the original structure in terms of peak and RMS values. Tables A26 to A42 presents the results of the passive and SA cases in terms of ratios. Ratios higher than one are underlined and those values with better results than (lower than) the best passive case (Pass1) are in bold. Finally, tables 43 to 45 summarize the data in terms of the average of the response ratios (Rao) for identification of the best cases for each type of input ground motion. The number of best cases have an associated suffix: 'a'-when all the cases are considered; 'b'-when the LQR2COO case is not taken in consideration; 'p'-when only the passive cases are considered. For example, the result '2p' means that two best cases for the solution are found when only the passive cases are considered. Table A46 summarizes the number of best cases for each solution. In the identification of the best cases, values with identical ratios are accounted as best cases for the respective solutions.

Type	A1				A2			
Accel.	Px_{ig} (mm)	Px_{sg} (mm)	Pa_i (m/s^2)	Pa_s (m/s^2)	Px_{ig} (mm)	Px_{sg} (mm)	Pa_i (m/s^2)	Pa_s (m/s^2)
1	63,44	4,02	0,511	0,439	47,17	3,66	0,534	0,391
2	58,21	3,92	0,544	0,423	48,68	3,43	0,505	0,385
3	51,06	3,41	0,460	0,375	53,28	4,99	0,822	0,554
4	48,48	3,15	0,361	0,362	51,51	3,86	0,498	0,420
5	47,40	3,01	0,393	0,355	49,06	3,06	0,389	0,362
6	40,49	3,10	0,432	0,344	32,98	3,06	0,515	0,326
7	45,23	3,42	0,481	0,352	41,33	2,73	0,429	0,306
8	49,79	3,53	0,504	0,424	41,16	3,67	0,535	0,406
9	41,58	2,72	0,346	0,321	52,20	3,49	0,533	0,406
10	40,94	2,52	0,282	0,288	30,64	2,67	0,371	0,299
Accel.	RMSx_{ig} (mm)	RMSx_{sg} (mm)	RMSa_i (m/s^2)	RMSa_s (m/s^2)	RMSx_{ig} (mm)	RMSx_{sg} (mm)	RMSa_i (m/s^2)	RMSa_s (m/s^2)
1	25,16	1,49	0,163	0,164	15,48	0,98	0,139	0,114
2	20,46	1,24	0,149	0,140	15,68	0,98	0,130	0,112
3	15,72	0,95	0,117	0,111	16,37	1,24	0,225	0,139
4	17,51	1,04	0,121	0,121	18,05	1,09	0,134	0,125
5	12,65	0,75	0,094	0,091	15,46	0,94	0,117	0,109
6	14,50	0,87	0,114	0,106	8,79	0,64	0,121	0,079
7	17,18	1,02	0,122	0,119	10,48	0,66	0,096	0,080
8	15,90	0,98	0,129	0,115	15,14	1,04	0,169	0,120
9	15,72	0,93	0,111	0,111	17,22	1,08	0,143	0,123
10	8,23	0,49	0,066	0,064	7,12	0,48	0,081	0,061

Table A24 - Original structure evaluation criteria with type 1 and 2 input ground motions, in experimental trials.

Type	FN/NS				FP/EW			
quake	Px_{ig} (mm)	Px_{sg} (mm)	Pa_i (m/s^2)	Pa_s (m/s^2)	Px_{ig} (mm)	Px_{sg} (mm)	Pa_i (m/s^2)	Pa_s (m/s^2)
ElCentro	39,75	2,37	0,295	0,266	37,70	2,69	0,432	0,310
Newhall	31,78	2,64	0,410	0,307	48,73	3,74	0,563	0,391
Rinaldi	30,83	1,92	0,235	0,240	39,14	2,56	0,329	0,282
Sylmar	54,43	3,40	0,434	0,383	39,04	2,53	0,300	0,274
Erzikan	35,95	2,94	0,396	0,318	29,45	2,57	0,385	0,294
Jiji	58,15	3,79	0,418	0,398	19,72	1,61	0,272	0,214
Kobe	38,06	3,17	0,397	0,331	40,74	3,25	0,477	0,345
quake	RMSx_{ig} (mm)	RMSx_{sg} (mm)	RMSa_i (m/s^2)	RMSa_s (m/s^2)	RMSx_{ig} (mm)	RMSx_{sg} (mm)	RMSa_i (m/s^2)	RMSa_s (m/s^2)
ElCentro	8,70	0,51	0,065	0,065	11,84	0,74	0,110	0,092
Newhall	6,74	0,49	0,086	0,060	14,11	0,92	0,129	0,104
Rinaldi	7,51	0,46	0,061	0,059	12,51	0,75	0,088	0,089
Sylmar	17,23	1,05	0,115	0,115	10,52	0,63	0,074	0,075
Erzikan	10,80	0,66	0,084	0,078	6,99	0,46	0,071	0,057
Jiji	20,32	1,23	0,133	0,135	5,49	0,33	0,050	0,047
Kobe	7,78	0,51	0,076	0,063	9,40	0,63	0,095	0,075

Table A25 - Original structure evaluation criteria with earthquake records, in experimental trials.

Accel 1	Type 1						Type 2					
Case	RPx_{ig}	RPx_{sg}	RPa_i	RPa_s	Rao	Pf/W	RPx_{ig}	RPx_{sg}	RPa_i	RPa_s	Rao	Pf/W
Pass0	0,42	**0,62**	**0,71**	**0,71**	**0,62**	0,004	0,65	**0,55**	**0,68**	**0,62**	**0,63**	0,003
Pass1	0,31	0,66	0,90	0,70	0,64	0,009	0,33	0,59	1,02	0,70	0,66	0,005
Pass5	**0,12**	1,28	1,30	1,43	1,03	0,031	**0,13**	1,44	1,81	1,62	1,25	0,031
DBB	**0,18**	0,91	1,13	0,96	0,79	0,030	**0,20**	0,82	1,73	0,83	0,90	0,028
MED	**0,18**	1,17	1,36	1,24	0,99	0,031	**0,13**	1,39	2,11	1,56	1,30	0,033
MHF	0,37	**0,65**	**0,84**	0,71	**0,64**	0,006	0,47	**0,56**	**0,70**	0,74	**0,61**	0,004
ICOO	**0,30**	**0,44**	**0,64**	**0,49**	**0,47**	0,012	**0,33**	**0,52**	**0,87**	**0,56**	**0,57**	0,014
LQRCOO	**0,28**	**0,41**	**0,53**	**0,48**	**0,42**	0,009	0,37	0,61	**0,81**	0,79	**0,65**	0,010
MPCCOO	**0,30**	**0,53**	0,92	**0,66**	**0,60**	0,009	0,38	**0,49**	**0,61**	**0,58**	**0,51**	0,005
LQR2COO	**0,26**	**0,34**	**0,59**	**0,47**	**0,41**	0,011	**0,31**	**0,40**	**0,73**	**0,56**	**0,50**	0,010
Case	RRx_{ig}	RRx_{sg}	RRa_i	RRa_s	Rao	RMSf/W	RRx_{ig}	RRx_{sg}	RRa_i	RRa_s	Rao	RMSf/W
Pass0	0,41	0,46	**0,63**	0,56	0,52	0,002	0,62	0,66	**0,69**	0,73	0,67	0,001
Pass1	0,22	0,42	0,68	0,53	0,46	0,003	0,34	0,62	0,88	0,72	0,64	0,002
Pass5	**0,09**	1,16	0,98	1,26	0,87	0,014	**0,12**	1,76	1,65	1,80	1,33	0,013
DBB	**0,15**	0,61	0,78	0,67	0,55	0,009	**0,24**	0,98	1,33	1,02	0,89	0,009
MED	**0,13**	0,94	0,86	1,01	0,73	0,012	**0,15**	1,51	1,53	1,54	1,18	0,012
MHF	0,27	**0,37**	**0,64**	**0,46**	**0,44**	0,002	**0,42**	**0,53**	**0,72**	**0,62**	**0,57**	0,002
ICOO	**0,21**	**0,29**	**0,49**	**0,39**	**0,34**	0,003	**0,34**	**0,48**	**0,72**	**0,59**	**0,53**	0,003
LQRCOO	**0,21**	**0,28**	**0,44**	**0,39**	**0,33**	0,002	0,35	**0,57**	**0,83**	**0,68**	**0,61**	0,003
MPCCOO	**0,22**	**0,33**	**0,60**	**0,43**	**0,39**	0,003	0,41	**0,49**	**0,64**	**0,60**	**0,54**	0,002
LQR2COO	**0,21**	**0,34**	**0,44**	**0,47**	**0,37**	0,004	**0,31**	**0,49**	**0,58**	**0,62**	**0,50**	0,003

Table A26 - Evaluation criteria with Accelerogram 1 under type 1 and 2 input ground motions, in experimental trials.

Accel 2	Type 1						Type 2					
Case	RPx_{ig}	RPx_{sg}	RPa_i	RPa_s	Rao	Pf/W	RPx_{ig}	RPx_{sg}	RPa_i	RPa_s	Rao	Pf/W
Pass0	0,54	0,72	0,93	0,78	0,74	0,004	0,67	**0,74**	**0,89**	**0,75**	**0,76**	0,004
Pass1	0,39	0,59	0,76	0,65	0,60	0,014	0,53	0,99	1,21	1,03	0,94	0,012
Pass5	**0,16**	1,40	1,53	1,56	1,16	0,032	**0,35**	2,26	2,64	2,37	1,91	0,037
DBB	**0,26**	1,02	1,13	1,09	0,88	0,033	**0,31**	1,06	1,87	1,07	1,08	0,034
MED	**0,15**	1,31	1,38	1,43	1,07	0,032	**0,34**	2,08	2,51	2,21	1,79	0,036
MHF	0,42	**0,57**	0,84	**0,65**	0,62	0,004	0,55	**0,83**	**1,09**	**0,89**	**0,84**	0,006
ICOO	**0,36**	**0,45**	**0,66**	**0,53**	**0,50**	0,016	**0,42**	**0,62**	**0,99**	**0,65**	**0,67**	0,016
LQRCOO	**0,32**	**0,53**	**0,57**	**0,59**	**0,50**	0,010	**0,44**	**0,77**	**1,17**	**0,76**	**0,78**	0,013
MPCCOO	0,42	**0,54**	0,85	**0,60**	**0,60**	0,013	**0,45**	**0,71**	**1,09**	**0,77**	**0,75**	0,011
LQR2COO	**0,32**	**0,56**	**0,50**	**0,59**	**0,49**	0,012	**0,47**	**0,54**	**0,76**	**0,67**	**0,61**	0,016
Case	RRx_{ig}	RRx_{sg}	RRa_i	RRa_s	Rao	RMSf/W	RRx_{ig}	RRx_{sg}	RRa_i	RRa_s	Rao	RMSf/W
Pass0	0,62	0,68	0,79	0,74	0,71	0,002	0,74	**0,80**	**0,88**	**0,86**	**0,82**	0,001
Pass1	0,34	0,53	0,74	0,65	0,57	0,004	0,47	0,81	1,26	0,89	0,86	0,004
Pass5	**0,13**	1,37	1,13	1,45	1,02	0,014	**0,26**	1,84	2,25	1,88	1,56	0,014
DBB	**0,23**	0,84	0,96	0,88	0,73	0,010	**0,31**	1,05	1,42	1,09	0,97	0,009
MED	**0,13**	1,29	1,09	1,38	0,97	0,014	**0,26**	1,74	2,12	1,79	1,47	0,014
MHF	0,41	**0,52**	0,77	**0,63**	0,58	0,002	0,50	**0,71**	**1,08**	**0,81**	**0,78**	0,002
ICOO	**0,29**	**0,36**	**0,54**	**0,46**	**0,41**	0,003	**0,42**	**0,57**	**0,89**	**0,68**	**0,64**	0,004
LQRCOO	**0,32**	**0,43**	**0,60**	**0,55**	**0,47**	0,003	**0,43**	**0,68**	**1,09**	**0,78**	**0,74**	0,003
MPCCOO	**0,32**	**0,42**	**0,68**	**0,52**	**0,48**	0,003	**0,43**	**0,60**	**0,98**	**0,70**	**0,68**	0,003
LQR2COO	**0,30**	**0,45**	**0,50**	**0,58**	**0,45**	0,004	**0,42**	**0,64**	**0,79**	**0,77**	**0,65**	0,004

Table A27 - Evaluation criteria with Accelerogram 2 under type 1 and 2 ground motions, in experimental trials.

Accel 3	Type 1						Type 2					
Case	RPx_{ig}	RPx_{sg}	RPa_i	RPa_s	Rao	Pf/W	RPx_{ig}	RPx_{sg}	RPa_i	RPa_s	Rao	Pf/W
Pass0	0,67	0,83	**0,90**	**0,84**	**0,81**	0,004	0,58	**0,54**	**0,55**	**0,56**	**0,56**	0,004
Pass1	0,55	0,77	1,12	0,87	0,83	0,007	0,48	0,55	0,75	0,62	0,60	0,013
Pass5	**0,18**	1,48	1,45	1,57	1,17	0,032	**0,15**	1,43	1,34	1,47	1,10	0,035
DBB	**0,29**	1,10	1,26	1,14	0,95	0,029	**0,26**	0,88	0,98	0,92	0,76	0,031
MED	**0,17**	1,33	1,55	1,48	1,13	0,034	**0,15**	1,36	1,33	1,42	1,06	0,034
MHF	0,58	0,93	1,37	0,94	0,96	0,006	0,56	0,65	**0,72**	0,65	0,64	0,007
ICOO	**0,54**	**0,59**	**0,75**	**0,70**	**0,64**	0,016	**0,44**	**0,43**	**0,52**	**0,52**	**0,48**	0,015
LQRCOO	**0,48**	**0,53**	**0,64**	**0,60**	**0,56**	0,011	**0,43**	**0,52**	**0,73**	**0,55**	**0,56**	0,014
MPCCOO	0,57	**0,75**	**0,94**	**0,82**	**0,77**	0,006	**0,48**	**0,46**	**0,62**	**0,54**	**0,53**	0,011
LQR2COO	**0,48**	**0,53**	**0,56**	**0,65**	**0,55**	0,015	**0,44**	**0,39**	**0,53**	**0,48**	**0,46**	0,014
Case	RRx_{ig}	RRx_{sg}	RRa_i	RRa_s	Rao	RMSf/W	RRx_{ig}	RRx_{sg}	RRa_i	RRa_s	Rao	RMSf/W
Pass0	0,72	0,79	**0,89**	0,86	0,81	0,001	0,71	0,66	0,56	0,73	0,66	0,001
Pass1	0,41	0,68	0,98	0,80	0,72	0,002	0,48	0,61	0,67	0,72	0,62	0,004
Pass5	**0,16**	1,75	1,36	1,80	1,27	0,014	**0,18**	1,52	1,38	1,59	1,16	0,014
DBB	**0,26**	1,02	1,17	1,05	0,87	0,009	**0,26**	0,85	0,91	0,90	0,73	0,010
MED	**0,20**	1,56	1,34	1,60	1,18	0,013	**0,16**	1,37	1,23	1,46	1,06	0,014
MHF	0,50	**0,63**	1,00	**0,73**	**0,71**	0,002	0,57	0,64	0,70	**0,72**	0,66	0,002
ICOO	0,43	**0,51**	**0,74**	**0,63**	**0,58**	0,004	**0,45**	**0,51**	**0,57**	**0,62**	**0,54**	0,004
LQRCOO	0,42	**0,53**	**0,70**	**0,67**	**0,58**	0,003	**0,43**	**0,58**	**0,66**	**0,67**	**0,58**	0,003
MPCCOO	0,49	**0,59**	**0,87**	**0,71**	**0,66**	0,002	**0,45**	**0,54**	**0,64**	**0,64**	**0,57**	0,003
LQR2COO	**0,40**	**0,59**	**0,64**	**0,74**	**0,59**	0,004	**0,41**	**0,54**	**0,47**	**0,67**	**0,52**	0,004

Table A28 - Evaluation criteria with Accelerogram 3 under type 1 and 2 input ground motions, in experimental trials.

Accel 4	Type 1						Type 2					
Case	RPx_{ig}	RPx_{sg}	RPa_i	RPa_s	Rao	Pf/W	RPx_{ig}	RPx_{sg}	RPa_i	RPa_s	Rao	Pf/W
Pass0	0,56	**0,79**	**0,95**	**0,83**	**0,78**	0,004	0,58	**0,65**	**0,78**	**0,72**	**0,68**	0,003
Pass1	0,32	0,82	1,24	0,84	0,81	0,005	0,39	0,67	1,20	0,76	0,75	0,006
Pass5	**0,17**	1,62	1,59	1,72	1,28	0,031	**0,15**	1,64	2,43	1,76	1,49	0,034
DBB	**0,19**	1,09	1,34	1,10	0,93	0,029	**0,32**	1,11	1,71	1,23	1,09	0,030
MED	**0,14**	1,56	1,66	1,65	1,25	0,032	**0,16**	1,56	2,24	1,69	1,41	0,036
MHF	0,43	**0,60**	**1,05**	**0,67**	**0,69**	0,005	0,44	0,69	**1,16**	**0,70**	**0,75**	0,004
ICOO	0,35	**0,46**	**0,71**	**0,49**	**0,50**	0,011	**0,38**	**0,46**	**1,05**	**0,53**	**0,61**	0,013
LQRCOO	**0,31**	**0,56**	**0,80**	**0,58**	**0,56**	0,010	**0,35**	**0,58**	**1,04**	**0,68**	**0,66**	0,014
MPCCOO	0,36	**0,60**	**0,89**	**0,63**	**0,62**	0,004	**0,39**	**0,61**	**1,05**	**0,69**	**0,68**	0,009
LQR2COO	**0,30**	**0,47**	**0,74**	**0,59**	**0,53**	0,012	**0,37**	**0,52**	**0,94**	**0,67**	**0,63**	0,015
Case	RRx_{ig}	RRx_{sg}	RRa_i	RRa_s	Rao	RMSf/W	RRx_{ig}	RRx_{sg}	RRa_i	RRa_s	Rao	RMSf/W
Pass0	0,48	**0,54**	**0,69**	**0,64**	0,59	0,002	0,64	0,69	**0,79**	0,76	0,72	0,001
Pass1	0,27	0,54	0,84	0,68	0,58	0,002	0,35	0,62	1,02	0,70	0,67	0,002
Pass5	**0,11**	1,45	1,19	1,47	1,05	0,012	**0,10**	1,62	2,13	1,67	1,38	0,013
DBB	**0,17**	0,85	1,03	0,88	0,73	0,008	**0,24**	0,90	1,35	0,96	0,86	0,009
MED	**0,10**	1,27	1,14	1,31	0,95	0,011	**0,11**	1,53	2,04	1,60	1,32	0,013
MHF	0,34	**0,47**	**0,81**	**0,60**	**0,55**	0,001	0,45	**0,58**	**0,93**	**0,68**	**0,66**	0,002
ICOO	0,28	**0,38**	**0,62**	**0,51**	**0,45**	0,003	**0,34**	**0,47**	**0,83**	**0,58**	**0,55**	0,004
LQRCOO	0,28	**0,41**	**0,61**	**0,57**	**0,47**	0,002	**0,33**	**0,55**	**0,92**	**0,65**	**0,61**	0,003
MPCCOO	0,34	**0,44**	**0,76**	**0,59**	**0,53**	0,002	**0,31**	**0,47**	**0,84**	**0,55**	**0,54**	0,003
LQR2COO	**0,26**	**0,45**	**0,58**	**0,62**	**0,48**	0,003	**0,29**	**0,48**	**0,65**	**0,59**	**0,50**	0,003

Table A29 - Evaluation criteria with Accelerogram 4 under type 1 and 2 ground motions, in experimental trials.

Accel 5	Type 1						Type 2					
Case	RPx_{ig}	RPx_{sg}	RPa_i	RPa_s	Rao	Pf/W	RPx_{ig}	RPx_{sg}	RPa_i	RPa_s	Rao	Pf/W
Pass0	0,67	0,76	**0,87**	0,83	0,78	0,004	0,68	0,96	**1,21**	0,93	0,95	0,003
Pass1	0,35	0,63	0,95	0,77	0,67	0,005	0,36	0,77	1,53	0,78	0,86	0,009
Pass5	**0,12**	1,59	1,34	1,62	1,16	0,032	**0,23**	1,91	3,01	1,88	1,76	0,033
DBB	**0,24**	1,07	1,39	0,98	0,92	0,030	0,38	0,95	2,86	0,96	1,29	0,029
MED	**0,22**	1,40	1,45	1,43	1,12	0,030	**0,22**	1,83	2,89	1,83	1,69	0,035
MHF	0,47	0,79	1,13	**0,76**	0,79	0,005	0,41	0,87	**1,48**	0,91	0,92	0,004
ICOO	0,37	**0,49**	**0,70**	**0,51**	**0,52**	0,011	**0,33**	**0,71**	**1,19**	**0,65**	**0,72**	0,014
LQRCOO	0,36	**0,52**	**0,71**	**0,63**	**0,56**	0,009	**0,34**	**0,67**	**1,15**	**0,75**	**0,73**	0,010
MPCCOO	0,43	**0,61**	**0,85**	**0,60**	**0,62**	0,005	**0,34**	0,81	**1,46**	0,90	0,87	0,008
LQR2COO	0,36	**0,46**	**0,55**	**0,56**	**0,48**	0,011	**0,31**	**0,50**	**1,04**	**0,65**	**0,63**	0,010
Case	RRx_{ig}	RRx_{sg}	RRa_i	RRa_s	Rao	RMSf/W	RRx_{ig}	RRx_{sg}	RRa_i	RRa_s	Rao	RMSf/W
Pass0	0,72	**0,79**	**0,91**	**0,88**	0,82	0,001	0,69	0,79	**0,98**	0,84	0,83	0,001
Pass1	0,40	0,80	1,10	0,95	0,81	0,002	0,37	0,71	1,12	0,82	0,75	0,003
Pass5	**0,12**	2,13	1,52	2,14	1,48	0,013	**0,18**	1,84	2,18	1,88	1,52	0,013
DBB	**0,31**	1,18	1,33	1,18	1,00	0,008	**0,32**	1,04	1,72	1,09	1,04	0,009
MED	**0,30**	1,83	1,49	1,80	1,36	0,012	**0,16**	1,73	2,02	1,78	1,42	0,013
MHF	0,52	**0,72**	1,12	**0,84**	**0,80**	0,002	0,40	**0,56**	**0,89**	**0,67**	**0,63**	0,002
ICOO	0,45	**0,59**	**0,86**	**0,74**	**0,66**	0,003	**0,37**	**0,49**	**0,80**	**0,60**	**0,56**	0,003
LQRCOO	0,42	**0,59**	**0,79**	**0,75**	**0,64**	0,003	**0,35**	**0,58**	**0,92**	**0,68**	**0,63**	0,003
MPCCOO	0,50	**0,62**	**0,91**	**0,76**	**0,70**	0,002	**0,34**	**0,51**	**0,91**	**0,60**	**0,59**	0,003
LQR2COO	0,41	**0,66**	**0,76**	**0,84**	**0,67**	0,004	**0,33**	**0,56**	**0,71**	**0,69**	**0,57**	0,004

Table A30 - Evaluation criteria with Accelerogram 5 under type 1 and 2 input ground motions, in experimental trials.

Accel 6	Type 1						Type 2					
Case	RPx_{ig}	RPx_{sg}	RPa_i	RPa_s	Rao	Pf/W	RPx_{ig}	RPx_{sg}	RPa_i	RPa_s	Rao	Pf/W
Pass0	0,73	0,71	0,84	0,83	0,78	0,003	0,86	0,87	0,88	0,97	0,90	0,003
Pass1	0,44	0,65	0,81	0,71	0,66	0,004	0,47	0,70	0,87	0,83	0,72	0,008
Pass5	**0,14**	1,64	1,31	1,72	1,20	0,033	**0,13**	1,82	1,61	2,00	1,39	0,033
DBB	**0,26**	1,02	1,29	1,06	0,91	0,025	**0,27**	1,01	1,41	1,06	0,94	0,028
MED	**0,18**	1,44	1,14	1,56	1,08	0,032	**0,15**	1,71	1,59	1,91	1,34	0,031
MHF	0,47	0,77	1,08	0,85	0,79	0,004	0,56	**0,67**	**0,68**	**0,75**	**0,67**	0,004
ICOO	**0,43**	**0,55**	**0,62**	**0,61**	**0,55**	0,011	**0,44**	**0,49**	**0,76**	**0,58**	**0,57**	0,010
LQRCOO	**0,43**	**0,48**	**0,54**	**0,61**	**0,51**	0,008	0,48	**0,60**	**0,70**	**0,80**	**0,65**	0,006
MPCCOO	0,56	0,69	1,02	0,77	**0,76**	0,004	**0,46**	**0,57**	**0,80**	**0,72**	**0,64**	0,007
LQR2COO	**0,41**	**0,43**	**0,49**	**0,53**	**0,46**	0,009	**0,38**	**0,42**	**0,80**	**0,59**	**0,55**	0,009
Case	RRx_{ig}	RRx_{sg}	RRa_i	RRa_s	Rao	RMSf/W	RRx_{ig}	RRx_{sg}	RRa_i	RRa_s	Rao	RMSf/W
Pass0	0,59	0,63	**0,68**	**0,71**	0,65	0,001	0,73	**0,81**	**0,85**	**0,89**	**0,82**	0,001
Pass1	0,30	0,60	0,79	0,72	0,60	0,001	0,42	0,96	1,09	1,05	0,88	0,002
Pass5	**0,10**	1,59	1,13	1,58	1,10	0,011	**0,14**	2,58	1,84	2,50	1,76	0,012
DBB	**0,22**	0,91	1,00	0,91	0,76	0,007	**0,32**	1,30	1,27	1,30	1,05	0,007
MED	**0,19**	1,44	1,11	1,44	1,04	0,011	**0,15**	2,31	1,70	2,26	1,60	0,011
MHF	0,41	**0,55**	0,81	**0,66**	0,61	0,001	0,51	**0,63**	**0,74**	**0,76**	**0,66**	0,001
ICOO	0,35	**0,44**	**0,64**	**0,57**	**0,50**	0,003	0,47	**0,63**	**0,76**	**0,77**	**0,65**	0,003
LQRCOO	0,34	**0,47**	**0,64**	**0,62**	**0,52**	0,002	0,47	**0,76**	**0,89**	**0,89**	**0,75**	0,002
MPCCOO	0,42	**0,51**	**0,76**	**0,65**	**0,58**	0,002	0,44	**0,65**	**0,84**	**0,76**	**0,67**	0,002
LQR2COO	0,32	**0,50**	**0,57**	**0,65**	**0,51**	0,003	**0,41**	**0,70**	**0,66**	**0,89**	**0,66**	0,003

Table A31 - Evaluation criteria with Accelerogram 6 under type 1 and 2 ground motions, in experimental trials.

Accel 7	Type 1						Type 2					
Case	RPx_{ig}	RPx_{sg}	RPa_i	RPa_s	Rao	Pf/W	RPx_{ig}	RPx_{sg}	RPa_i	RPa_s	Rao	Pf/W
Pass0	0,76	0,84	**0,78**	0,92	0,83	0,004	0,78	1,07	**1,01**	1,07	0,98	0,003
Pass1	0,44	0,70	0,92	0,83	0,72	0,006	0,54	0,87	1,17	1,00	0,89	0,010
Pass5	**0,13**	1,46	1,30	1,70	1,15	0,033	**0,20**	2,46	2,11	2,46	1,81	0,034
DBB	**0,26**	1,09	1,27	1,20	0,96	0,030	**0,40**	1,20	1,61	1,21	1,10	0,032
MED	**0,22**	1,41	1,37	1,66	1,16	0,032	**0,20**	2,25	2,12	2,35	1,73	0,035
MHF	0,50	**0,66**	**0,90**	**0,77**	**0,71**	0,004	**0,52**	**0,73**	1,25	**0,89**	**0,85**	0,005
ICOO	**0,44**	**0,49**	**0,56**	**0,58**	**0,52**	0,012	**0,50**	**0,68**	**0,97**	**0,75**	**0,72**	0,013
LQRCOO	**0,42**	**0,40**	**0,61**	**0,54**	**0,49**	0,010	**0,46**	**0,71**	**0,85**	**0,85**	**0,72**	0,011
MPCCOO	0,55	**0,63**	**0,71**	**0,72**	**0,65**	0,005	**0,50**	**0,85**	**1,04**	**0,96**	**0,84**	0,009
LQR2COO	**0,39**	**0,39**	**0,49**	**0,58**	**0,46**	0,011	**0,45**	**0,63**	**1,07**	**0,74**	**0,72**	0,013
Case	RRx_{ig}	RRx_{sg}	RRa_i	RRa_s	Rao	RMSf/W	RRx_{ig}	RRx_{sg}	RRa_i	RRa_s	Rao	RMSf/W
Pass0	0,60	0,66	**0,76**	0,72	0,68	0,001	0,72	**0,87**	**1,04**	**0,94**	**0,89**	0,001
Pass1	0,31	0,59	0,89	0,71	0,62	0,002	0,46	0,95	1,36	1,06	0,96	0,003
Pass5	**0,12**	1,48	1,21	1,53	1,08	0,012	**0,19**	2,76	2,64	2,70	2,07	0,014
DBB	**0,18**	0,88	1,05	0,92	0,76	0,008	**0,37**	1,39	1,76	1,40	1,23	0,008
MED	**0,17**	1,37	1,21	1,42	1,04	0,012	**0,20**	2,38	2,36	2,35	1,82	0,012
MHF	0,39	**0,52**	**0,83**	**0,64**	**0,60**	0,002	0,54	**0,79**	**1,17**	**0,91**	**0,85**	0,001
ICOO	0,34	**0,42**	**0,64**	**0,54**	**0,48**	0,004	0,47	**0,69**	**1,02**	**0,82**	**0,75**	0,003
LQRCOO	**0,31**	**0,42**	**0,61**	**0,56**	**0,47**	0,003	**0,45**	**0,80**	**1,14**	**0,92**	**0,83**	0,003
MPCCOO	0,37	**0,47**	**0,72**	**0,58**	**0,54**	0,002	**0,45**	**0,74**	**1,17**	**0,86**	**0,80**	0,002
LQR2COO	**0,30**	**0,48**	**0,58**	**0,63**	**0,50**	0,003	**0,42**	**0,77**	**0,87**	**0,93**	**0,75**	0,003

Table A32 - Evaluation criteria with Accelerogram 7 under type 1 and 2 input ground motions, in experimental trials.

Accel 8	Type 1						Type 2					
Case	RPx_{ig}	RPx_{sg}	RPa_i	RPa_s	Rao	Pf/W	RPx_{ig}	RPx_{sg}	RPa_i	RPa_s	Rao	Pf/W
Pass0	0,64	0,76	0,90	0,77	0,77	0,003	0,73	**0,77**	**0,87**	**0,76**	0,78	0,003
Pass1	0,44	0,68	0,84	0,67	0,65	0,005	0,45	0,79	0,96	0,83	0,76	0,009
Pass5	**0,13**	1,34	1,25	1,32	1,01	0,030	**0,19**	1,51	2,02	1,62	1,33	0,035
DBB	**0,25**	0,93	1,11	0,89	0,79	0,028	**0,35**	1,23	1,36	1,20	1,04	0,032
MED	**0,13**	1,22	1,19	1,24	0,94	0,030	**0,19**	1,52	1,80	1,61	1,28	0,035
MHF	0,46	**0,55**	0,79	**0,56**	**0,59**	0,005	0,54	**0,59**	**0,94**	**0,65**	**0,68**	0,005
ICOO	**0,41**	**0,40**	**0,59**	**0,41**	**0,45**	0,011	**0,44**	**0,48**	**0,78**	**0,52**	**0,55**	0,013
LQRCOO	**0,38**	**0,43**	**0,56**	**0,50**	**0,47**	0,009	0,49	**0,53**	**0,88**	**0,61**	**0,63**	0,011
MPCCOO	0,45	**0,51**	**0,61**	**0,53**	**0,53**	0,005	0,47	**0,52**	**0,81**	**0,64**	**0,61**	0,009
LQR2COO	**0,35**	**0,41**	**0,48**	**0,48**	**0,43**	0,011	0,46	**0,45**	**0,89**	**0,55**	**0,59**	0,012
Case	RRx_{ig}	RRx_{sg}	RRa_i	RRa_s	Rao	RMSf/W	RRx_{ig}	RRx_{sg}	RRa_i	RRa_s	Rao	RMSf/W
Pass0	0,65	0,71	**0,78**	0,78	0,73	0,001	0,70	0,74	**0,79**	0,79	0,76	0,001
Pass1	0,35	0,61	0,83	0,74	0,63	0,002	0,43	0,69	0,84	0,79	0,69	0,004
Pass5	**0,10**	1,61	1,17	1,64	1,13	0,013	**0,17**	1,77	1,61	1,81	1,34	0,014
DBB	**0,25**	0,94	1,03	0,97	0,80	0,009	**0,27**	1,01	1,10	1,04	0,86	0,009
MED	**0,10**	1,54	1,14	1,58	1,09	0,013	**0,17**	1,63	1,49	1,69	1,24	0,013
MHF	0,41	**0,53**	**0,77**	**0,65**	**0,59**	0,002	0,50	**0,58**	**0,72**	**0,67**	**0,62**	0,002
ICOO	**0,34**	**0,44**	**0,64**	**0,57**	**0,50**	0,004	**0,39**	**0,49**	**0,63**	**0,60**	**0,53**	0,004
LQRCOO	**0,34**	**0,46**	**0,62**	**0,61**	**0,51**	0,003	**0,41**	**0,58**	**0,74**	**0,68**	**0,60**	0,003
MPCCOO	0,41	**0,49**	**0,70**	**0,63**	**0,56**	0,002	**0,38**	**0,51**	**0,69**	**0,61**	**0,55**	0,003
LQR2COO	**0,32**	**0,50**	**0,55**	**0,66**	**0,51**	0,003	**0,38**	**0,54**	**0,56**	**0,68**	**0,54**	0,004

Table A33 - Evaluation criteria with Accelerogram 8 under type 1 and 2 ground motions, in experimental trials.

Accel 9	Type 1						Type 2					
Case	RPx_{ig}	RPx_{sg}	RPa_i	RPa_s	Rao	Pf/W	RPx_{ig}	RPx_{sg}	RPa_i	RPa_s	Rao	Pf/W
Pass0	0,77	0,81	**0,88**	0,87	0,83	0,004	0,65	1,01	1,15	1,01	0,96	0,004
Pass1	0,40	0,82	1,25	0,83	0,82	0,004	0,48	0,76	1,10	0,87	0,80	0,012
Pass5	**0,14**	1,77	1,64	1,84	1,35	0,031	**0,16**	1,93	2,13	1,89	1,53	0,035
DBB	**0,25**	1,29	1,85	1,22	1,15	0,030	**0,34**	1,05	1,50	1,04	0,98	0,033
MED	**0,19**	1,66	1,56	1,61	1,25	0,032	**0,21**	1,56	1,99	1,51	1,32	0,035
MHF	0,47	0,88	**1,22**	0,91	0,87	0,004	0,53	0,83	1,21	**0,82**	0,85	0,006
ICOO	**0,36**	**0,54**	**0,77**	**0,60**	**0,57**	0,011	**0,46**	**0,63**	**1,04**	**0,65**	**0,70**	0,015
LQRCOO	**0,38**	**0,57**	**0,92**	**0,63**	**0,63**	0,009	**0,47**	**0,74**	1,15	**0,76**	**0,78**	0,013
MPCCOO	0,45	**0,72**	**1,14**	**0,76**	**0,77**	0,004	0,49	**0,76**	1,11	**0,78**	**0,78**	0,010
LQR2COO	**0,35**	**0,48**	**0,67**	**0,60**	**0,52**	0,011	**0,44**	**0,60**	**0,97**	**0,67**	**0,67**	0,013
Case	RRx_{ig}	RRx_{sg}	RRa_i	RRa_s	Rao	RMSf/W	RRx_{ig}	RRx_{sg}	RRa_i	RRa_s	Rao	RMSf/W
Pass0	0,69	0,75	**0,84**	0,80	0,77	0,001	0,65	1,01	1,15	1,01	0,96	0,004
Pass1	0,32	0,64	0,93	0,77	0,67	0,002	0,48	0,76	1,10	0,87	0,80	0,012
Pass5	**0,12**	1,75	1,35	1,76	1,25	0,013	**0,16**	1,93	2,13	1,89	1,53	0,035
DBB	**0,21**	0,95	1,17	0,98	0,83	0,008	**0,34**	1,05	1,50	1,04	0,98	0,033
MED	**0,18**	1,49	1,23	1,49	1,10	0,012	**0,21**	1,56	1,99	1,51	1,32	0,035
MHF	0,42	**0,56**	**0,89**	**0,69**	**0,64**	0,001	0,53	0,83	1,21	**0,82**	0,85	0,006
ICOO	0,36	**0,47**	**0,72**	**0,61**	**0,54**	0,004	**0,46**	**0,63**	**1,04**	**0,65**	**0,70**	0,015
LQRCOO	0,35	**0,48**	**0,70**	**0,63**	**0,54**	0,003	**0,47**	**0,74**	1,15	**0,76**	**0,78**	0,013
MPCCOO	0,44	**0,54**	**0,85**	**0,67**	**0,62**	0,002	0,49	**0,76**	1,11	**0,78**	**0,78**	0,010
LQR2COO	**0,32**	**0,54**	**0,65**	**0,70**	**0,55**	0,004	**0,44**	**0,60**	**0,97**	**0,67**	**0,67**	0,013

Table A34 - Evaluation criteria with Accelerogram 9 under type 1 and 2 input ground motions, in experimental trials.

Accel 10	Type 1						Type 2					
Case	RPx_{ig}	RPx_{sg}	RPa_i	RPa_s	Rao	Pf/W	RPx_{ig}	RPx_{sg}	RPa_i	RPa_s	Rao	Pf/W
Pass0	0,81	0,89	**1,10**	0,91	0,92	0,003	0,92	0,84	**0,83**	0,85	0,86	0,003
Pass1	0,40	0,71	1,26	0,79	0,79	0,005	0,46	0,71	1,30	0,83	0,83	0,009
Pass5	**0,11**	1,80	1,98	1,88	1,44	0,033	**0,15**	1,96	2,06	2,08	1,56	0,032
DBB	**0,28**	1,33	1,88	1,36	1,21	0,026	**0,33**	1,09	1,68	1,04	1,03	0,029
MED	**0,12**	1,71	1,97	1,82	1,40	0,034	**0,20**	1,69	2,13	1,85	1,47	0,031
MHF	0,45	0,73	1,39	0,91	0,87	0,004	0,73	0,79	**0,96**	0,87	0,84	0,005
ICOO	**0,34**	**0,53**	**0,85**	**0,55**	**0,57**	0,011	0,54	**0,60**	**0,78**	**0,67**	**0,65**	0,011
LQRCOO	**0,40**	**0,55**	**0,98**	**0,61**	**0,63**	0,009	0,47	**0,59**	**0,94**	**0,83**	**0,71**	0,008
MPCCOO	0,50	**0,69**	**1,08**	**0,74**	**0,75**	0,004	0,59	**0,68**	**0,97**	**0,81**	**0,76**	0,008
LQR2COO	**0,33**	**0,49**	**0,64**	**0,66**	**0,53**	0,010	**0,44**	**0,50**	**0,80**	**0,68**	**0,60**	0,009
Case	RRx_{ig}	RRx_{sg}	RRa_i	RRa_s	Rao	RMSf/W	RRx_{ig}	RRx_{sg}	RRa_i	RRa_s	Rao	RMSf/W
Pass0	0,80	**0,90**	**1,13**	**1,06**	**0,97**	0,001	0,83	**0,90**	**0,95**	**1,01**	**0,92**	0,001
Pass1	0,46	0,99	1,33	1,16	0,98	0,001	0,44	1,04	1,24	1,16	0,97	0,002
Pass5	**0,16**	2,95	1,92	2,77	1,95	0,012	**0,14**	3,09	2,38	2,86	2,12	0,011
DBB	**0,38**	1,75	1,72	1,68	1,38	0,008	**0,40**	1,62	1,69	1,56	1,32	0,007
MED	**0,21**	2,76	1,89	2,61	1,87	0,012	**0,23**	2,59	2,16	2,46	1,86	0,010
MHF	0,59	**0,86**	1,36	**1,03**	**0,96**	0,001	0,62	**0,76**	**0,95**	**0,91**	**0,81**	0,001
ICOO	0,47	**0,70**	**1,07**	**0,87**	**0,78**	0,003	0,50	**0,72**	**0,92**	**0,89**	**0,76**	0,003
LQRCOO	0,50	**0,74**	**1,00**	**0,96**	**0,80**	0,002	0,47	**0,77**	**0,94**	**0,92**	**0,78**	0,002
MPCCOO	0,60	**0,80**	**1,21**	**1,00**	**0,90**	0,001	0,51	**0,80**	**1,04**	**0,94**	**0,82**	0,002
LQR2COO	**0,45**	**0,82**	**0,93**	**1,07**	**0,82**	0,003	0,47	**0,87**	**0,90**	**1,10**	**0,83**	0,003

Table A35 - Evaluation criteria with Accelerogram 10 under type 1 and 2 ground motions, in experimental trials.

El Centro	FN						FP					
Case	RPx_{ig}	RPx_{sg}	RPa_i	RPa_s	Rao	Pf/W	RPx_{ig}	RPx_{sg}	RPa_i	RPa_s	Rao	Pf/W
Pass0	0,76	**0,91**	**1,08**	**0,94**	**0,92**	0,003	0,77	0,96	0,96	1,07	0,94	0,003
Pass1	0,50	1,04	1,21	1,13	0,97	0,004	0,51	0,83	0,89	0,85	0,77	0,007
Pass5	**0,20**	2,43	2,56	2,58	1,94	0,032	**0,26**	2,20	1,47	2,26	1,55	0,035
DBB	**0,19**	1,51	1,65	1,52	1,22	0,030	**0,36**	1,22	1,25	1,15	0,99	0,027
MED	**0,19**	2,10	2,48	2,27	1,76	0,030	**0,29**	1,97	1,14	2,04	1,36	0,035
MHF	0,57	**0,93**	1,42	**1,01**	0,99	0,006	0,71	1,00	1,34	1,02	1,02	0,007
ICOO	**0,43**	**0,87**	**1,06**	**0,84**	**0,80**	0,012	0,57	**0,69**	**0,77**	**0,67**	**0,68**	0,016
LQRCOO	**0,46**	**0,70**	**0,99**	**0,79**	**0,74**	0,008	0,61	**0,60**	**0,68**	**0,67**	**0,64**	0,010
MPCCOO	0,56	**0,84**	**1,37**	**0,91**	**0,92**	0,004	0,58	**0,82**	1,10	**0,83**	0,83	0,007
LQR2COO	**0,41**	**0,59**	**0,94**	**0,69**	**0,66**	0,011	0,57	**0,61**	**0,62**	**0,75**	**0,64**	0,012
Case	RRx_{ig}	RRx_{sg}	RRa_i	RRa_s	Rao	RMSf/W	RRx_{ig}	RRx_{sg}	RRa_i	RRa_s	Rao	RMSf/W
Pass0	0,68	**0,77**	**0,94**	**0,86**	**0,81**	0,001	0,67	0,72	**0,72**	0,78	0,72	0,001
Pass1	0,35	0,84	1,14	0,97	0,83	0,001	0,35	0,67	0,78	0,77	0,64	0,002
Pass5	**0,15**	2,26	1,71	2,20	1,58	0,009	**0,13**	1,54	1,00	1,49	1,04	0,009
DBB	**0,27**	1,34	1,39	1,32	1,08	0,006	**0,35**	0,85	0,83	0,84	0,72	0,006
MED	**0,16**	1,98	1,61	1,95	1,42	0,008	**0,14**	1,36	0,94	1,35	0,95	0,008
MHF	0,47	**0,67**	**1,09**	**0,82**	**0,76**	0,001	0,47	**0,58**	**0,74**	**0,67**	**0,62**	0,001
ICOO	0,38	**0,59**	**0,92**	**0,71**	**0,65**	0,002	0,36	**0,50**	**0,65**	**0,60**	**0,53**	0,003
LQRCOO	0,39	**0,63**	**0,90**	**0,79**	**0,68**	0,002	0,39	**0,50**	**0,60**	**0,63**	**0,53**	0,002
MPCCOO	0,49	**0,70**	**1,11**	**0,83**	**0,78**	0,001	0,43	**0,58**	**0,74**	**0,68**	**0,60**	0,002
LQR2COO	0,37	**0,71**	**0,88**	**0,90**	**0,71**	0,002	0,37	**0,55**	**0,58**	**0,70**	**0,55**	0,003

Table A36 - Evaluation criteria with El Centro earthquake, in experimental trials.

Newhall	FN						FP					
Case	RPx_{ig}	RPx_{sg}	RPa_i	RPa_s	Rao	Pf/W	RPx_{ig}	RPx_{sg}	RPa_i	RPa_s	Rao	Pf/W
Pass0	0,92	0,91	**0,86**	0,93	0,90	0,003	0,68	**0,73**	**0,87**	0,88	0,79	0,003
Pass1	0,64	0,77	1,10	0,82	0,84	0,006	0,40	0,75	0,97	0,79	0,73	0,006
Pass5	**0,51**	2,04	2,44	1,99	1,74	0,034	**0,22**	1,33	2,26	1,54	1,34	0,032
DBB	**0,60**	1,35	2,21	1,23	1,35	0,036	**0,36**	1,00	1,86	1,05	1,07	0,030
MED	**0,52**	2,02	2,18	2,04	1,69	0,033	**0,22**	1,26	2,22	1,46	1,29	0,032
MHF	0,68	1,02	1,24	1,00	0,99	0,006	0,46	**0,71**	**0,85**	**0,77**	**0,70**	0,005
ICOO	0,66	**0,66**	**0,87**	**0,71**	**0,73**	0,016	0,44	**0,61**	1,21	**0,75**	0,75	0,017
LQRCOO	**0,58**	**0,60**	**0,60**	**0,65**	**0,61**	0,014	0,41	**0,67**	1,02	**0,78**	**0,72**	0,012
MPCCOO	0,66	0,82	**0,99**	**0,81**	**0,82**	0,006	0,45	**0,64**	**0,79**	**0,77**	**0,67**	0,006
LQR2COO	**0,57**	**0,66**	**0,47**	**0,80**	**0,62**	0,014	0,41	**0,56**	**0,89**	**0,68**	**0,64**	0,012
Case	RRx_{ig}	RRx_{sg}	RRa_i	RRa_s	Rao	RMSf/W	RRx_{ig}	RRx_{sg}	RRa_i	RRa_s	Rao	RMSf/W
Pass0	0,89	0,83	**0,71**	0,92	0,84	0,001	0,74	0,79	0,86	0,85	0,81	0,001
Pass1	0,49	0,77	0,77	0,88	0,73	0,001	0,30	0,49	0,71	0,60	0,52	0,002
Pass5	**0,30**	1,83	1,14	1,76	1,26	0,007	**0,11**	1,14	1,06	1,19	0,88	0,008
DBB	**0,44**	1,13	0,92	1,12	0,90	0,005	**0,23**	0,68	0,88	0,72	0,63	0,006
MED	**0,27**	1,69	1,04	1,64	1,16	0,007	**0,10**	1,08	1,04	1,15	0,84	0,008
MHF	0,64	0,79	0,94	0,89	0,82	0,001	0,36	**0,46**	**0,64**	**0,58**	**0,51**	0,001
ICOO	0,51	**0,56**	**0,62**	**0,67**	**0,59**	0,002	**0,27**	**0,37**	**0,57**	**0,47**	**0,42**	0,003
LQRCOO	0,56	**0,66**	**0,61**	**0,79**	**0,66**	0,002	**0,30**	**0,43**	**0,66**	**0,54**	**0,48**	0,002
MPCCOO	0,62	**0,72**	0,81	**0,83**	0,74	0,001	0,34	**0,41**	**0,59**	**0,53**	**0,47**	0,001
LQR2COO	0,51	**0,68**	**0,51**	**0,81**	**0,63**	0,002	**0,28**	**0,39**	**0,50**	**0,52**	**0,42**	0,002

Table A37 - Evaluation criteria with Newhall earthquake, in experimental trials.

Rinaldi	FN						FP					
Case	RPx_{ig}	RPx_{sg}	RPa_i	RPa_s	Rao	Pf/W	RPx_{ig}	RPx_{sg}	RPa_i	RPa_s	Rao	Pf/W
Pass0	0,97	**1,03**	**1,27**	**0,99**	**1,07**	0,002	0,74	0,80	0,93	0,88	0,84	0,002
Pass1	0,85	1,51	1,79	1,42	1,39	0,006	0,29	0,49	0,79	0,61	0,55	0,004
Pass5	**0,54**	2,89	4,12	2,76	2,58	0,033	**0,08**	1,46	1,62	1,63	1,20	0,028
DBB	**0,67**	2,02	2,52	1,82	1,76	0,030	**0,20**	1,14	0,96	1,14	0,86	0,025
MED	**0,57**	2,88	4,10	2,79	2,59	0,033	**0,08**	1,29	1,45	1,47	1,07	0,027
MHF	**0,76**	**1,37**	**1,70**	**1,35**	**1,29**	0,006	0,43	0,58	0,80	0,68	0,62	0,004
ICOO	**0,66**	**0,93**	**1,58**	**1,01**	**1,05**	0,015	**0,28**	0,56	**0,70**	**0,56**	**0,52**	0,011
LQRCOO	**0,63**	**0,91**	**1,27**	**0,88**	**0,92**	0,014	0,35	**0,38**	**0,76**	**0,64**	**0,53**	0,005
MPCCOO	**0,77**	**1,22**	**1,51**	**1,20**	**1,17**	0,006	0,35	**0,48**	**0,71**	**0,61**	**0,54**	0,005
LQR2COO	**0,65**	**0,96**	**0,93**	**1,12**	**0,92**	0,016	0,33	**0,39**	**0,48**	**0,58**	**0,45**	0,007
Case	RRx_{ig}	RRx_{sg}	RRa_i	RRa_s	Rao	RMSf/W	RRx_{ig}	RRx_{sg}	RRa_i	RRa_s	Rao	RMSf/W
Pass0	0,84	0,85	**0,90**	0,95	0,89	0,001	0,62	0,65	0,72	0,71	0,68	0,001
Pass1	0,58	0,82	0,93	0,90	0,81	0,001	0,20	0,38	0,57	0,51	0,41	0,001
Pass5	**0,41**	1,91	1,86	1,80	1,49	0,007	**0,05**	0,85	0,85	0,91	0,66	0,005
DBB	**0,36**	1,00	1,16	1,00	0,88	0,004	**0,13**	0,59	0,71	0,64	0,52	0,004
MED	**0,44**	1,79	1,80	1,70	1,43	0,007	**0,05**	0,78	0,78	0,85	0,61	0,005
MHF	0,65	**0,67**	**0,87**	**0,79**	**0,75**	0,001	0,33	0,39	0,60	0,50	0,45	0,001
ICOO	**0,53**	**0,66**	**0,88**	**0,76**	**0,71**	0,002	0,22	**0,29**	**0,51**	**0,41**	**0,36**	0,002
LQRCOO	**0,57**	**0,68**	**0,82**	**0,81**	**0,72**	0,002	0,26	**0,32**	**0,55**	**0,47**	**0,40**	0,001
MPCCOO	**0,52**	**0,62**	**0,77**	**0,73**	**0,66**	0,001	0,28	**0,33**	**0,56**	**0,46**	**0,41**	0,001
LQR2COO	**0,53**	**0,70**	**0,75**	**0,84**	**0,70**	0,002	0,24	**0,34**	**0,49**	**0,50**	**0,40**	0,002

Table A38 - Evaluation criteria with Rinaldi earthquake, in experimental trials.

Sylmar	FN						FP					
Case	RPx_{ig}	RPx_{sg}	RPa_i	RPa_s	Rao	Pf/W	RPx_{ig}	RPx_{sg}	RPa_i	RPa_s	Rao	Pf/W
Pass0	0,61	**0,80**	**0,97**	**0,87**	**0,81**	0,003	0,67	**0,78**	**1,02**	**0,91**	0,85	0,003
Pass1	0,44	0,90	1,15	1,02	0,88	0,006	0,40	0,83	1,10	0,94	0,82	0,004
Pass5	**0,09**	1,60	1,62	1,68	1,25	0,029	**0,14**	2,17	1,82	2,37	1,63	0,032
DBB	**0,33**	**0,86**	1,51	**0,84**	**0,88**	0,029	**0,26**	1,23	1,80	1,20	1,12	0,027
MED	**0,10**	1,48	1,45	1,56	1,15	0,029	**0,15**	1,98	1,72	2,20	1,51	0,030
MHF	**0,41**	**0,82**	**1,04**	**0,90**	**0,79**	0,006	0,52	**0,66**	1,21	0,89	**0,82**	0,005
ICOO	**0,38**	**0,48**	**0,78**	**0,51**	**0,54**	0,013	**0,32**	**0,60**	**0,96**	**0,70**	**0,65**	0,012
LQRCOO	**0,37**	**0,66**	**1,09**	**0,71**	**0,71**	0,010	**0,40**	**0,45**	**0,82**	**0,55**	**0,55**	0,007
MPCCOO	0,45	**0,74**	**1,10**	**0,87**	**0,79**	0,006	0,47	**0,61**	**0,94**	**0,73**	**0,69**	0,005
LQR2COO	**0,35**	**0,48**	**0,56**	**0,62**	**0,50**	0,013	**0,37**	**0,46**	**0,69**	**0,72**	**0,56**	0,009
Case	RRx_{ig}	RRx_{sg}	RRa_i	RRa_s	Rao	RMSf/W	RRx_{ig}	RRx_{sg}	RRa_i	RRa_s	Rao	RMSf/W
Pass0	0,49	0,52	0,63	0,58	0,56	0,001	0,55	0,59	0,74	0,68	0,64	0,001
Pass1	0,25	0,34	0,52	0,43	0,39	0,001	0,23	0,45	0,65	0,58	0,48	0,001
Pass5	**0,03**	0,60	0,56	0,67	0,47	0,005	**0,09**	1,08	0,83	1,12	0,78	0,005
DBB	**0,16**	0,37	0,56	**0,42**	**0,38**	0,004	**0,15**	0,55	0,66	0,58	**0,48**	0,003
MED	**0,04**	0,57	0,55	0,65	0,45	0,005	**0,11**	0,96	0,78	1,02	0,72	0,005
MHF	0,29	0,35	0,55	0,45	0,41	0,002	0,34	**0,44**	0,75	**0,57**	0,52	0,001
ICOO	**0,21**	**0,22**	**0,35**	**0,31**	**0,28**	0,002	**0,21**	**0,33**	**0,53**	**0,47**	**0,38**	0,002
LQRCOO	**0,20**	**0,25**	**0,42**	**0,33**	**0,30**	0,001	0,26	**0,34**	**0,57**	**0,49**	**0,41**	0,001
MPCCOO	0,27	**0,31**	**0,52**	**0,39**	**0,37**	0,001	0,30	**0,39**	0,70	**0,53**	**0,48**	0,001
LQR2COO	**0,19**	**0,25**	**0,34**	**0,34**	**0,28**	0,002	0,28	**0,41**	**0,58**	0,59	**0,46**	0,002

Table A39 - Evaluation criteria with Sylmar earthquake, in experimental trials.

Erzikan	NS						EW					
Case	RPx_{ig}	RPx_{sg}	RPa_i	RPa_s	Rao	Pf/W	RPx_{ig}	RPx_{sg}	RPa_i	RPa_s	Rao	Pf/W
Pass0	0,79	0,70	0,84	0,73	0,77	0,003	0,76	**0,63**	**0,71**	**0,64**	**0,68**	0,002
Pass1	0,40	0,53	0,60	0,60	0,54	0,005	0,34	0,70	1,08	0,72	0,71	0,005
Pass5	**0,05**	1,05	0,88	1,20	0,79	0,026	**0,09**	1,54	0,99	1,60	1,06	0,029
DBB	**0,23**	0,75	1,16	0,82	0,74	0,025	**0,32**	0,98	1,40	1,04	0,94	0,026
MED	**0,06**	1,00	0,92	1,16	0,79	0,025	**0,11**	1,42	1,07	1,52	1,03	0,028
MHF	0,49	0,66	0,82	0,74	0,68	0,005	0,56	**0,53**	**0,88**	0,73	**0,67**	0,004
ICOO	0,43	**0,51**	**0,55**	**0,59**	**0,52**	0,011	0,44	**0,42**	**0,83**	**0,46**	**0,54**	0,010
LQRCOO	0,43	**0,45**	**0,52**	**0,53**	**0,48**	0,006	0,48	**0,43**	**0,66**	**0,49**	**0,52**	0,006
MPCCOO	0,51	**0,51**	0,65	**0,59**	0,56	0,005	0,54	**0,51**	**0,82**	**0,56**	**0,61**	0,005
LQR2COO	0,43	**0,40**	**0,39**	**0,47**	**0,42**	0,008	0,37	**0,38**	**0,44**	**0,55**	**0,44**	0,007
Case	RRx_{ig}	RRx_{sg}	RRa_i	RRa_s	Rao	RMSf/W	RRx_{ig}	RRx_{sg}	RRa_i	RRa_s	Rao	RMSf/W
Pass0	0,60	0,63	0,73	0,68	0,66	0,001	0,67	0,68	**0,64**	0,75	0,68	0,001
Pass1	0,25	0,37	0,45	0,47	0,38	0,001	0,27	0,55	0,71	0,69	0,56	0,001
Pass5	**0,02**	0,50	0,43	0,57	**0,38**	0,003	**0,06**	1,50	0,76	1,48	0,95	0,006
DBB	**0,14**	0,44	0,49	0,47	**0,38**	0,003	0,32	0,77	0,74	0,78	0,65	0,004
MED	**0,03**	0,45	0,42	0,52	**0,35**	0,003	**0,07**	1,42	0,75	1,43	0,92	0,006
MHF	0,32	0,38	0,53	0,45	0,42	0,001	0,46	**0,52**	**0,66**	**0,69**	0,58	0,001
ICOO	0,27	**0,29**	**0,39**	**0,38**	**0,33**	0,002	0,35	**0,41**	**0,53**	**0,55**	**0,46**	0,002
LQRCOO	0,26	**0,29**	**0,40**	**0,40**	**0,34**	0,001	0,39	**0,44**	**0,58**	**0,64**	**0,51**	0,001
MPCCOO	0,34	**0,36**	0,51	**0,46**	0,42	0,001	0,43	**0,46**	**0,61**	**0,62**	**0,53**	0,001
LQR2COO	0,26	**0,31**	**0,38**	**0,41**	**0,34**	0,001	0,32	**0,40**	**0,48**	**0,60**	**0,45**	0,001

Table A40 - Evaluation criteria with Erzikan earthquake, in experimental trials.

Jiji	NS						EW					
Case	RPx_{ig}	RPx_{sg}	RPa_i	RPa_s	Rao	Pf/W	RPx_{ig}	RPx_{sg}	RPa_i	RPa_s	Rao	Pf/W
Pass0	0,53	0,57	**0,67**	0,65	0,61	0,003	0,53	**0,58**	**0,71**	**0,66**	**0,62**	0,002
Pass1	0,23	0,38	0,68	0,52	0,45	0,007	0,34	0,66	0,83	0,74	0,64	0,007
Pass5	**0,03**	0,84	**0,65**	0,92	0,61	0,026	**0,10**	1,39	0,65	1,26	0,85	0,020
DBB	**0,13**	0,40	**0,66**	**0,45**	**0,41**	0,016	0,49	1,06	0,97	0,85	0,84	0,019
MED	**0,03**	0,78	**0,52**	0,87	0,55	0,024	**0,12**	1,36	0,68	1,23	0,85	0,020
MHF	0,33	0,48	**0,67**	0,53	0,50	0,004	0,52	**0,55**	**0,73**	**0,63**	**0,61**	0,003
ICOO	0,31	**0,37**	**0,49**	**0,45**	**0,41**	0,014	0,52	**0,62**	**0,63**	**0,65**	**0,60**	0,011
LQRCOO	0,36	**0,36**	**0,48**	**0,41**	**0,40**	0,007	0,48	**0,45**	**0,59**	**0,57**	**0,52**	0,004
MPCCOO	0,34	0,45	**0,61**	0,53	0,48	0,007	0,51	**0,60**	**0,68**	**0,66**	**0,61**	0,007
LQR2COO	0,29	**0,31**	**0,38**	**0,37**	**0,34**	0,008	0,41	**0,40**	**0,59**	**0,60**	**0,50**	0,005
Case	RRx_{ig}	RRx_{sg}	RRa_i	RRa_s	Rao	RMSf/W	RRx_{ig}	RRx_{sg}	RRa_i	RRa_s	Rao	RMSf/W
Pass0	0,37	0,38	0,47	0,45	0,42	0,001	0,51	**0,54**	0,79	0,80	0,66	0,001
Pass1	0,13	0,20	0,31	0,29	0,23	0,002	0,23	0,63	0,73	0,76	0,59	0,002
Pass5	**0,02**	0,30	**0,28**	0,36	0,24	0,003	**0,10**	1,05	0,73	0,98	0,72	0,003
DBB	**0,11**	0,22	**0,28**	**0,28**	**0,22**	0,003	0,58	0,89	0,73	0,86	0,76	0,003
MED	**0,02**	0,27	**0,27**	0,34	**0,23**	0,003	**0,12**	0,95	0,69	0,94	0,68	0,003
MHF	0,20	0,23	0,36	0,32	0,28	0,001	0,42	**0,49**	0,77	**0,76**	0,61	0,001
ICOO	0,19	**0,17**	**0,25**	**0,24**	**0,22**	0,002	0,47	**0,63**	**0,68**	**0,76**	0,63	0,002
LQRCOO	0,19	**0,19**	**0,30**	**0,29**	0,24	0,001	0,36	**0,44**	**0,66**	**0,70**	**0,54**	0,001
MPCCOO	0,20	0,22	0,34	0,31	0,27	0,002	0,34	**0,56**	0,74	**0,73**	**0,59**	0,002
LQR2COO	0,16	**0,18**	**0,27**	**0,27**	**0,22**	0,002	0,34	**0,46**	**0,66**	**0,73**	**0,55**	0,001

Table A41 - Evaluation criteria with Jiji earthquake, in experimental trials.

Kobe	NS						EW					
Case	RPx_{ig}	RPx_{sg}	RPa_i	RPa_s	Rao	Pf/W	RPx_{ig}	RPx_{sg}	RPa_i	RPa_s	Rao	Pf/W
Pass0	0,83	**0,82**	**0,89**	**0,89**	**0,86**	0,003	0,82	**0,90**	**0,96**	**1,00**	**0,92**	0,003
Pass1	0,74	0,82	1,64	0,90	1,02	0,006	0,61	1,05	1,05	1,13	0,96	0,007
Pass5	**0,53**	2,22	2,78	2,49	2,00	0,034	**0,51**	2,36	2,49	2,45	1,95	0,036
DBB	**0,41**	1,51	2,43	1,74	1,52	0,036	**0,59**	1,39	1,55	1,40	1,23	0,032
MED	**0,53**	2,16	2,71	2,42	1,96	0,034	**0,48**	2,32	2,38	2,48	1,92	0,038
MHF	**0,71**	**0,74**	**1,42**	**0,87**	**0,93**	0,006	0,71	1,11	1,39	1,22	1,11	0,007
ICOO	**0,55**	**0,58**	**0,82**	**0,66**	**0,65**	0,015	0,63	**0,57**	**0,84**	**0,70**	**0,69**	0,016
LQRCOO	**0,54**	**0,76**	**0,92**	**0,89**	**0,78**	0,016	0,62	**0,77**	**0,96**	**0,86**	**0,80**	0,015
MPCCOO	**0,67**	**0,62**	**0,99**	**0,80**	**0,77**	0,006	0,68	**0,88**	1,12	**0,96**	**0,91**	0,007
LQR2COO	**0,58**	**0,71**	**0,74**	**0,94**	**0,74**	0,018	0,67	**0,77**	**0,82**	**0,95**	**0,80**	0,018
Case	RRx_{ig}	RRx_{sg}	RRa_i	RRa_s	Rao	RMSf/W	RRx_{ig}	RRx_{sg}	RRa_i	RRa_s	Rao	RMSf/W
Pass0	0,85	**0,87**	**0,83**	**0,92**	**0,87**	0,001	0,84	**0,87**	**0,88**	**0,95**	**0,89**	0,001
Pass1	0,60	0,99	1,14	1,06	0,95	0,001	0,63	0,93	1,06	1,02	0,91	0,002
Pass5	**0,51**	2,43	1,92	2,33	1,80	0,010	**0,38**	2,20	1,87	2,17	1,66	0,011
DBB	**0,38**	1,55	1,41	1,51	1,21	0,007	**0,41**	1,33	1,29	1,34	1,09	0,007
MED	**0,49**	2,24	1,84	2,17	1,68	0,009	**0,36**	2,09	1,79	2,08	1,58	0,010
MHF	0,64	**0,79**	**0,97**	**0,88**	**0,82**	0,001	0,66	**0,88**	1,14	**0,95**	**0,91**	0,002
ICOO	**0,53**	**0,68**	**0,81**	**0,79**	**0,70**	0,002	**0,51**	**0,62**	**0,74**	**0,73**	**0,65**	0,003
LQRCOO	**0,55**	**0,88**	**0,93**	**0,98**	**0,84**	0,003	**0,56**	**0,81**	**0,87**	**0,91**	**0,79**	0,003
MPCCOO	0,61	**0,75**	**0,91**	**0,85**	**0,78**	0,001	0,64	**0,79**	**1,01**	**0,88**	**0,83**	0,002
LQR2COO	**0,51**	**0,87**	**0,74**	**0,99**	**0,78**	0,003	**0,55**	**0,81**	**0,70**	**0,94**	**0,75**	0,004

Table A42 - Evaluation criteria with Kobe earthquake, in experimental trials.

Type 1 - Peak values											
Case	Acc. 1	Acc. 2	Acc. 3	Acc. 4	Acc. 5	Acc. 6	Acc. 7	Acc. 8	Acc. 9	Acc. 10	#best
Pass0	**0,62**	0,74	**0,81**	**0,78**	0,78	0,78	0,83	0,77	0,83	0,92	3p
Pass1	0,64	0,60	0,83	0,81	0,67	0,66	0,72	0,65	0,82	0,79	7p
Pass5	1,03	1,16	1,17	1,28	1,16	1,20	1,15	1,01	1,35	1,44	
DBB	0,79	0,88	0,95	0,93	0,92	0,91	0,96	0,79	1,15	1,21	
MED	0,99	1,07	1,13	1,25	1,12	1,08	1,16	0,94	1,25	1,40	
MHF	**0,64**	0,62	0,96	**0,69**	0,79	0,79	**0,71**	**0,59**	0,87	0,87	
ICOO	**0,47**	**0,50**	**0,64**	**0,50**	**0,52**	**0,55**	**0,52**	**0,45**	**0,57**	**0,57**	1a/6b
LQRCOO	**0,42**	**0,50**	**0,56**	**0,56**	**0,56**	**0,51**	**0,49**	**0,47**	**0,63**	**0,63**	5b
MPCCOO	**0,60**	**0,60**	**0,77**	**0,62**	**0,62**	**0,76**	**0,65**	**0,53**	**0,77**	**0,75**	
LQR2COO	**0,41**	**0,49**	**0,55**	**0,53**	**0,48**	**0,46**	**0,46**	**0,43**	**0,52**	**0,53**	9a
Type 1 - RMS values											
Case	Acc. 1	Acc. 2	Acc. 3	Acc. 4	Acc. 5	Acc. 6	Acc. 7	Acc. 8	Acc. 9	Acc. 10	#best
Pass0	0,52	0,71	0,81	0,59	0,82	0,65	0,68	0,73	0,77	**0,97**	1p
Pass1	0,46	0,57	0,72	0,58	0,81	0,60	0,62	0,63	0,67	0,98	9p
Pass5	0,87	1,02	1,27	1,05	1,48	1,10	1,08	1,13	1,25	1,95	
DBB	0,55	0,73	0,87	0,73	1,00	0,76	0,76	0,80	0,83	1,38	
MED	0,73	0,97	1,18	0,95	1,36	1,04	1,04	1,09	1,10	1,87	
MHF	**0,44**	0,58	**0,71**	**0,55**	**0,80**	0,61	**0,60**	**0,59**	**0,64**	**0,96**	
ICOO	**0,34**	**0,41**	**0,58**	**0,45**	**0,66**	**0,50**	**0,48**	**0,50**	**0,54**	**0,78**	7a/7b
LQRCOO	**0,33**	**0,47**	**0,58**	**0,47**	**0,64**	**0,52**	**0,47**	**0,51**	**0,54**	**0,80**	5a/5b
MPCCOO	**0,39**	**0,48**	**0,66**	**0,53**	**0,70**	**0,58**	**0,54**	**0,56**	**0,62**	**0,90**	
LQR2COO	**0,37**	**0,45**	**0,59**	**0,48**	**0,67**	**0,51**	**0,50**	**0,51**	**0,55**	**0,82**	

Table A43 - Summary of average ratios (Rao) and number of best cases (#best) under type 1 seismic actions, in experimental trials.

Type 2 - Peak values											
Case	Acc. 1	Acc. 2	Acc. 3	Acc. 4	Acc. 5	Acc. 6	Acc. 7	Acc. 8	Acc. 9	Acc. 10	#best
Pass0	**0,63**	**0,76**	**0,56**	**0,68**	0,95	0,90	0,98	0,78	0,96	0,86	4p
Pass1	0,66	0,94	0,60	0,75	0,86	0,72	0,89	0,76	0,80	0,83	6p
Pass5	1,25	1,91	1,10	1,49	1,76	1,39	1,81	1,33	1,53	1,56	
DBB	0,90	1,08	0,76	1,09	1,29	0,94	1,10	1,04	0,98	1,03	
MED	1,30	1,79	1,06	1,41	1,69	1,34	1,73	1,28	1,32	1,47	
MHF	**0,61**	**0,84**	0,64	**0,75**	0,92	**0,67**	**0,85**	**0,68**	0,85	0,84	
ICOO	**0,57**	**0,67**	**0,48**	**0,61**	**0,72**	**0,57**	**0,72**	**0,55**	**0,70**	**0,65**	3a/9b
LQRCOO	**0,65**	**0,78**	**0,56**	**0,66**	**0,73**	**0,65**	**0,72**	**0,63**	**0,78**	**0,71**	1a/1b
MPCCOO	**0,51**	**0,75**	**0,53**	**0,68**	0,87	**0,64**	**0,84**	**0,61**	**0,78**	**0,76**	1b
LQR2COO	**0,50**	**0,61**	**0,46**	**0,63**	**0,63**	**0,55**	**0,72**	**0,59**	**0,67**	**0,60**	8a
Type 2 - RMS values											
Case	Acc. 1	Acc. 2	Acc. 3	Acc. 4	Acc. 5	Acc. 6	Acc. 7	Acc. 8	Acc. 9	Acc. 10	#best
Pass0	0,67	**0,82**	0,66	0,72	0,83	**0,82**	**0,89**	0,76	0,96	**0,92**	4p
Pass1	0,64	0,86	0,62	0,67	0,75	0,88	0,96	0,69	0,80	0,97	6p
Pass5	1,33	1,56	1,16	1,38	1,52	1,76	2,07	1,34	1,53	2,12	
DBB	0,89	0,97	0,73	0,86	1,04	1,05	1,23	0,86	0,98	1,32	
MED	1,18	1,47	1,06	1,32	1,42	1,60	1,82	1,24	1,32	1,86	
MHF	**0,57**	**0,78**	0,66	**0,66**	**0,63**	**0,66**	**0,85**	**0,62**	0,85	**0,81**	
ICOO	**0,53**	**0,64**	**0,54**	**0,55**	**0,56**	**0,65**	**0,75**	**0,53**	**0,70**	**0,76**	6a/9b
LQRCOO	**0,61**	**0,74**	**0,58**	**0,61**	**0,63**	**0,75**	**0,83**	**0,60**	**0,78**	**0,78**	
MPCCOO	**0,54**	**0,68**	**0,57**	**0,54**	**0,59**	**0,67**	**0,80**	**0,55**	**0,78**	**0,82**	1b
LQR2COO	**0,50**	**0,65**	**0,52**	**0,50**	**0,57**	**0,66**	**0,75**	**0,54**	**0,67**	**0,83**	5a

Table A44 - Summary of average ratios (Rao) and number of best cases (#best) under type 2 seismic actions, in experimental trials.

Peak val.	El Centro		Newhall		Rinaldi		Sylmar		Erzikan		Jiji		Kobe		
Case	FN	FP	FN	FP	FN	FP	FN	FP	NS	EW	NS	EW	NS	EW	#best
Pass0	**0,92**	0,94	0,90	0,79	**1,07**	0,84	**0,81**	0,85	0,77	**0,68**	0,61	**0,62**	**0,86**	**0,92**	7p
Pass1	0,97	0,77	0,84	0,73	1,39	0,55	0,88	0,82	0,54	0,71	0,45	0,64	1,02	0,96	7p
Pass5	1,94	1,55	1,74	1,34	2,58	1,20	1,25	1,63	0,79	1,06	0,61	0,85	2,00	1,95	
DBB	1,22	0,99	1,35	1,07	1,76	0,86	**0,88**	1,12	0,74	0,94	**0,41**	0,84	1,52	1,23	
MED	1,76	1,36	1,69	1,29	2,59	1,07	1,15	1,51	0,79	1,03	0,55	0,85	1,96	1,92	
MHF	0,99	1,02	0,99	**0,70**	**1,29**	0,62	**0,79**	**0,82**	0,68	**0,67**	0,50	**0,61**	**0,93**	1,11	
ICOO	**0,80**	**0,68**	**0,73**	0,75	**1,05**	**0,52**	**0,54**	**0,65**	**0,52**	**0,54**	**0,41**	**0,60**	**0,65**	**0,69**	2a/4b
LQRCOO	**0,74**	**0,64**	**0,61**	**0,72**	**0,92**	**0,53**	**0,71**	**0,55**	**0,48**	**0,52**	**0,40**	**0,52**	**0,78**	**0,80**	3a/9b
MPCCOO	**0,92**	0,83	**0,82**	**0,67**	**1,17**	**0,54**	**0,79**	**0,69**	0,56	**0,61**	0,48	**0,61**	**0,77**	**0,91**	1b
LQR2COO	**0,66**	**0,64**	**0,62**	**0,64**	**0,92**	**0,45**	**0,50**	**0,56**	**0,42**	**0,44**	**0,34**	**0,50**	**0,74**	**0,80**	10a
RMS val.	El Centro		Newhall		Rinaldi		Sylmar		Erzikan		Jiji		Kobe		
Case	FN	FP	FN	FP	FN	FP	FN	FP	NS	EW	NS	EW	NS	EW	#best
Pass0	**0,81**	0,72	0,84	0,81	0,89	0,68	0,56	0,64	0,66	0,68	0,42	0,66	**0,87**	**0,89**	3p
Pass1	0,83	0,64	0,73	0,52	0,81	0,41	0,39	0,48	0,38	0,56	0,23	0,59	0,95	0,91	11p
Pass5	1,58	1,04	1,26	0,88	1,49	0,66	0,47	0,78	**0,38**	0,95	0,24	0,72	1,80	1,66	
DBB	1,08	0,72	0,90	0,63	0,88	0,52	**0,38**	**0,48**	**0,38**	0,65	**0,22**	0,76	1,21	1,09	
MED	1,42	0,95	1,16	0,84	1,43	0,61	0,45	0,72	**0,35**	0,92	**0,23**	0,68	1,68	1,58	
MHF	**0,76**	**0,62**	0,82	**0,51**	**0,75**	0,45	0,41	0,52	0,42	0,58	0,28	0,61	**0,82**	**0,91**	
ICOO	**0,65**	**0,53**	**0,59**	**0,42**	**0,71**	**0,36**	**0,28**	**0,38**	**0,33**	**0,46**	**0,22**	0,63	**0,70**	**0,65**	11a/13b
LQRCOO	**0,68**	**0,53**	**0,66**	**0,48**	**0,72**	**0,40**	**0,30**	**0,41**	**0,34**	**0,51**	0,24	**0,54**	**0,84**	**0,79**	2a/2b
MPCCOO	**0,78**	**0,60**	0,74	**0,47**	**0,66**	**0,41**	**0,37**	**0,48**	0,42	**0,53**	0,27	**0,59**	**0,78**	**0,83**	
LQR2COO	**0,71**	**0,55**	**0,63**	**0,42**	**0,70**	**0,40**	**0,28**	**0,46**	**0,34**	**0,45**	**0,22**	**0,55**	**0,78**	**0,75**	5a

Table A45 - Summary of average ratios (Rao) and number of best cases (#best) under earthquake records, in experimental trials.

Peak values					
Case	Type 1	Type 2	Type 1&2	Earthquakes	All
Pass0	3p	4p	7p	7p	14p
Pass1	7p	6p	13p	7p	20p
Pass5					
DBB					
MED					
MHF					
ICOO	1a/6b	3a/9b	4a/15b	2a/4b	6a/19b
LQRCOO	5b	1a/1b	1a/6b	3a/9b	4a/15b
MPCCOO		1b	1b	1b	2b
LQR2COO	9a	8a	17a	10a	27a
RMS values					
Case	Type 1	Type 2	Type 1&2	Earthquakes	All
Pass0	1p	4p	5p	3p	8p
Pass1	9p	6p	15p	11p	26p
Pass5					
DBB					
MED					
MHF					
ICOO	7a/7b	6a/9b	13a/16b	11a/13b	24a/29b
LQRCOO	5a/5b		5a/5b	2a/2b	7a/7b
MPCCOO		1b	1b		1b
LQR2COO		5a	5a	5a	10a

Table A46 - Number of best cases (#best) for each solution, in experimental trials.

A3 Comparison of Experimental and Numerical Results

This section presents a comparison of results in terms of frequency response functions (FRFs) obtained from the numerical and experimental data. The FRFs were evaluated using the collected response time data resulting from artificial accelerograms (10 type 1 and 10 type 2 accelerograms) as inputs, with the H1 estimator, using a hanning window with 4096 points, which results in 0,05 Hz of frequency resolution.

The FRFs presented relate the output relative displacements and accelerations with the input ground acceleration: X_{ig}/A_g; X_{si}/A_g; A_i/A_g; A_s/A_g. The comparison is made for all the solutions under study:

- Original structure;
- MR damper in passive mode: with 0 V – Pass0; w/1 V – Pass1; and w/5 V – Pass5;
- MR damper in Semi-active mode with the strategies under study: Decentralized Bang-Bang control – DBB; Maximum Energy Dissipation algorithm – MED; Modulated Homogeneous Friction – MHF; the Integral control, two Linear Quadratic Regulator controllers and the Model Predictive Control plus a Clipped On-Off algorithm, referred as ICOO, LQRCOO, LQR2COO and MPCCOO respectively.

Figures A1 to A11 show the comparison of results in terms of FRFs (magnitude and phase).

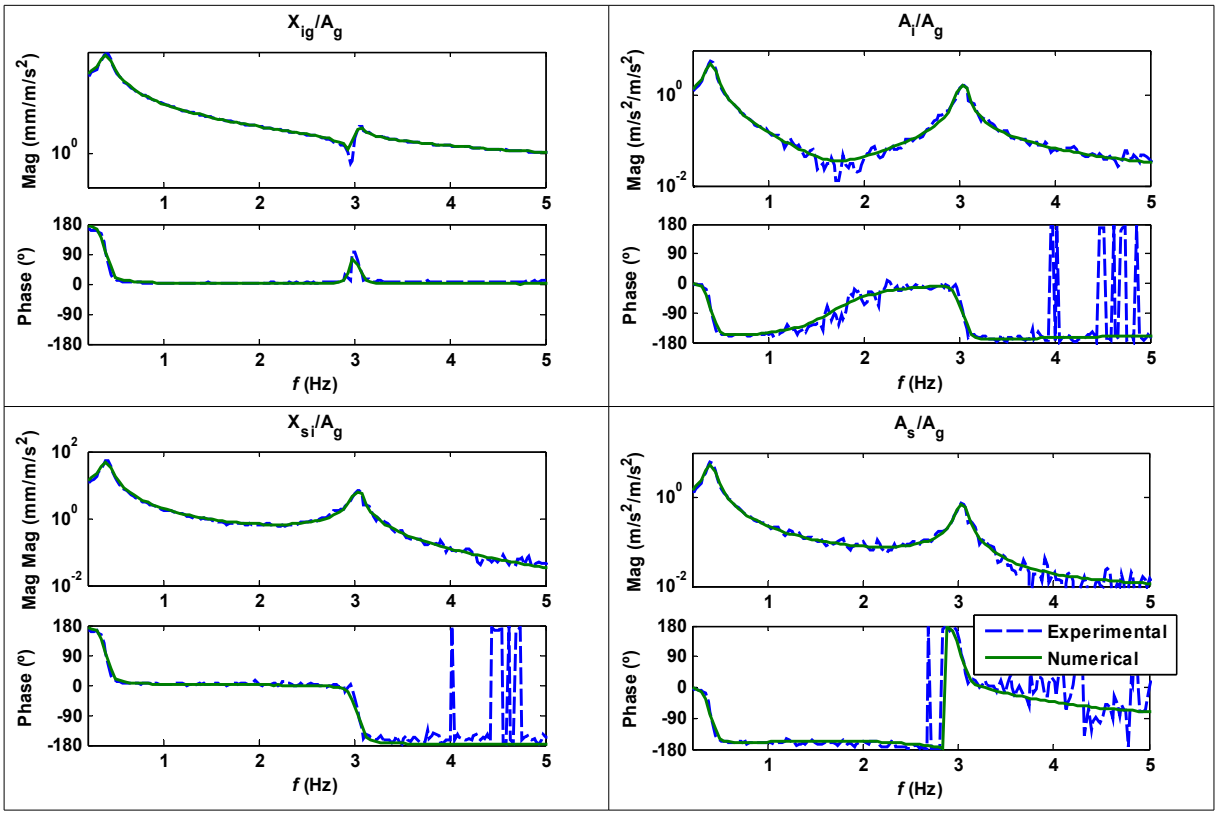

Figure A1 - Comparison between the numerical and experimental FRFs for the Original structure, obtained using the artificial accelerograms as input.

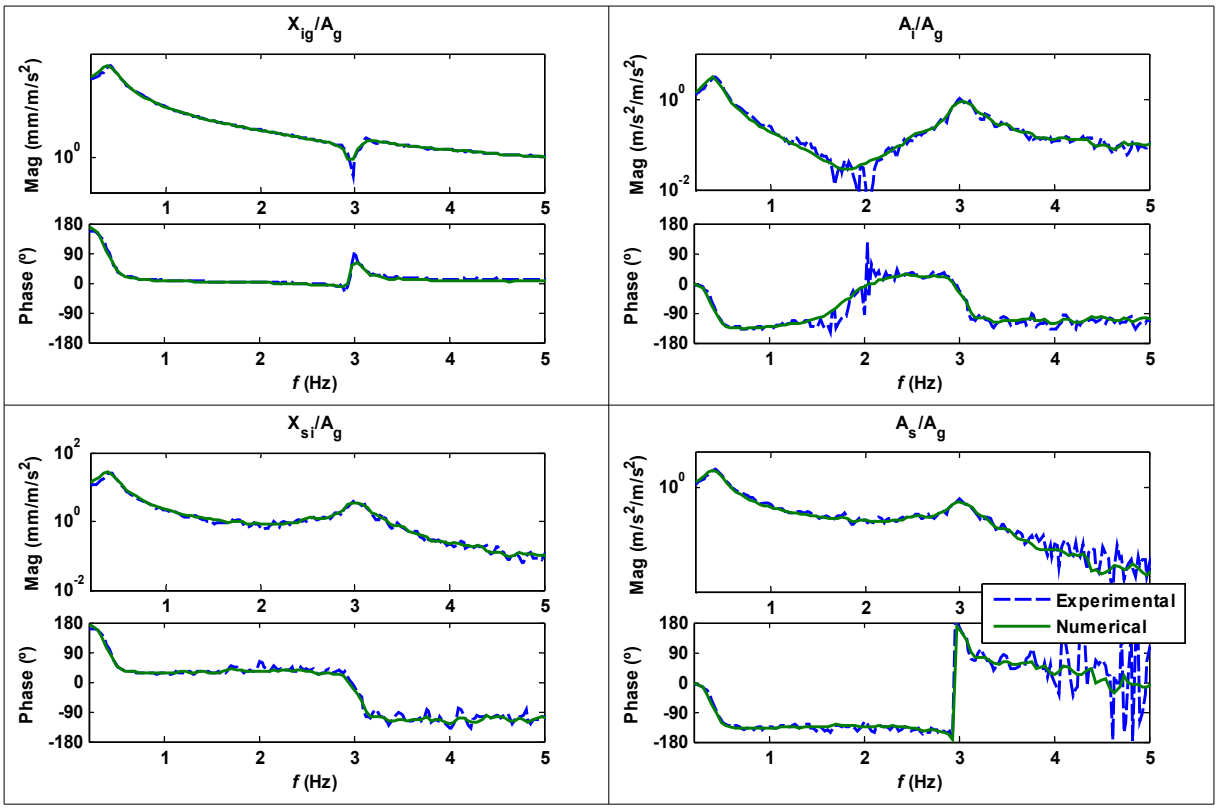

Figure A2 - Comparison between the numerical and experimental FRFs for the Pass0 case, obtained using the artificial accelerograms as input.

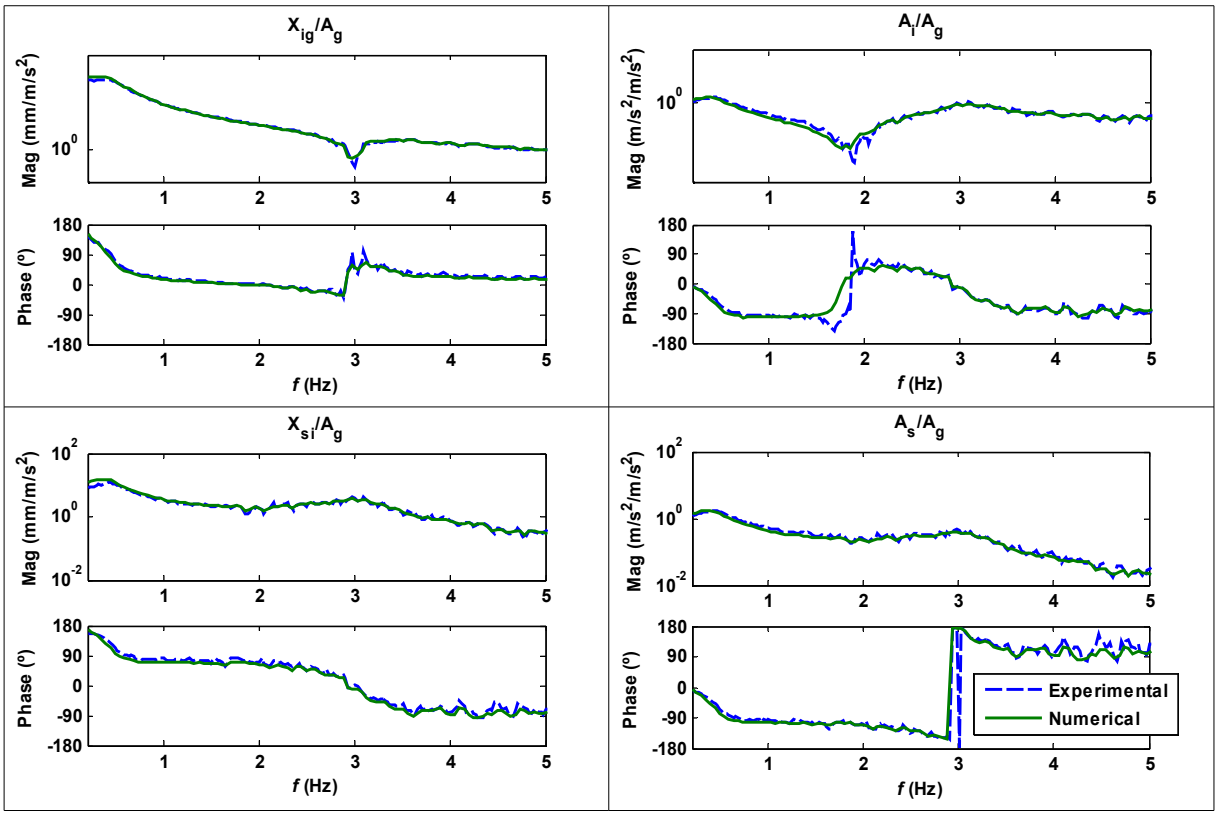

Figure A3 - Comparison between the numerical and experimental FRFs for the Pass1 case, obtained using the artificial accelerograms as input.

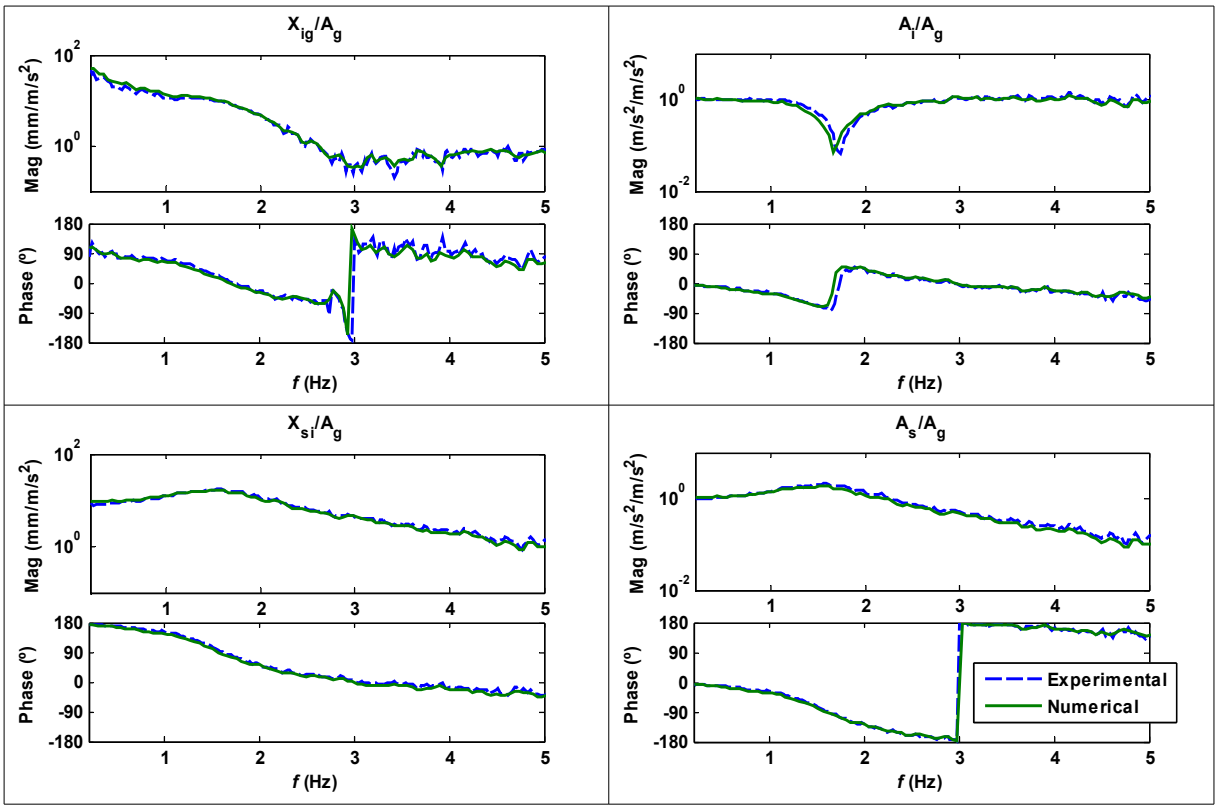

Figure A4 - Comparison between the numerical and experimental FRFs for the Pass5 case, obtained using the artificial accelerograms as input.

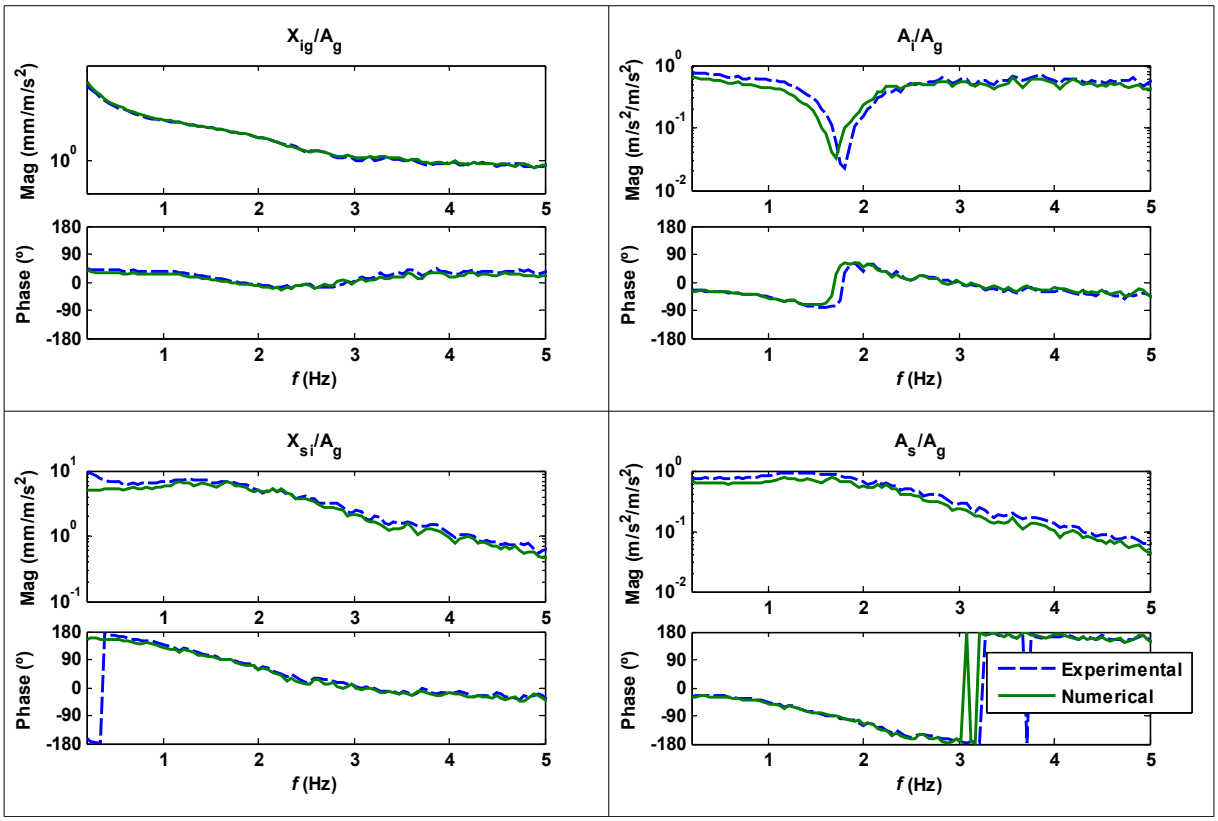

Figure A5 - Comparison between the numerical and experimental FRFs for the DBB case, obtained using the artificial accelerograms as input.

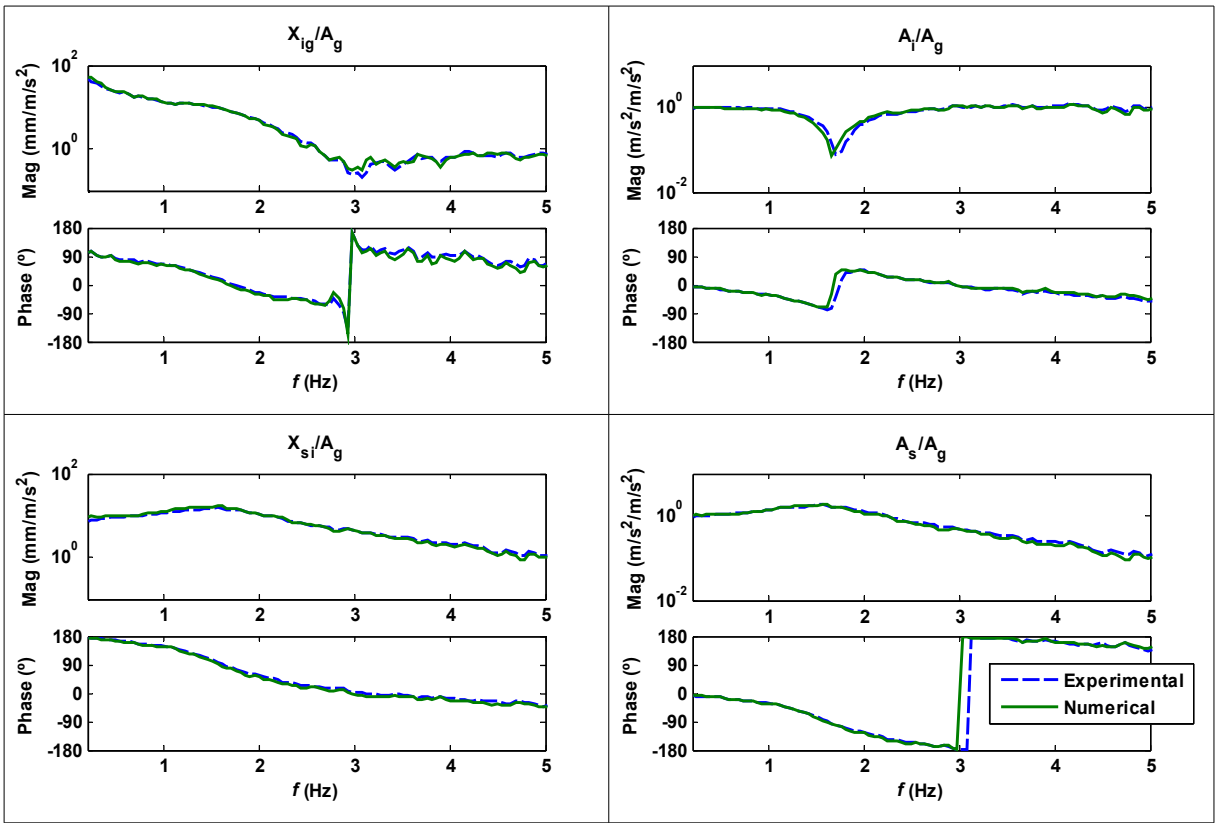

Figure A6 - Comparison between the numerical and experimental FRFs for the MED case, obtained using the artificial accelerograms as input.

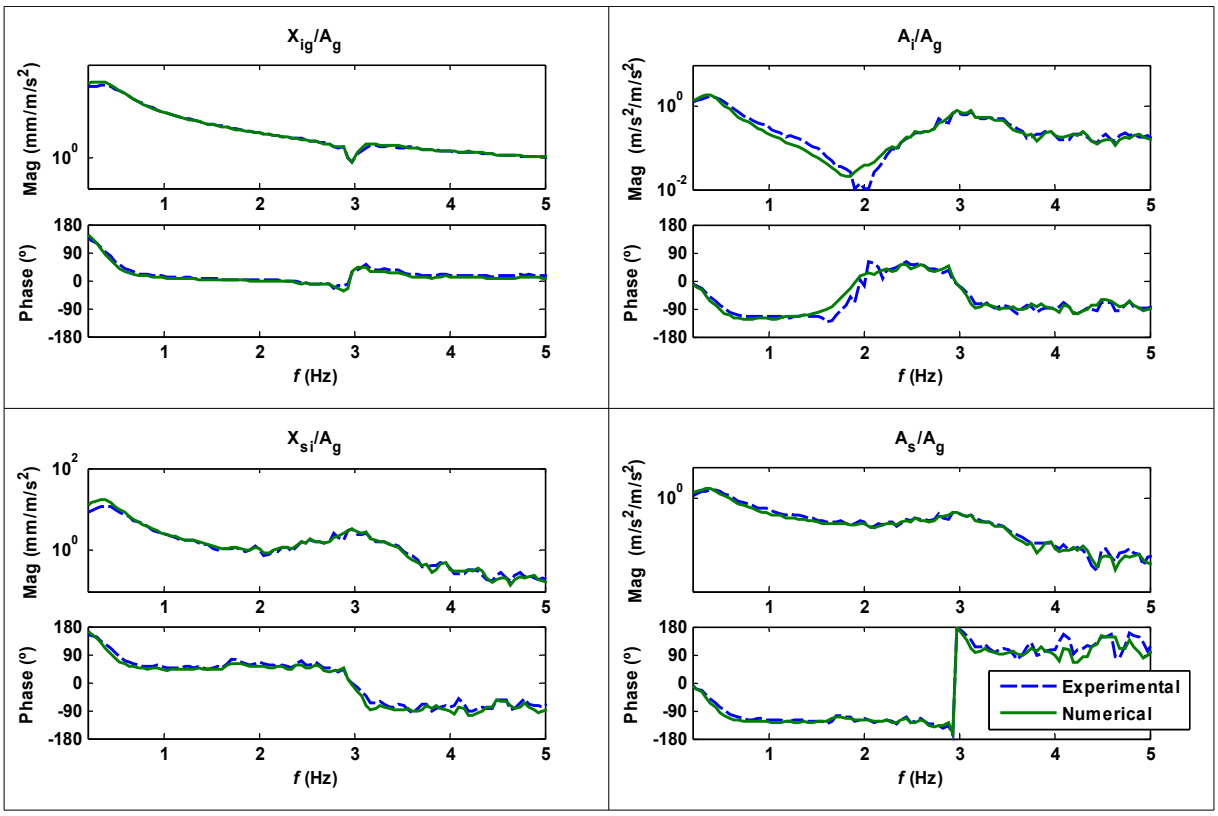

Figure A7 - Comparison between the numerical and experimental FRFs for the MHF case, obtained using the artificial accelerograms as input.

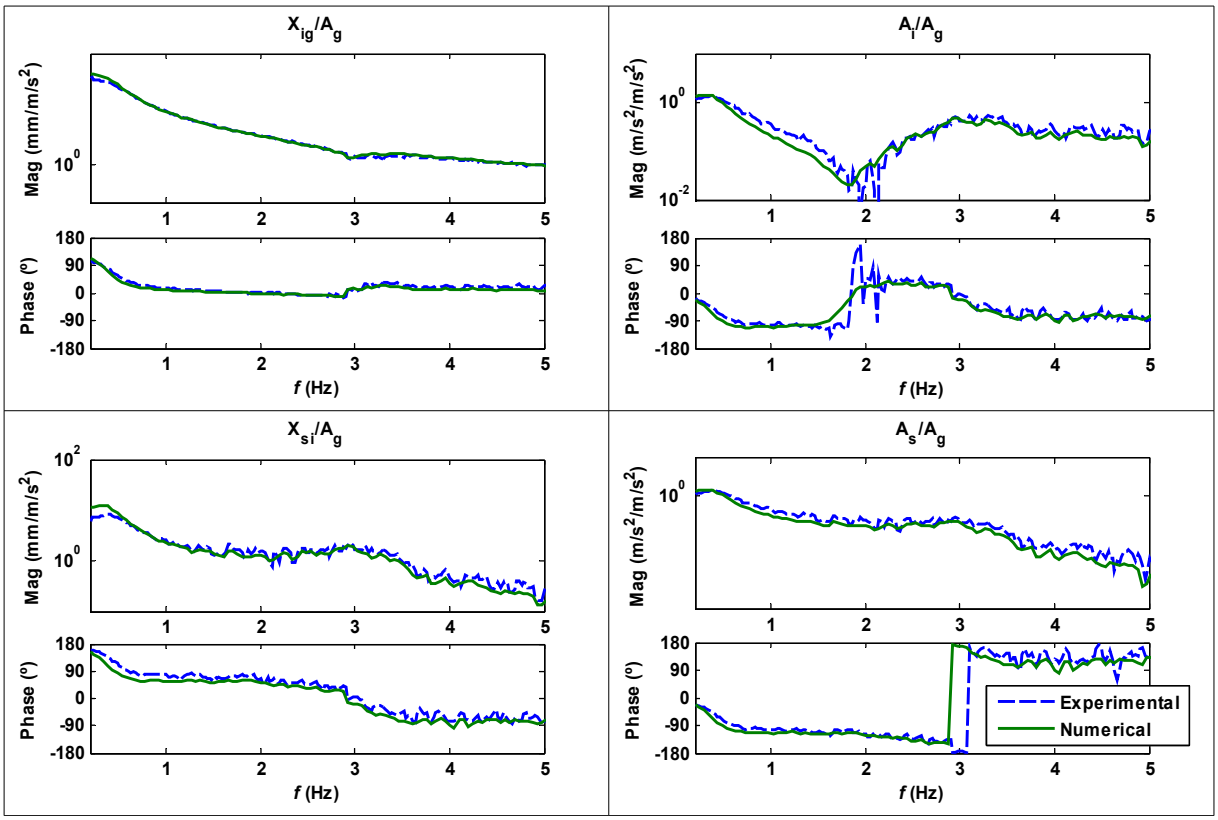

Figure A8 - Comparison between the numerical and experimental FRFs for the ICOO case, obtained using the artificial accelerograms as input.

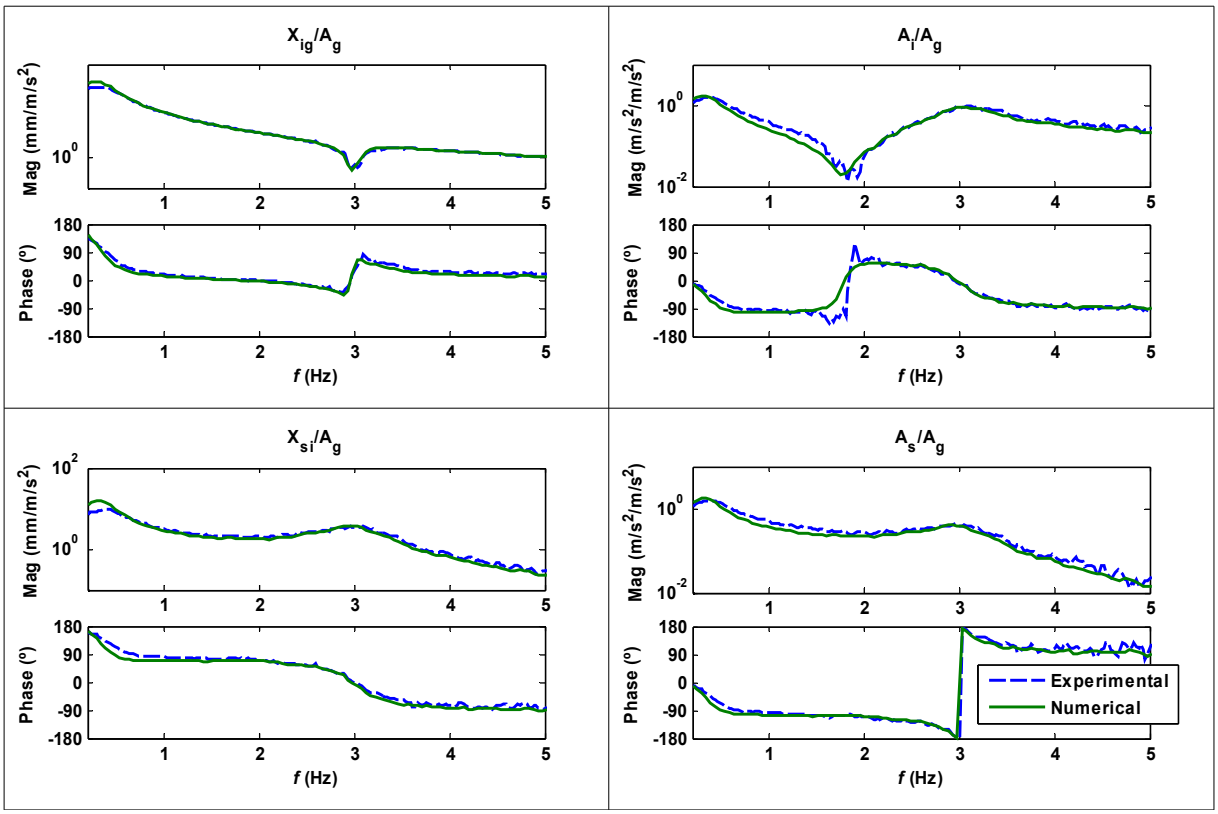

Figure A9 - Comparison between the numerical and experimental FRFs for the LQRCOO case, obtained using the artificial accelerograms as input.

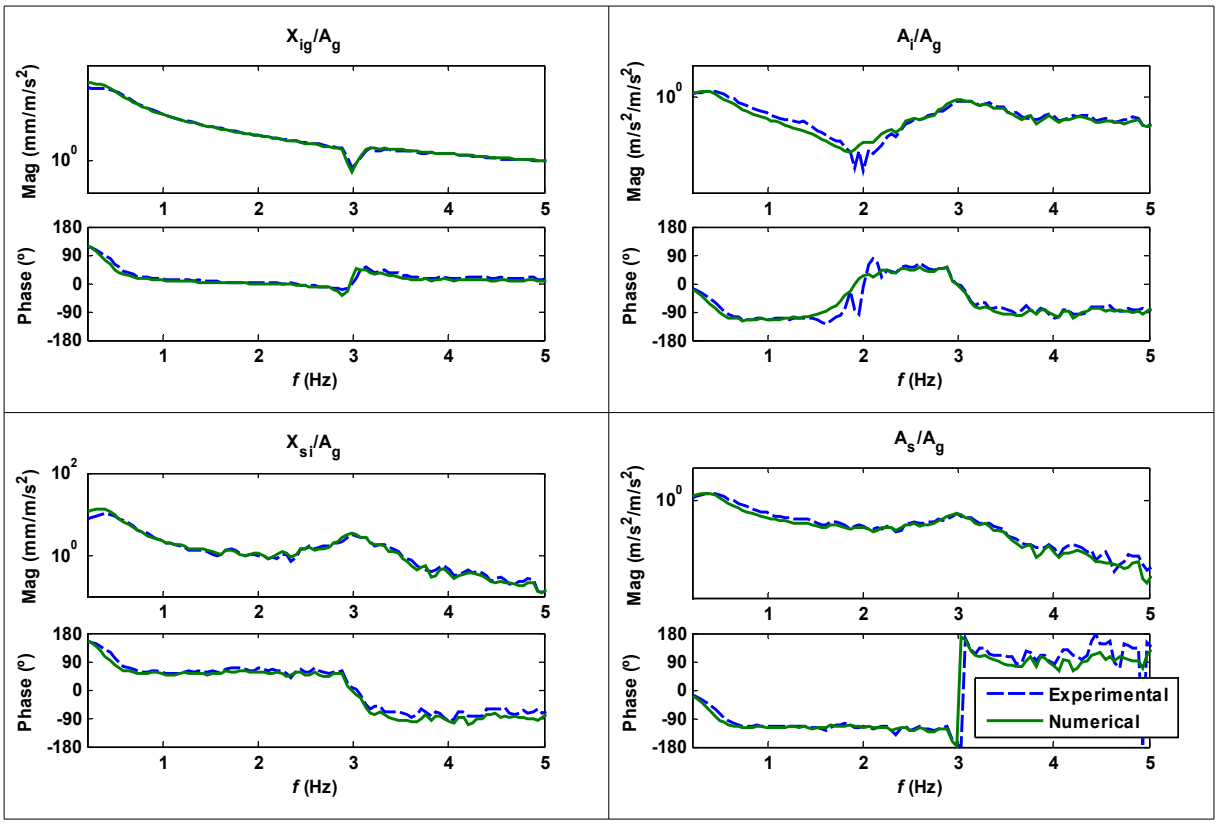

Figure A10 - Comparison between the numerical and experimental FRFs for the MPCCOO case, obtained using the artificial accelerograms as input.

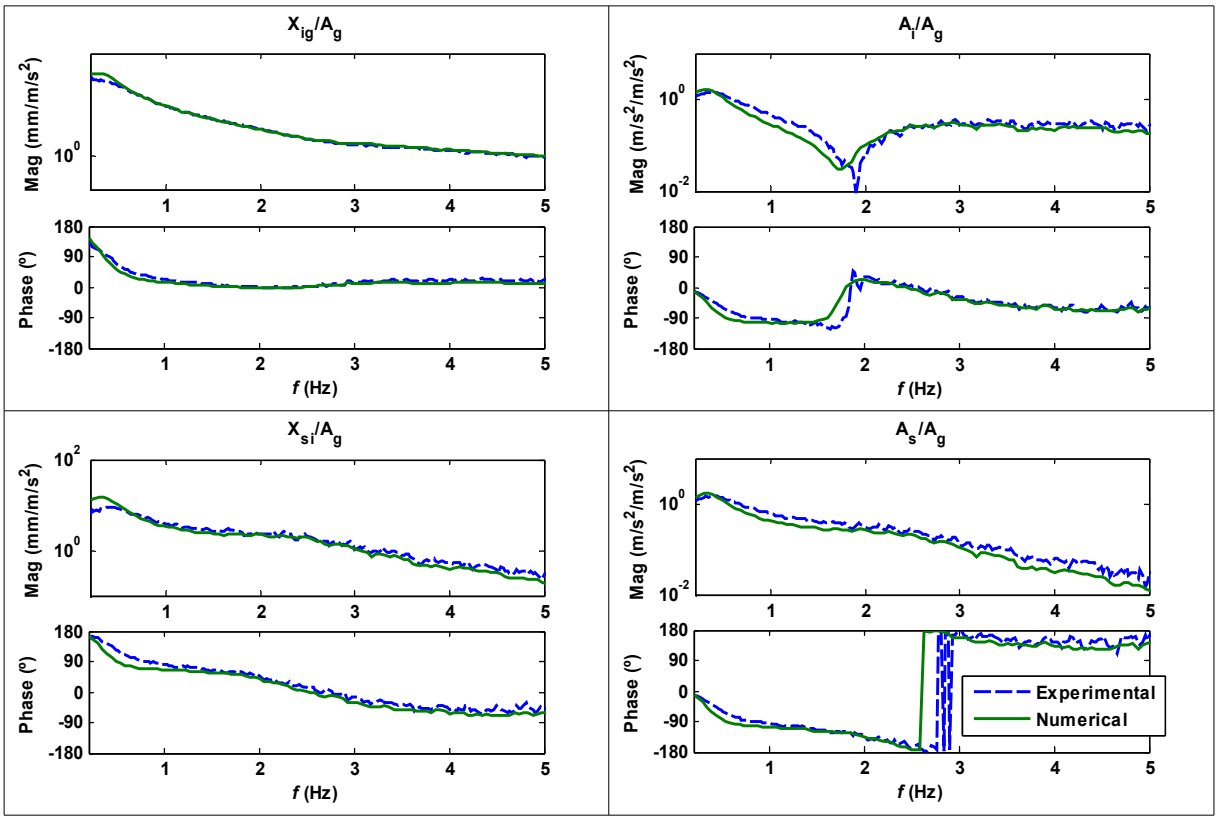

Figure A11 - Comparison between the numerical and experimental FRFs for the LQR2COO case, obtained using the artificial accelerograms as input.